LEABHARLANN CHOLÁISTE NA TRÍONÓIDE, BAILE ÁTHA CLIATH | TRINITY COLLEGE LIBRARY DUBLIN
Ollscoil Átha Cliath | The University of Dublin

Terms and Conditions of Use of Digitised Theses from Trinity College Library Dublin

Copyright statement

All material supplied by Trinity College Library is protected by copyright (under the Copyright and Related Rights Act, 2000 as amended) and other relevant Intellectual Property Rights. By accessing and using a Digitised Thesis from Trinity College Library you acknowledge that all Intellectual Property Rights in any Works supplied are the sole and exclusive property of the copyright and/or other IPR holder. Specific copyright holders may not be explicitly identified. Use of materials from other sources within a thesis should not be construed as a claim over them.

A non-exclusive, non-transferable licence is hereby granted to those using or reproducing, in whole or in part, the material for valid purposes, providing the copyright owners are acknowledged using the normal conventions. Where specific permission to use material is required, this is identified and such permission must be sought from the copyright holder or agency cited.

Liability statement

By using a Digitised Thesis, I accept that Trinity College Dublin bears no legal responsibility for the accuracy, legality or comprehensiveness of materials contained within the thesis, and that Trinity College Dublin accepts no liability for indirect, consequential, or incidental, damages or losses arising from use of the thesis for whatever reason. Information located in a thesis may be subject to specific use constraints, details of which may not be explicitly described. It is the responsibility of potential and actual users to be aware of such constraints and to abide by them. By making use of material from a digitised thesis, you accept these copyright and disclaimer provisions. Where it is brought to the attention of Trinity College Library that there may be a breach of copyright or other restraint, it is the policy to withdraw or take down access to a thesis while the issue is being resolved.

Access Agreement

By using a Digitised Thesis from Trinity College Library you are bound by the following Terms & Conditions. Please read them carefully.

I have read and I understand the following statement: All material supplied via a Digitised Thesis from Trinity College Library is protected by copyright and other intellectual property rights, and duplication or sale of all or part of any of a thesis is not permitted, except that material may be duplicated by you for your research use or for educational purposes in electronic or print form providing the copyright owners are acknowledged using the normal conventions. You must obtain permission for any other use. Electronic or print copies may not be offered, whether for sale or otherwise to anyone. This copy has been supplied on the understanding that it is copyright material and that no quotation from the thesis may be published without proper acknowledgement.

PREPARATION AND CHARACTERISATION OF SPRAY DRIED COMPOSITES OF PHARMACEUTICAL MATERIALS

by

Deirdre Olive Corrigan, B.Sc. (Pharm.), Dip. Stat. Q.I., M.P.S.I.

being a thesis submitted for

the degree of Doctor of Philosophy in Pharmaceutics

at

University of Dublin

Trinity College

under the supervision and direction of

A. M. Healy, B.Sc. (Pharm.), Ph.D., M.P.S.I.

November 2002

TRINITY COLLEGE
13 MAR 2003
LIBRARY DUBLIN
THESIS
7172

DECLARATION

This thesis is submitted by the undersigned to the University of Dublin, Trinity College, for examination for the degree of Doctor of Philosophy. It has not been submitted for a degree at any other university. I myself carried out all the practical work except where duly acknowledged. This manuscript was written by me with the help of editorial advice from Dr. A. M. Healy.

I give permission for the Library to lend or copy this thesis upon request.

Deirdre Corrigan

Science is built up of facts,
as a house is built of stones;
but an accumulation of facts is no more a science
than a heap of stones is a house.

Henri Poincaré

TABLE OF CONTENTS

Acknowledgements i

Presentations and Publications associated with this thesis ii

Abbreviations and Symbols iii

Summary vii

INTRODUCTION

Origin and scope of the thesis 1

CHAPTER 1. INTRODUCTION

1.1 Spray Drying 2

1.2 Solid State Phases 7

1.2.1 Amorphous forms 7

1.2.2 Polymorphism 8

1.2.3 Pseudopolymorphism 9

1.3 Solid Dispersions 9

1.3.1 Classification of Solid Dispersions 11

1.3.1.1 Eutectics 11

1.3.1.2 Solid solutions 12

1.3.1.3 Glass solutions and suspensions 14

1.3.1.4 Amorphous precipitations in crystalline carriers 14

1.3.1.5 Compound and complex formation 15

1.3.1.6 Combinations of the above systems 15

1.3.2 Methods of preparation of solid dispersions 15

1.3.3 Methods of Characterisation of Solid State Forms 17

1.3.3.1 Thermal Analysis 17

1.3.3.2 Powder X-ray Diffraction (XRD) 18

1.3.3.3 Fourier Transform Infrared Spectroscopy (FTIR) 21

1.3.3.4 Hot Stage Microscopy 21

1.3.3.5 Intrinsic Dissolution Rate Studies 21

1.4 Excipients used in this work 22
1.4.1 Polyethylene glycols (PEGs) 22
1.4.2 Lactose 24
1.4.3 Chitosan 28
1.5 Drugs used in the current work 34
1.5.1 Bendroflumethiazide 34
1.5.2 Salbutamol base 35
1.5.3 Salbutamol sulphate 35
1.5.4 Ipratropium bromide monohydrate 36
1.5.5 Budesonide 36
1.5.6 Formoterol fumarate dihydrate 37
1.6 Dry powder inhaler delivery 37

EXPERIMENTAL

CHAPTER 2. MATERIALS AND METHODS

2.1 Materials 43
2.2 Methods 45
2.2.1 Spray drying 45
2.2.2 Solid Dispersion Production 45
2.2.3 Powder X-Ray Diffraction 45
2.2.4 Differential Scanning Calorimetry Analysis 45
2.2.5 Thermogravimetric Analysis 46
2.2.6 Hot Stage Microscopy 46
2.2.7 Light microscopy 46
2.2.8 Scanning Electron Microscopy 46
2.2.9 Energy Dispersive X-Ray Analysis 46
2.2.10 Fourier Transform Infrared Spectroscopy 47
2.2.11 Gel Permeation Chromatography (GPC) 47
2.2.12 High Performance Liquid Chromatography 48
2.2.13 UV Analysis 49
2.2.14 *In Vitro* Aerosol Characterisation 49
2.2.15 Assay for Degree of Deacetylation of Chitosan 50

2.2.16 *In Vitro* Release Studies 51
2.2.16.1 Dissolution studies on BFMT and BFMT/PEG systems 51
2.2.16.2 Release from chitosan/salbutamol sulphate systems 52
2.2.16.3 Release from particles 52
2.2.17 Statistical Analysis 52
2.2.18 Particle Size Measurement 53
2.2.19 Density Measurements 53
2.2.20 Preparation of Formaldehyde Solution for use as the Crosslinking Agent 53
2.2.21 Production of 5-Trifluoromethyl-2,4-disulphamoylaniline 53
2.2.22 Creation of Defined Relative Humidity (RH) Conditions 54
2.2.23 Phagocytosis Study 54
2.2.24 Modelling Drug Release 55

RESULTS AND DISCUSSION

CHAPTER 3. CO-SPRAY DRIED LACTOSE/PEG 4000 SYSTEMS

3.1. Introduction 57
3.2. Individual components spray dried alone 58
3.2.1. Lactose 58
3.2.2. PEG 4000 60
3.3. Co-spray dried lactose/PEG 4000 systems 63
3.3.1. Lactose/PEG 4000 5% 63
3.3.2. Lactose/PEG 4000 10% 64
3.3.3. Lactose/PEG 4000 20% 67
3.3.4. Lactose/PEG 4000 30% 68
3.4. Effect of storage on physicochemical properties of spray dried systems 69
3.4.1. Spray dried lactose 69
3.4.2. PEG 4000 72
3.4.3. Co-spray dried systems 76
3.5. Conclusions 90

CHAPTER 4. CO-SPRAY DRIED BENDROFLUMETHIAZIDE/PEG SYSTEMS

4.1. Introduction 93

4.2. Co-spray dried BFMT/PEG 4000 systems 94

4.2.1. Physical stability of BFMT/PEG 4000 systems 100

4.2.2. Chemical stability of BFMT/PEG 4000 systems 104

4.3. Co-spray dried BFMT/PEG 20,000 and PEO 300,000 systems 105

4.3.1. Spray dried PEG 20,000 106

4.3.2. Co-spray dried BFMT/PEG 20,000 systems 108

4.3.3. Spray dried PEO 300,000 111

4.3.4. Co-spray dried BFMT/PEO 300,000 systems 113

4.4. Phase Diagrams 117

4.5. Conclusions 122

CHAPTER 5. SPRAY DRIED DRUG MIXTURES FOR USE IN DRY POWDER INHALER FORMULATIONS

5.1. Introduction 124

5.2. Salbutamol and ipratropium bromide systems 125

5.2.1. Salbutamol sulphate 125

5.2.2. Salbutamol base 130

5.2.3. Ipratropium bromide monohydrate 132

5.2.4. Co-spray dried salbutamol sulphate and ipratropium bromide 136

5.2.5. Co-spray dried salbutamol base and ipratropium bromide 144

5.2.6. Analysis of Respirable Fraction using Twin Stage Impinger Apparatus (TSI) 148

5.2.6.1. Introduction 148

5.2.6.2. Results of TSI experiments 148

5.2.7. Conclusions 150

5.3. Budesonide and formoterol fumarate systems 152

5.3.1. Budesonide 152

5.3.2. Formoterol fumarate dihydrate 154

5.3.3. Co-spray dried formoterol fumarate:budesonide systems 157

5.3.4. Factorial Design Study 160

5.3.5. Conclusions 165

CHAPTER 6. CO-SPRAY DRIED EXCIPIENT-CONTAINING SYSTEMS FOR DRY POWDER INHALER (DPI) DELIVERY

6.1. Introduction 167
6.2. Salbutamol sulphate/lactose systems 168
6.3. Salbutamol sulphate/PEG 4000 systems 172
6.4. Salbutamol sulphate/PEG 20,000 systems 175
6.5. Chitosan Systems 179
6.5.1. Introduction 179
6.6. Salbutamol sulphate/chitosan systems (not crosslinked) 184
6.7. Crosslinked salbutamol sulphate/chitosan systems 187
6.8. Conclusions 189
6.9. Analysis of Respirable Fraction using the Twin Stage Impinger (TSI) 190
6.9.1. Conclusions for TSI 194
6.10. *In vitro* release of salbutamol sulphate from salbutamol sulphate/chitosan systems 196
6.10.1. *In vitro* release from compressed discs 196
6.10.2. *In vitro* release from microparticles 206
6.10.3. Conclusion 207
6.11. Chitosan/PEG systems for "stealth effect" 207
6.11.1. Chitosan/PEG 4000 systems 208
6.11.2. Phagocytosis study 211
6.11.2.1. Introduction 211
6.11.2.2. Results of phagocytosis experiments 211

CHAPTER 7. GENERAL DISCUSSION

7.1 Introduction 215
7.2 Crystallinity of systems spray dried alone 215
7.3 Crystallinity of co-spray dried systems 222
7.4 Spray dried systems for inhalation 233
7.5 Main findings 240
7.6 Future Work 241

REFERENCES 242

APPENDICES

APPENDIX I 263

APPENDIX II 270

APPENDIX III 271

APPENDIX IV 272

APPENDIX V 277

APPENDIX VI 278

APPENDIX VII 277

APPENDIX VIII 284

ACKNOWLEDGEMENTS

I would like to thank my supervisor Dr. Anne Marie Healy for all her guidance and support during the course of my research and in the preparation of this thesis.

I wish to thank the Trinity Trust for the postgraduate award and for travel grants which allowed me to attend two international conferences. I would also like to thank Leo Laboratories and IVAX Pharmaceuticals for supplying the raw drug materials used in this thesis. I want to thank the Centre for Microscopy and Analysis (CMA) for the bursary which allowed me to perform the energy dispersive X-ray analysis work. I am grateful to Neal Leddy of the CMA for all his help.

I would like to thank Nick Hawkins from TA Instruments for running the modulated DSC experiments. I would also like to thank Mark Hanlon for help with the synthesis of TFSA and Mark, Meadhbh Lally and John O'Brien for running the NMR samples. I am grateful to Rhona Prendergast for the FTIR work. Thanks are also due to David Doff, formerly of the Department of Geology, for advice re XRD and for letting me use Geology's XRD when the XRD in the physics department was out of action. Thanks to Caitriona O'Driscoll for the use of the Waters GPC system and to Brendan for all the advice re HPLC. I am grateful to Fiona for giving me the macrophage cells, providing the positive control and for all the help with cell culture techniques. I would like to thank John Gilmer for his chemistry advice.

Thanks to my lab mate Karl and to postgrads Helena, Fiona, Meadhbh and Catríona for all the fun lunches! Thanks to Emma, Lidia, Rob, Dave, Anne, Anthony and Karl for all the coffee breaks and to the old gang Karen, Nicole, Bronagh, Rosario, Len, Sallyann, Shane and Tina for help in year one. Thanks to Rob and new Fiona for giving me first access to the pycnometer and vacuum oven. Special thanks also have to go to the pharmacognosy lads and Patrick and the PharmChem crowd for the parties and the fun trips away.

Thanks to my Mom, Dad and two sisters Éadaoin and Gemma for all their encouragement. I would like to thank Caroline, Eimir and Audrey for distractions and Conall for posh lunches. Finally I would like to thank Jack for his untiring understanding and for all the special care and attention.

PRESENTATIONS AND PUBLICATIONS ASSOCIATED WITH THIS THESIS

Oral Presentation

"An Investigation of the amorphous nature of PEG/Lactose and PEG/Bendroflumethiazide co-spray dried systems" at the 6th European Intensive Course on New Forms and New Routes of Administration for Drugs, University of Santiago de Compostela, Spain, February, 2000. [D.O. Corrigan, N. Allman, O.I. Corrigan, and A.M. Healy]

Poster Presentations

"The Influence of Processing by Spray Drying on the Physicochemical Properties of Pharmaceutical Composites" at the 23rd Joint Research Seminar, Trinity College Dublin, March, 2000. [D.O. Corrigan, N. Allman, O.I. Corrigan and A.M. Healy]

"Preliminary Characterisation of Chitosan Co-spray Dried Systems" at the Annual Postgraduate research Seminar, Trinity College Dublin, March, 2001. [D.O. Corrigan, O.I. Corrigan and A.M. Healy]

"The effect of spray drying solutions of bendroflumethiazide/polyethylene glycol on the physicochemical properties of the resultant materials" at the 4th World Meeting of Pharmaceutics, Biopharmaceutics and Pharmaceutical Technology, Florence, Italy, April 2002. [Deirdre O. Corrigan, Natalie Allman, Owen I. Corrigan and Anne Marie Healy]

Publication

"The effect of spray drying solutions of polyethylene glycol (PEG) and lactose/PEG on their physicochemical properties", Int. J. Pharm., 235 (2002) 193-205. [Deirdre O. Corrigan, Anne Marie Healy and Owen I. Corrigan]

ABBREVIATIONS AND SYMBOLS

θ	angle of incidence
ρ	density
μ	mass absorption coefficient
μ_m	mass absorption coefficient of a matrix
µm	micrometre
ε	porosity
™	trademark
λ	wavelength
ΔH	change in enthalpy
-	to
~	approximately
®	registered trademark
τ	tortuosity
∞	infinity
°	degree
°C	degree celcius
A	surface area
ANOVA	analysis of variance
aq	aqueous solution
BFMT	bendroflumethiazide
B.P.	British Pharmacopoeia
C_s	solubility of a solute
c.p.m.	cycles per minute
CoDet	coefficient of determination
cm	centimetre
cm^{-1}	frequency
CPS	counts per second
D	diffusivity
DMEM	dulbecco's modified eagles medium
DPI	dry powder inhaler
DSC	differential scanning calorimetry
DTA	differential thermal analysis

EDXA	energy dispersive X-ray analysis
EtOH	ethanolic solvent (95%)
exo	exothermic direction
FTIR	fourier transform infrared spectroscopy
g	gram
GPC	gel permeation chromatography
h	diffusion layer thickness
HFMT	hydroflumethiazide
F	fraction or percent crystallinity
H	hydrogen
Ha	enthalpy change of component a
Hb	enthalpy change of component b
H_20	water
HCl	hydrochloric acid
hr	hour
HSM	hot stage microscopy
I	peak intensity
I_{max}	peak intensity at time infinity
J/g	joules per gram
K	degrees Kelvin
KBr	potassium bromide
l/hr	litres/hour
M	moles per litre
MDI	metered dose inhaler
PMDI	pressurised metered dose inhaler
MPa	melting temperature of component a
MPb	melting temperature of component b
m.p.	melting point
mcg	microgram per ml
mg	milligram
min	minute
ml	millilitre
mm	millimetre
mM	millimolar
mW	milliwatt

Mn	number average molecular weight
Mw	weight average molecular weight
MSC	model selection criterion
N	nitrogen
N_2	nitrogen gas
nm	nanometre
nx	not crosslinked
NMR	nuclear magnetic spectroscopy
PEG	polyethylene glycol
PEO	polyethylene oxide
Ph.Eur	European Pharmacopoeia
PM	physical mix
X	solubility (mole fraction)
XRD	X-ray diffraction (powder)
pH	minus log of hydrogen ion concentration
PVP	polyvinylpyrollidone
RH	relative humidity
r.p.m.	revolutions per minute
R^2	correlation coefficient
R	ideal gas constant (8.314J/K/mol)
S^2	the variance
SB	salbutamol base
SD	spray dried
SE	standard error
SEM	scanning electron microscopy
SS	salbutamol sulphate
SS:IB	salbutamol sulphate:ipratropium bromide
SS water	salbutamol sulphate spray dried from aqueous solution
SS ethanol	salbutamol sulphate spray dried from ethanolic solution
SSlac	salbutamol sulphate/lactose co-spray dried systems
SSP4000	salbutamol sulphate/PEG 4000 co-spray dried systems
SSP20,000	salbutamol sulphate/PEG 20,000 co-spray dried systems
sschi	salbutamol sulphate/chitosan co-spray dried systems
sschixx	spray dried salbutamol sulphate/crosslinked chitosan
T	temperature

t	time
t_0	an induction time
TFSA	5-trifluoromethyl-2,4-disulphamoylaniline
TGA	thermogravimetric analysis
T_g	glass transition temperature
$T_{g\,mix}$	glass transition temperature of a mix of two components
T_m	melting temperature
TSI	twin stage impinger
UV	ultraviolet spectroscopy
U.S. F.D.A.	United States Food and Drug Administration
vs	versus
v/v	volume in volume
w/v	weight in volume
w/w	weight in weight
W	weight
x	crosslinked
xx	crosslinked

SUMMARY

The solid state properties of a range of spray dried excipients and drugs and co-spray dried excipient/excipient, drug/excipient and drug/drug, systems were investigated. The excipients investigated were lactose, polyethylene glycol 4000, polyethylene glycol 20,000, polyethylene oxide 300,000 and chitosan. The drugs investigated were bendroflumethiazide, salbutamol sulphate, salbutamol base, ipratropium bromide monohydrate, budesonide and formoterol fumarate dihydrate.

The methods of analysis used to characterise the spray dried systems were powder X-ray diffraction (XRD), differential scanning calorimetry (DSC), thermogravimetric analysis (TGA), Fourier Transform Infrared spectroscopy (FTIR) and scanning electron microscopy (SEM). Energy dispersive X-ray analysis was performed on some samples to determine the presence of certain elements. The effect of co-spray drying lactose with PEG 4000 on the recrystallisation rate of lactose was studied under differing temperature and humidity conditions. Release studies were performed on BFMT/PEG 4000 systems to assess the effect of the modification of the solid-state properties on the dissolution behaviour of BFMT present in the BFMT/PEG co-spray dried composites. Twin stage impinger (TSI) experiments were carried out on systems which had potential for inhalation therapy.

Lactose, chitosan, BFMT, salbutamol sulphate and budesonide spray dried alone were X-ray amorphous. Formoterol fumarate was not spray dried alone in this work but was known to form an amorphous composite on spray drying. Chitosan starting material was amorphous while the other materials were crystalline prior to spray drying. The polyethylene glycol/oxides of various molecular weights, salbutamol base and ipratropium bromide did not form X-ray amorphous phases on spray drying. Some reduction in crystallinity was observed for PEG 4000, PEO 300,000 and salbutamol base. Salbutamol base did consist of some amorphous material as evidenced by a recrystallisation exotherm by DSC. Ipratropium bromide spray dried from aqueous solution consisted of mainly the anhydrous form while spray drying from ethanolic solvent showed mainly the monohydrate form by XRD.

Co-spray drying lactose with PEG 4000 resulted in systems of differing crystallinity depending on the concentration of PEG included. 5% PEG-containing systems showed the presence of crystalline β-lactose and some crystalline PEG. 10% PEG-containing systems were amorphous with respect to PEG and consisted of mainly amorphous lactose with the suggestion of the presence of a small amount of crystalline lactose. 20% and 30% PEG-containing systems were not completely amorphous but consisted of crystalline PEG which was reduced in crystallinity compared to equivalent physical mixes. The 20% and 30%

PEG 4000-containing systems also consisted of some crystalline α-anhydrous lactose. Storage at high relative humidities resulted in conversion of anhydrous lactose to lactose monohydrate. The rate of conversion to the monohydrate was modelled using the Avrami equation.

Co-spray drying BFMT with PEG 4000, PEG 20,000 and PEO 300,000 resulted in completely amorphous systems, over the concentration range of polymer studied of 10-30% polymer.

Co-spray drying salbutamol sulphate with ipratropium bromide resulted in X-ray amorphous composites for the three weight ratios studied of 10:1, 5:1 and 2:1 salbutamol sulphate:ipratropium bromide monohydrate. Co-spray drying salbutamol base with ipratropium bromide resulted in increasing proportions of amorphous material as the concentration of ipratropium bromide in the systems was increased. Co-spray drying budesonide and formoterol fumarate resulted in amorphous systems.

The crystallinity of co-spray dried salbutamol sulphate/excipient systems depended on the type of excipient used. When salbutamol sulphate was spray dried with lactose, which forms an amorphous phase when spray dried alone, amorphous composites resulted. Co-spray drying salbutamol sulphate with PEGs resulted in completely amorphous systems only at the lower concentrations of the excipients but inclusion of PEGs at a concentration of 40% by weight of total solids resulted in crystalline PEG, the salbutamol sulphate remaining amorphous. Chitosan when spray dried remained amorphous and co-spray dried salbutamol sulphate/chitosan systems were amorphous.

The Gordon-Taylor equation was used to calculate the glass transition temperatures of the mixed two component systems. The Gordon-Taylor equation appeared to be useful in predicting the likely physical stability of amorphous composites and indicated that even materials with apparently low T_gs may be stabilised by a suitable material with a sufficiently high T_g.

The particle morphology and size varied depending on the systems spray dried and the spray drying parameters used. Spray drying proved a successful method of producing microspherical particles which for many of the systems, deposited in the lower region of the twin stage impinger (TSI) indicating that they were in the respirable range.

Preliminary investigations using a macrophage cell line indicated that spray dried chitosan was not phagocytosed and therefore might be a useful carrier for sustained drug delivery to the lung.

INTRODUCTION

ORIGIN AND SCOPE

Spray drying is a method of powder production whereby a feed material is transformed from a fluid state into a dried particulate form in a one step process. It is known that spray drying often results in the production of amorphous materials. Amorphous materials have properties that can be of advantage in the formulation of drugs. The production of a drug in its amorphous high energy form can result in increased solubility (Hancock and Parks, 2000), increased dissolution rate (Corrigan et al., 1984) and hence increased bioavailability (Fukuoka et al., 1987) over its crystalline equivalent. Corrigan et al. (1984) spray dried a number of thiazide diuretics and while the majority were rendered amorphous, chlorthiazide formed an amorphous phase only when spray dried with PVP. PVP is an amorphous hydrophilic material. PEG is an alternative hydrophilic polymeric excipient. PEGs have been used in the formulation of solid dispersions with poorly soluble drugs to increase their dissolution rates (Chiou and Riegelman, 1971). Spray drying of PEGs alone has not previously been reported in the literature. The effect of co-spray drying with PEG as opposed to PVP on the crystallinity of systems was investigated in this thesis. Relatively little investigation into the physicochemical properties of co-spray dried systems has been reported in the literature. Co-spray drying components should prove a useful method of obtaining well mixed systems since composite particles should form on spray drying. The small particle size of spray dried materials makes spray drying an attractive method of producing powders for inhalation.

Various excipients and drugs were co-spray dried for this thesis. The primary objectives of the thesis were:

1) To investigate the effect of co-spray drying lactose with PEG on the crystal structure of the resultant systems.
2) To study the effect of co-spray drying a poorly soluble drug (bendroflumethiazide) with PEG on the crystallinity of the resultant systems and to determine the effects of any change in crystallinity on the dissolution properties of the poorly soluble drug.
3) To use spray drying as a method for production of co-spray dried two component systems with properties suitable for use in dry powder inhalers.
4) To examine the potential of co-spray drying drugs for inhalation with excipients, thereby overcoming the need for mixing of therapeutic agents with flow aids or alternatively to achieve sustained release of therapeutic agents in the deep lung.
5) To investigate the stability of co-spray dried systems.

1.1 Spray Drying

Spray drying involves the transformation of a feed material from a liquid state into a dried particulate form in a one step process. The process involves atomisation of feed material, spray-gas contact, drying of the spray material and separation of the material from the gas stream. A schematic diagram of a spray drier is shown in Figure 1.1.

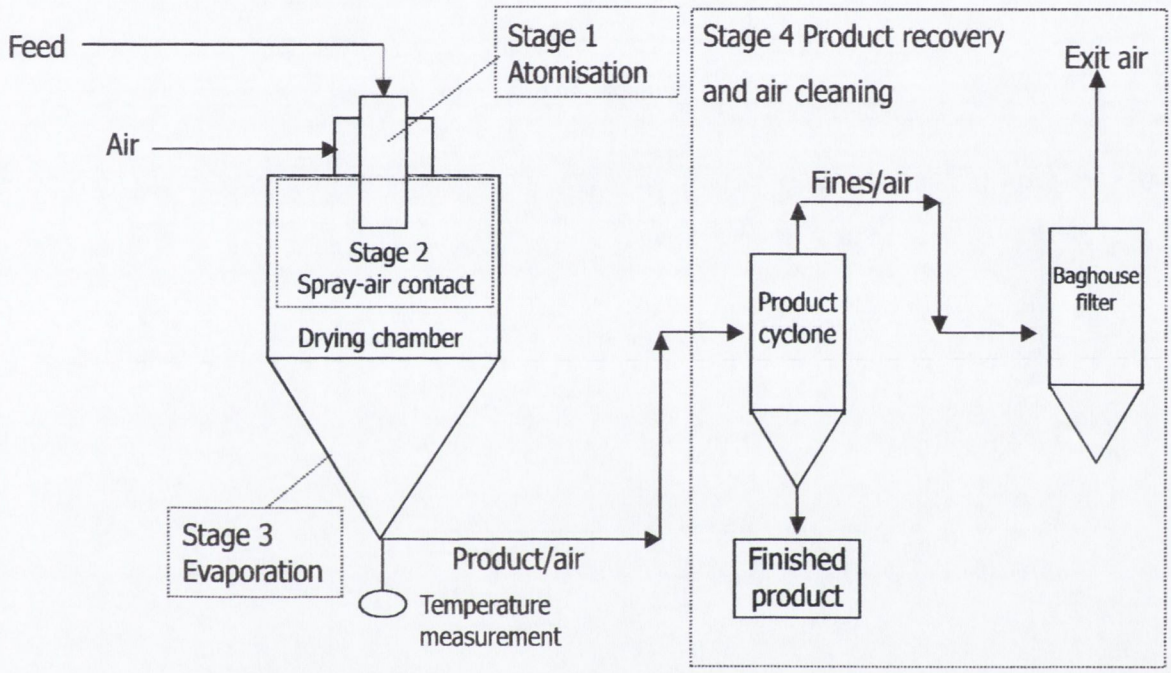

Figure 1.1 Schematic diagram of a co-current spray drier.

Spray drying is not a new technology in relation to processing of pharmaceuticals, being in use since the early 1940s. It has been used for excipient production, microencapsulation, granulation, complex formation, modification of biopharmaceutical properties, solid dispersion production, dry powder aerosol formulation and processing of heat sensitive materials (Broadhead et al., 1992).

The spray drying process involves four stages (Masters, 1985):

(a) Atomisation of feed into a spray
(b) Spray-gas contact
(c) Drying of spray (evaporation)
(d) Separation of dried product from the gas (usually air)

Atomisation involves the exertion of a force onto a liquid resulting in droplet formation. A variety of atomisation systems exist depending on the type of spray drier and these can be classified according to nozzle design. Types of atomisation include rotary atomisation, pressure atomisation or two-fluid (pneumatic) atomisation. Rotary atomisation involves the introduction of the liquid feed into the drying chamber through a rotating wheel or spinning disc which creates a spray of droplets (the size and shape depending on the size, shape and speed of the rotating wheel or disc). Pressure atomisation involves the feed being delivered to the nozzle under pressure which results in the dispersion of the fluid into droplets as it leaves the nozzle. In the case of two-fluid nozzles, the liquid feed and compressed gas are passed separately to the nozzle where they are mixed and create a spray of droplets. The Büchi Mini Spray Drier, a laboratory scale spray drier, contains a two fluid (pneumatic) atomizer. Spray driers can operate with either co-current drying, counter-current drying or with the spray gas contact being somewhere intermediate between co- and counter-current. The Büchi Mini spray drier operates co-current drying (i.e. the spray feed materials and drying air pass through the dryer in the same direction). Co-current is less economical in terms of heat utilisation but it is preferable for heat sensitive materials since the dry product is in contact with only the coolest air (Masters, 1985). Counter-current drying involves the spray and the drying gas entering the dryer at opposite ends. This arrangement offers dryer performance with excellent heat utilisation but subjects the driest powder to the hottest air stream and therefore is not appropriate for heat sensitive materials. While air is the most common drying gas, the drying air can be replaced by an inert gas, usually nitrogen, when using closed cycle spray dryers (Broadhead et al., 1992). Spray drying can also be used for aseptic processing by filtration of the liquid feed material and the atomising air, careful drier design and operating in a clean plant facility.

Following atomisation of the feed, evaporation from the droplet begins. There are two stages of evaporation, firstly the constant rate period and secondly the falling rate period (Masters, 1985). The constant rate period occurs when there is sufficient moisture within

the droplet to replenish the moisture being lost at the surface of the droplet. Diffusion of moisture from within the droplet maintains the saturated surface and evaporation takes place at a constant rate until the critical point is reached. At the critical point, surface saturation cannot be maintained by migration from the droplet core and a dried crust forms at the surface of the droplet. Evaporation then depends upon the rate of diffusion of moisture through the dried surface crust. During the second stage of drying, the falling rate period, the thickness of the dried crust increases with time and results in a decrease in the rate of evaporation. A considerable part of the droplet evaporation occurs when the droplet surfaces are saturated and cool and thus the temperature of the drying product is lower than the drying air leaving the evaporating chamber. During the falling rate drying period, when the surface skin restricts evaporation, the temperature of the particles starts to rise and they become more sensitive to heat. However degradation is largely prevented since the evaporating moisture absorbs most of the available heat.

Processing conditions can affect the properties of resultant powders in relation to appearance, particle size and size distribution, bulk density, particle density, porosity, moisture content, flowability, stability, dispersability, friability, compressibility and retention of activity, aroma and flavour (Masters, 1985).

Feed concentration and spray flow primarily govern particle size of the spray dried product. However there is interdependency between the various operating parameters which can be controlled on the spray drier. Masters (1985) describes an equation (Equation 1.1) for determining the mean spray size (D) generated by pneumatic nozzles.

$$D = \frac{A}{\left(V_{rel}^2 \rho_a\right)^{\alpha}} + B\left(\frac{M_{air}}{M_{liq}}\right)^{-\beta} \qquad \text{Equation 1.1}$$

where V_{rel} is the relative velocity between the gas and the liquid at the nozzle head, M_{air}/M_{liq} is the mass ratio of the gas and liquid, α and β are constants related to nozzle design and A and B are constants related to both nozzle design and liquid properties. According to this equation, increasing the relative velocity reduces the particle size. A rise in viscosity increases mean droplet size. Values of the ratio M_{air}/M_{liq} range from 0.1 to 10.0. Below 0.1 atomisation deteriorates. As the value increases smaller particles are produced. Further increases in the ratio above the value of 10 do not result in marked decreases in droplet size (Masters, 1985). Therefore increasing the spray flow reduces the droplet size and in turn the particle size of the end product up to a certain point beyond

which increases in airflow will not significantly affect particle size. Bodmeier and Chen (1988) described the formation of fibres when spray drying polylactic acid systems and attributed the fibre formation to there being insufficient atomisation forces present to break up the liquid filament into droplets during spray drying. Clarke et al. (1998) described similar fibre production when spray drying polylactic co-glycolic acid systems and found that lowering the feed concentrations resulted in microparticle production.

The rate of drying, and the rigidity and porosity of the solid initially produced on drying, affects the final morphology of spray dried product. Masters (1985) describes the shape and changes that spray dried droplets can undergo based on single component spray drying. Shape and texture of the dried product are described as falling into two groups depending on whether the drying air temperature was above or below the boiling point of the droplets. Figure 1.2 and Figure 1.3 show the visual characteristics of the two groups.

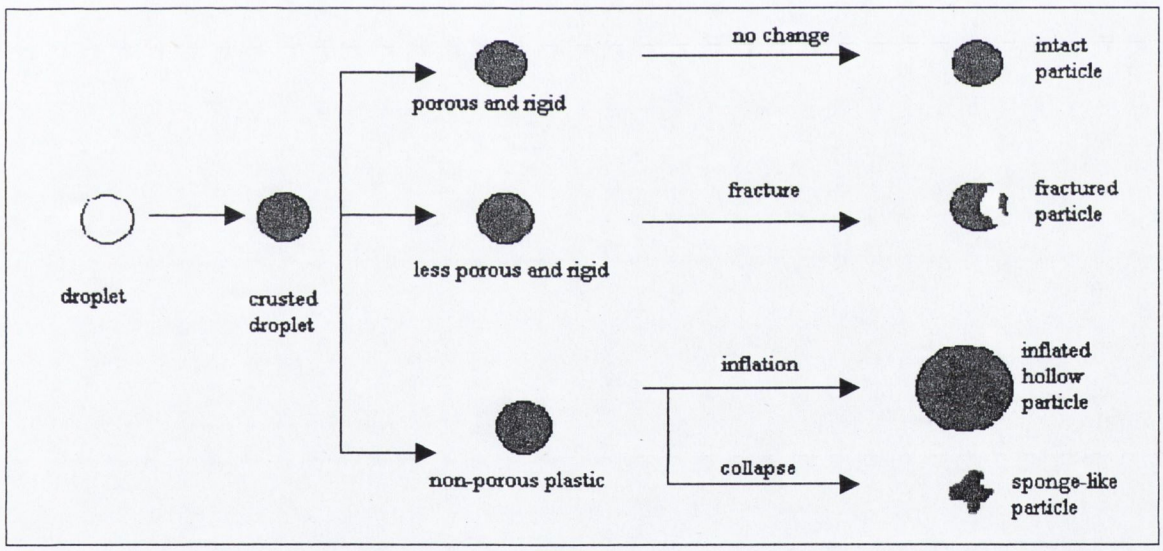

Figure 1.2 The visual characteristics of droplets dried using a drying air temperature above the boiling point of the droplets (adapted from Masters, 1985).

Rigid/porous materials form spheres while less porous and rigid materials tend to fracture. Less porous and rigid materials can also result in particles with surface crystals when dried below the droplets boiling point. Non-porous materials dried above their boiling point can either form inflated hollow particles or collapsed sponge-like particles. Pliable materials dried below their boiling point can result in sponge-like collapsed particles.

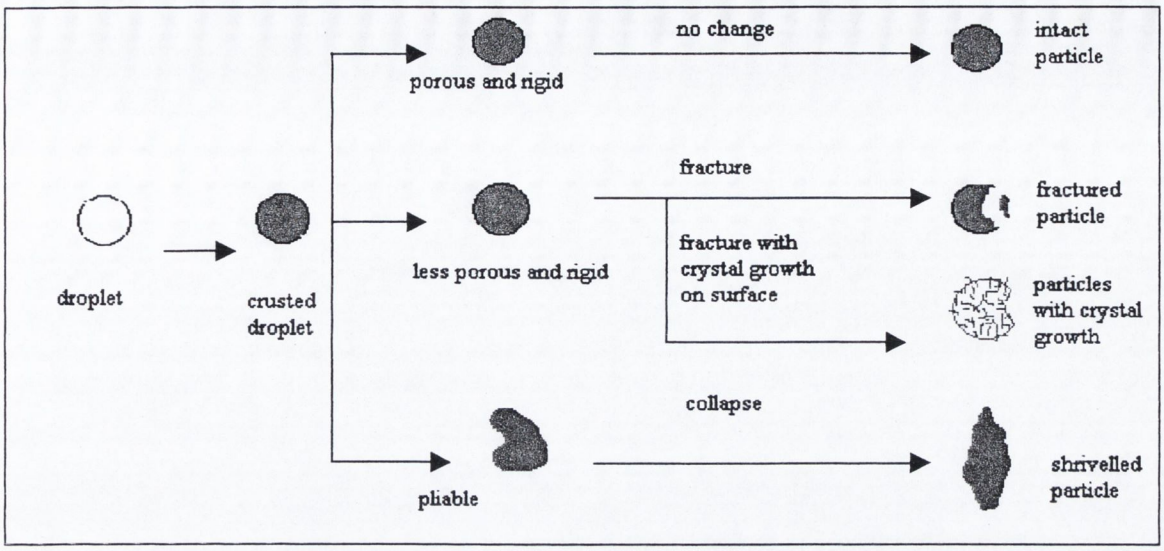

Figure 1.3 The visual characteristics of droplets dried using a drying air temperature below the boiling point of the droplets (adapted from Masters, 1985).

Spray drying can result in the production of polymorphic, pseudopolymorphic and amorphous forms of a drug or excipient. It is still not possible to predict how spray drying will affect the solid-state properties of a given compound. For example, spray drying of several thiazide diuretics was performed by Corrigan et al., (1984) and while bendroflumethiazide, hydrochlorthiazide, hydroflumethiazide and cyclopenthiazide resulted in amorphous forms, one thiazide, chlorthiazide, remained crystalline.

Spray drying has numerous applications in pharmaceutical processing (Broadhead et al., 1992) in relation to both excipient and drug production. Spray dried lactose is the most commonly encountered spray dried pharmaceutical excipient. Changes in the solid state of materials can result from the formation of less ordered systems on spray drying. A crystal lattice is generally considered to be a highly ordered structure repeating itself in three dimensions. However lattice imperfections exist, such as point defects, line defects and plane defects. The levels of such defects are generally recognised to increase with rapid drying processes such as spray drying (Corrigan, 1995). Spray drying can result in polymorphic changes, solvate formation and in some cases the formation of amorphous systems. The four most common methods of inducing amorphous character in a solid are shown in Figure 1.4 (Hancock and Zografi, 1997).

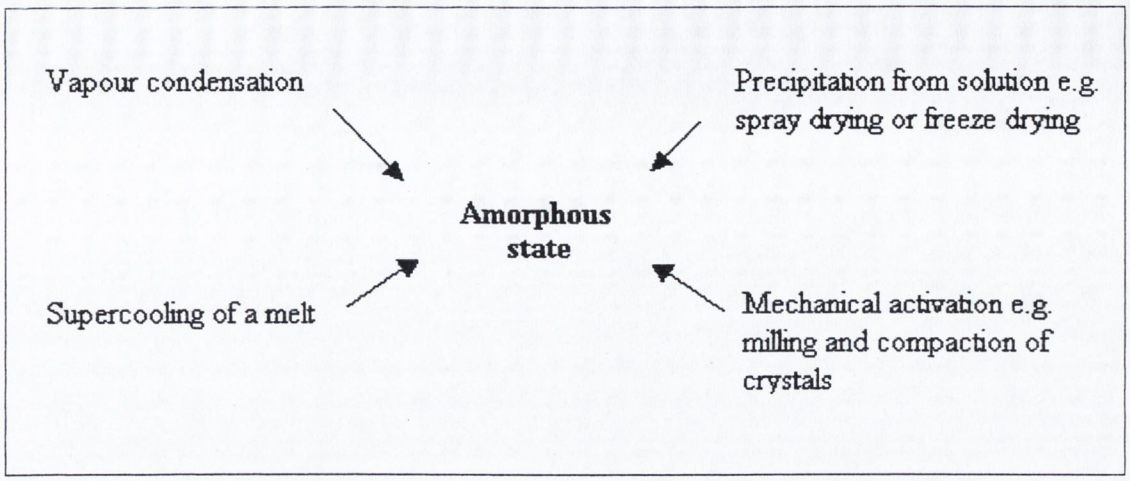

Figure 1.4 Schematic diagram of the most common methods whereby amorphous character is induced in pharmaceutical systems.

1.2 Solid State Phases

1.2.1 Amorphous forms

The three-dimensional long-range order characteristic of crystalline materials is absent in amorphous systems, which more resemble the liquid state of randomly orientated molecules. Amorphous solids do show some degree of short-range order typically over a few molecular dimensions. The amorphous state is defined by Hancock and Zografi (1997) as resulting from the rapid cooling of a liquid below its melting point leading to the structural characteristics of a liquid, but with a much greater viscosity. The amorphous state is considered an equilibrium "supercooled" liquid. Giron (1995) described amorphous forms of drugs as forms that solidify in a non-ordered random fashion related to the liquid state. The rapid drying that occurs using spray drying can lead to solidification of materials in a non-ordered fashion resulting in the production of amorphous materials. Although the amorphous state is a high-energy state it is thermodynamically metastable and recrystallisation is theoretically inevitable. The glass transition is the point whereby cooling of the amorphous system results in a change from the "rubbery state" to the "glass state". The two amorphous states differ greatly in molecular mobility, with the glassy form having the lower molecular mobility. When present as the glass, the system is, in effect, "frozen" and the system loses its molecular mobility. Absorbed moisture is known to be able to reduce the glass transition temperature of amorphous materials (i.e. a plasticising effect) thereby allowing crystallisation of materials to occur at lower temperatures (Hancock and Zografi, 1997). Absorption of

water resulting in the lowering of the glass transition temperature can result in collapse and densification of a material. Collapse occurs as the material changes structure from the glassy to the rubbery state (Buckton and Darcy, 1996). Prior to collapse, absorbed water can be easily removed by lowering the storage humidity of a sample. However, once the material collapses, water release will only occur by slow diffusion.

The presence of even small amounts of amorphous material can have dramatic effects on the resultant product's stability. Ahlneck and Zografi (1990) described the amplification effect whereby even a residual moisture content of 0.5% can have serious consequences if the sample contains even a small amount of amorphous material. The residual water will be preferentially absorbed in the amorphous regions and therefore an apparently small water content averaged over the complete sample mass will, in effect, be a high water content when localised in a small amorphous region and therefore will influence the physical and chemical stability of that region. The second issue regarding water content is that dried materials, which have some amorphous material in the collapsed state, will only release water by slow diffusion (Buckton and Darcy, 1996). The resultant effects on stability of pharmaceuticals during storage needs to be considered.

1.2.2 Polymorphism

Polymorphism is the ability of an element or compound to crystallise in more than one distinct crystal form. Polymorphic forms of a substance differ in crystalline structure but are identical in the liquid or gaseous state (Haleblian and McCrone, 1969). As a result of their different structures, polymorphic forms of the same substance usually differ in properties such as density, hardness, vapour pressure, melting point and solubility. Spray drying has been previously shown to change the polymorphic form of drugs (Matsuda et al., 1980; Corrigan et al., 1983; Kawashima et al., 1983; Matsuda et al., 1984). Polymorphs can exhibit enantiotropy or monotropy. Enantiotropy describes the situation where transition from one polymorphic form to another is reversible. Monotropy occurs when the transition between two polymorphic forms is irreversible (Giron, 1995). In the case of enantiotropy the lower melting form is the stable form at temperatures below the transition temperature (the temperature at which one form transforms to the other form) and the higher melting form is the most stable form at temperatures above the transition temperature. The higher melting form is always the most thermodynamically stable form in monotropic polymorphs. The form of a compound with the lowest free energy and the lowest solubility, is the thermodynamically most stable form (Giron, 1995).

1.2.3 Pseudopolymorphism

The term pseudopolymorphism describes solvated crystal forms and distinguishes them from true polymorphic forms of a compound. During crystallisation, if the solvent molecules become incorporated into the crystalline compound, a pseudopolymorphic form of the crystal results. When the solvent molecule in the crystal lattice is water, the pseudopolymorphic form is termed a hydrate. Hydrates are generally more stable than anhydrate forms, exhibiting reduced solubility and bioavailability (Haleblian, 1975).

1.3 Solid Dispersions

A solid dispersion refers to the dispersion of one or more materials in another material at solid state prepared by the melt, solvent evaporation, or melt-solvent evaporation method. The dispersion of one solid material in another solid material by traditional physical mixing is not included in the category of solid dispersion (Chiou and Riegelman, 1971). Dispersion of a poorly soluble material in a readily water soluble material results in a fast release of the poorly soluble material since the dissolution rate of a component from a surface is affected by the second component in a two component mixture (Higuchi, 1967). Formation of solid dispersions is a means whereby the dissolution of poorly soluble drugs can be improved. The rate determining step in the absorption process for drugs of low solubility is generally the dissolution rate of such drugs in the gastro-intestinal fluids rather than the rate of diffusion across the gastrointestinal wall. Nernst and Brunner (1904) applied Fick's first law of diffusion to quantify the dissolution rate of a solid dissolving in a solvent described by Equation 1.2.

$$\frac{dM}{dt} = \frac{DA(C_s - C)}{h} \qquad \text{Equation 1.2}$$

where $\frac{dM}{dt}$ is the dissolution rate of the drug, D is the diffusion coefficient, A is the surface area of the drug, C_s is the solubility of the solute in the dissolution medium, C is the concentration of solute in the bulk solution at time t and h is the thickness of the diffusion boundary layer.

Increasing the solubility or increasing the surface area will increase the dissolution. Approaches to improving the solubility or increasing the surface area available for dissolution include physical modifications and chemical modifications. Examples of

physical modifications which could improve solubility or increase surface area include decreasing the particles size by micronisation, modification of solid state form, complexation/solubilisation and drug dispersion in carriers. Chemical modifications include production of prodrugs and salt forms. Reduction in particle size by milling, spray drying and other methods may not result in increases in dissolution rate due to agglomeration of the fine particles because of their high surface energy. In fact Lin et al. (1968) found that the *in vitro* dissolution rate of micronised griseofulvin was actually lower than that of drug samples with larger particle sizes.

There are a range of possible reasons why solid dispersion preparation can result in enhanced dissolution rates (Craig, 2002). The first is as a result of particle size reduction and reduced agglomeration.

In a solid dispersion, one component is present as a microfine dispersion within the other. The production of solid dispersions consisting of a poorly soluble drug in a readily soluble material can maximise the surface area of the poorly soluble drug that comes into contact with the dissolution medium as the readily soluble material dissolves. When a eutectic system consisting of a poorly soluble component in a highly water soluble component comes into contact with an aqueous dissolution medium, the highly water soluble component may dissolve rapidly releasing very fine crystals of the poorly soluble component. The large surface area of the resulting suspension of the poorly soluble component should result in increased dissolution rate and thus enhanced bioavailability. The production of a solid solution of a poorly soluble component in a highly water soluble component should further increase the oral bioavailability of the poorly soluble component compared to when present as a eutectic. Solid solutions consist of one component dispersed at the molecular level within the other component. The particle size of the poorly soluble component is reduced to molecular dimensions and the dissolution rate is determined by the dissolution rate of the highly soluble component (Leuner and Dressman, 2002). After the highly soluble component has dissolved, the drug is molecularly dispersed in the dissolution medium i.e. it is present in solution form. Another theory for the improvement in the dissolution rate is that the drug has no crystal structure in the solid solution and therefore the energy required to break up the crystalline structure of the drug, before it can dissolve, is not an issue (Taylor and Zografi, 1997). It has been suggested that the presentation of particles to the dissolution medium as physically separate entities may reduce agglomeration. The dissolution rate of a drug in drug/polymer systems may be controlled by the dissolution rate of the polymer i.e. carrier-controlled dissolution (Corrigan 1985, 1986; Dubois and Ford, 1985).

Increased solubility of the drug through the formation of a different polymorphic or amorphous form during solid dispersion production is another mechanism whereby dissolution may be increased. Amorphous systems are known to often show higher solubilities due to their metastable high energy state. However, this is often short-lived due to conversion to their more stable crystalline conformations. Production of solid dispersions can lead to the formation of amorphous materials, due to the often rapid cooling of the melts, or rapid evaporation of the solvent, in the production process.

1.3.1 Classification of Solid Dispersions

Chiou and Riegelman (1971) described a classification of solid dispersions prepared from two component systems consisting of six groups as outlined below.

1.3.1.1 Eutectics

Eutectics are two phase systems in which the two solid components are miscible in all proportions in the liquid state but are totally immiscible in the solid state. A eutectic system consists of a microfine dispersion of two solid components which are intimately blended. The eutectic has a unique melting point, which is lower than that of either of the melting points of the two pure components. The melting points of each component in excess of the eutectic composition are depressed with respect to the pure materials. The reduction in particle size of the drug, the absence of aggregation and agglomeration and improved bulk wettability and dispersibility (Chiou and Riegelman, 1971; Sekiguchi and Obi, 1961) generally result in an increased dissolution rate relative to that of the pure drug. It is important to recognise that unless an exact eutectic composition is achieved, the system will consist of a mixture of the microfine eutectic and another separate phase of one or other component.

Figure 1.5 shows a schematic of a typical phase diagram of a model binary eutectic system. There are four regions: (a) a single liquid phase, (b) a region containing solid component A and a conjugate liquid phase, (c) a region in which solid component B is in equilibrium with a conjugate liquid phase and (d) a region in which components A and B are both present as pure solid phases. The eutectic point is the lowest temperature at which a liquid phase can exist in the A-B system. At this point three phases coexist: liquid, solid A and solid B.

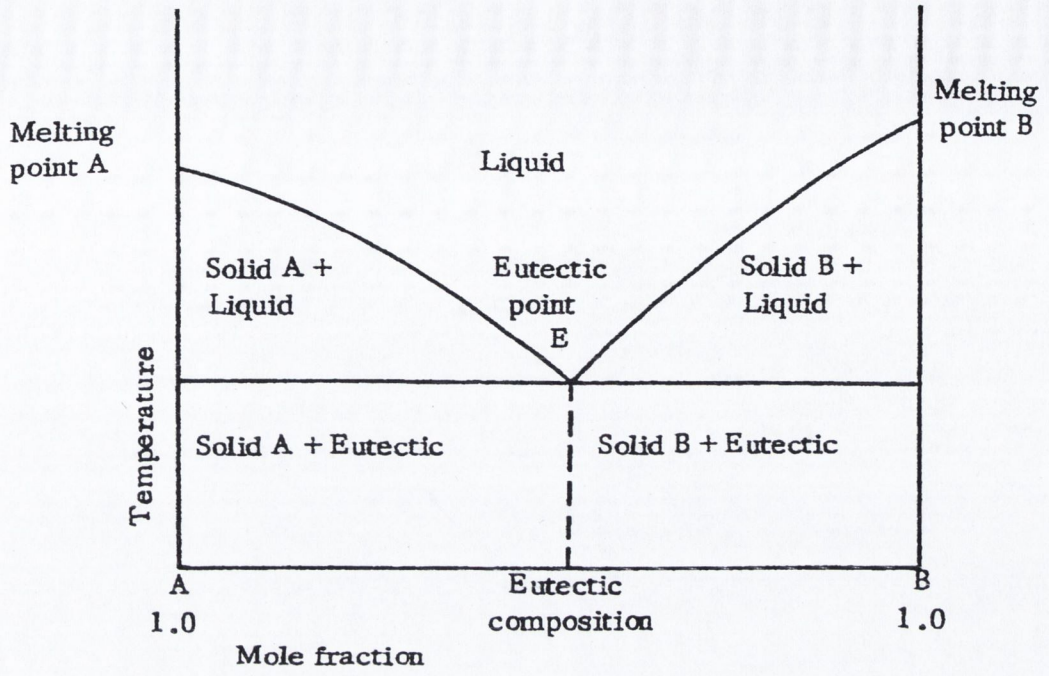

Figure 1.5 Schematic diagram of a simple binary eutectic system (adapted from Chatham, 1985).

1.3.1.2 Solid solutions

Solid solutions are one phase systems in which a solid solute is dissolved in a solid solvent. Two types of solid solutions exist, discontinuous and continuous, depending on the miscibility of the two components. In continuous solid solutions the two components are miscible in all proportions in the solid state. This means that the bonding strength between the two components is stronger than the bonding strength between the molecules of each of the individual components. Continuous solid solutions have not been reported in the pharmaceutical literature to date. Discontinuous solid solutions are systems where the two components show only partial miscibility with each other. A typical phase diagram for a discontinuous binary solid solution system is shown in Figure 1.6.

Solid solutions can also be classified according to their crystalline structure into substitutional or interstitial solid solutions. In substitutional solid solutions the solute molecule substitutes for the solvent molecule in the crystal lattice of the solid solvent (Figure 1.7). The size of the solute and the solvent molecules must be very similar in order for the formation of substitutional solid solutions (Hume-Rotherly and Raynor, 1954). Also significant is the degree of lattice distortion produced in the solvent by steric effects or chemical interactions. For example, naphthalene is capable of forming solid solutions with its β-derivatives substituted with halogens, hydroxyl, or amino groups but can only form eutectic mixtures with its α-substituted derivatives (Chiou and Riegelman, 1971).

This indicates the degree of molecular similarity necessary for the formation of substitutional solid solutions and means substitutional solid solutions are unlikely to occur in pharmaceutical systems consisting of a carrier and a drug.

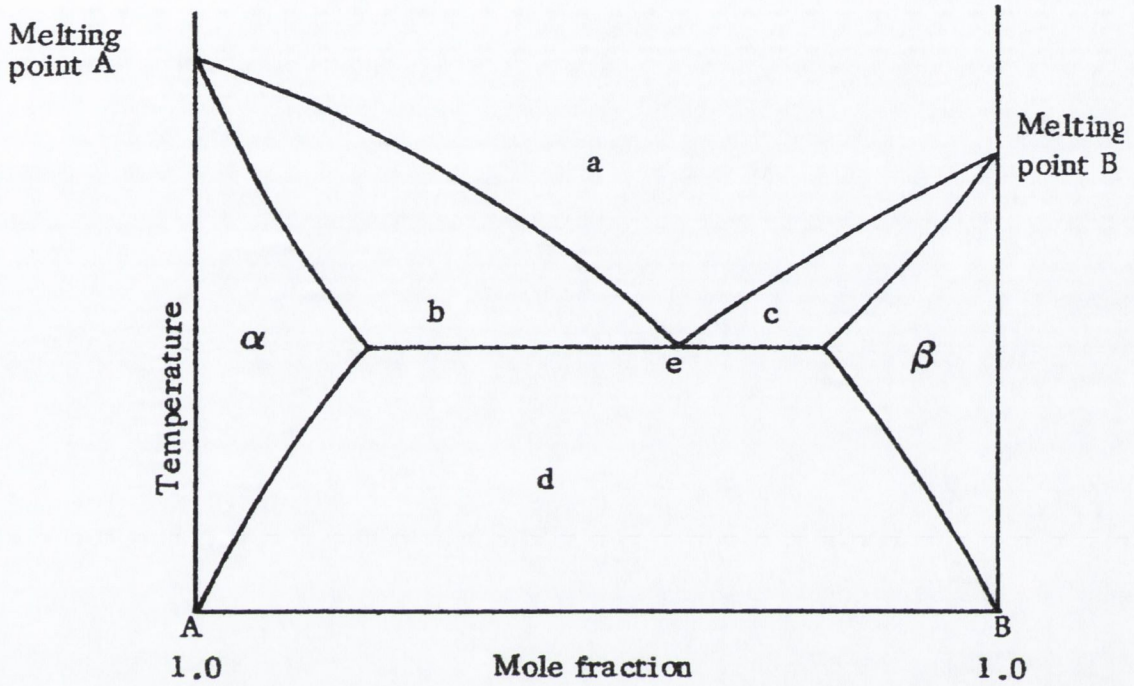

Figure 1.6 Schematic phase diagram of a discontinuous solid solution of a binary system, A and B (adapted from Chatham, 1985). α and β are the regions of true solid solutions. In these regions one of the solid components is completely dissolved in the other solid component. a is liquid, b is solid solution α and liquid, c is solid solution β and liquid, d is two conjugate solid solutions and e is the eutectic point.

In interstitial solid solutions the solute molecule occupies the interstitial space of the solvent lattice (Figure 1.8). The solute molecules in interstitial crystalline solid solutions should have a molecular diameter that is no greater than 0.59 of the solvent molecule's molecular diameter (Reed-Hill, 1964). The volume of the solute is also critical. In order to fit into the interstices, the solute molecules volume should be less than 20% of that of the solvent. Water-soluble crystalline polymers of high molecular weight were described as logical choices for interstitial solid solution formation since the molecular weight of most organic drugs is usually less than 1000 (Chiou and Riegelman 1971). Given that PEG polymers consist of two parallel helixes, on solidification of PEG/drug systems, significant amounts of drug should be trapped in the helical interstitial space.

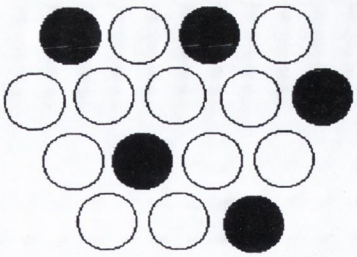

Figure 1.7 Schematic representation of a substitutional solid solution. Black circles represent solute atoms or molecules and white circles represent solvent atoms or molecules.

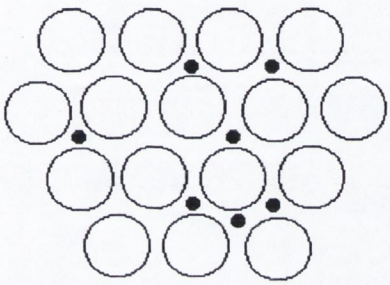

Figure 1.8 Schematic representation of an interstitial solid solution. Black circles represent solute atoms or molecules and white circles represent solvent atoms or molecules.

1.3.1.3 Glass solutions and suspensions

A glass solution is described as a homogeneous, glassy system in which a solute dissolves in a glassy solvent (Chiou and Riegelman, 1971). Leuner and Dressman (2000) describe a glassy system consisting of an amorphous solid solution in which the solute molecules are dispersed molecularly but irregularly within the amorphous solvent. Glass suspensions consist of precipitated drug particles suspended in a glassy solid solvent. These systems may offer dissolution advantages over even solid solutions since amorphous forms of compounds have the highest free energy. Associated with this high free energy metastable state is the tendency of amorphous systems to revert to their more thermodynamically stable but less soluble crystalline form.

1.3.1.4 Amorphous precipitations in crystalline carriers

This type of system results when a drug does not crystallise but is precipitated in the amorphous form within a crystalline carrier. As described above, the amorphous form is the highest energy form and therefore should result in faster dissolution than the crystalline drug. However the system may convert to the more stable crystalline form. The carrier used substantially influences the final structure of the drug dispersed within it. For example the viscous nature of the melt produced with PEGs may retard crystallisation of

the drug due to the difficulties of nucleation and crystal growth in such a medium (Chatham, 1985). The properties of the drug are also important. Chiou and Riegelman (1971) describe that if the drug supercools to a large extent then it will be more likely to solidify as the amorphous form.

1.3.1.5 Compound and complex formation

Complexes formed between carriers and drugs have been reported to enhance or retard the dissolution of the drugs. Chiou and Riegelman (1971) describe that in comparison with pure, insoluble solid drugs, the rates of dissolution and gastro-intestinal absorption can be increased by the formation of a soluble complex with a low association constant.

1.3.1.6 Combinations of the above systems

A solid dispersion may be made up of combinations of systems. The observed increase in dissolution rate may therefore be as a result of contributions of different mechanisms.

1.3.2 Methods of preparation of solid dispersions

Sekiguchi and Obi (1961) were the first to propose the melt method for the preparation of fast-release solid dispersions. They heated a physical mixture of drug and carrier to just higher than its melting point and then solidified the melt using an ice bath while vigorously stirring. The resultant solid mass was pulverised and sieved. Other variations on this method involve mainly changes in the rate of cooling of the solid dispersion. The melt method, as a method of solid dispersion production, is limited by the thermostability of the components of the solid dispersion. Additionally, the miscibility of one component in the other in the molten form, is necessary. The solvent evaporation method offers an alternative method of production to the melt method, overcoming the issues of miscibility in the molten state and may be advantageous for more thermolabile materials. Tachibana and Nakamura (1965) were the first to use the solvent evaporation method. This method involves the dissolution of both components in a common solvent followed by evaporation of the solvent to produce the solid dispersion. The term co-precipitate is often used to describe solid dispersions produced by the solvent evaporation method. Tachibana and Nakamura (1965) used the solvent evaporation method to produce a solid solution of the highly lipophilic material β-carotene in the highly water soluble carrier polyvinylpyrrolidone (PVP). The solvent method overcame some of the problems associated with the melt method, i.e. the solvent method enabled the preparation of solid

dispersions of thermolabile materials (Leuner and Dressman, 2000). Many polymers which were unsuitable for formulation by the melt method due to their high melting points, for example, PVP, could be used to formulate solid dispersions using the solvent evaporation method. Due to the good solubility of PVP in a wide range of organic solvents, PVPs were especially suitable for the preparation of solid dispersions and many solid dispersions containing PVP were prepared by the solvent evaporation method (Leuner and Dressman, 2000). Corrigan and Timoney (1975) prepared hydroflumethiazide-PVP systems by the solvent evaporation method. The systems consisted of a high energy amorphous drug phase when greater than 40% PVP was included. Doherty and York (1989) produced X-ray amorphous frusemide-PVP solid dispersions consisting of 60% PVP. Corrigan and Holohan (1984) spray dried hydroflumethiazide resulting in the production of an amorphous form. Amorphous hydroflumethiazide produced by spray drying converted to a crystalline form within 12 days of processing. However co-spray drying with 1% PVP extended the conversion time to six months. Co-spray drying with higher concentrations of PVP resulted in amorphous hydroflumethiazide composites which were stable for over one year (Corrigan and Holohan, 1984). Spray drying is effectively a solvent evaporation technique. Spray drying drugs with PVP can increase the stability of the amorphous systems produced. Spray drying of indomethacin from ethanolic solution resulted in the formation of a viscous liquid phase. This viscous liquid formed an amorphous solid on contact with the walls of the cyclone of the spray drier. The amorphous form recrystallised within one week. Co-spray drying indomethacin with PVP in concentrations greater that 20%, using the same solvent, retarded the recrystallisation of the drug and resulted in the production of microparticles which deposited in the collection vessel of the spray drier (Corrigan et al., 1985). Ketoprofen and ibuprofen were also spray dried by Corrigan et al. (1985). These drugs have lower melting points than indomethacin and resulted in viscous transparent liquids when spray dried. Co-spray drying with 50-75% PVP resulted in the production of stable amorphous forms of both ketoprofen and ibuprofen. While spray drying single component systems can result in amorphous systems or polymorphism, co-spray drying with PVP promoted the formation of amorphous material. Polyethylene glycols (PEGs) are other hydrophilic polymeric compounds which do not appear to have yet been co-spray dried with poorly soluble drugs. PEGs have been described by Chiou and Riegelman (1971) as the logical choice as carriers for solid dispersions due to their non-toxicity and compatibility with most drugs.

A third method for the production of solid dispersion systems is the melt/solvent evaporation method. The melt/solvent evaporation method involves first dissolving a drug in a suitable liquid solvent and then incorporating the solution directly into the melt of the second component (for example polyethylene glycol) without removing the liquid. This method was used by Bajpai and Varma (1981). They dissolved amphotericin B in propylene glycol before incorporating it into molten PEG 4000 and PEG 6000. A limitation of this technique is the problem of finding a solvent for the first component which is also miscible with the melt component.

1.3.3 Methods of Characterisation of Solid State Forms

1.3.3.1 Thermal Analysis

Thermal analysis refers to any method that involves the heating of a sample and the measurement of changes in some physical property. Differential scanning calorimetry (DSC) involves subjecting a sample and reference to a controlled temperature programme. In power compensated DSC both the sample and the reference cell are maintained at the same temperature throughout the temperature programme and any energy difference in the independent supplies to the sample and reference during the temperature programme is recorded against the programme temperature. Thermal events in the sample appear as deviations from the baseline and are either endothermic (e.g. melting, boiling, sublimation, vaporisation, desolvation, solid-solid phase transitions, chemical degradation, etc.) or exothermic (crystallisation, oxidative decomposition, etc.) depending on whether more or less energy has to be supplied to the sample relative to the reference material.

DSC results are generally plotted as the differential power input against temperature. The area of a DSC peak is directly proportional to the heat change resulting from a thermal event and can be integrated to give the heat of reaction. DSC can be used in the study of polymers. Polymers which are formed by rapid cooling to a low temperature (quenching) from the melt may initially be present in a glassy state. The transition from the glassy state to the rubbery state, the glass transition, is accompanied by a change in heat capacity but no change in enthalpy. The glass transition is an example of a second order phase transition (Martin, 1993). A glass transitions appears by DSC as a discontinuity in the baseline which may be accompanied by a small relaxation endotherm.

Modulated Temperature DSC involves the superimposition of a sinusoidal signal on a linear heating programme. The response is then deconvoluted into the reversing and non-reversing components. Samples which have been cooled at a rate very different from their

subsequent heating rate often show enthalpic relaxation peaks in the glass transition region (Verdonck et al., 1999). Enthalpic relaxation peaks may conceal the variation in heat capacity which occurs at the glass transition. Modulated temperature DSC separates the heat flow into reversing and non-reversing and therefore allows better interpretation of simultaneous thermal events such as the glass transition (detected from the reversible heat capacity signal) and relaxation endotherms, which may occur over the same temperature range (detected in the non-reversing signal).

Thermogravimetric analysis (TGA) measures weight loss over time as a sample is subjected to a heating programme. Thermogravimetry is not as useful as DSC since it is restricted to transitions that involve either a gain or a loss of mass. TGA is useful however in conjunction with DSC to clarify whether or not thermal events are associated with weight loss. For example, an endothermic peak observed by DSC might be either due to desolvation or melting of a crystalline system. If weight loss is not observed by TGA in the same temperature region as the event by DSC then the thermal event cannot be due to desolvation and is most likely due to melting.

The main use of DSC in the investigation of pharmaceutical solid dispersions has been the determination of thaw and melting point temperatures over a range of compositions of the two components. DSC thermograms over ranges of composition can be used for the construction of phase diagrams. Exothermic peaks prior to melting endothermic peaks indicate recrystallisation and therefore the presence of amorphous material in the sample.

Solution Calorimetry investigates processes which involve enthalpy changes. The heat change which occurs on mixing a solute with a solvent is termed the heat of solution (ΔH_{soln}). A compound which exists in different solid state forms with different lattice energies will give different heats of solution in any given solvent. The difference in the heats of solution of two polymorphic forms of the same substance will reflect the difference in lattice energy of the solids (Giron, 1995). The difference in heat of solution between the two forms is equal to the heat of transition, ΔH_t.

1.3.3.2 Powder X-ray Diffraction (XRD)

The diffraction of X-rays by a crystal occur because the wavelength of X-rays are of the same order of magnitude as the spacings between planes of crystalline lattices. The Bragg equation (Equation 1.3) describes the scattering of X-rays by a crystal (Cullity, 1978).

$$N\lambda = 2dSin\theta$$ Equation 1.3

A monochromatic X-ray beam (wavelength λ) is diffracted by a set of parallel equally spaced planes (spacings d) within a crystal. Diffraction occurs only in precise directions (the angle θ) with respect to the planes, for each of several orders of diffraction (N). Therefore the pattern and intensity of X-ray diffraction by a material measured as a function of diffraction angle is characteristic of the material.

For XRD analysis of powder samples, a randomly orientated sample is prepared so as to expose all the planes of the sample and is irradiated with monochromatic X-ray radiation. The scattering angle θ is determined by slowly rotating the sample and using a scintillation counter to measure the angle of the diffracted rays with respect to the angle of the incident beam. Alternatively, the detector can be moved and the angle between the sample and source kept fixed. Knowledge of the wavelength of the incident beam allows calculation of the spacing between the planes (d spacings) be calculated using Bragg's law. Patterns of peaks from powder samples can be compared to reference materials to establish the identity of the powder since every compound produces its own characteristic powder pattern owing to the unique crystallography of its structure. XRD analysis can be used qualitatively to determine the type of material present and distinguish polymorphic and amorphous forms (Black and Lovering, 1977). XRD analysis can also be used quantitatively for the determination of phase composition in a mix of crystalline solids (Doff et al., 1986). The intensity of diffracted X-rays is a function of the amount of diffracting material present. Quantitative XRD of organic materials can often be performed using a simple calibration curve since variations in mass absorption coefficients of organic materials are low unlike for inorganic materials where the differences in mass absorption coefficients of compounds of interest and surrounding matrix can lead to nonlinear relationships between the amount of diffracting material and diffracted intensity (Shell, 1963; Klug and Alexander, 1974). Alternatively internal standards (e.g. lithium fluoride) can be included in the samples for analysis to correct for absorption (Phadnis, 1997). The use of X-ray diffraction quantitatively assumes the particle size of the materials is sufficiently small so that extinction and micro-absorption effects are negligible and relies on the minimisation of preferred orientation of the sample.

Single crystal X-ray crystallography yields a precise identification and description of a crystalline substance. Unit cell dimensions and angles conclusively establish the crystalline lattice system. Unfortunately single X-ray crystallography requires relatively

large high quality single crystals, which are not generally readily available, and therefore powder XRD is more commonly performed (Klug and Alexander, 1974).

Chiou and Riegelman (1971) describe how the powder XRD method can be used to determine the different types of solid dispersion systems as outlined below. In simple eutectic systems peaks due to the presence of each crystalline component will be observed by XRD. If a substitutional solid solution is present, the lattice parameter of the solvent crystal may be either increased, decreased or unchanged, depending on the relative size of the solute atom or molecule. A gradual shift in the positions of the diffraction lines occurs with changes in composition and is generally recognised as evidence for the presence of a solid solution, since shifts occur due to the changes in the lattice parameter of the solvent crystal. A shift in the diffraction lines from the position of one component to those of the other is evidence of a continuous solid solution. In an interstitial solid solution the diffraction lines due to the solvent component may or may not change while those of the solute component disappear. XRD can be used to detect amorphous systems which result in diffuse halos (due to the lack of long range order) and the absence of peaks indicative of crystallinity. XRD can also be used to detect the presence of complex formation since the spectra produced will be decidedly different from mixes of the pure components (Chiou and Riegelman, 1971). The main weakness of the XRD method is its inability to discriminate between amorphous precipitation in a crystalline carrier and solid solution/molecular dispersion if the lattice parameter of the solvent is not changed. In both types of solid dispersion the diffraction peaks of the solute are not visible. Chiou and Niazi (1971) investigated sulfathiazole-urea solid dispersions. XRD showed the absence of sulfathiazole diffraction peaks. Differential thermal analysis of the solidified eutectic system of sulfathiazole-urea showed a broad melting peak as opposed to a sharp melting peak as found for the equivalent physical mix. The melting of the solidified eutectic occurred over a lower melting range. They attributed this to the presence of amorphous sulfathiazole rather than a solid solution of sulfathiazole in urea. They postulated that the presence of crystalline forms of both urea and sulfathiazole in the solid dispersion should not result in a considerable decrease in the thaw point and a wider range of melting. This was substantiated by differential thermal analysis (DTA) studies and XRD studies on aged systems. These systems showed increasing melting temperatures by DTA and appearance of peaks due to sulfathiazole by XRD implying the recrystallisation over time of the amorphous drug. DTA is a method of analysis similar to DSC except that the heat differences between a sample and reference cell are measured as a function of the heating programme. DSC differs from DTA in that both cells are maintained at the same

temperature in DSC and the heat flow required to keep the equality in temperature is measured.

1.3.3.3 Fourier Transform Infrared Spectroscopy (FTIR)

The vibrational spectra of solid materials reflects details of the crystal structure and therefore FTIR can be used in the investigation of polymorphic and pseudopolymorphic forms (Brittain, 1999). The energies associated with the vibrational modes of a chemical compound lie within 400-4000 cm^{-1}. The pattern of absorption bands is diagnostic of a particular compound. The vibrational spectra of solid materials reflects details of the crystal structure and therefore FTIR can be used to detect polymorphic forms of compounds. If shifts in the IR bands are not observed this indicates the absence of marked interactions between both components.

1.3.3.4 Hot Stage Microscopy

Hot stage microscopy, also referred to as thermal microscopy, involves heating and cooling a small amount (a few milligrams) of a substance on a microscope slide and observing the sample visually during the heating or cooling process. The optical properties of crystals usually undergo drastic change during phase transformation (Newman and Brittain, 1995). Solvated systems can be detected by hot stage microscopy by mounting the samples in oil; the evolution of gases (desolvation) during heating is evidenced by the generation of bubbles (Newman and Brittain, 1995). Fine particles of crystallisation in a glassy matrix can be easily detected by the polarizing microscopy. Hot stage microscopy has been used for the construction of phase diagrams. However Chiou and Riegelman (1971) describe this method as suffering from some subjectivity.

1.3.3.5 Intrinsic Dissolution Rate Studies

Equation 1.3 described the factors affecting the dissolution rate of a solid in a solute. If the surface area is kept constant (for example by preparing discs and exposing only one surface to the dissolution medium) the difference in solubility of two different solid state forms will be reflected in their different dissolution rates (since the diffusivity and boundary layer will be the same). The intrinsic dissolution rate method can be used for comparison of the dissolution rates of different solid state forms from constant-surface discs made from the materials to be compared. The application of this method requires the observed dissolution rate to be proportional to the surface area and a reasonably large

difference to exist between the dissolution rate of the different solid state forms (Chiou and Riegelman, 1971).

1.4 Excipients used in this work

1.4.1 Polyethylene glycols (PEGs)

PEGs are hydrophilic synthetic polymers, which have the general formula $HOCH_2(CH_2OCH_2)_nCH_2OH$ where $_n$ is the number of oxyethylene groups. Their relatively low price, water solubility and favourable toxicity have resulted in their use in a wide variety of pharmaceutical formulations (Handbook of Pharmaceutical Excipients, 1994). These include parenteral, topical, ophthalmic, oral, and rectal preparations. PEG grades 200-600 are liquids while grades 1000 and above are solids at ambient temperatures. In solid-dosage formulations, higher molecular weight PEGs can be used to enhance the effectiveness of tablet binders, to impart plasticity to granules, in film coatings as plasticisers, as lubricants, in the preparation of urethane hydrogels, as controlled release agents (Handbook of Pharmaceutical Excipients, 1994) and in matrices for fast-release dosage forms of poorly soluble drugs (Chiou and Riegelman, 1971). More recently PEGs have been found to be useful in prolonging circulation time (Harris and Zalipsky, 1997) of drugs by decreasing biomolecule adsorption and consequently inhibiting the uptake of the drug by cells of the reticuloendothelial system. Interest in the development of "stealth" nanoparticles or long-circulating nanoparticles as drug carriers stems from the many advantages that such delivery systems would enjoy, namely less uptake by cells of the mononuclear phagocyte system, extended half-life and increased efficacy for targeted controlled release of therapeutic agents (Torchillin, 1998). "Stealth" drug delivery systems can be prepared by modification of their surface with hydrophilic, flexible and non-ionic polymers such as PEG (Gref et al., 1994). Gref et al. (1994) prepared injectable nanoparticulate carriers from PLGA, polycaprolactone and co-polymers of the two materials with PEG covalently attached. They found that blood circulation times in mice of the model drug lidocaine, incorporated into these carriers were dramatically increased. This was explained by the presence of the PEG coating which prevented opsonisation and subsequent recognition by the macrophages of the reticuloendothelial system. Illum et al. (1986) investigated uptake of polystyrene microspheres, coated with secretory immunoglobulin A, egg lecithin or poloxamers, by mouse murine macrophages. They found uptake was lowest for the poloxamer systems while highest uptake occurred for the

uncoated microspheres. The protective effect of PEG is assumed to be due to the steric barrier produced by its flexible chains which create a "conformational cloud" protecting other macromolecules from interaction at the surface (Torchillin, 1998). Tobío et al. (1998) described "stealth" PLA-PEG nanoparticles as protein carriers for nasal administration. From their results with tetanus toxoid as a model therapeutic agent they proposed that the PLA-PEG nanoparticles were partially taken up by the M cells of the nasal associated lymphoid tissue as well as via other routes and that the long persistence of the toxoid in the bloodstream could be explained by slow removal of the particles by the mononuclear phagocyte system.

PEGs used for solid dispersion production are usually in the molecular weight range 3000-20,000. PEGs in this range are semi-crystalline solids containing crystalline and amorphous regions. The crystalline regions are present as double helices and the helices are arranged as lamellae with the hydroxyl end groups rejected onto the surface (Buckley and Kovacs, 1975). The chains within the lamellae may be extended or folded, the latter being metastable with respect to the former (Kambe, 1980; Chatham, 1985). The lamellae are arranged in spherical structures known as spherulites (Bailey and Koleske, 1976). Extended chain crystals are found in PEGs of molecular weights up to approximately 4000 at which point folded chain crystals begin to form. At molecular weights above PEG 6000, folded chain PEGs are the predominant form present. PEG 4000 can crystallise as extended or once folded chain crystals, the latter being metastable with respect to the former and therefore melting at lower temperatures (Kovacs, 1977; Kambe, 1980). Polymers do not show a unique melting point but melt over a range of temperatures, the melting temperature range increasing with increasing molecular weight up to PEG 6000 due to the increase in chain length. Beyond 6000 the melting point becomes dependent on the thickness of the lamellae rather than the length of the chains (Chatham, 1985). Melting can be considered to be a function of molecular order or crystallinity and therefore is affected by factors such as previous temperature of crystallisation (Chatham, 1985). The previous thermal history influences the degree of crystallinity and the crystal form of PEG 4000, i.e. the relative proportions of extended and once folded chain crystals (Kambe, 1980; Chatham, 1985). Factors that affect the structure of PEG include time in the molten state and temperature of melting, cooling rate and ageing (Chatham, 1985). The time in the molten state and temperature of melting affects the number of surviving nuclei. The cooling rate affects the nucleation and growth rate. In the melt, polymer chains are randomly orientated and, on cooling, nucleation and growth occur by chain diffusion through the melt. If the sample is cooled quickly the time for diffusion decreases and the

rapid increase in viscosity limits the growth of the nuclei. In the case of flash cooling of polymers the chains can become frozen in their random orientation resulting in an amorphous system. Samples which have been rapidly cooled will contain many small crystallites with crystal imperfections which tend to lower the melting point of the substance (Meares, 1965; Chatham, 1985). Slow cooling causes formation of only a few nuclei resulting in the growth of large spherulites. Ageing involves a slow and continual increase in crystallinity due to perfecting of the existing crystal structure and recrystallisation of amorphous regions. Kambe (1980) reported the conversion of metastable once folded PEG 4000 crystals to the extended chain conformation over time. Chatham showed that the dissolution rate of PEG 4000 was influenced by its degree of crystallinity and that, as this increased on ageing, the dissolution rate of the polymer decreased. After completion of the primary crystallisation process, secondary processes are known to occur. While a continual increase in crystallinity occurs over months due to perfecting of the existing crystal structure on ageing (Chatham, 1985), total crystallinity is never achieved (i.e. PEGs are semicrystalline).

PEG 4000 turns yellow when kept at high temperatures for long periods. Chatham observed this with polymer melts kept for 10 hours at 100°C and 200°C. The instability of PEG 4000 on prolonged heating is attributed to the break up of the polymer chains into lower molecular weight fragments. These result in a larger fraction of amorphous material because the chains cannot pack effectively into the crystals and tend to be rejected during the crystallisation process. This is reflected in decreased heats of fusion. According to Chatham, long melting periods at high temperatures are required before appreciable break up occurs and, below 100°C, degradation of polymer chains is minimal. Chatham attempted to produce an amorphous form of PEG by quenching it in both solid carbon dioxide and liquid nitrogen. A completely amorphous form of PEG 4000 did not result following such quenching methods, although the crystallinity was somewhat reduced when compared to the starting material.

1.4.2 Lactose

Lactose is another commonly used excipient in pharmaceutical systems. Spray dried lactose has quite different properties to conventional lactose (Fell, 1971). Lactose consists of one galactose and one glucose moiety. It exists in two isomeric forms: α- and β-lactose. α-lactose can be both hydrous (α-lactose monohydrate) and anhydrous but β-lactose can only exist in its anhydrous form. According to the British Pharmacopoeia (B.P., 2002)

lactose monohydrate may be modified as to its physical characteristics and may contain varying proportions of amorphous lactose. The B.P. states that anhydrous lactose is β-lactose or a mixture of α-lactose and β-lactose. Figure 1.9 shows the structures of α-anhydrous lactose and β-anhydrous lactose.

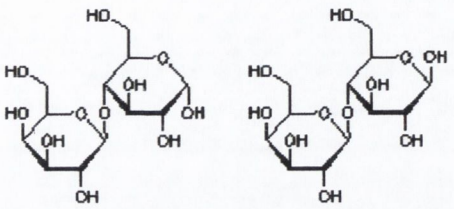

Figure 1.9 Structures of α-anhydrous lactose (left) and β-anhydrous lactose (right).

Chidavaenzi et al. (1997) investigated the impact of feed concentration on the amorphous content of spray dried lactose. Solutions of lactose when spray dried by Chidavaenzi et al. (1997) were amorphous as found previously by many groups (Briggner et al., 1994; Buckton and Darcy, 1995; Elamin et al., 1995). However Chidavaenzi et al. found that spray drying suspensions of lactose resulted in powders with higher amorphous contents than that which could have resulted solely from the amount of dissolved lactose and they therefore concluded that there was a milling effect on the suspended lactose particles in the atomiser resulting in the production of amorphous lactose.

Briggner et al. (1994) used isothermal microcalorimetry to study changes in crystallinity induced during processing of lactose. They found that the recrystallisation of amorphous lactose, produced by spray drying, occurred spontaneously throughout the entire powder bed. They concluded that the water vapour is taken up by the powder at the surface and then transported into the powder bed. When the entire bed is saturated, recrystallisation occurs simultaneously throughout the bed of powder, described by Briggner et al. (1994) as a co-operative process. The time delay before recrystallisation occurred was affected by the weights of powder beds used in the study. Longer times were required for crystallisation to occur as the weight of the powder beds was increased. A larger powder bed requires more uptake of water vapour in order to saturate the material and result in simultaneously co-operative recrystallisation. Briggner et al. (1994) found that spray dried lactose recrystallised to a mixture of α-lactose monohydrate and β-lactose. When the X-ray diffraction peaks for pure α-lactose monohydrate, pure β-lactose and recrystallised spray dried lactose samples were compared, the content of β-lactose in the recrystallised samples was determined to be 15%. Lactose recrystallisation experiments were performed

at 25°C and varying relative humidities from 53% to 85% relative humidity (RH). Spray dried lactose stored at humidities of 47% or below, during the time frame of an overnight experiment, did not produce peaks indicative of recrystallisation. It was also observed from samples which did recrystallise that, if the recrystallised samples were retained in a microcalorimeter after the recrystallisation peaks, the anhydrous lactose transformed to α-lactose monohydrate.

Kinetics of water sorption by amorphous lactose at 40% RH and 50% RH have been shown to be biphasic (Buckton and Darcy, 1996). Water generally lowers the glass transition temperature (T_g) until eventually the material is able to crystallise. As water plasticises the amorphous material the T_g approaches the temperature of the experiment, the material starts to change structure, which results in a collapse and densification prior to crystallisation. Buckton and Darcy (1996) found that equilibration at 40% RH resulted in an equilibrium uptake of 7% water, which was not sufficient to lower the T_g of lactose and cause collapse. Desorption from the uncollapsed material was rapid on lowering the RH, the rate being proportional to the extent to which the RH was lowered. If amorphous lactose was equilibrated to 50% RH the water content exceeded that which lowered the T_g below the temperature of the experiment resulting in collapse of the amorphous structure, but not in instantaneous crystallisation. Collapse occurred when the glassy material had converted to the rubbery state and due to absorption of water the rubbery material was unable to support its own weight under gravity. Water desorption from the collapsed amorphous structure was slow, following square root of time dependency. The rate of desorption was not altered by changing the external RH. After reducing the RH the water content of the collapsed structure remained high, but the recrystallisation was greatly delayed. Buckton and Darcy (1996) found that water was rapidly absorbed and desorbed by the structure prior to collapse, but water sorption to and from the collapsed structure was slow and controlled by diffusion in the solid, rather than external humidity.

Additives can affect the recrystallisation of lactose. Buckton and Darcy (1995) investigated the recrystallisation of amorphous lactose when the amorphous material was divided firstly by a layer of glass beads (an inert additive), then by a layer of magnesium stearate (hydrophobic excipient) and finally a layer of microcrystalline cellulose (hygroscopic excipient). They found significant differences in the time required for recrystallisation to occur in these systems. The glass beads had only a small effect whereas the magnesium stearate caused an increased lag time prior to the recrystallisation event. The lactose recrystallised all at one time in both cases even though it was physically divided into two separate regions by the additives. The sample with the microcrystalline

cellulose layer showed the longest lag time and the authors postulated that the two distinct peaks visible by microcalorimetry were likely due to two regions of lactose recrystallising at different times (due to upper and lower layers) or could be as a result of gradual crystallisation. When recrystallisation of a uniform mix of lactose and microcrystalline cellulose was investigated the response showed a single recrystallisation event. Buckton and Darcy (1995) concluded that the cooperative mechanism for recrystallisation observed in the divided layered systems was probably due to rapid availability of water vapour to the lower layer as the upper layer recrystallised. This rapid availability of water to the lower layers caused the lower layers of the sample to recrystallise almost immediately following the recrystallisation of the upper layer. They stated that physically separated samples still gave the impression of cooperativity even though there was no physical contact between the powder layers.

Gravimetry can be used to study recrystallisation (Buckton and Darcy, 1995b). Amorphous material absorbs water which lowers the glass transition temperature of the material to that of the experiment and allows sufficient freedom of molecular movement to facilitate crystallisation. Upon crystallisation the water that was absorbed is expelled from the material with subsequent weight loss (Buckton and Darcy, 1995b). Stubberud and Forbes (1998) used gravimetry for studying the effect of additives on the moisture-induced recrystallisation of amorphous lactose above its glass transition temperature i.e. at 25°C 75% RH and 55°C and 75% RH. Initially absorption of moisture caused a weight increase. After peak moisture uptake was attained, the corresponding time to the onset of weight loss of the sample i.e. the "apparent recrystallisation" was determined. Stubberud and Forbes (1998) sieved their spray dried lactose through a 0.425 mm sieve and physically mixed it with PVP. Mixing with PVP was found to delay the time for the onset of weight loss, i.e. the "apparent" recrystallisation. It is thought that PVP acts as an internal dessicant. The time for recrystallisation was found to be decreased when non-hygroscopic excipients were added. This was explained by an isolation and deaggregating effect on the amorphous lactose. The two non-hygroscopic materials used were lactose monohydrate and silicon dioxide. The isolation effect appeared greater for the silicon dioxide than the lactose monohydrate and this was attributed to the fact that the particles were smaller and were better able to penetrate the amorphous lactose powder and bring about a higher level of dispersion of the primary amorphous lactose particles. Both Briggner et al. (1994) and Stubberud and Forbes (1998) found that the time to onset of weight loss, i.e. the time to apparent onset of recrystallisation, decreased with increasing humidity and also when the sample weight was increased, the time to onset of recrystallisation was prolonged

(probably because recrystallisation occurs as a co-operative process throughout the powder bed). PVP was not shown to modify the crystal form of lactose produced when the mixes of amorphous lactose and PVP recrystallised under the conditions of 25°C and humidity of 50 and 75%, i.e. a mixture of anhydrous β-lactose and α-monohydrate was formed. When spray dried amorphous lactose was exposed to 50% RH (following drying) in order to induce different amounts of collapse in the amorphous structure (Darcy and Buckton, 1997) it was found that collapsed lactose crystallised at a much lower temperature by DSC (indicated by an exotherm at 70°C) compared to non-collapsed material which crystallised at significantly higher temperature (indicated by an exotherm at approximately 180°C). The collapsed lactose yielded mostly β-lactose and some α-lactose monohydrate. The non-collapsed lactose yielded mostly α-lactose and some β-lactose. TGA showed three distinct water loss peaks for the collapsed structure; two were believed to be due to crystallisation occurring and the final one due to loss of water of crystallisation.

Jouppila et al. (1997) investigated lactose crystallisation in skim milk powder and found that samples of freeze-dried skim milk containing amorphous lactose recrystallised largely as an anhydrous mixture of α and β-lactose in a molar ratio of 5:3. They did find other crystal forms at high relative humidities. They successfully modelled the rate of crystallisation using the Avrami equation (Avrami, 1940) when relative humidity was $\geq$66.2%.

1.4.3 Chitosan

Chitin, derived from the exoskeletons of crustaceans, is the second most abundant natural polymer in the world after cellulose. Upon deacetylation, it yields the novel biomaterial chitosan. Chitins which have been deacetylated to a degree of between 40% and 98% are regarded as chitosan (Illum, 1998). Chitosan is formed by demineralising chitin in dilute hydrochloric acid, deproteination in dilute sodium hydroxide solution and then finally deacetylation to become chitosan in a concentrated sodium hydroxide solution at boiling point (Paula and Sharma, 2000). The structure of chitosan is shown in Figure 1.10.

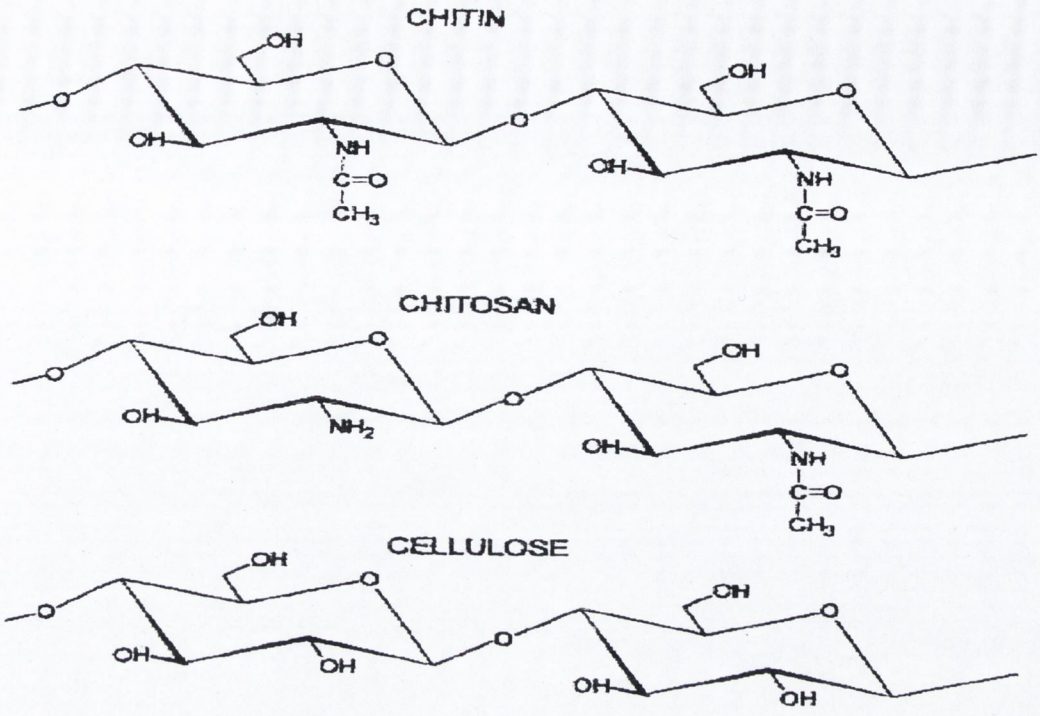

Figure 1.10 Structure of chitin, chitosan and cellulose.

Depending on the degree of deacetylation chitosans contain different numbers of acetyl groups. The degree of deacetylation of chitosan is important since it affects its crystallinity. Chitin is a crystalline material and as it is deacetylated it becomes more amorphous. Kurita et al. (1993) showed that, although shrimp derived chitosan with a degree of deacetylation of 0.8-0.89 was amorphous, further deacetylation caused crystallisation again, the sample with a degree of deacetylation of 0.95 being highly crystalline indicated by XRD peaks at 20 and 11° 2θ. Chitin is insoluble in water due to strong inter and intramolecular H-bonding. Exposure of chitosan to acidic aqueous media results in protonation of the amino groups of chitosan rendering the polymer positively charged and thereby overcoming associative forces between the chains. As chitin becomes deacetylated the overall charge density due to the presence of ammonium groups increases resulting in a decrease in the crosslinking density related to hydrogen bonding and hydrophobic interactions (Vachoud et al., 2000). An increase in the degree of deacetylation results in increased swelling due to an increase in the number of ionic sites and their counter-ions (Vachoud et al., 2000).

Chitosan is insoluble at neutral and alkaline pH values but forms salts with inorganic and organic acids such as glutamic acid, hydrochloric acid, lactic acid and acetic acid (Illum, 1998).

Paul and Sharma (2000), Dodane and Vilivalam (1998) and Illum (1998) have published review articles on the uses of chitosan. More recently Bernkop-Schnürch (2000) published a review article on potential uses of chitosan and its derivatives for peroral peptide delivery.

Paul and Sharma describe medical and pharmaceutical applications of chitosan which include drug delivery, wound healing ointments and dressings, artificial skin, haemostatic agents, enzyme immobilization, dialysis membranes, contact lenses or eye bandages, orthopaedics, surgical sutures and dentistry. Chitosan is described as digestible, making it promising for drug delivery systems. Chitosan has a lipid-lowering effect, is biocompatible, non-toxic and biodegradable. Chitosan molecules are strongly positively charged at pHs of <6.5 and also form gels with polycations at low pH. They are described as having antacid properties and anti-ulcer activity which may reduce drug irritation in the stomach. The U.S. F.D.A have approved chitosan as a food additive in animal feed and it is a generally recognised as safe (GRAS) substance. A study by Miura et al. (1995) showed that chitosan as a food additive in normal and neonatal streptozotocin-induced diabetic mice significantly reduced blood glucose, cholesterol and triglyceride levels. Therefore chitosan may be useful for treatment of lean type non-insulin-dependent diabetes mellitus. Intramuscular injection of chitosan as microspheres in rats showed tissue compatibility. Also documented are side effect reports following oral and parenteral administration in mice (Tanaka et al., 1997) and implantation in Wistar rats (Jameela and Jayakrishnan, 1995).

Chitosan has been used to aid the dissolution of poorly soluble drugs. Griseofulvin and prednisolone when ground with chitosan showed enhanced dissolution properties (Sawayanagi et al., 1982; Sawayanagi et al., 1983) consistent with a reduction in crystallinity of the drugs. Chitosan and chitosan glutamate have been shown to enhance the dissolution properties of the poorly water soluble drug nifedipine (Portero et al., 1998). Portero et al. (1998) used various methods to disperse nifedipine within the polymers. The chitosan:nifedipine solid mixes were ordered according to the efficiency of improving drug dissolution as follows: solid dispersion > kneaded mix > co-ground mix > physical mix. The solid dispersion production method was described as a casting/drying technique in which the polymer solutions were prepared and then the drug was either directly dispersed or firstly dissolved in a small volume of ethanol and then added. The drug-containing polymer solutions were cast on glass petri dishes and the solvent dried. The drug dissolution enhancement was attributed to the decreased drug crystallinity and size and also polymer wetting. Genta et al. (1995) demonstrated the ability of chitosan to improve

the dissolution rate of dexamethasone from spray dried chitosan microspheres. Genta et al. described that the entrapment of dexamethasone in the chitosan polymeric network using the spray drying method led to an improvement in dissolution rate of the drug which did not occur in the equivalent physical mix. They attributed this to a reduction in crystallinity of the drug entrapped in chitosan in the spray dried microspheres. Sawayanagi et al. (1982) described chitosan as an excipient for direct compression of tablets with 50% chitosan resulting in rapid disintegration. Ritthidej et al. (1994) showed that when chitosan was included in tablets in a concentration higher than 5% it was superior as a disintegrant to corn starch and microcrystalline cellulose. Efficiency as a disintegrant depended on chitosan crystallinity, degree of deacetylation, molecular weight and particle size. Chitosan was found to be a better tablet binder than methylcellullose and sodium carboxymethylcellulose by Upadrashta et al. (1992).

In contrast to using chitosan to aid dissolution, chitosan has been used for the preparation of sustained release systems. Nigalaye et al. (1990) produced theophylline sustained release tablets containing chitosan, carbomer-93P and citric acid. Chitosan, when used at concentrations of greater than 50% of the tablet weight, resulted in an insoluble non-erosion type matrix. At concentrations less than 33% a fast releasing matrix system was produced and at concentrations of less than 10% chitosan acted as a disintegrant. Takeuchi et al. (2000) prepared composite particles from an aqueous solution of lactose and sodium alginate and an acetic acid solution of chitosan concomitantly fed to the rotary atomiser of a spray drier. They found the composites had good compacting properties and when used as coating for tablets the coated tablets, showed excellent acid resistance and prolonged induction periods of drug release (the model drug was acetaminophen). The induction period for drug release was increased with an increase in the degree of deacetylation of chitosan and with an increase in the amount of chitosan in the formulation. Dangprasirt and Pongwai (1998) demonstrated the controlled release of diclofenac sodium from freeze dried solid dispersions with ethylcellulose and chitosan as single and combination carriers. Giunchedi et al. (1998) described the preparation and characterisation of ampicillin loaded chitosan and methylpyrrolidinone chitosan microspheres by a spray drying technique. Spray drying ampicillin with both chitosan and methylpyrrolidinone chitosan resulted in amorphous ampicillin. Nevertheless release of ampicillin from chitosan ampicillin microspheres was slower than from pure ampicillin. The activity of the antibiotic was not reduced by the spray drying technique. Giunchedi et al. (1998) also investigated the effect of heat treatment at 90°C and 150°C for 2 and 4 hours on the release of ampicillin from methylpyrrolidinone/chitosan microspheres (1:1 drug/polymer ratio) since heat treatment is

known to induce the formation of crosslinks in chitosan increasing its water resistance (Lim and Wan, 1995). They found only a slightly slower drug release from all thermally treated microspheres in comparison to untreated microparticles, which they decided was not significant. Ganza-Gonzalez et al. (1999) demonstrated the controlled release of metoclopramide when spray dried with chitosan using formaldehyde as a crosslinking agent. He et al. (1999) spray dried chitosan base and chitosan hydrochloride alone with the drugs cimetidine, famotidine and nizatadine with and without the crosslinking agents formaldehyde and glutaraldehyde. Non-crosslinked chitosans swelled and dissolved in contact with water and crosslinking chitosan was found to be necessary to maintain the integrity of the microspheres. Crosslinking affected the particle size and the zeta potential of the particles. As the amount of crosslinking agent was increased the particle size was decreased and the zeta potential also decreased. The model drugs were shown by DSC to be molecularly dispersed within the chitosan. Loading was found to be decreased with an increasing amount of the crosslinking agent. The effect of changing molecular weight of chitosan on the release rate was negligible.

The likely mechanisms whereby glutaraldehyde and formaldehyde crosslink chitosan are shown in Figure 1.11 and Figure 1.12 based on the mechanisms whereby glutaraldehyde and formaldehyde crosslink collagen (Khor, 1997).

Chitosan's permeation enhancing effect (Artursson et al., 1994; Illum et al., 1994; Lueβen et al., 1996), enzyme inhibitory capabilities (Bernkop-Schnürch, 2000) and mucoadhesive properties (Lehr et al., 1992) make it and its derivatives important polymers for peroral peptide delivery. Chitosans with a high degree of deacetylation and high molecular mass display the comparatively highest increase in epithelial permeability (Bernkop-Schnürch, 2000).

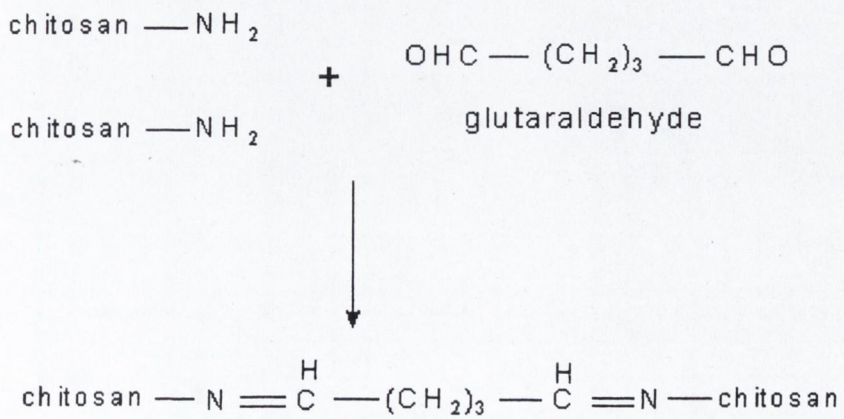

Figure 1.11 Mechanism whereby glutaraldehyde crosslinks chitosan. Chitosan-NH_2 is chitosan showing the reactive group, NH_2.

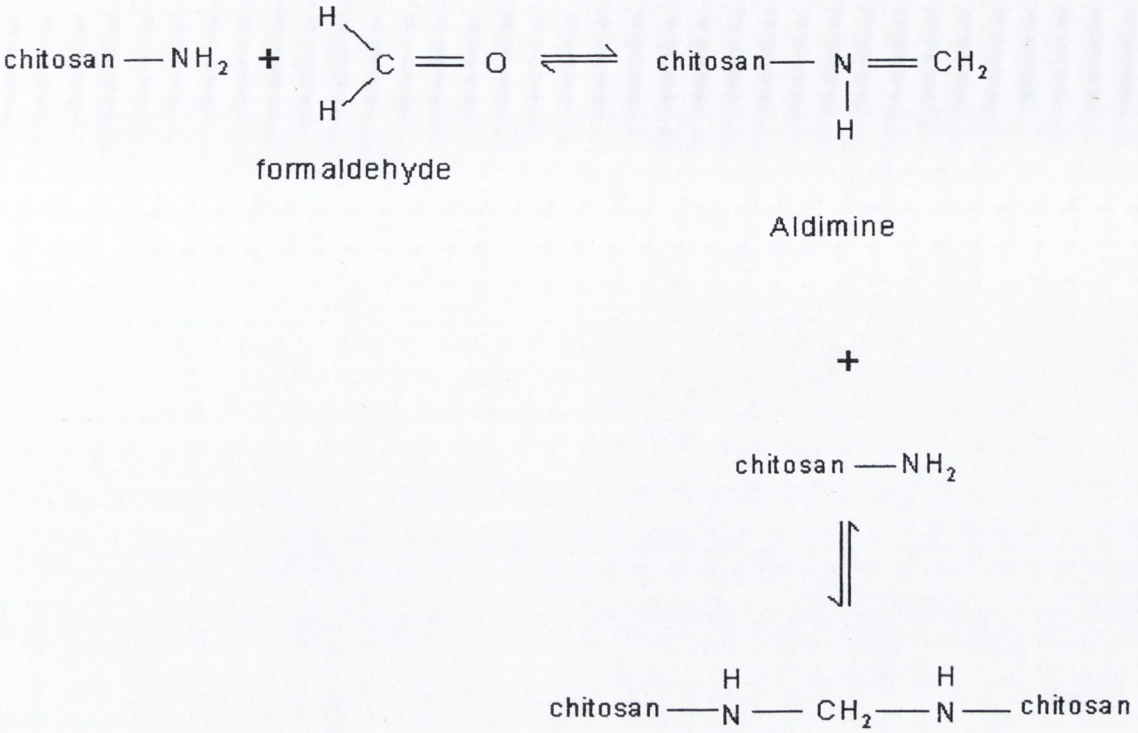

Figure 1.12 Mechanism whereby formaldehyde crosslinks chitosan. Chitosan-NH_2 is chitosan showing the reactive group, NH_2.

Tozaki et al. (1997) investigated colon-specific insulin delivery with chitosan capsules. They evaluated intestinal absorption of insulin by measuring plasma insulin levels and insulin's hypoglycaemic affect after oral administration in chitosan capsules. A hypoglycaemic effect was observed which started 8 hours after the administration of chitosan capsules, which corresponded to the time the capsules entered the colon, evaluated by transit time experiments with chitosan capsules. Tozaki et al. (1997) described how, by targeting the drug to the colon, where there is a relatively low activity of proteolytic enzymes, sufficient drug was absorbed to produce a hypoglycaemic effect. Aiedeh et al. (1997) used chitosan microcapsules as controlled release systems for insulin, insulin being incorporated, based on an interfacial crosslinking of chitosan by ascorbyl palmitate, in a water in oil dispersion. A 100% entrapment efficiency was obtained and release showed kinetics approaching zero order. Release rate could be increased by decreasing the chitosan content in the preparative solution. Takeuchi et al. (1996) used insulin-loaded liposomes coated with chitosan to improve the enteral absorption of insulin. They tested for mucoadhesion *in vitro* and *in vivo* in orally administered rats via an intragastric tube. As the chitosan concentration was increased in the coating, the mucoadhesion was reported to improve and also the absorption of insulin was increased. Ohya et al. (2000) investigated the incorporation of insulin as a model peptide drug into

PEG-grafted chitosan nanoparticles. They found that the nanoparticles incorporated a certain quantity of insulin molecules spontaneously but this was dependant on the degree of introduction of PEG chains on chitosan. The degree of introduction of PEG chains also affected the release rate of insulin *in vitro*. Chitosan/ethylene oxide-propylene oxide copolymers (Calvo, 1997) were tested for the controlled release of protein vaccines. Tetanus toxoid was released *in vitro* at a constant rate in its active form for 15 days from these nanoparticles.

The use of chitosans in parenteral drug delivery has also been investigated. Jameela and Jayakrishnan (1995) prepared microspheres containing mitoxantrone and crosslinked chitosan and found drug release was controlled by the crosslinking, with only approximately 25% of drug release occurring over 36 days when microspheres with a high degree of crosslinking were analysed. These microspheres were not biodegraded in the muscles of rats.

Williams et al. (1998) investigated microspheres made of chitosan as potential carriers for delivery of proteins, peptides and plasmid DNA to the lung via pressurised metered dose inhalers (MDIs). They found chitosan to be compatible with the non-chlorofluorocarbon propellant P134a and to have favourable physicochemical characteristics for use in pressurised aerosol formulations.

With the growth of newer biotechnological products, which tend to be larger molecules and tend to have stability problems, spray drying has a potential role in the development of solid dosage forms of such protein or peptide products. Spray drying may prove a useful alternative to lyophilisation for the drying of pharmaceutical proteins, since spray dried powders are usually microspherical and much more amenable to further processing than lyophilised powders. The recent move towards dry powder inhalers has led to increased interest in novel methods of powder production and control. Spray drying of drug/drug and drug/excipient systems has potential in this area.

1.5 Drugs used in the current work

1.5.1 Bendroflumethiazide

Bendroflumethiazide (BFMT) is used therapeutically as a diuretic and is available in tablet form for oral administration. Bendroflumethiazide is practically insoluble in water, soluble in acetone and soluble in alcohol (European Pharmacopoeia (Ph. Eur., 2002). Ph. Eur. grade bendroflumethiazide is a white or almost white crystalline powder. The melting

point of the crystalline material is between 221-226°C (Merck Index, 1996). Corrigan et al. (1984) reported that spray drying BFMT results in an amorphous material. The structure of BFMT is shown in Figure 1.13

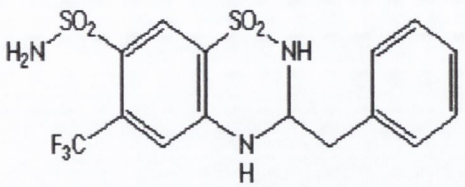

Figure 1.13 Structure of BFMT.

1.5.2 Salbutamol base

Salbutamol is a β_2-agonist used in the treatment of asthma by inhalation. It is a crystalline material which melts at 155°C with decomposition (Ph. Eur., 2002). It is sparingly soluble in water and soluble in alcohol. The structure of salbutamol base is shown in Figure 1.14.

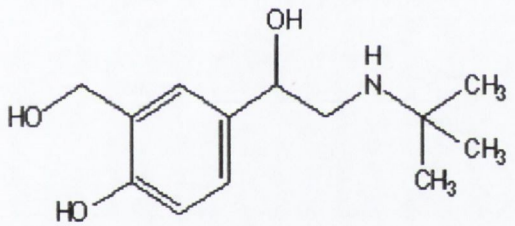

Figure 1.14 Structure of salbutamol base.

1.5.3 Salbutamol sulphate

Salbutamol sulphate, a salt of salbutamol base is also used primarily as a β_2-agonist in the treatment of asthma. Salbutamol sulphate is available in inhalation formulations as well as in oral and injectable formulations. Salbutamol sulphate is a crystalline material which is freely soluble in water, slightly soluble in alcohol and very slightly soluble in methylene chloride (Ph. Eur., 2002). Spray drying of salbutamol sulphate from aqueous solution results in an amorphous material (Chawla et al., 1994). The melting point of salbutamol sulphate was reported as 200°C (Ward and Schultz, 1995). The structure of salbutamol sulphate is shown in Figure 1.15.

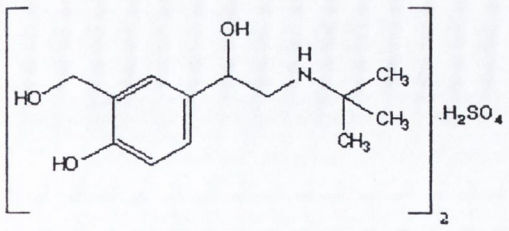

Figure 1.15 Structure of salbutamol sulphate.

1.5.4 Ipratropium bromide monohydrate

Ipratropium bromide is a muscarinic receptor antagonist, a quaternary ammonium ion analogue of atropine. It is used as a bronchodilator and is taken by the inhaled route to minimise systemic side effects. It is not available as an oral formulation (for systemic action). Ipratropium bromide is a crystalline material. It is soluble in water, freely soluble in methanol and slightly soluble in alcohol (Ph. Eur., 2002). The structure of ipratropium bromide monohydrate is shown in Figure 1.16. The melting point of ipratropium bromide is approximately 230°C (Ph. Eur., 2002), melting occurring with decomposition (Ph. Eur., 2002).

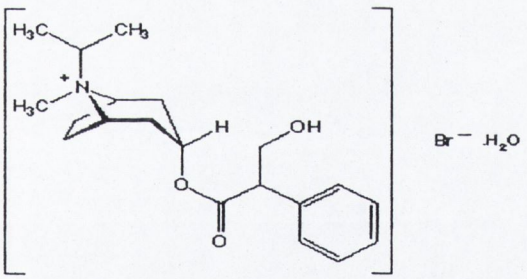

Figure 1.16 Structure of ipratropium bromide monohydrate.

1.5.5 Budesonide

Budesonide is a corticosteroid used as an anti-inflammatory and immunosupressive agent. It is used by inhalation in the preventative treatment of asthma. It is a crystalline powder which is practically insoluble in water, freely soluble in methylene chloride and sparingly soluble in alcohol (Ph. Eur., 2002). Budesonide melts at 221-232°C (Merck Index, 1996). Budesonide exists as a mix of two isomers, the S-isomer making up 40-51% of the mix. The structure of budesonide is given in Figure 1.17.

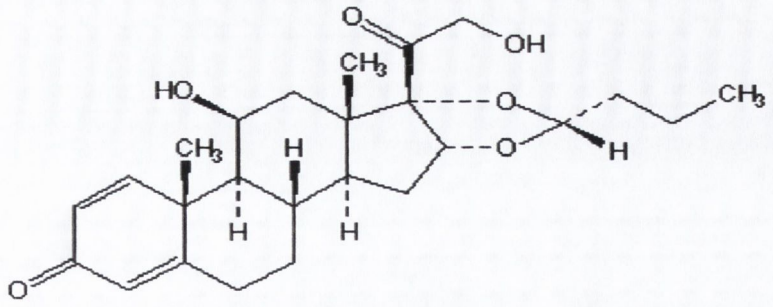

Figure 1.17 Structure of budesonide.

1.5.6 Formoterol fumarate dihydrate

Formoterol is a directly acting sympathomimetic with predominantly β-adrenoceptor stimulant activity, specific to β_2 receptors. Formoterol fumarate dihydrate is the salt form used in this thesis and is a crystalline material. Formoterol fumarate exists in two racemic forms, the A racemate melting at 138-140°C and the B racemate melting at 154-155°C (Merck Index, 1996). The structure of formoterol fumarate dihydrate is given in Figure 1.18.

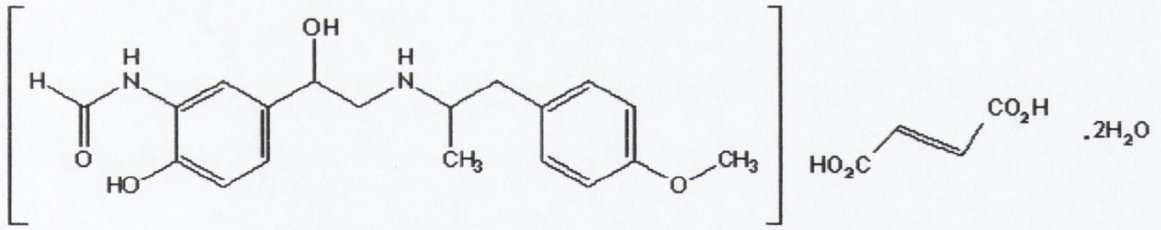

Figure 1.18 Structure of fomoterol fumarate dihydrate.

1.6 Dry powder inhaler delivery

There are three main applications of inhalation formulations in drug therapy.

(a) Local action (for example asthma),

(b) Respiratory infection (a localised delivery reducing the systemic drug toxicity),

(c) Systemic action (for example delivery of anaesthetics and delivery of proteins and peptides, i.e. therapeutics which would be degraded or show poor bioavailability when given orally).

A major factor governing the effectiveness of the deposition in the respiratory tract is the size of the inspired particles. The aerodynamic equivalent diameter is the diameter of a sphere of unit density (1 g/cm^3) which has the same settling velocity as the particle in question (Hickey, 1992). The aerodynamic diameter is a function of the size, shape and density of the particles. The airways consist of a series of dividing passageways originating at the trachea and terminating at the alveolar sacs. Only particles of an aerodynamic diameter below 5 μm reach the deep lung region because the bifurcating passageways lead to inertial impaction and sedimentation of larger particles (Hickey, 1992; Hickey, 1996). The deep lung alveoli region is the region of interest for targeting inhalables for systemic delivery. Particles larger than 10 μm generally deposit in the upper respiratory tract while particles less than 0.5 μm aerodynamic diameter are either exhaled or adhere to the walls of the mouth during the exhalation phase (Timsina et al., 1994).

With regard to inhalables for local action, attention has focused on reducing pharyngeal deposition to reduce the risks associated with local side effects and also systemic side effects resulting from swallowed drugs. In general therefore, whether designing a formulation for systemic or local drug delivery the optimum particle size range is regarded as 0.5-5 μm (aerodynamic equivalent diameter) (Timsina et al., 1994). The physicochemical properties of both the drug and the carrier particles used in a dry powder formulation for inhalation influence the dispersion and subsequent deposition of the drug particles in the respiratory tract. Other influences on the site of deposition and the deposition pattern of inhaled aerosols from dry powder inhalers (DPIs) include the patient (anatomical and physiological aspects of the respiratory tract and user technique) and design of the DPI device (Timsina et al., 1994).

The twin impinger is a simple device for assessing the delivery of drugs from inhalers (Hallworth and Westmoreland, 1987). In the case of the twin impinger, operated at a flow rate of 60 litres/minute, particles which collect in the lower stage are taken to have an aerodynamic diameter of less than 6.4 μm. The twin impinger is included in the European Pharmacopoeia (Ph. Eur., 2002, apparatus A) and British Pharmacopoeia (B.P. 2002, apparatus A) for the aerodynamic assessment of fine powder fractions (respirable fractions) of preparations for inhalation. Figure 1.19 shows a schematic diagram of the twin stage impinger.

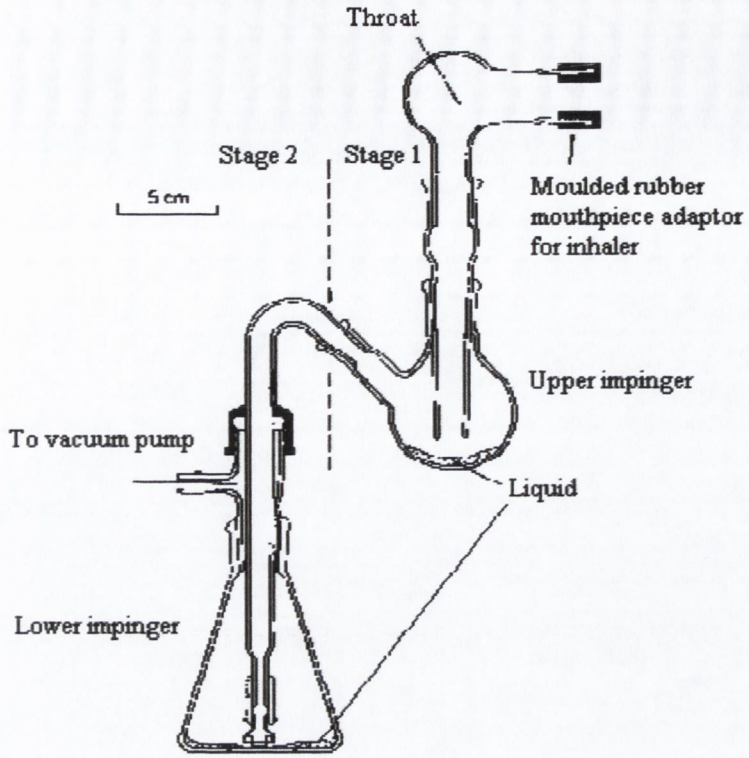

Figure 1.19 Schematic diagram of twin stage impinger.

For research purposes, two methods are generally used to calculate the respirable fraction. The first is to calculate the amount of drug in the lower impinger as a percentage of the nominal dose and the second is to calculate the amount of drug collected in the lower impinger as a percentage of drug collected in both chambers (Timsina et al., 1994). Timsina et al. (1994) state that the latter method is to be preferred since it represents the redispersion or deaggregation ability of the dry powder inhaler (DPI) device and also takes account of only the drug being delivered into the "airways".

Dry powder formulations for inhalation usually consist of micronised drug (1-5 μm) and inert coarse carrier particles (50-200 μm). The carrier particles are included in the formulation to aid flow and dispersibility of drug particles which can be highly cohesive when micronised (Kawashima et al., 1998). Typical formulations consist of micronised drug particles and carriers in a ratio of 1:67.5. The most commonly used carrier excipient is lactose monohydrate. It has been shown that the surface morphology of a carrier can affect the respirable fractions of a drug due to different strengths of adhesion between the drug and the carrier (Zeng et al., 2000). Zeng et al. (2000) blended lactose crystals of different shapes but similar surface-volume mean diameters with salbutamol sulphate. An increase in either the surface smoothness or the elongation ratio of lactose crystals increased the potentially respirable fraction of salbutamol sulphate from both a

Cyclohaler® and Rotahaler® device. Timsina et al. (1994) state that a test on the homogeneity of drug-carrier mixtures for DPIs should be carried out if a carrier is added in the powder formulation. Co-spray drying is a useful method of producing composite particles thus avoiding problems of non-homogeneity of mixing. While lactose is the obvious excipient of choice, since it is already the most commonly used excipient in DPIs, PEGs have also been investigated recently as carriers. Lucas et al. (1998) added micronised PEG 6000 instead of fine particle lactose to mixtures of co-spray dried bovine serum albumin/maltodextrin and coarse lactose and found that PEG 6000 was capable of improving the *in vitro* deposition of the model therapeutic agent measured using a Rotahaler® attached to a twin stage impinger. PEGs are generally recognised as safe (GRAS) by the U.S. F.D.A.

Spray drying has been previously used by Vidgrén et al. (1989) to produce particles for inhalation. They spray dried sodium cromoglycate and compared the product to mechanically micronised material *in vitro*. Whilst both methods of powder preparation resulted in about the same proportion of material (approximately 40%) having an acceptable particle size for inhalation (i.e. 0.5-7 μm), the spray dried material consisted of a greater proportion of particles in the 0.5-3.3 μm size range than the micronised material. Formulation of increased proportions of particles in the 0.5-3.3 μm size range compared to particles in the 5-7 μm is not necessary for drugs intended to act locally, for example on bronchial smooth muscle. However, it is important for drugs intended for systemic action.

The pulmonary route for delivery of therapeutic agents for systemic action has received much attention due to the many advantages this route possesses over oral delivery. The capacity of the lung to metabolise drugs is not as high as that of the liver (Hickey, 1996). Pulmonary delivery is non-invasive and provides an alternative route to parenteral administration for delivery of proteins and peptides which show unfavourable bioavailability by the oral route (Gonda, 1996). The high mucosal surface area and extensive blood supply together with the lower concentrations of extracellular enzymes in the lung compared with the gastrointestinal tract has resulted in research in the area of pulmonary delivery for systemic action (Byron, 1990). Some examples of peptide drugs which have been investigated for pulmonary delivery and were found to have acceptable bioavailability by this route are insulin (Colthorpe et al., 1992), human y-interferon, parathyroid hormone and salmon and human calcitonin (Patton, 1994). Spray drying has been used previously for the production of proteins for use in DPIs, for example Broadhead et al. (1996) investigated the deposition of spray dried β-galactosidase from a DPI.

In order to achieve systemic action the drug needs to reach the alveoli. Approximately 95% of the alveolar surface area is covered by a single layer of epithelial type 1 pneumocytes which are joined by tight junctions (Hickey, 1996). For systemic delivery the drug must reach the alveoli, avoid phagocytosis by macrophages and then cross the epithelium lining. Alveolar macrophages migrate around the alveoli (usually 3-4 per alveolus) beneath the surfactant layer (Morén et al., 1985).

As described in section 1.4.3, chitosan has been shown to act as a permeation enhancer, both *in vitro* by Artursson et al. (1994) and *in vivo* by Illum et al. (1994) who showed it to greatly enhance the absorption of insulin across the nasal mucosa of rat and sheep. Lueβen et al. (1996) also showed chitosan to have permeation enhancing effects at mucosal epithelia. Chitosan is known to be mucoadhesive and biodegradable (Lehr et al., 1992; Illum, 1998).

For a controlled release DPI to be effective, the product must first reach the deep lung and then be retained in the lung for a prolonged period to release the active substance. The ability of particles to escape detection and uptake by alveolar macrophages would ultimately determine the success of a sustained release drug delivery system.

Edwards et al. (1997) investigated the use of large porous particles for pulmonary delivery of insulin and found they produced a sustained suppression of systemic glucose levels for 96 hours compared to an effect lasting only 4 hours produced by nonporous insulin particles. The porous particles were larger in mean geometric diameter than the non-porous particles but because of their high porosity had the same aerodynamic diameters as the non-porous particles. The large porous nature of the particles was shown to result in more efficient aerosolisation from a DPI than smaller nonporous particles, resulting in higher respirable fractions. Edwards et al. (1997) used macrophages to investigate phagocytosis of the two different types of particles and found that the large porous particles were phagocytosed to a much lesser extent than nonporous particles due to their larger geometric diameters. They attributed the delayed appearance of insulin in the bloodstream, following the administration of the large porous particles, to the low phagocytosis of these particles by alveolar macrophages. Evora et al. (1998) investigated the effect of inclusion of 1,2-dipalmitoylphosphatidylcholine in PLGA microspheres on phagocytosis using lung macrophages obtained by intratracheal lavage of Wistar rats. They concluded that 1,2-dipalmitoylphosphatidylcholine reduced phagocytic uptake of the microspheres.

Lacasse et al. (1998) investigated macrophage phagocytosis of biodegradable polyanhydride PLA and PLGA microspheres prepared by both the spray drying and

solvent evaporation techniques. They measured the extent of phagocytosis by fluorescence determination and optical microscopy. The effect of PEG derivatives on phagocytosis was determined using PEG distearate incorporated into the microspheres. On incubation of microspheres with murine macrophages, PEG-distearate was found to inhibit phagocytosis when present in the microspheres at appropriate levels, i.e. 0.1% w/w inhibited phagocytosis but higher levels i.e. >1% w/w resulted in enhanced association with macrophages even in the presence of the phagocytosis inhibitor, cytochalasin D. The microsphere particle sizes studied ranged from 0.9 to 3.2 μm in diameter.

EXPERIMENTAL

2.1 Materials

Material	Supplier/manufacturer
Acetic Acid	Merck
Acetone	Merck
Acetonitrile	Riedel de Haën
Alpha lactose monohydrate	BDH
Bendroflumethiazide (BFMT)	Leo Laboratories
Budesonide	IVAX Pharmaceuticals, Ireland.
Chitosan low molecular weight (first batch : batch and filling code 38370311 32599)	Fluka
Chitosan low molecular weight (second batch : batch and filling code 40756811 50100)	Fluka
Deuterated water	Apollo Scientific Ltd.
Deuterated acetic acid	Apollo Scientific Ltd.
Deionised water	Purite Prestige Analyst HP water purification system
Diethyl ether	Cooley Distillery
Dulbecco's Modified Eagles Medium (DMEM)	Sigma
Ethanol	Cooley Distillery
Formoterol fumarate dihydrate	IVAX Pharmaceuticals, Ireland.
Gentamicin	Sigma
HPLC Grade water	Purite Prestige Analyst HP water purification system
Hydrochloric acid (HCl)	BDH
Ipratropium bromide monohydrate	IVAX Pharmaceuticals, Ireland.
Lactose monohydrate	BDH
Lactose anhydrous	Sheffield Products (a divison of Quest International)
L-Glutamine	Sigma
Methanol (HPLC Grade)	Riedel de Haën
Magnesium chloride hexahydrate ($MgCl_2.6H_2O$)	Merck
Ninhydrin Reagent	Sigma
Paraformaldehyde	Sigma
Polyethylene glycol 4000 (PEG 4000)	Riedel-de Haën
Polyethylene glycol 20,000 (PEG 20,000)	Fluka
Polyox resin WSRN-750 NF	Union Carbide

Polyethylene glycol standard (molecular weight 1,470)	Fluka
Polyethylene glycol standard (molecular weight 4,120)	Fluka
Polyethylene oxide standard (molecular weight 22,800)	Fluka
Polyethylene oxide standard (molecular weight 112,100)	Fluka
Polyethylene oxide standard (molecular weight 276,300)	Fluka
Potassium chloride (KCl)	Merck
Potassium nitrate (KNO_3)	BDH Chemicals
Pullulan standard (molecular weight 11,800)	Polymer Laboratories
Pullulan standard (molecular weight 22,800)	Polymer Laboratories
Pullulan standard (molecular weight 47,300)	Polymer Laboratories
Pullulan standard (molecular weight 112,000)	Polymer Laboratories
Pullulan standard (molecular weight 212,000)	Polymer Laboratories
Pullulan standard (molecular weight 404,000)	Polymer Laboratories
Salbutamol sulphate	IVAX Pharmaceuticals, Ireland.
Salbutamol base	IVAX Pharmaceuticals, Ireland.
Silica Gel	Lennox laboratory Suppliers
Sodium acetate trihydrate	Sigma
Sodium chloride (NaCl)	Merck
Sodium dihydrogen phosphate dihydrate	Merck
di-sodium hydrogen phosphate dodecahydrate	Merck
Sodium dihydrogen phophate monohydrate	Merck
Sodium hydroxide	Riedel de Haën
Sulphuric acid	Riedel de Haën
Tetrahydrofuran	Riedel de Haën
Trypsin	Sigma
Ventolin Rotacaps®	Allen & Hanburys

2.2 Methods

2.2.1 Spray drying

All systems were spray dried as solutions using a Büchi Mini Spray Dryer 190 or 191 (Büchi Laboratoriums-Technik AG, Switzerland). The concentrations of feed solutions and spray drying parameters used for the various spray dried systems are given in Appendix I.

2.2.2 Solid Dispersion Production

Method 1. Both components were dissolved and spray dried using a Büchi Minispray Dryer 190 or 191.

Method 2. Melt method. Melts of BFMT:PEG 4000 10:90 were prepared according to the method of Frontini and Mielck (1997a). Both components were heated over a water bath to a temperature of 80°C while stirring. When a clear melt had formed the mixture was poured onto aluminium foil and left to solidify for one hour. It was then removed and milled with a mortar and pestle.

2.2.3 Powder X-Ray Diffraction

Powder X-ray diffraction measurements (XRD) were made on samples in low background silicon mounts, which consisted of cavities 0.5 mm deep and 9 mm in diameter (Bruker AXS, UK). A Siemens D500 Diffractometer was used. This consists of a DACO MP wide-range goniometer with a 1.0° dispersion slit, a 1.0° anti-scatter slit and a 0.15° receiving slit. The Cu anode X-ray tube was operated at 40 kV and 30 mA in combination with a Ni filter to give monochromatic Cu Kα X-rays. Measurements were generally taken from 5° to 35° on the 2 theta scale at a step size of 0.05° per second for qualitative analysis. For quantitative analysis a step size of 0.02° was used with a count time of 5 seconds.

2.2.4 Differential Scanning Calorimetry Analysis

Differential scanning calorimetry (DSC) (Mettler Toledo DSC 821°) was performed using closed 40 µl aluminium pans with three vent holes on accurately weighed samples (5-10 mg). Samples were run at a heating rate of 10°C/minute under nitrogen purge.

Mettler Toledo STAR^e software Version 5.1 or Version 6.1 was used for analysis of thermodynamic events.

Modulated temperature DSC experiments to determine glass transition temperatures of BFMT/PEG spray dried composites were carried out using a Q1000 Tzero^{TM} TA Instruments DSC, version 6.2, build 204. Samples were run from –60 to 220°C using a heating rate of 5°C/minute, a modulation amplitude of 0.5°C and a period of 50 seconds. Samples were run in aluminium pans with three vent holes under nitrogen purge.

2.2.5 Thermogravimetric Analysis

Thermogravimetric analysis (TGA) was performed using a Mettler TG 50 linked to a Mettler MT5 balance. Data was processed using Mettler Toledo STAR^e software Version 5.1 or Version 6.1. Accurately weighed samples between 5 and 10 mg were analysed using open pans under nitrogen purge. The scans were generally run from 30 to 350°C at a heating rate of 10°C/minute.

2.2.6 Hot Stage Microscopy

Hot stage microscopy (HSM) was performed using a Reichert hot stage mounted on a MEOPTA microscope. Samples were mounted in silicon oil (to detect desolvation) and in air.

2.2.7 Light microscopy

Light microscopy was carried out using an Olympus BX 60 light microscope.

2.2.8 Scanning Electron Microscopy

Samples were mounted on aluminium stubs and sputtered with gold. Scanning electron microscopy (SEM) was performed using a Hitachi S-3500N variable pressure scanning electron microscope. The images were formed from the collection of secondary electrons.

2.2.9 Energy Dispersive X-Ray Analysis

Energy Dispersive X-Ray Analysis (EDXA) was carried out using Pungsten Gamma Tech Imix-PTS EDX analysis on the Hitachi S-3500N variable pressure SEM with a 10 mm^2

UTW detector. For qualitative EDXA, powder samples were utilised and an area mapped for the presence of the atom being analysed. For quantitative EDXA discs composed of either spray dried material or standards were prepared from 150 mg weights of powder. The standards were prepared from non-spray dried material. Point analysis was used to determine the weight percent of the atom present in the various discs. Count times of 5 minutes per analysis were employed for both qualitative and quantitative analysis.

2.2.10 Fourier Transform Infrared Spectroscopy

Fourier Transform Infrared Spectroscopy (FTIR) was carried out using a Perkin Elmer Paragon 1000 fourier transform infra-red spectrometer. KBr discs were prepared based on 1 mg % sample loading. Discs were prepared by grinding the sample with KBr in an agate mortar and pestle, placing the sample in an evacuable KBr die and applying 8 tons of pressure, in a Graseby Specac IR press. Two FTIR spectra were obtained for each system.

2.2.11 Gel Permeation Chromatography (GPC)

Gel Permeation Chromatography (GPC) was performed using a Plaquagel-OH Mixed 8 μm 300 x 7.5 mm column (Polymer Laboratories Ltd., UK). One of two systems was used:

a) For analysis of PEG systems the method was supplied by Polymer Laboratories (Technical Bulletin TB598). Water was used as the solvent and mobile phase. The mobile phase flow rate was 1 ml/minute. Calibration curves were prepared using polyethylene glycol and polyethylene oxide narrow standards. 0.2% w/v concentrations of standards and samples were prepared and volumes of 200 μl were injected in triplicate. A Waters 410 Refractive index detector was used. Analysis was performed using Waters Millenium 32 software. A sample calibration curve is shown in Appendix II.

b) For analysis of chitosan systems the method supplied by Polymer Laboratories (Technical Bulletin TB581) was followed substituting potassium nitrate for sodium nitrate. The mobile phase consisted of potassium nitrate 0.5 M and sodium phosphate monosodium 0.01 M brought to pH 2 with concentrated HCl. The mobile phase flow rate was 1 ml per minute. Samples were prepared as 0.05 to 0.10% w/v solutions in concentrated HCL and brought to volume with mobile phase. Pullulan polysaccharides were used as standards and prepared as 0.05 to 0.10% w/v solutions in mobile phase. 200 μl volumes of samples or standards were injected in triplicate. The detector used was a Waters 410 differential

refractometer. Analysis was performed using Shimadzu Class VP software (version 6.10) with GPC for Class VP (version 1.02). A sample calibration curve is shown in Appendix II.

Number average molecular weight (*Mn*) and weight average molecular weight (*Mw*) were determined as shown in Equations 2.1 and 2.2 respectively.

$$Mn = \frac{\sum NxMx}{\sum Nx}$$ Equation 2.1

$$Mw = \frac{\sum WxMx}{\sum Wx} = \frac{\sum NxMx^2}{\sum NxMx}$$ Equation 2.2

where *Mx* is the molecular weight of a molecule corresponding to a degree of polymerisation *x*, *Nx* and *Wx* are the total number and weight of the molecules of "length" *x*, respectively.

2.2.12 High Performance Liquid Chromatography

High Performance Liquid Chromatography (HPLC) was performed using one of two systems:

a) HPLC analysis of BFMT and 5-Trifluoromethyl-2,4-disulphamoylaniline (TFSA) were performed according to the method of Frontini and Mielck (1992). The method involved the use of a phenyl column (Ubondapak 10 Phenyl, Labquip) enclosed in an oven at 37°C. The mobile phase consisted of 40:60 methanol:water. The solvent phase was prepared by dissolving 750 mg of KCl in 10 ml of 1N HCl, adding approximately 400 ml of water, adding 400 ml of methanol, mixing and bringing to 1000 ml with water. The flow rate was 1.5 ml per minute and samples were analysed at 270 nm with aufs setting at 0.005. For analysis of spray dried samples for TFSA content the samples were prepared using the solvent described above. However when analysing BFMT release during dissolution studies the sample dissolution medium was identical to the solvent phase described except it did not include methanol. Samples, mobile phase and solvent phase were filtered through 0.45 μm membrane filters prior to use. Samples were manually injected into a 20 μl rheodyne injection port using a 50 μl needle. The system consisted of a Waters 484 Absorbance Detector attached to a Waters 745 Data Module. Samples were injected at

least in duplicate. A calibration curve was prepared each day. A sample calibration curve and sample chromatograms are shown in Appendix IV.

b) HPLC analysis of salbutamol sulphate was performed using a variation of the USP Pharmacopeia (USP Pharmacopeia 2000) method for HPLC analysis of salbutamol sulphate. Sodium-1-heptane-sulfonic acid was used in the preparation of the mobile phase instead of sodium-1-hexane-sulfonic acid. Preparation of the mobile phase involved dissolving 1.13 g of sodium 1-heptanesulfonic acid in 1200 ml of water and adding 12 ml of glacial acetic acid to produce solution A. This was then mixed with methanol in a ratio 60:40 solution A:methanol. 50 µl volumes of samples or standards were injected. A calibration curve was prepared each day by making standard solutions of salbutamol sulphate raw material which were injected in duplicate. Samples were also injected in duplicate. A C18 column (Techopak 10 C18, Labquip) attached to a Shimadzu LC-10 AT VP liquid chromatograph with a Shimadzu SCL-10A system controller, a Shimadzu SPD-10A VP UV-VIS detector, a Shimadzu DGU-14 degasser and a SIL-10AD VP autoinjector was used and the system was operated at a flow rate of 1 ml per minute. The solvent phase for salbutamol sulphate samples was either isotonic phosphate buffer pH 7 (if analysing salbutamol sulphate release from discs or particles, section 2.2.16.2 and section 2.2.16.3) or water or acetic acid 1% v/v (if analysing salbutamol sulphate deposition in twin impinger experiments, section 2.2.14). Samples were analysed using Shimadzu Class VP software (version 6.10). A sample calibration curve and sample chromatogram is shown in Appendix IV.

2.2.13 UV Analysis

UV measurements were made using a Hewlett Packard 8452A photodiode array UV/VIS spectrophotometer using 10 mm quartz cuvettes (Spectrosil). Absorbances were measured at 274 nm for BFMT analyses or at 276 nm for salbutamol sulphate analyses. Concentrations were determined by reference to a calibration curve prepared from dilutions of stock solutions of the particular drug (Appendix V). UV analysis was also used for ninhydrin analysis as described in section 2.2.15 b.

2.2.14 In Vitro Aerosol Characterisation

In vitro deposition of dry powders for inhalation were determined using a twin impinger (Glaxo Type single stage impactor, Copley Instruments (Nottingham) Ltd.). The

instrument complied with specifications for apparatus A of the European Pharmacopoeia (Ph. Eur., 2002) and British Pharmacopoeia (B.P., 2002). 60 mg samples of powder were weighed and loaded into size 3 soft gelatin capsules which were individually installed in a Rotahaler device (Glaxo Wellcome, Inc., NC). The rotahaler was attached to the impinger which contained 7 and 30 mls of collecting solvents in stages 1 and 2, respectively. The solvent used was water except in the analysis of salbutamol/chitosan systems in which case the solvent used was acetic acid 1% v/v. The capsules contents were released by twisting the rotahaler and the system was vacuumed to produce air streams of 60 litres/min for 5 seconds. The liquids in stages 1 and 2 were collected and diluted as appropriate and measured by UV spectrophotometry (section 2.2.13) or HPLC (2.2.12). Each deposition experiment involved the aerosolisation of one capsule. All systems were analysed in triplicate. Statistical analysis was carried out using Minitab^{TM} statistical software (Version 13.1).

2.2.15 Assay for Degree of Deacetylation of Chitosan

The degree of deacetylation of chitosan was determined by one of two methods:

a) ^{1}H-Nuclear Magnetic Resonance Spectroscopy (^{1}H-NMR)

Samples for ^{1}H-NMR were prepared using the method of Hirai et al (1991). 20 mg samples were dissolved in 2 mls of 2% w/w deuterated acetic acid in deuterated water solution. The solutions were heated to 70°C to aid dissolution and filtered through cotton wool. Samples were analysed using a Bruker 400 megahertz NMR. The degree of deacetylation was determined by Equation 2.3 (Hirai et al., 1991) using the integral intensity, ICH_3, of the CH_3 residue and the sum of integral intensities $IH_2 - H_6$ of the H_2, H_3, H_4, H_5, H_6' and H_6 protons.

$$\text{Degree of deacetylation (\%)} = \{1 - (\frac{1}{3} ICH_3 / \frac{1}{6} IH_2 - H_6)\} x100 \qquad \text{Equation 2.3}$$

b) Ninhydrin Assay

A ninhydrin colorimetric test based on that described by Curotto and Aros (1993) was used for quantification of chitosan and subsequent determination of the percentage of free amino groups. The method involved preparation of calibration curves by preparing solutions of chitosan and of D glucosamine (0.1 mg/ml in 2% acetic acid). 0.1, 0.2, 0.3, 0.4, 0.5 ml of these solutions were pipetted into separate test tubes. Acetic/acetate buffer (0.5 ml; pH

5.5, 4 M) was added to each tube and the volume adjusted to 1 ml with deionised water. Finally, 2 ml of ninhydrin reagent (20 g/litre ninhydrin, 3 g/litre hydrindantin, dimethylsulfoxide 75% and lithium acetate 1 mole/litre pH 5.2) was added and the tubes were agitated vigorously. They were then heated for 10 minutes in a boiling water bath, cooled for 15 minutes and their absorbances read by UV at 570 nm. All plots were linear. A value of 100% of free amino groups was assigned to the slope of the D-glucosamine calibration curve and correspondingly the values for the slopes obtained with solutions of chitosan and processed chitosans gave the percentages of free amino groups. Samples were analysed in triplicate.

2.2.16 In Vitro Release Studies

2.2.16.1 Dissolution studies on BFMT and BFMT/PEG systems

Dissolution studies were performed using the USP 24 paddle apparatus (USP Pharmacopeia 2000). Dissolution studies were performed for BFMT, spray dried BFMT/PEG 4000 systems and equivalent physical mix systems. Powders for physical mixes were sieved through a 63 μm laboratory test sieve (Endecotts Ltd.). The appropriate ratios were weighed and mixed in a Turbula® mixer (Glen Creston Ltd.) for five minutes. Discs were prepared from 200 mg of powder using a 13 mm punch and die set and compressing in a Perkin Elmer hydraulic press at a pressure of 7 tonnes for 1 to 2 minutes depending on the system (since some discs cracked if compressed for too long). The discs were mounted in stainless steel cylindrical holders with one end filled with paraffin wax so that only one surface was exposed to the dissolution medium. The dissolution medium consisted of 400 ml of buffer pH 2. The low pH was used to avoid degradation of BFMT during the timecourse of the experiment (Frontini and Mielck, 1992). The pH 2 buffer was prepared by dissolving 750 mg KCl in 10 ml of 1N HCl and bringing to 1000 ml with water. Dissolutions were carried out in a Sotax AT7 dissolution bath at 37°C with paddles operating at 50 r.p.m.. 5 ml aliquots were withdrawn at appropriate time intervals, filtered through 0.45 μm filters (Gelman Sciences) and analysed for drug content. 5 ml samples of fresh buffer at 37°C were used to replace the medium removed at each sample point. The medium was analysed for BFMT content initially by both UV analysis as described in section 2.2.13 and HPLC analysis as described in section 2.2.12. Once it was established that no significant increase in TFSA (main degradation product) occurred over the time course of the experiment then UV analysis was used for all further analysis of BFMT.

2.2.16.2 Release from chitosan/salbutamol sulphate systems

These studies were performed using the USP 24 paddle apparatus (USP Pharmacopeia 2000). For analysis of chitosan/salbutamol systems intrinsic dissolution tests could not be performed since discs of the spray dried materials swelled in the dissolution medium and were not retained in the steel holders. Powders of a particle size less than 63 μm were used for preparation of non spray dried discs and discs of physical mixes. The chitosan raw material was first milled (in a Retsch centrifugal mill with a 0.08 mm sieve ring attachment) prior to sieving through the laboratory test sieve (Endecotts Ltd.). Powders which were to be used in physical mixes were mixed in a Turbula® mixer as in section 2.2.16.1. Discs of chitosan/salbutamol sulphate were prepared by weighing 150 mg of powder and compressing in a 13 mm punch and die set using a Perkin Elmer hydraulic press operated at 7 tonnes for 5 minutes. Discs of pure crystalline salbutamol sulphate discs averaged 126.5 mg in weight. Dissolutions were carried out in a Sotax AT7 dissolution bath at 37°C with paddles operating at 50 r.p.m.. The dissolution medium used was 500 mls of Sφrensens modified isotonic phosphate buffer pH 7 (Pharmaceutical Handbook, 1980). 5 ml samples were taken, filtered through a 0.2 μm filter and replaced with 5 ml of fresh medium at 37°C as described in section 2.2.16.1. Samples were analysed by HPLC (see section 2.2.12).

2.2.16.3 Release from particles

Salbutamol sulphate release from chitosan/salbutamol sulphate co-spray dried systems was performed using a variation of the method of Heelan et al. (1997). The method involved adding 50 mg of powder to a 100 ml conical followed by the addition of 20 ml of isotonic phosphate buffer pH 7 (already heated to 37°C). The conical was stoppered and placed into a horizontal shaker water bath maintained at 37°C and shaken at 100 cycles per minute. 2 ml samples were withdrawn at appropriate time intervals and filtered through a 0.2 μm filter. 2 ml of fresh medium at 37°C was washed through the filter holder back into the conicals having first removed the filters. The filters were added into the conicals after each sample point to avoid loss of particles from the medium. Samples were analysed by HPLC as described in section 2.2.12.

2.2.17 Statistical Analysis

Minitab™ statistical software release 13.1 was used for all statistical analysis.

2.2.18 Particle Size Measurement

Particle size was measured by scanning electron microscopy (SEM) (Lee et al., 1996). SEM photographs were taken and imported into Adobe Photoshop version 6.0. The Photoshop measuring tool was used to measure the diameter of 100 particles of each system. In the factorial design experiment of spray dried formoterol fumarate:budesonide (Chapter 5) the results of particle size measurements for replicates were combined so that a total of 200 particle diameters were counted for each variation of parameter setting. All particles were spherical so width and length measurements were not necessary. A one-way analysis of variance performed by Minitab was used to compare the particle sizes produced for the different spray drying conditions.

2.2.19 Density Measurements

True density measurements were performed by helium pycnometry using a calibrated AccuPyc 1330 instrument (Micromeritics, USA). Prior to analysis, the samples were dried overnight to a constant weight in a vacuum oven at 50 °C with a vacuum pressure of 600 mbar. The mass of each sample was accurately determined using a MT5 microbalance (Mettler Toledo, Switzerland). Each sample was analysed in duplicate.

2.2.20 Preparation of Formaldehyde Solution for use as the Crosslinking Agent

Commercial formaldehyde solutions ("formalin") contain 10-15% methanol to prevent the formaldehyde from polymerising during storage. To produce methanol free formaldehyde, paraformaldehyde was added to water and heated in a water bath to 55-60°C until the paraformaldehyde dissolved. The resulting formaldehyde solution is stable for use for approximately 2 weeks if stored under refrigeration. (This method was obtained from Sigma Product Information for Sigma Product Number P6148).

2.2.21 Production of 5-Trifluoromethyl-2,4-disulphamoylaniline

5-Trifluoromethyl-2,4-disulphamoylaniline (TFSA) (the main degradation product of BFMT) was prepared according to the method of Hassan (1983). Frontini and Mielck (1997a) found that TFSA produced by the method of Hassan had a purity of 99.6%,

determined using the BP-CRS material. Preparation of TFSA involved refluxing approximately 100 mg of bendroflumethiazide with 25 ml of 20% sodium hydroxide solution for one hour. After cooling to room temperature, 50 ml of water was added and the pH adjusted to between 7 and 8 with dilute sulphuric acid. The solution was transferred to a separating funnel and extracted with diethyl ether (3 x 30 ml). The ether extracts were combined, washed with water, the volume transferred to a round bottomed flask and evaporated to dryness (using a Büchi Rotavapor R-114 attached to a Büchi Waterbath B-480). The residue was then redissolved in 5 ml of methanol and evaporated to dryness, resulting in TFSA.

2.2.22 Creation of Defined Relative Humidity (RH) Conditions

Conditions of 4°C 34% RH, 30°C 32% RH and 45°C 31% RH were created using saturated magnesium chloride solutions stored at 4°C, 30°C and 45°C respectively (Nyqvist, 1983). Higher relative humidity conditions of 75% RH were created by storing saturated sodium chloride solutions at 4°C, 30°C and 45°C (Nyqvist, 1983).

2.2.23 Phagocytosis Study

The macrophage cell culture line, J774A.1, was already in use for phagocytosis experiments by Fiona Brennan, a Ph.D student in the department of Pharmaceutics and Pharmaceutical Technology. The cell line was originally obtained from ATCC (USA). The J774A.1 cell line is a mouse macrophage cell line. The cell line was grown in a 5% CO_2 incubator (Nuaire, USA) at 37°C in Dulbecco's Modified Eagles Medium (DMEM), which was supplemented with L-glutamine (2 mM), foetal calf serum (10% v/v) and gentamicin (100 mg/ml). The cells were grown in 75 ml flasks (Grenier), passaged approximately once weekly and the growth media was replaced with fresh growth media twice weekly.

Passaging of cells

The supplemented DMEM present in the flasks was removed (in order to remove the trypsin inhibitor present in the foetal calf serum) and the cells were washed with 10 ml of unsupplemented DMEM. 1 ml of trypsin was added and the flasks were shaken vigorously to cause detachment of the cells from the flask wall. 10 ml of supplemented DMEM was added and the mixture was centrifuged for 5 minutes at 1000 r.p.m.. The pellet was

resuspended in 6 ml of supplemented DMEM and cell density determined using a haemocytometer. Cells were seeded at a density of 1–2 x 10^6 cm^2.

Phagocytosis assay

Phagocytosis of chitosan or chitosan/PEG 4000 microspheres by macrophages was measured by observing the number of microspheres internalised (Kimura et al., 1994 and Wang et al., 1999). The method was as follows: Macrophage cells were cultured in 24-well culture plates (Grenier) seeded at a density of 2 x 10^5 cells/well in supplemented DMEM (1 ml volume) and incubated for 24 hours in a 5% CO_2 atmosphere at 37°C. After 24 hours incubation 0.5 mg of microspheres suspended in 200 µl of DMEM media was added to each well and culture plates were incubated for different time periods up to 24 hours. At various time points culture plates were removed from the incubators, washed three times with phosphate buffered saline (pH 7.4) to remove non phagocytosed cells and examined by phase contrast microscopy (Zeiss, Germany). Photographs were taken using a RTS Kontax camera attached to the phase contrast microscope. Negative controls consisted of wells to which had been added 200 µl of DMEM media, while positive controls consisted of polylactic/glycolic acid (PLGA) microspheres (0.5 mg/200µl). The positive control experiments were performed by Fiona Brennan (both studies being performed using the same passage of J774A-1 cells and at the same time). PLGA microspheres have previously been shown to be phagocytosed by J774A.1 macrophages in the literature (Wang et al., 1999).

2.2.24 Modelling Drug Release

The experimental release data from salbutamol sulphate/chitosan microspheres were fitted to theoretical equations using MicoMath® Scientist® for Windows™ software. The various equations examined are described in Chapter 6. The ability of an equation to describe the experimental data was assessed using both the Coefficient of Determination (CoDet) and Model Selection Criterion (MSC). The CoDet is a measure of the fraction of the total variance taken into account by the model and is viewed as a measure of goodness of fit. Values of CoDet can vary from –1 to 1 with 1 describing a perfect fit. The CoDet is defined in Equation 2.4.

$$CoDet = \frac{\sum_{i=1}^{n} w_i\left(Yobs_i - \overline{Y}obs\right)^2 - \sum_{i=1}^{n} w_i\left(Yobs_i - Ycalc_i\right)^2}{\sum_{i=1}^{n} w_i\left(Yobs_i - \overline{Y}obs\right)^2} \qquad \text{Equation 2.4}$$

where n is the number of points, w_i is the weight applied to each point, $\overline{Y}obs$ is the weighted mean of the observed data, $Yobs_i$ is the observed values of dependent variable and $Ycalc_i$ is the calculated values of dependent variable.

The MSC is a representation of the "information content" of a given set of parameter estimates by relating the CoDet to the number of parameters, i.e. the number of degrees of freedom used in obtaining the fit. Equation 2.5 is used to determine the MSC.

$$MSC = \ln\left[\frac{\sum_{i=1}^{n} w_i(Yobs_i - \overline{Y}obs)^2}{\sum_{i-1}^{n} w_i(Yobs_i - Ycalc_i)^2}\right] - \frac{2p}{n} \qquad \text{Equation 2.5}$$

where p is the number of parameters estimated. When comparing two models which have different numbers of parameters, the model selection criterion places the burden on the model with the greater number of parameters to have a better CoDet. When judging the fit of a particular model to experimentally derived data, the model with the highest MSC is the most appropriate.

RESULTS AND DISCUSSION

CO-SPRAY DRIED LACTOSE/PEG 4000 SYSTEMS

3.1. Introduction

It is well known that the spray drying of pure lactose produces an amorphous product with significantly altered functional properties compared to those of the conventional crystalline forms of the sugar (Gunsel and Lachman, 1963; Vromans, 1986; Sebhatu and Alderborn, 1999). It has also been shown that additives added after the formation of amorphous lactose can influence the recrystallisation of amorphous spray dried lactose (Buckton and Darcy, 1995), PVP delaying the onset of recrystallisation (Stubberud and Forbes, 1998). Chidavaenzi et al. (1997) spray dried 10, 20, 30 and 40 g/100ml feed concentrations of lactose. The 10 g/100ml system yielded amorphous lactose, the 20 and 30 g/100ml feed concentrations yielded amorphous lactose and some α-anhydrous lactose and the 40 g/100ml feed concentration yielded some amorphous material, some α-anhydrous lactose and some lactose monohydrate. Chidavaenzi et al. (1997) reported that the amount of amorphous lactose produced from the 30 and 40 g/100ml suspension feeds was higher than the amount of lactose in solution and that the increase in the amount of amorphous lactose produced was due to a milling effect in the atomiser of the spray drier. Chidavaenzi et al. (2001) prepared 10, 20, 30 and 40 g/100ml lactose feed concentrations to which they added 12% PEG 4000 by weight of lactose. Spray drying of these systems resulted in crystalline systems as evidenced by powder X-ray diffraction (XRD) and differential scanning calorimetry (DSC). The 10 and 20 g/100ml lactose systems showed the presence of α-lactose monohydrate and β-lactose. The PEG melting endotherms observed by DSC supported the presence of the extended chain polymorphic form (Chatham (1985). The crystallisation of PEG into its different polymorphic forms (the metastable once folded chain conformation and the stable extended chain form) has been studied by Chatham (1985). The 30 and 40 g/100ml PEG-containing lactose systems were described by Chidavaenzi et al. (2001) as consisting of α-lactose monohydrate and α-anhydrous lactose but no β-lactose, the PEG again being present in the extended chain conformation. Lactose/PEG systems containing lower PEG contents were also spray dried, containing 1, 2 and 4% PEG (by weight of lactose). The materials produced were crystalline and β-lactose was absent from the systems. It was postulated that the presence of the PEG 4000 slowed the solidification rate of the lactose during the drying process, allowing both components to crystallise. Rapid conversion of any α-anhydrous lactose present to lactose monohydrate occurred on storage at 40°C 75% RH. Chidavaenzi et al. (2001) stated that they were surprised that spray drying with PEG produced predominantly crystalline products given that spray drying indomethacin/PVP systems (Corrigan et al., 1985)

resulted in amorphous materials. Both PVP and PEG are water soluble polymers. However PVP is an amorphous excipient while PEG is a semi-crystalline material. Chidavaenzi et al. (2001) did not spray dry PEG alone to ascertain whether spray drying results in the formation of amorphous PEG.

In the current thesis, the preparation and properties of spray dried PEG 4000 and lactose/PEG 4000 composites of 5, 10, 20 and 30% PEG by weight of total solids spray dried as 10% w/v solutions, were investigated. The physical stability of these systems under different storage conditions was also examined.

3.2. Individual components spray dried alone

3.2.1. Lactose

A 10% w/v lactose solution was prepared from lactose monohydrate and spray dried using the parameters shown in Appendix I. The DSC scan of spray dried lactose is shown in Figure 3.1 (scan a).

Figure 3.1 DSC scans of (a) spray dried lactose; (b) lactose monohydrate and (c) anhydrous lactose.

Spray dried lactose was amorphous, as expected, as evidenced by the presence of an exotherm representative of recrystallisation of the amorphous form. The spray dried lactose sample showed a melting endotherm at approximately 217°C indicative of melting of α-lactose (Angberg, 1995; Chidavaenzi et al., 2001). Figure 3.1 also shows a DSC scan of commercial grade anhydrous lactose with a melting endotherm in the 230°C region, indicative of β-lactose (scan c) (Angberg, 1995; Chidavaenzi et al., 2001). A slight depression was evident at approximately 140°C suggesting that some monohydrate may be present in the commercial sample. The DSC scan of lactose monohydrate shows a dehydration endotherm in the 140°C region and an α-lactose melting endotherm at approximately 217°C (Figure 3.1 scan b).

Figure 3.2 shows the XRD scans of lactose monohydrate and lactose after spray drying. Spray dried lactose was amorphous, as expected, indicated by the halo and lack of peaks indicative of crystallinity in the XRD scan (Briggner et al., 1994).

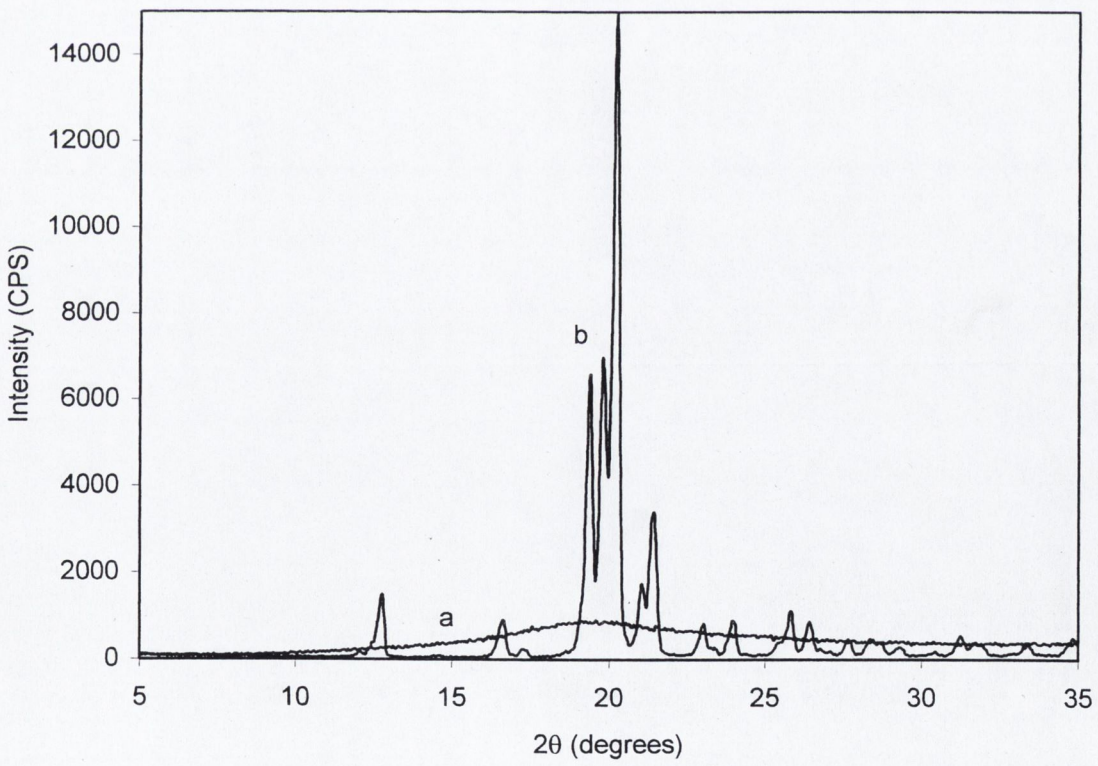

Figure 3.2 XRD scans of (a) spray dried lactose and (b) lactose monohydrate.

Scanning electron microscopy (SEM) of the spray dried lactose showed smooth spherical particles approximately 1-4 μm in diameter.

3.2.2. PEG 4000

Attempts to spray dry PEG 4000 from water were unsuccessful since an outlet temperature below that of PEG's melting temperature could not be achieved. Therefore PEG was spray dried from ethanol 95%, using inlet temperatures of 75-77°C which allowed outlet temperatures of less than 47°C to be attained i.e. temperatures which were sufficiently low to allow solidification of PEG.

Figure 3.3 shows the XRD scans of PEG before and after spray drying, both showing peaks indicative of crystallinity. The reduction in magnitude of the XRD peaks in the spray dried sample (Figure 3.3, scan a), together with a reduction in enthalpy change for the melting endotherm by DSC (Figure 3.4, scan a), was consistent with some reduction in PEG crystallinity on spray drying. XRD showed peak intensities of 8039 counts per second (CPS) at 19.2°(2θ) and 9120 CPS at 23.4° for non-spray dried PEG compared to lower CPS of 6959 and 7108 for the spray dried PEG. The enthalpy changes by DSC were 192 J/g (+/- 2.35 J/g) for the commercial PEG and 173 J/g (+/- 0.65 J/g) for the spray dried sample. Therefore it appears that a reduction in crystallinity of approximately 10-15% was achieved on spray drying.

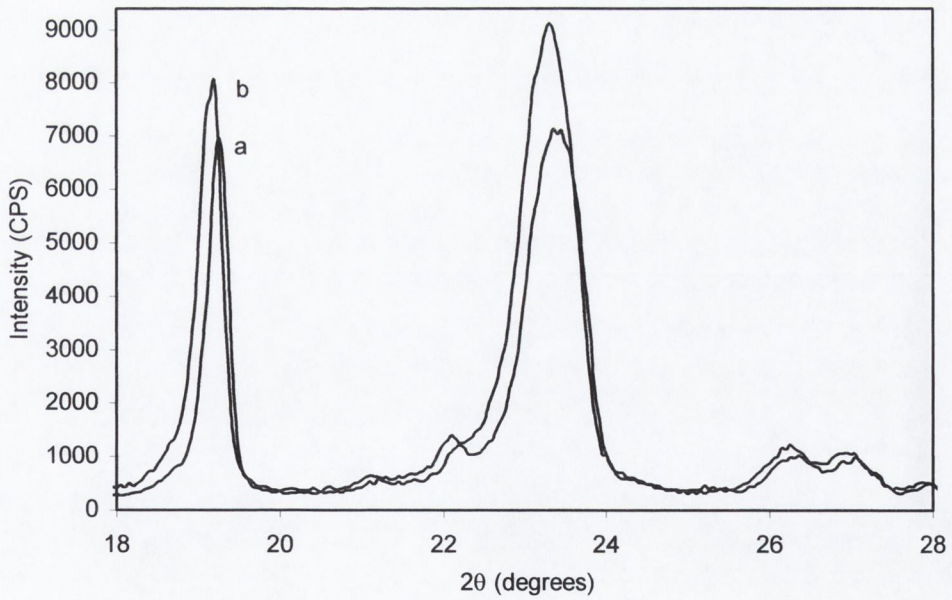

Figure 3.3 XRD scans of (a) spray dried PEG 4000 and (b) commercial sample of PEG 4000.

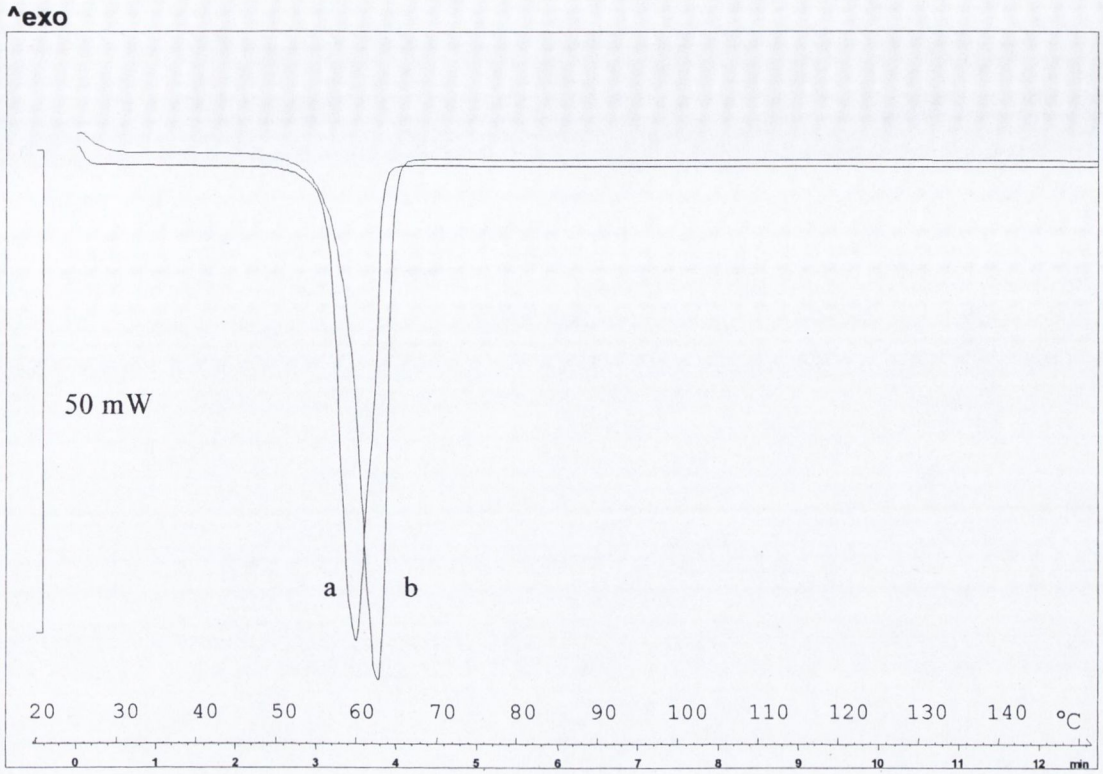

Figure 3.4 DSC scans of (a) spray dried PEG 4000 and (b) commercial sample of PEG 4000.

PEG 4000 is known to exist in extended or once folded chain conformations, the latter being metastable with respect to the former (Chatham, 1985; Kambe, 1980). Once folded chain PEG melts at a lower temperature, approximately 5°C lower by DSC than the extended form (Chatham, 1985; Kambe, 1980). Double peaks are observed by DSC when the sample consists of mixtures of once folded and extended chain PEG (Chatham, 1985; Kambe, 1980). DSC analysis of the spray dried PEG sample resulted in a single peak having a slightly lower PEG melting temperature than non spray dried PEG. This could be due to the presence of some amorphous polymer and/or PEG being present in the once folded chain form.

Figure 3.5 shows SEM micrographs of spray dried PEG. Particle morphology was highly dependent on the processing conditions. Thus, depending on the spray drying conditions, either sphere-like particles with nodules or twig-like particles were produced. The sphere-like particles were produced when the outlet temperature was 45-46°C, and these were quite large, approximately 50-70 μm in diameter. Their surfaces were not smooth, as is often the case with amorphous spray dried products, but were rather 'convoluted', of large surface area, appearing like aggregates of attached smaller particles (Figure 3.5 (top)). If

the spray drying conditions were such that the outlet temperature was greater than 47°C melting occurred, while outlet temperatures of 41-44°C tended to produce elongated twig-like particles (Figure 3.5 (bottom)).

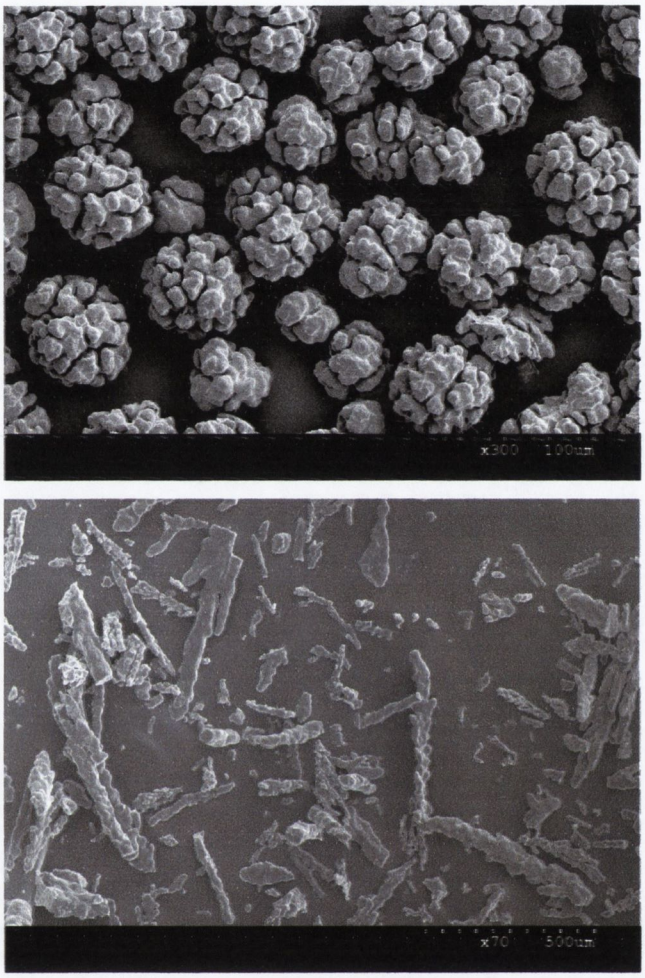

Figure 3.5 SEM micrographs of PEG 4000 spray dried with an outlet temperature of 45-46°C (top) and PEG 4000 spray dried with an outlet temperature of 41-44°C (bottom).

The number average molecular weight (Mn) and weight average molecular weight (Mw) by gel permeation chromatography (GPC) of the commercial PEG and spray dried PEG were as follows: Mn: 2626 (+/- 33.5) and 2644 (+/- 65.6); Mw: 3856 (+/- 110) and 3824 (+/- 28.1) respectively. There was no significant difference in molecular weights before and after spray drying of PEG, indicating that the heat involved in the spray drying procedure did not result in any significant polymer chain scission/breakdown (two sample t-tests; $P>0.05$).

3.3. Co-spray dried lactose/PEG 4000 systems

3.3.1. Lactose/PEG 4000 5%

The XRD pattern of co-spray dried lactose/PEG 5% is shown in Figure 3.6. The spray dried composite contained crystalline β-lactose indicated by peaks at 10.5° (2θ) and 17.7° (Buma and Wiegers, 1967), peaks not shown by α-lactose monohydrate or anhydrous α-lactose. The maximum intensity β-lactose peaks (at 19.2° and 21°) are close to the maximum peak intensities of α-lactose monohydrate, stable anhydrous α- and unstable anhydrous α-lactose at 19.9°, 19.4° and 19.0° respectively (Buma and Wiegers, 1967). PEG also shows a peak at 19.2°. This spray dried composite contained amorphous PEG as indicated by the reduction in peak intensity in the 23.3° region compared to the physical mix, shown in Figure 3.6 (scan c). Co-spray dried lactose/PEG 4000 5% shows a peak at 19.2° consistent with the presence of β-lactose and possibly some crystalline PEG. Crystallisation of PEG on storage is also evident (Figure 3.6, scan b) confirming the initial presence of some amorphous PEG. The arrow in Figure 3.6 indicates the peaks at approximately 23° indicative of crystalline PEG.

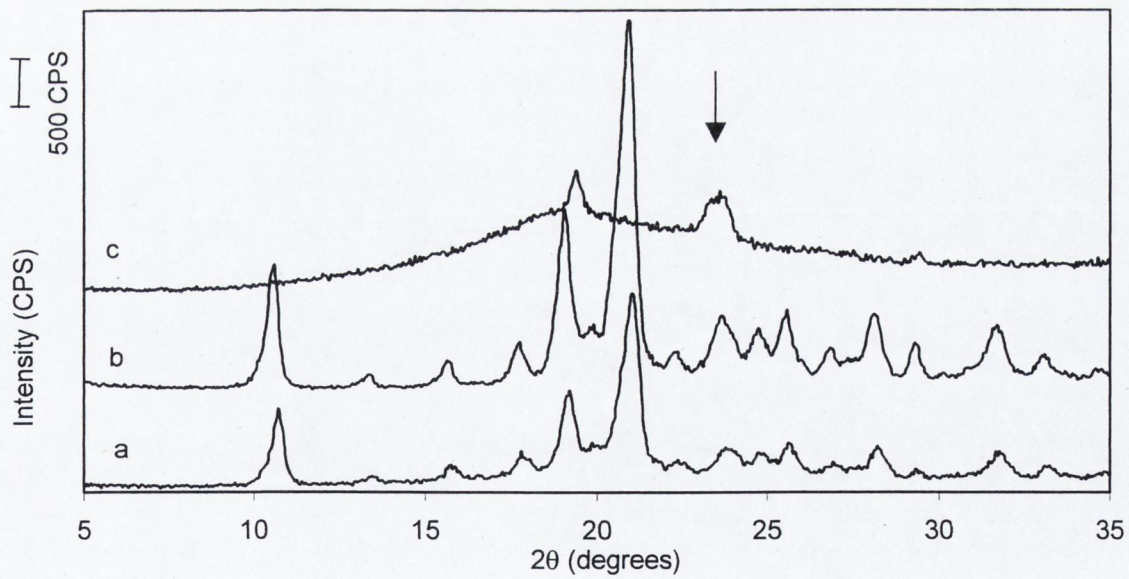

Figure 3.6 XRD scans of (a) spray dried lactose/PEG 4000 5%; (b) spray dried lactose/PEG 4000 5% stored for 16 days at 4°C 34% RH and (c) physical mix of amorphous lactose/PEG 4000 5%. The arrow indicates the position of the peak attributable to crystalline PEG.

The DSC scan of spray dried lactose/PEG 5% is shown in Figure 3.7 (scan a). No distinct PEG melting peak was observed in comparison to the physical mixes (Figure 3.7, scan e and f), indicating the absence of detectable crystalline PEG. An exotherm is present, consistent with recrystallisation of amorphous lactose. The lactose melting endotherm occurs at approximately 231°C indicative of the melting of β-lactose at this temperature.

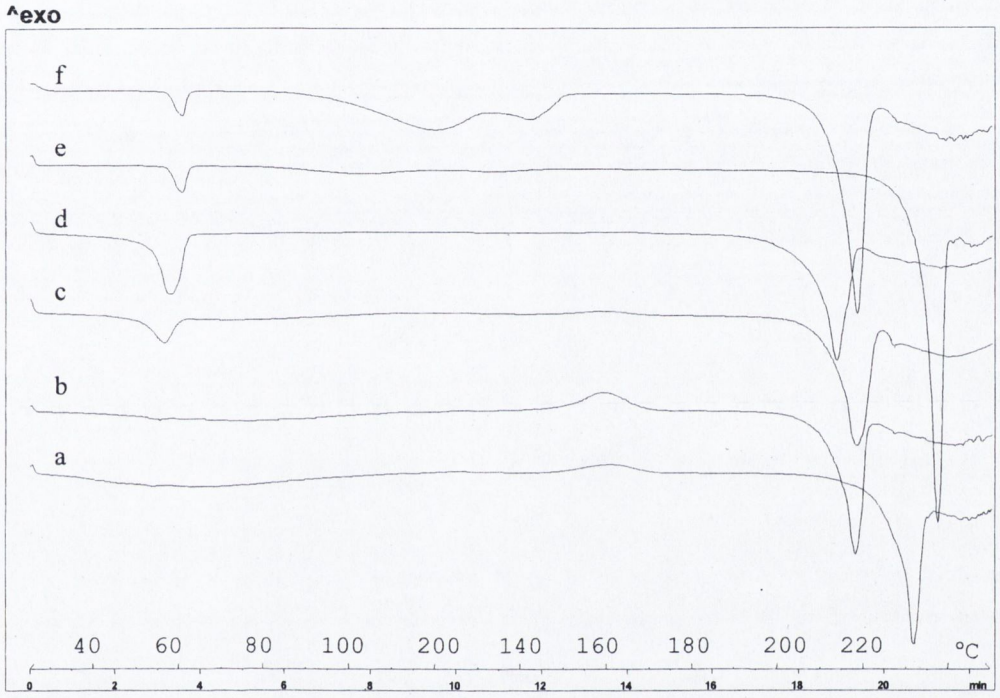

Figure 3.7 DSC scans of (a) spray dried lactose/PEG 4000 5%; (b) spray dried lactose/PEG 4000 10%; (c) spray dried lactose/PEG 4000 20%; (d) spray dried lactose/PEG 4000 30%; (e) physical mix anhydrous lactose/PEG 4000 5% and (f) physical mix lactose monohydrate/PEG 4000 5%.

3.3.2. Lactose/PEG 4000 10%

The XRD scan of spray dried lactose/PEG 4000 10% is compared to a range of physical mixtures of equivalent composition in Figure 3.8. The spray dried system is practically amorphous, just showing low intensity broad peaks in the ranges 12-13° and 19-20°. These peaks could indicate traces of crystalline stable α-anhydrous lactose (Buma and Wiegers, 1967). No β- or monohydrate lactose forms were evident initially. Crystalline PEG is also apparently absent.

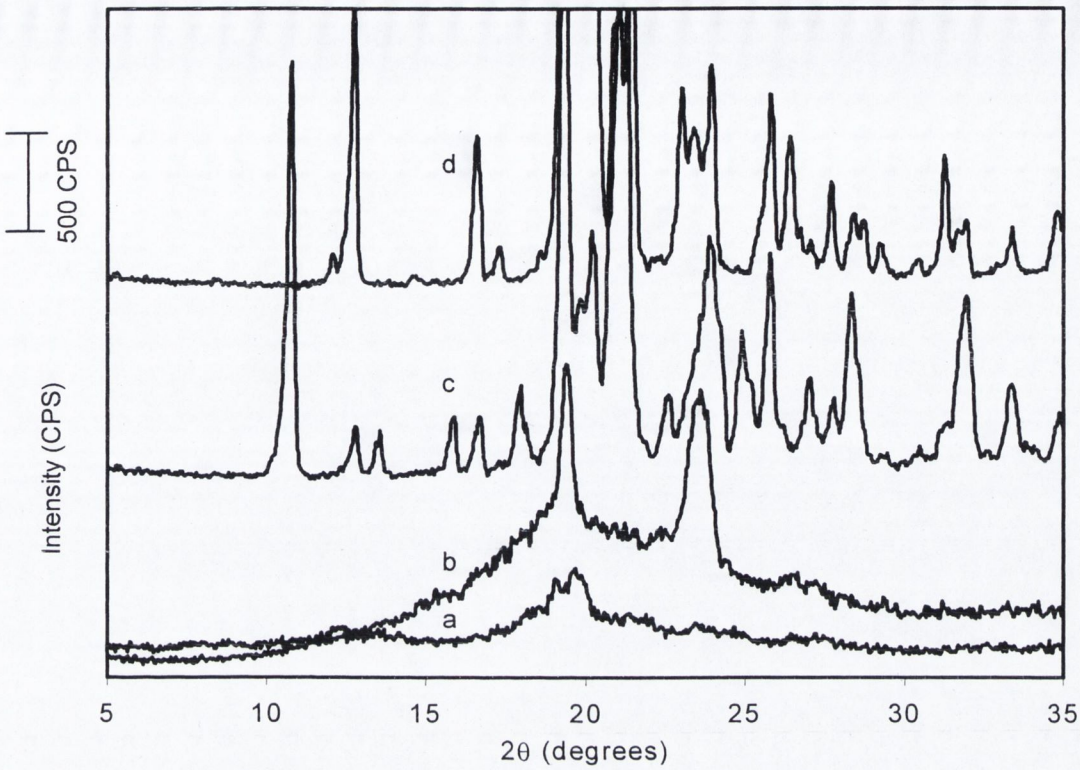

Figure 3.8 XRD scans of (a) spray dried lactose/PEG 4000 10%; (b) physical mix amorphous lactose/PEG 4000 10%; (c) physical mix anhydrous lactose /PEG 4000 10% and (d) physical mix lactose monohydrate/PEG 4000 10%.

The DSC scan of spray dried lactose/PEG 4000 10% is included in Figure 3.7 (scan b). A very slight depression in the PEG melting endotherm region is observable by DSC, which could be attributed to some of the once folded chain conformation (Chatham, 1985). Alternatively the presence of the large amount of a second component (lactose) could also lower the position of the melting endotherm. On storage it was observed that the PEG melting endotherm shifted to a higher temperature which would be consistent with conversion to the more stable extended chain form. An exotherm due to recrystallisation of amorphous lactose was observed and the lactose melting endotherm occurred at 214°C consistent with α-lactose. A thermogravimetric analysis (TGA) scan of spray dried lactose/PEG 10% and lactose monohydrate is shown in Figure 3.9. The spray dried system showed a weight loss consistent with the loss of absorbed water (amorphous material is known to be hygroscopic). This absorbed water is likely to be responsible for the broad endotherm visible by DSC prior to 100°C. No weight loss was observed in the

monohydrate temperature region indicating the absence of any detectable monohydrate lactose in the spray dried sample (already evidenced by the lack of a dehydration endotherm in the monohydrate region by DSC).

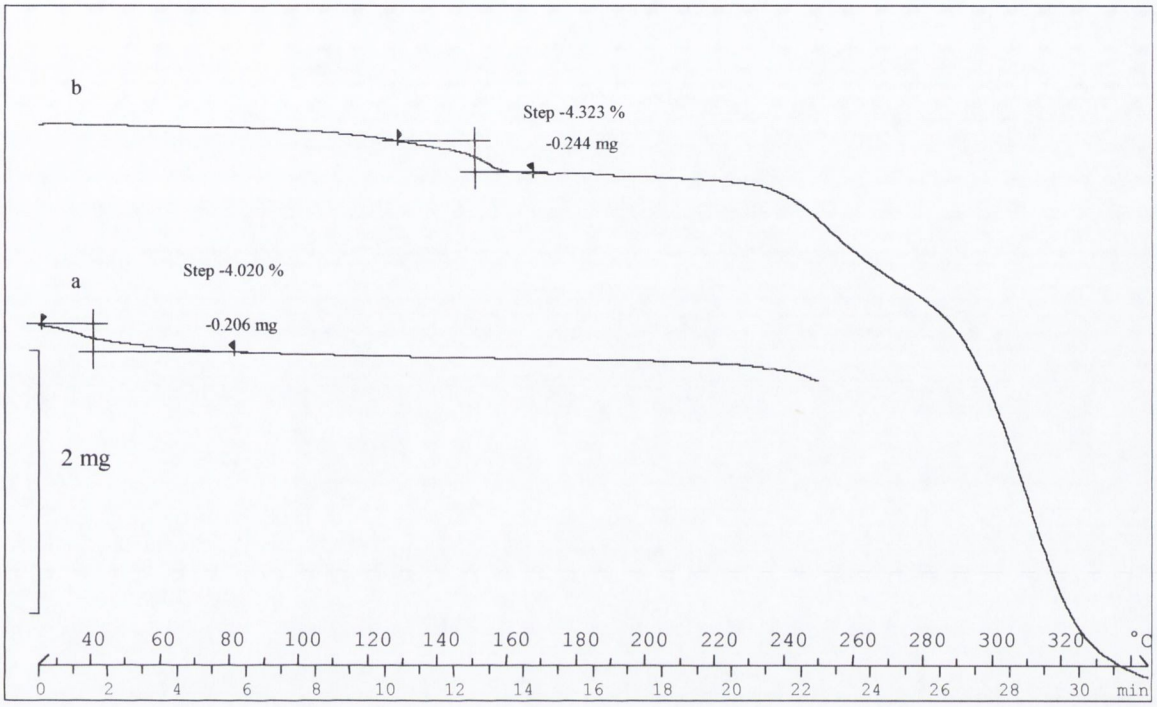

Figure 3.9 TGA scans of (a) spray dried lactose/PEG 4000 10% and (b) lactose monohydrate.

A scanning electron micrograph of the spray dried sample, the most amorphous of the lactose/PEG composites prepared, is shown in Figure 3.10.

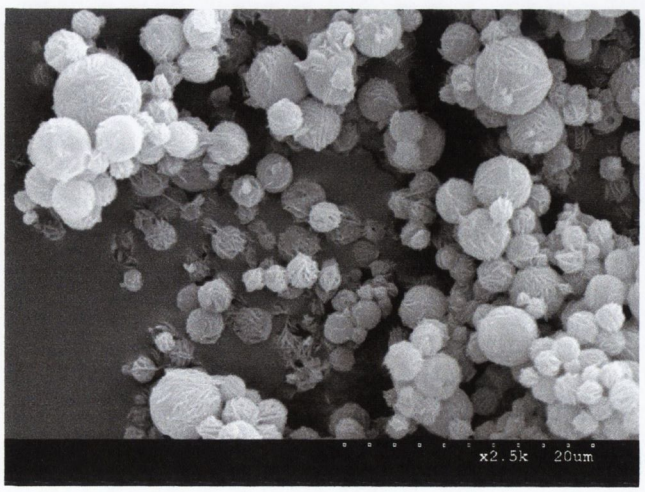

Figure 3.10 SEM micrograph of spray dried lactose/PEG 4000 10%.

The product, relative to pure PEG, consists of relatively smooth microspheres of a much smaller size, being 2-5 μm in diameter consistent with Chidavaenzi et al. (2001) who reported spray dried lactose/PEG particles with a particle size of roughly 2-10 μm in diameter. The lactose/PEG composite particles are similar in size to those obtained on spray drying pure lactose but are less smooth.

3.3.3. Lactose/PEG 4000 20%

The XRD and DSC scans of spray dried lactose/PEG 4000 20% are included in Figure 3.11 and Figure 3.7 (scan c) respectively. This system was more crystalline than that prepared with 10% PEG. Spray dried lactose/PEG 4000 20% consists mainly of amorphous lactose with some crystalline α-anhydrous lactose and some crystalline PEG. The DSC shows a low PEG melting point (which could be indicative of once folded PEG). A small exotherm indicative of amorphous lactose and an endotherm corresponding to melting of α-lactose are also evident. The enthalpy change, due to the melting of PEG, was not as large as that of the corresponding physical mix. SEM showed similar particle morphologies to the co-spray dried lactose/PEG 10% system.

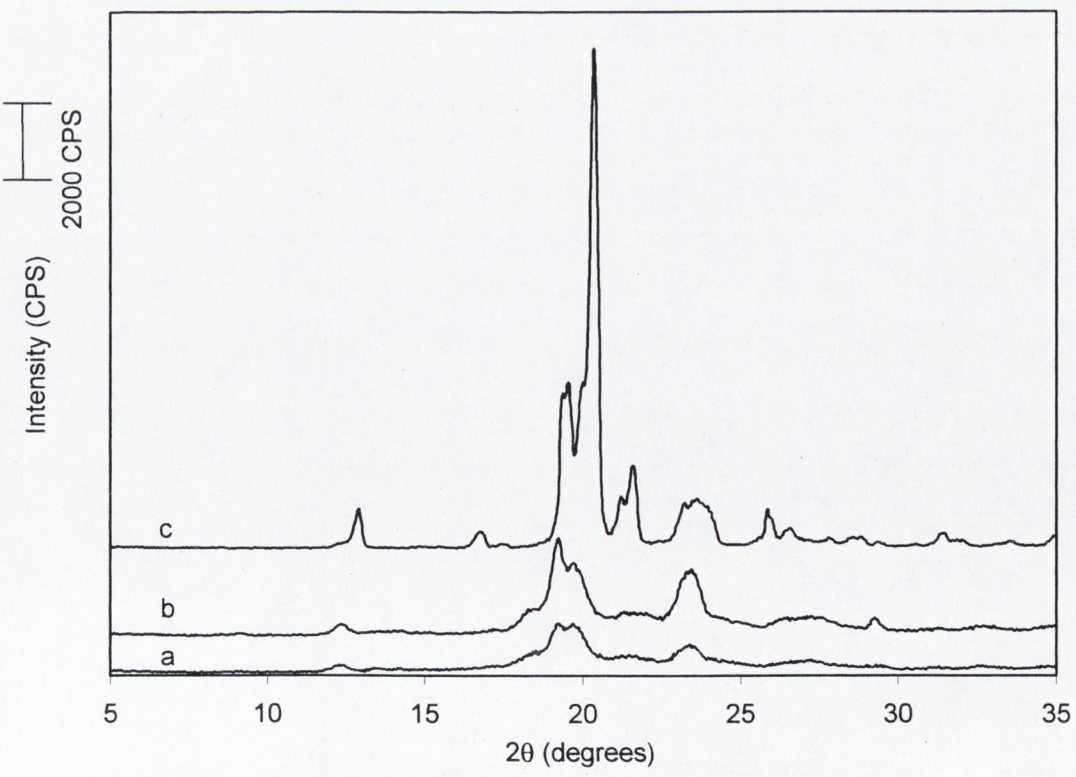

Figure 3.11 XRD scans of (a) spray dried lactose/PEG 4000 20%; (b) spray dried lactose/PEG 4000 30% and (c) physical mix of lactose monohydrate and PEG 4000 20%.

3.3.4. Lactose/PEG 4000 30%

XRD and DSC scans of spray dried lactose/PEG 4000 30% are included in Figure 3.11 and Figure 3.7 (scan d) respectively. This system had similar characteristics to the 20% PEG system showing the presence of both crystalline α-anhydrous lactose and amorphous lactose and a slight reduction in PEG crystallinity when compared to physical mix samples. SEM showed similar spherical particles to the other lactose/PEG co-spray dried systems. An exotherm indicative of recrystallisation of amorphous lactose was observable by DSC at higher resolution.

In summary, immediately following spray drying, all spray dried systems showed some amorphous lactose. The crystallinity of PEG was much reduced as indicated by the comparative sizes of the melting endotherms (Figure 3.7). Lactose monohydrate was not present in any system, evidenced by the absence of dehydration endotherms in the DSC scans and lack of appropriate XRD peaks, for example the characteristic peak at 16.4°. TGA experiments also confirmed the absence of the monohydrate. The physical mix of lactose monohydrate/PEG 5% showed an unusual dehydration endotherm, having two endothermic peaks. The form of lactose initially present in the spray-dried systems was dependent on the percentage of PEG in the composite. When 5% PEG was incorporated β-lactose was the only form of crystalline lactose present. When the PEG content was increased to 10% and above, the crystalline form of lactose when present was that of α-anhydrous lactose. PEG 4000 appeared to be amorphous when present as 10% of the composite. While DSC scans showed no detectable melting endotherm for the 5% PEG system, some crystalline PEG was suggested by XRD. Decreased PEG crystallinity was evident when systems containing 20% and 30% PEG were spray dried.

All lactose/PEG systems spray dried in this work showed the presence of some amorphous material in contrast to the findings of Chidavaenzi et al. (2001). Chidavaenzi et al. did not comment on the time period or storage conditions of the spray dried samples prior to first analysis. It is possible that their composites may have changed in structure before analysis by XRD and DSC. All spray dried samples in this work were analysed immediately after production by DSC and within 24 hours by XRD, samples being stored in dessicators if not analysed immediately by XRD.

3.4. Effect of storage on physicochemical properties of spray dried systems

3.4.1. Spray dried lactose

Spray dried lactose stored at 4°C 34% RH did not recrystallise during the storage period of 8 weeks (evidenced by XRD). The DSC scan of spray dried lactose following 8 weeks of storage at 4°C 34% RH is shown in Figure 3.12 (scan a).

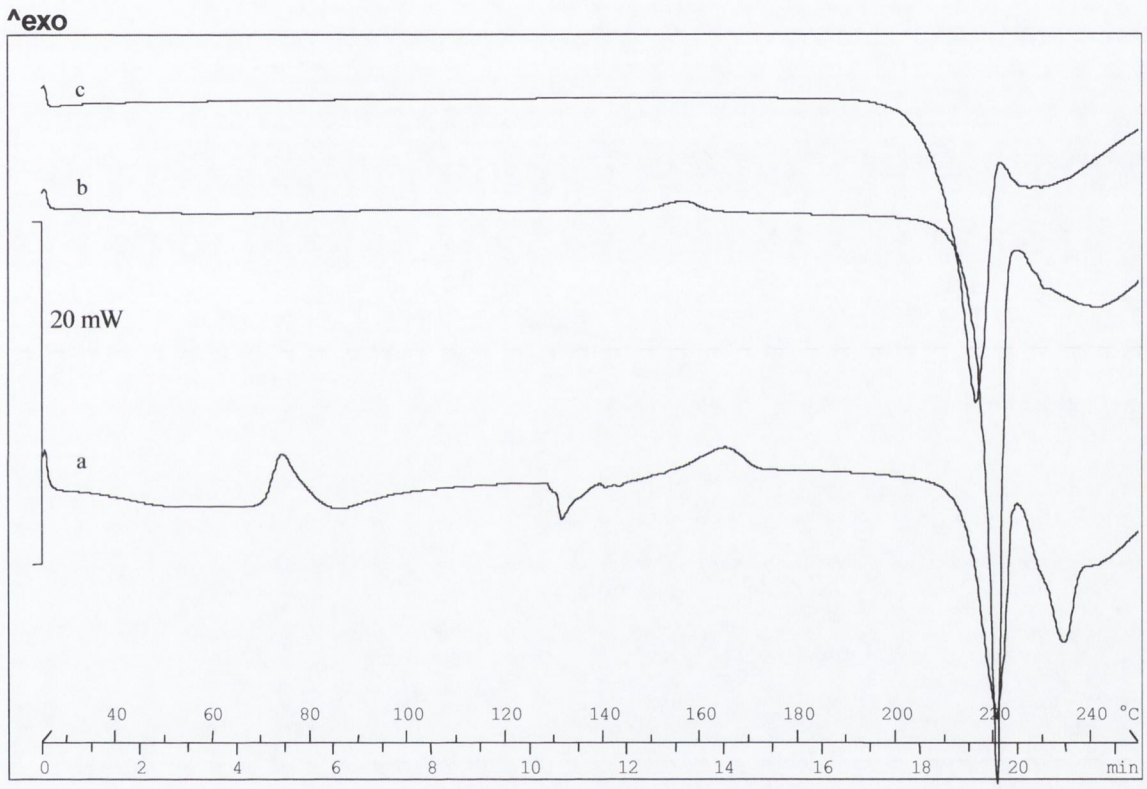

Figure 3.12 DSC scans of spray dried lactose stored for 8 weeks at (a) 4°C 34% RH; (b) 30°C 32% RH and (c) 45°C 31% RH.

The DSC scan shown in Figure 3.12 (scan a) is similar to that shown by Darcy and Buckton (1997) describing a system containing some collapsed amorphous lactose. Amorphous systems are hygroscopic and absorb water which acts as a plasticiser and lowers the glass transition temperature. As water plasticises the material and the glass transition approaches the storage temperature of the material, the material changes structure which results in a collapse and densification prior to crystallisation (Buckton and Darcy, 1996). Recrystallisation is not instantaneous but the fact that the material has collapsed means that crystallisation is more imminent. The exotherm at approximately

70°C in Figure 3.12, scan a, is due to recrystallisation of collapsed lactose and the endotherms at approximately 130°C, in Figure 3.12 (scan a) are due to water loss from the collapsed structure (Darcy and Buckton, 1997). The exotherm in the 160°C region in Figure 3.12 scan a is recrystallisation of the amorphous material which had not yet collapsed. Therefore, while the XRD patterns of spray dried lactose stored at 4°C 34% RH imply no change in the system during the storage period, the DSC scans show that the material has collapsed but not yet recrystallised. Spray dried samples stored at 30°C 32% RH and 45°C 31% RH showed no dehydration endotherms by DSC (Figure 3.12, scans b and c) indicating the absence of lactose monohydrate. By 8 weeks of storage at 30°C 32% RH some amorphous lactose remained, indicated by the exotherm in Figure 3.12 (scan b). However the exotherm was much reduced in magnitude and XRD scans of the 30°C 32% RH sample were consistent with the presence of some crystalline anhydrous lactose.

The XRD scans of the 30°C 32% RH and 45°C 31% RH stored samples were similar; the XRD scan of the 45°C 31% RH sample is shown in Figure 3.13 (scan a). No β-lactose was present in either sample indicated by the absence of a peak in the XRD scans at 10.5°. XRD also confirmed the absence of lactose monohydrate indicated by the absence of a peak at 16.5°. According to Buma and Wiegers (1967) stable α-anhydrous lactose shows peaks at 9.0° and 22.1°, peaks not shown by the other forms of lactose. The XRD patterns of spray dried lactose stored at 30°C 32% RH and 45°C 31% RH were consistent with the presence of only anhydrous α-lactose. The arrow in Figure 3.13 (scan a) indicates a peak due to α-anhydrous lactose. Buma and Wiegers (1967) describe an unstable crystalline anhydrous α-lactose which shows a peak at 11.6° which is not shown for other lactose forms. No peak by XRD at 11.6° was visible for the low humidity samples in the current work indicating the absence of unstable anhydrous α-lactose.

Figure 3.14 shows the DSC scans of spray dried lactose stored at 4°C 75% RH, 30°C 75% RH and 45°C 75% RH for 8 weeks. Dehydration endotherms at approximately 140°C were visible confirming the presence of lactose monohydrate in the samples. Two melting endotherms for lactose, one in the α melting region and one in the β melting region, were also visible by DSC. The XRD scans of the samples stored at 75% RH showed peaks at approximately 10.5° and 16.5°; the XRD scan of the 45°C 75% RH sample is shown in Figure 3.13 (scan b). The arrow in Figure 3.13 (scan b) indicates the peak due to the presence of β-lactose.

The recrystallisation of amorphous lactose at a relative humidity of 75% was consistent with previous reports of recrystallisation of lactose to a mix of β-lactose and α-lactose

monohydrate when stored at humidities greater than 50% (Briggner et al., 1994; Drapier-Beche et al., 1997). Following 8 weeks of storage the peak at approximately 10.5° was still present in the samples stored at 4°C 75% RH and 30°C 75% RH but was no longer visible in the samples stored at 45°C 75% RH (Figure 3.13, scan c). This indicates that β-lactose converts to lactose monohydrate on storage at 45°C 75% RH. The DSC of the 45°C 75% RH sample stored for 8 weeks still showed melting due to β-lactose. This is likely due to mutarotation of α to β-lactose on heating by DSC (Angberg, 1995) since XRD showed absence of β-lactose at this time period.

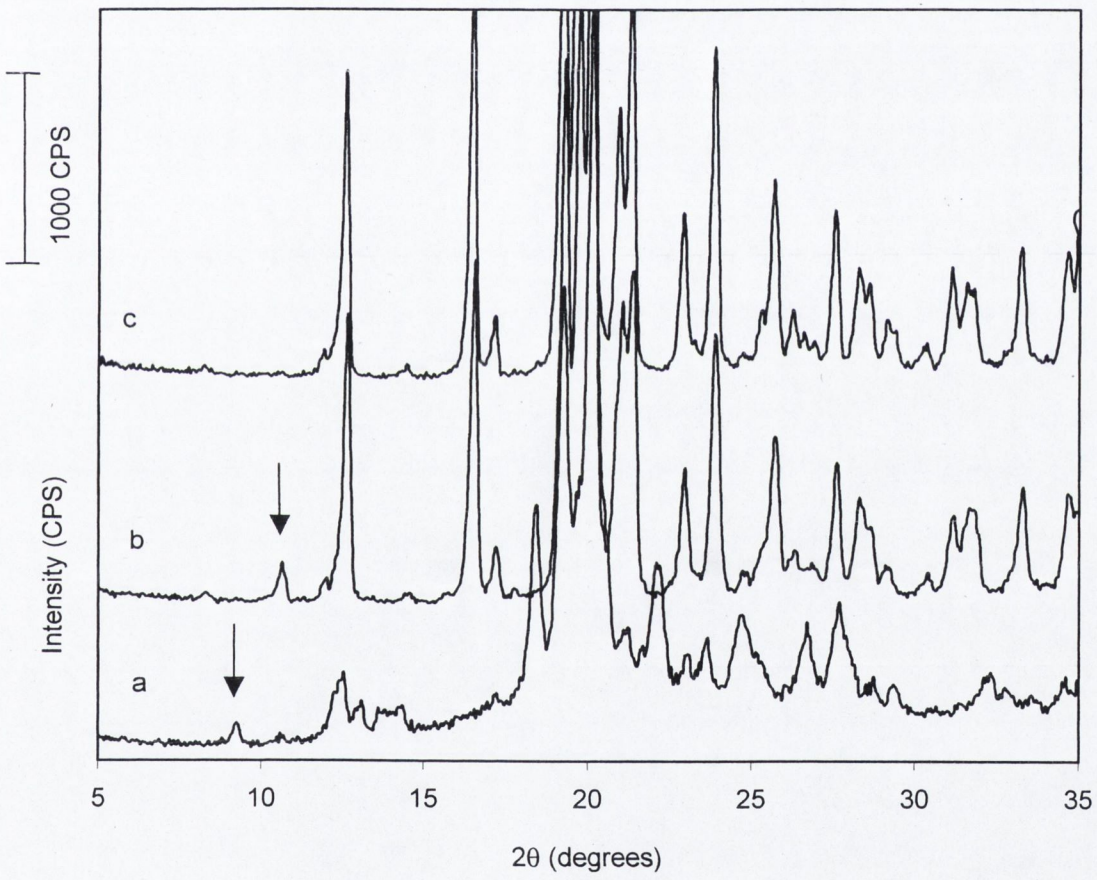

Figure 3.13 XRD scans of spray dried lactose after storage at (a) 45°C 31% RH for 16 days; (b) 45°C 75% RH for 16 days and (c) 45°C 75% RH for 8 weeks. The arrows indicate differences in the scans, the arrow at approximately 9° 2θ indicating a peak due to stable anhydrous α-lactose and the arrow at approximately 10.5° 2θ indicating a peak due to β-lactose.

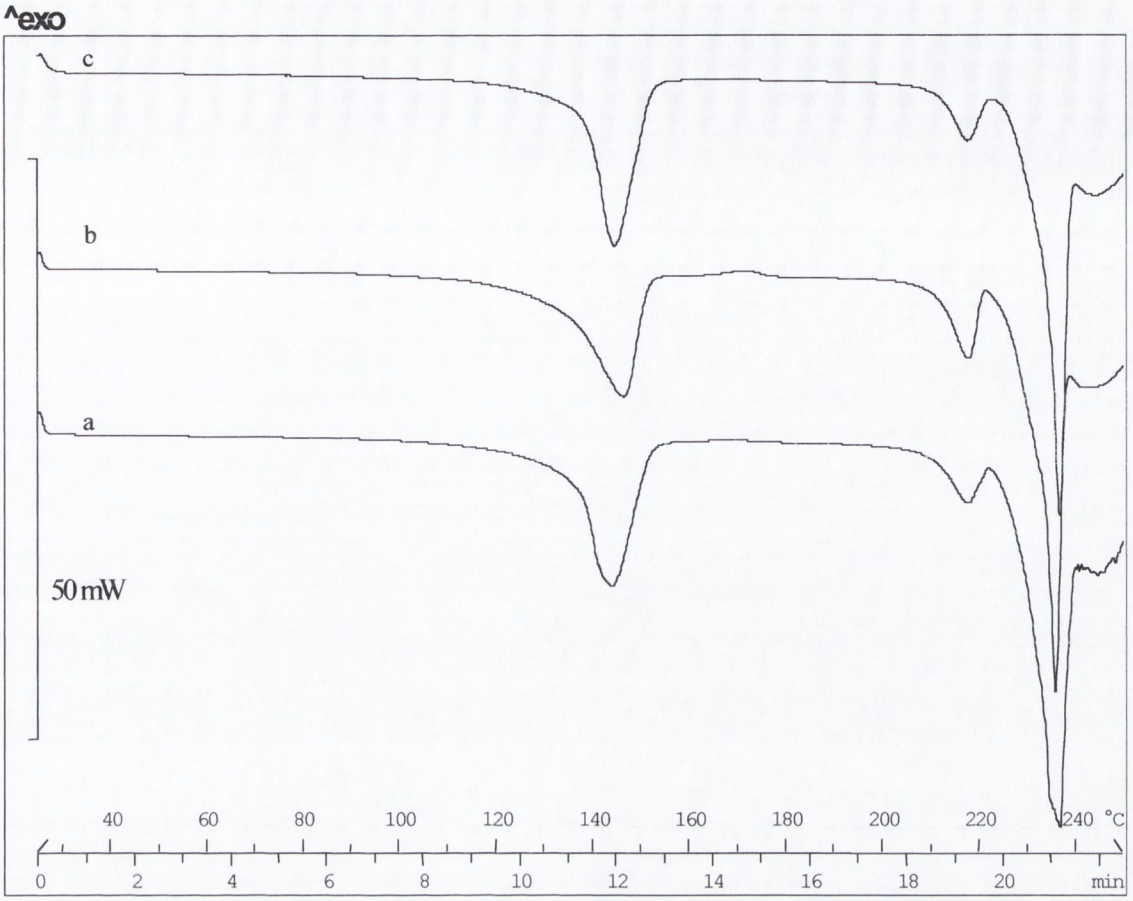

Figure 3.14 DSC scans of spray dried lactose stored for 8 weeks at (a) 4°C 75% RH; (b) 30°C 75% RH and (c) 45°C 75% RH.

3.4.2. PEG 4000

Only a 10-15% reduction in PEG 4000 crystallinity occurred on spray drying (section 3.2.2) and therefore recrystallisation under different storage conditions was not studied. However unprocessed PEG 4000 was stored at 45°C 75% RH to determine its stability to high temperatures and humidities. DSC analysis and gel permeation chromatography (GPC) were performed after 8 days and 58 weeks of storage. DSC of PEG stored for 58 weeks showed no melting endotherms when initially analysed by DSC from 25°C to 140°C (Figure 3.15).

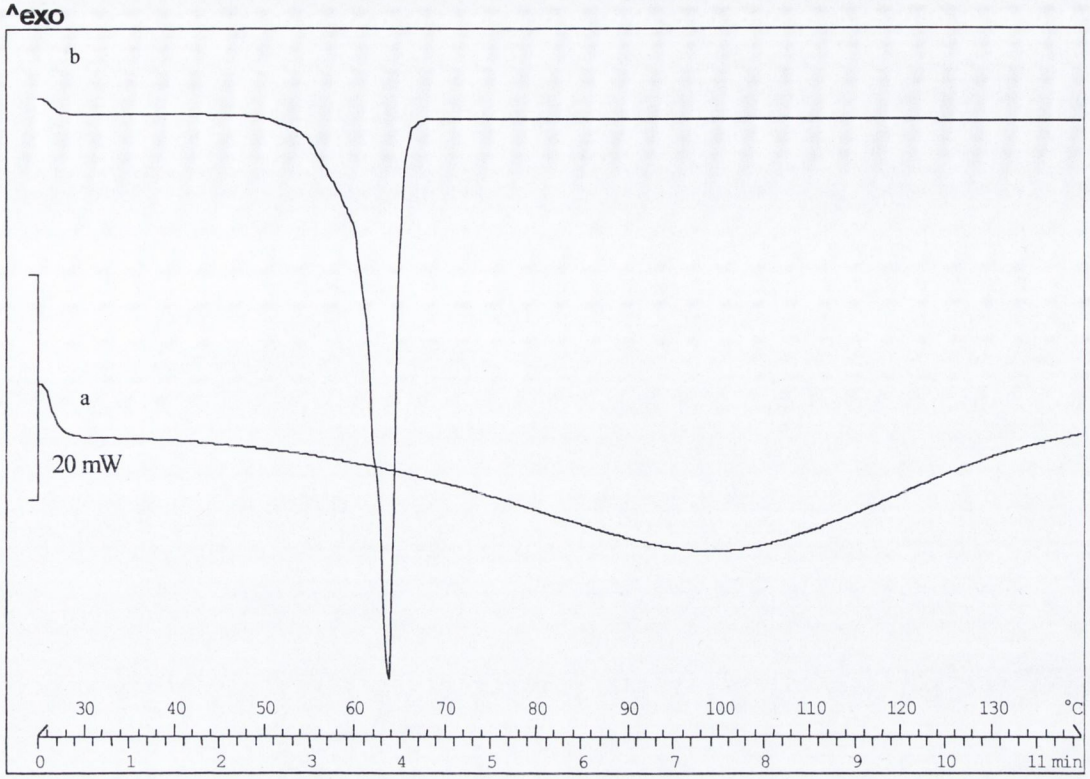

Figure 3.15 DSC scans of (a) PEG 4000 stored for 58 weeks at 45°C 75% RH and (b) PEG 4000 starting material.

The broad endotherm observed in Figure 3.15, peaking at 100°C, is due to the loss of moisture as confirmed by TGA (Figure 3.16).

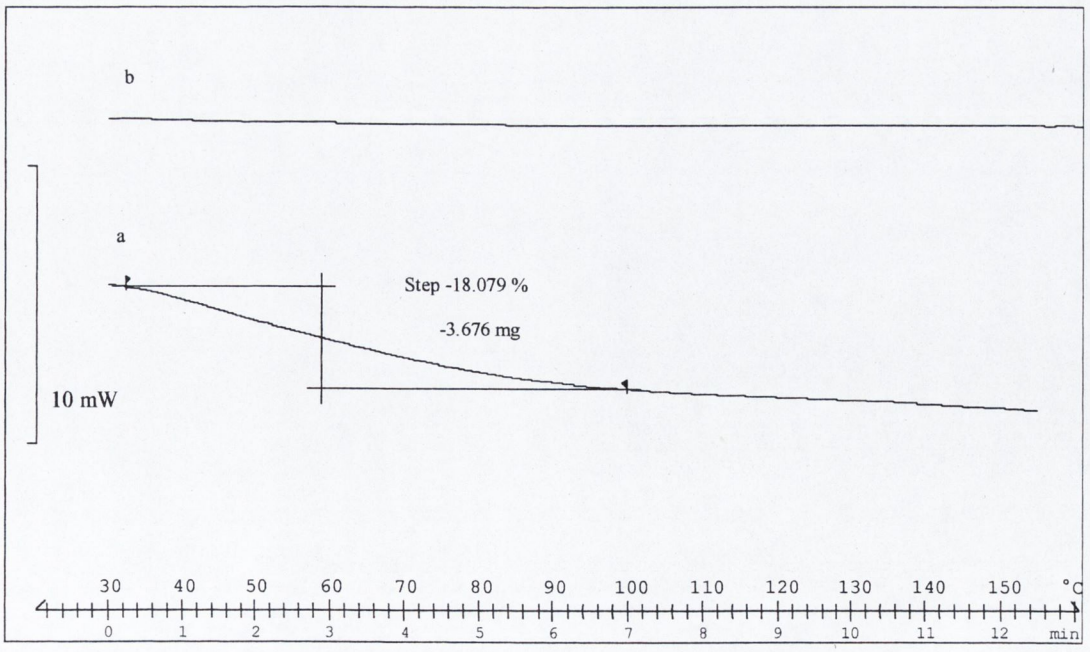

Figure 3.16 TGA scan of (a) PEG 4000 stored at 45°C 75% RH for 58 weeks and (b) PEG 4000 starting material.

It was not surprising that no melting endotherms were observed by DSC since the sample appeared molten when removed from the 45°C 75% RH chamber. Lower molecular weight PEGs are known to be liquids at room temperature.

The samples were cooled to 0°C and run to 100°C by DSC so that they would initially be solids and, on heating, the melting temperature and the shape of the melting endotherms could be observed. The DSC scans of the samples stored at 45°C 75% RH for 8 days and 58 weeks, cooled to 0°C and run to 100°C by DSC are shown in Figure 3.17.

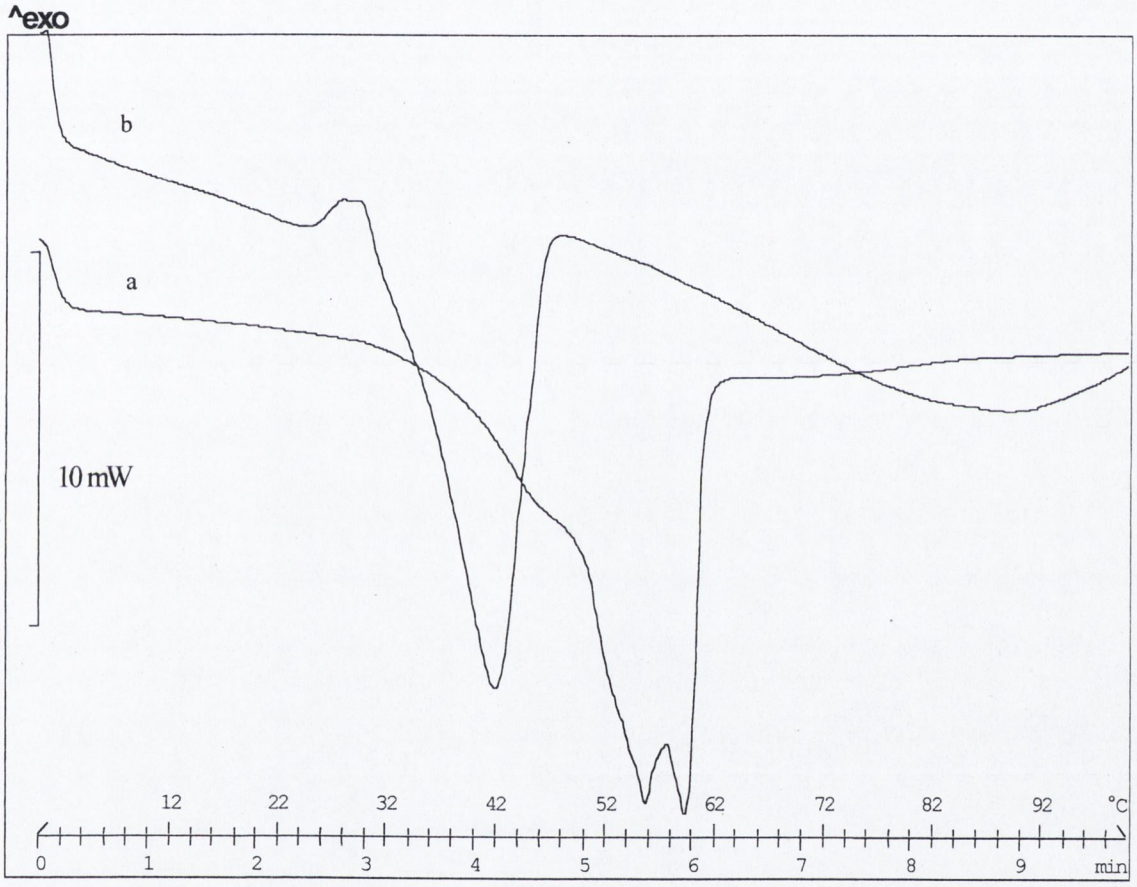

Figure 3.17 DSC scans of samples stored at 45°C 75% RH. (a) PEG 4000 stored for 8 days and (b) PEG 4000 stored for 58 weeks.

The PEG 4000 sample stored for 58 weeks appeared to show two melting endotherms, the first peaking at approximately 25°C and the second broad endotherm peaking at approximately 42°C. These peaks are consistent with the presence of lower molecular weight PEGs which melt at lower temperatures. The broad nature of the peaks indicated a wide distribution of molecular weights which therefore melt over a broader temperature range. The sample stored for 8 days also showed lower melting point peaks when

compared to PEG 4000 which had not been exposed to storage at 45°C 75% RH. The presence of a broad endotherm containing two peaks at 56°C and 60°C and the shoulder on the low temperature side of the peaks indicates the presence of a broad range of molecular weight PEGs.

GPC results of number average molecular weights and weight average molecular weights of PEG starting material, PEG stored for 8 days and PEG stored for 58 weeks at 45°C 75% RH are shown in Table 3.1 and Table 3.2 respectively. Brackets denote the 95% confidence interval. Where brackets of different systems overlap the systems are not statistically different from each other.

Table 3.1 ANOVA results for GPC analysis of number average molecular weight of PEG 4000 starting material and PEG 4000 stored at 45°C 75% RH for 58 weeks and 8 days.

Level	N	Mean	StDev	Individual 95% Confidence Intervals For Mean Based on Pooled StDev
PEG 4000	3	3209.0	147.6	(*)
58wks 45C75	3	717.0	35.7	(*)
8days 45C75	3	3482.7	22.0	(*)
Pooled StDev =		88.6		1000 2000 3000 4000

PEG 4000 refers to the material prior to storage, 58wks 45C75 refers to PEG 4000 which had been stored for 58 weeks at 45°C 75% RH, 8days 45C75 refers to PEG 4000 which had been stored for 8 days at 45°C 75% RH.

Table 3.2 ANOVA results for GPC analysis of weight average molecular weight of PEG 4000 starting material and PEG 4000 stored at 45°C 75% RH for 58 weeks and 8 days.

Level	N	Mean	StDev	Individual 95% Confidence Intervals For Mean Based on Pooled StDev
PEG 4000	3	5174.0	83.5	(----*-----)
58wks 45C75	3	1803.0	1049.9	(-----*-----)
8days 45C75	3	4458.0	7.8	(-----*----)
Pooled StDev =		608.1		1500 3000 4500 6000

PEG 4000 refers to the material prior to storage, 58wks 45C75 refers to PEG 4000 which had been stored for 58 weeks at 45°C 75% RH, 8days 45C75 refers to PEG 4000 which had been stored for 8 days at 45°C 75% RH.

GPC analysis showed that storage for 8 days and 58 weeks at 45°C 75% RH resulted in systems with significantly different number average molecular weights. The weight average molecular weights were compared and the 8 days sample was found not to be statistically different from the PEG starting material. However the sample stored for greater than 1 year at 45°C 75% RH showed significantly lower molecular weight. Chatham (1985) states that high temperatures during processing (rather than storage) of PEG can result in polymer chain scission resulting in lower molecular weight fragments. However Chatham states that below 100°C the effect is unlikely to be significant. It has been shown in the current work by GPC and DSC that PEG 4000 is not stable when exposed to a temperature of 45°C and a relative humidity of 75%. Exposure to such conditions results in degradation to lower molecular weight fragments i.e. chain scission. Frontini and Mielck (1995) described the degradation of PEG to formaldehyde when present in a solid dispersion with bendroflumethiazide. They postulated an oxidative decomposition of the polyoxyethylene chains. The reaction was described as needing water to form ethylene glycol in the first step, which may then be oxidised to formaldehyde.

3.4.3. Co-spray dried systems

Lactose/PEG 4000 5%

The physical instability of these high energy lactose/PEG composites was evident from the XRD data in Figure 3.6, which showed recrystallisation of PEG in the 5% PEG system when stored at 4°C 34% RH for 16 days. Figure 3.18 shows DSC scans of spray dried lactose/PEG 5% stored under a range of temperature and RH conditions. Some recrystallisation of PEG had occurred after 5 days when stored at 4°C 34% RH (probably recrystallising to the metastable once folded PEG conformation). The exotherm due to crystallisation of amorphous lactose was no longer present. Lactose remained as the β form for the 10 month duration of storage under these conditions, as evidenced by peaks at 10.5° by XRD and the melting temperature by DSC. DSC and XRD data (Figure 3.18 and Figure 3.19) indicated that storage at the higher temperature and RH of 30°C and 75% RH, resulted in conversion of lactose to a mixture of α-lactose monohydrate and β-lactose by 24 hours, followed by conversion to α-lactose monohydrate alone. This behaviour is consistent with findings from section 3.4.1 for lactose spray dried alone. PEG recrystallises and apparently transforms to the more stable extended chain form on storage at higher temperatures and humidity as can be seen from the DSC data in Figure 3.18. The

characteristic PEG double endotherms are clearly present after one and 5 days storage at 30°C and 75% RH (Figure 3.18, scans e, f). Recrystallisation to some once folded chain PEG that melts at lower temperatures is observed and on further storage a single endotherm representative of melting of the more stable extended chain conformation is evident after 16 days (Figure 3.18, scan g).

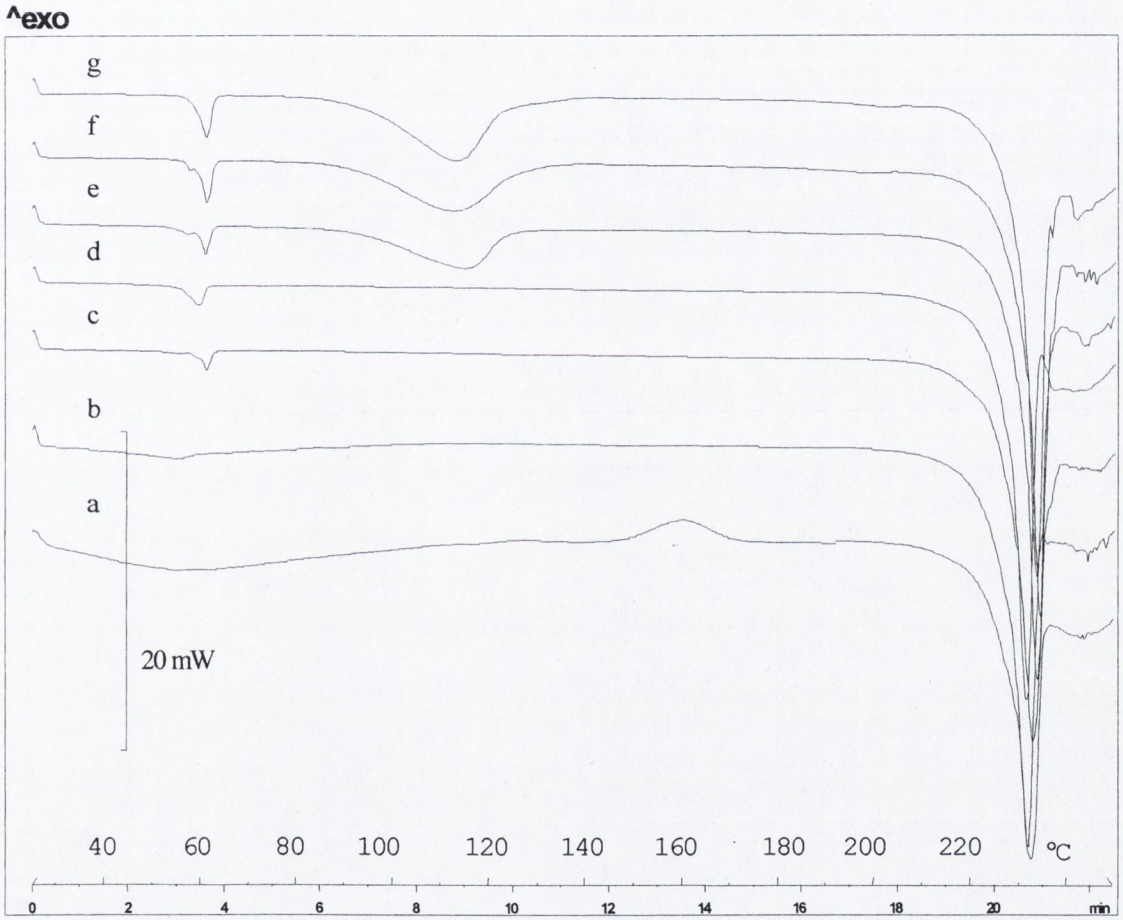

Figure 3.18 DSC scans of lactose/PEG 4000 5% following storage. (a) spray dried lactose/PEG 4000 5%; (b) spray dried lactose/PEG 4000 5% stored at 4°C 34% RH for 5 days; (c) spray dried lactose/PEG 4000 5% stored at 45°C 31% RH for 1 day; (d) spray dried lactose/PEG 4000 5% stored at 30°C 32% RH for 5 days; (e) spray dried lactose/PEG 4000 5% stored at 30°C 75% RH for 1 day; (f) spray dried lactose/PEG 4000 5% stored at 30°C 75% RH for 5 days and (g) spray dried lactose/PEG 4000 5% stored at 30°C 75% RH for 16 days.

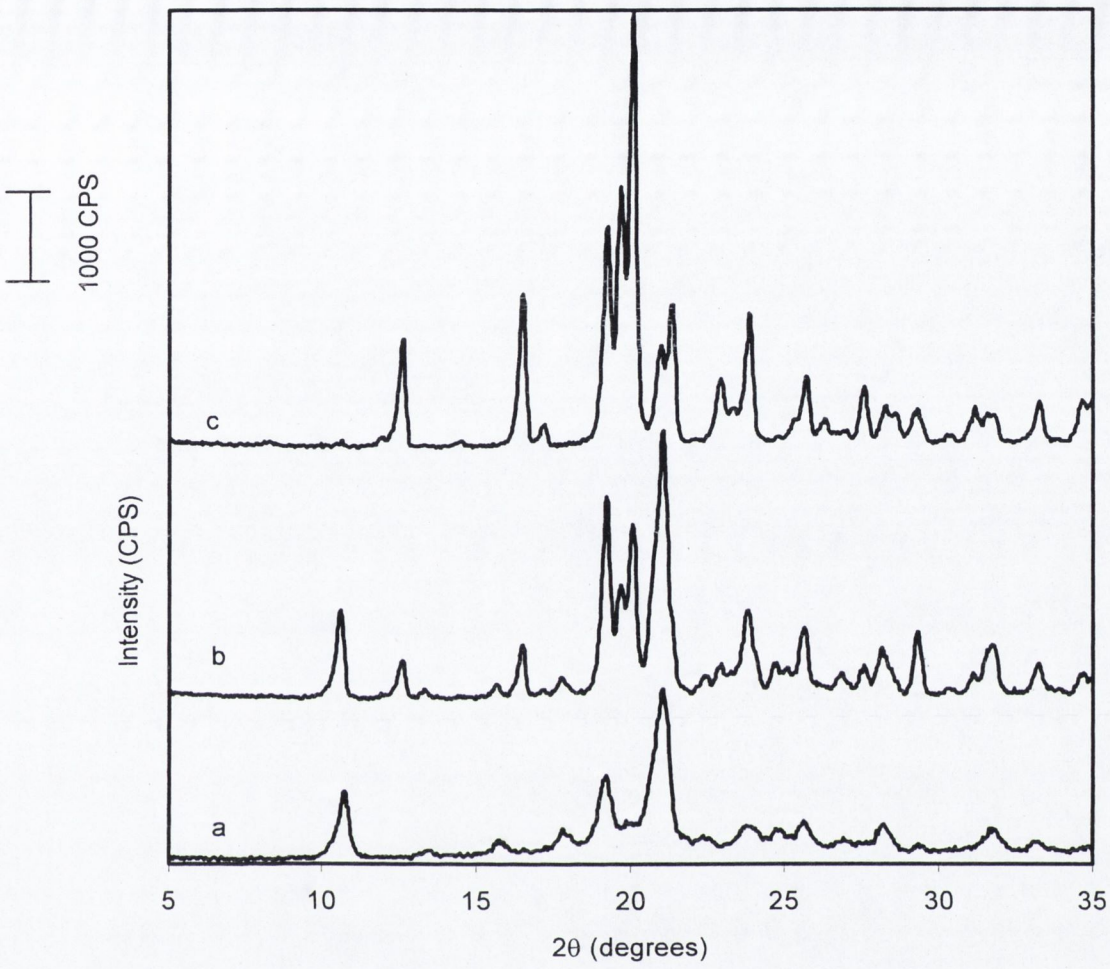

Figure 3.19 Effect of storage conditions on the XRD pattern of spray dried lactose/PEG 4000 5%. (a) spray dried lactose/PEG 4000 5%; (b) spray dried lactose/PEG 4000 5% stored for 1 day at 30°C 75% RH and (c) spray dried lactose/PEG 4000 5% stored for 7 weeks at 30°C 75% RH.

Lactose/PEG 4000 10%

Figure 3.20 shows DSC scans obtained on storage of spray dried lactose/PEG 10% at 45°C 75% RH. Recrystallisation of PEG occurred, firstly (after 6 hours at 45°C 75% RH) to the once folded form and then to a mixture of once folded and extended chain form (by 22 hours). By 46 hours, at 45°C and 75% RH, the presence of some α-lactose monohydrate was observable by DSC (Figure 3.20, scan d) and by XRD.

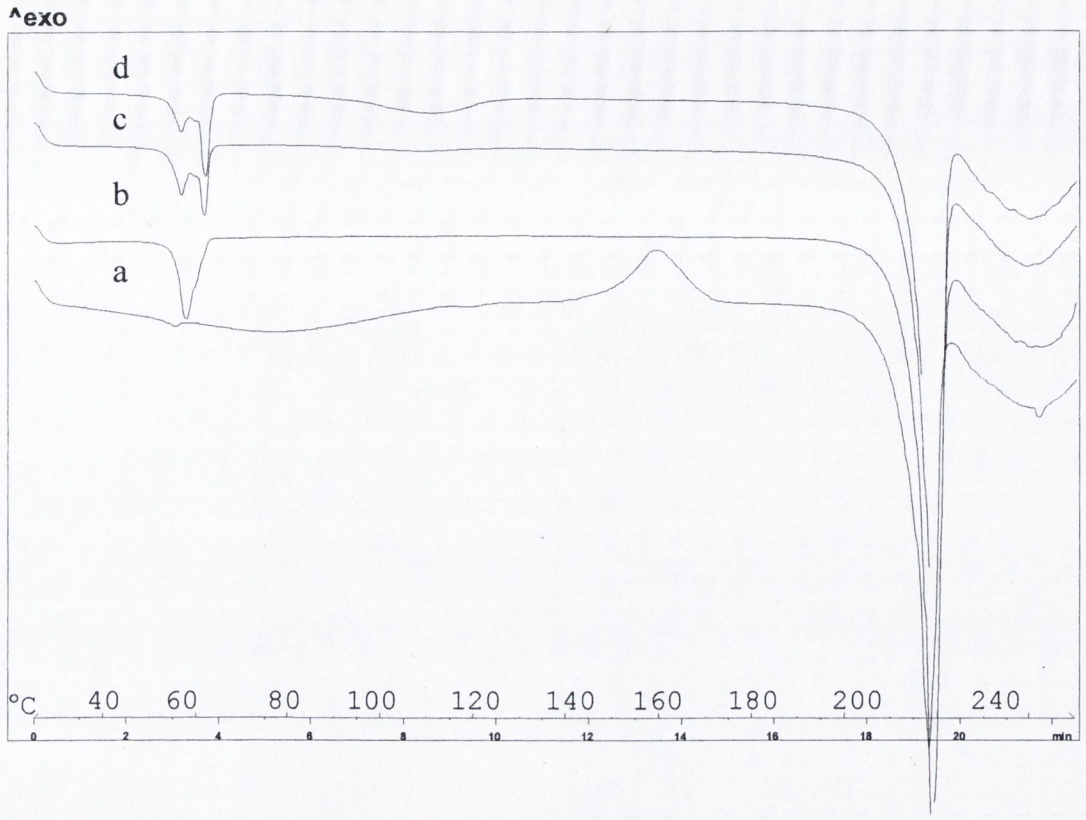

Figure 3.20 DSC scans of spray dried lactose/PEG 4000 10% stored at 45°C 75% RH showing beginning of conversion of PEG to more stable extended form by 22hrs. (a) spray dried lactose/PEG 4000 10% prior to storage; (b) spray dried lactose/PEG 4000 10% after 6 hours storage at 45°C 75% RH; (c) spray dried lactose/PEG 4000 10% after 22 hours storage at 45°C 75% RH and (d) spray dried lactose/PEG4000 10% after 46 hours storage at 45°C 75% RH.

Lactose/PEG 4000 20%

The DSC scans of spray dried lactose/PEG 20% are shown in Figure 3.21. Initially the PEG onset melting temperature was lower than that seen on storage and in physical mixes. This could be due to the lowered crystallinity and/or some PEG being present in the metastable once folded form. Following storage for one year at 4°C 34% RH the PEG does not appear to have recrystallised to the extended chain conformation. At 4°C 34% RH no increase in lactose crystallinity was observed on storage. By week 15 a low temperature exotherm was observed in the 45°C 31% RH sample, implying collapse of amorphous lactose, consistent with findings of Darcy and Buckton (1997) and section 3.4.1 for lactose present alone. However by one year this collapsed lactose does not appear to have recrystallised. Any crystalline lactose present remains in the low humidity stored samples as the anhydrous α form. Storage at low humidity but higher temperatures results

in recrystallisation of PEG to the extended chain form, the rate of recrystallisation increasing with increasing storage temperature.

Figure 3.21 shows the DSC scans of freshly spray dried, stored spray dried (45°C 75% RH) and physical mixtures of lactose/PEG 20%. Storage at high humidity resulted in conversion to α-lactose monohydrate as evidenced by the dehydration endotherm. Conversion to α-lactose monohydrate occurred by 3 days storage even when stored at 4°C. When stored at 4°C 75% RH for one year a shoulder on the low temperature side of the PEG 4000 melting peak was observed suggesting some PEG was still present in the once folded conformation (Figure 3.22, scan c). When the samples stored at 30°C and 45°C were analysed after storage for 3 days PEG melting was seen to be that of the extended chain form only.

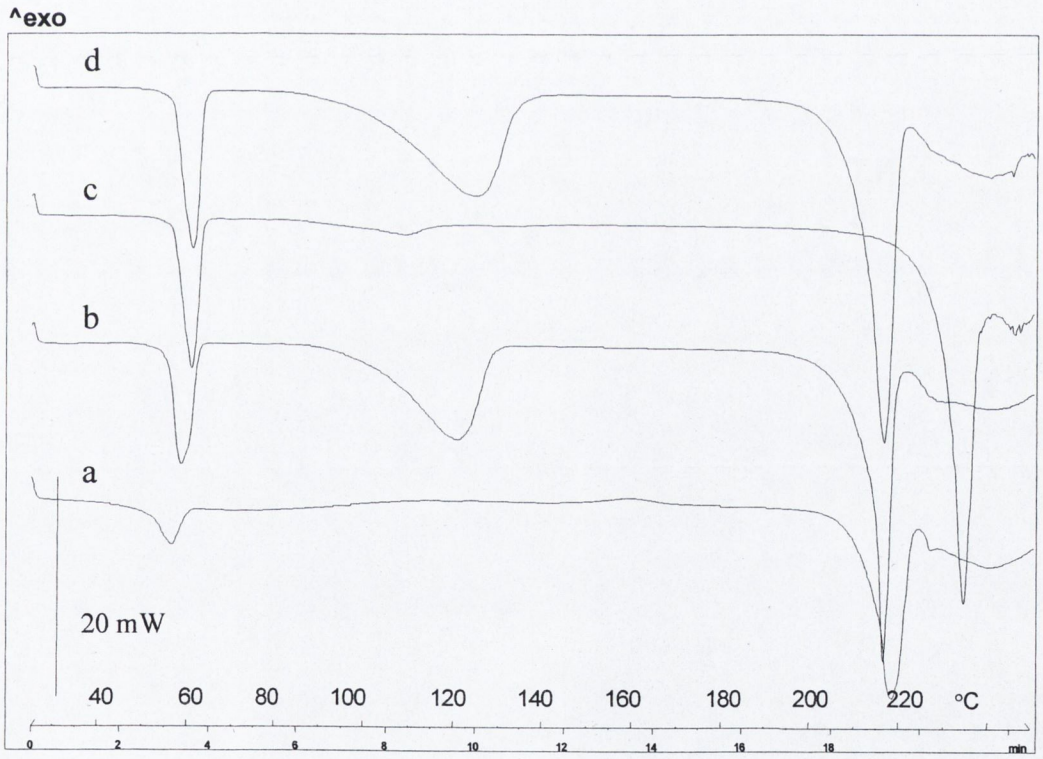

Figure 3.21. DSC scans of (a) spray dried lactose/PEG 4000 20% prior to storage; (b) spray dried lactose/PEG 4000 20% stored for 3 days at 45°C 75%RH; (c) physical mix of anhydrous lactose/PEG 4000 20% and (d) physical mix of lactose monohydrate/PEG 4000 20%.

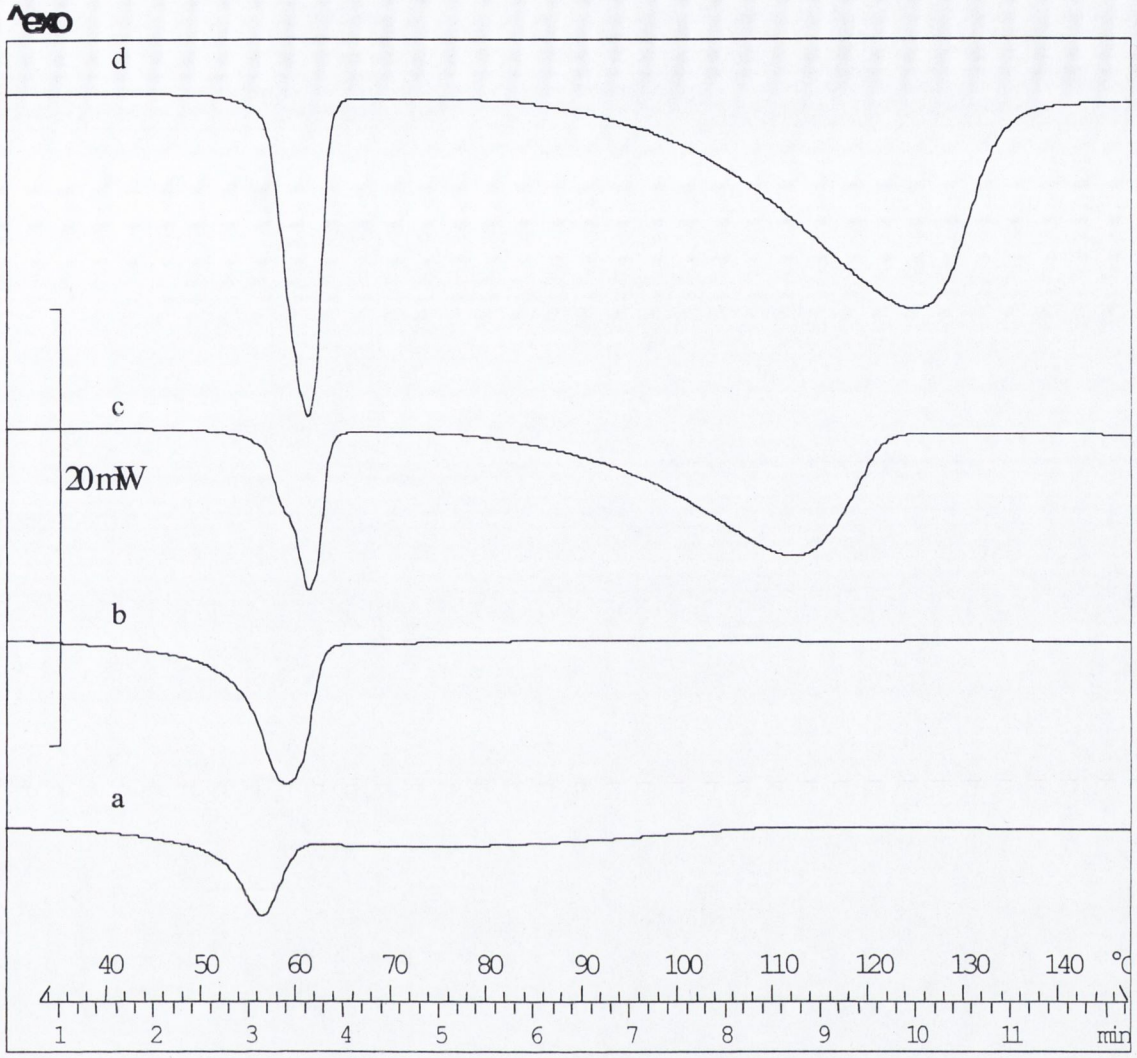

Figure 3.22 DSC scans of (a) spray dried lactose/PEG 4000 20% prior to storage; (b) spray dried lactose/PEG 4000 20% after one years storage at 4°C 34% RH; (c) spray dried lactose/PEG 4000 20% after one years storage at 4°C 75% RH and (d) physical mix of lactose monohydrate/PEG 4000 20%.

XRD of lactose/PEG 4000 20% over time showed an increase in the intensity of PEG peaks (at approximately 19° and 23.4° 2θ) which was consistent with the increase in heats of fusion found by DSC indicating recrystallisation of PEG. The XRD scans of spray dried lactose/PEG 20% stored at 4°C 75% RH for various times are shown in Figure 3.23.

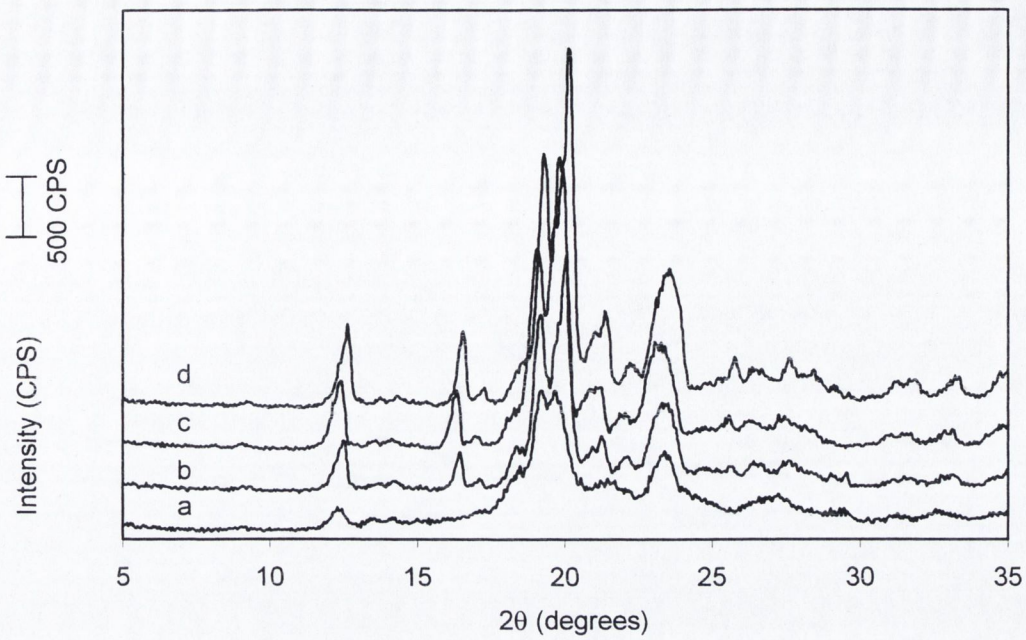

Figure 3.23 XRD scan of spray dried lactose/PEG 20% (a) prior to storage; (b) following 3 days storage at 4°C 75% RH; (c) following 10 days storage at 4°C 75% RH and (d) following 21 days storage 4°C 75% RH.

Enthalpy changes for endothermic and exothermic peaks by DSC were plotted against time for the various storage conditions. Figure 3.24 shows the enthalpy changes by DSC for spray dried lactose and co-spray dried lactose/PEG 5% and 20% when stored at 4°C 34% RH (scans a, b and c) and 4°C 75% RH (scans d, e and f). Figure 3.25 shows the enthalpy changes by DSC for the same systems stored at 45°C 75% RH.

Spray dried lactose on storage at 4°C 34% RH (Figure 3.24, scan a) showed a gradual decrease in the magnitude of the exothermic event over time indicative of recrystallisation. The endotherm due to melting of α-anhydrous lactose increased initially on storage as more lactose recrystallised. A fall in the magnitude of the α-lactose melting endotherm occurred following the initial increase and this fall was accompanied on storage by a peak due to β-lactose (the DSC scan showing the β-lactose melting endotherm is shown in Figure 3.12). XRD scans of spray dried lactose stored at 4°C 34% RH showed an amorphous form up to the 8 weeks of storage. Therefore the α-anhydrous lactose and β-lactose which were observed by DSC were consistent with crystalline lactose produced from recrystallisation of the amorphous material during the DSC heating programme. α-lactose is known to mutarotate to β-lactose during heating by DSC (Angberg, 1995).

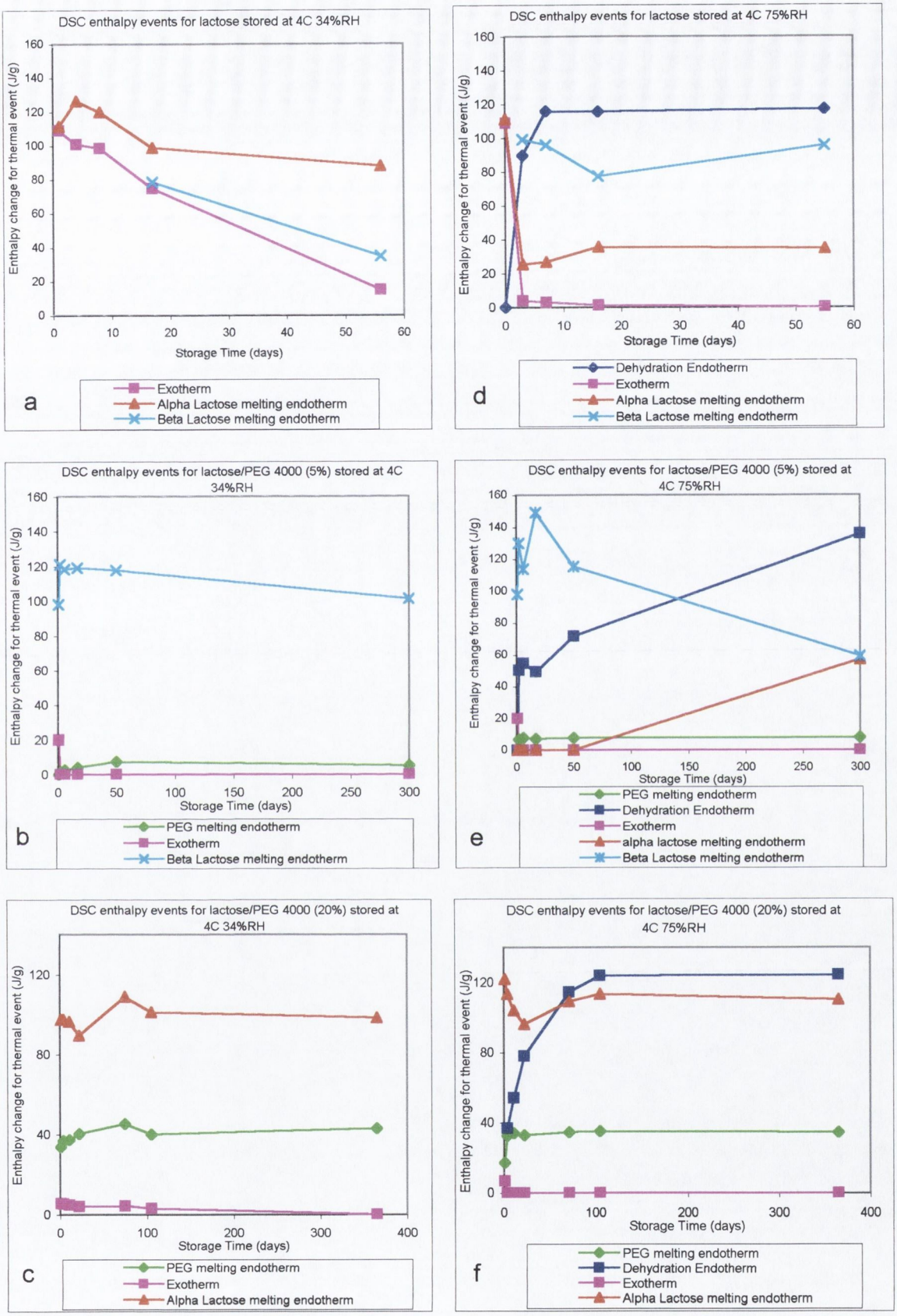

Figure 3.24 Graphs of DSC enthalpy changes for spray dried lactose and co-spray dried lactose/PEG 5% and 20% systems stored at 4°C 34% RH and 4°C 75% RH for different periods of time.

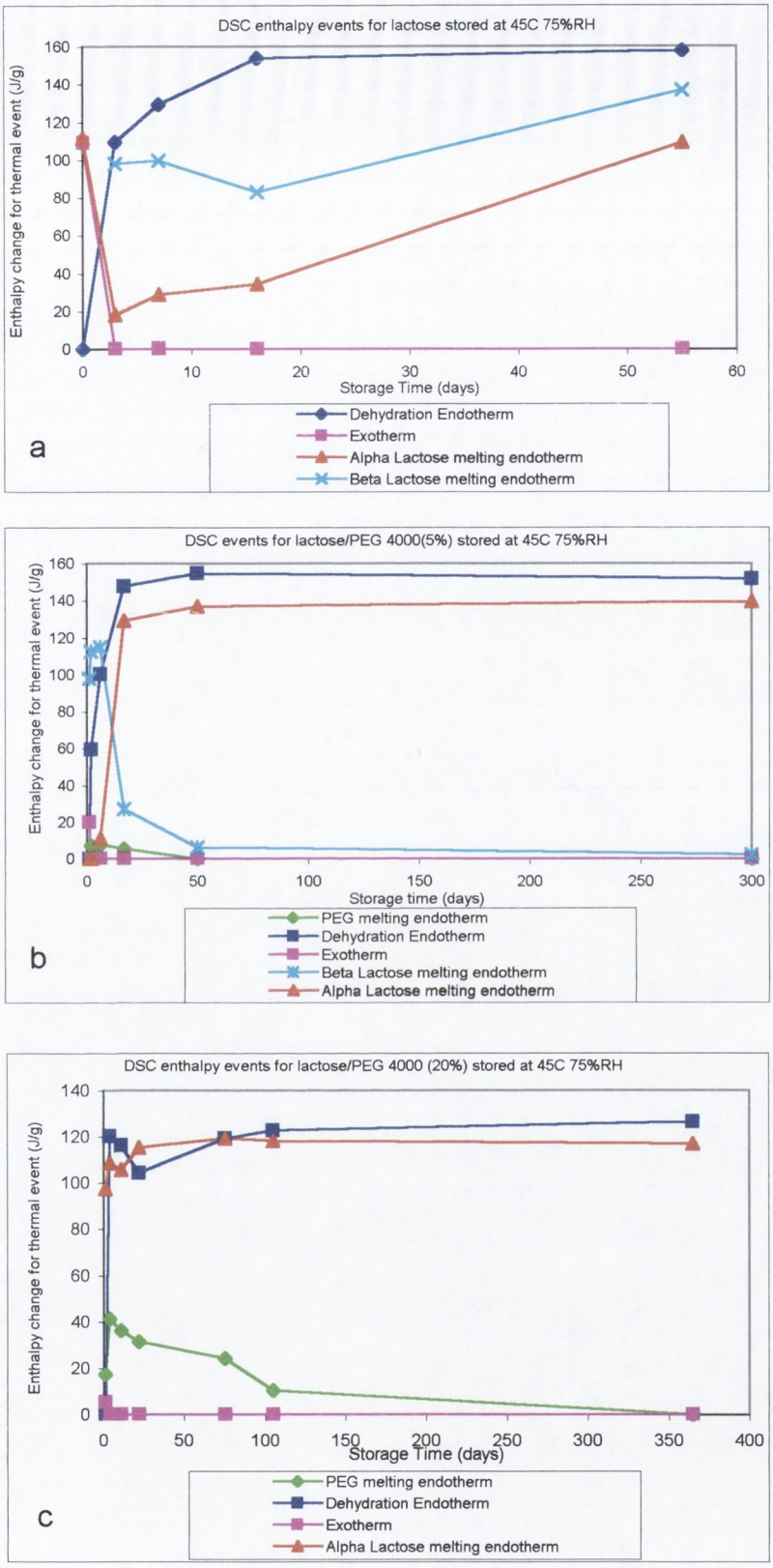

Figure 3.25 Graphs of DSC enthalpy changes for spray dried lactose and co-spray dried lactose/PEG 5% and 20% systems stored at 45°C 75% RH for different periods of time.

On storage at the higher humidity of 75% (Figure 3.24 scan d) the exotherm due to recrystallisation of amorphous lactose decreased in magnitude more rapidly than in the 4°C 34% RH and while initially recrystallised amorphous lactose melted as the α-anhydrous form, on storage a peak due to β-lactose and a dehydration peak representative of the presence of monohydrate lactose were visible (as seen in Figure 3.14). XRD scans of samples stored at 4°C 75% RH showed the presence of β-lactose indicating it was not just formed from mutarotation during heating by DSC. As the dehydration peak grew the α-anhydrous lactose melting peak also increased. DSC enthalpy events for spray dried lactose stored at 45°C 75% RH are shown in Figure 3.25 (scan a). Events were similar to the 4°C 75% RH stored sample but decreases in exotherms and increases in endotherms occurred at faster rates.

DSC enthalpy events on storage at 4°C of the spray dried lactose/PEG 5% system are shown in Figure 3.24 (scans b and e). Storage at 4°C 34% RH showed a reduction in the exothermic peak rapidly to zero and an initial increase in the β-lactose melting peaks and PEG melting peaks. The sample stored at 4°C 75% RH also showed a rapid decrease in the exothermic event to zero. A peak due to dehydration of monohydrate lactose grew in magnitude on storage at 75% RH. Initially when the lactose monohydrate dehydration endotherm was visible, no α-lactose melting endotherm was present; instead the β-endotherm increased in magnitude consistent with some mutarotation of the dehydrated α-lactose to β-lactose. At later time periods α-anhydrous lactose melting was visible. The sample stored at 45°C 75% RH (Figure 3.25, scan b) showed similar events but these occurred over shorter time periods and by 300 days storage β-lactose had decreased to zero. Interestingly the melting endotherm due to PEG also decreased to zero in the 45°C 75% RH stored sample.

DSC enthalpy events for spray dried lactose/PEG 20% are shown in Figure 3.24 (scans c and f). The sample stored at 4°C 34% RH showed a gradual reduction in the magnitude of the lactose exotherm indicating a slower recrystallisation of amorphous lactose than for the 5% PEG system. The 4°C 75% RH sample showed no exotherm after first analysis following storage (time point 3 days) indicating an increased rate in recrystallisation of amorphous lactose when the humidity was increased. The magnitude of the α-lactose melting endotherm initially decreased. As lactose recrystallised to the monohydrate, indicated by the increase in the dehydration endotherm, the α-lactose melting endotherm increased. The sample stored at 45°C 75% RH (Figure 3.25, scan c) showed faster production of the dehydration endotherm. Interestingly the PEG melting endotherm

decreased in magnitude on storage at 45°C 75% RH to zero as seen for the spray dried lactose/PEG 5% system.

Recrystallisation of amorphous material can also be monitored using XRD. XRD can be used in a quantitative manner since the intensity of diffracted X-rays is a function of the amount of diffracting material present. The relationship underlying all quantitiative analysis using XRD is described by Equation 3.1 (Klug and Alexander, 1974).

$$I = \frac{Kx}{\rho[x(\mu - \mu_m) + \mu_m]} \qquad \text{Equation 3.1}$$

where I is the diffracted X-ray intensity arising from a component of a mixture, K is a constant depending on the nature of the component, x is the mass fraction of the component, ρ the density, μ the mass absorption coefficient and μ_m the mass absorption coeffictient of the matrix.

For mixtures in which the absorbing power of the unknown component is the same as that of the entire mixture, for example in mixtures of polymorphs of the same substance, then $\mu=\mu_m$ and Equation 3.1 simplifies to

$$I = \left(\frac{K}{\rho\mu}\right)x \quad \text{or} \quad I = Kx \qquad \text{Equation 3.2}$$

where the intensity is directly proportional to the concentration and the constant K is a measure of the sensitivity. In such systems direct linear analysis is possible.

In situations where $\mu \neq \mu_m$ the intensity-concentration curve will no longer be linear because of the inequality in the absorbing powers of the sample and matrix. Direct analysis is possible however by reference to a calibration curve prepared from mixes of the two components. Since variations in mass absorption coefficients of organic materials are low, unlike for inorganic materials, quantitative XRD of organic materials can be easily performed using simple calibration curves (Shell, 1963; Klug and Alexander, 1974).

Calibration curves were prepared from physical mixes of PEG 4000 and either lactose monohydrate, anhydrous lactose or spray dried lactose. Linear relationships between peak intensity and concentration were observed. The calibration curve prepared from physical mixes of PEG 4000 and spray dried amorphous lactose is included in Appendix III. The relative intensities of PEG peaks were determined by comparing peak heights of PEG in

the physical mixes to peak heights of PEG alone. The calibration curves were linear. From the calibration curve of PEG peak intensity in physical mixes with spray dried lactose the amount of crystalline PEG present in the spray dried lactose/PEG 20% and 30% systems was estimated at approximately 14% and 19% respectively. DSC enthalpy changes for spray dried systems were not compared to calibration curves prepared from physical mixes since spray dried systems were considered to show melting endotherms due to some once folded chain PEG forms (see Figure 3.20) and since the spray dried systems showed melting at lower temperatures to the physical mixes direct comparisons were not possible.

An attempt was made to quantify the recrystallisation of amorphous lactose on storage. Attempts to fit the disappearance of the lactose recrystallisation exotherm or the recrystallisation of PEG by DSC failed due to the fast rates of these events, which prevented sufficient data points for fitting.

Jouppila et al. (1997) have shown that the transformation of amorphous lactose in freeze-dried skim milk, at relative humidities of 66.2% and greater, can be quantified using the Avrami equation (Avrami, 1940) and XRD peak intensity at 19°, 20° and 22° as a measure of the extent of transformation. This equation may be written as

$$I = I^{max} . [1 - e^{-(K(t-t_0))^n}] \qquad \text{Equation 3.3}$$

where I is the peak intensity at time t, t_0 is an induction time, I^{max} is the peak intensity at time infinity, K is the crystallisation rate constant, and n is the Avrami exponent which depends on the nucleation mechanism and the number of dimensions in which growth is occurring. Similarly Schmitt et al. (1999) used an equation of this form, having the value of 3 for n on the assumption of three-dimensional growth, to quantify spray dried lactose recrystallisation at a relative humidity of 57.5%, using gravimetry data. Thus in the absence of an induction time and expressing crystallinity as fraction or percent, Equation 3.3 may be simplified to Equation 3.4.

$$F = 1 - e^{-(Kt)^3} \qquad \text{Equation 3.4}$$

where F is the fraction or percentage crystallinity. From the storage data obtained at 75% RH and 45°C, it is evident from the growth in XRD peak intensities of the lactose/PEG composites that the amorphous lactose converts to crystalline lactose monohydrate. Since

PEG shows strong broad XRD peaks at 19.2° and 23.3°, the peak considered to best represent lactose monohydrate recrystallisation was that at 16.4° (Buma et al., 1967). Percent crystallinity, based on this peak for the spray dried lactose/PEG 10% composite, the most amorphous sample, is plotted in Figure 3.26. Also included in Figure 3.26 is the fitted line obtained using Equation 3.4 (using MicroMath® Scientist®). The data gave a reasonably good fit with K = 0.239 days^{-1} (+/-0.0127), R^2 = 0.986. The crystallisation of monohydrate is also evident from the DSC data in that it resulted in an increase in the endothermic peak at approximately 140°C on the DSC scan. Thus the enthalpy change (ΔH) for the dehydration endotherm could also be used to monitor the rate of recrystallisation of the monohydrate. This data is also shown in Figure 3.26 for the 10% PEG system. A better fit to Equation 3.4 was obtained giving a K estimate of 0.222 days^{-1} +/-0.006 (R^2 = 0.997), close to that obtained by XRD.

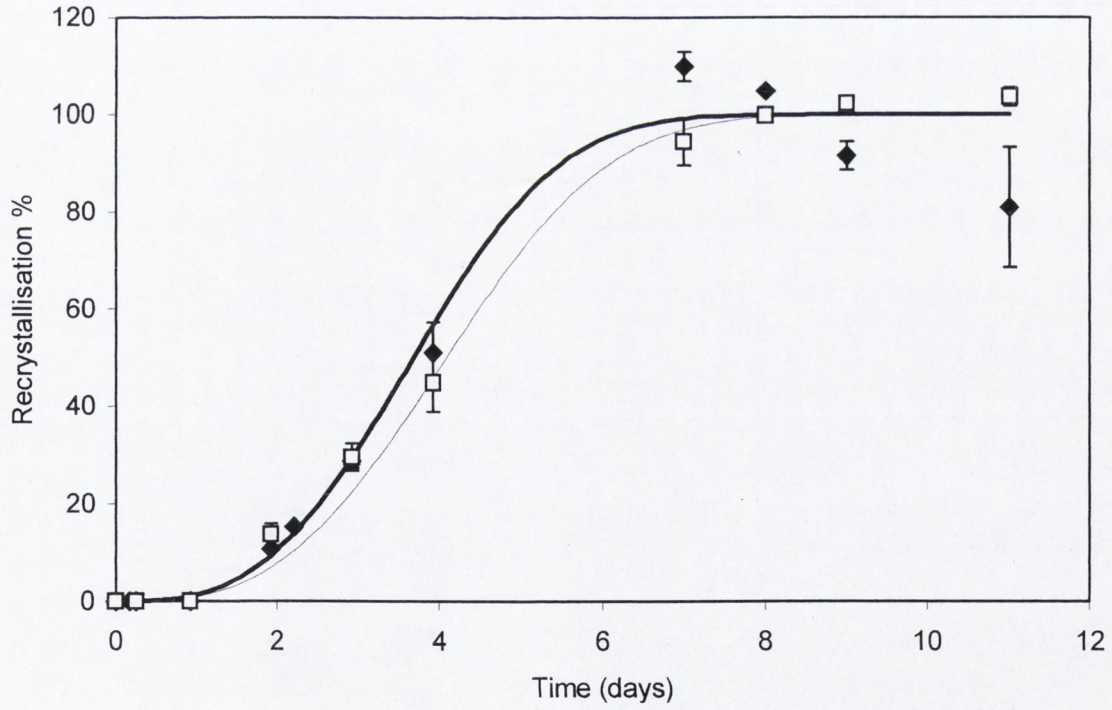

Figure 3.26 Rate of recrystallisation of α-lactose monohydrate from spray dried lactose/PEG (10%). (◆) XRD; (□) DSC; (▬) fitted XRD; (—) fitted DSC.

Similar analysis of the ΔH of dehydration by DSC for pure lactose, lactose/PEG 5% and lactose/PEG 20% spray dried systems gave K values of 0.369 (+/-0.026), 0.207 (+/-0.033)

and 0.565 (+/-0.143) respectively. This limited data suggests that the presence of PEG at low concentrations (when it is mainly amorphous) may retard crystallisation of lactose to lactose monohydrate compared to lactose in which no PEG is present. At higher PEG concentrations lactose recrystallisation may be accelerated.

Analysis of the co-spray dried samples over prolonged time periods showed that, for some samples, XRD peaks due to PEG disappeared. At similar time points endothermic peaks were no longer visible on heating by DSC implying the absence of PEG 4000. Figure 3.27 shows the XRD scans of spray dried lactose/PEG 4000 20% and a physical mix of lactose monohydrate/PEG 20%. Following storage for 75 days the peak by XRD which had been present due to PEG 4000 at approximately 23.4° (indicated by the arrow in Figure 3.27) was no longer detectable but instead only peaks due to lactose monohydrate were visible.

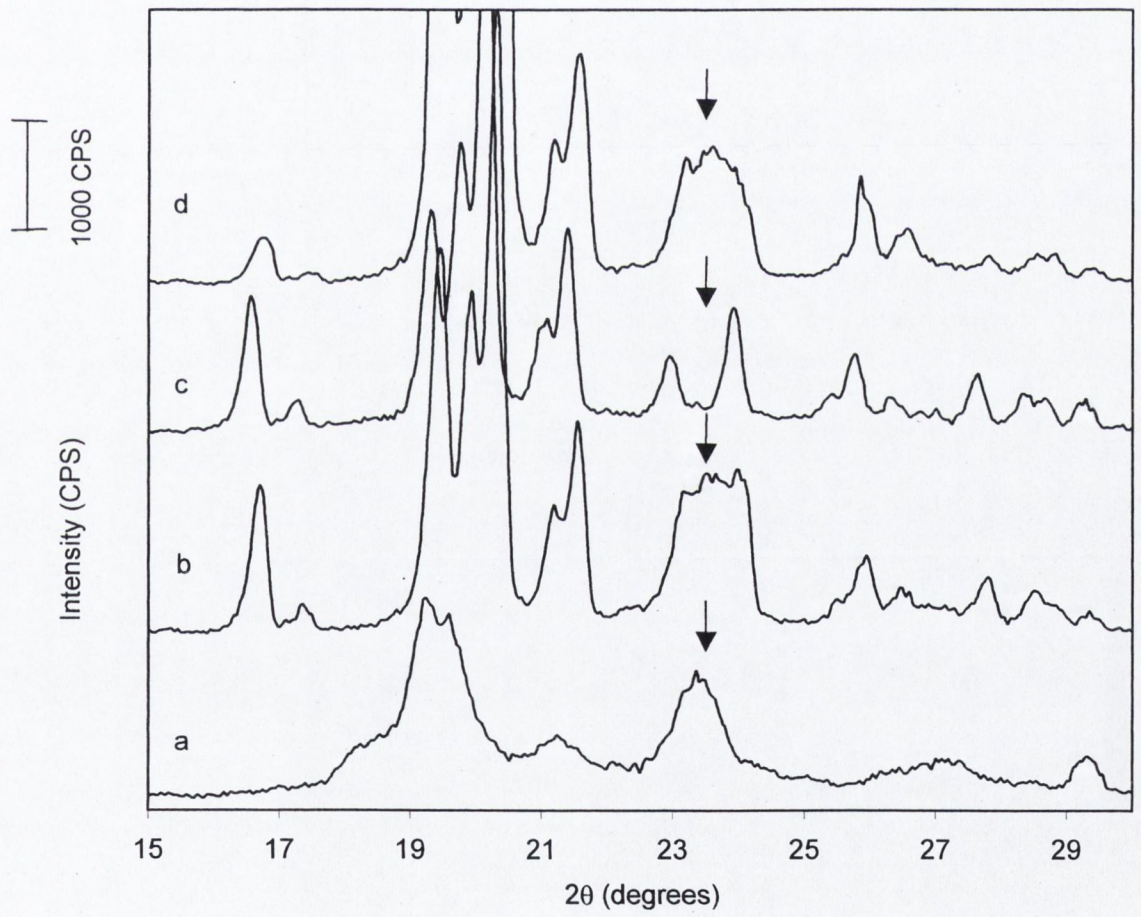

Figure 3.27. XRD scan of (a) spray dried lactose/PEG 4000 20% prior to storage; (b) spray dried lactose/PEG 4000 20% stored at 45°C 75% RH for 22 days; (c) spray dried lactose/PEG 20% stored at 45°C 75% RH for 75 days and (d) physical mix of lactose monohydrate/PEG 20%. The arrows indicate the region of the PEG peak.

Figure 3.28 shows DSC scans of spray dried lactose/PEG 4000 20%. Melting due to PEG 4000 was absent by day 75 of storage at 45°C 75% RH (Figure 3.28, scan c). Samples of spray dried lactose/PEG 20% stored at 30°C 75% RH, 45°C 31% RH and 45°C 75% RH all showed a reduction in PEG peak intensity by XRD and heat change by DSC on storage (after an initial increase due to recrystallisation). The spray dried lactose/PEG 20% 45°C 31% RH sample showed absence of PEG by 1 year of storage and the 45°C 75% RH sample showed absence of PEG by 75 days of storage. The spray dried lactose/PEG 4000 5% and 10% systems also showed evidence of the loss of PEG during storage at high temperature and humidity conditions. GPC was performed on these samples and no PEG was detected. It is probable that the high humidity resulted in chain scission followed by oxidation to formaldehyde which is gaseous and therefore evaporates.

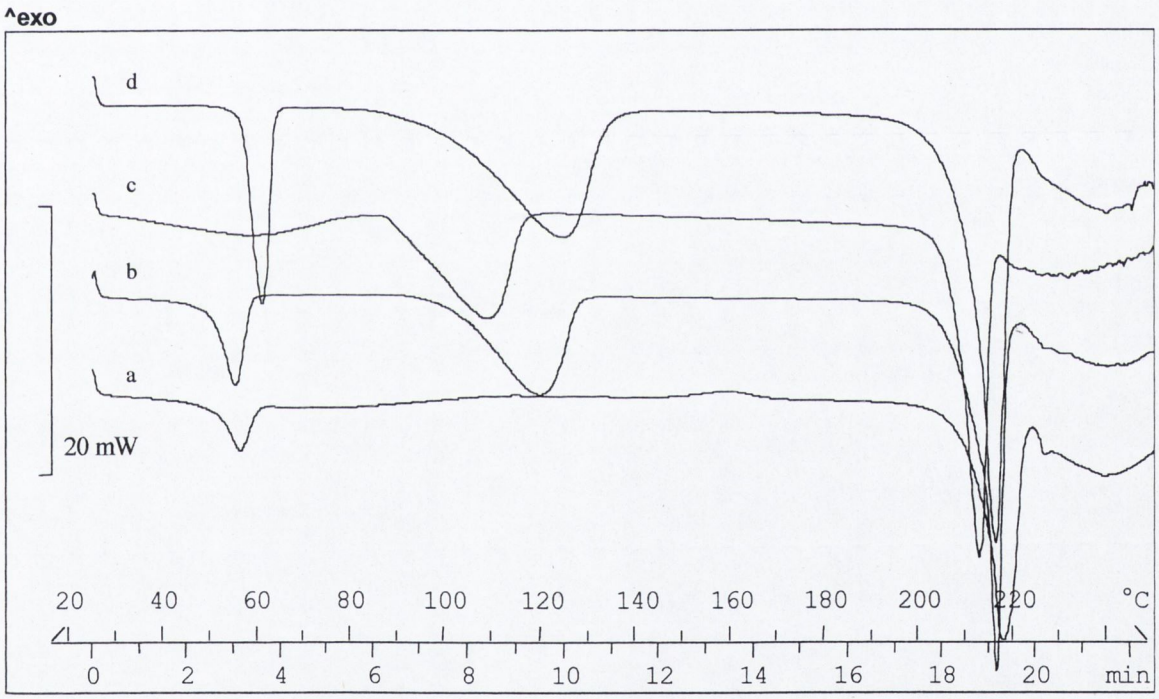

Figure 3.28. DSC scans of (a) spray dried lactose/PEG 4000 20% prior to storage; (b) spray dried lactose/PEG 4000 20% stored at 45°C 75% RH for 22 days; (c) spray dried lactose/PEG 20% stored at 45°C 75% RH for 75 days and (d) physical mix of lactose monohydrate/PEG 20%.

3.5. Conclusions

The crystallinity of co-spray dried lactose/PEG 4000 composites varied depending on the percentage of PEG present. All co-spray dried systems analysed contained amorphous lactose together with varying amounts of crystalline lactose. The crystalline lactose was

initially present as β-lactose (i.e. in the lactose/PEG 5% system), or as anhydrous α-lactose (i.e. in the lactose/PEG 4000 10, 20, 30% systems). The lactose/PEG 4000 10% system was initially the least crystalline of the spray dried composites prepared. Chidavaenzi et al. (2001) found crystalline β-lactose present when 12% PEG was spray dried by weight of lactose (i.e. 10.7% by weight of total solids) but not when 1, 2 or 4% PEG was present. β-lactose was found to be present, in the current work, when 5% PEG (by weight of total solids) was spray dried with lactose but was absent for 10, 20, 30% PEG systems. Chidavaenzi et al. (2001) found some crystalline α-lactose monohydrate present in all their spray dried lactose/PEG systems. None of the systems spray dried in the current work showed the initial presence of α-lactose monohydrate. On storage at low humidity, XRD and DSC data showed no conversion to lactose monohydrate, the initial amorphous lactose recrystallising to α-anhydrous lactose, or in the case of lactose/PEG 5% to β-lactose alone. Storage of the spray dried lactose/PEG composites at high humidity resulted in conversion to α-lactose monohydrate, consistent with the findings of Briggner et al. (1994) for recrystallisation of spray dried lactose alone.

The crystallinity of PEG 4000 depended on its concentration in the composites. When spray dried alone it remained crystalline with 10-15% reduction in peak intensities. DSC analysis showed a slight reduction in melting temperature which could be due to the presence of some once folded chains or result from the slight reduction in crystallinity. PEG is known to be unstable when exposed to prolonged heating (Chatham, 1985). Spray drying of PEG did not result in polymer chain breakdown or in discoloration, which is typical of over exposure to heat. GPC showed no significant difference in PEG molecular weight before and after spray drying. PEG was shown to be amorphous when spray dried with lactose at a concentration of 10% PEG. For all other concentrations of PEG studied, some crystalline PEG was likely to be present on spray drying but a non-crystalline form was also present as evidenced by the increase in PEG crystallinity on storage, as detected by both XRD and DSC. PEG appeared to recrystallise as the extended chain form when stored at temperatures and humidity higher than 4°C 34% RH. DSC data suggested that initially the once folded form recrystallised on storage followed by recrystallisation/conversion to the more stable extended chain conformation. Chidavaenzi et al. (2001) found that PEG spray dried with lactose was present in the extended chain conformation consistent with our results of spray dried lactose/PEG following storage. The apparent lower crystallinity of the lactose/PEG systems prepared in the current work compared to those of Chidavaenzi et al. (2001) may be related to the differing spray drying

conditions employed, namely their use of a higher inlet temperature and a lower airflow rate in the spray drier. Alternatively their systems may not have been analysed soon enough after production and recrystallisation may have occurred before DSC and XRD analysis was performed. The timing of first analysis of spray dried systems is critical for accurate determination of their initial crystallinity since rapid recrystallisation may occur.

PEG whether alone or present in co-spray dried systems degraded when exposed to high temperature and humidity conditions (45°C 75% RH or 45°C 30% RH). It was observed from storage of co-spray dried systems that as temperature and humidity conditions are increased PEG degrades at an increasing rate.

CO-SPRAY DRIED BENDROFLUMETHIAZIDE/POLYMER SYSTEMS

4.1. Introduction

Previously it has been shown that co-precipitates of hydroflumethiazide with the water soluble amorphous polymer PVP, in appropriate proportions, result in high energy amorphous composites with enhanced dissolution relative to corresponding compressed physical mixtures at polymer contents of 20-70% (Corrigan and Timoney, 1975). In contrast much lower enhancements were observed when the water soluble crystalline polymer, PEG, was used to form coprecipitates and these systems were crystalline (Corrigan and Timoney, 1976). Co-spray drying drug/PVP systems extended the composition range over which amorphous systems were obtained and further increased the energy of the systems (Corrigan and Holohan, 1984). In Chapter 3 it was shown that spray drying lactose with PEG promoted amorphous PEG formation, in contrast to previous experience with coprecipitate drug/PEG systems in which both the drug and PEG were crystalline (Corrigan and Timoney, 1976). Therefore it was of interest to spray dry drug/PEG systems in an attempt to prepare totally amorphous systems. Such amorphous systems are likely to have higher energy and therefore show increased solubility (Hancock and Parks, 2000) and increased dissolution rates (Corrigan et al., 1984) when compared to their crystalline counterparts and therefore should show higher bioavailability (Fukuoka et al., 1987). It has previously been shown that spray drying the thiazide diuretics hydroflumethiazide and bendroflumethiazide from ethanol resulted in amorphous products with increased solubility (Corrigan et al., 1984). Several other thiazide diuretics were spray dried such as chlorthiazide, hydrochlorthiazide and cyclopenthiazide. The lower molecular weight thiazides (i.e. chlorthiazide, hydrochlorthiazide and hydroflumethiazide) formed amorphous phases less readily and had poor physical stability. Chlorthiazide only formed an amorphous phase when spray dried with PVP while hydrochlorthiazide spray dried alone was stable for only 24 hours. The larger molecular weight thiazides such as bendroflumethiazide and cyclopenthiazide readily gave amorphous phases on spray drying and were physically stable even after 12 months (Corrigan et al., 1984). Bendroflumethiazide (BFMT) was therefore chosen as a model drug with low solubility since the spray drying of it results in a relatively stable amorphous system and also it was readily available (donation from Leo Laboratories). The objective of this work was to spray dry BFMT/PEG systems to ascertain if amorphous drug/PEG composites could be formed with improved dissolution characteristics relative to BFMT alone.

4.2. Co-spray dried BFMT/PEG 4000 systems

Systems containing 0, 10, 20, 30 and 90% PEG by weight of total solids were spray dried. The spray drying conditions are given in Appendix I. The lack of peaks by XRD confirmed that BFMT spray dried alone was amorphous, as found previously by Corrigan et al. (1984). This conclusion was supported by DSC data shown in Figure 4.1 (scan a). A relaxation endotherm indicative of the glass transition temperature with an onset temperature at approximately 120°C was visible followed by an exotherm (recrystallisation of the amorphous state) and then the melting endotherm which had an onset temperature at approximately 220°C. The DSC scan of unprocessed BFMT is shown in Figure 4.1 (scan b), showing one sharp endotherm with an onset temperature at 229°C indicative of melting of the crystalline material.

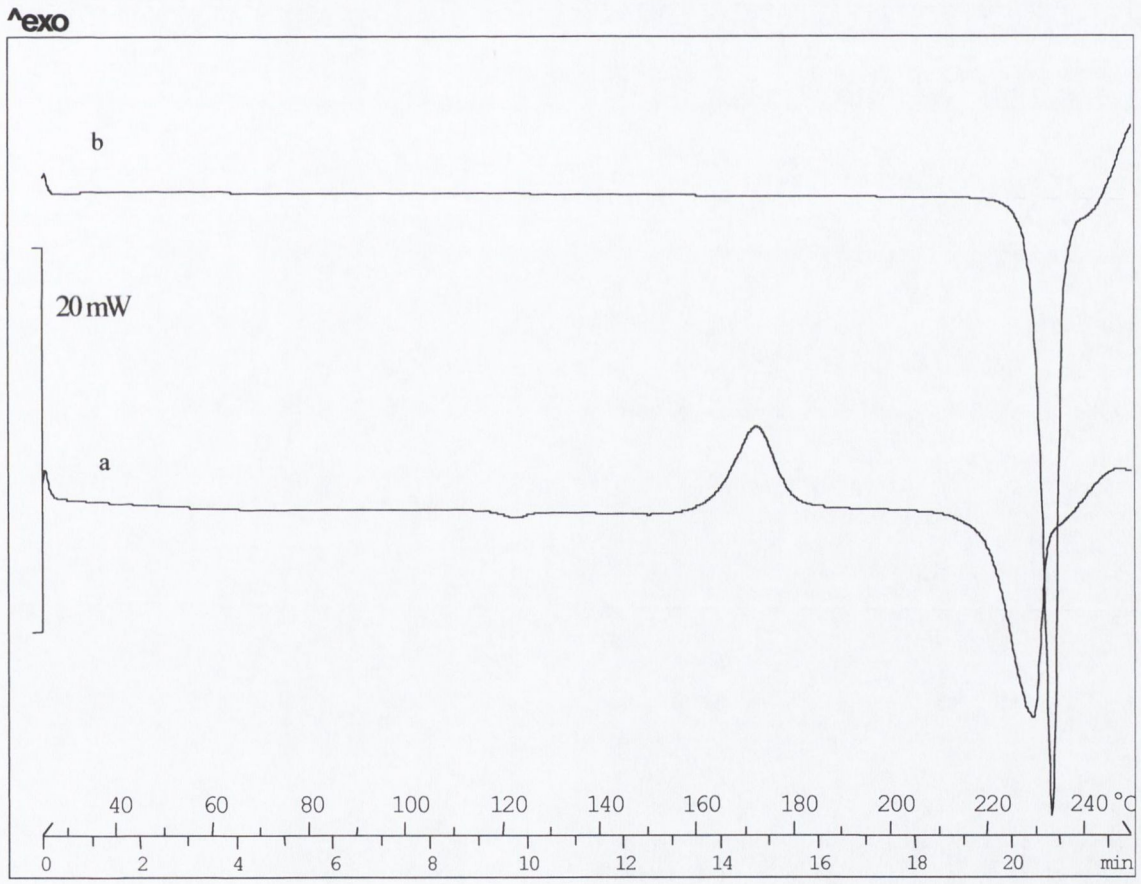

Figure 4.1 DSC scan of (a) spray dried BFMT and (b) BFMT starting material.

Figure 4.2 shows the XRD scan of co-spray dried BFMT/PEG 4000 composites (containing 10, 20 and 30% PEG). The systems were all amorphous, indicated by the lack of peaks indicative of crystallinity. No peaks indicative of crystalline PEG were visible which contrasts with the XRD data shown in Chapter 3 for lactose/PEG systems containing

20 and 30% PEG in which peaks indicative of crystalline PEG were apparent (although somewhat reduced in magnitude).

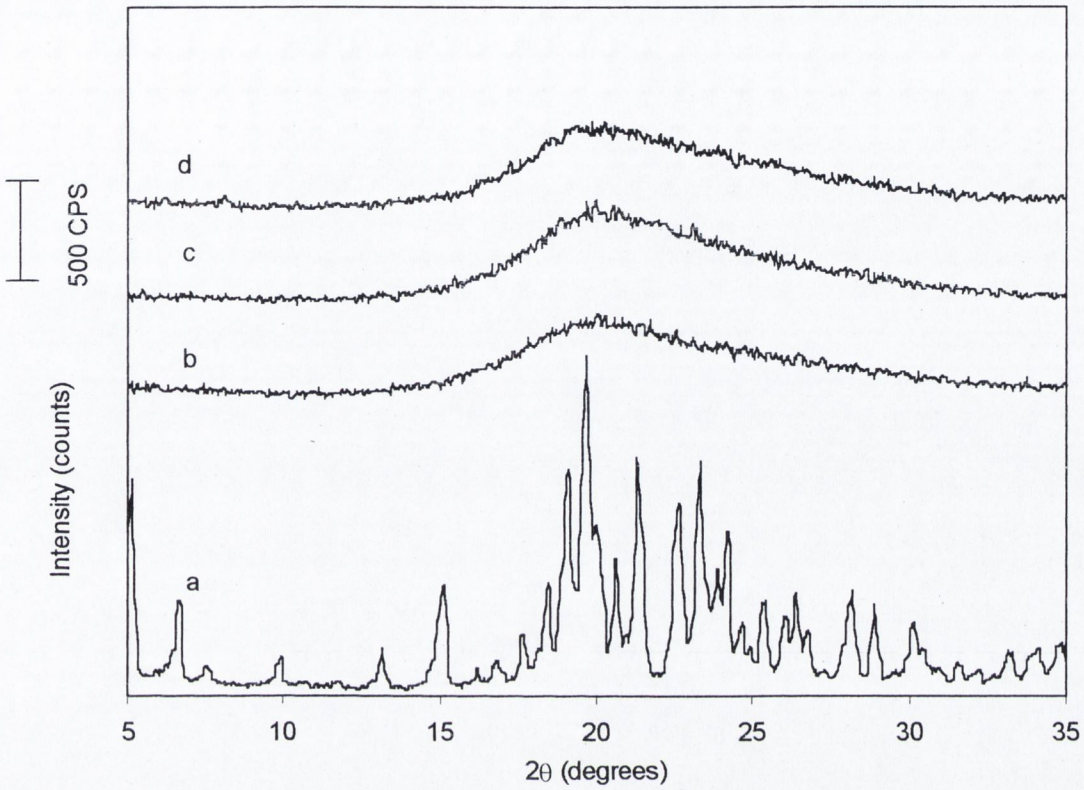

Figure 4.2 XRD scans of (a) physical mix BFMT/PEG 4000 10% (b) spray dried BFMT/PEG 4000 10%; (c) spray dried BFMT/PEG 4000 20% and (d) spray dried BFMT/PEG 4000 30%.

DSC scans of the co-spray dried samples are shown in Figure 4.3. The 10% PEG system showed two very small overlapping endotherms with onset temperatures at approximately 205 and 210°C. A broad endotherm at approximately 90°C was observed. This endotherm is at too high a temperature to be due to the melting of PEG. A DSC scan of a physical mix of BFMT/PEG 10% is shown in Figure 4.3 (scan d), the endotherm in the PEG melting region indicating that DSC can readily detect such a concentration of PEG in a mixed system. The spray dried BFMT/PEG 20% system (Figure 4.3, scan b) showed a small melting endotherm at approximately 170°C followed by a broader double endotherm at approximately 200°C. A broad endotherm is present at approximately 70°C which is also at too high a temperature to be due to the presence of PEG. No exotherms or endotherms in the PEG melting region were observed in either the 10% or 20% PEG system. The 30% PEG-containing system (Figure 4.3, scan c) showed an exotherm at

approximately 120°C prior to the melting of BFMT which occurred at approximately 150°C followed by a second endotherm which peaked at approximately 200°C. A change in the baseline was visible in the PEG melting region but did not resemble melting of PEG as seen in the equivalent physical mix, the physical mix of BFMT/PEG 30% also being shown in Figure 4.3 (scan e). The onset melting temperature of pure unprocessed BFMT by DSC was 229°C (Figure 4.1). Physical mixes of BFMT with PEG 4000 (Figure 4.3) resulted in the BFMT melting endotherms occurring at lower onset temperatures than BFMT alone indicating that the presence of PEG reduced the temperature of BFMT melting. The physical mixes showed a second melting endotherm following or overlapping with the BFMT melting endotherm as was the case with the spray dried systems. This second endotherm is likely due to degradation of BFMT on heating.

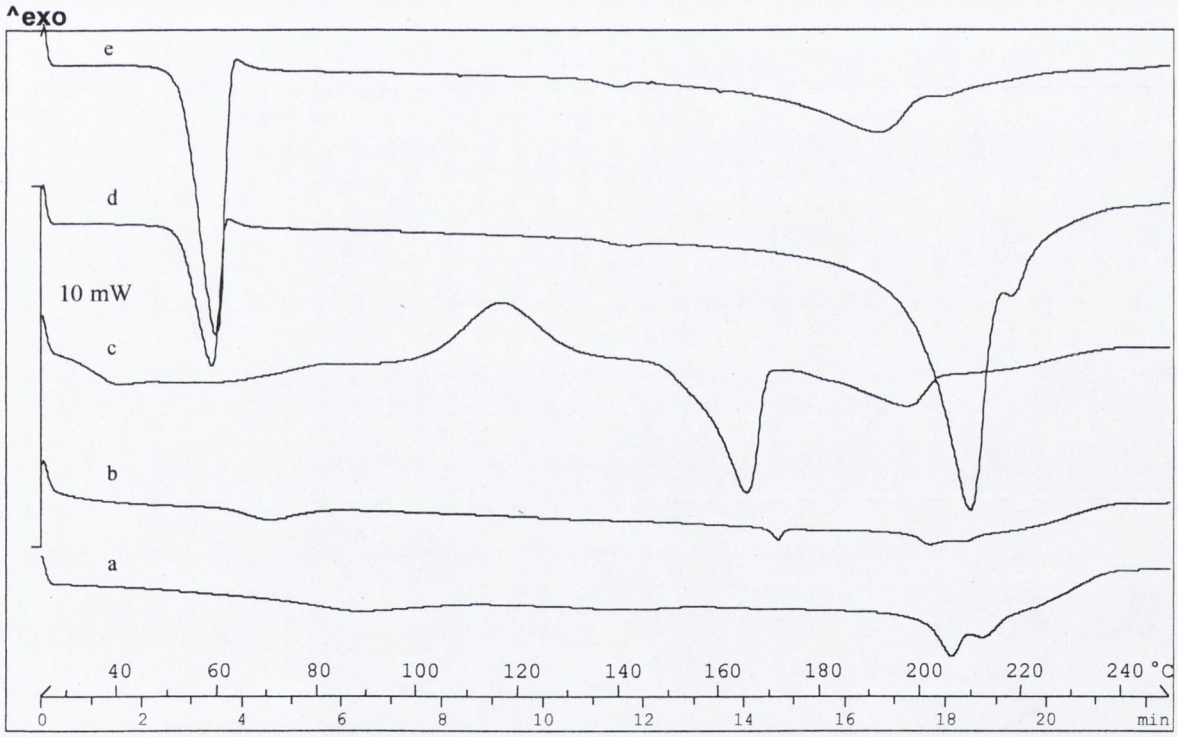

Figure 4.3 DSC scans of (a) spray dried BFMT/PEG 4000 10%; (b) spray dried BFMT/PEG 4000 20%; (c) spray dried BFMT/PEG 4000 30%; (d) physical mix BFMT/PEG 4000 10% and (e) physical mix BFMT/PEG 4000 30%.

No obvious glass transitions were visible in the spray dried BFMT/PEG systems, although changes in the baseline were observed in the 40-90°C temperature region. A change in the baseline was especially obvious in the 30% PEG system and this could have been due to the glass transition. Modulated temperature differential scanning calorimetry, which is

known to be superior to conventional DSC for measuring glass transitions (Craig, 1995), was performed on spray dried BFMT/PEG 10%, 20% and 30% systems. Figure 4.4 shows the total heat flows recorded using the modulated temperature DSC for analysis of the different BFMT/PEG 4000 weight ratios. Samples which have been cooled at a rate very different from their subsequent heating rate often show enthalpic relaxation peaks in the glass transition region (Verdonck et al., 1999). Verdonck et al. (1999) report that this relaxation peak can be large enough to conceal the variation of the heat capacity at the glass transition, and the glass transition may be misinterpreted as a melting transition. Figure 4.5 shows the separation of reversing and non-reversing heat flow signals for the modulated DSC scan of the 30% PEG sample, showing separation of the change in heat capacity at the glass transition (shown in the reversing heat flow in Figure 4.5) from the enthalpic relaxation (shown in the non-reversing heat flow in Figure 4.5).

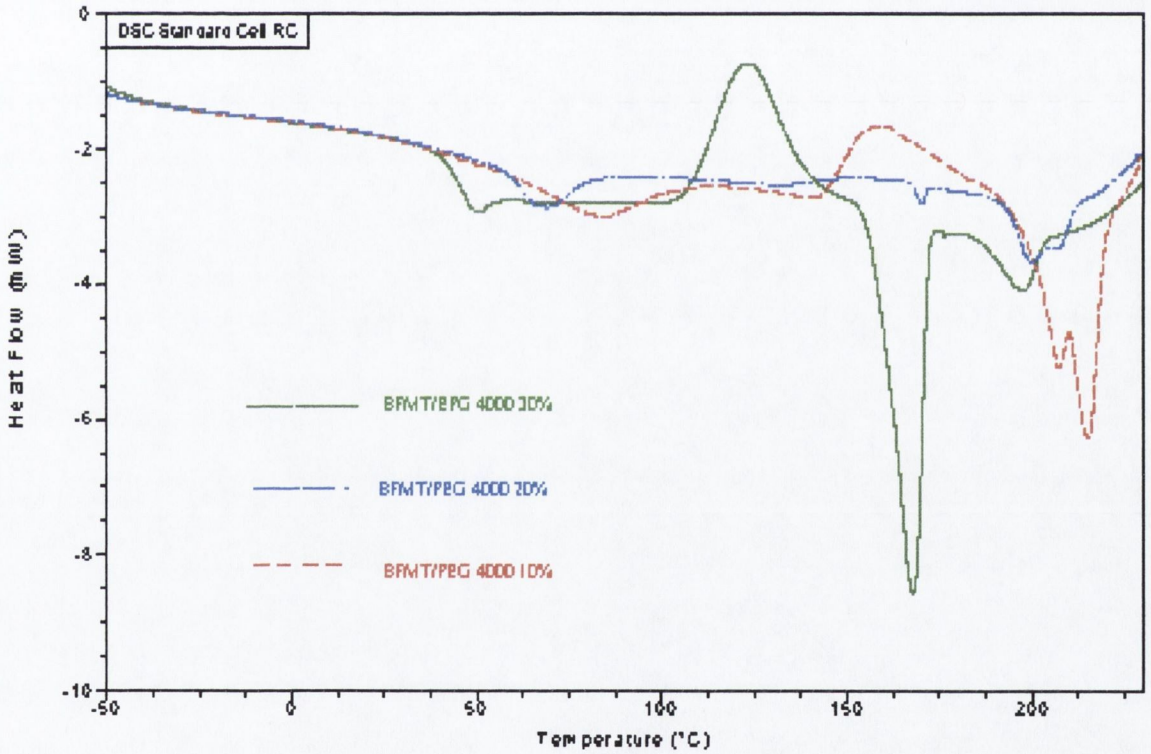

Figure 4.4 Modulated temperature DSC scan of spray dried BFMT/PEG 4000 10%, 20% and 30%.

From the modulated DSC experiments it appeared that the endotherms observed by conventional DSC in the 40-90°C temperature region were due to enthalpic relaxations which masked the glass transitions. The glass transition temperatures appeared to decrease as the amount of PEG in the composites was increased. The BFMT/PEG 4000 10%

system showed a glass transition at approximately 83°C, the BFMT/PEG 4000 20% showed a glass transition at approximately 69°C and the BFMT/PEG 4000 30% systems showed a glass transition at approximately 45°C.

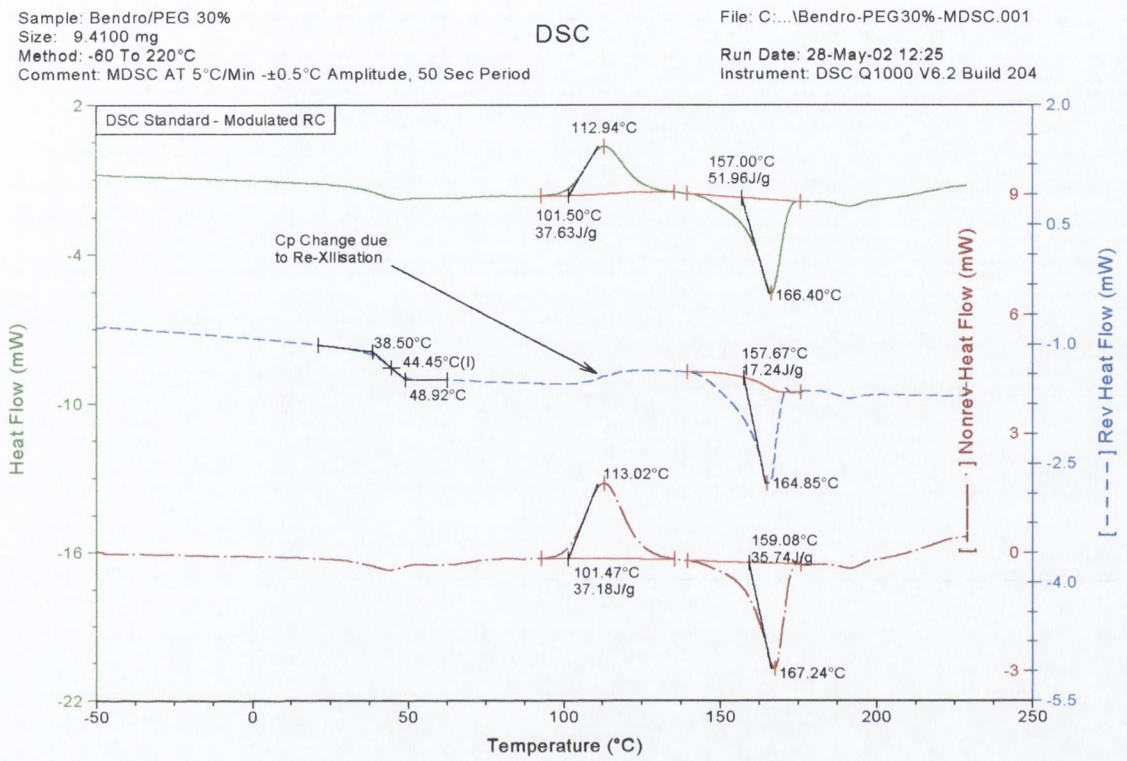

Figure 4.5 Modulated DSC scan of spray dried BFMT/PEG 30% showing separation of reversing and non-reversing heat flows.

SEM micrographs of spray dried BFMT/PEG 4000 systems are shown in Figure 4.6. BFMT/PEG 4000 10% and 20% systems consisted of smooth spherical particles approximately 0.5 to 4 μm in diameter. The spheres present in the 10% PEG system although smooth surfaced did show some surface dimpling. The BFMT/PEG 4000 30% composite did not consist of distinct spheres but appeared to consist of flakes of fused material.

Intrinsic dissolution studies were performed as described in Chapter 2. Prior to dissolution testing discs were analysed by XRD to determine whether the compression process had affected the crystallinity of the systems. All spray dried systems remained amorphous following compression into discs and discs of physical mixes showed similar XRD patterns to powders of physical mixes.

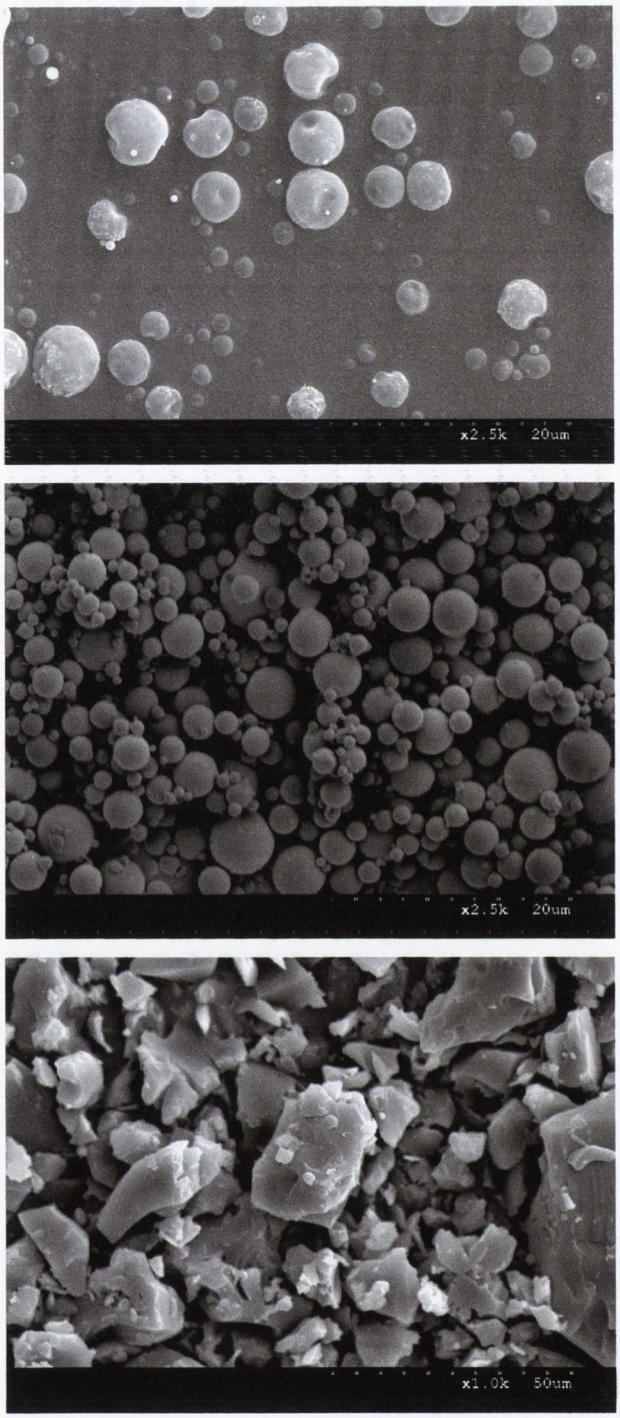

Figure 4.6 SEM micrographs of spray dried BFMT/PEG 4000 systems. BFMT/PEG 4000 10% (top); BFMT/PEG 4000 20% (middle); BFMT/PEG 4000 30% (bottom). Note the lower magnification of the BFMT/PEG 4000 30% micrograph.

Dissolution studies were performed on crystalline and spray dried BFMT, and equivalent physically mixed BFMT/PEG and co-spray dried systems. The BFMT/PEG 30% discs swelled and could not be retained in the holders. The dissolution profiles for the other systems are shown in Figure 4.7.

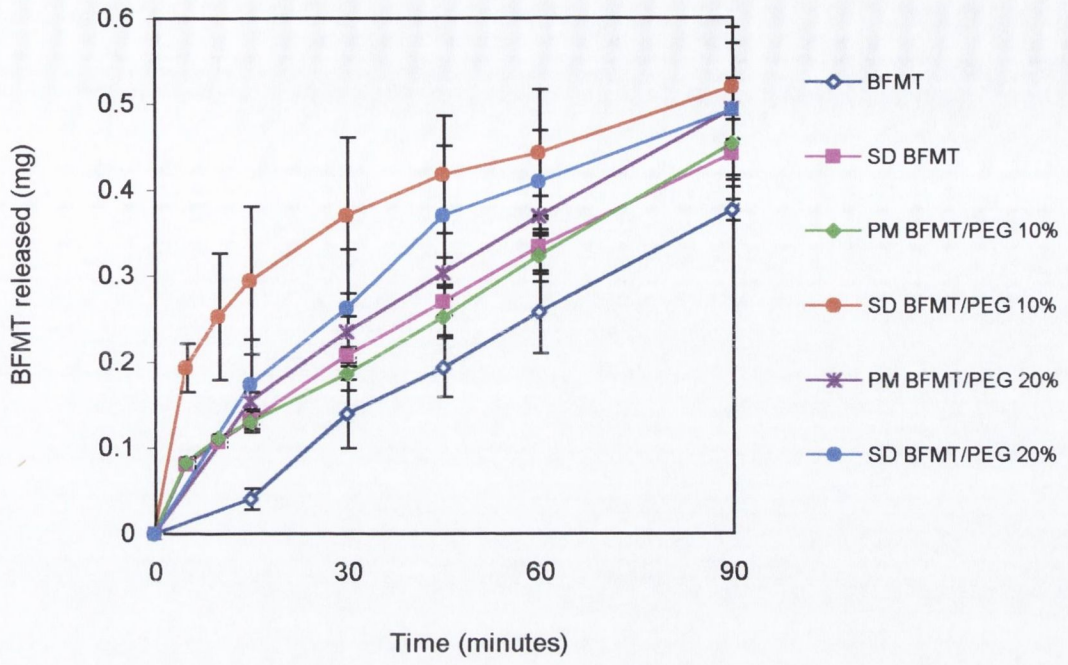

Figure 4.7 Dissolution of spray dried (SD) and physical mixes (PM) of BFMT/PEG 4000, SD BFMT and BFMT alone at 37°C in pH 2 media.

The spray dried BFMT/PEG 10% system gave a significantly higher release rate, over the first 15 minutes, than the 20% PEG spray dried system or the physical mix BFMT/PEG systems, which in turn gave significantly higher release rates than micronised BFMT. Profiles of the spray dried systems were nonlinear, the dissolution rate declining over time, reflecting recrystallisation of the components and the more rapid dissolution of the polymer. This was confirmed by XRD of the discs following dissolution testing which showed the presence of crystalline BFMT but no evidence of the presence of PEG 4000. Discs of the physical mixes after dissolution testing were analysed by XRD and while crystalline BFMT was visible, peaks due to PEG 4000 were not observed.

4.2.1. Physical stability of BFMT/PEG 4000 systems

Samples of spray dried BFMT and co-spray dried BFMT/PEG 4000 10%, 20% and 30% were stored at 30°C and at a relative humidity of 75% (using saturated salt solutions as described by Nyqvist, 1983). DSC analysis was used to monitor recrystallisation of the samples after storage at 30°C 75% RH for various time periods. Spray dried BFMT remained amorphous for over 6 months, while the 10% PEG 4000 system showed a

recrystallisation exotherm after 29 days but no exotherm by day 31 of storage. The 20% PEG 4000 system still showed a recrystallisation exotherm at 10 days of storage but no recrystallisation exotherm thereafter. The 30% PEG system was first analysed following 18 hours of storage and displayed no recrystallisation exotherm. The presence of PEG in the composites appeared to destabilise the amorphous BFMT with higher weight ratios of PEG causing faster recrystallisation.

Figure 4.8 shows a plot of the DSC enthalpy changes of the exotherms versus time for spray dried BFMT and spray dried BFMT/PEG 4000 systems when stored at 30°C 75% RH. The recrystallisation exotherm was not initially evident in the 10 and 20% PEG systems following spray drying which may indicate that initially these systems are stable on heating. On storage exotherms became evident and the enthalpy change associated with these exotherms increased initially prior to decreasing eventually to zero when the samples had fully recrystallised. The 20% PEG system was the slowest to reach its maximum enthalpy change associated with the recrystallisation exotherm. Recrystallisation in the 10% PEG system stored at 30°C 75% RH did not appear to be a co-operative process but appeared gradual with exothermic peaks becoming smaller over time (Figure 4.8). Buckton and Darcy (1995) described the recrystallisation of amorphous lactose as occurring simultaneously throughout the powder bed in a co-operative process. They studied the recrystallisation of amorphous lactose when the amorphous material was divided by different additives and found that the lactose recrystallised all at one time even when it was physically divided into two separate regions by the additives.

From the modulated DSC experiments (Figure 4.4) it appeared that the glass transition temperatures of the systems decreased with increasing PEG content (i.e. PEG acts as a plasticiser). Absorbed water generally acts as a plasticiser, lowering the glass transition of amorphous materials until eventually when enough water is absorbed the glass transition becomes lowered to the storage temperature and the material recrystallises. Since the 30% PEG system has the lowest glass transition temperature, the time for the absorption of water to lower this already lowered glass transition will be faster than for the other systems with higher initial glass transition temperatures. Therefore since the glass transition temperatures of the spray dried systems decreased with increasing PEG, the system with the highest amount of PEG (the lowest glass transition) will recrystallise first and that with the lowest amount of PEG (i.e. the highest initial glass transition) will take the longest time to recrystallise. This was shown to be the case in the storage study at 30°C 75% RH (Figure 4.8).

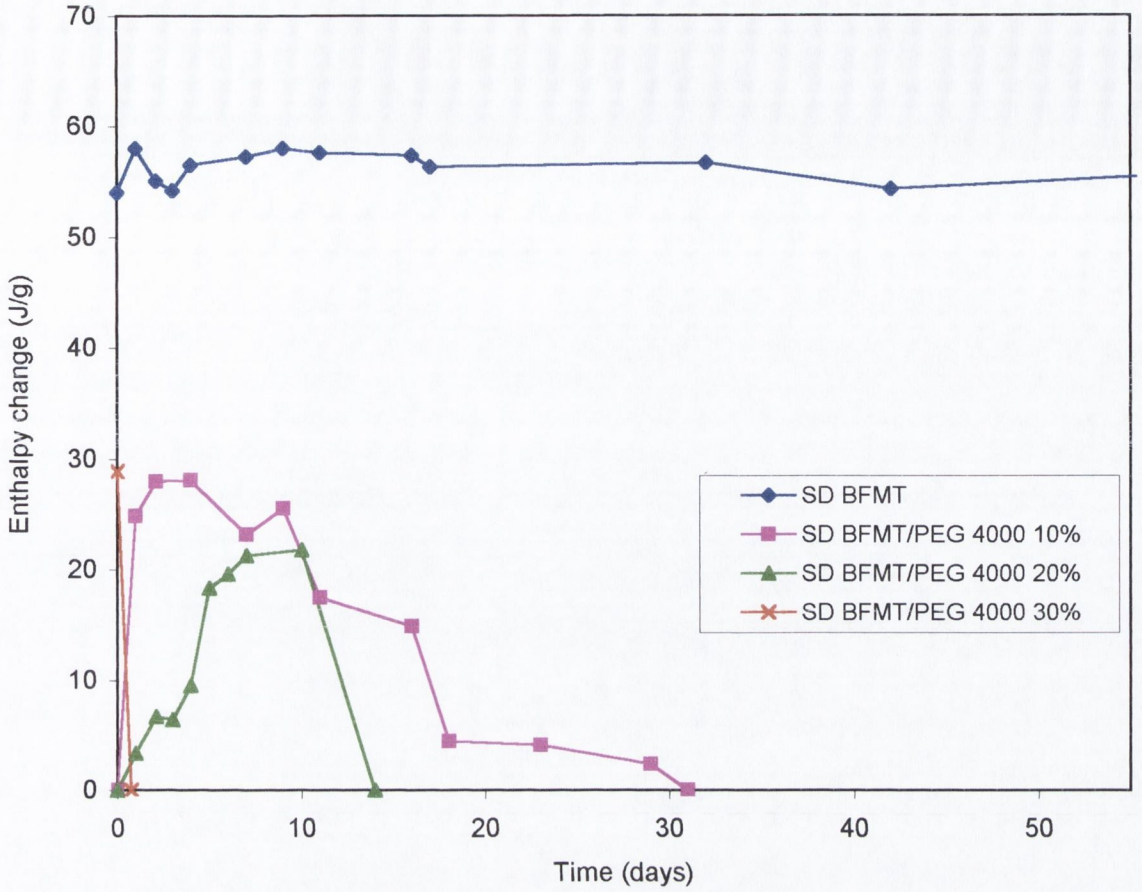

Figure 4.8 DSC recrystallisation data (based on exothermic enthalpy change) for spray dried BFMT and BFMT/PEG 4000 systems at 30°C 75% RH.

It is likely that the spray dried BFMT/PEG systems exist as glass solutions and that on storage the PEG may recrystallise first leaving the remaining amorphous BFMT to recrystallise. Alternatively the PEG may degrade leaving the BFMT to recrystallise.

From XRD scans of spray dried BFMT/PEG 20% it was observed that the sample stored at 30°C 75% RH remained amorphous following 7 days of storage. XRD following 5 weeks of storage showed peaks indicative of crystallinity (Figure 4.9 (scan e)). No peaks indicative of PEG were visible in the stored samples by XRD. A physical mix of BFMT/PEG 20% is shown in Figure 4.9 (scan b), the peak at approximately 23.4 °θ being due to the presence of PEG. DSC of the 30°C 75% RH sample following 5 weeks of storage also failed to show peaks indicative of the presence of PEG.

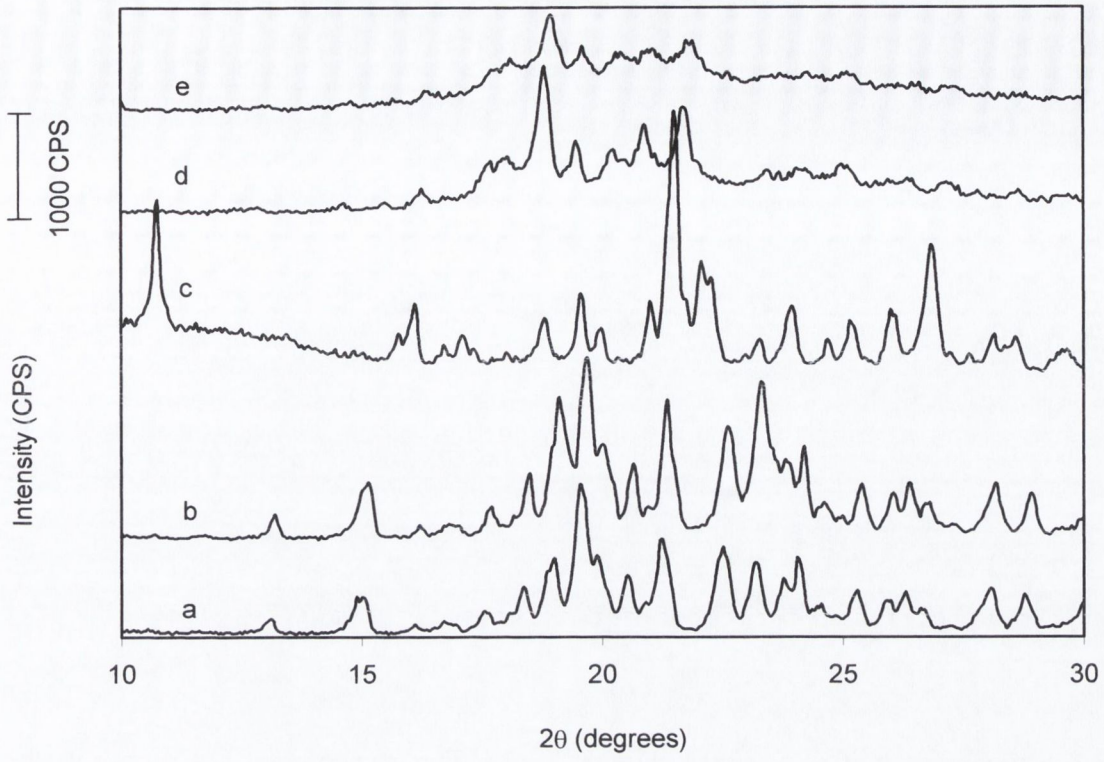

Figure 4.9 XRD of (a) BFMT; (b) physical mix of BFMT/PEG 4000 20%; (c) TFSA; (d) spray dried BFMT/PEG 4000 20% stored at 45°C 75% RH for 4 days and (e) spray dried BFMT/PEG 4000 20% stored at 30°C 75% RH for 5 weeks.

No peaks by XRD (Figure 4.9 (scan d)) nor by DSC were visible for PEG in the BFMT/PEG 20% samples stored at the 45°C 75% RH for 4 days. GPC analysis of amorphous spray dried BFMT/PEG systems confirmed the presence of PEG 4000 in the composites. Following storage, when recrystallised samples failed to show presence of PEG by DSC and XRD, GPC of these samples also did not detect the presence of PEG. It is likely that the PEG has degraded as occurred when lactose/PEG samples were stored at high temperatures and high relative humidities (Chapter 3).

The stored spray dried samples shown in Figure 4.9 had not fully recrystallised as indicated by the lack of many peaks corresponding to crystalline BFMT and the background halo underlying the peaks which were present. An XRD scan of TFSA, the main degradation product of BFMT, is shown in Figure 4.9 (scan c), showing peaks not visible in the recrystallising BFMT/PEG samples (at approximately 11° and 27° 2θ). Therefore amorphous BFMT does not appear to recrystallise to its degradation product TFSA.

4.2.2. Chemical stability of BFMT/PEG 4000 systems

Frontini and Mielck (1997a) prepared solid dispersions of BFMT/PEG 6000 using both a melt method and a solvent evaporation method. They used drug:carrier weight ratios of 10:90 BFMT:PEG 6000 and described their system as x-ray amorphous. Frontini and Mielck (1997c) also described the chemical instability of BFMT in the presence of PEG with hydrolysis of the BFMT to TFSA and hydroflumethiazide (HFMT). In our laboratory we prepared a similar weight ratio of BFMT:carrier using the melt method described by Frontini and Mielck (1997a) but replacing PEG 6000 with PEG 4000. The product obtained was cream to yellow in appearance. XRD analysis showed the BFMT to be amorphous but the PEG 4000 to be crystalline. For comparison purposes a 10:90 weight ratio BFMT:PEG 4000 was spray dried. Figure 4.10 shows the XRD scans of the systems prepared by both methods (i.e. the spray drying method and the melt method). The spray drying method gave similar results to the melt method by XRD i.e. peaks indicative of crystalline PEG but no peaks indicative of crystalline BFMT. However the spray drying method did result in significantly lower intensity peaks indicative of a reduction of PEG crystallinity by this method of production.

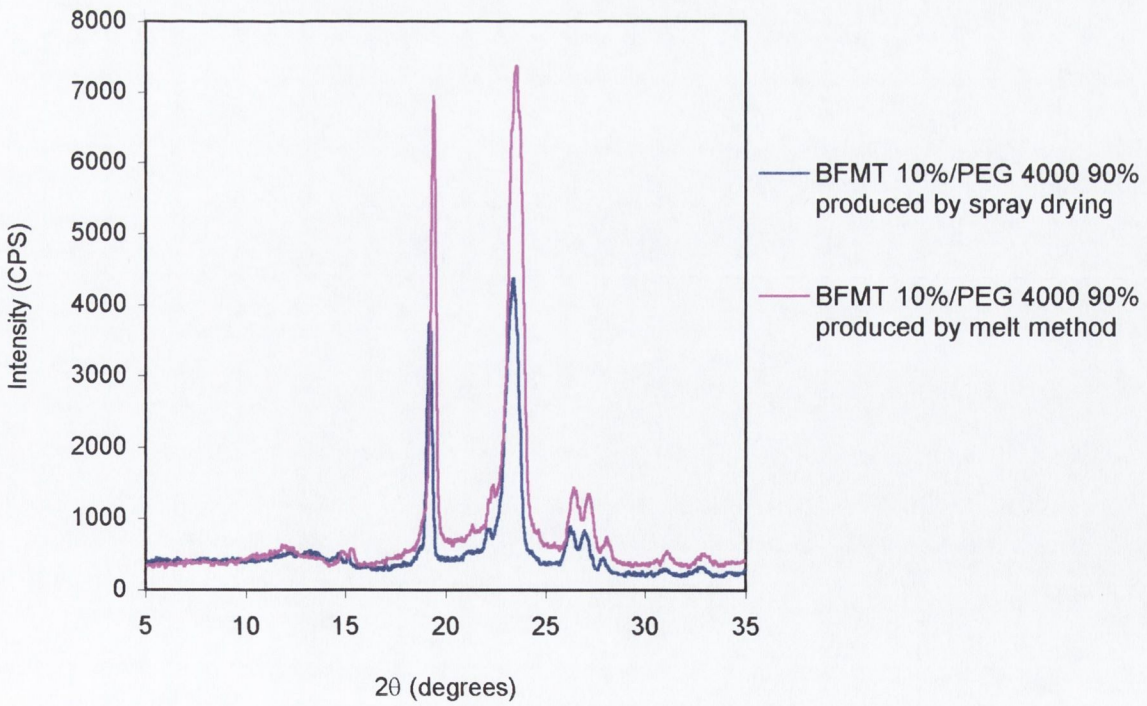

Figure 4.10 XRD scans of BFMT/PEG 4000 90% prepared by both the spray dried and melt method.

The spray dried BFMT/PEG 90% system appeared white in colour, similar to the other spray dried systems containing different weight ratios, in contrast to the creamy/yellow system obtained by the melt method. HPLC analysis was performed on both systems using the method of Frontini and Mielck (1992) and a significant amount of TFSA (main degradation product) was found in the sample prepared by the melt method. TFSA for HPLC was prepared as outlined in Chapter 2. HPLC of the melt produced system consisted of 0.5% w/w TFSA. This was approximately 64 times the amount present in the equivalent spray dried system. The other spray dried BFMT/PEG 4000 systems were also analysed by HPLC to determine whether the spray drying method resulted in degradation of the drug. All systems showed no significant increase in TFSA compared to the starting material.

The melt method involved heating to 80°C whilst spray drying involved an inlet temperature of 78-80°C. An inlet temperature of 78-80°C however resulted in an outlet temperature of only 57-62°C. It is generally recognised that spray drying is a suitable method for processing many heat sensitive materials (Broadhead et al., 1992). Generally the particles reach a maximum temperature which is well below the outlet temperature of the spray drier (Masters, 1985). The superiority of the spray drying method over the melt method for production of BFMT/PEG composites with respect to TFSA production is probably due to the short drying times and minimum exposure to heat.

4.3. Co-spray dried BFMT/PEG 20,000 and PEO 300,000 systems

The production of composites with completely amorphous PEG 4000 from systems containing 10-30% PEG and BFMT was surprising. There are few examples of PEG-amorphous drug solid dispersion systems (Law et al., 2001; Chutimaworapan et al., 2000; Aldén et al., 1992; Chatham, 1985; Frontini and Mielck, 1997a) and to our knowledge there are no examples in the literature of amorphous PEG-amorphous drug solid dispersion systems. Spray drying of PEG 4000 alone as shown in Chapter 3 did not result in an amorphous system. Chatham (1985) quenched PEG 4000 in liquid nitrogen and solid carbon dioxide in an attempt to produce amorphous material but peaks, although lower in intensity than for the starting material, were clearly evident by XRD. Chatham also investigated the effect of temperature on PEG 4000 and found that long melting periods at high temperatures were required before appreciable break up of polymer chains into lower molecular weight fragments occurred. She states that below 100°C degradation of the polymer chains is minimal. Spray drying was shown in Chapter 3 not to result in

degradation of PEG (i.e. molecular weights of PEG before and after spray drying were not significantly different). GPC of amorphous BFMT/PEG systems showed that co-spray drying PEG 4000 with BFMT did not affect the molecular weight of PEG 4000. Therefore, since degradation of the polymer is not responsible for the lack of peaks by XRD or DSC the polymer must be present in an amorphous form. To investigate whether co-spray drying BFMT with higher molecular weight polymers could also result in amorphous systems, BFMT/PEG 20,000 and BFMT/PEO 300,000 co-spray dried systems were produced. PEG 20,000 and PEO 300,000 were also spray dried alone.

4.3.1. Spray dried PEG 20,000

PEG 20,000 was spray dried from 95% ethanol as a 1% w/v solution. Spray drying conditions are given in Appendix I. The XRD scans of spray dried PEG 20,000 and PEG 20,000 starting material are shown in Figure 4.11. Spray drying PEG 20,000 alone did not result in the production of an amorphous material, the spray dried material showed slightly higher peak intensities than the starting material indicating if anything a slight increase in crystallinity.

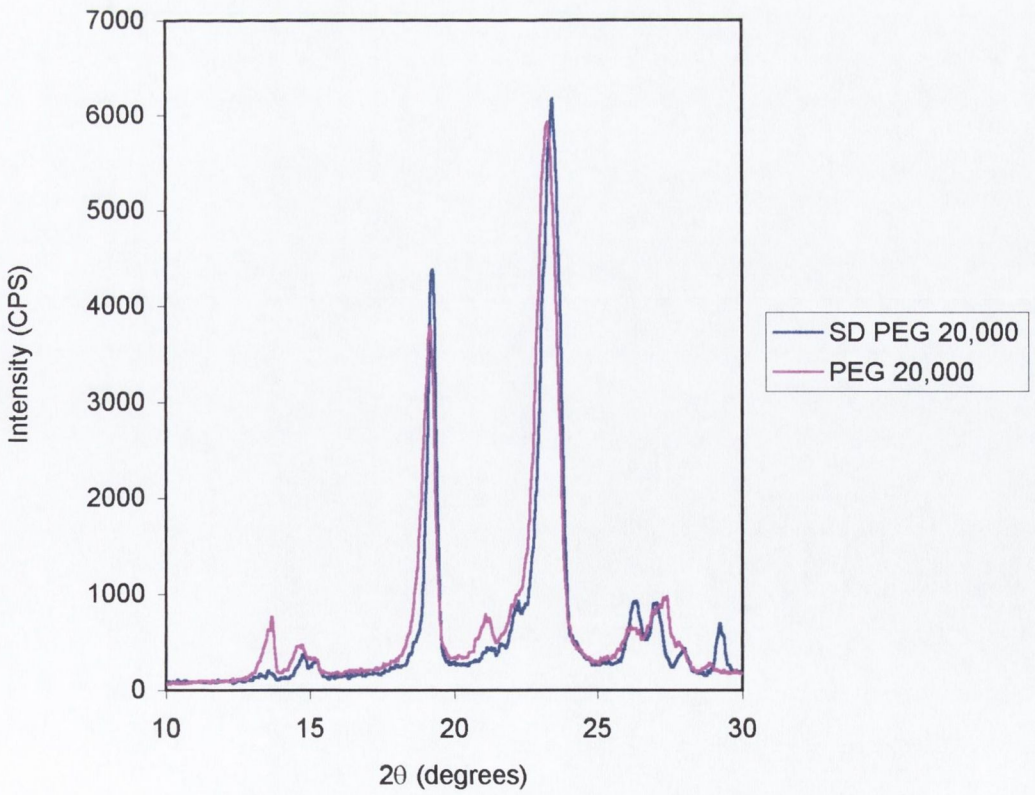

Figure 4.11 XRD scans of spray dried PEG 20,000 (SD) and PEG 20,000 starting material.

DSC scans of spray dried PEG 20,000 and PEG 20,000 starting material are shown in Figure 4.12. The starting material showed an onset melting temperature of 62.15°C, a peak melting temperature of 65.2°C and an enthalpy change due to melting of 178 J/g. The spray dried material showed an onset temperature of 62.5°C, a peak melting temperature of 67.7°C and a heat change of 184.1 J/g indicating slightly higher crystallinity.

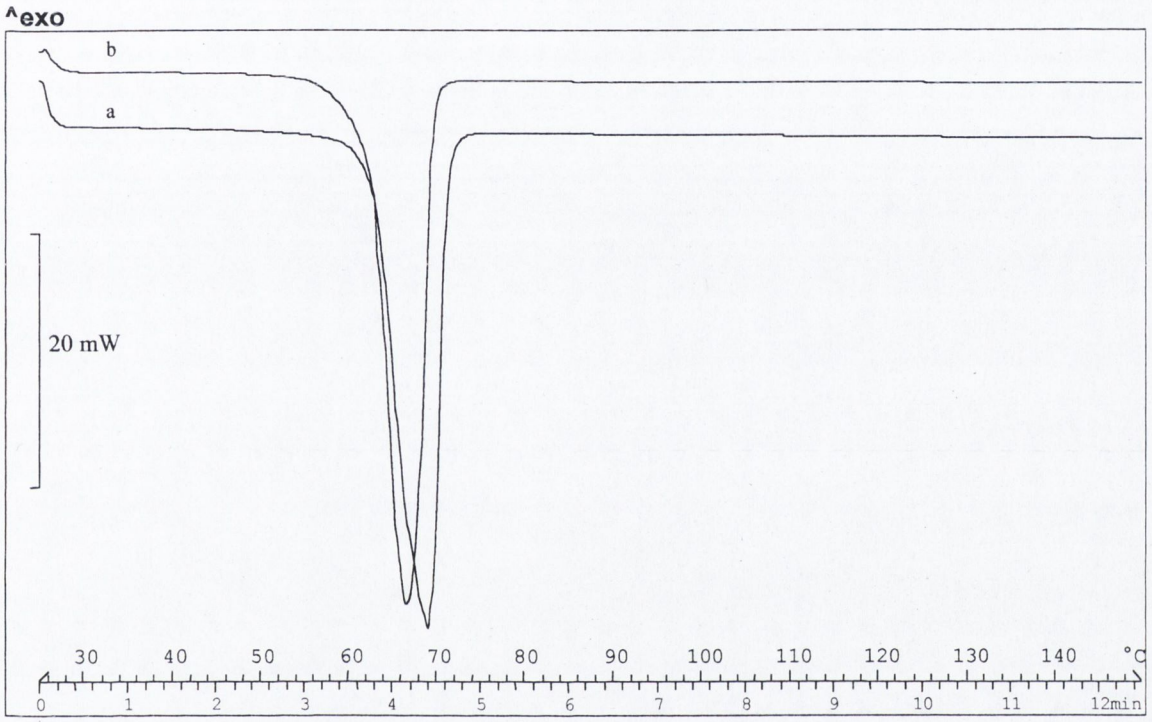

Figure 4.12 DSC scans of (a) spray dried PEG 20,000 and (b) PEG 20,000.

A SEM micrograph of spray dried PEG 20,000 is shown in Figure 4.13. Spray dried PEG 20,000 appeared to consist of fused aggregates with some aggregates appearing to be made up of many smaller spheres. Some of the aggregates were larger than 50 μm and some of the spheres were as small as approximately 2 μm in diameter.

The number average (Mn) and weight average (Mw) molecular weights by GPC of the PEG 20,000 starting material and spray dried PEG 20,000 were as follows: Mn; 10605 (+/- 704) and 11088 (+/- 158), Mw; 22869 (+/- 163) and 22921 (+/- 275), respectively. There was no significant difference in molecular weights before and after spray drying of PEG, indicating that the heat involved in the spray drying procedure did not result in any significant polymer chain breakdown (two sample t-tests; $P>0.05$).

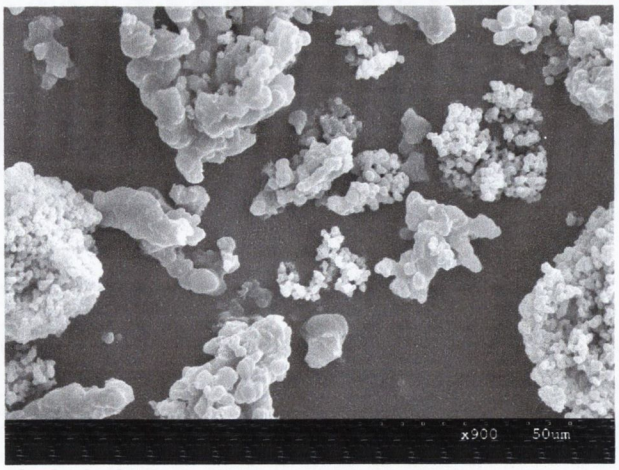

Figure 4.13 SEM micrograph of spray dried PEG 20,000.

4.3.2. Co-spray dried BFMT/PEG 20,000 systems

Systems containing 10, 20 and 30% PEG 20,000 by weight of total solids were spray dried from ethanolic solutions (as 2.5% w/v solids). Spray drying conditions are given in Appendix I. All systems showed halos by XRD with no distinct peaks indicating lack of crystallinity (Figure 4.14).

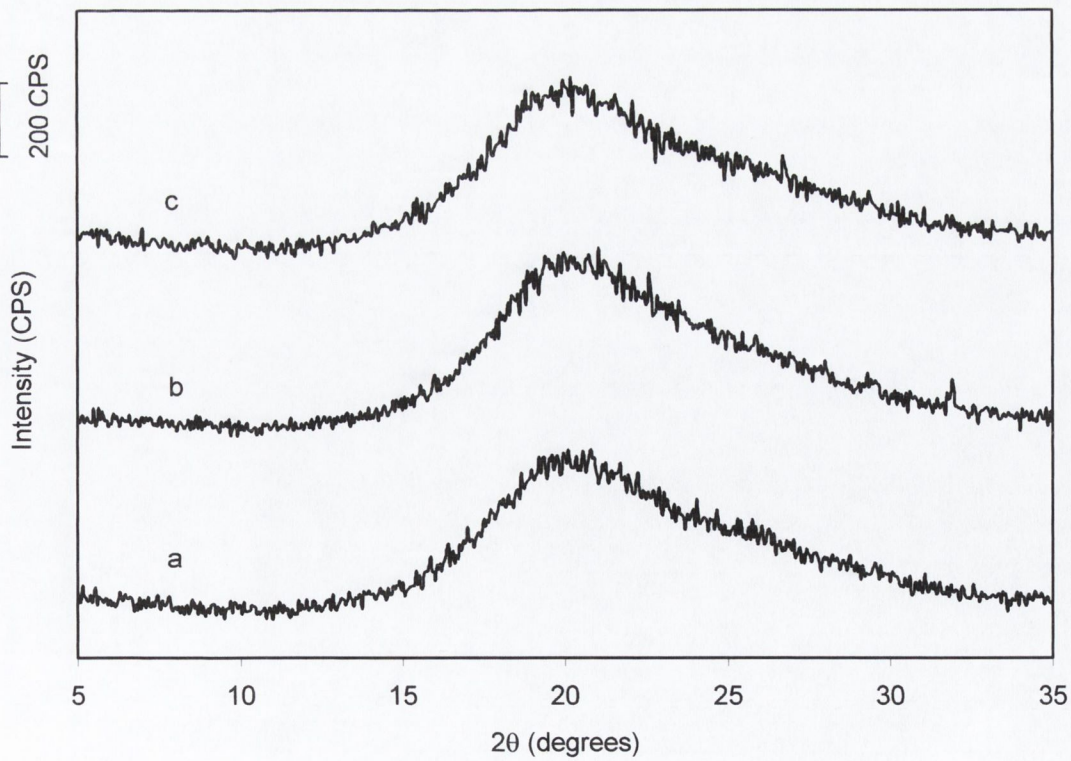

Figure 4.14 XRD scans of (a) spray dried BFMT/PEG 20,000 10%; (b) spray dried BFMT/PEG 20,000 20% and (c) spray dried BFMT/PEG 20,000 30%.

Figure 4.15 shows the DSC scans of spray dried BFMT/PEG 20,000 systems. A broad endotherm was seen for all spray dried systems in the 40-70°C regions followed by a recrystallisation exotherm and a melting endotherm. The onset temperatures for the recrystallisation exotherms decreased as the percentage of PEG 20,000 increased indicating that increasing the PEG content destabilises the system. The melting endotherms also decreased in onset temperature as the PEG content increased, similar to that which was observed for the PEG 4000 systems.

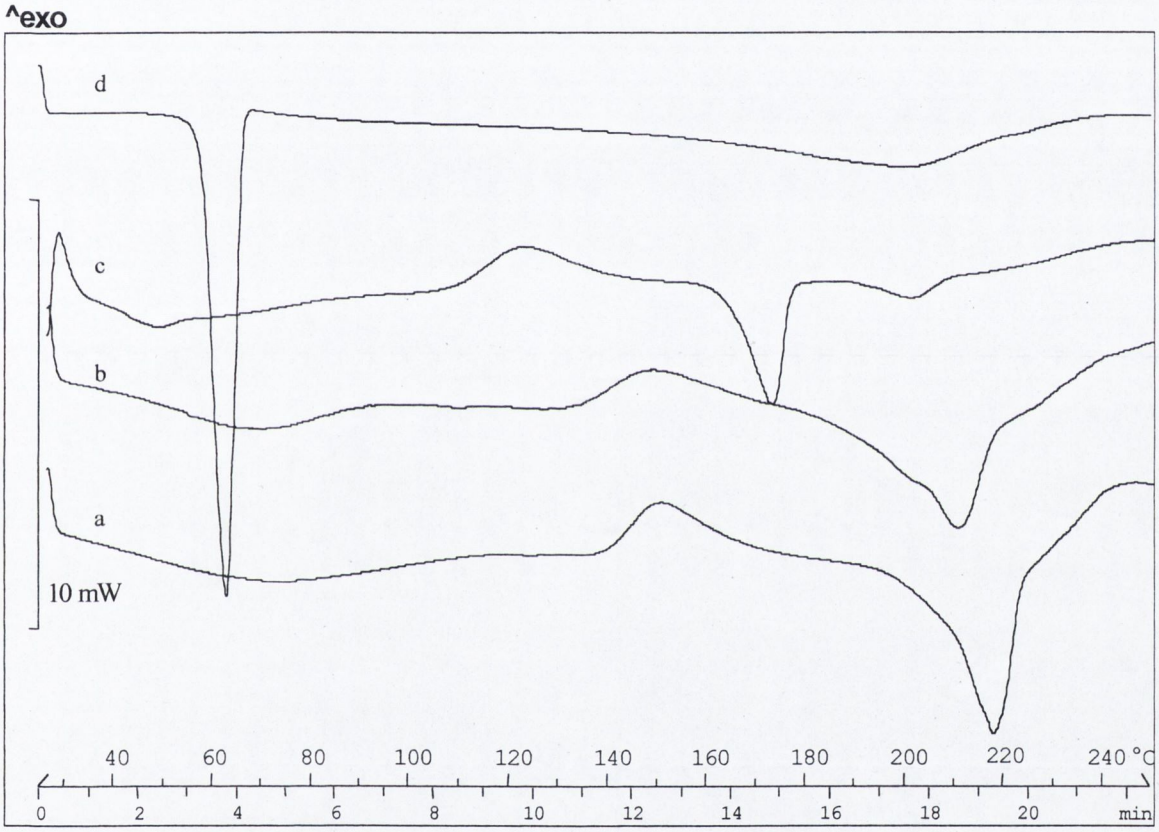

Figure 4.15 DSC scans of (a) spray dried BFMT/PEG 20,000 10%; (b) spray dried systems BFMT/PEG 20,000 20%; (c) spray dried BFMT/PEG 20,000 30% and (d) physical mix BFMT/PEG 20,000 30%.

SEM micrographs of spray dried BFMT/PEG 20,000 10%, 20% and 30% are shown in Figure 4.16 showing smooth spherical particles under 6 μm in diameter, the 10% and 20% systems showing surface indentations.

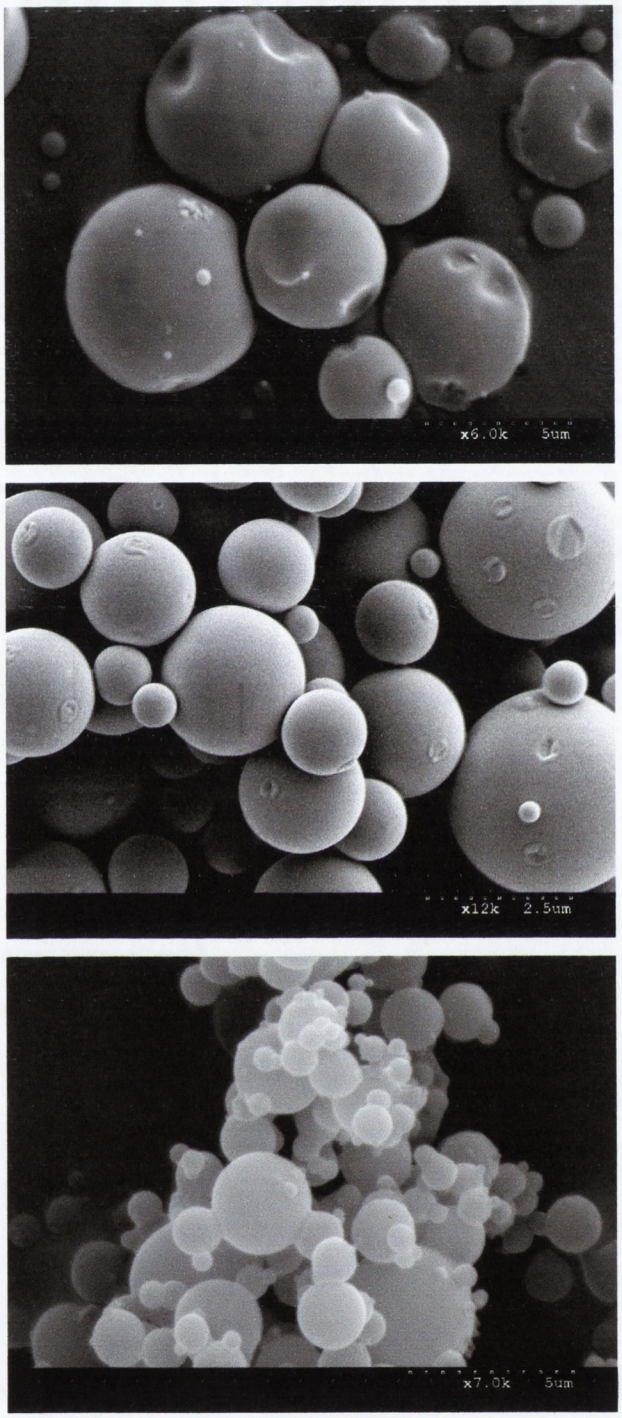

Figure 4.16 SEM micrographs of spray dried BFMT/PEG 20,000 10% (top), 20% (middle) and 30% (bottom).

4.3.3. Spray dried PEO 300,000

PEO 300,000 was spray dried from 95% ethanol as a 0.5% w/v solution. The spray drying conditions are given in Appendix I. The XRD scans of spray dried PEO 300,000 and PEO 300,000 starting material are shown in Figure 4.17. The intensity of the peaks produced by XRD of the spray dried sample were much lower than those due to the starting material indicating a reduction in polymer crystallinity.

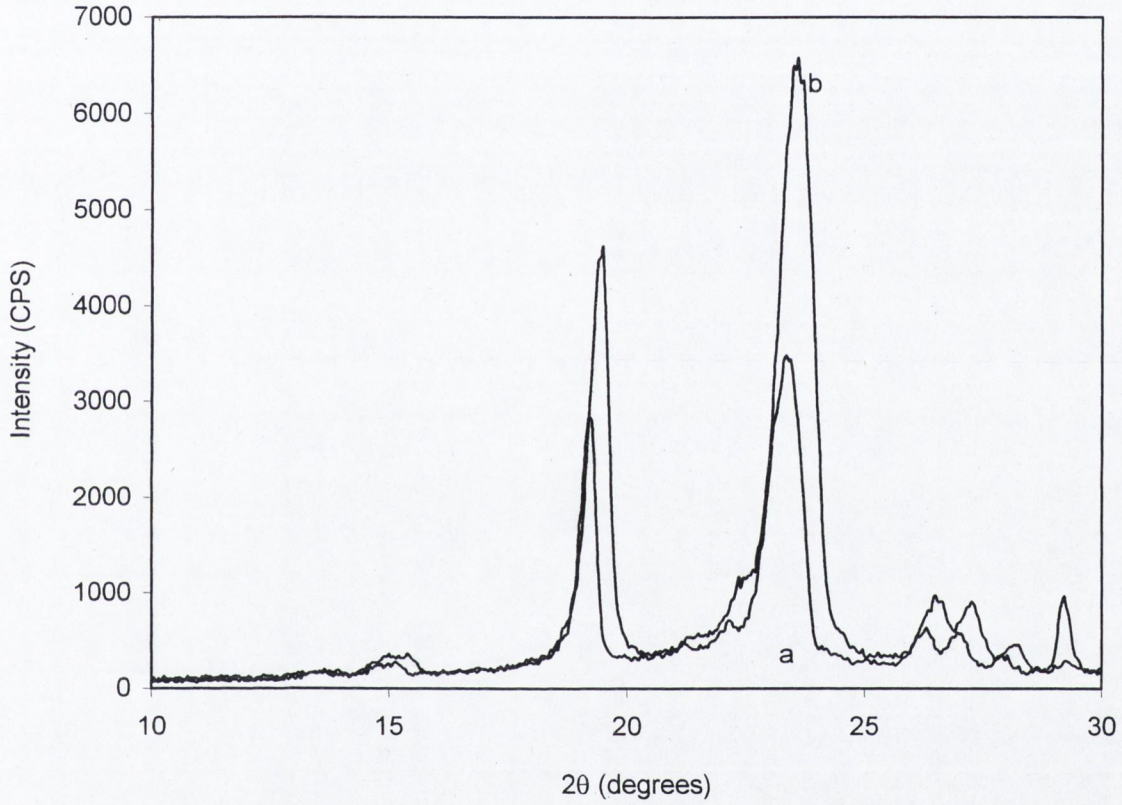

Figure 4.17 XRD of (a) spray dried PEO 300,000 and (b) PEO 300,000 starting material.

The DSC scans of spray dried PEO 300,000 and PEO 300,000 starting material are shown in Figure 4.18. The onset and peak melting temperatures and the enthalpy change due to melting were lower for the spray dried material when compared to the starting material, the enthalpy change being 139.4 J/g compared to 176.2 J/g, indicating a reduction in crystallinity on spray drying.

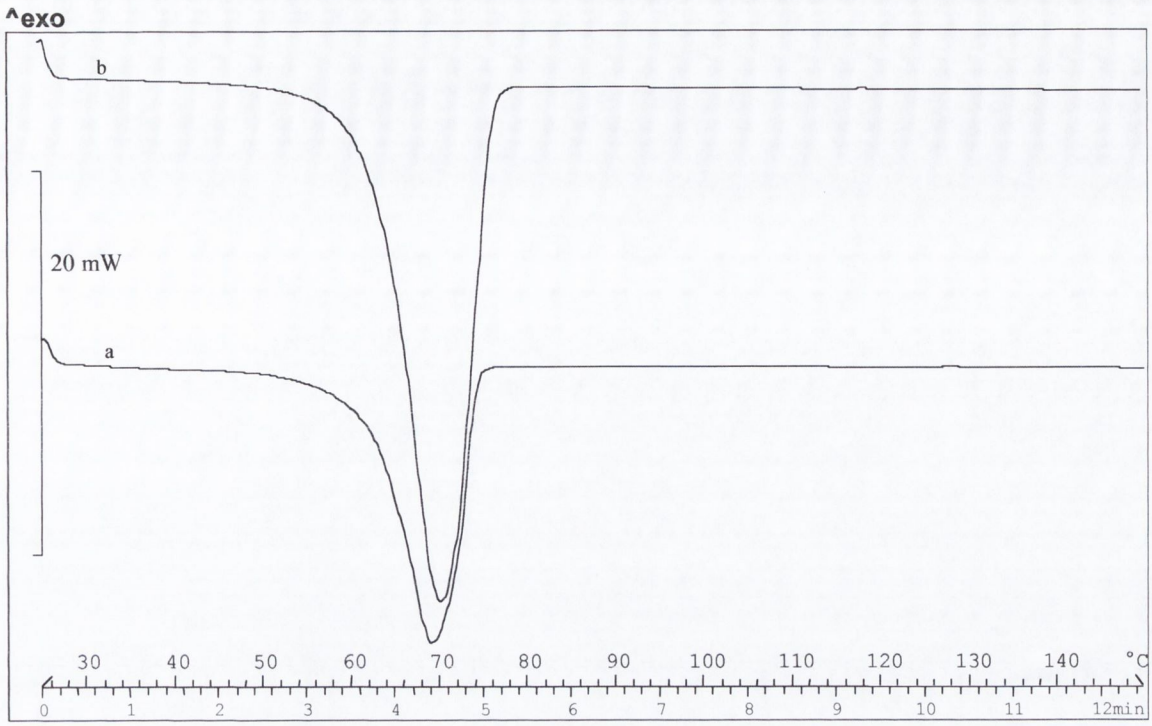

Figure 4.18 DSC scan of (a) spray dried PEO 300,000 and (b) PEO 300,000 starting material.

A SEM micrograph of spray dried PEO 300,000 is shown in Figure 4.19. Spray dried PEO 300,000 by SEM consisted of spherical particles approximately 2-8 μm in diameter. Also present were fibre-like particles.

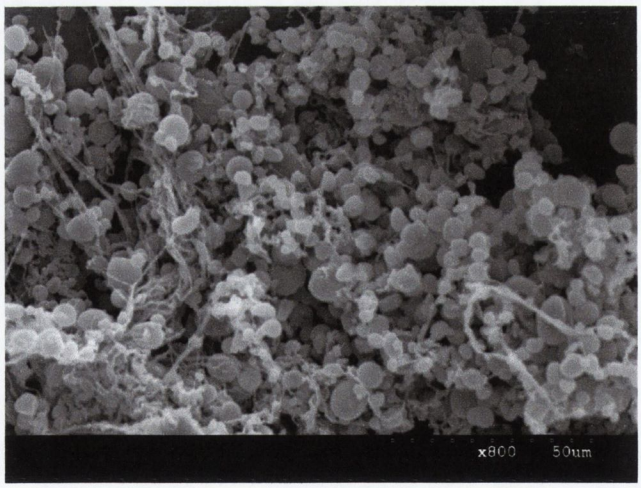

Figure 4.19 SEM micrograph of spray dried PEO 300,000.

The number average (Mn) and weight average (Mw) molecular weights by GPC of the commercial PEO and spray dried PEO were as follows: Mn; 46,011 (+/- 8457) and 13,378 (+/- 6565), Mw; 547,649 (+/- 108541) and 662,032(+/-68,944), respectively. There was a significant difference in number average molecular weights before and after spray drying

of PEO. There was no significant difference in weight average molecular weight (two sample t-tests; $P>0.05$). Chain scission of a polymer results in a larger number of smaller molecular weight species. Number average molecular weight is calculated based on "sharing" the total weight, of all the species present, equally amongst each of the species. Therefore an increase in the number of species can result in large differences in the calculated number average molecular weights. The weight average molecular weight does not "count" species just by their number but takes into consideration their total weight. Therefore a small increase in the number of species due to a small amount of chain scission will not affect the weight average molecular weight to as large an extent as it would the number average molecular weight. The difference in number average molecular weight before and after spray drying PEO is consistent with some chain scission having occurred.

4.3.4. Co-spray dried BFMT/PEO 300,000 systems

A BFMT/PEO system containing 10% PEO 300,000 by weight of total solids was spray dried from ethanolic solution as a 2.5% w/v solution. Spray drying conditions are given in Appendix I. XRD scans of the spray dried system showed a diffuse halo indicating that the spray dried system was amorphous (Figure 4.20 (scan a)).

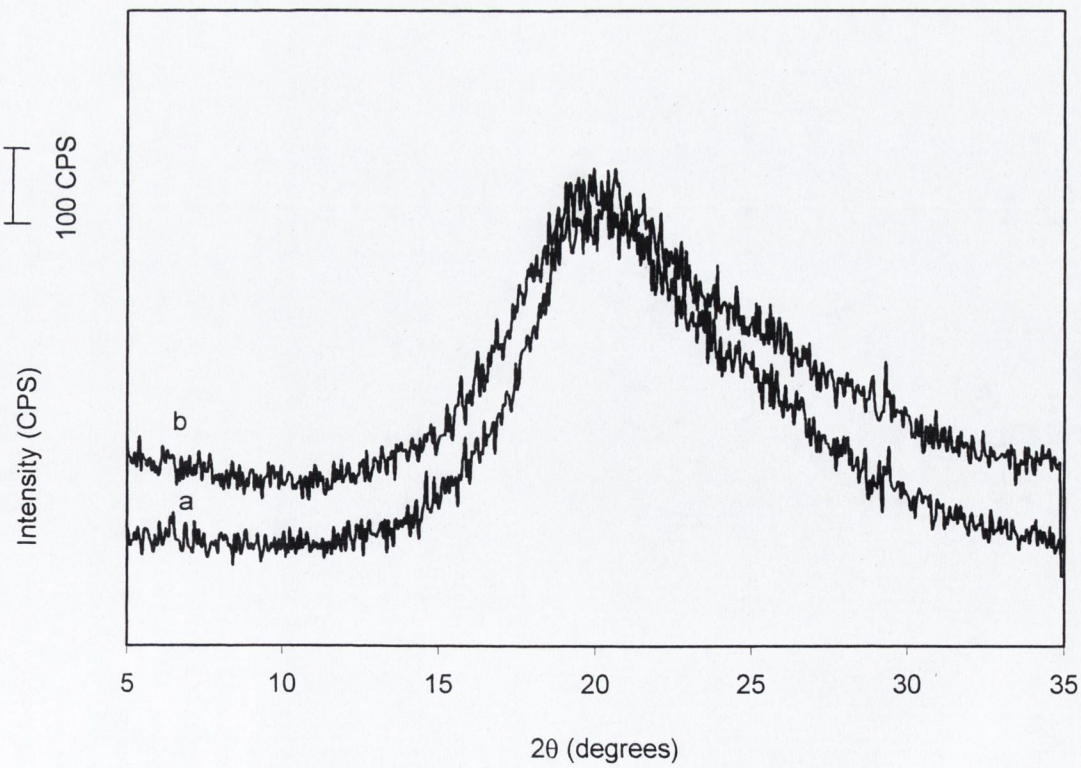

Figure 4.20 XRD of (a) spray dried BFMT/PEO 300,000 10% and (b) spray dried BFMT/PEO 300,000 30%.

DSC scans showed no distinctive peak indicative of melting of PEO. An exotherm indicative of recrystallisation of amorphous material prior to the BFMT melting endotherm was observed (Figure 4.21 (scan a)).

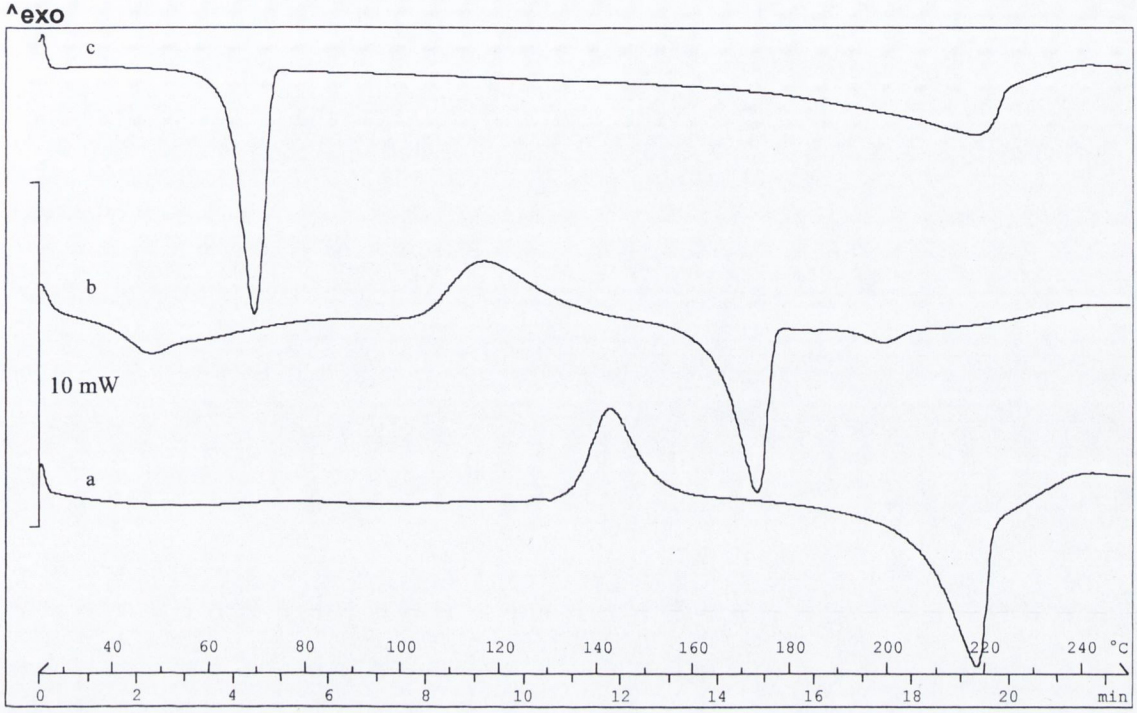

Figure 4.21 DSC scan of (a) spray dried BFMT/PEO 300,000 10%; (b) spray dried BFMT/PEO 300,000 30% and (c) physical mix BFMT/PEO 300,000 30%.

The SEM micrograph is shown in Figure 4.22. The differing particle morphologies by SEM indicated that the system may not have been homogeneous. It was thought that it may have consisted of pure BFMT particles represented by the smooth spheres, particles consisting of mixtures of BFMT and polymer represented by the particles with the folded surfaces, and particles composed of pure polymer represented by the long fibre-like particles. Spray drying of PEO 300,000 alone had produced long fibre-like particles (Figure 4.19) while spray drying of PEG 4000 alone resulted in particles with a folded "convoluted" surface (Chapter 3).

The BFMT/PEO 300,000 10% system was investigated further by energy dispersive x-ray analysis (EDXA). Figure 4.23 shows the EDXA map of sulphur atoms detected in the BFMT/PEO 10% system spray dried as a 2.5% w/v solution. The presence of sulphur atoms in particles of all types confirmed the presence of BFMT and was consistent with the existence of drug in all the different particle morphologies.

Figure 4.22 SEM micrograph of BFMT/PEO 300,000 10% spray dried as a 2.5% w/v solution.

A physical mix of BFMT and PEO was prepared and EDXA was performed on the sample, the scan is shown in Figure 4.23 (right). The "X" symbols show areas where PEO particles were present and therefore where no sulphur was detected (apart from background counts).

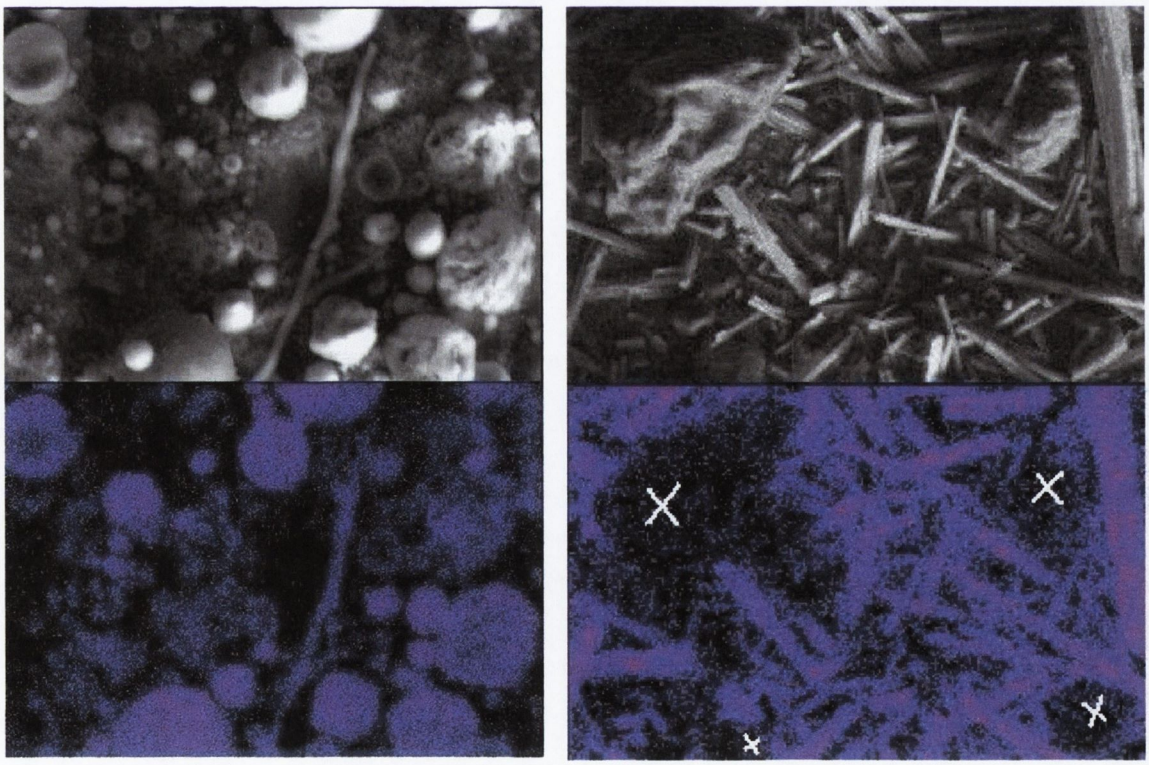

Figure 4.23. EDXA map of sulphur atoms present in BFMT/PEO 300,000 10% spray dried as a 2.5% w/v solution (left) and sulphur atoms present in a physical mix of BFMT/PEO 10% (right). X symbols correspond to regions where PEO particles are present and therefore sulphur is not detected (apart from low background counts). The top pictures show SEM micrographs, of the samples being analysed, and the bottom pictures show the areas of detectable sulphur.

Clarke et al. (1998) investigated spray drying of polylactic acid and polylactic-co-glycolic acid microspheres and found that for high molecular weight polymers, microparticle formation was only possible at lower viscosity, involving spray drying at lower feed concentrations. At higher feed concentrations fibres were formed. Therefore the BFMT/PEO 10% system was prepared a second time using a lower feed concentration of 0.8% w/v. This resulted in microspherical particles without the presence of fibre-like material (Figure 4.24). XRD and DSC scans of the BFMT/PEO 10% system spray dried as a 0.8% w/v solution were similar to those obtained for the equivalent 2.5% w/v system. A BFMT/PEO 300,000 30% system was also spray dried, at a feed concentration of 0.8% w/v, and SEM showed homogeneous spheres were produced (Figure 4.24).

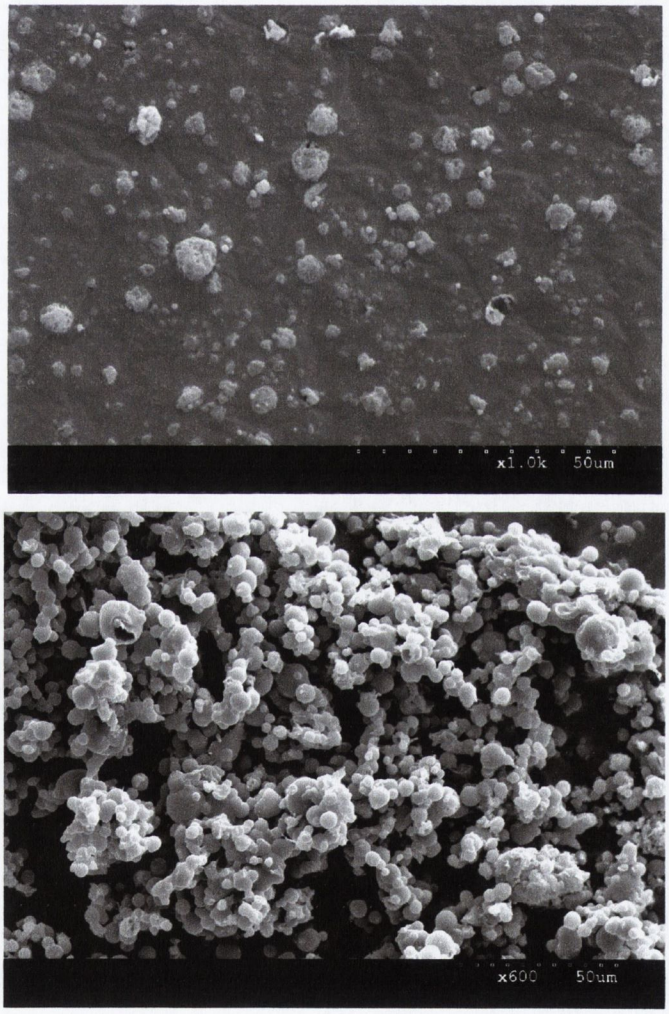

Figure 4.24 SEM micrograph of BFMT/PEO 300,000 10% spray dried as a 0.8% w/v solution (top) and BFMT/PEO 300,000 30% spray dried as a 0.8% w/v solution (bottom).

The DSC scans of the spray dried and physical mix 30% PEO systems were shown in Figure 4.21. The spray dried 30% PEO system did not show a sharp PEO melting

endotherm. Instead a small broad endotherm was visible at approximately 45°C which could be due to melting of some crystalline PEO, however the endotherm was greatly reduced in enthalpy change and had a much lower melting temperature than the equivalent physical mix (also shown in Figure 4.21). An exotherm was seen indicative of recrystallisation of amorphous BFMT. This occurred at a lower temperature than in the spray dried 10% system which indicates that the amorphous phase present in the 30% system may be less stable than in the 10% spray dried system. The melting endotherm observed in the spray dried 30% system was also shifted to a lower temperature than in the physical mix or 10% spray dried system which indicates that not all the BFMT may have recrystallised and that the melting may be due to the amorphous form. Chiou and Niazi (1971) described a broader lower onset melting point for sulfathiazole urea solid dispersions when compared to the equivalent physical mix and described that this was due to the sulfathiazole being present in the amorphous form (even though a small exotherm was observed earlier in the thermal scan). They described that the presence of crystalline forms of both urea and sulfathiazole in the solid dispersion should not result in a considerable decrease in the thaw point and a wider range of melting. Their claim of amorphous sulfathiazole being present as opposed to a solid solution was substantiated by differential thermal analysis (DTA) studies and XRD studies on aged systems which showed increasing melting temperatures by DTA and appearance of peaks due to sulfathiazole by XRD implying the recrystallisation over time of the amorphous drug.

4.4. Phase Diagrams

Phase diagrams are used to characterise the phases present in binary systems. Phase diagrams produced from melting data obtained from thermal analysis of physical mixtures have been shown to correlate well with those produced from fused or evaporated mixtures (Guillory et al., 1969). Physical mixes of BFMT/PEG 4000 were prepared and heated by DSC. Melting point data was obtained from the heating cycle as opposed to the cooling cycle since BFMT degrades when heated past its melting point. Both onset melting temperatures and peak melting temperatures were plotted separately against mole fraction PEG (based on unit molecular weight PEG).

Eutectic systems are two phase systems where the two components are miscible in all proportions in the liquid state but are totally immiscible in the solid state (Reisman, 1970). The eutectic point is the composition which gives the lowest melting point which is below

that of either of the two pure components and when that composition melts it gives a single melting event.

The solubility of an ideal solid is given by Equation 4.1.

$$\ln X = \frac{Hm}{R}\left(\frac{1}{T} - \frac{1}{T_1}\right) \qquad \text{Equation 4.1}$$

where X is the ideal mole fraction solubility, Hm is the enthalpy of fusion, R is the gas constant, T is the temperature and T_1 is the melting point.

Application of Equation 4.1 to both components of a mixture and rearrangement results in Equation 4.2 and Equation 4.3, the Le Chatelier-Schroder-van Laar equations (Smith, 1976) which describe the melting curves of eutectic binary systems.

$$\text{Melting curve Ta: } T = \frac{MPa}{1 - \frac{RMPa}{Ha}\ln X} \qquad \text{Equation 4.2}$$

where MPa is the melting temperature of component a and Ha is the enthalpy change of component a.

$$\text{Melting curve Tb: } T = \frac{MPb}{1 - \frac{RMPb}{Hb}\ln(1 - X)} \qquad \text{Equation 4.3}$$

where MPb is the melting temperature of component b and Hb is the enthalpy change of component b.

For BFMT and PEG the values of the melting point and the heat of fusion were determined experimentally and used to generate the phase diagram using Equation 4.2 and Equation 4.3. R, the gas constant was 8.315. The experimentally derived melting temperature and heats of fusion used to generate the phase diagram are shown in Table 4.1.

Table 4.1. Values used in equation for production of simulation of BFMT/PEG 4000 phase diagram. Values of Ha (enthalpy change of component a) and MPa (melting point of component a) were obtained from DSC scans of PEG 4000. Values of Hb (enthalpy change of component b) and MPb (melting point of component b) were obtained from DSC scans of BFMT. CoDet is the coefficient of determination, the values produced by MicroMath® Scientist® for sum of squared observations and CoDet are shown for the physical mix data fitted to the simulated line.

Melting data type used	Ha (J/mol)	Hb (J/mol)	MPa (K)	MPb (K)	Sum of squared observations	CoDet
Peak melting temperature	8448	44925	334.04	503.36	2951510	0.676
Onset melting temperature	8448	44925	330.68	498.88	2678426	0.927

Firstly peak melting temperature data was simulated and the simulation together with the actual data points for physical mixes and spray dried systems is shown in Figure 4.25. The simulation did not resemble a eutectic system and the peak melting data did not fit the simulated line very well giving a sum of squared observations and a coefficient of determination value of 2,951,510 and 0.676 respectively.

The peak melting point data from the spray dried samples appeared to better fit the simulated line than data from the equivalent physical mixes (Figure 4.25) giving sum of squared observations and coefficient of determination values of 986,495 and 0.991 respectively.

The experimental values for the physical mix systems tended to be above those predicted by the simple eutectic model. Onset melting data is generally taken as the true melting temperature rather than peak melting temperature since peak melting temperature is only the temperature at which the difference between sample and reference is largest. Therefore onset melting temperature data was plotted versus composition and the predicted profile from Equation 4.2 and Equation 4.3 is shown in Figure 4.26 together with the actual data points for physical mixes and spray dried systems. The sum of squared observations and coefficient of determination values produced from fitting the onset melting physical mix data were quite good, being 2,678,426 and 0.927 respectively. The sum of squared observations and coefficient of determination values obtained when onset melting data from spray dried systems was fitted to the simulated eutectic equation were 965,019 and 0.991 respectively.

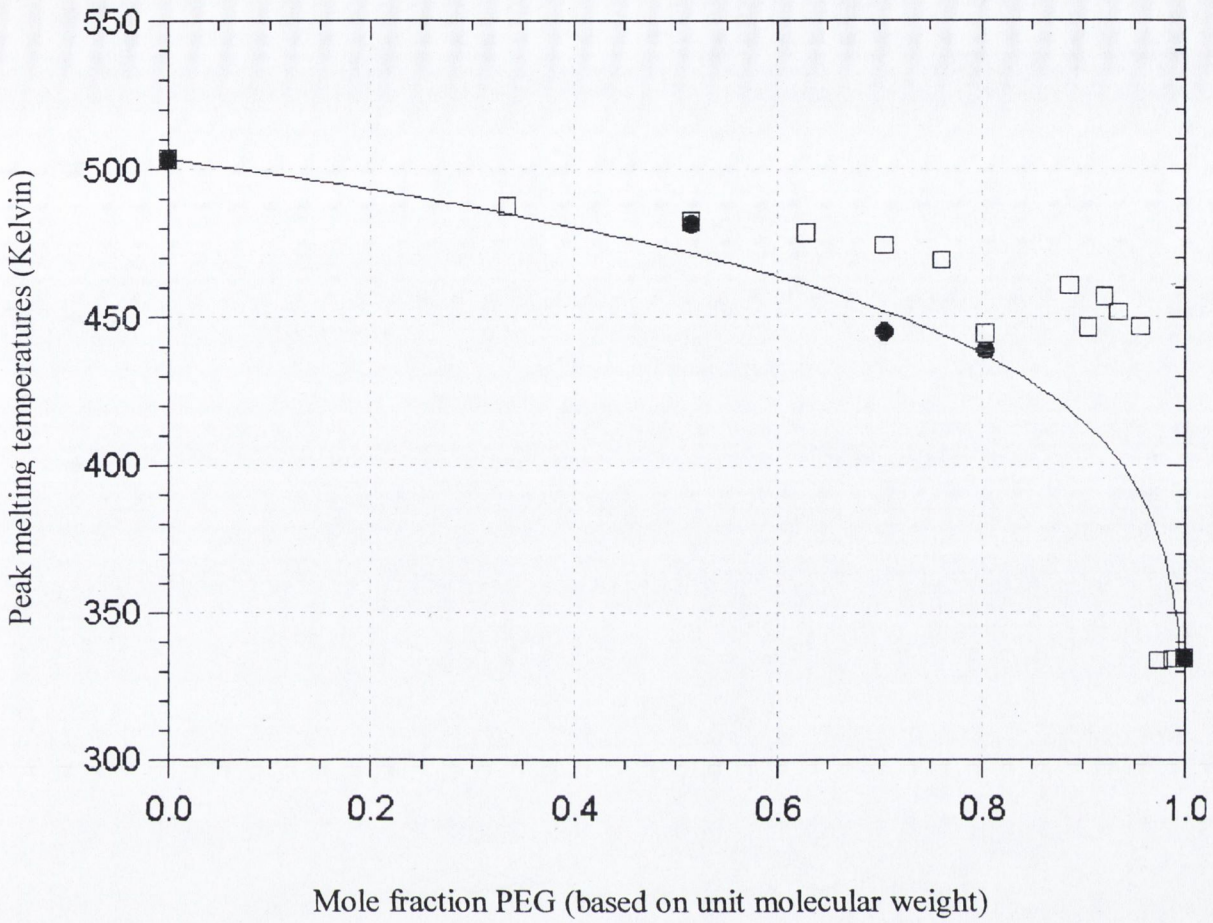

Figure 4.25. MicroMath® Scientist® simulation of BFMT/PEG 4000 eutectic system and actual data for physical mixes and spray dried BFMT/PEG 4000 systems obtained using peak melting temperatures.

□ = data from physical mixes

● = data from spray dried systems

——— = simulation

The phase diagrams did not resemble simple eutectic systems as shown schematically in Chapter 1. Monotectic systems have been described by several authors (Kaur et al., 1980; Chatham, 1985; Craig, 1989; Venkataram and Rogers, 1984 and Najib et al., 1989). Monotectic systems have been described as eutectic systems where one "arm" of the diagram is missing and the lower melting component replaces the eutectic composition. The BFMT/PEG phase diagrams appeared to resemble monotectic systems. However closer examination of Figure 4.26 gives Figure 4.27, an expansion of the right side of Figure 4.26. The system does in fact conform to a eutectic profile with the eutectic point being reached when the mole fraction PEG is 0.996.

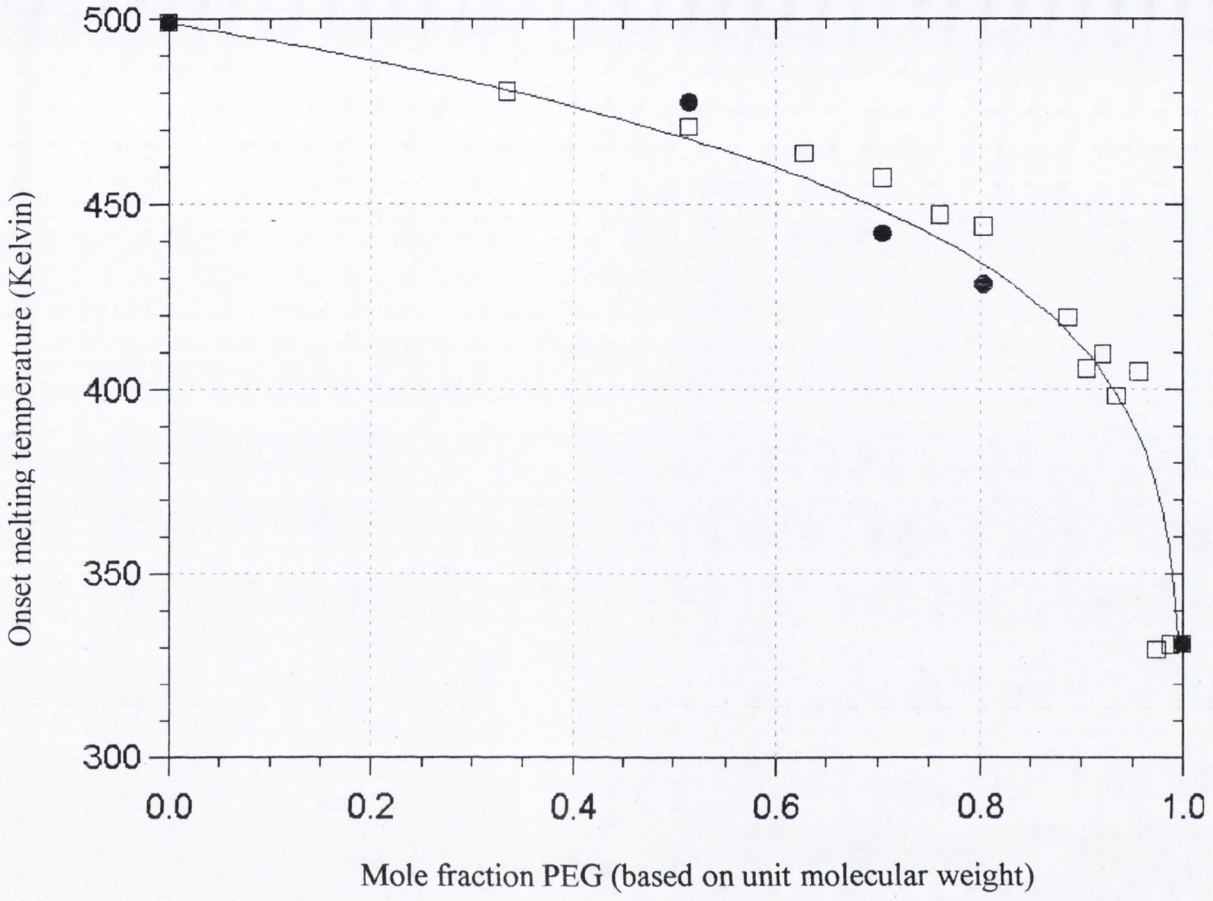

Figure 4.26. MicroMath® Scientist® simulation of BFMT/PEG 4000 eutectic system and actual data for physical mixes and spray dried BFMT/PEG 4000 systems obtained using onset melting temperatures.

□ = data from physical mixes

● = data from spray dried systems

——— = simulation

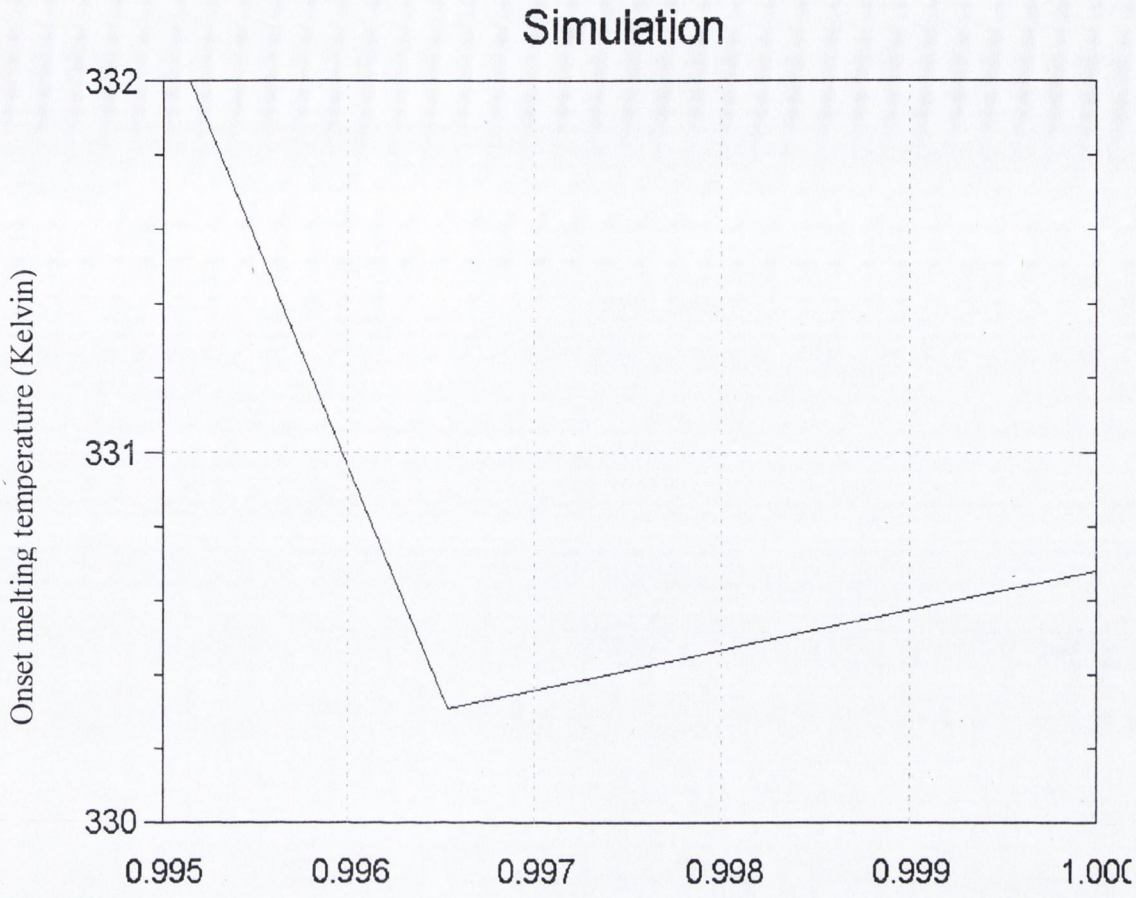

Figure 4.27. Expansion of Figure 4.26 showing MicroMath® Scientist® simulation of BFMT/PEG 4000 eutectic system obtained using onset melting temperatures.

4.5. Conclusions

Spray drying of BFMT with the normally crystalline polymer PEG, at concentrations of 10, 20 and 30% PEG by weight of BFMT, can result in amorphous composites. Spray drying results in no significant production of the main BFMT degradant, TFSA, and for composites consisting of 90% PEG 4000 by weight of total solids spray drying appears a superior method of production than the melt method which results in significant BFMT degradation.

The physical stability of amorphous BFMT is reduced on inclusion of PEG 4000, recrystallisation occurring more quickly with increasing amount of PEG 4000 in the composites.

All BFMT/PEG compressed discs showed initial increased release of BFMT compared to discs of micronised BFMT alone with the spray dried BFMT/PEG 4000 10% system showing initial rates two to three times that of BFMT alone.

When the molecular weight of PEG was increased the resultant systems were also amorphous. The morphology of the particles produced remained smooth and spherical except for the spray dried BFMT/PEO 300,000 systems spray dried as a 2.5% w/v solutions which showed non-homogeneous shaped particles. On spray drying at a lower feed concentration homogeneous spherical particles were produced. Spray drying PEG 20,000 and PEO 300,000 from ethanol does not result in the production of completely amorphous polymers.

The BFMT/PEG systems are thought to form eutectic mixtures where both components are completely miscible when liquid but solidify on cooling as two separate phases.

SPRAY DRIED DRUG MIXTURES FOR USE IN DRY POWDER INHALER FORMULATIONS

5.1. Introduction

In Chapter 4 it was shown that processing of the model drug BFMT with excipients by spray drying could result in the production of very small uniformly shaped particles, depending on the concentration of polymer used. Spray drying should prove a useful method for the production of mixtures of powders for use in dry powder formulations for inhalation since, not only does spray drying result in the production of an intimate mix of components (solid dispersions), but the solids produced are often microspherical (thereby potentially resulting in systems with good flow properties), are of a narrow particle size distribution, and the particles produced are often in the inhalation size range (0.5-5 μm aerodynamic diameter). The move away from pressurised aerosol formulations, due to restriction in chlorofluorocarbon production and use, has led to an increased interest in dry powder inhaler formulations as inhalable delivery systems. A major drawback of the standard pressurised metered dose inhaler (pMDI) lies in the necessity for synchronisation of discharge from the device and inspiration. Ganderton and Jones (1992) state that as many as 30% of users are unable to use the device effectively even after careful instruction. An advantage of dry powder inhaler (DPI) systems is that the patient's inspiration provides the energy to fluidise the dose thus avoiding the problem of synchronisation of discharge with inspiration. Typically DPI formulations consist of a micronised active mixed with an inert diluent or carrier, such as lactose, to facilitate dispersion (Ganderton and Jones, 1992). When formulations consisting of more than one active are to be produced, good mixing is essential to ensure dose uniformity.

The use of spray drying to produce powders of drugs used in the treatment of asthma was investigated. Already marketed is a pressurised inhalation combination formulation of salbutamol:ipratropium bromide, used in a 5:1 ratio in Combivent™, Boehringer Ingelheim. This formulation contains chlorofluorocarbons and therefore alternative formulations need to be developed. Salbutamol:ipratropium bromide systems produced by spray drying were investigated for potential use in dry powder inhalers as an alternative to the pressurised aerosol formulation.

5.2. Salbutamol and ipratropium bromide systems

Salbutamol sulphate, salbutamol base and ipratropium bromide monohydrate (the monohydrate being the form used in the commercial Combivent™ formulation) were supplied as micronised crystalline powders. They were spray dried alone from ethanolic solutions and from aqueous solutions (except for the salbutamol base which was not soluble in water). 10:1, 5:1 and 2:1 weight ratios of salbutamol (as the sulphate or the base):ipratropium bromide monohydrate were spray dried. Appendix I lists the conditions used for spray drying the various systems.

5.2.1. Salbutamol sulphate

The XRD scans of crystalline salbutamol sulphate and spray dried salbutamol sulphate (from both solvents) are shown in Figure 5.1. Salbutamol sulphate was spray dried from a 75% ethanol 25% aqueous solution due to its low solubility in ethanol.

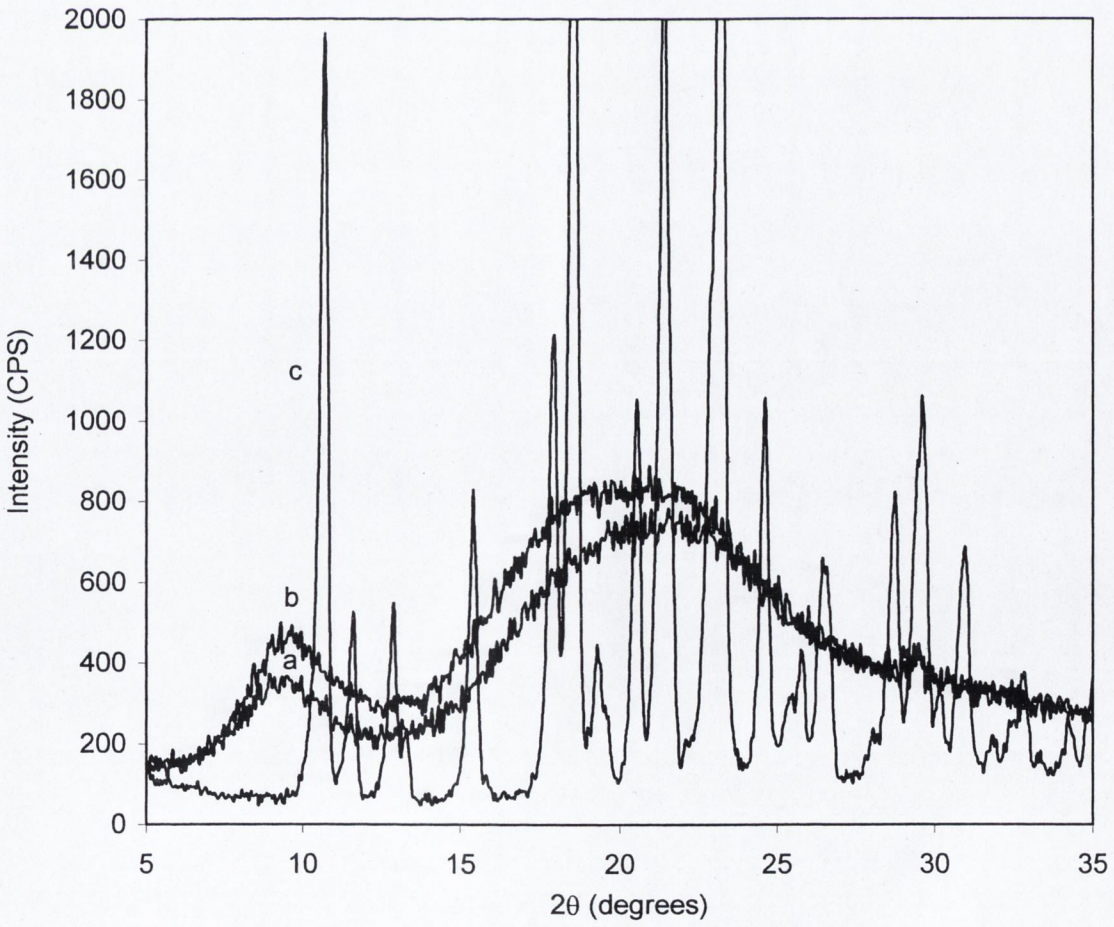

Figure 5.1 XRD scan of (a) salbutamol sulphate spray dried from ethanolic solution (75%); (b) salbutamol sulphate spray dried from aqueous solution and (c) salbutamol sulphate starting material.

Salbutamol sulphate spray dried from aqueous solution resulted in the production of an amorphous system evidenced by the halo shown by XRD. The production of amorphous salbutamol sulphate on spray drying from aqueous solution was previously reported by Chawla et al. (1994). Spray drying of salbutamol sulphate from ethanolic solution also yielded an amorphous system as indicated by the broad halo and lack of peaks indicative of crystallinity by XRD.

DSC scans of salbutamol sulphate and spray dried salbutamol sulphate systems are shown in Figure 5.2. The starting material showed a melting peak which had an onset temperature at approximately 200°C. Ward and Schultz (1995) found salbutamol sulphate melted by DSC with degradation near 200°C.

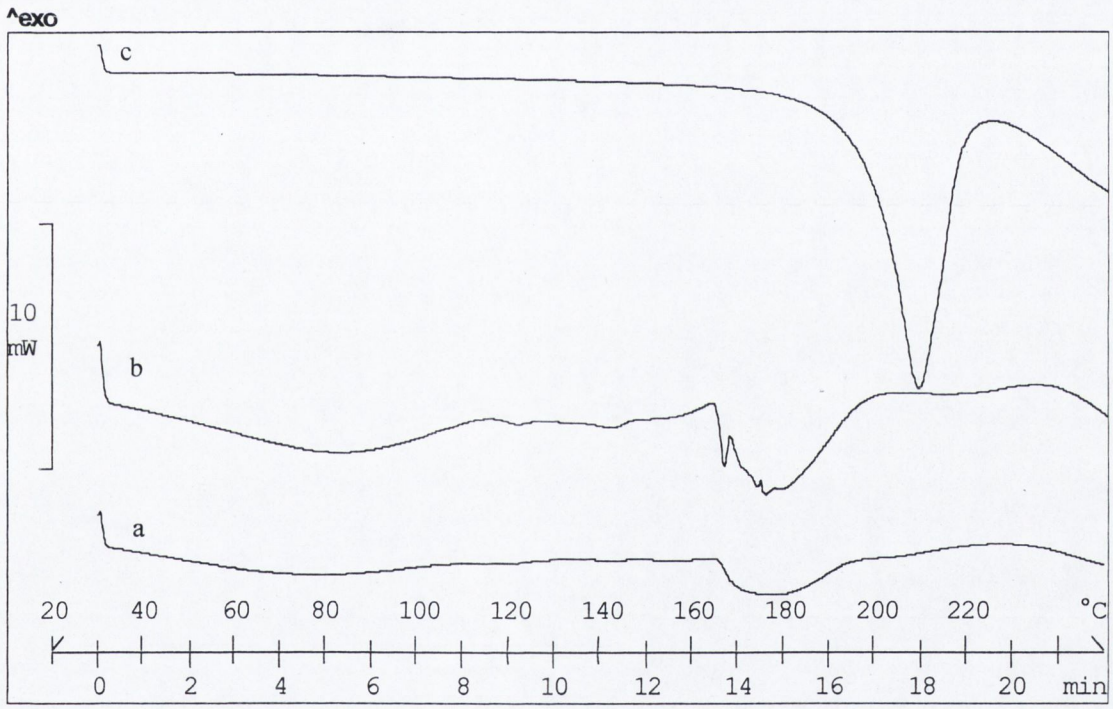

Figure 5.2 DSC scans of (a) spray dried salbutamol sulphate spray dried from ethanolic solution (75%); (b) salbutamol sulphate spray dried from aqueous solution and (c) salbutamol sulphate starting material.

The spray dried salbutamol sulphate systems (from both solvents) showed no obvious exotherms by DSC which would indicate recrystallisation of the amorphous form. This could indicate that the amorphous systems were relatively stable on heating. Broad endotherms, consistent with melting, were observed with onset temperatures at approximately 160°C. Hot stage microscopy of the spray dried samples showed melting at approximately 145°C. Chiou and Niazi (1971) described broad endotherms due to melting of sulfathiazole in sulfathiazole/urea solid dispersions, the broad appearance of the melting

endotherm indicating an increase in disorder of the system. No sharp crystalline melting peaks were observed. Ward and Shultz (1995) micronised salbutamol sulphate using an air jet micronisation technique. The micronised material was not X-ray amorphous, showing only minor differences in peak intensities. A small exotherm was detected by DSC for the micronised material followed by a melting endotherm occurring at approximately 200°C (a heating rate of 10°/minute was employed, the same as that used for DSC of the spray dried salbutamol sulphate analysed in this thesis). It is likely that the crystalline material present in their micronised sample acted as seed crystals promoting the recrystallisation of any amorphous material which was present. The lack of visible exotherms, together with the lower and broader melting endotherms, obtained by DSC of spray dried salbutamol sulphates, indicated that the materials remained amorphous on heating.

FTIR of the samples spray dried from ethanolic and aqueous solution showed similar spectra but differed from salbutamol sulphate starting material in the OH region (3100-3600 cm^{-1}) (Appendix VIII). Peaks in the OH region are indicative of the presence of water molecules (Lin-Vien et al., 1991). Nguyen et al. (1994) and Ledwidge et al. (1996) described peaks in this region for carbovir hydrates and diclofenac N-(2-hydroxyethyl)pyrrolidine hydrate respectively. Morris et al. (1994) described sharp absorption bands in this region for some polymorphs of SQ-33600 as indicative of the OH stretching mode associated with either strongly bound or crystalline water. This band was evident in samples stored at their lowest humidity storage condition of 6% relative humidity. The non specific desolvation found by TGA and the absence of a dehydration endotherm by DSC indicated the presence of noncrystalline water. Spray dried salbutamol sulphate systems were amorphous and amorphous forms are known to be hygroscopic, therefore the change in the FTIR spectra of the spray dried materials relative to the equivalent physical mixes were consistent with the absorption of water by the amorphous system. The broad endotherm in the DSC scan prior to 100 °C and the low temperature weight loss by TGA (Figure 5.3) indicated the presence of absorbed moisture in the sample. No dehydration endotherms were observed by DSC indicating the absence of hydrate formation in the spray dried systems. Chawla et al. (1994) spray dried salbutamol sulphate from aqueous solution and compared the infrared spectra to that of their starting material. They concluded that spray drying did not appear to alter salbutamol sulphate chemically. HPLC of spray dried salbutamol sulphate was performed and indicated that spray dried salbutamol sulphates were not altered chemically by the process. IVAX Pharmaceuticals also analysed the spray dried systems and found the process not to result in a significant increase in degradation products. EDXA detected sulphur atoms in the

spray dried material consistent with the spray dried material remaining as the sulphate salt form (Appendix VII).

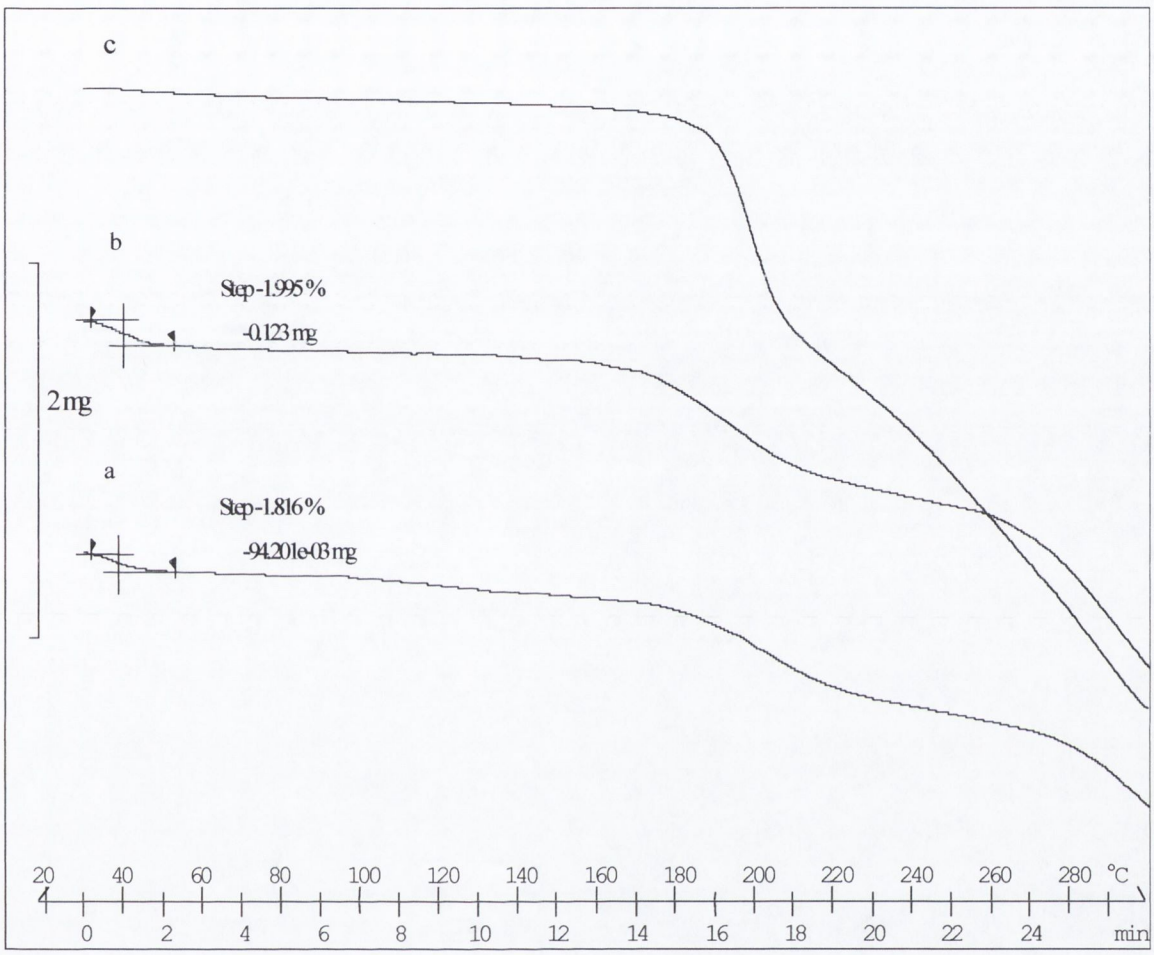

Figure 5.3 TGA scans of (a) salbutamol sulphate spray dried from ethanolic solution; (b) salbutamol sulphate spray dried from aqueous solution and (c) salbutamol sulphate starting material.

SEM micrographs of the spray dried material showed small spherical particles with diameters ranging from approximately 1 to 7 μm for the aqueous spray dried salbutamol sulphate system and approximately 1 to 3 μm for particles produced from ethanolic solvent (Figure 5.4). The surfaces of the particles in both cases were slightly dimpled.

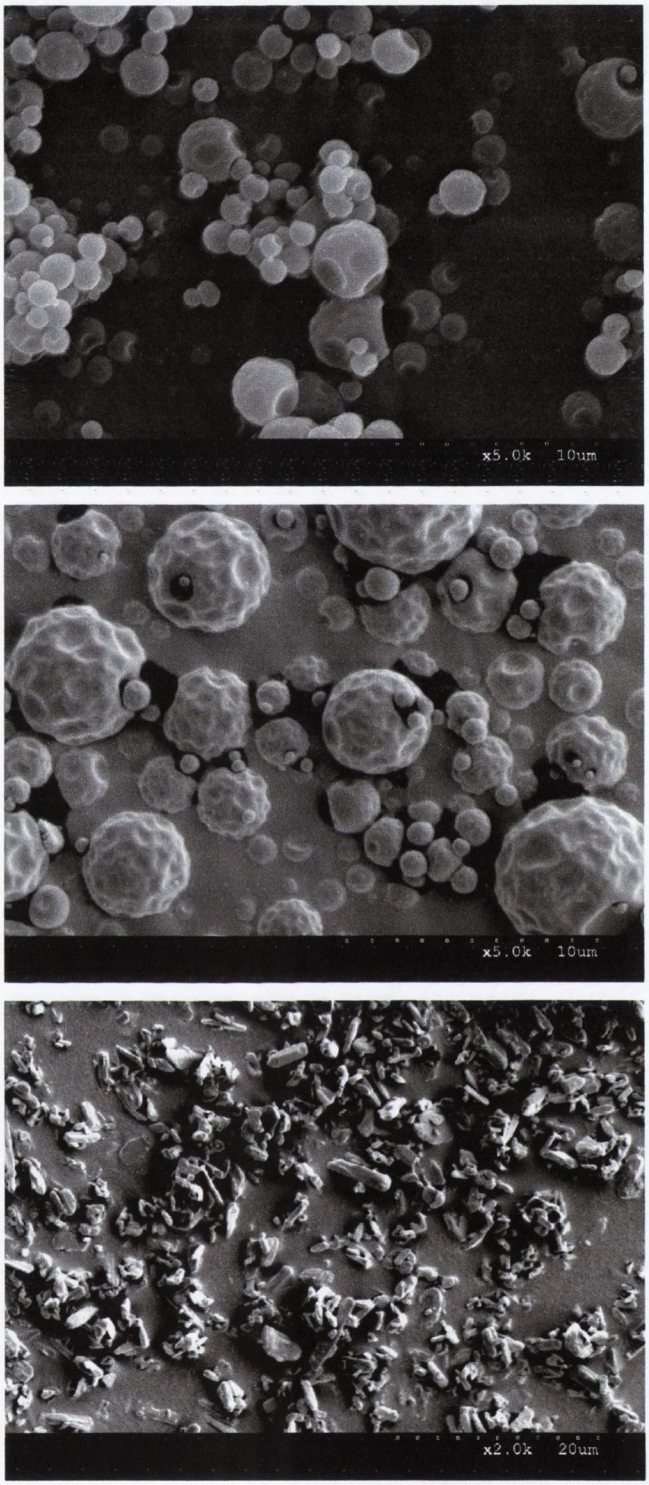

Figure 5.4 SEM micrographs of salbutamol sulphate spray dried from ethanolic solution (top); salbutamol sulphate spray dried from aqueous solution (middle) and micronised salbutamol sulphate (bottom).

5.2.2. Salbutamol base

Figure 5.5 shows the XRD scans of salbutamol and spray dried salbutamol base. Salbutamol base is insoluble in aqueous solvent therefore it was spray dried only from ethanolic solution (95%). Spray drying did not result in a completely amorphous product. Peaks of lower intensity were present for the spray dried powder together with an underlying halo indicating that the spray drying process did cause some decrease in crystallinity.

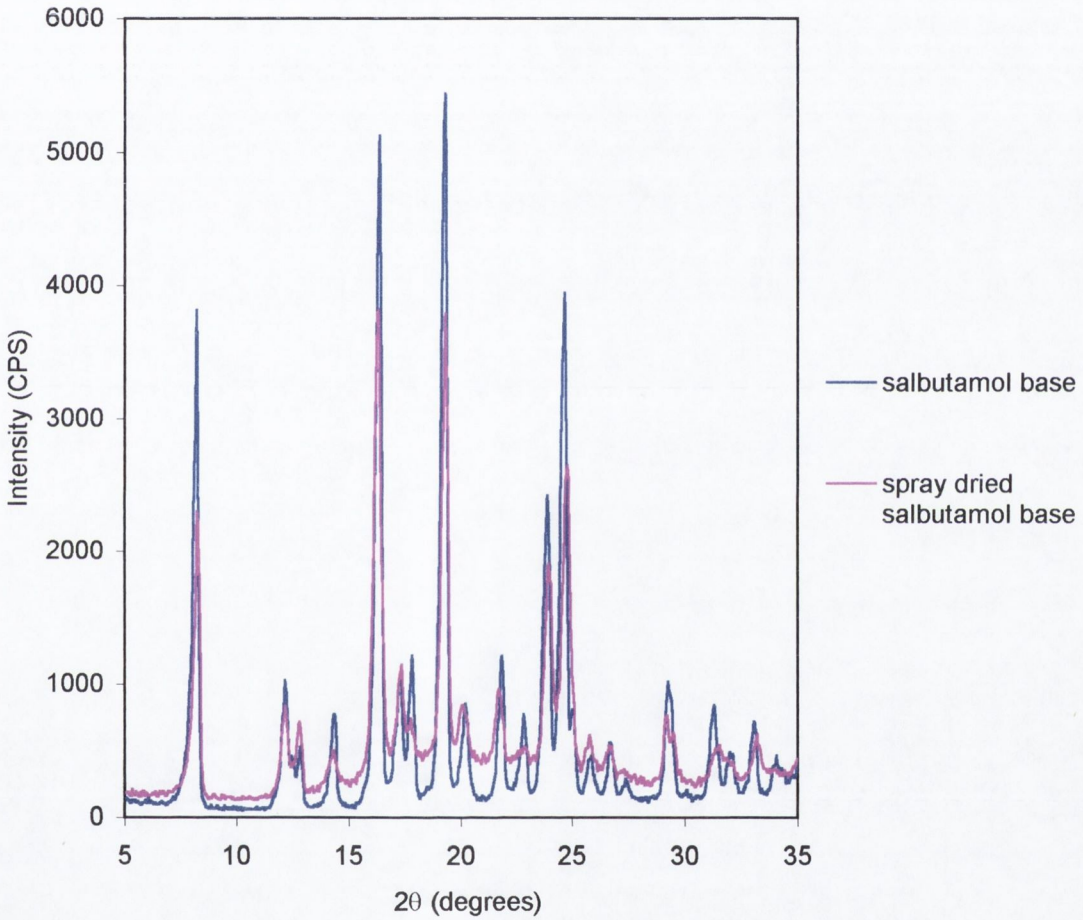

Figure 5.5 XRD scans of spray dried salbutamol base and salbutamol base starting material.

The DSC scan of spray dried salbutamol base is shown in Figure 5.6. An exotherm was observed with an onset at approximately 60°C. This indicated the presence of some amorphous material which recrystallises upon heating.

The infrared spectrum (Appendix VIII) of the spray dried system was a good match to the spectrum of the original material confirming the XRD data which showed the crystalline form present in the spray dried material to be the same as that of the starting material.

Spray dried salbutamol base showed rough irregular shaped fused particles by SEM, with diameters ranging from less than 1 μm to approximately 6 or 7 μm. Figure 5.7 shows the SEM micrographs of spray dried salbutamol base and salbutamol base starting material.

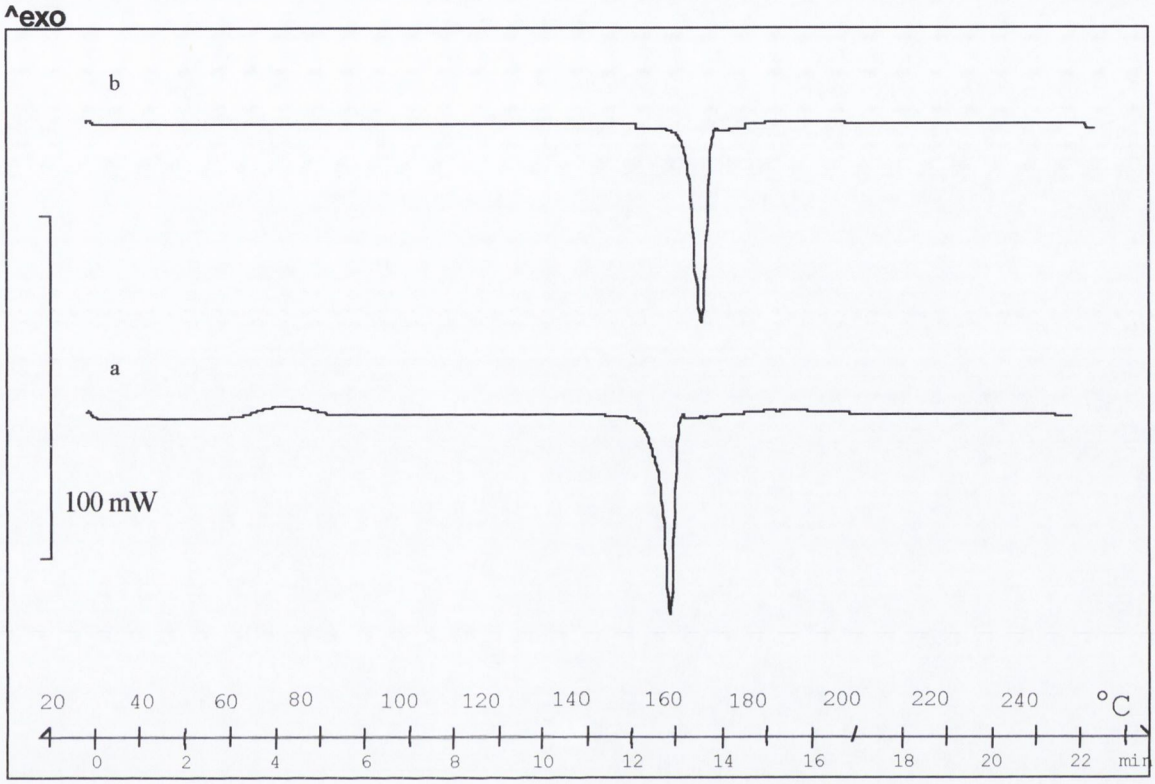

Figure 5.6 DSC scans of (a) spray dried salbutamol base and (b) salbutamol base starting material.

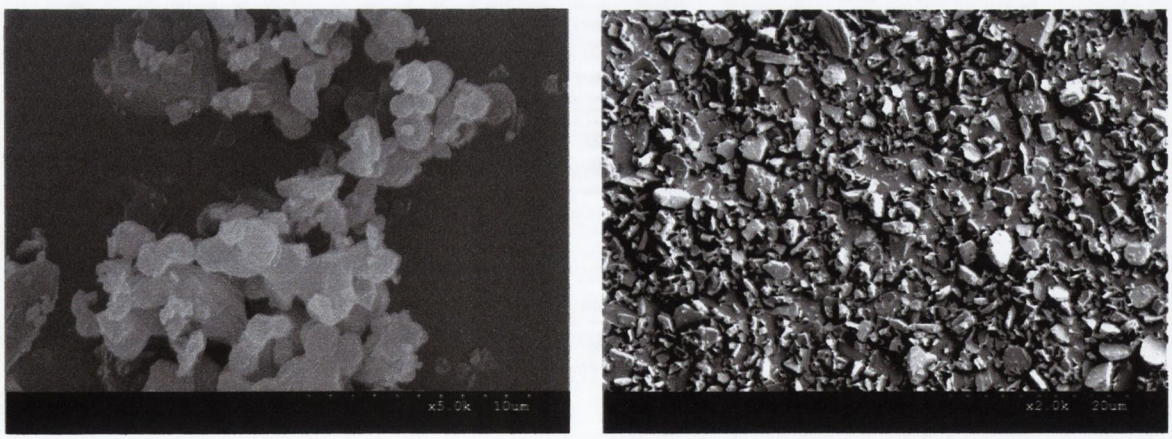

Figure 5.7 SEM micrographs of spray dried salbutamol base (left) and salbutamol base starting material (right). Note the spray dried material is at a higher magnification than the starting material.

5.2.3. Ipratropium bromide monohydrate

Spray drying ipratropium bromide alone from either aqueous solution or ethanolic solution did not result in the production of an amorphous system, though some changes in the XRD pattern were apparent, especially for the system spray dried from aqueous solution, indicating some change in the crystal form. Figure 5.8 shows the XRD scans of the two spray dried systems and the starting material. The arrows in the XRD scans indicate positions where peaks differ between the three samples.

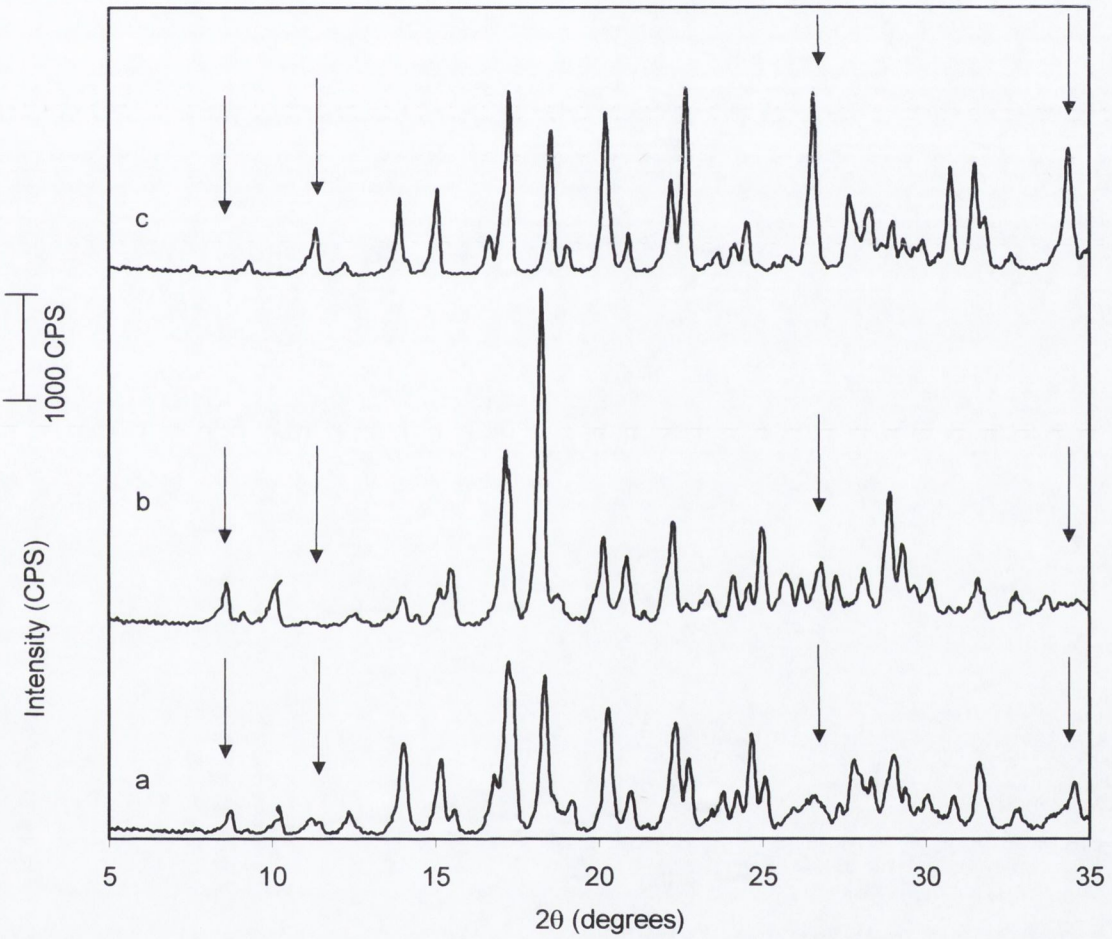

Figure 5.8 XRD scans of (a) ipratropium bromide spray dried from ethanolic solution (95%); (b) ipratropium bromide spray dried from aqueous solution and (c) ipratropium bromide monohydrate starting material. The arrows in the XRD scans indicate positions where peaks differ between the three samples.

DSC scans of ipratropium bromide are shown in Figure 5.9. The starting material showed a major endotherm with a peak at approximately 237°C which was attributed to melting. Two further lower temperature overlapping endotherms between 80 and 120°C were visible (when the DSC was viewed at a higher magnification) and were likely due to the loss of the monohydrate.

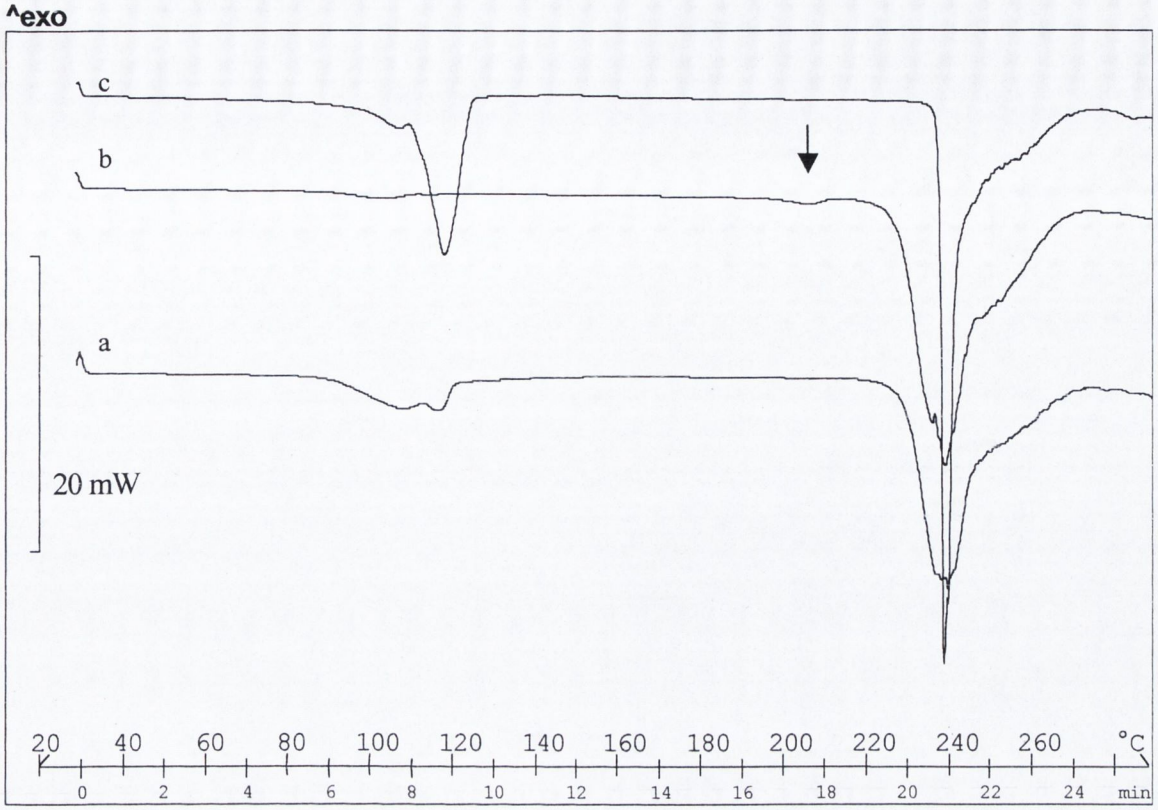

Figure 5.9 DSC of (a) ipratropium bromide spray dried from ethanolic solution; (b) ipratropium bromide spray dried from aqueous solution and (c) ipratropium bromide monohydrate starting material. The arrow indicates an endotherm at approximately 208°C in scan b.

A TGA scan of ipratropium bromide monohydrate is shown in Figure 5.10. TGA analysis of ipratropium bromide monohydrate showed a loss of approximately 4% of total solid mass in the same temperature region as the dehydration endotherm by DSC. This weight loss is consistent with the loss of a monohydrate (the loss of one water molecule corresponds to a loss of 4% by weight of ipratropium bromide monohydrate when determined on a molecular weight basis).

The DSC of the aqueous spray dried material (Figure 5.9, scan b) showed two low temperature endotherms between approximately 85 and 120°C (at higher magnification), however, TGA did not detect any mass loss associated with these peaks (Figure 5.10, scan b). The combined energy change associated with the two lower endotherms was ~ 4 J/g compared to ~122 J/g for the starting material. The sample appeared to consist of mainly the anhydrous form, indicated by the lack of weight loss by TGA in the monohydrate region. The presence of the endotherm in the monohydrate region by DSC, which was greatly reduced in magnitude compared to the monohydrate starting material, indicated that a small percentage of monohydrate material may be present in the sample. The absence of

weight loss by TGA associated with the small endotherm in the DSC implies that the amount present was too low to be detected by TGA. Another small endothermic peak was visible in the aqueous spray dried material at approximately 208°C just before the larger melting endotherm (indicated by the arrow in Figure 5.9). This melting endotherm may be indicative of the presence of a polymorphic form of ipratropium bromide. The DSC scan of ipratropium bromide spray dried from ethanolic solution (Figure 5.9, scan a) was similar to the DSC scan of the starting material showing two low temperature endothermic peaks as well as the higher melting endotherm. No peak at approximately 208°C was observed. The energy change associated with the lower temperature endotherms was smaller than that associated with the starting materials low temperature endotherms i.e. it was ~49 J/g compared to ~122 J/g but larger than that of ipratropium bromide spray dried from aqueous solution. TGA of the ethanolic spray dried system did show weight loss indicative of the monohydrate of approximately 2.6% (Figure 5.10, scan a) indicating that not all the sample was present as the monohydrate. The DSC was also consistent with not all the material being present as the monohydrate. It is likely that some anhydrous ipratropium bromide is formed, the small amount present not changing the XRD pattern to a large extent.

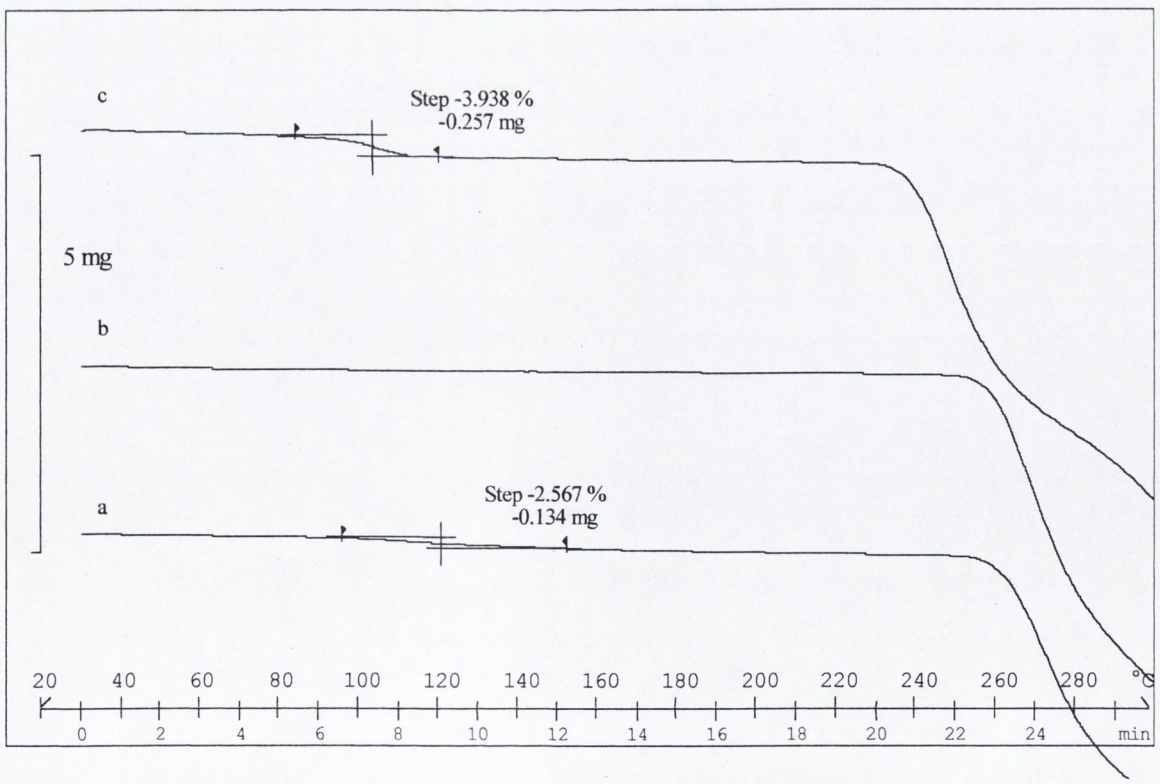

Figure 5.10 TGA scans of (a) ipratropium bromide spray dried from ethanolic solvent; (b) ipratropium bromide spray dried from aqueous solvent and (c) ipratropium bromide monohydrate starting material.

FTIR showed similar spectra for ipratropium bromide spray dried from ethanol and ipratropium bromide monohydrate starting material (Appendix VIII). However ipratropium bromide spray dried from aqueous solution showed changes in the OH region. Changes in the OH region are indicative of changes in the hydrate form of the drug and were consistent with DSC and TGA experiments which indicated the presence of predominantly the anhydrous form. The DSC scan of the aqueous spray dried system indicated the possibility of the presence of an additional polymorphic form. While some polymorphic forms of drugs show quite large differences by FTIR, the spectra of many polymorphic systems are often found to be only slightly different indicating that the pattern of molecular vibrations is not grossly affected by the differences in crystal structure (Brittain et al., 1999). FTIR of the aqueous spray dried system did not show peaks, other than in the OH region, which were significantly different from the starting material.

EDXA of the spray dried materials showed the presence of bromine consistent with the spray dried material remaining as the bromide salts (Appendix VII).

SEM micrographs of ipratropium bromide spray dried from ethanolic and aqueous solvents and ipratropium bromide monohydrate starting material are shown in Figure 5.11.

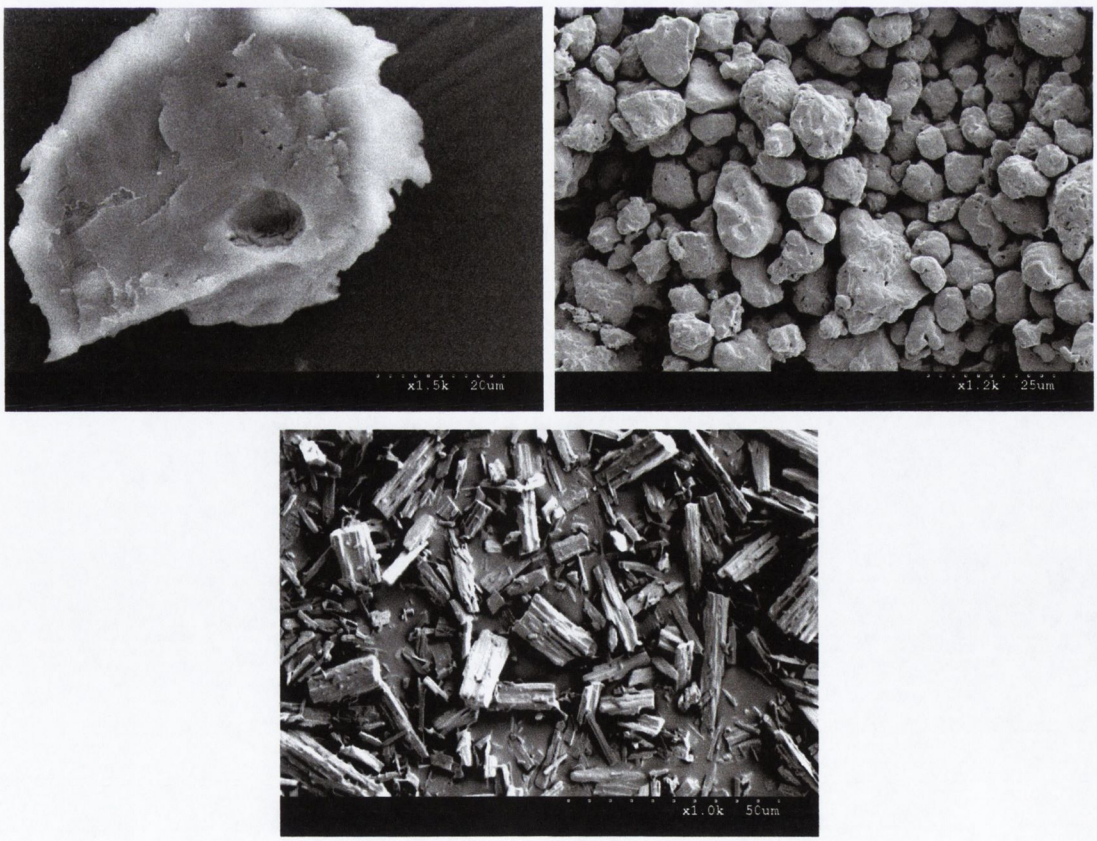

Figure 5.11 SEM micrographs of ipratropium bromide spray dried from 95% ethanolic solution (top left); ipratropium bromide spray dried from aqueous solution (top right) and micronised ipratropium bromide (bottom).

The aqueous spray dried systems showed rough irregular shaped particles with diameters ranging from approximately 5 to 20 μm. Ipratropium bromide spray dried from ethanolic solvent showed larger particles with diameters of the order of 60 μm and larger.

5.2.4. Co-spray dried salbutamol sulphate and ipratropium bromide

Salbutamol sulphate:ipratropium bromide 10:1, 5:1 and 2:1 weight ratios were spray dried from aqueous as well as ethanolic solutions. The 10:1 weight ratio was spray dried from 84% ethanol, the 5:1 ratio from 85% ethanol and the 2:1 ratio from 89% ethanol since as the percentage of salbutamol sulphate decreased a lower percentage of water was needed in the solvent to form a solution. XRD scans of the physical mixes compared with the systems spray dried from aqueous solution are shown in Figure 5.12.

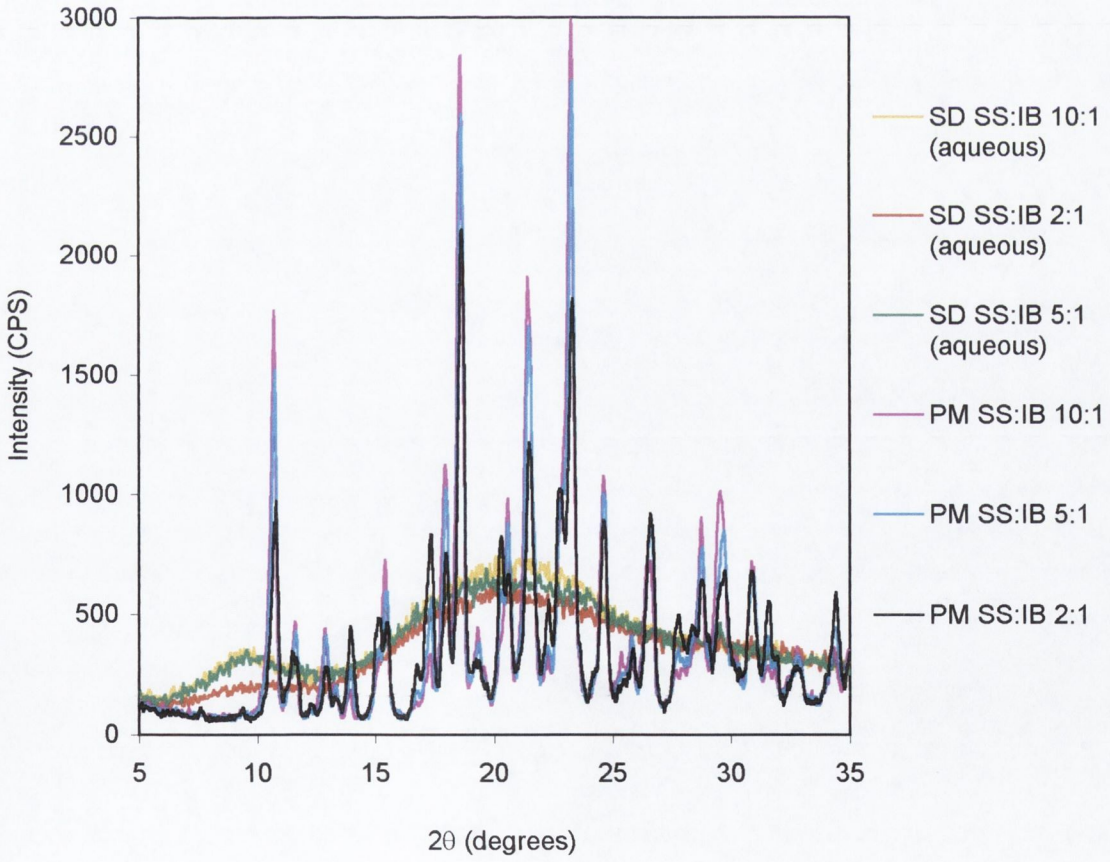

Figure 5.12 XRD scans of salbutamol sulphate:ipratropium bromide (SS:IB) 10:1, 5:1 and 2:1 systems spray dried (SD) from aqueous solutions and salbutamol sulphate:ipratropium bromide monohydrate 10:1, 5:1 and 2:1 physical mixes (PM).

All three weight ratios when spray dried resulted in amorphous powders, regardless of the solvent used in production, as evidenced by the lack of peaks in the XRD scans. The systems spray dried from ethanolic solution showed similar amorphous halos to those shown for the aqueous spray dried systems.

DSC scans of salbutamol sulphate:ipratropium bromide systems spray dried from aqueous solution are shown in Figure 5.13. DSC scans were similar to those of salbutamol sulphate spray dried alone except for small endotherms in the 100 to 120°C region. Physical mixes of crystalline ipratropium bromide monohydrate and amorphous salbutamol sulphate were prepared, the DSC scans of the 2:1 and 10:1 mixes are shown in Figure 5.14.

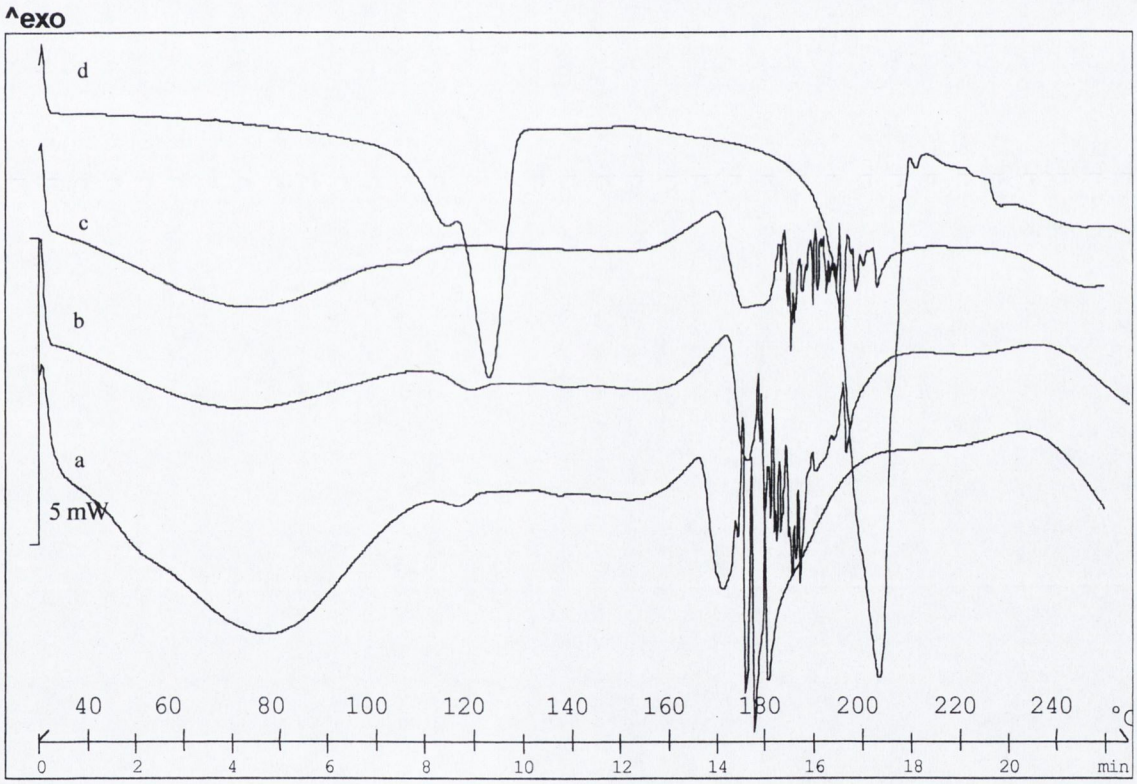

Figure 5.13 DSC scans of (a) salbutamol sulphate:ipratropium bromide 10:1 spray dried from aqueous solution; (b) salbutamol sulphate:ipratropium bromide 5:1 spray dried from aqueous solution; (c) salbutamol sulphate:ipratropium bromide 2:1 spray dried from aqueous solution and (d) salbutamol sulphate:ipratropium bromide monohydrate 2:1 physical mix.

The small endotherms in the co-spray dried systems did not resemble the dehydration endotherm observed for the physical mix of crystalline ipratropium bromide monohydrate and crystalline salbutamol sulphate (Figure 5.13, scan d). However the single peaked

dehydration endotherms observed when crystalline ipratropium bromide monohydrate was physically mixed with amorphous salbutamol sulphate (Figure 5.14) did resemble the endotherms visible for the co-spray dried systems. The magnitude of the dehydration endotherms in the co-spray dried systems were reduced in size compared to physical mixes indicating that less monohydrate ipratropium bromide was present.

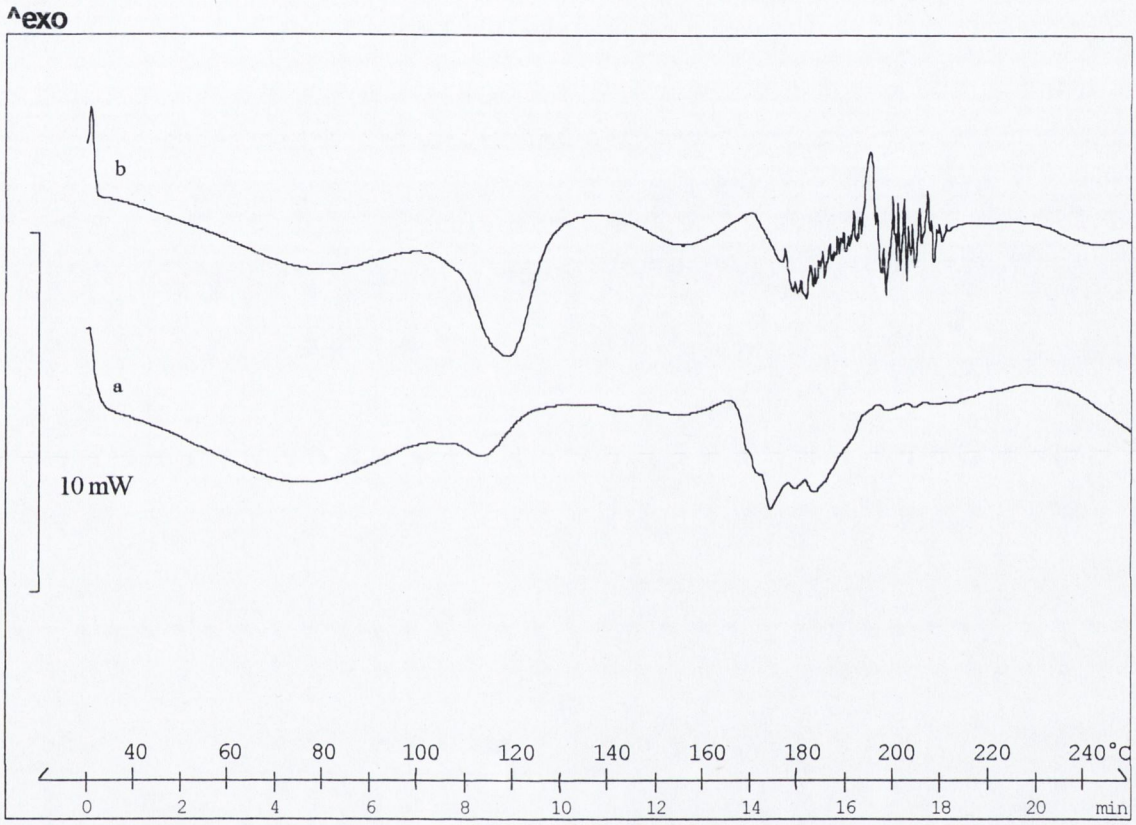

Figure 5.14 DSC scans of (a) physically mixed amorphous salbutamol sulphate:crystalline ipratropium bromide monohydrate 2:1 and (b) physically mixed amorphous salbutamol sulphate:crystalline ipratropium bromide monohydrate 10:1

Since ipratropium bromide does not show a tendency to form an amorphous phase alone and the evidence of a typical exotherm is lacking by DSC, it was thought that the ipratropium bromide in this system may be present as crystalline material suspended in the amorphous salbutamol sulphate as a glass suspension. An XRD scan of a physical mix of crystalline ipratropium bromide monohydrate in amorphous salbutamol sulphate was run to establish whether crystalline ipratropium bromide suspended in amorphous salbutamol sulphate would be detectable by XRD. The 10:1 physical mix is shown in Figure 5.15 (i.e. the mix with the lowest proportion of ipratropium bromide monohydrate). Peaks due to ipratropium bromide were clearly present, even at this low concentration of crystalline

material (9% w/w ipratropium bromide monohydrate). Ipratropium bromide is likely present predominantly in the amorphous state, the small endotherms visible by DSC may have been a result of trace amounts of crystalline ipratropium bromide which may have formed on preparation or during the DSC run.

No typical exotherms indicative of recrystallisation of amorphous material were observed by DSC for any of the systems co-spray dried from aqueous solution. Increases in the baseline prior to the degradation peaks may be indicative of recrystallisation prior to degradation or could be part of the degradation peaks.

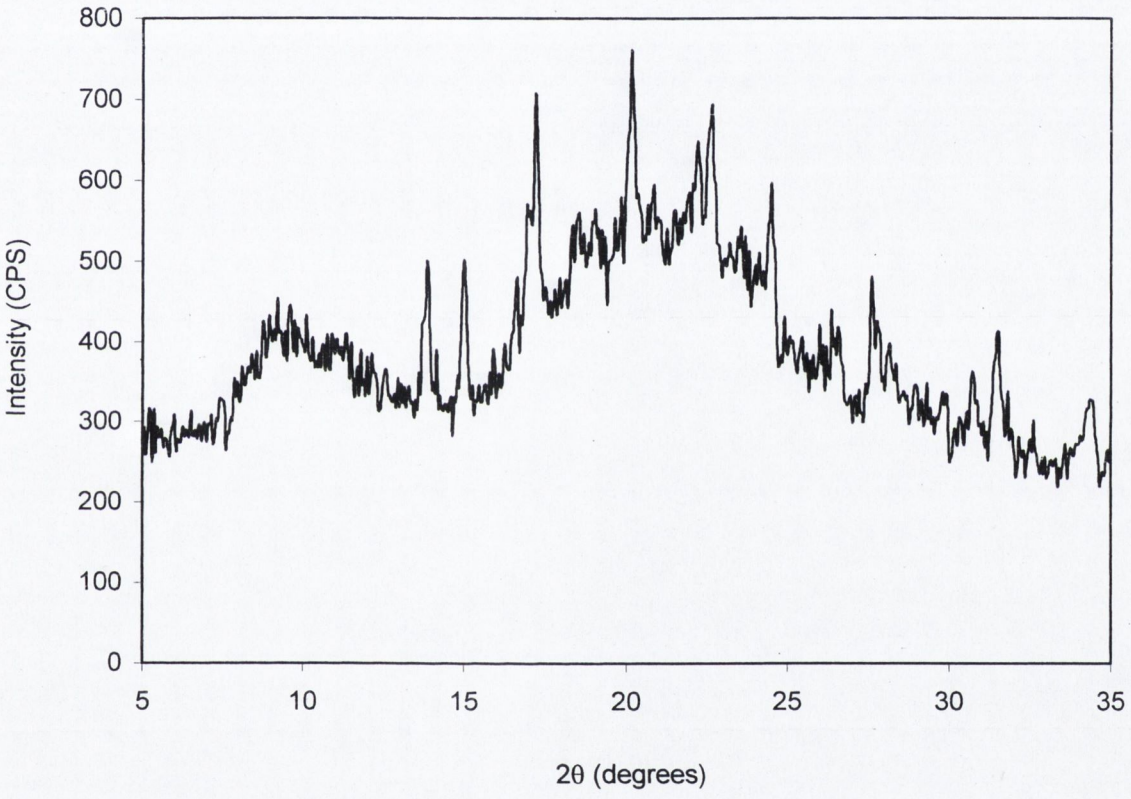

Figure 5.15 XRD scan of a physical mix of spray dried amorphous salbutamol sulphate:crystalline ipratropium bromide monohydrate 10:1.

DSC scans of salbutamol sulphate:ipratropium bromide systems spray dried from ethanolic solvent are shown in Figure 5.16. All spray dried systems resembled salbutamol sulphate spray dried alone from ethanol. There were suggestions of exothermic events just prior to the main endothermic events at ~170°C. The melting endotherms for salbutamol sulphate were shifted to lower temperatures than in the physical mixes and for two of the systems appeared to consist of two overlapping endotherms. No peaks indicative of degradation were observed unlike for the salbutamol sulphate:ipratropium bromide systems spray dried

from aqueous solution indicating that spray drying from ethanolic solvent may result in more stable systems. Endothermic peaks prior to approximately 120°C were not as pronounced as in the equivalent systems spray dried from aqueous solution. These peaks may possibly be due to trace amounts of crystalline ipratropium bromide monohydrate.

TGA was consistent with the broad endotherms visible by DSC, in the aqueous and ethanolic spray dried systems prior to approximately 100°C, being due to loss of absorbed water. TGA showed weight loss (1-3%) in this region for the spray dried systems which was not observed for the physical mixes. (Amorphous materials are often hygroscopic).

No weight losses were visible in the region of loss of water of hydration in the TGA scans of the co-spray dried systems. TGA of the 5:1 and 2:1 physical mix systems showed weight losses indicative of the loss of monohydrate water, however a weight loss was not detectable in the 10:1 system indicating that TGA could not detect weight loss when ipratropium bromide was present as such a low concentration of the mix. DSC of the physical mixes showed the presence of an endotherm due to loss of the monohydrate was detectable even for the 10:1 system indicating that DSC could detect loss of the monohydrate when present at a lower concentration than TGA could.

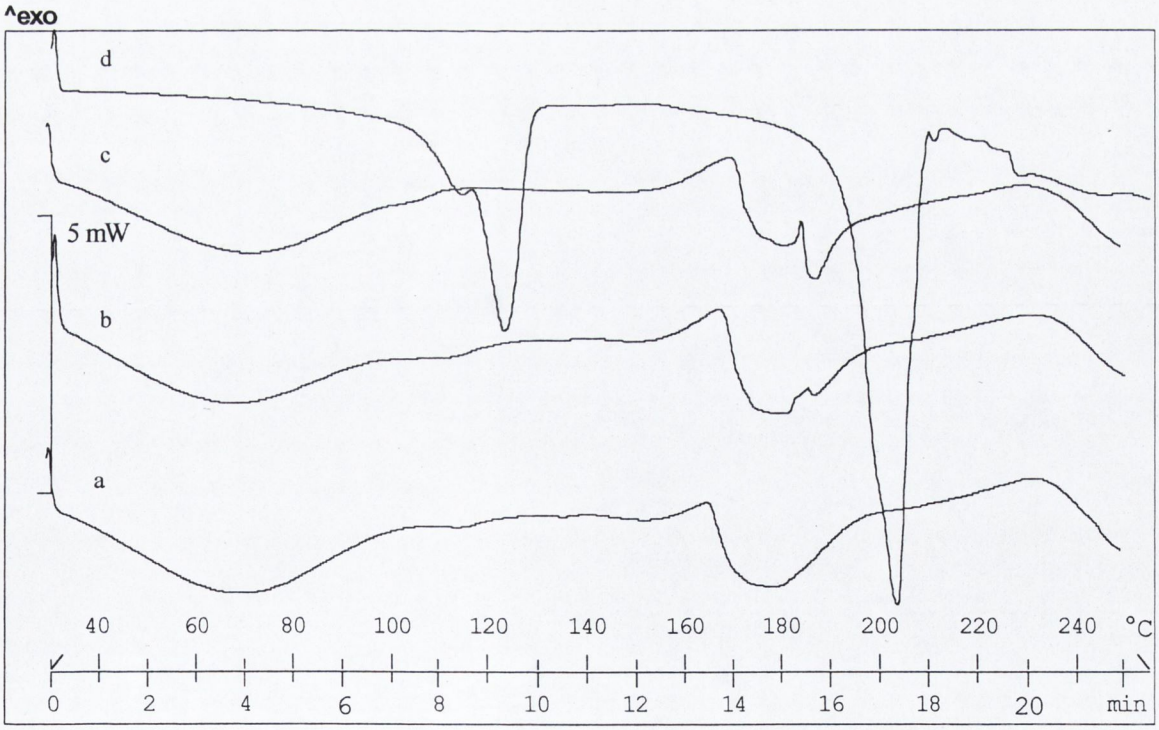

Figure 5.16 DSC scans of (a) salbutamol sulphate:ipratropium bromide 10:1 spray dried from ethanol; (b) salbutamol sulphate:ipratropium bromide 5:1 spray dried from ethanol; (c) salbutamol sulphate:ipratropium bromide 2:1 spray dried from ethanol and (d) physical mix of salbutamol sulphate:ipratropium bromide 2:1.

FTIR of the systems spray dried from either solvent showed changes in the OH region and in the 1000-1060 cm^{-1} region compared to equivalent physical mixes. The changes in the OH region are consistent with the change in ipratropium bromide from the monohydrate to an anhydrous form. FTIR of all spray dried samples showed no peak at 1031, a peak which was shown by the physical mix systems and additional peaks at 1044 and 1003, peaks not shown by the physical mix systems. Changes in the region 1020-1060 cm^{-1} have been described to be due to the C-N(H) stretching mode (Brittain, 1999). Differences in bands in the C-N(H) region were apparent for six polymorphic forms of mexiletine hydrochloride (Brittain, 1999). Salbutamol sulphate contains a C-N(H) group and ipratropium bromide contains a nitrogen atom bonded to carbon atoms. Differences observed in the spectra of spray dried salbutamol sulphate:ipratropium bromide systems compared to equivalent physical mixes are likely due to the change in ipratropium bromide from the monohydrate form to an anhydrous form on spray drying. When solvent molecules are removed from a crystal lattice the new structure is often different enough that the change in molecular vibrations are detectable (Khankari et al., 1995).

Figure 5.17 shows the SEM micrographs of the salbutamol sulphate:ipratropium bromide systems spray dried from aqueous solutions. Figure 5.18 shows the SEM micrographs of the salbutamol sulphate:ipratropium bromide systems spray dried from ethanolic solutions. SEM of the aqueous spray dried systems showed small spherical particles for the three systems. The 10:1 sample showed slightly dimpled particles approximately 0.5-3 μm in diameter. The 5:1 systems showed particles that were more significantly dimpled with diameters of approximately 0.5-5μm and the 2:1 system displayed smooth spherical particles approximately 1-6 μm in diameter. As the concentration of ipratropium bromide is increased the size of the particles also increases.

The salbutamol sulphate:ipratropium bromide systems spray dried from ethanolic solution appeared as hemispheres embedded in the gold coating (Figure 5.18). SEM of these samples was repeated and the same result obtained. These atypical SEM micrographs are most likely due to the hygroscopic nature of the material. Later in Chapter 6, similar atypical SEM micrographs were obtained. When the powders resulting in the atypical micrographs were observed prior to gold coating, using a light microscope, spherical particles were initially observed but these particles appeared to join up resembling the appearance of the atypical micrographs. Preparation of the samples for gold coating without delay resulted in more typical SEM micrographs showing spherical particles.

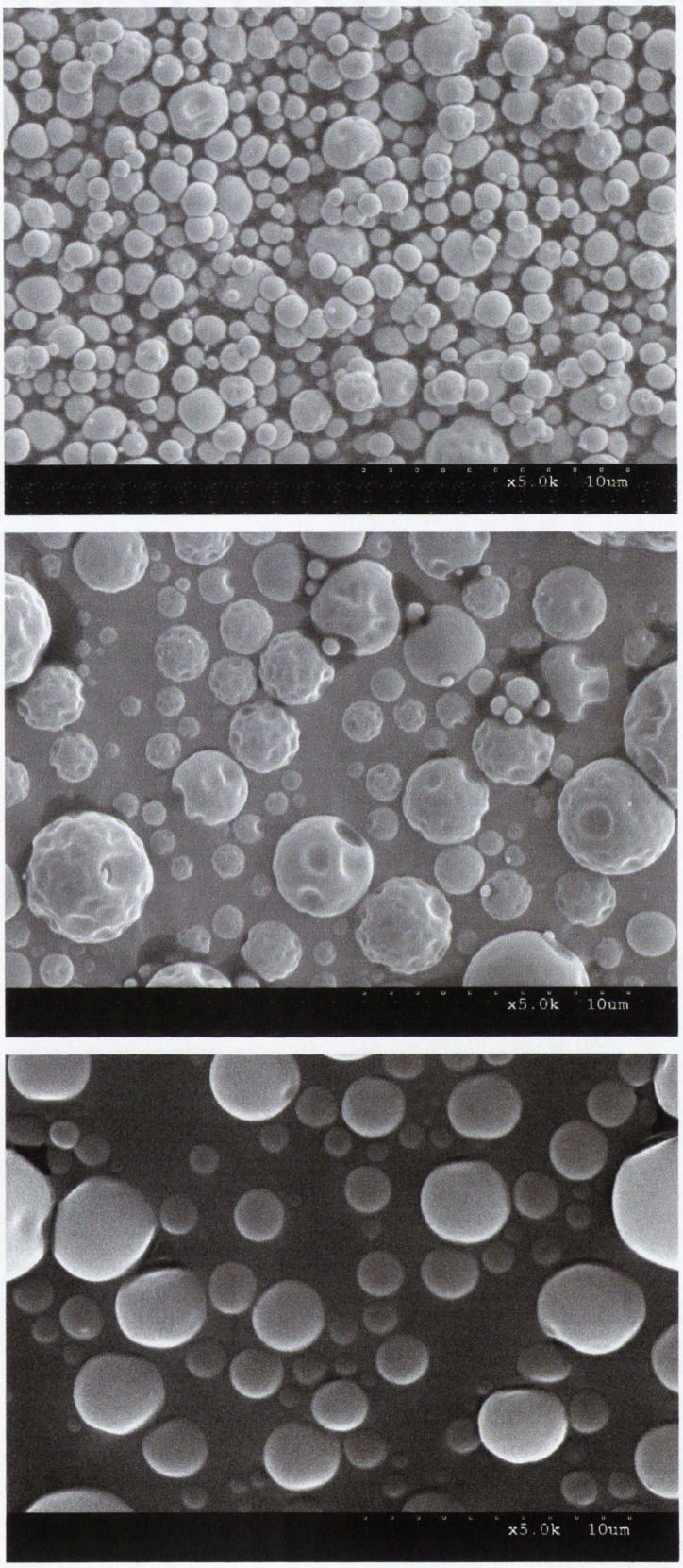

Figure 5.17 SEM micrographs of salbutamol sulphate:ipratropium bromide systems 10:1 (top); 5:1 (middle) and 2:1 (bottom) spray dried from aqueous solutions.

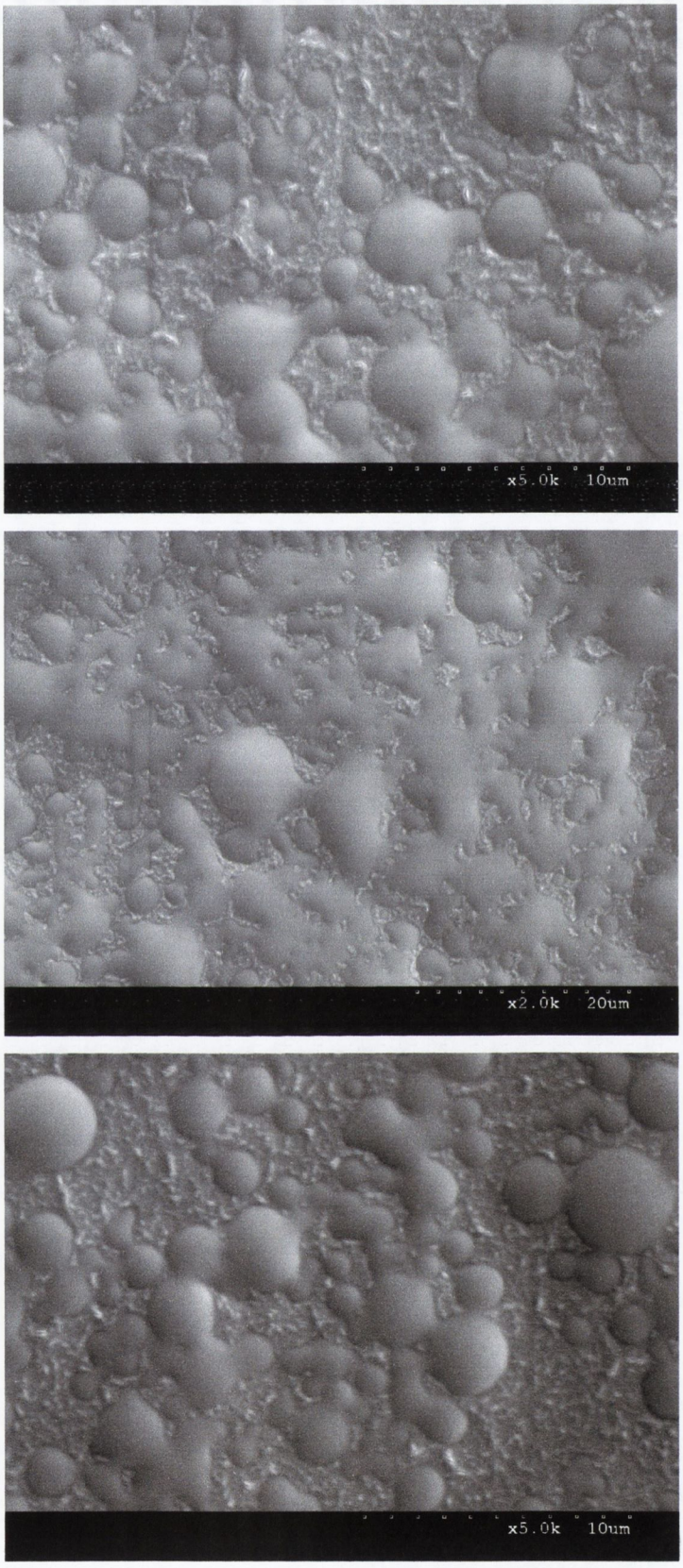

Figure 5.18 SEM micrographs of salbutamol sulphate:ipratropium bromide systems 10:1 (top); 5:1 (middle) and 2:1 (bottom) spray dried from ethanolic solutions.

5.2.5. Co-spray dried salbutamol base and ipratropium bromide

Figure 5.19 shows the XRD scans of the different weight ratios of spray dried salbutamol base:ipratropium bromide compared to equivalent physical mixes. The 10:1 and 5:1 salbutamol:ipratropium bromide co-spray dried systems were crystalline as shown by XRD scans, however the peaks indicative of crystallinity were of lower intensity than in the equivalent physical mixes and there were suggestions of underlying amorphous halos in the XRD scans. The 2:1 co-spray dried system was amorphous as evidenced by a halo and the absence of peaks indicative of crystallinity.

DSC scans of spray dried salbutamol:ipratropium bromide systems are shown in Figure 5.20. All spray dried systems showed exotherms indicative of recrystallisation of amorphous material followed by melting endotherms. The magnitude of the exotherms increased as did their onset temperature as the weight ratio of ipratropium bromide increased. The recrystallisation exotherm observed in salbutamol base spray dried alone showed an onset temperature at approximately 60°C (Figure 5.6). Higher onset recrystallisation temperatures were observed for the co-spray dried systems with the 2:1 salbutamol base:ipratropium bromide showing the highest onset and peak recrystallisation temperatures. This imples that as the weight ratio of ipratropium bromide is increased, it may have a stabilising effect on the amorphous system, since a higher temperature is needed to result in recrystallisation. Glass transition related events, which would have clarified whether ipratropium bromide acted as an antiplasticiser (i.e. whether it resulted in an increase in the glass transition temperature) were not large enough or occurred at lower temperatures and therefore were not detected by DSC.

The DSC scans of the co-spray dried salbutamol base:ipratropium bromide 2:1 system showed the broadest and lowest temperature melting endotherm when compared to the other co-spray dried salbutamol base:ipratropium bromide weight ratios. The broader appearance of the 2:1 spray dried system compared to its equivalent physical mix implies a more disordered system (Chiou and Niazi, 1971) and was consistent with the XRD scan showing an amorphous system (Figure 5.19, bottom scan). The melting endotherms observed for all weight ratios consisted of two overlapping peaks, these overlapping peaks were also observed in physical mixes of the systems and could be due to the melting of both crystalline salbutamol base and ipratropium bromide.

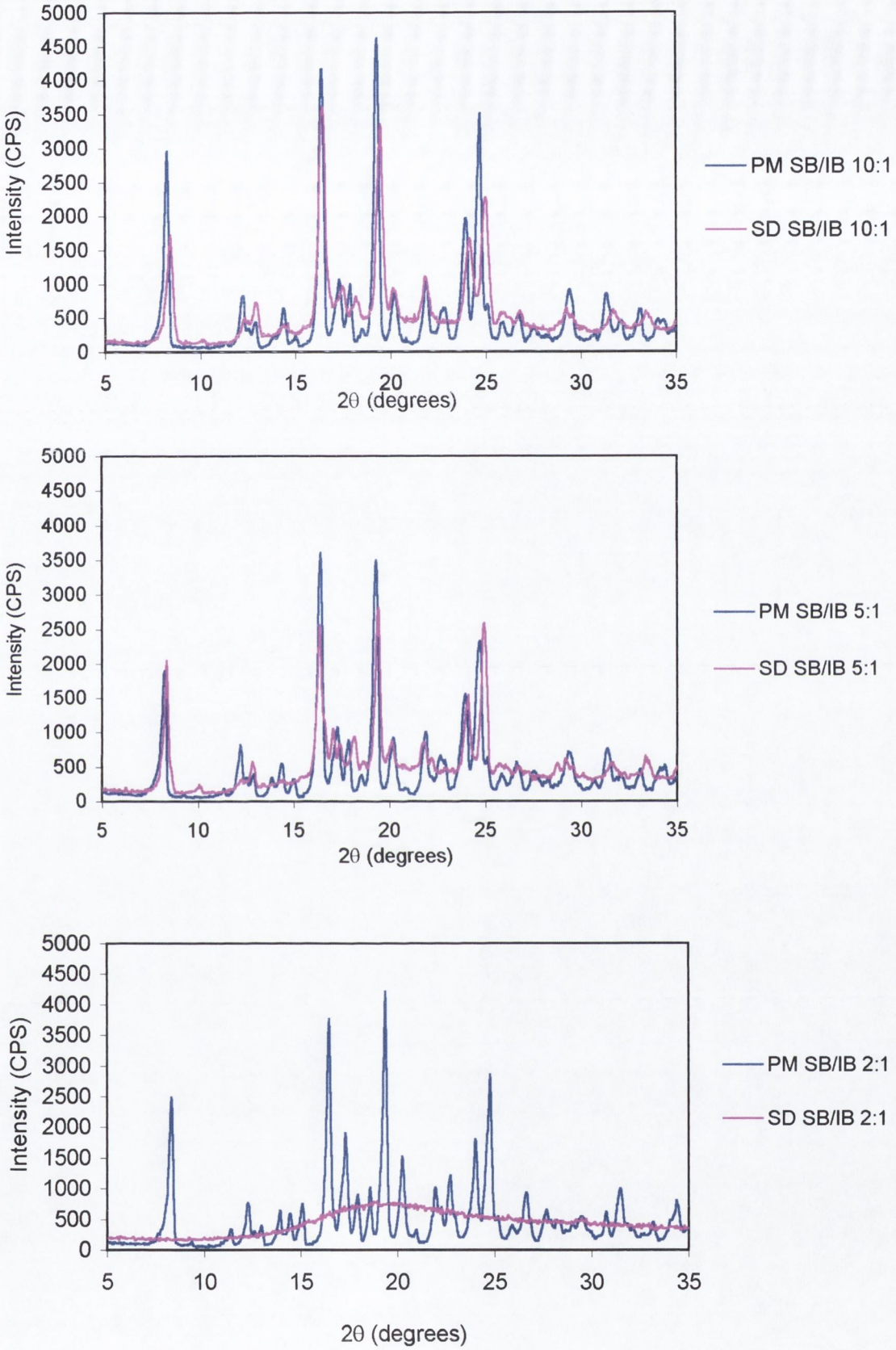

Figure 5.19 XRD scans of co-spray dried salbutamol:ipratropium bromide and equivalent physical mixes: 10:1 (top); 5:1 system (middle) and 2:1 system (bottom).

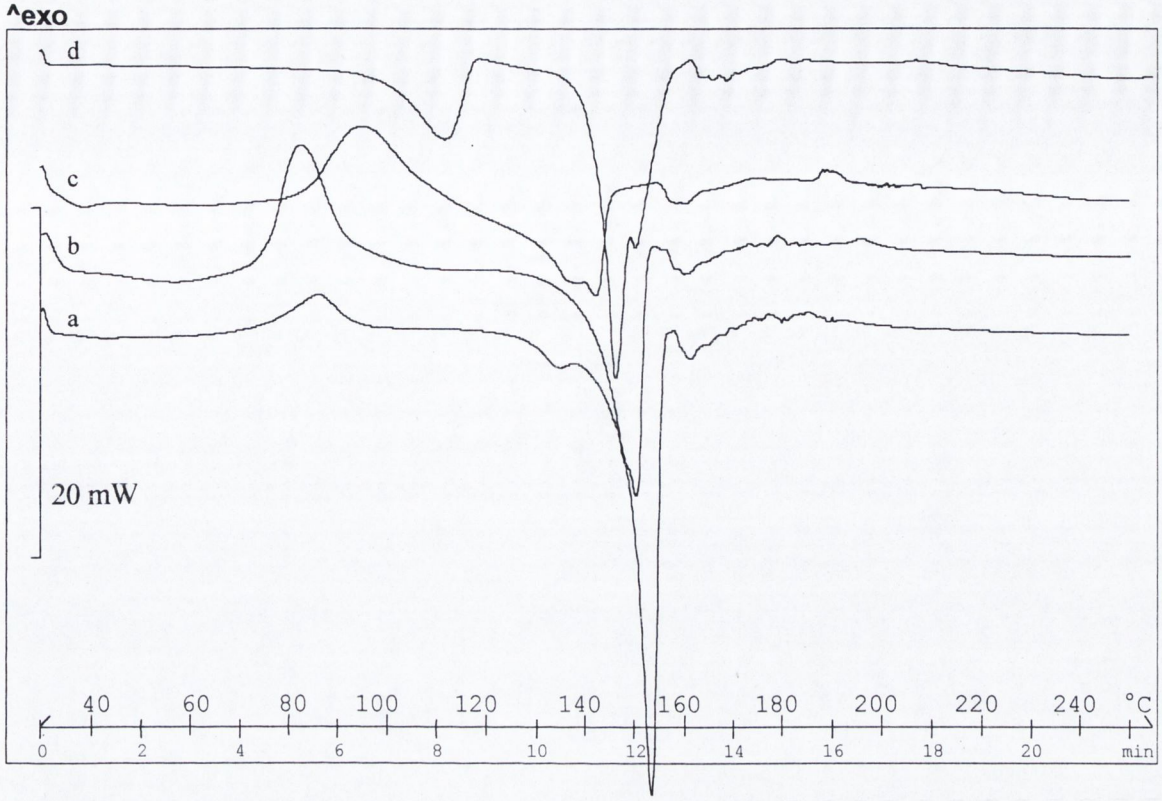

Figure 5.20 DSC scans of (a) spray dried salbutamol base:ipratropium bromide 10:1; (b) spray dried salbutamol base:ipratropium bromide 5:1; (c) spray dried salbutamol base:ipratropium bromide 2:1 and (d) physical mix of salbutamol base:ipratropium bromide 2:1.

TGA of physical mixes of salbutamol base:ipratropium bromide monohydrate showed detectable weight loss due to the loss of the monohydrate for the 5:1 and 2:1 systems. No weight loss was detectable for the 10:1 system indicating that TGA is not sensitive to detect hydrate loss from ipratropium bromide when it is present in such a low concentration of a mix. DSC could detect the loss of monohydrate in the 10:1 physical mix system. TGA of the spray dried systems showed no weight losses which could be attributed to loss of monohydrate water indicating that ipratropium bromide monohydrate was not present in sufficient amounts to be detectable by TGA.

The infrared spectrum of the 10:1 spray dried system was a good match to the equivalent physical mix, however the change in monohydrate to anhydrous ipratropium bromide at such a low level of ipratropium bromide might not be detectable by FTIR. The 5:1 and 2:1 systems showed a broad peak in the OH region when compared to the physical mixes. TGA was consistent with a change in hydrate form which is likely responsible for the change in the OH region observed by FTIR. The changes observed in this region may also be due to absorbed water (Morris et al., 1994). The 5:1 and 2:1 spray dried systems consist

of large amounts of amorphous material which may absorb significant quantities of water. TGA showed a weight loss prior to 70°C representative of a loss of absorbed moisture.

SEM micrographs of spray dried salbutamol base:ipratropium systems are shown in Figure 5.21. SEM of the 10:1 system showed a flaky mass. The 5:1 system by SEM was shown to consist of large irregular shaped agglomerated particles.

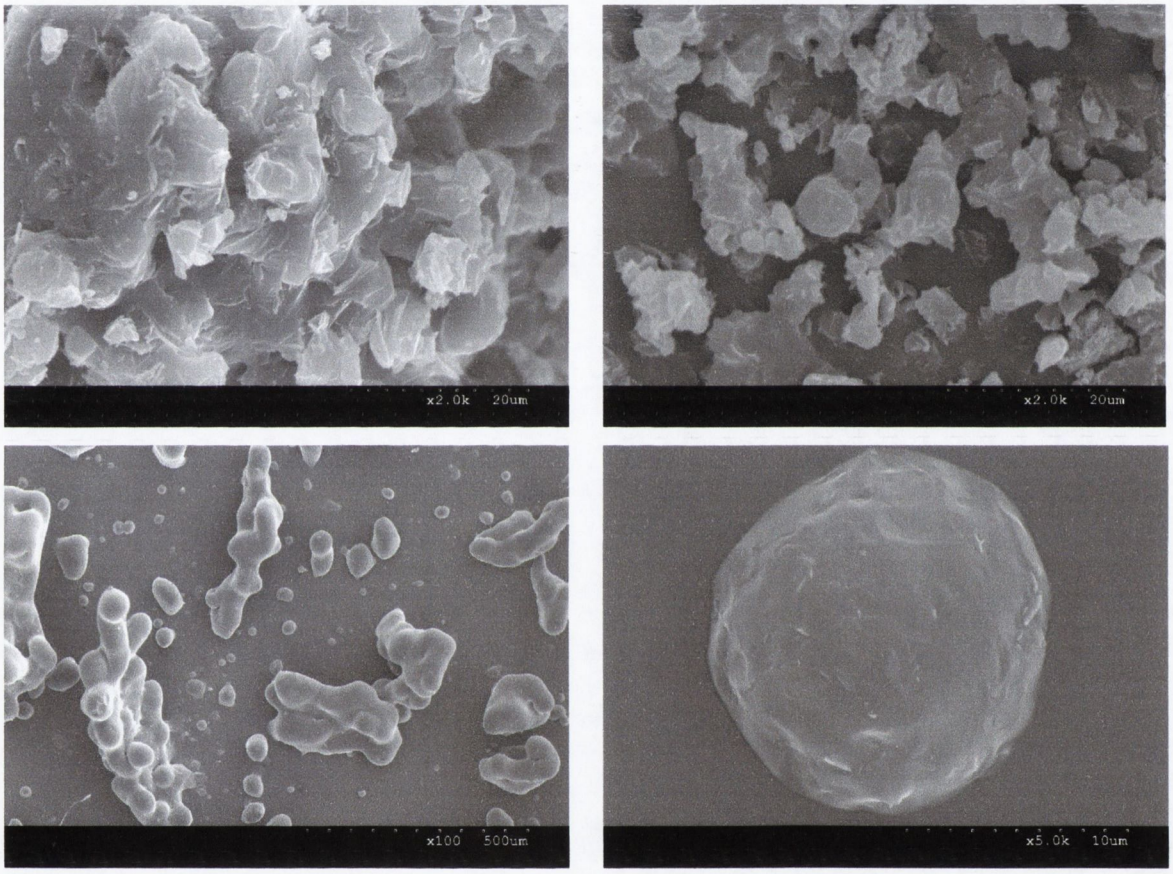

Figure 5.21 SEM micrographs of spray dried salbutamol /ipratropium bromide systems 10:1 (top left), 5:1 (top right) and 2:1 (bottom left and right)

The 2:1 system consisted of roughly spherical particles of diameters less than ~70 μm with some as small as 15 μm in diameter. Larger masses of agglomerated material also appeared to be present (Figure 5.21, bottom left).

5.2.6. Analysis of Respirable Fraction using Twin Stage Impinger Apparatus (TSI)

5.2.6.1. Introduction

Detailed descriptions of the twin stage impinger are available in the British Pharmacopoeia (B.P., 2002, apparatus A) and European Pharmacopoeia (Ph. Eur., 2002, apparatus A). When operated at 60 litres/minute, stage two of the device is claimed to collect fine particles with aerodynamic diameters < 6.4 μm with larger particles remaining in stage 1 (Hallworth and Westmoreland, 1987). The respirable fraction was calculated as the amount deposited in the lower stage of the impinger as a percentage of the emitted dose (the dose emitted into the upper and lower stage excluding the amount remaining in the device). Another method for expressing the respirable fraction is to calculate the amount deposited in the lower impinger as a percentage of the total dose in the capsule. All the respirable fractions stated in the text to follow are based on the emitted dose since respirable fraction calculated as a percentage of total dose is dependent on the amount filled into the capsules. Vanbever et al. (1999) found that half-filled capsules emitted the largest amount of powder when performing in vitro deposition experiments on excipient-drug spray dried systems. Chawla et al. (1994) investigated *in vitro* aerosol deposition of salbutamol sulphate powder which had been spray dried from aqueous solution. They weighed 50-60 mg quantities of powder into size 3 gelatin capsules for *in vitro* deposition studies. Therefore, in this work, 60 mg of powder was used to fill size 3 gelatin capsules for experiments. *In vitro* deposition experiments were performed on the systems that showed favourable particles by SEM for use in dry powder inhalers (DPIs), i.e. systems which did not consist of large fused aggregates by SEM.

5.2.6.2. Results of TSI experiments

Salbutamol sulphate capsules consisting of either micronised salbutamol sulphate, spray dried salbutamol sulphate (spray dried from both solvents), co-spray dried salbutamol sulphate:ipratropium bromide systems (spray dried from aqueous solution) or the commercial product Ventolin Rotacaps® (containing salbutamol sulphate and lactose) were analysed by the TSI. Micronised salbutamol sulphate showed the lowest mean respirable fraction giving a respirable fraction of 1.5%. Salbutamol sulphate, spray dried from aqueous or ethanolic solution, gave higher respirable fractions of 21.7% and 19.6% respectively. The co-spray dried salbutamol sulphate:ipratropium bromide systems gave

higher respirable fractions than micronised salbutamol sulphate but not as high as salbutamol sulphate spray dried alone. The respirable fractions obtained by the twin impinger experiments were compared by analysis of variance (ANOVA) using Minitab™, the results of which are shown in Table 5.1. The brackets around the mean denote the 95% confidence interval, where brackets overlap there is no statistical difference between systems.

Table 5.1 ANOVA comparing respirable fractions of salbutamol sulphate obtained from twin impinger experiments of micronised salbutamol sulphate, spray dried salbutamol sulphate from aqueous solvent (water) and from ethanolic solvent (ethanol), co-spray dried salbutamol sulphate:ipratropium bromide systems spray dried from aqueous solvent and the commercial product Ventolin Rotacaps®. SS = salbutamol sulphate, SD = spray dried, SS:IB = salbutamol sulphate: ipratropium bromide, water = spray dried from aqueous solvent, ethanol = spray dried from ethanolic solvent.

System	N	Mean	StDev	Individual 95% Confidence Intervals For Mean Based on Pooled StDev
micronised SS	3	1.540	0.286	(-*-)
SD SS (water)	3	21.676	2.352	(-*--)
SD SS (ethanol)	3	19.627	5.140	(-*-)
10 1 SD SS:IB	3	9.071	2.559	(-*-)
5 1 SD SS:IB	3	11.767	1.465	(-*-)
2 1 SD SS:IB	3	5.237	1.767	(-*--)
Rotacaps®	2†	39.964	1.855	(--*-)
Pooled StDev =		2.648		0 15 30 45

†Data from the third replicate was discarded as an outlier since during the experiment the capsule did not release the contents on the first twist but appeared to stick. Inclusion of data from the third replicate would have resulted in a standard deviation for rotacaps of 15.36 which was deemed unrealistic for a commercial product.

Table 5.1 shows that micronised salbutamol sulphate results in the lowest respirable fraction, however this is not statistically different from the co-spray dried salbutamol sulphate:ipratropium bromide 2:1 system. The salbutamol sulphate:ipratropium bromide 2:1 system showed larger particles by SEM than the 10:1 or 5:1 spray dried weight ratios (i.e. the 2:1 systems showed particles approximately 1-6 μm in diameter while the 10:1 and 5:1 systems showed approximate diameters of 0.5-3 μm and 0.5-5 μm). Additionally the 10:1 and 5:1 systems consisted of spherical particles with surface dimpling while the 2:1 system consisted of smooth spheres. The 10:1 and 5:1 systems showed statistically higher respirable fractions than micronised salbutamol sulphate but not as high as salbutamol sulphate systems spray dried alone from either ethanol or water. The salbutamol sulphate systems spray dried from aqueous and ethanolic solvents gave mean respirable fractions of 21.7% and 19.6% respectively, which was a large improvement over micronised salbutamol sulphate which gave a mean respirable fraction of 1.5%. The Ventolin

Rotacap® formulation resulted in the highest respirable fraction. This was not surprising since the Ventolin Rotacap® formulation consisted of micronised salbutamol sulphate with the carrier lactose. Dry powder formulations for inhalation usually consist of a micronised drug (1-5μm) and inert coarse carrier particles (30-90μm) (Timsina et al., 1994). The carrier particles are included in the formulation to aid flow and dispersibility of drug particles which can be highly cohesive when micronised. Chawla et al. (1994) found no significant difference in respirable fractions between micronised salbutamol sulphate and aqueous spray dried salbutamol sulphate assessed using a Spinhaler® device attached to the TSI. It is well known that the design of the dry powder inhaler device plays a significant role in the deposition pattern of the powder formulation (Timsina et al., 1994; Steckel et al., 1997) since every type of dry powder inhaler has a specific air flow resistance that limits flow. Therefore the results of Chawla et al. (1994) cannot be directly compared to results using a different inhaler device. Further work could investigate the effect of inclusion of coarse carrier particles on the deposition of spray dried salbutamol sulphate systems.

5.2.7. Conclusions

Spray drying salbutamol sulphate from aqueous solution resulted in an amorphous system as previously shown by Chawla et al. (1994). Spray drying salbutamol sulphate from ethanolic solution also resulted in an amorphous system. Spray drying salbutamol base resulted in a powder of reduced crystallinity with some amorphous content. Spray drying ipratropium bromide from aqueous solvent resulted in a crystalline material with altered XRD peaks when compared to ipratropium bromide starting material. DSC of the spray dried material showed a large reduction in the endotherm attributable to the presence of the monohydrate and an additional endotherm prior to the melting endotherm shown by the starting material. TGA of the spray dried sample was consistent with the presence of anhydrous ipratropium bromide since no weight loss was observed, unlike for the starting material. FTIR also showed differences in the OH region of the spectra when ipratropium bromide spray dried from aqueous solvent and ipratropium bromide starting material were compared. Therefore it is likely that mainly anhydrous ipratropium bromide is produced on spray drying ipratropium bromide from aqueous solvent with the presence of low amounts of the monohydrate and possibly the production of another polymorphic form of ipratropium bromide. Spray drying ipratropium bromide from ethanolic solvent resulted in a crystalline material with an XRD pattern different from that of the material spray dried

from aqueous solvent and more similar to the ipratropium bromide starting material. DSC showed only the one melting endotherm and an endotherm in the dehydration region which was reduced in magnitude compared to the starting material. FTIR of the ethanolic spray dried material showed similar spectra to the starting material and was different from the aqueous spray dried spectra. The ipratropium bromide spray dried from ethanolic solvent could consist of ipratropium bromide monohydrate with perhaps some anhydrous ipratropium bromide or an ethanolic solvate.

Co-spray drying salbutamol sulphate with ipratropium bromide resulted in amorphous composites, regardless of solvent used.

Co-spray drying salbutamol base with ipratropium bromide resulted in the production of systems of reduced crystallinity. As the weight ratio of ipratropium bromide was increased the crystallinity reduced, with a 2:1 ratio of salbutamol:ipratropium bromide resulting in an amorphous composite.

Spray dried salbutamol sulphate (from either solvent) and co-spray dried salbutamol sulphate:ipratropium bromide sprayed from aqueous solution, showed spherical particles by SEM which were of a size suitable for inhalation. Salbutamol sulphate:ipratropium bromide systems sprayed from ethanolic solution resulted in a powder product, however by SEM the particles appeared fused. It is likely that salbutamol sulphate:ipratropium bromide systems sprayed from ethanolic solution are more hygroscopic than the equivalent systems spray dried from aqueous solutions and this may be responsible for the unusual appearance of the particles by SEM. SEM analysis of co-spray dried salbutamol base:ipratropium bromide systems showed fused aggregates which were considered too large to be suitable for inhalation.

Twin impinger studies, without the use of a carrier excipient, showed an increase in respirable fraction of spray dried salbutamol sulphate compared to micronised salbutamol sulphate regardless of solvent used in the spray drying process. Co-spray dried salbutamol sulphate:ipratropium bromide 10:1 and 5:1 systems also showed an increase in respirable fraction compared to micronised salbutamol sulphate. The respirable fraction of the 2:1 co-spray dried system was not significantly different from that of micronised salbutamol sulphate alone.

It is recognised that by changing various parameters on the spray drier, particles can be produced with different particle sizes (Conte et al., 1994, Chawla et al., 1994). Since particle size is crucial for the success of an inhalation product, optimisation of the process would be necessary to obtain the best particle size. Optimising yield is also important for an economically viable process. A factorial design experiment would elucidate the effects

of changing various parameters on the important physicochemical properties of the systems.

5.3. Budesonide and formoterol fumarate systems

Solutions of budesonide alone and formoterol fumarate dihydrate:budesonide mix, 6:100 weight ratio and 6:400 weight ratio were prepared in ethanol 95% and spray dried using the spray drying parameters given in Appendix I.

5.3.1. Budesonide

Budesonide was supplied as a micronised powder. Figure 5.22 shows the XRD scans of spray dried budesonide and budesonide starting material. Budesonide starting material was crystalline. Spray drying budesonide resulted in an amorphous product as evidenced by the absence of peaks and the presence of a diffuse halo in the XRD scan.

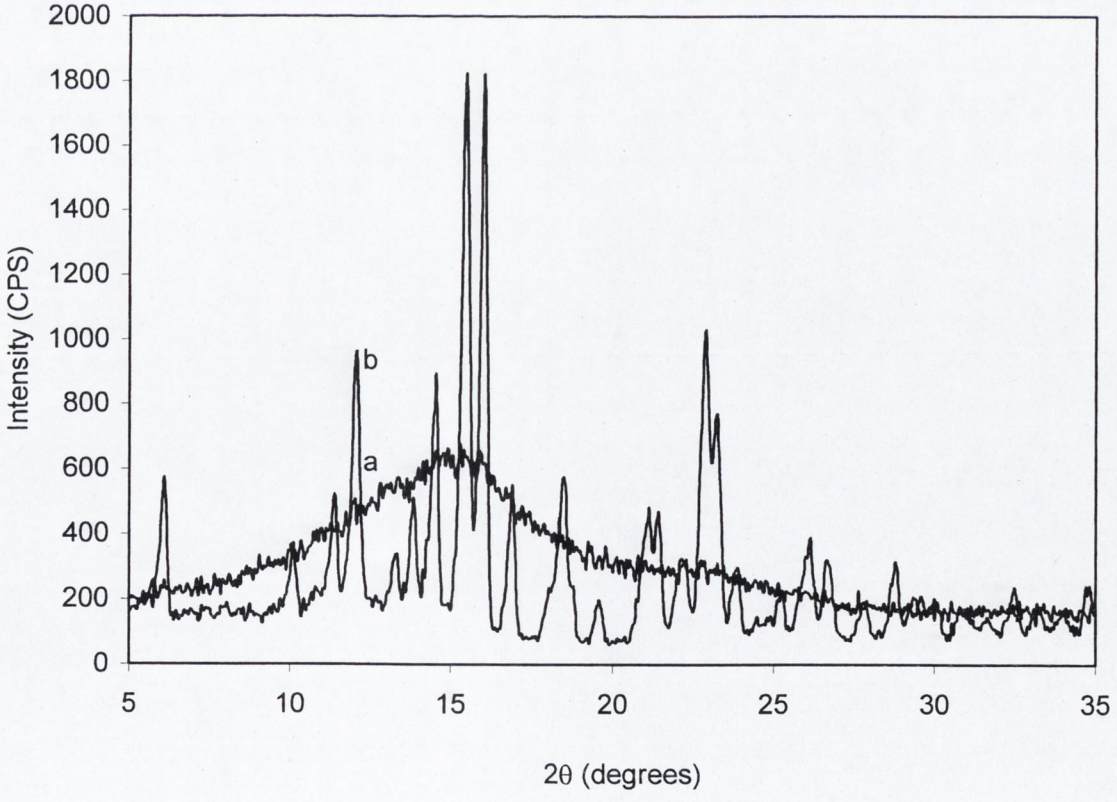

Figure 5.22 XRD scans of (a) spray dried budesonide and (b) budesonide.

Figure 5.23 shows the DSC scans of spray dried budesonide and budesonide starting material. The amorphous material recrystallised on heating as evidenced by the exotherm in the DSC scan, which had an onset temperature at approximately 113 °C. Prior to this exotherm a small endotherm was visible at approximately 90°C (at higher magnification) which may be attributed to the glass transition. The presence of the glass transition at approximately 90°C is in good agreement with the estimated temperature of 102°C, obtained by calculating 0.7 times the melting temperature in degrees Kelvin (Hancock and Zografi, 1994; Britain, 1999). The budesonide crystalline melting endotherm occurs with an onset temperature of 262°C in both the spray dried material and the starting material.

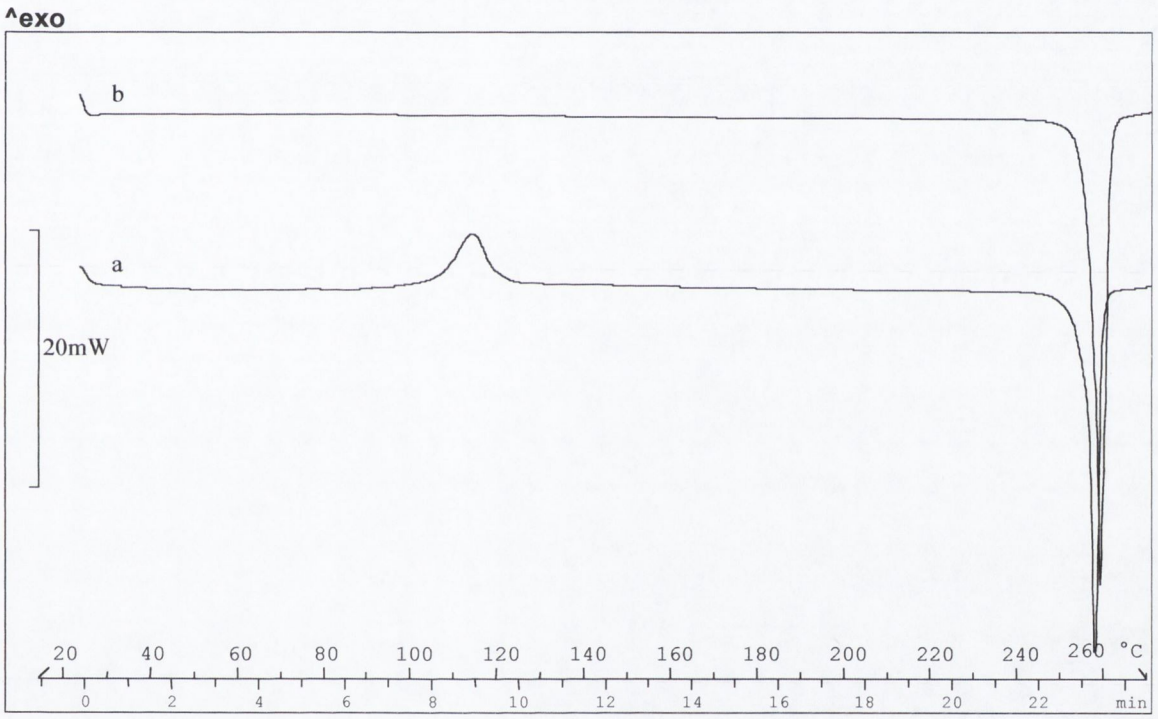

Figure 5.23 DSC scans of (a) spray dried budesonide and (b) budesonide starting material.

No differences between spray dried budesonide and budesonide starting material were detected by TGA and FTIR.

SEM showed that spray drying resulted in spherical particles which had a mainly smooth surface morphology apart from a few imperfections. Spray dried budesonide particles were approximately 0.5-5 μm in diameter. In comparison with the starting material the spray dried particles were more uniform in shape. The particles of budesonide starting material were approximately 0.5-7 μm in diameter. Figure 5.24 shows the SEM micrographs of spray dried budesonide and budesonide starting material.

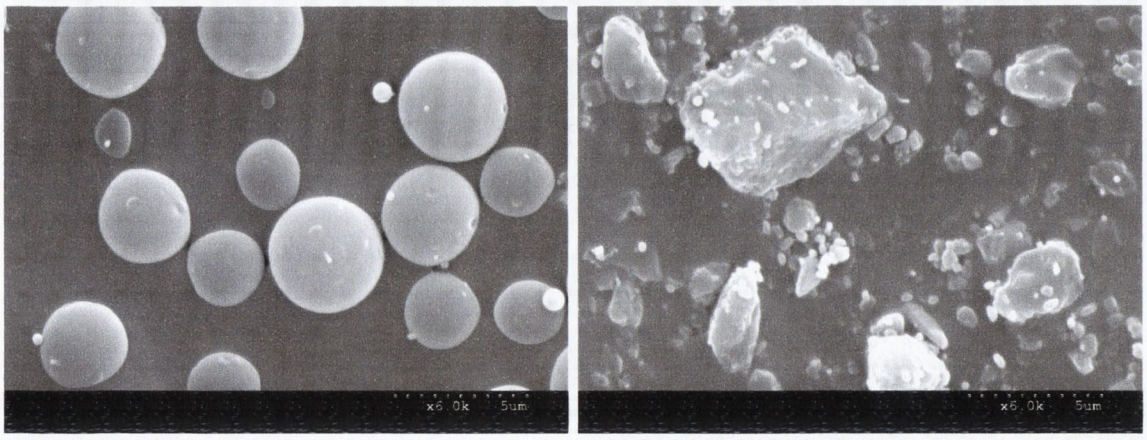

Figure 5.24 SEM micrographs of spray dried budesonide (left) and budesonide starting material (right).

5.3.2. Formoterol fumarate dihydrate

Formoterol fumarate dihydrate was supplied as a micronised powder. The XRD trace, showing peaks indicative of crystallinity, is shown in Figure 5.25. Due to the limited availability of this high cost material formoterol fumarate dihydrate was not spray dried alone.

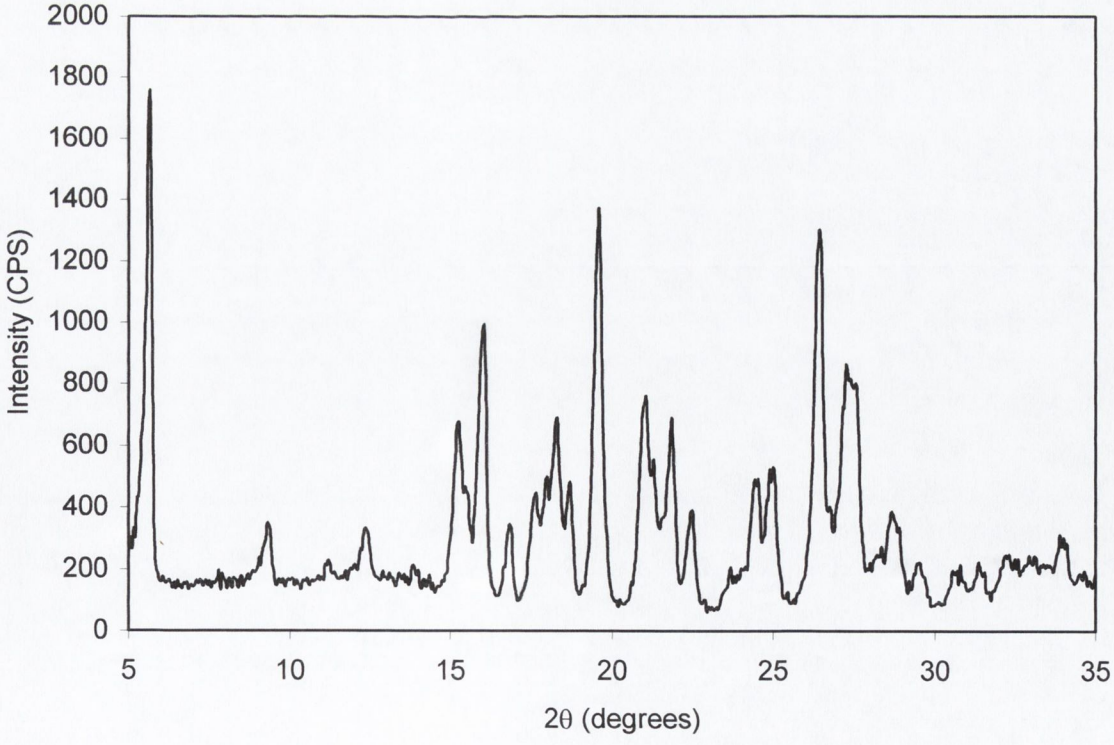

Figure 5.25 XRD scan of formoterol fumarate dihydrate starting material.

A DSC scan of the starting material is shown in Figure 5.26. The DSC shows an endotherm at approximately 120°C, consistent with the loss of crystalline water, followed by an endotherm at approximately 140°C and an endotherm at approximately 155°C. The Merck Index (1996) states that formoterol fumarate consists of two racemates, one which melts at 138-140°C and the second which melts at 154-155°C. Therefore the melting endotherms observed in these regions by DSC are consistent with melting of the two racemates. Degradation followed the melting endotherms. TGA showed weight loss at approximately 100°C corresponding to a weight loss of approximately 4% (Figure 5.27 scan c). This weight loss corresponds to the loss of the two water molecules since the weight of two water molecules expressed as a percentage of total weight of formoterol fumarate dihydrate is 4%. A TGA scan of formoterol fumarate dihydrate starting material is shown in Figure 5.27, scan c. A weight loss occurred beyond 155°C consistent with degradation.

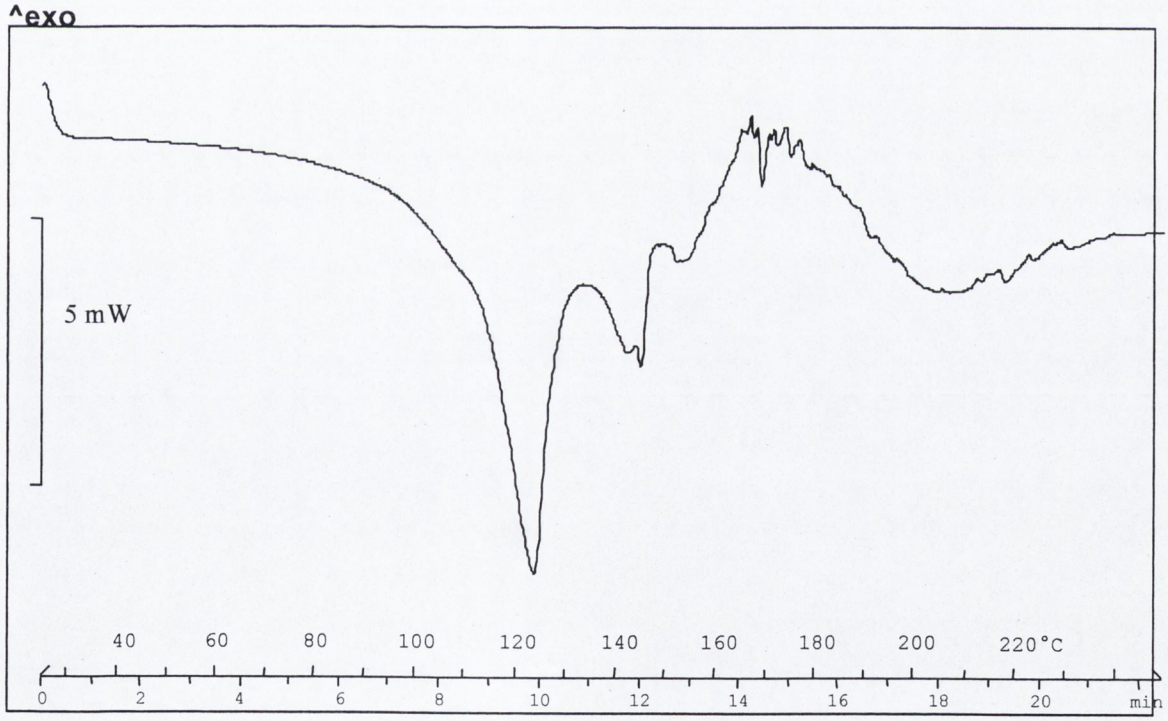

Figure 5.26 DSC scan of formoterol fumarate dihydrate.

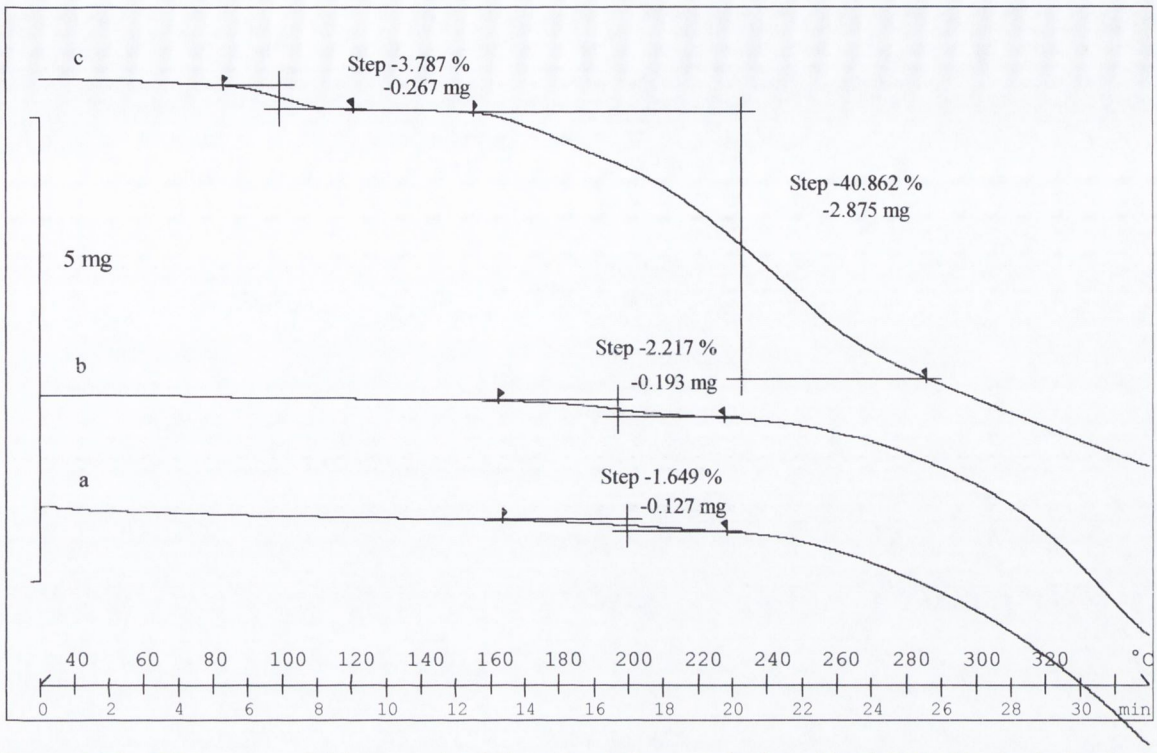

Figure 5.27 TGA scans of (a) spray dried formoterol fumarate:budesonide 6:100; (b) physical mix of formoterol fumarate dihydrate:budesonide 6:100 and (c) formoterol fumarate dihydrate.

SEM of formoterol fumarate dihydrate starting material showed irregular shaped particles under 5 μm in diameter (Figure 5.28).

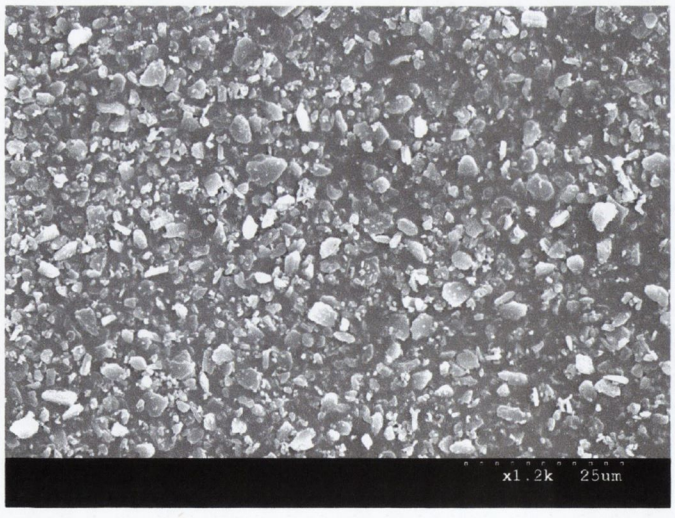

Figure 5.28 SEM micrograph of formoterol fumarate dihydrate.

5.3.3. Co-spray dried formoterol fumarate:budesonide systems

Formoterol fumarate dihydrate:budesonide mixtures on spray drying resulted in amorphous systems as evidenced by diffuse halos by XRD (Figure 5.29). XRD scans of the physical mixtures were identical to XRD scans of budesonide alone. No peaks indicative of formoterol fumarate could be detected in the physical mixes due to the low concentrations of formoterol fumarate present.

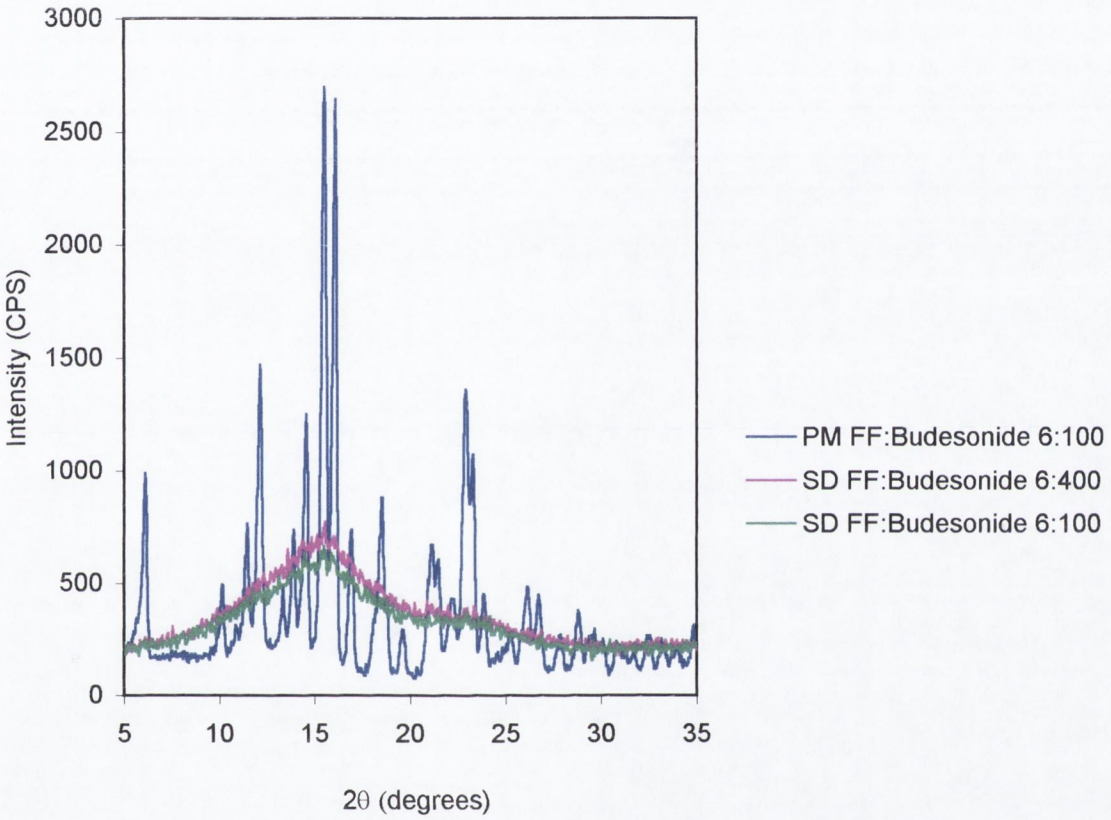

Figure 5.29 XRD scans of spray dried (SD) formoterol fumarate (FF):budesonide 6:100, SD formoterol fumarate:budsonide 6:400 and physical mix (PM) of formoterol fumarate dihydrate: budesonide 6:100 system.

The DSC scans of the co-spray dried systems and their equivalent physical mixes are shown in Figure 5.30.

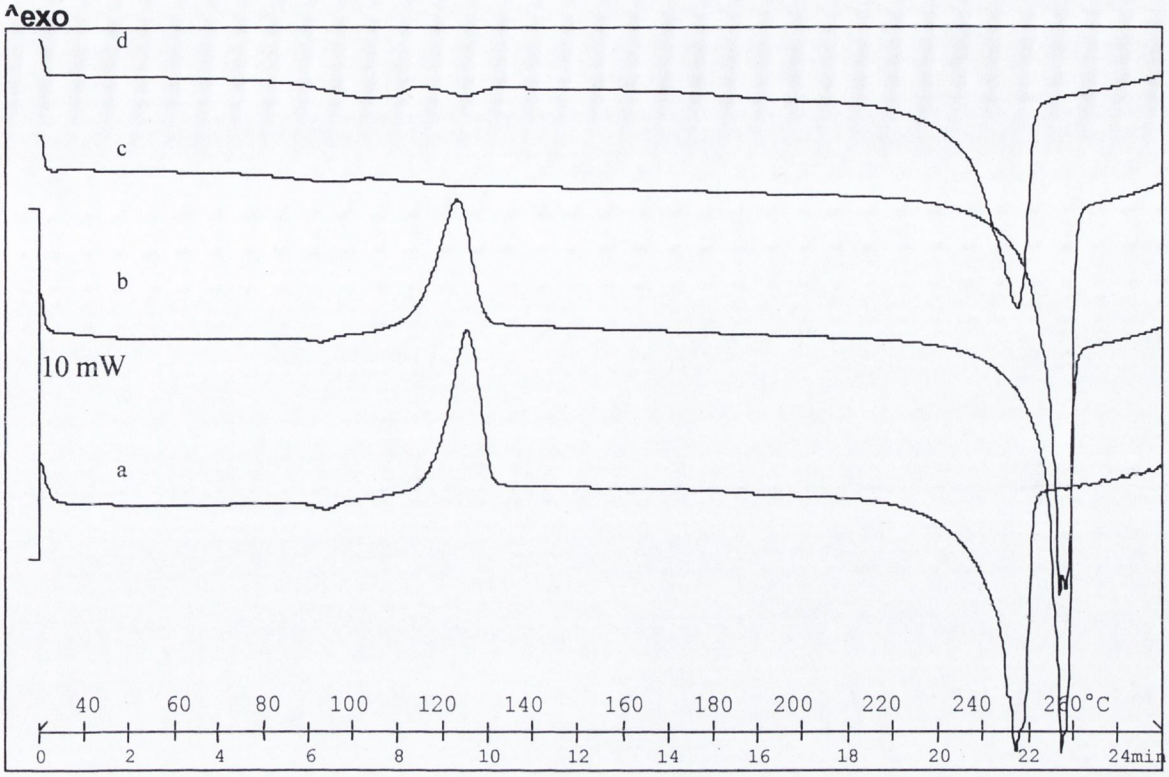

Figure 5.30 DSC scans of (a) spray dried formoterol fumarate:budesonide 6:100; (b) spray dried formoterol fumarate:budesonide 6:400; (c) physical mix of formoterol fumarate dihydrate:budesonide 6:400 and (d) physical mix of formoterol fumarate dihydrate:budesonide 6:100.

DSC scans of the physical mixtures showed evidence of the presence of both components. The presence of the two endotherms due to formoterol fumarate dihydrate were more easily observed in the DSC scan at higher resolution as shown in Figure 5.31. The two endotherms from formoterol fumarate dihydrate, as well as the melting endotherm for budesonide, occurred at lower temperatures than when either component was analysed alone. The co-spray dried systems showed a small endotherm, at approximately 90°C, which could be a relaxation endotherm associated with the glass transition (seen at similar temperature in spray dried budesonide alone) but could also be due to the presence of formoterol fumarate dihydrate. A budesonide recrystallisation exotherm was observed beginning at 118°C for the 6:100 mix and 114°C for the 6:400 system. The higher temperature recrystallisation exotherm, observed in the 6:100 system compared to the 6:400 system and spray dried budesonide alone, implies that the higher amount of formoterol fumarate present in this system may act as an antiplasticiser, i.e. an additive which raises the glass transition temperature of a substance (Hancock and Zografi, 1994) thereby increasing the stability of the amorphous system. Formoterol fumarate may be present in the anhydrous form in the spray dried composite and may preferentially absorb

any available moisture thus preventing moisture from plasticising the amorphous budesonide.

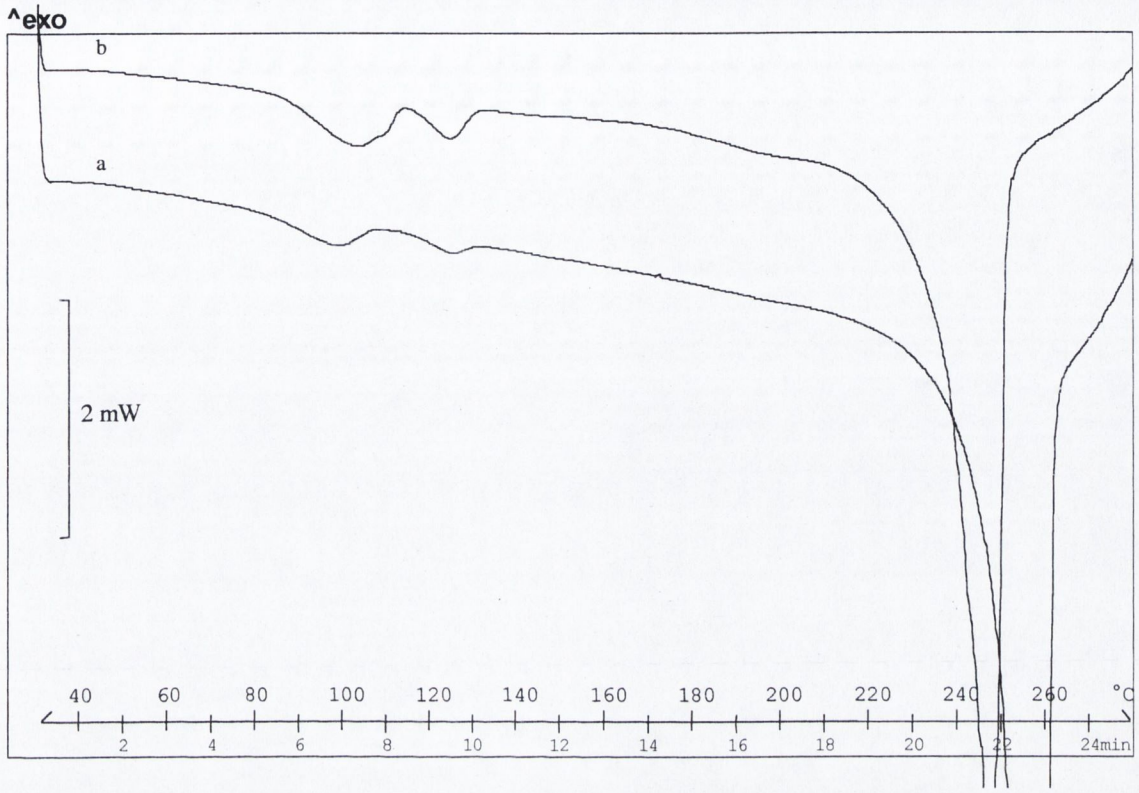

Figure 5.31 DSC scans of (a) physical mix of formoterol fumarate dihydrate:budesonide 6:400 and (b) physical mix of formoterol fumarate dihydrate:budesonide 6:100, at a higher magnification than in Figure 5.30.

TGA scans of formoterol fumarate dihydrate:budesonide 6:100 physical mix and equivalent spray dried system are shown in Figure 5.27. Weight losses consistent with loss of hydrates were not observed for physical mix or co-spray dried systems. TGA of the 6:100 physical mix showed weight loss occurring after 175°C corresponding to a loss of approximately 2.2%. A weight loss of approximately 1.6% was seen in the same region for the co-spray dried 6:100 system. No such loss was detected for either of the 6:400 systems. This loss, probably due to degradation of formoterol fumarate, was not detected in the 6:400 systems possibly due to the very low amount of formoterol fumarate dihydrate present. The absence of a weight loss consistent with loss of the dihydrate implies that TGA is not sensitive enough to detect such small weight losses.

FTIR showed no apparent difference between physical mixes and co-spray dried systems for both weight ratios investigated.

Figure 5.32 shows the SEM micrographs of the co-spray dried systems. SEM showed the physical mixes to consist of irregular shaped particles of roughly 0.5 to 5 μm in diameter. The co-spray dried particles were uniform smooth spheres of approximately 1-5.5 μm in diameter.

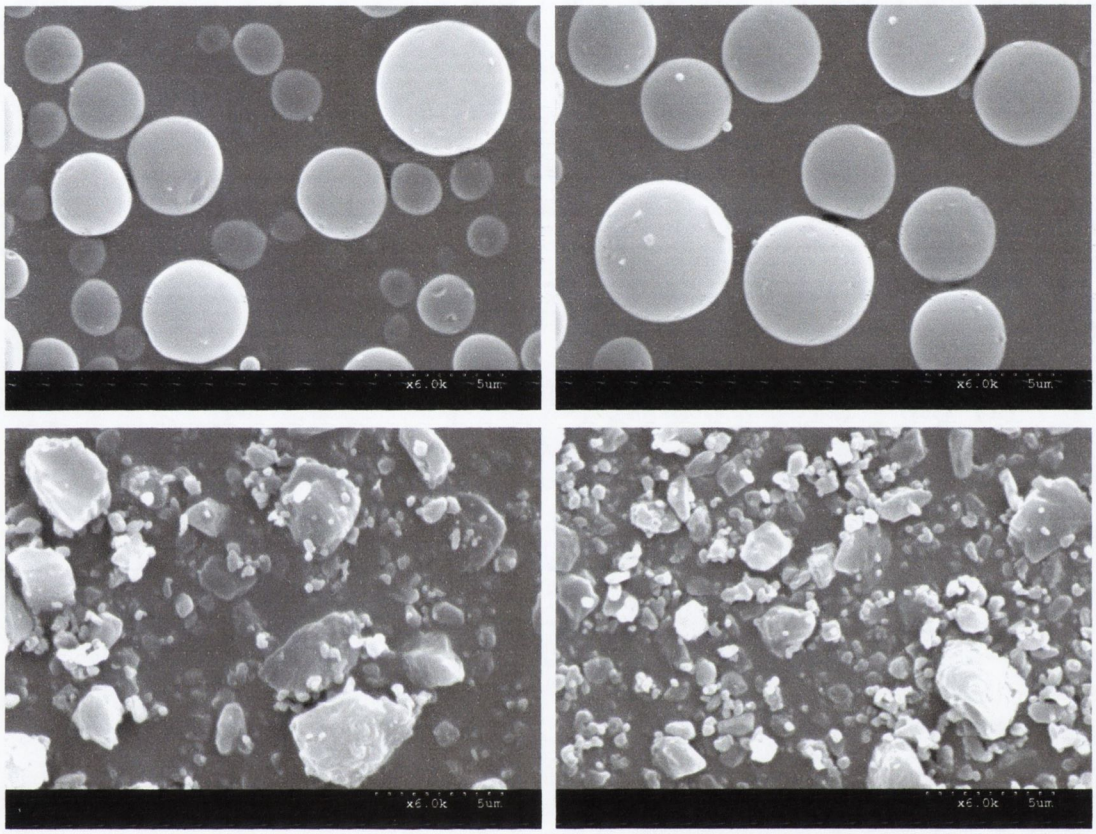

Figure 5.32 SEM micrographs of spray dried formoterol fumarate:budesonide 6:100 (top left), 6:400 (top right) and physical mixes of formoterol fumarate dihydrate:budesonide 6:100 (bottom left) and 6:400 (bottom right).

5.3.4. Factorial Design Study

A factorial design is a statistical design strategy for the systematic investigation of complex systems. Spray drying involves setting four different parameters on the spray drier and additionally a fifth parameter, the feed concentration, can also be altered.
The four parameters which can be set on the Büchi spray drier are:

Inlet temperature
Pump rate
Air (spray) flow rate
Aspirator rate

Outlet temperature is dependent on the settings of the above parameters and cannot be set directly. Therefore to assess the affect of the five variables the most complete experimental design would be a 2^5 factorial design. This would look at all factors at two levels – a high level and a low level and would allow all interaction effects to be observed. However 32 experimental runs would be necessary to run all the factors at both levels once, not accounting for any replicate runs. Formoterol fumarate:budesonide 6:100 system was chosen as a model two component system for the factorial design study since it contained a higher concentration of the formoterol fumarate than the 6:400 system and formoterol fumarate:budesonide spray dried systems showed favourable particles for potential use in inhalation formulations. Yield and particle size are important for the production of a powder formulation for inhalation. The feed concentration was kept constant at 1.75% w/v (highest concentration at which both components were soluble). Inlet temperature was kept constant at 78-79°C (high enough to result in evaporation of the solvent but low enough to minimise risks from explosion and thermal degradation). Aspirator rate should be kept at a maximum, if possible, since it is responsible for sucking the drying air through the spray dryer and regulates the quantity of the heated air (or gas) in the apparatus. The energy available for evaporation varies according to the amount of air (or gas) in the apparatus meaning that the aspirator setting has a major influence on spray drying performance. It may not be practical to set the aspirator at maximum for certain products. Very fine products with low specific weight may require lower aspirator performance since high aspirator rate can result in light powders being carried through the apparatus towards the filters resulting in poor yields. The two parameters which were deemed most likely to affect yield and particle size were airflow rate and pump rate. Therefore a 2^2 factorial design was carried out to determine the effects of altering airflow rate and pump rate on the yield and particle size of the resultant powder using the formoterol fumarate dihydrate:budesonide 6:100 system as a model. The Büchi spray drier was operated using the parameters shown in Table 5.2. Yield was expressed as a percentage of starting material with approximately 1.06 g being spray dried for each set of parameters. Minitab™ was used to generate a random experimental run order. Each combination of parameters were spray dried in duplicate and the percentage yield for each replicate is shown in Table 5.2

Table 5.2 Results of yield obtained for the different experimental design points.

Air flow rate (l/hr)	Pump rate %	% Yield Replicate 1	% Yield Replicate 2	Mean % Yield	Standard Deviation
400 (-)	10 (-)	56.2	49.4	52.8	4.81
800 (+)	10 (-)	42.5	37.5	40.0	3.36
400 (-)	40 (+)	33.0	42.3	37.65	6.58
800 (+)	40 (+)	49.5	53.4	51.45	2.76

Figure 5.33 shows a graphical representation of the mean percentage yields for the different experimental design points.

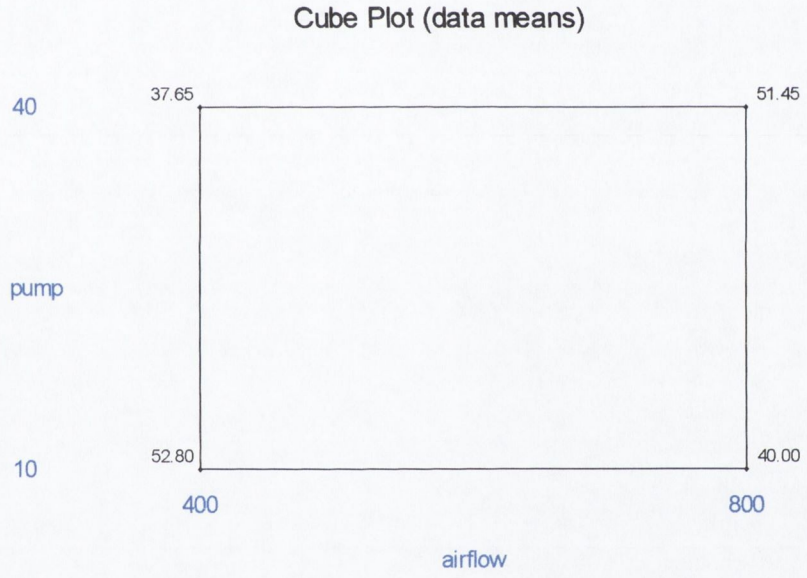

Figure 5.33 Cube plot of the mean percentage yields of spray dried formoterol fumarate:budesonide obtained using the different processing parameters.

The model for the analysis using the factorial design assumes that, while the average response may vary from design point to design point, the standard deviation of replicate results will be the same for all design points. Assuming this, the standard deviations of each design point are combined to give an overall pooled value.

Interactions occur when the effect of changing one factor depends on the level of a second factor.

The Minitab™ analyses showed a P value of 0.016 for the interaction term. Therefore, since this interaction is significant (i.e. less than 0.05), neither parameter can be considered alone since the effect of one is dependent on the effect of the other. When airflow is low an increase in pump rate results in a decreased yield. When airflow is high an increase in pump results in an increased yield.

To determine whether the changes in yield are statistically significant appropriate t-tests are carried out. The estimated standard error (SE) is calculated using Equation 5.1.

$$\text{SE}\left(\text{difference between two averages}\right) = \sqrt{\frac{2s^2}{N}} \qquad \text{Equation 5.1}$$

N is the number of observations on which the mean is based (in this case N is 2). s^2 is obtained from the pooled standard deviation for the yield data as shown in Equation 5.2.

$$s^2 = \frac{s_1^2 + s_2^2 + s_3^2 + s_4^2}{4} \qquad \text{Equation 5.2}$$

The estimated SE of any difference is 4.62. The pooled standard deviation has 4 degrees of freedom associated with it, therefore if $\alpha = 0.05$ then the relevant t value is 2.78. The differences between each design point are divided by the SE (4.62) and if the value obtained lies outside the critical value of +/-2.78 the difference in yield obtained by changing from one set of parameters to another is deemed significant, if it lies within +/-2.78 it is deemed not significant.

The difference between low and high pump at low airflow is 15.15 therefore 15.15/4.62 = 3.28 which is significant because it is greater than 2.78. The difference between low and high pump at high airflow is 11.45, 11.45/4.62 = 2.48, which is not significant. The difference between low and high airflow at low pump is 12.8, 12.8/4.62 = 2.77 which is just not significant and the difference between high and low airflow at high pump is 13.8, 13.8/4.62 = 2.98 which is significant. The nature of the interaction is now clearer. When airflow is 400 changing pump rate from 10% to 40% causes a reduction in yield that is statistically significant. When airflow is 800 increasing pump rate from 10 to 40% results in no significant change in the yield. When pump is at 40% changing the airflow from 400 to 800 l/hr results in a significant increase in yield. When pump rate is at 10%, increasing airflow from 400 to 800 l/hr does not significantly change the yield.

For the purposes of maximising production yield in a timely manner high pump and high airflow would be chosen. A confidence interval for the long run response at the chosen combination of factors studied is determined using Equation 5.3.

$$\overline{Y}_1 \pm t\sqrt{\frac{s^2}{n}} \qquad \text{Equation 5.3}$$

where $\overline{Y}_1$ is the mean of the chosen operating condition, t is the critical value based on the number of degrees of freedom associated with the standard deviation, in this case t is 2.78, and n is the number of observations on which $\overline{Y}_1$ is based, i.e. 2 in this case.

The expected percentage yield under these conditions would be estimated at between 42.37 and 60.53% (i.e. 51.45 ± 9.08, using a 95% confidence interval).

An increase in the number of replicates could reduce the standard deviation and allow more of an insight into whether changing airflow from low to high at low pump was significant since a value of 2.77 is only just inside the critical limits.

Since particle size is also of interest the effect of changing the airflow and pump speed on particle size was investigated. Airflow is known to affect particle size with higher airflow resulting in smaller particles (Masters, 1985). It was thought that pump speed might affect the particle size since a low pump would result in less liquid being passed to the evaporating chamber and therefore perhaps result in faster evaporation thereby resulting in a smaller particle size.

Particle size measurements were carried out as described in Chapter 2. An ANOVA performed by Minitab™, was used to compare the particle sizes of the systems prepared using the different spray drying parameters, the results of the ANOVA are shown in Table 5.3.

Morphologically all particles appeared similar with respect to shape and surface characteristics. The results of the particle size study showed that airflow setting controlled the particle size in this study irrespective of pump setting. High airflows resulted in particles with smaller diameters than did low airflows. Systems spray dried at different pump rates were not found to produce particle sizes that were significantly different from each other. Since low pump rates result in longer processing times, higher pump speeds would result in more efficient processing without affecting particle size significantly. All processing parameters investigated produced particles within the respirable range (0.5–5 μm diameter). Therefore considering the yield and particle size information the optimum

processing conditions for the production of the smallest particles in a timely manner would be high airflow and high pump rate.

Table 5.3 Anova results for particle diameters obtained from spray drying formoterol fumarate:budesonide 6:100 using the following varying spray drying parameters: airflow 400 l/hr, pump 40% (a400p40); airflow 800 l/hr, pump 40% (a800p40); airflow 400 l/hr, pump 10% (a400p10) and airflow 800 l/hr, pump 10% (a800p10).

Level	N	Mean	StDev	Individual 95% Confidence Intervals For Mean (μm) Based on Pooled StDev
a400p40	200	2.345	1.593	(---*--)
a800p40	200	1.537	0.959	(---*--)
a400p10	200	2.513	1.622	(---*--)
a800p10	200	1.343	0.627	(---*--)
Pooled StDev =		1.273		1.50 2.00 2.50

5.3.5. Conclusions

Spray drying of budesonide and formoterol fumarate dihydrate:budesonide systems resulted in the production of microspherical particles. All systems appeared amorphous by XRD. However formoterol fumarate dihydrate in the physical mix systems was below the detection level by XRD due to its low concentration in the physical mixes and therefore it is possible that the co-spray dried systems may consist of amorphous budesonide and crystalline formoterol fumarate. Due to the limited availability of formoterol fumarate dihydrate it was not spray dried alone in this study. Spray drying of formoterol fumarate dihydrate alone was performed in a later study by Lidia Tajber (a Pharmaceutics and Pharmaceutical Technology Ph.D. research student) and resulted in the production of an amorphous phase, as evidenced by a halo by XRD. The preparation of a physical mix of crystalline formoterol fumarate dihydrate with amorphous budesonide, would clarify if crystalline formoterol fumarate dihydrate, present in such a low concentration in a mix, would be detectable by XRD. Due to the limited availability of formoterol fumarate due to its high cost this was not performed. However since formoterol fumarate spray dried alone resulted in an amorphous system it is likely that it was present in an amorphous state in the co-spray dried formoterol fumarate:budesonide systems. No distinct exotherm was visible when spray dried formoterol fumarate alone was analysed by DSC. It was not possible by DSC to confirm the presence/absence of crystalline formoterol fumarate in the co-spray dried systems since the dehydration and melting endothermic peaks of formoterol fumarate dihydrate occur in the same region as the budesonide glass transition and the budesonide recrystallisation exotherm. The particle size distribution appeared narrower by SEM for

the spray dried systems when compared to the physical mixes with fewer particles in the less than 0.5 μm size range (particles which would be too light to deposit in the lungs and would be exhaled). Spray dried formoterol fumarate:budesonide systems were analysed by IVAX Pharmaceuticals, Ireland, using a multistage impinger to determine respirable fractions and the results obtained were favourable for potential use in DPIs.

Alteration of spray drying parameters is likely to affect the resultant products. Since particle size and particle size distribution are crucial for the potential use of the resultant powder as an inhalation product, the effects of alteration of pump rate and airflow rate was determined. While a high airflow rate was necessary to result in smaller particles, either low pump rate and low airflow rate or high pump rate and high airflow rate was necessary for high yields. Therefore to produce smaller particles with high yields a high airflow rate and a high pump rate should be used.

CO-SPRAY DRIED EXCIPIENT-CONTAINING SYSTEMS FOR DRY POWDER INHALER DELIVERY

6.1. Introduction

Dry powder inhaler (DPI) formulations generally consist of micronised drug and inert coarse carrier particles. The carrier excipients are included to aid flow and dispersiblity of drug particles which may be highly cohesive when micronised (Timsina et al., 1994). Inclusion of a carrier also overcomes the problem of dose metering if fractions of a milligram of a potent medicament are to be delivered (Ganderton and Jones, 1992). Typical formulations consist of carriers and micronised drug in a ratio of 1:67.5 (Zeng et al., 2000). Adequate mixing is essential for dose uniformity and formulations consisting of a drug and a carrier need to be tested for homogeneity of mixing (Timsina et al., 1994). Co-spray drying drugs with excipients should avoid problems of non-homogeneity of mixing of drug and carriers, while overcoming dose metering problems if small amounts of medicament need to be administered.

The adhesion of particles is a surface phenomenon, the morphology of the surface having a significant effect on the adhesion of particles (Ganderton and Jones, 1992). The relatively smooth surfaced powders which often result from spray drying, may potentially improve respirable fractions of drugs, compared to equivalent micronised systems.

Zeng et al. (2000) reported that carrier morphology can influence drug delivery by DPI, demonstrating that lactose crystals with an increased surface smoothness or elongation ratio resulted in an increased respirable fraction of salbutamol sulphate *in vitro*, measured using a twin impinger. Carriers should possess sufficient adhesion to result in mixtures which do not segregate during the handling and filling processes, but which release the drug when inhaled. Co-spray drying overcomes the problems of segregation of the drug and carrier during handling and filling and overcomes the problems of excessive adhesion of drug to carrier which would result in the drug staying adhered to the carrier and not reaching the site of action.

Since co-spray drying for inhalation delivery appears to have advantages, the model drug salbutamol sulphate was co-spray dried with various excipients. Table 6.1 shows the two component systems investigated. The spray drying conditions for each system are listed in Appendix I.

Table 6.1. Two component systems investigated

Component A	Component B	Percentage of Component B
Salbutamol sulphate	Lactose monohydrate	5%, 20% and 40% lactose
Salbutamol sulphate	PEG 4000	5%, 20% and 40% PEG 4000
Salbutamol sulphate	PEG 20,000	5%, 20% and 40% PEG 20,000
Salbutamol sulphate	Chitosan (low molecular weight)	60%, 80% and 90% chitosan
Salbutamol sulphate	Chitosan (crosslinked with formaldehyde*)	60%, 80% and 90% chitosan
Chitosan (non-crosslinked)	PEG 4000	10%, 20% and 30% PEG 4000

* 1.6% v/v of a 1% formaldehyde solution was used to crosslink the chitosan

6.2. Salbutamol sulphate/lactose systems

Salbutamol sulphate/lactose systems consisting of 5%, 20% and 40% lactose by weight of total solids were spray dried as 10% w/v aqueous solutions. The 20% lactose system was also spray dried at a feed concentration of 2.5% w/v from an aqueous solution. The 20% systems showed similar XRD and DSC scans regardless of the feed concentration at which they were spray dried. The 5%, 20% and 40% systems were all amorphous as evidenced by XRD analysis. Figure 6.1 shows the XRD scans of the various spray dried systems showing diffuse halos, in contrast to a physical mix of salbutamol sulphate/lactose 20% which shows peaks attributable to both crystalline components.

Figure 6.2 shows the DSC scans of spray dried salbutamol sulphate/lactose composites and a DSC scan of a physical mix of salbutamol sulphate/lactose 20%. The DSC scans of the spray dried systems did not show exothermic events indicative of recrystallisation of amorphous material. The spray dried systems did show degradation of salbutamol sulphate on heating which did not occur in the physical mixes. This implies that spray drying may result in some degradation or some instability in the systems which on heating results in degradation. The DSC scans of the spray dried salbutamol sulphate/lactose systems appeared very similar to the scans of salbutamol sulphate spray dried alone or indeed spray dried salbutamol sulphate:ipratropium bromide systems spray dried from aqueous solution (Chapter 5). The spray dried salbutamol sulphate/lactose systems showed broad endotherms prior to 100°C consistent with loss of absorbed moisture. Two very small endotherms at approximately 120°C and 140°C and a broad melting peak starting at approximately 165°C, with jagged peaks indicating degradation, were also observed. The lactose used in the physical mix was lactose monohydrate, therefore the endotherm visible

in the DSC scan of the physical mix at approximately 150°C is due to the dehydration of the monohydrate. The melting endotherm of spray dried lactose alone by DSC has an onset temperature at 217°C (Chapter 3). In the co-spray dried salbutamol sulphate/lactose systems no distinct peak was observed at this temperature. The melting of lactose may have shifted to a lower temperature and be obscured by the melting of salbutamol sulphate. In the case of the physical mix of salbutamol sulphate/lactose, the broad endotherm at approximately 200°C is likely to be due to the melting of lactose which may occur at a lower temperature than when present alone. The melting of salbutamol sulphate may overlap with the melting of lactose and this may be responsible for the broad melting endotherm that is observed.

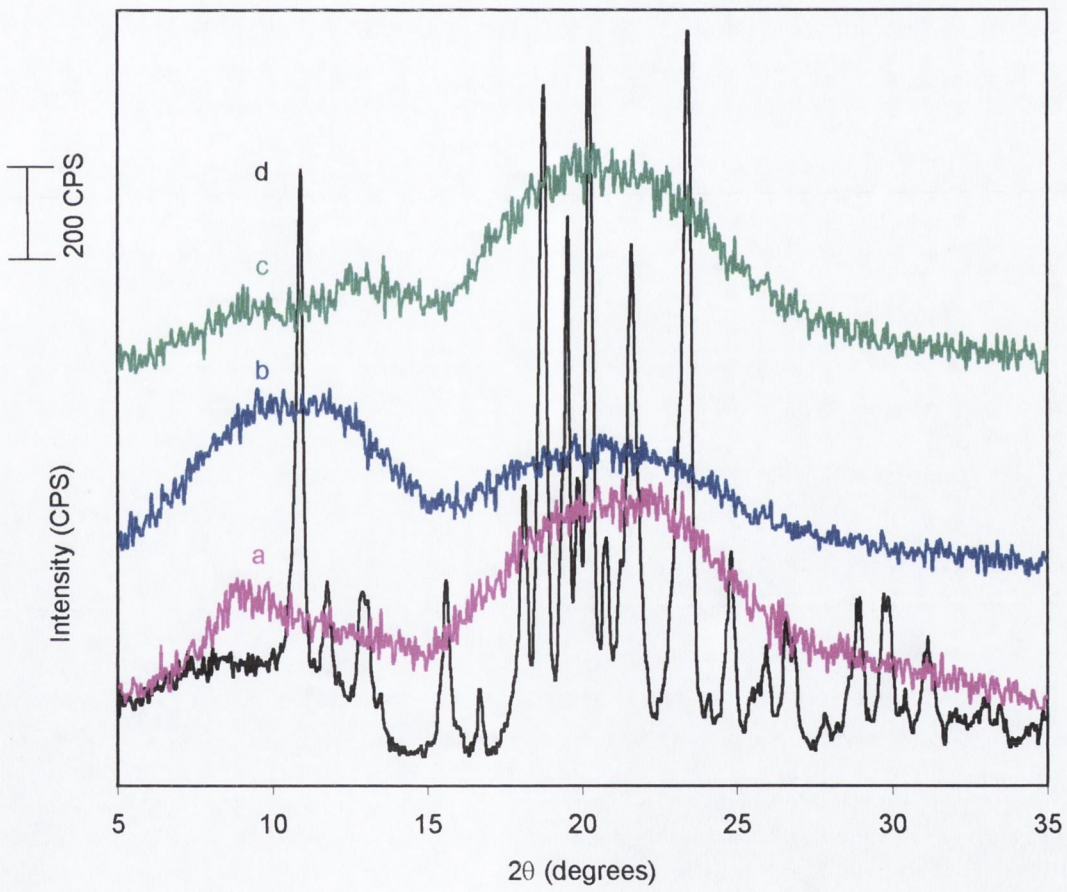

Figure 6.1 XRD scans of (a) spray dried salbutamol sulphate/lactose 5%; (b) spray dried salbutamol sulphate/lactose 20%; (c) spray dried salbutamol sulphate/lactose 40% and (d) physical mix of salbutamol sulphate/lactose 20%.

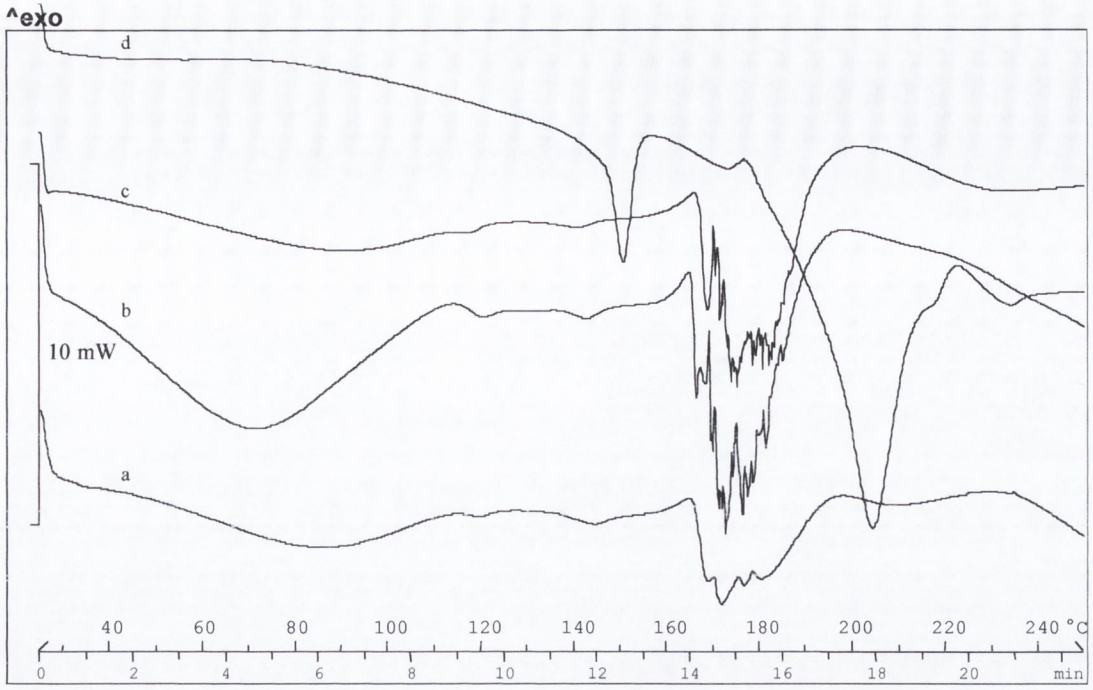

Figure 6.2 DSC scans of (a) spray dried salbutamol sulphate/lactose 5%; (b) spray dried salbutamol sulphate/lactose 20%; (c) spray dried salbutamol sulphate/lactose 40% and (d) physical mix of salbutamol sulphate/lactose monohydrate 20%.

Spray drying salbutamol sulphate/lactose solutions produced a powder, however SEM micrographs of the samples did not show particles but showed a bubbling melted surface (Figure 6.3).

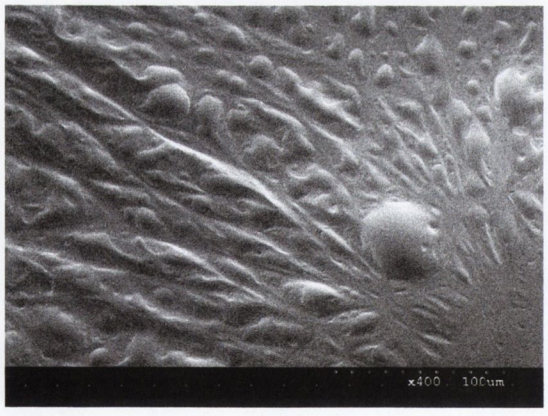

Figure 6.3 SEM micrograph of spray dried salbutamol sulphate/lactose 20%.

The mounting and gold coating was repeated but no distinct particles were evident. Samples were carbon coated and mounted without coating and again SEM showed atypical pictures. Samples were then taken straight from the dessicator and looked at under a light microscope (Olympus BX 60). While being observed under the microscope, spherical

particles could be seen which appeared to absorb moisture and merge together within a matter of seconds.

Samples were then mounted on stubs for gold coating immediately and examined without delay. SEM micrographs of the immediately coated particles are shown in Figure 6.4. The 5% and 20% lactose systems consisted of spheres with slightly indented surfaces. The 40% lactose system also showed spheres but many of these were fused and had started merging together prior to SEM analysis, appearing in some areas similar to the previous samples which had been exposed to the environment for too long during preparation.

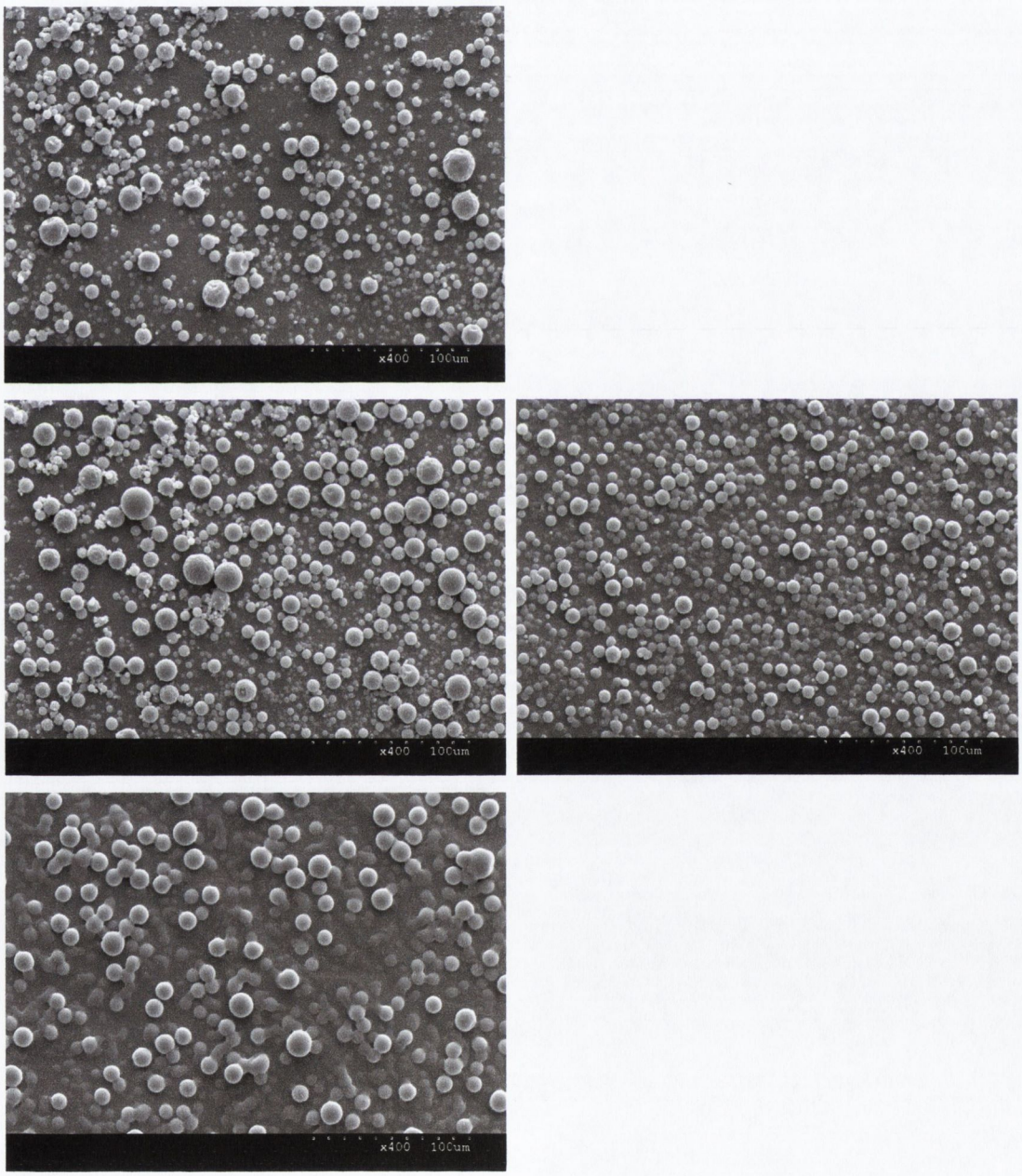

Figure 6.4 SEM micrographs of immediately coated spray dried salbutamol sulphate/lactose 5% (top), spray dried salbutamol sulphate/lactose 20% (middle left; spray dried as a 10% w/v solution, middle right; spray dried as a 2.5% w/v solution) and spray dried salbutamol sulphate/lactose 40% (bottom).

The particles of the salbutamol sulphate/lactose 5% system were approximately 1 to 15 μm in diameter. Particles of the 20% system spray dried as a 10% w/v solution were approximately 1 to 20 μm in diameter. Salbutamol sulphate/lactose 20% spray dried at the lower feed concentration of 2.5% w/v resulted in particles with a narrower size distribution, particles being approximately 2 to 10 μm in diameter. The salbutamol sulphate/lactose 40% system resulted in particles 5 to 15 μm in diameter. However these particles had already started to merge by the time they were gold coated, therefore their true size is expected to be smaller.

6.3. Salbutamol sulphate/PEG 4000 systems

Figure 6.5 shows the XRD scans of spray dried salbutamol sulphate/PEG 4000 composites (containing 5, 20 and 40% PEG 4000 by weight of total solids).

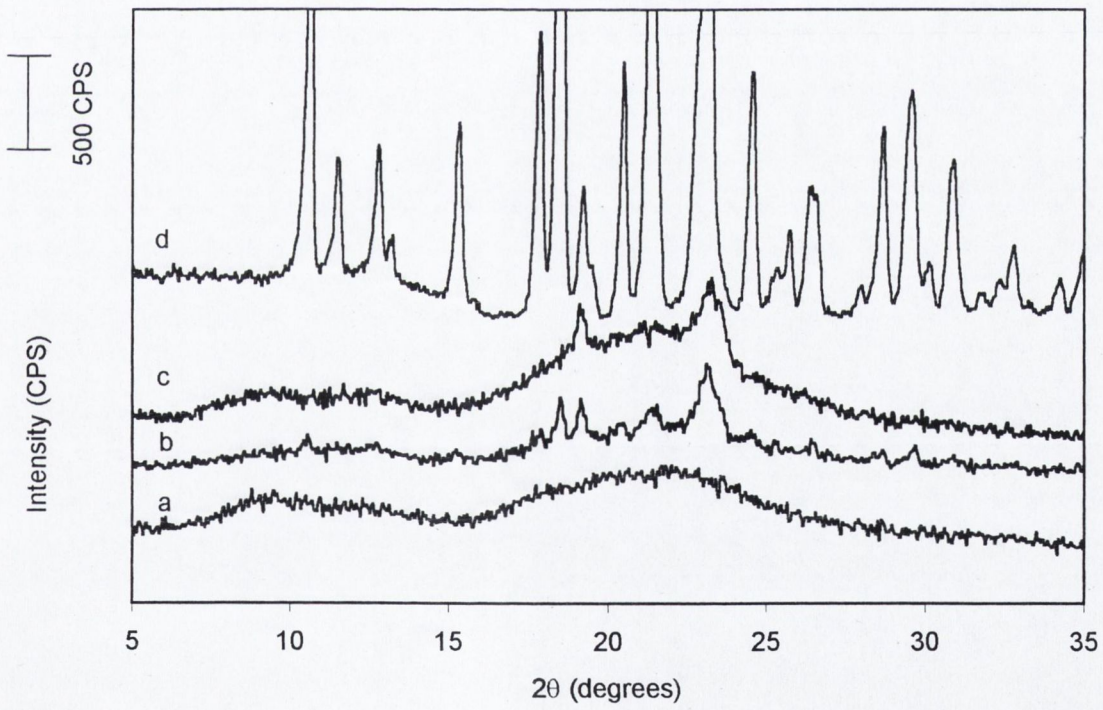

Figure 6.5 XRD scans of (a) spray dried salbutamol sulphate/PEG 4000 5%; (b) spray dried salbutamol sulphate/PEG 4000 20%; (c) spray dried salbutamol sulphate/PEG 4000 40% and (d) physical mix of salbutamol sulphate/PEG 4000 5%.

No peaks indicative of crystallinity were apparent by XRD for the 5% system. The 20 and 40% PEG 4000 systems did show some peaks indicative of the presence of some

crystalline PEG, however these peaks were of very low intensity compared to a physical mix, indicating some reduction in crystallinity of PEG 4000 during processing. The 20% PEG 4000 system appeared to contain some crystalline salbutamol sulphate unlike the 40% system which showed only the two peaks at approximately 19° and 23° 2θ, attributable to crystalline PEG 4000.

DSC scans of salbutamol sulphate/PEG 4000 systems are shown in Figure 6.6.

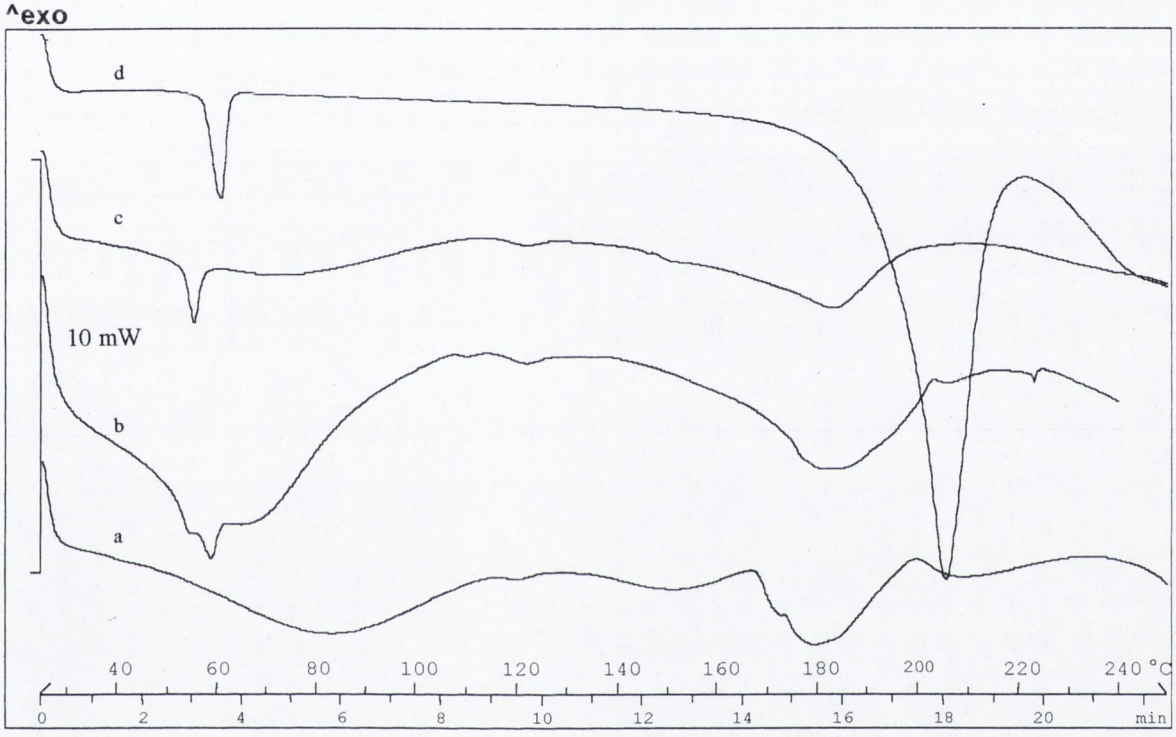

Figure 6.6 DSC scans of (a) spray dried salbutamol sulphate/PEG 4000 5%; (b) spray dried salbutamol sulphate/PEG 4000 20%; (c) spray dried salbutamol sulphate/PEG 4000 40% and (d) physical mix of salbutamol sulphate/PEG 4000 5%.

No melting endotherm for PEG 4000 is visible in the DSC scan of the spray dried 5% system, however a melting endotherm for PEG 4000 can be seen for the 5% physical mix. This indicates that DSC can detect the presence of crystalline PEG 4000 at this level and therefore spray drying has resulted in amorphous PEG 4000. The 20% PEG 4000 system showed two melting endotherms for PEG 4000 which could represent melting of some once folded PEG (metastable) as well as melting of the extended chain form of PEG (Chatham, 1985, Kambe, 1980). The 40% PEG 4000 system showed a PEG melting peak which occurred at a slightly lower temperature than in the equivalent physical mix (possibly due to the presence of the once folded metastable form). The magnitude of the PEG endotherm in the 40% system was less than for the 5% physical mix implying less

than 5% crystalline PEG is present. No recrystallisation exotherms are visible by DSC for any of the spray dried systems and the melting endotherms of salbutamol sulphate are broader and reduced in onset temperature compared to the physical mixes.

SEM micrographs showed spherical salbutamol sulphate/PEG 4000 5% particles with diameters of 4-10 μm (Figure 6.7). The salbutamol sulphate/PEG 4000 20% system appeared to consist of fused aggregates of spheres (Figure 6.8). Large fused aggregates had diameters of approximately 25-30 μm. Individual spheres were approximately 2-6 μm in diameter. The salbutamol sulphate/PEG 4000 40% SEM micrographs showed spherical structures of approximately 70 μm in diameter, consisting of many tiny particles as well as separate spherical individual particles approximately 1-5 μm in diameter (Figure 6.9).

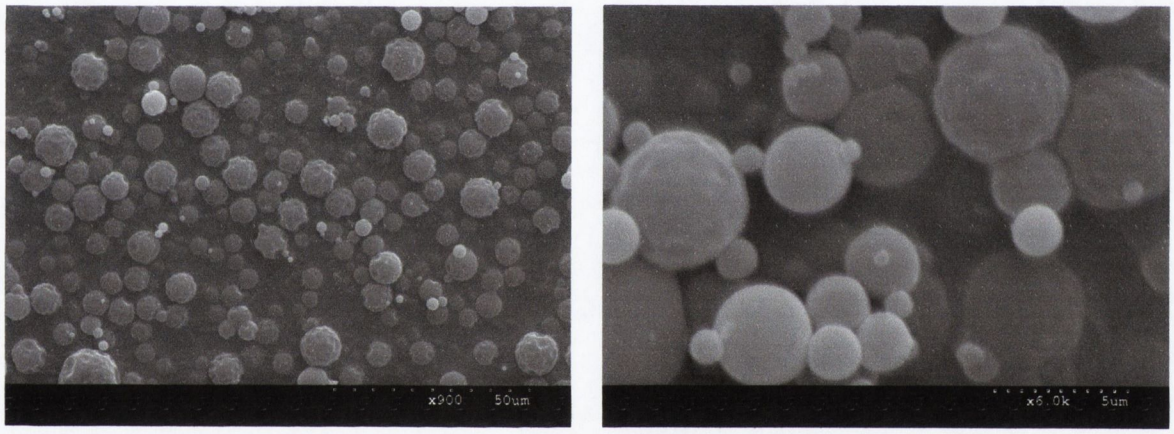

Figure 6.7 SEM micrographs of spray dried salbutamol sulphate/PEG 4000 5%.

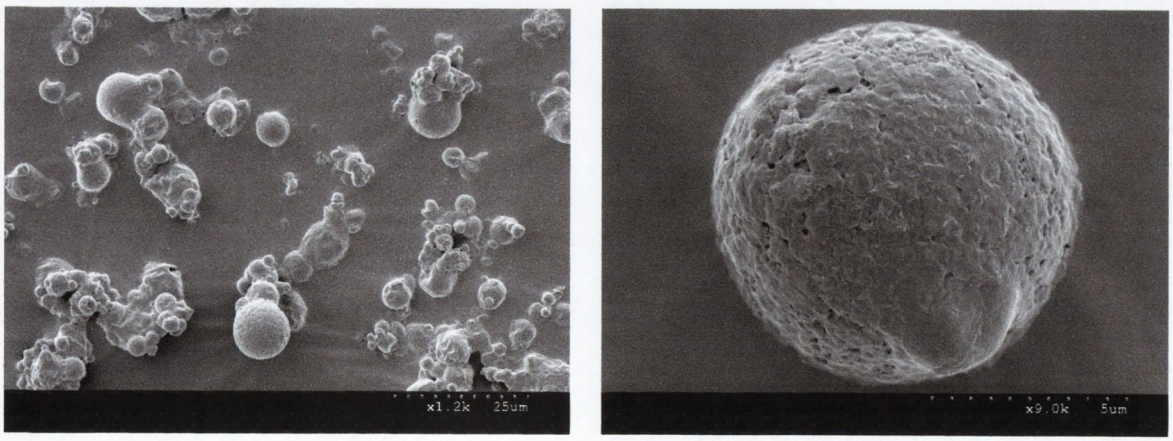

Figure 6.8 SEM micrographs of spray dried salbutamol sulphate/PEG 4000 20%.

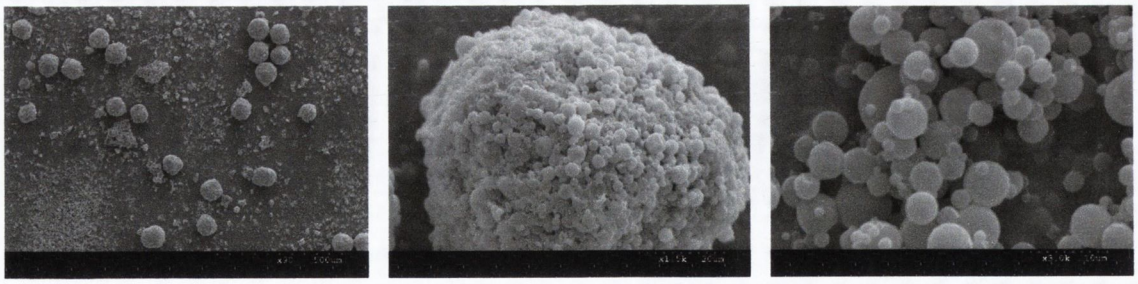

Figure 6.9 SEM micrographs of spray dried salbutamol sulphate/PEG 4000 40%.

6.4. Salbutamol sulphate/PEG 20,000 systems

Figure 6.10 shows the XRD scans of the spray dried salbutamol sulphate/PEG 20,000 systems. The 5% and 20% systems were completely amorphous by XRD with respect to salbutamol sulphate and polymer. The 40% PEG 20,000 system showed peaks indicative of crystalline PEG 20,000. These peaks were smaller in magnitude than the equivalent physical mix. No peaks were present for crystalline salbutamol sulphate in the 40% system indicating that it is either amorphous or present as a molecular dispersion within the PEG 20,000.

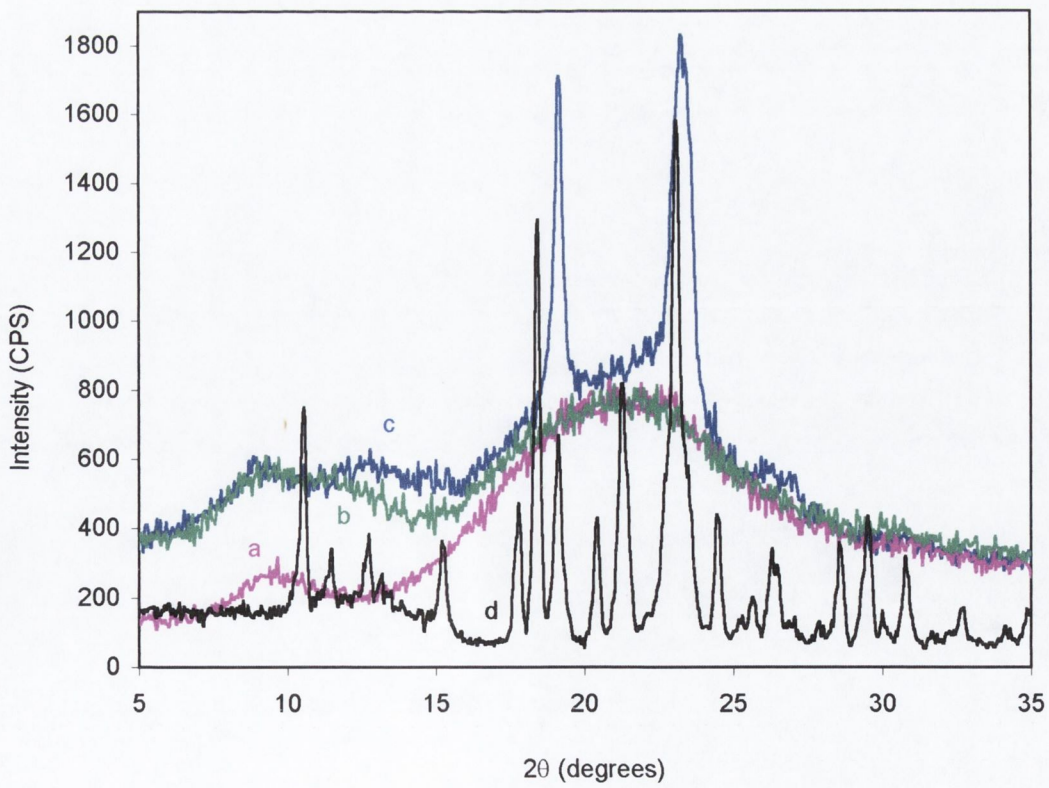

Figure 6.10 XRD scans of (a) spray dried salbutamol sulphate/PEG 20,000 5%; (b) spray dried salbutamol sulphate/PEG 20,000 20%; (c) spray dried salbutamol sulphate/PEG 20,000 40% and (d) physical mix of salbutamol sulphate/PEG 20,000 20%.

Figure 6.11 shows the DSC scans of the various spray dried salbutamol sulphate/PEG 20,000 systems. Neither the 5% nor the 20% system show an endotherm indicative of melting of crystalline PEG. The 40% PEG 20,000 system does show a melting endotherm in the PEG region but this is much reduced in enthalpy compared to the 40% PEG 20,000 physical mix, being less than half the magnitude of the PEG melting endotherm of the 20% PEG physical mix shown in Figure 6.11 (scan d). The spray dried PEG 20,000 20% system showed a distinct exotherm by DSC indicating recrystallisation of amorphous salbutamol sulphate prior to the salbutamol sulphate melting endotherm (indicated by the arrow in Figure 6.11 (scan b)).

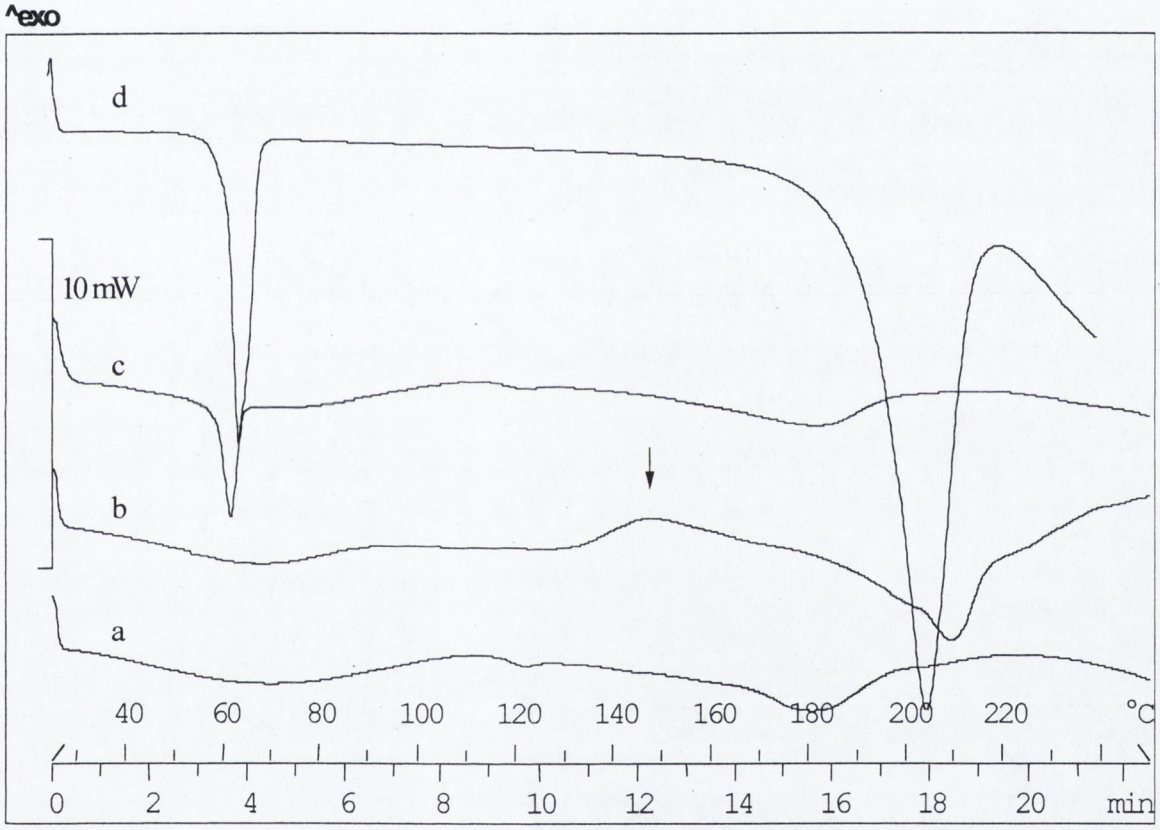

Figure 6.11 DSC scans of (a) spray dried salbutamol sulphate/PEG 20,000 5%; (b) spray dried salbutamol sulphate/PEG 20,000 20%; (c) spray dried salbutamol sulphate/PEG 20,000 40% and (d) physical mix of salbutamol sulphate/PEG 20,000 20%. The arrow indicates the exothermic peak.

The salbutamol sulphate/PEG 20,000 20% system was the first spray dried system containing salbutamol sulphate to show a visible recrystallisation exotherm during heating by DSC. The 5% and 40% systems do not show obvious exotherms. Salbutamol sulphate systems spray dried alone did not show recrystallisation exotherms by DSC, nor did previous salbutamol sulphate co-spray dried systems. The melting endotherm for salbutamol sulphate in the 20% PEG 20,000 system is therefore due to the presence of

some recrystallised salbutamol sulphate as opposed to melting of an amorphous form. This melting endotherm occurs at a higher temperature, much closer in peak melting temperature to the physical mix systems, than any of the other salbutamol sulphate containing co-spray dried systems. The endotherm for the 20% system is quite broad when compared to a physical mix implying that the salbutamol sulphate is perhaps not as crystalline as that in the physical mix. The fact that other salbutamol sulphate spray dried systems show broad lower temperature endotherms which are not preceded by exothermic events implies that the salbutamol sulphate is present as a glass which does not recrystallise on heating. The 20% PEG 20,000 system therefore is consistent with the presence of amorphous salbutamol sulphate rather than a solid solution of salbutamol sulphate in PEG 20,000.

Chiou and Niazi (1971) investigated solid dispersions of sulfathiazole and urea prepared by the melt method. XRD analysis of the solid dispersion systems showed no peaks indicative of sulfathiazole indicating that it may be present either as a solid solution or as an amorphous phase. Differential thermal analysis of the solid dispersion showed an exotherm followed by a melting endotherm, the melting endotherm occurring at a lower melting temperature than in equivalent physical mixes. On storage the melting endotherm gradually increased in onset melting temperature and weak diffraction lines attributable to sulfathiazole appeared by XRD. Chiou and Niazi (1971) concluded that sulfathiazole was likely to have been present as an amorphous phase rather than as a molecular dispersion based on the fact that sulfathiazole alone shows a tendency to supercool to a glassy state and because of the presence of a DSC exotherm, a lower onset melting endotherm and the appearance of peaks by XRD following storage.

SEM micrographs of spray dried salbutamol sulphate/PEG 20,000 systems are shown in Figure 6.12. The 5% and 40% PEG 20,000 consisted of smooth spherical particles with numerous indentations. The 20% system showed particles that were spherical but with fibrous surfaces. The 5% and 20% PEG 20,000 particles were approximately 2 to 8 μm in diameter. The 40% PEG 20,000 system consisted of particles with diameters from approximately 2 to 10 μm.

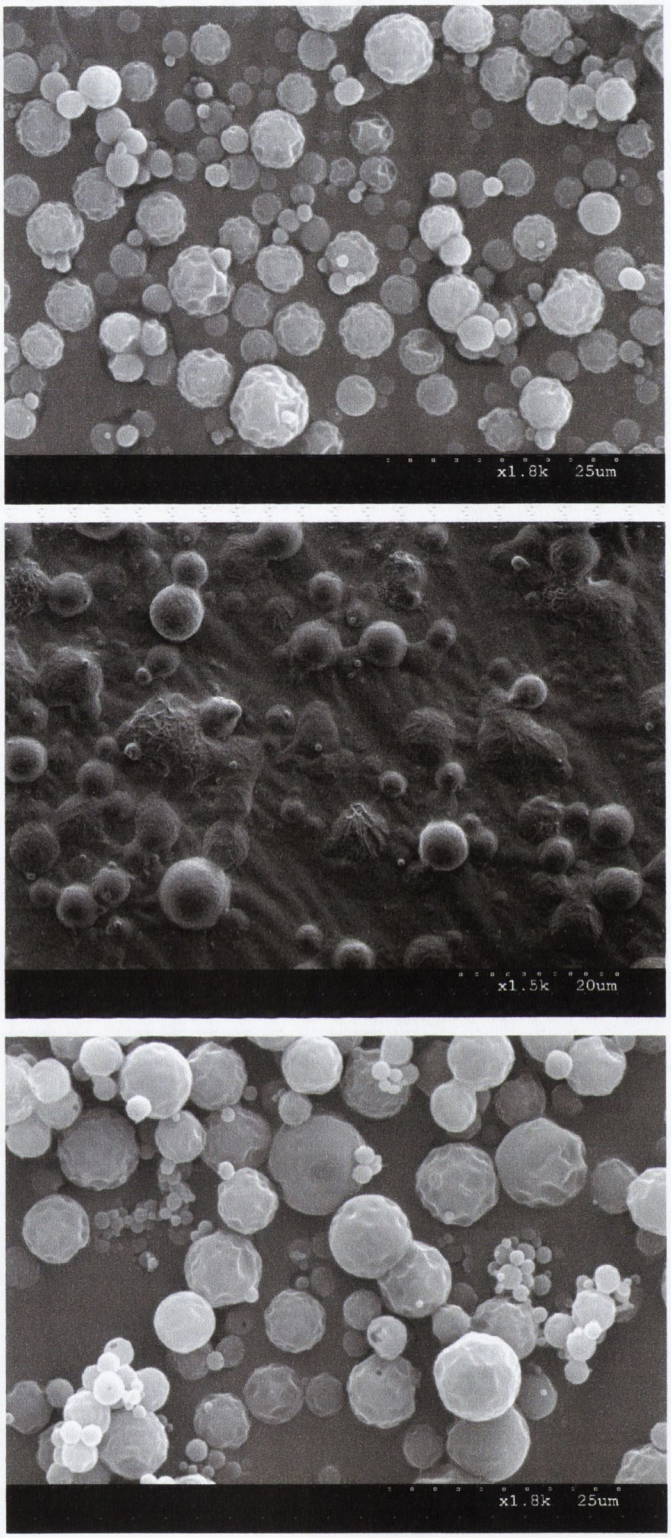

Figure 6.12 SEM micrographs of spray dried salbutamol sulphate/PEG 20,000 5% (top), 20% (middle) and 40% (bottom).

6.5. Chitosan Systems

6.5.1. Introduction

Williams et al. (1998) investigated microspheres made of chitosan as potential carriers, for proteins, peptides and plasmid DNA, for administration to the lung from pressurised metered dose inhalers (MDIs). They investigated both non-crosslinked chitosan and crosslinked chitosan. They found non-crosslinked chitosan and glutaraldehyde-crosslinked chitosan microspheres to be potential candidates for carrying biotherapeutic compounds to the lung via MDIs due to their compatibility with the non-CFC propellant P134a and their favourable physicochemical characteristics. Carrión-Recio et al. (2002) investigated chitosan microspheres prepared by a double emulsion microencapsulation technique as potential pulmonary delivery systems. They incorporated the model proteins insulin and bovine serum albumin and found the chitosan microspheres to have suitable morphological and aerodynamic properties for lung delivery.

Co-spray dried chitosan salbutamol sulphate systems for use in dry powder inhalers (DPI) were investigated in this work. Formaldehyde was used instead of glutaraldehyde as a crosslinking agent due to its lower toxicity (apparent from comparison of material safety data sheets). 0.2% w/v solutions of chitosan (prepared in 1% v/v acetic acid with and without formaldehyde as a crosslinking agent) were spray dried based on the method of He et al. (1999). Chitosan was also spray dried from a 0.8% w/v solution of hydrochloric acid (HCl). XRD scans of chitosan starting material and processed chitosans are shown in Figure 6.13. All systems showed diffuse halos with two regions of short-range order. Zong et al. (2000) describe XRD scans of chitosan raw material and a chitosan cast film prepared from its solution in water/acetic acid. They describe two crystal forms of chitosan, form I showing strongest reflection at 10° 2θ and form II showing strongest reflection at 20° 2θ by XRD, both forms being orthorhombic. Production of the cast film resulted in a change in the relative intensity of the peaks at 20° and 10° 2θ indicating a partial change from crystal form II to form I.

DSC scans of chitosan starting material and spray dried chitosan are shown in Figure 6.14. No sharp endotherms were visible. The unprocessed chitosan showed only one broad endotherm. All other chitosans showed two broad endotherms. Lee et al. (2000) described that although chitosan has crystalline regions, the crystalline melting temperature is not found because of the rigid-rod polymer backbone having strong inter and/or intra molecular H-bonding. Kim et al. (1994) describe this behaviour for chitin and

hydroxypropyl chitin. They state that rigid-rod-type polymers show glass transitions followed by rapid thermal degradation and that in general DSC does not provide information of glass transition temperatures or melting temperatures of polysaccharides. Using dynamic mechanical analysis they found glass transitions of chitin at 236°C.

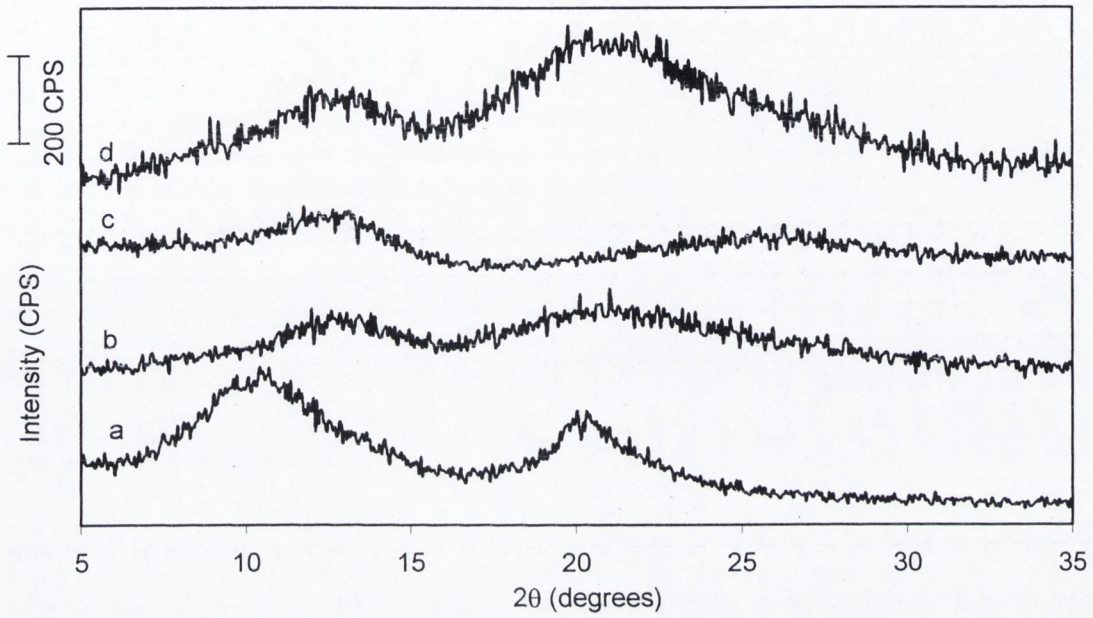

Figure 6.13 XRD scans of (a) chitosan starting material; (b) chitosan spray dried from 1% v/v acetic acid; (c) chitosan spray dried from 0.8% w/v HCl and (d) crosslinked chitosan spray dried from 1% v/v acetic acid.

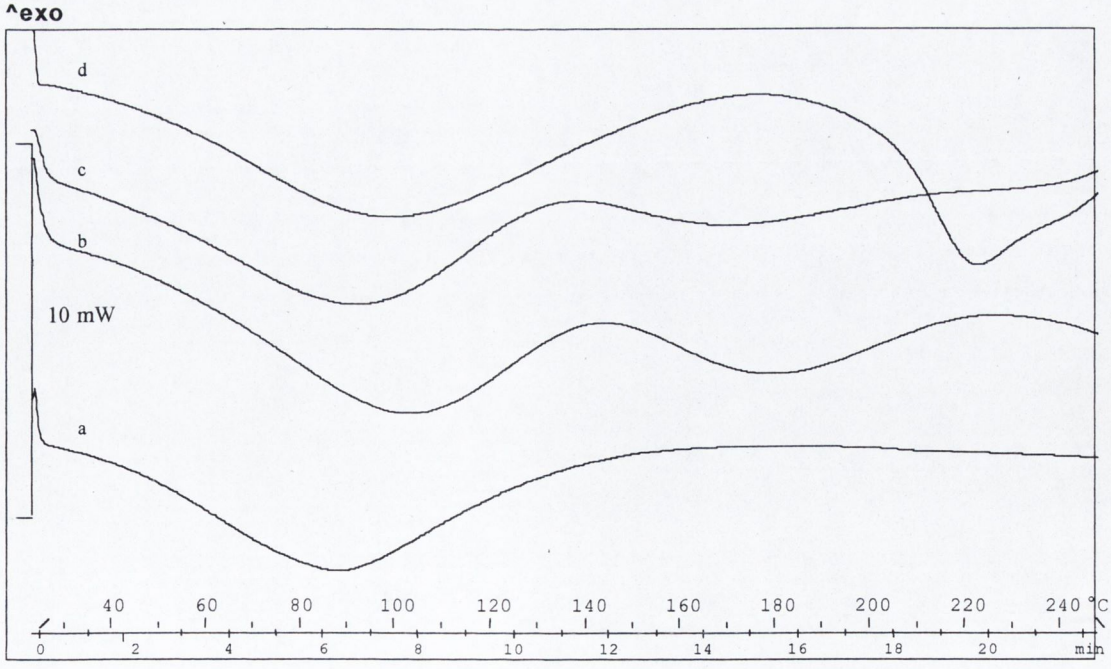

Figure 6.14 DSC scans of (a) chitosan; (b) chitosan spray dried from 1% v/v acetic acid solution; (c) chitosan spray dried from 0.8% w/v hydrochloric acid solution and (d) crosslinked chitosan spray dried from 1% v/v acetic acid.

Analysis by SEM showed that spray drying chitosan reduced the particle size and changed the particle morphology. The particle morphology depended on the solvent from which the chitosan was spray dried. SEM micrographs are shown in Figure 6.15. Spray drying from acetic acid solution resulted in uniform spherical particles, which had a roughened folded surface with diameters ranging from 1 to 4 μm. Crosslinking chitosan did not change the particle shape or surface characteristics and resulted in particles of a similar size range as the non-crosslinked chitosan spray dried from acetic acid. Spray drying form HCl resulted in concave collapsed particles with smooth surfaces. The longest dimension of these particles was approximately 5 μm.

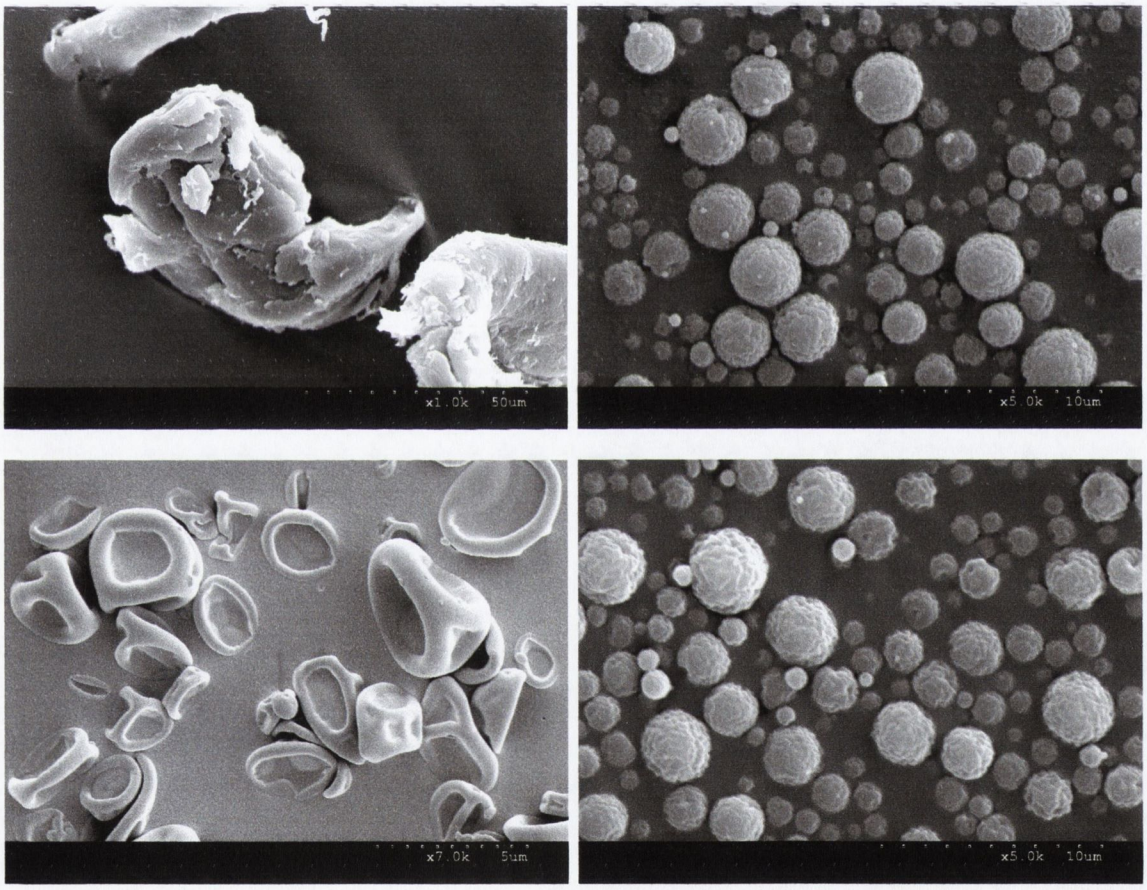

Figure 6.15 SEM micrographs of milled chitosan (top left); chitosan spray dried from acetic acid (top right); chitosan spray dried from HCl (bottom left) and spray dried crosslinked chitosan spray dried from acetic acid (bottom right).

Two different batches of chitosan raw material were used in the work for this thesis. The first batch was used for chitosan/PEG 4000 work and the second batch was used for the chitosan salbutamol sulphate work. Chitosan is obtained from the deacetylation of chitin which is obtained from natural sources and therefore batch to batch variability can be high.

Hence both batches were characterised with respect to molecular weight and degree of deacetylation.

Table 6.2 and Table 6.3 show the number average and weight average molecular weight results for chitosan raw materials and spray dried chitosans determined using GPC. Included in Table 6.2 and Table 6.3 is the analysis of variance (ANOVA) of the molecular weight data for number average molecular weights and weight average molecular weights, performed using Minitab^{TM} for Windows (Version 13.1).

Table 6.2 ANOVA comparing number average molecular weight for raw material and spray dried chitosan systems.

Level	N	Mean	StDev	Individual 95% Confidence Intervals For Mean Based on Pooled Standard Deviation
B1	3	165595	6968	(-----*----)
SD B1	3	171314	28887	(-----*----)
B2	3	164651	59154	(-----*------)
SD B2	3	161390	5504	(----*----)
SD B1 from HCl	3	26298	1334	(----*-----)
Pooled StDev =		24334		0 60000 120000 180000

SD = spray dried, B1 and B2 refer to batch 1 and batch 2 (the different batches of chitosan raw material), from HCl refers to chitosan spray dried from HCl.

Table 6.3 ANOVA comparing weight average molecular weight for raw material and spray dried chitosan systems.

Level	N	Mean	StDev	Individual 95% Confidence Intervals For Mean Based on Pooled Standard Deviation
B1	3	837375	76394	(-----*-----)
SD B1	3	720426	19439	(-----*----)
B2	3	643611	343857	(----*-----)
SD B2	3	784513	37215	(----*-----)
SD B1 from HCl	3	78574	6235	(-----*-----)
Pooled StDev =		158667		0 350000 700000 1050000

SD = spray dried, B1 and B2 refer to batch 1 and batch 2 (the different batches of chitosan raw material), from HCl refers to chitosan spray dried from HCl.

Both batches of chitosan raw material were spray dried from acetic acid 1% v/v. No significant differences were found between batches of raw material or between unprocessed chitosan and chitosan spray dried from acetic acid. This is indicated in the ANOVA by the overlapping confidence intervals. Chitosan spray dried from HCl showed a much lower number and weight average molecular weight. Chitosan spray dried from HCl was prepared as for the other chitosan samples (i.e. in concentrated HCl and then brought to volume with mobile phase) but additionally using just water as the solvent and analysed by GPC. It showed a significantly lower molecular weight than unprocessed

chitosan or chitosan processed from 1% v/v acetic acid regardless of the method of sample preparation. Crosslinked chitosans are not included in Table 6.2 and Table 6.3 since a suitable solvent could not be found, the crosslinked chitosans being insoluble in acetic acid, acetonitrile and tetrahydrofuran.

The degree of deacetylation affects the physicochemical properties of chitosan such as solubility and viscosity of chitosan solutions (Illum, 1998). The effect of spray drying on the degree of deacetylation was investigated. The degree of deacetylation was initially determined by ninhydrin assay (which detects the $-NH_2$ group on the glycoside repeating unit of chitosan) and also by ^{1}H-NMR. The results of analyses of degree of deacetylation of chitosan raw materials and spray dried chitosans are shown in Table 6.4. Ninhydrin assay gave consistently lower values for the degree of deacetylation than ^{1}H-NMR. This difference between ninhydrin and ^{1}H-NMR has been previously described in the literature with the higher results obtained using ^{1}H-NMR being generally recognised as the more accurate (Tan et al., 1998). Since ninhydrin analysis gave lower values for the degree of deacetylation of chitosan raw material than that described by the manufacturer's specifications, ^{1}H-NMR was adopted as the method of choice for determining degree of deacetylation in this work. The two different batches of chitosan purchased from Fluka, were stated to have a degree of deacetylation of 75-85%. When analysed by ^{1}H-NMR they were both found to have a degree of deacetylation of 82%. Spray drying chitosan from acetic acid resulted in a reduction in the degree of deacetylation. Deacetylation values of 50% and 55% (for batches 1 and 2 of raw material) were obtained by ^{1}H-NMR. When the ninhydrin values for degree of deacetylation of raw material and material spray dried from acetic acid were compared, the spray dried material resulted in a significantly lower value (only spray dried material from the first batch was analysed). Chitosan spray dried from 0.8% w/v HCl was shown to have a degree of deacetylation of 79% by ^{1}H-NMR and 51% by ninhydrin (i.e. no significant change from unprocessed chitosan which gave deacetylation values of 82% by ^{1}H-NMR but deacetylation values of 50% by ninhydrin analysis). These studies indicate that spray drying chitosan from acetic acid results in a reduction in the degree of deacetylation unlike spray drying from 0.8% w/v HCl solution. It is likely that chitosan spray dried from acetic acid forms some chitosan acetate and therefore the amino groups are no longer available for detection. Crosslinking chitosan during spray drying resulted in a dramatic reduction in the degree of free amino groups measured as degree of deacetylation. A value of 1% deacetylation (in fact 1% free amino groups) was obtained for crosslinked chitosan by ^{1}H-NMR analysis. Non-crosslinked

chitosan is water soluble as the salt with various acids on the amino group of the D-glucosamine unit (Sugimoto, 1998). Crosslinking chitosan removes the functional group necessary for salt formation thus reducing chitosans ability to form water soluble salts. This would explain the crosslinked chitosans insolubility during sample preparation for GPC analysis.

Table 6.4 Results of analyses of percentage deacetylation of chitosan and spray dried chitosans.

System	^{1}H-NMR analysis	Ninhydrin analysis
Chitosan raw material batch 1	82%	50%
Chitosan spray dried from acetic acid using raw material from batch 1	50%	40%
Chitosan raw material batch 2	82%	Not performed
Chitosan spray dried from acetic acid using raw material from batch 2	55%	Not performed
Chitosan (batch 1) spray dried from HCl	79%	51%
Crosslinked chitosan spray dried from acetic acid (batch 2)	1% *	Not performed

*Test analyses free amino groups, in this case groups which may have been deacetylated to give free amino groups are no longer free because they have been crosslinked.

6.6. Salbutamol sulphate/chitosan systems (not crosslinked)

The XRD scans of spray dried salbutamol sulphate/chitosan systems containing 10%, 20% and 40% salbutamol sulphate are shown in Figure 6.16. All systems were shown to be amorphous by XRD with two regions of short range order. The DSC scans of the spray dried systems and a physical mix of crystalline salbutamol sulphate and chitosan are shown in Figure 6.17. All spray dried systems show two broad endotherms similar to the DSC scan obtained for chitosan alone. The physical mix shows a salbutamol sulphate melting endotherm peaking at approximately 205°C. No such melting endotherms are visible in this region for the spray dried systems. He et al. (1999) spray dried chitosan with cimetidine and famotidine with and without crosslinking agent and found no endothermic peaks indicative of melting of either drug. They concluded that the lack of endotherms for the drug indicated that the drugs were dispersed inside the matrix of chitosan as a solid solution. Since DSC of salbutamol sulphate/chitosan co-spray dried systems showed no sharp endotherms indicative of melting of crystalline material, and XRD also showed no peaks indicative of crystallinity, the salbutamol sulphate/chitosan co-spray dried systems exist as glass solutions.

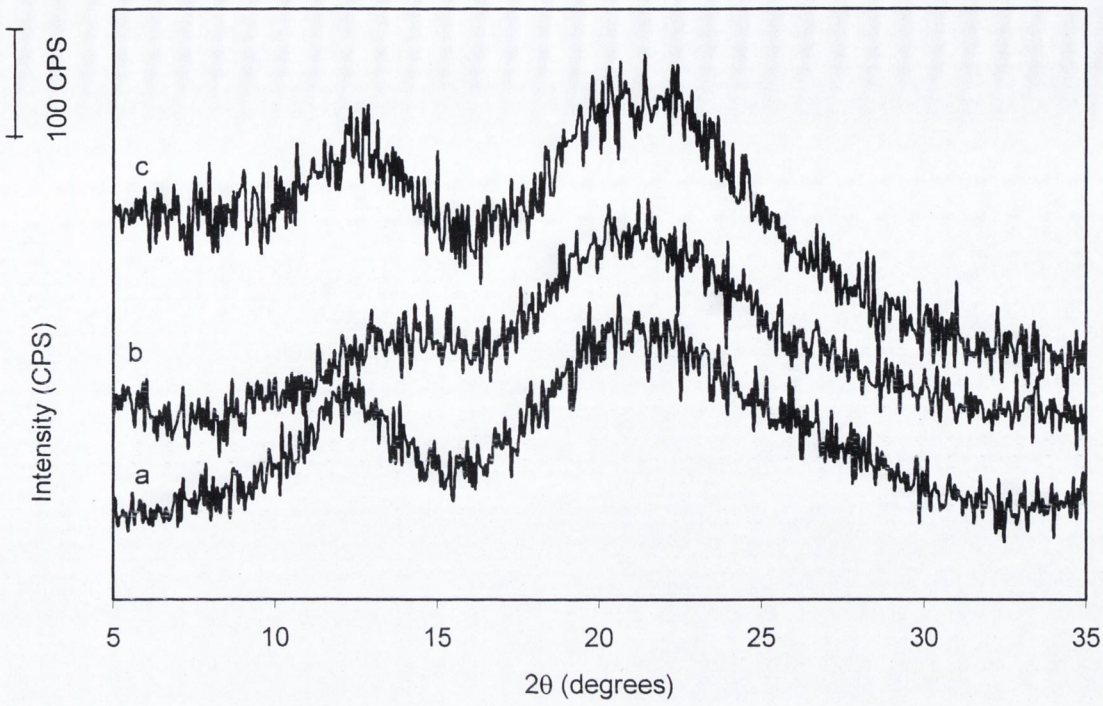

Figure 6.16 XRD scans of (a) spray dried 10% salbutamol sulphate/chitosan; (b) spray dried 20% salbutamol sulphate/chitosan and (c) spray dried 40% salbutamol sulphate/chitosan.

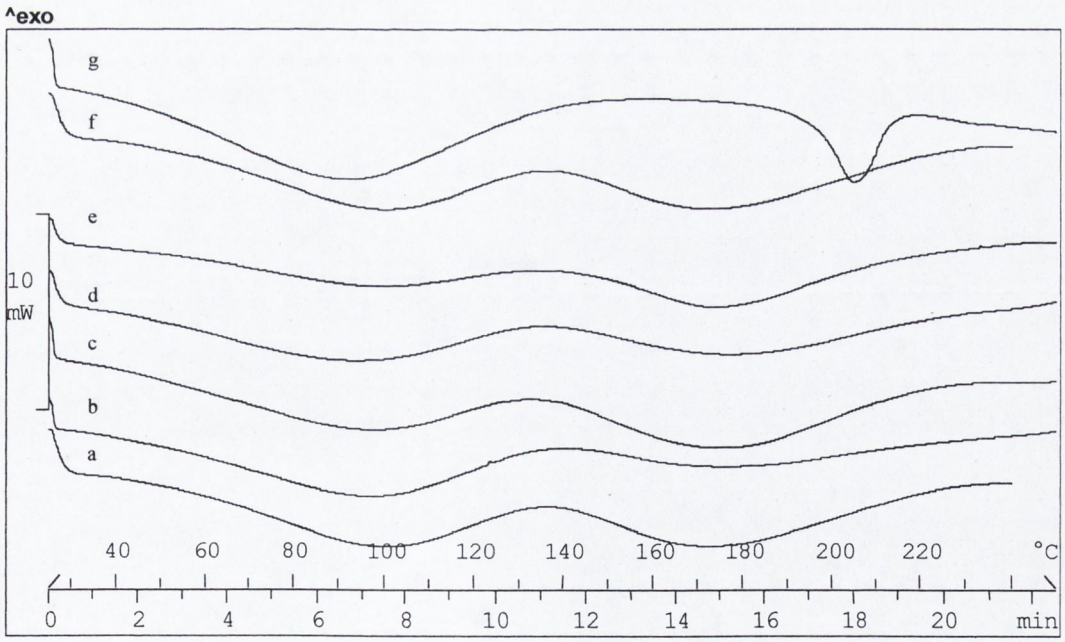

Figure 6.17 DSC scans of (a) spray dried 10% salbutamol sulphate/chitosan; (b) spray dried 10% salbutamol sulphate/crosslinked chitosan; (c) spray dried 20% salbutamol sulphate/chitosan; (d) spray dried 20% salbutamol sulphate/crosslinked chitosan; (e) spray dried 40% salbutamol sulphate/chitosan; (f) spray dried 40% salbutamol sulphate/crosslinked chitosan and (g) physical mix of 20% crystalline salbutamol sulphate/chitosan.

SEM micrographs of salbutamol sulphate/chitosan spray dried composites are shown in Figure 6.18. SEM micrographs of the 10% and 20% salbutamol sulphate systems showed particles with a similar morphology to chitosan spray dried alone, with diameters of approximately 1 to 4 μm. Particles were spherical with a roughened surface. SEM of the 40% salbutamol sulphate/chitosan system showed particles of a different morphology. They were collapsed but smooth surfaced, the lengths of the largest particles being approximately 5 μm.

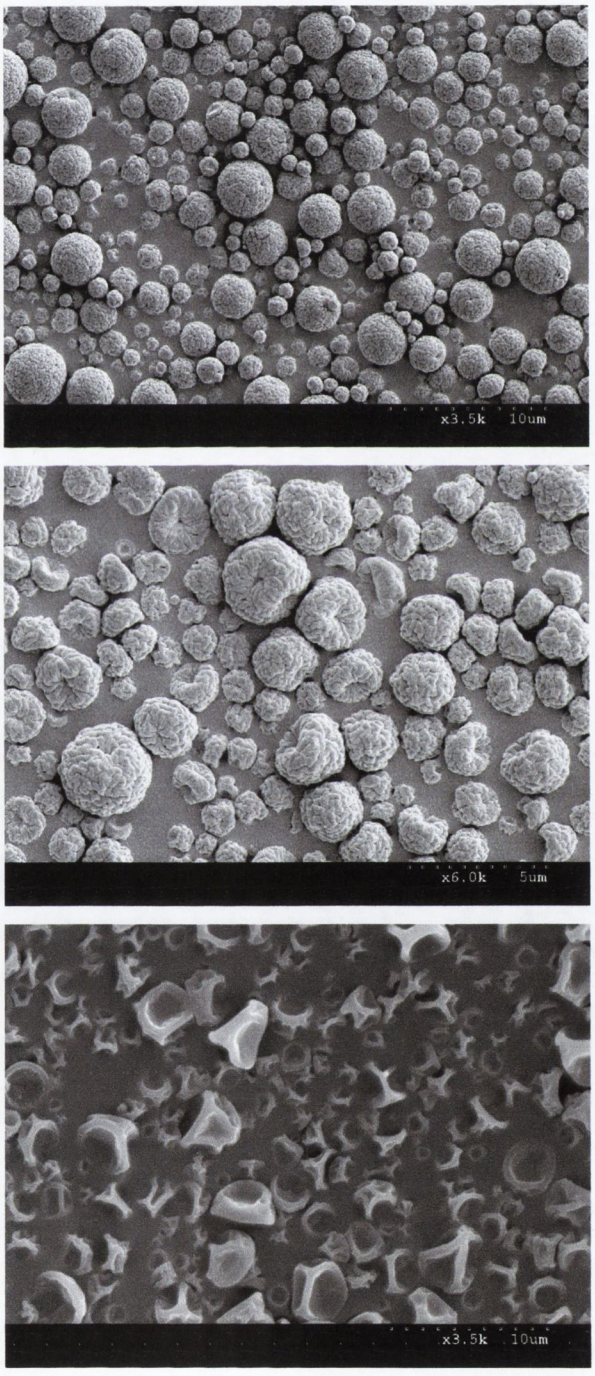

Figure 6.18 SEM micrographs of spray dried (a) 10% salbutamol sulphate/chitosan; (b) 20% salbutamol sulphate/chitosan and (c) 40% salbutamol sulphate/chitosan.

6.7. Crosslinked salbutamol sulphate/chitosan systems

Crosslinking of chitosans is known to result in sustained release systems (He et al., 1999; Remuñán-López et al., 1997). Sustained release formulations for lung delivery have, in the past, focused on incorporation of drugs into liposomes, production of biodegradable microspheres (using albumin microspheres or polyglycolide and/or lactide microspheres) and utilisation of the pro-drug approach (Zeng et al., 1995). Due to the instability of liposomal formulations in inhaler devices, dry powder delivery via microparticulates for sustained release appears the simplest option. The use of crosslinked chitosan for possible sustained release was investigated.

The XRD scans of 10%, 20% and 40% salbutamol sulphate/chitosan systems, which were spray dried with the crosslinking agent formaldehyde, are shown in Figure 6.19. All systems were amorphous indicated by the lack of peaks by XRD. Each system showed two regions of short range order.

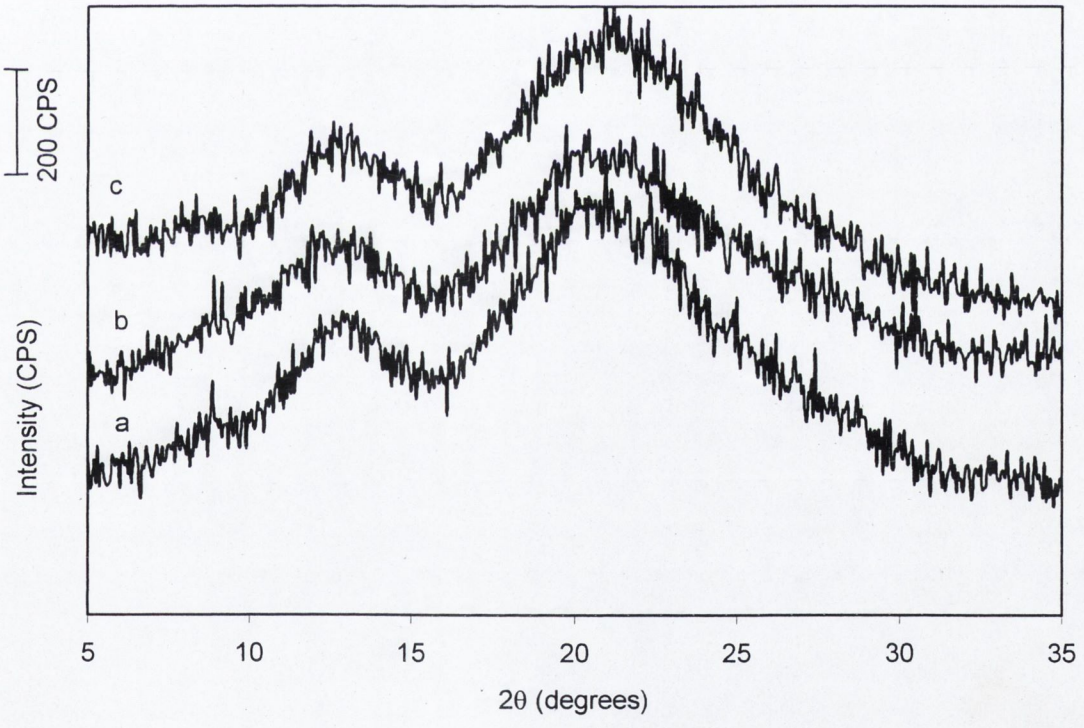

Figure 6.19 XRD scans of spray dried (a) 10% salbutamol sulphate/crosslinked chitosan; (b) 20% salbutamol sulphate/crosslinked chitosan and (c) 40% salbutamol sulphate/crosslinked chitosan.

The DSC scans were shown previously in Figure 6.17 and were similar to spray dried non-crosslinked chitosan/salbutamol sulphate systems.

SEM micrographs of spray dried salbutamol sulphate/crosslinked chitosan systems are shown in Figure 6.20. SEM micrographs of the 10% and 20% drug systems showed

particles with a similar morphology to chitosan spray dried alone and equivalent weight ratios of spray dried non-crosslinked systems. Particles were spherical with a roughened surface. The SEM micrographs of the 40% salbutamol sulphate/crosslinked chitosan system were similar to that of the 40% salbutamol sulphate/chitosan system and different to the systems containing lower percentages of salbutamol sulphate. Particles size ranges were similar to non-crosslinked salbutamol sulphate/chitosan spray dried systems.

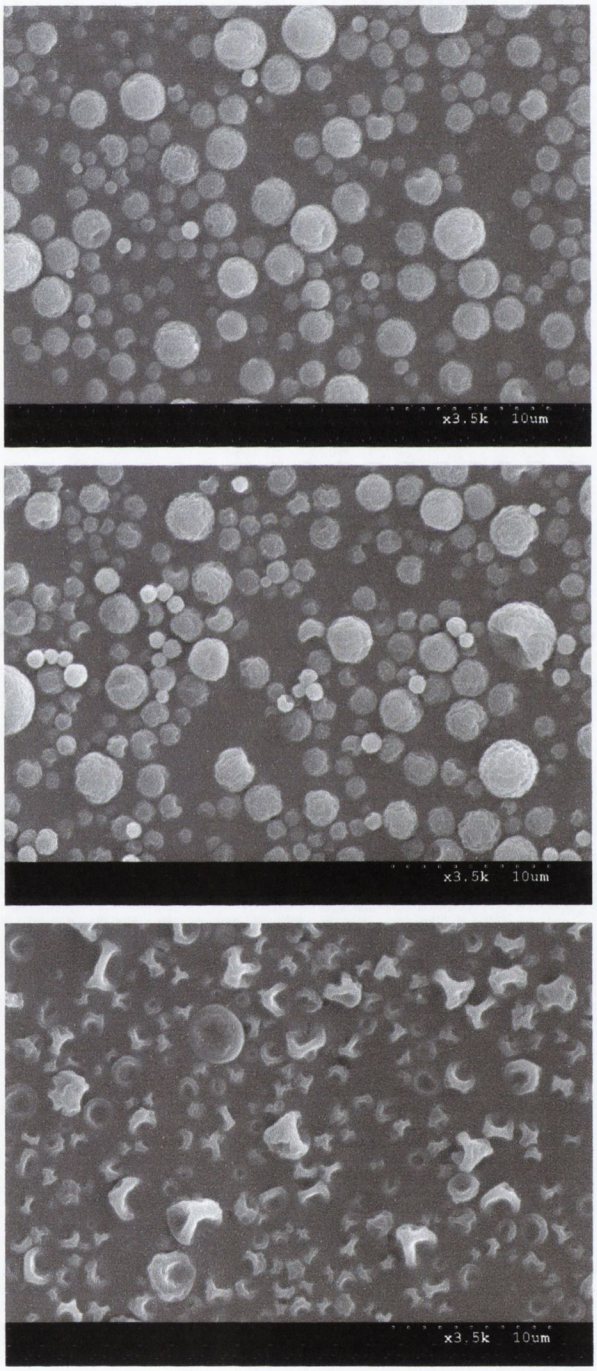

Figure 6.20 SEM micrographs of spray dried 10% salbutamol sulphate/crosslinked chitosan (top); 20% salbutamol sulphate/crosslinked chitosan (middle) and 40% salbutamol sulphate/crosslinked chitosan (bottom).

Co-spray dried salbutamol sulphate/chitosan systems were spray dried from 1% v/v acetic acid as described in Appendix I. To determine whether the salbutamol present in the resultant composites remained in the sulphate form, quantitative EDXA was performed on discs prepared from physical mixes and spray dried salbutamol sulphate/chitosan systems. Results showed no difference in sulphur content between spray dried and physical mix systems, consistent with no change in the salt form occurring on spray drying (Appendix VII).

6.8. Conclusions

Co-spray drying salbutamol sulphate with the excipients lactose and chitosan, which were amorphous when spray dried alone, resulted in amorphous composites. Co-spray drying salbutamol sulphate with PEG 4000 and PEG 20,000, which do not form amorphous systems when spray dried alone, resulted in systems of varying crystallinity, the crystallinity depending on the weight ratio of polymer to drug. For 5% PEG 4000 or 20,000 amorphous composites resulted. The salbutamol sulphate/PEG 4000 20% system consisted of some crystalline PEG and some crystalline drug. Some amorphous drug was present in this system evidenced by the recrystallisation exotherm in the DSC scan. This was the only system containing salbutamol sulphate to show an obvious exotherm by DSC and it showed a higher melting endotherm than other spray dried salbutamol sulphate systems. The presence of some crystalline salbutamol sulphate in the powder may have acted as seed crystals to facilitate recrystallisation during heating by DSC of the amorphous material also present in the powder. It appeared that the other salbutamol sulphate co-spray dried systems, which all consisted of completely amorphous salbutamol sulphate, do not recrystallise during the DSC heating cycle. No other systems showed the presence of crystalline salbutamol sulphate after spray drying. The salbutamol sulphate/PEG 20,000 20% powder was completely amorphous while the salbutamol sulphate/PEG 4000 40% and salbutamol sulphate/PEG 20,000 40% systems both showed some crystalline polymer but the absence of crystalline salbutamol sulphate. The peaks by XRD and the endotherms by DSC were reduced in magnitude compared to equivalent physical mixes indicating a reduction in crystallinity.

Salbutamol sulphate/chitosan systems resulted in the smallest particles with the narrowest particle size distribution. Due to the low solubility of chitosan these systems were spray dried at the lowest feed concentration, i.e. a feed concentration of 0.2% w/v. The other systems were all spray dried at feed concentrations of 2.5% w/v or higher. Feed

concentration is a major factor in determining particle size of the resultant powders. The difference in size and size distribution for different feed concentrations was demonstrated by spray drying salbutamol sulphate/lactose 20% at two different feed concentrations. When the SEM micrographs of the two systems were compared it was apparent that a change in feed concentration from 10% w/v to 2.5% w/v could result in the production of smaller diameter particles with a narrower size distribution. All salbutamol sulphate/excipient systems were spray dried at the same airflow setting but as shown in the factorial study in Chapter 5, varying airflow can also change the particle size of the resultant powder. Depending on the particle size required, factorial design studies could be helpful in choosing appropriate spray drying conditions to engineer the desired size.

Depending on the percentage of excipient, differing particle morphologies were found for some systems. The 5% PEG 4000 systems resulted in homogeneous spherical particles. The 20% PEG 4000 system resulted in fused particles and the 40% system resulted in large spherical aggregates consisting of many smaller spheres, together with separate spheres. Spray drying salbutamol sulphate with 5% and 40% PEG 20,000 resulted in particles with a smooth surface with indentations unlike the 20% PEG 20,000 system, which had a fibrous surface. Spray dried salbutamol sulphate 10% and 20% with chitosan resulted in spheres with a folded roughened surface similar to the morphology of chitosan spray dried alone. When the concentration of salbutamol sulphate was increased to 40% by weight of total solids the particle morphology changed to that of collapsed spheres. The morphology of salbutamol sulphate/chitosan spray dried systems was not altered by crosslinking.

6.9. Analysis of Respirable Fraction using the Twin Stage Impinger (TSI)

Use of the twin impinger for analysis of respirable fraction is described in Chapter 1. The respirable fraction was calculated as the amount deposited in the lower stage of the impinger as a percentage of the emitted dose (the amount emitted into the upper and lower stage excluding the amount remaining in the device).

The respirable fractions obtained for co-spray dried salbutamol sulphate/excipient systems are shown in Table 6.5. The respirable fraction determined for micronised salbutamol sulphate, the commercial Ventolin Rotacaps® formulation and spray dried salbutamol sulphate are also included for comparison purposes. Since the Ventolin Rotacaps®

formulation consists of a carrier (described in Chapter 5) it was expected to show superior respirable fractions.

Table 6.5 Mean respirable fractions and standard deviations of salbutamol sulphate from capsules of salbutamol sulphate raw material, Ventolin Rotacaps®, capsules of spray dried salbutamol sulphate and capsules of co-spray dried salbutamol sulphate/excipient composites obtained using the twin impinger.

System	Mean Respirable % (n=3)	Standard Deviation (n=3)
Micronised salbutamol sulphate	1.54	0.29
Ventolin Rotacaps®	39.97*	1.86*
Spray dried salbutamol sulphate (from aqueous solution)	21.68	2.35
Spray dried salbutamol sulphate (from ethanolic solution 95%)	19.63	5.14
Spray dried salbutamol sulphate/lactose 5%	11.17	3.40
Spray dried salbutamol sulphate/lactose 20%	13.54	1.33
Spray dried salbutamol sulphate/lactose 20% as 2.5% w/v feed solution	25.69	4.13
Spray dried salbutamol sulphate/lactose 40%	13.14	1.43
Spray dried salbutamol sulphate/PEG 4000 5%	8.25	1.41
Spray dried salbutamol sulphate/PEG 4000 20%	0.93	0.12
Spray dried salbutamol sulphate/PEG 4000 40%	4.55	0.18
Spray dried salbutamol sulphate/PEG 20,000 5%	4.80	0.15
Spray dried salbutamol sulphate/PEG 20,000 20%	7.35	2.07
Spray dried salbutamol sulphate/PEG 20,000 40%	1.95	0.30
Spray dried 10% salbutamol sulphate/chitosan 90%	28.41	1.70
Spray dried 20% salbutamol sulphate/chitosan 80%	32.01	1.40
Spray dried 40% salbutamol sulphate/chitosan 60%	32.99	10.40
Spray dried 10% salbutamol sulphate/ crosslinked chitosan	36.13	7.04
Spray dried 20% salbutamol sulphate/ crosslinked chitosan	29.29	4.82
Spray dried 40% salbutamol sulphate/ crosslinked chitosan	36.46	4.10

(*n=2)

An ANOVA was performed using Minitab to compare the respirable fractions of all co-spray dried systems. The respirable fractions obtained for micronised salbutamol sulphate, spray dried salbutamol sulphate and the commercial Rotacaps® formulation are included for comparison purposes. The results are shown in Table 6.6.

Table 6.6 ANOVA of respirable fractions of salbutamol sulphate obtained from micronised salbutamol sulphate, spray dried salbutamol sulphate, spray dried salbutamol sulphate/excipient systems and the Ventolin Rotacaps® formulation. All combination systems listed are spray dried composites. The following abbreviations apply: SS = salbutamol sulphate, water indicates spray drying from aqueous solution, ethanol indicates spray drying from ethanolic solution; SSlac = salbutamol sulphate/lactose systems; P4000 = PEG 4000, P20,000 = PEG 20,000, xxchit = crosslinked chitosan.

Level	N	Mean	StDev	Individual 95% Confidence Intervals For Mean Based on Pooled StDev
Micronised SS	3	1.540	0.286	(--*--)
SS water	3	21.676	2.352	(-*--)
SS ethanol	3	19.627	5.140	(--*--)
SSlac 5%	3	11.167	3.401	(-*--)
SSlac20%	3	13.536	1.329	(--*--)
SSlac20%†	3	25.694	4.126	(--*--)
SS lac40%	3	13.140	1.429	(--*--)
SSP40005%	3	8.253	1.406	(--*-)
SSP400020%	3	0.932	0.120	(--*--)
SSP400040%	3	4.553	0.165	(--*--)
SSP20,000 5%	3	4.803	0.153	(--*--)
SSP20,00020%	3	7.353	2.077	(--*--)
SSP20,00040%	3	1.952	0.296	(--*--)
SS10%chitosan	3	28.414	1.699	(--*--)
SS20%chitosan	3	32.007	1.402	(--*--)
SS40%chitosan	3	32.989	10.423	(--*--)
SS10%xxchit	3	36.132	7.041	(--*--)
SS20%xxchit	3	29.288	4.819	(--*-)
SS40%xxchit	3	36.464	4.098	(--*--)
Rotacaps®	2	39.964	1.855	(---*--)
Pooled StDev		3.760		0 15 30 45

† Denotes the salbutamol sulphate/lactose 20% system spray dried at a feed concentration of 2.5% w/v unlike the other salbutamol sulphate/lactose systems, which were spray dried as 10% w/v solutions.

The salbutamol sulphate/chitosan co-spray dried systems gave high respirable fractions, with no significant differences existing between crosslinked and non-crosslinked systems or between systems of different weight ratios of salbutamol sulphate to chitosan. Respirable fractions were comparable with the commercial Ventolin Rotacaps® formulation.

Salbutamol sulphate/lactose systems spray dried as 10% w/v solutions gave significantly higher respirable fractions than micronised salbutamol sulphate but not as high as salbutamol sulphate/chitosan systems. The salbutamol sulphate/lactose 20% system spray dried as a 2.5% w/v solution gave significantly higher respirable fractions than the other salbutamol sulphate/lactose systems spray dried as 10% w/v solutions. This was consistent with the smaller particle sizes produced on spray drying using the lower feed concentration. The 20% system spray dried as a 2.5% w/v solution gave respirable fractions comparable to most of the salbutamol sulphate/chitosan systems. The spray dried PEG-containing systems did not appear significantly different from each other when

analysed with all the other systems in the ANOVA shown in Table 6.6. ANOVA uses a standard deviation determined from the pooling of the standard deviations of all the samples and assumes that all the systems have equal variance. Considering the differences between the various systems with respect to composition, production parameters etc. it might be more informative to compare each salbutamol sulphate/excipient group to micronised salbutamol sulphate by separate ANOVAs so that real differences are not masked by the overall pooled standard deviation. The results of a Minitab ANOVA comparing salbutamol sulphate/PEG 4000 5%, 20% and 40% and micronised salbutamol sulphate are shown in Table 6.7.

Table 6.7 ANOVA of respirable fractions of micronised salbutamol sulphate and co-spray dried salbutamol sulphate/PEG 4000 composites.

```
                                        Individual 95% Confidence Intervals
                                          For Mean Based on Pooled StDev
Level            N    Mean     StDev  -+---------+---------+---------+-----
micronised SS    3  1.5397  0.2855      (--*--)
SSP40005%        3  8.2534  1.4057                              (---*--)
SSP400020%       3  0.9318  0.1200    (--*--)
SSP400040%       3  4.5533  0.1649               (--*--)
                                       -+---------+---------+---------+-----
Pooled StDev =   0.7244               0.0       3.0       6.0       9.0
SS = salbutamol sulphate, SD = spray dried, P4000 = PEG 4000.
```

The PEG 4000 20% system had the lowest respirable fraction and this was not statistically different to micronised salbutamol sulphate. It was not surprising that the PEG 4000 20% system had a significantly lower respirable fraction than the 5% or 40% systems since it consisted of fused agglomerates. The salbutamol sulphate/PEG 4000 5% system showed the highest respirable fraction, being statistically higher than micronised salbutamol sulphate or the 20% and 40% systems. The 40% system gave a significantly higher respirable fraction than micronised salbutamol sulphate or the 20% system but not as high as the 5% system.

The results of a Minitab ANOVA comparing salbutamol sulphate/PEG 20,000 5%, 20% and 40% and micronised salbutamol sulphate are shown in Table 6.8. The PEG 20,000 40% system gave respirable fractions that were not statistically different from micronised salbutamol sulphate. This was not unexpected since the 40% system showed particles as large as 10 μm in diameter unlike the 5% and 20% systems in which all particles were less than 8 μm in diameter. The 5% and 20% systems showed higher respirable fractions than

micronised salbutamol sulphate, these two systems not being statistically different from each other with respect to respirable fraction.

Table 6.8 ANOVA of respirable fractions of micronised salbutamol sulphate and co-spray dried salbutamol sulphate/PEG 20,000 composites.

```
                                    Individual 95% Confidence Intervals
                                    For Mean Based on Pooled StDev
Level           N    Mean     StDev ----------+---------+---------+------
micronised SS   3   1.540     0.286  (----*-----)
SSP20,000 5%    3   4.803     0.153               (----*-----)
SSP20,00020%    3   7.353     2.077                          (----*-----)
SSP20,00040%    3   1.952     0.296    (-----*----)
                                    ----------+---------+---------+------
Pooled StDev =      1.061                 2.5       5.0       7.5
SS = salbutamol sulphate, SD = spray dried, P20,000 = PEG 20,000.
```

The results of the Minitab ANOVA comparing spray dried salbutamol sulphate/chitosan systems are shown in Table 6.9. The chitosan systems resulted in respirable fractions which were not significantly different from each other.

Table 6.9 ANOVA of respirable fractions of micronised salbutamol sulphate and co-spray dried salbutamol sulphate/chitosan composites.

```
                                      Individual 95% Confidence Intervals
                                      For Mean Based on Pooled StDev
Level           N      Mean     StDev ----+---------+---------+---------+--
micronised SS   3     1.540     0.286  (---*---)
SS10%chitosan   3    28.414     1.699                  (----*---)
SS20%chitosan   3    32.007     1.402                    (---*----)
SS40%chitosan   3    32.989    10.423                     (---*---)
SS10%xxchit     3    36.132     7.041                       (---*----)
SS20%xxchit     3    29.288     4.819                   (----*---)
SS40%xxchit     3    36.464     4.098                       (---*----)
                                    ----+---------+---------+---------+--
Pooled StDev =      5.387               0        15        30        45
SS = salbutamol sulphate and xxchit = crosslinked chitosan.
```

6.9.1. Conclusions for TSI

Spray drying of salbutamol sulphate alone results in a powder which shows a higher *in vitro* respirable fraction than micronised salbutamol sulphate when tested with a Rotahaler® device attached to a twin stage impinger. Co-spray drying salbutamol sulphate with PEG excipients resulted in a small improvement in respirable fraction over micronised salbutamol sulphate for the 5% and 40% PEG 4000 systems, the 5% system

giving the higher respirable fraction. The 5% system consisted of spheres with numerous indentations appearing to have a very similar surface morphology to spray dried salbutamol sulphate alone. The 40% system consisted of smooth spheres with no indentations as well as larger spherical bodies consisting of many smaller spheres. The 20% PEG 4000 system did not show an improvement in respirable fraction over micronised salbutamol sulphate alone, however this was not surprising since it consisted of many fused agglomerated particles and was the only system which showed evidence by XRD of crystalline salbutamol sulphate. The 5% PEG 4000 system was totally amorphous with respect to drug and polymer. The 20% PEG 4000 system consisted of crystalline drug and crystalline polymer and the 40% PEG 4000 system consisted of crystalline polymer but amorphous drug. Co-spray dried salbutamol sulphate/PEG 20,000 systems consisting of 10% and 20% PEG 20,000 showed slight improvements in respirable fraction over micronised salbutamol sulphate, these systems being completely amorphous with respect to drug and polymer. The 40% PEG 20,000 did not show any improvement in respirable fraction, the system consisted of some crystalline PEG unlike the 10 and 20% systems in which the PEG appeared amorphous. The 40% PEG 20,000 system consisted of larger particles than the 5% or 20% PEG 20,000 systems.

The co-spray dried salbutamol/chitosan systems gave favorable respirable fractions with high mean results. The average respirable fraction for spray dried salbutamol sulphate from aqueous and ethanolic solutions was 21.7% and 19.7% respectively while all salbutamol/chitosan systems showed average respirable fractions higher than 28%, with four out of the six systems giving average fractions over 32% of the emitted dose. No significant difference in respirable fractions was found between different ratios of salbutamol sulphate/chitosan systems or between crosslinked and non-crosslinked salbutamol sulphate/chitosan systems, even though the particle morphology of the 40% salbutamol sulphate/chitosan systems was very different to the morphology of the 10 and 20% salbutamol sulphate/chitosan systems.

Co-spray drying salbutamol sulphate with lactose at feed concentrations of 10% w/v also resulted in an improvement in respirable fraction over micronised salbutamol sulphate alone. The salbutamol sulphate/lactose systems spray dried as 10% w/v feed solutions showed respirable fractions of 11% to 13.5%, compared to 1.5% for micronised salbutamol sulphate. The salbutamol sulphate/lactose 20% system, which was spray dried at a 2.5% w/v feed concentration, showed a significantly better respirable fraction than the 10% w/v spray dried systems. This was not unexpected considering that its particle size by SEM

was smaller and the powder appeared to have a narrower size distribution. The respirable fraction of the 20% lactose system spray dried as a 2.5% w/v solution was 25.7% of the emitted dose which was not significantly different to the respirable fractions obtained with most of the co-spray dried chitosan-containing systems.

Zeng et al. (2000) prepared blends of salbutamol sulphate:lactose, 1:67.5 w/w (i.e. the same ratio employed in commercial Ventolin® formulations) and analysed the respirable fraction emitted using a rotahaler and twin stage impinger. They filled size 3 gelatin capsules with 33.0 mg (+/- 1.5 mg) of powder so that each capsule contained 481 μg (+/- 22 μg) salbutamol sulphate, which was similar to the unit dose contained in Ventolin Rotatcaps®. They found respirable fractions (ratio of lower impinger to emitted dose) of between 19.4% and 34.1% depending on the lactose used. They compared 8 different lactose systems, Lactochem^R (Borculo Whey Ltd., UK) and lactose batches they prepared themselves using different crystallisation conditions. They concluded that increasing either the surface smoothness or the elongation ratio of lactose crystals increased the potentially respirable fraction of salbutamol sulphate from dry powder formulations for inhalation. It has been shown in this thesis that co-spray drying salbutamol sulphate with lactose gives similar respirable fractions without the need for elaborate mixing and checking of uniformity of mixing. When the actual dose of salbutamol sulphate deposited in the lower impinger was calculated for the different spray dried systems, it was found that, depending on the excipient used, co-spray dried systems deposited 4 to 43 times the amount of salbutamol sulphate that the Ventolin Rotacaps® formulation deposited. Alteration of the amount filled into the capsules, depending on the excipient used could result in therapeutic doses similar to Ventolin Rotacaps® being delivered.

6.10. *In vitro* release of salbutamol sulphate from salbutamol sulphate/chitosan systems

6.10.1. *In vitro* release from compressed discs

To determine the likely ability of chitosan to retard drug release, and the possible mechanisms involved in such drug release, compressed discs were prepared in order to control the surface area. Discs were prepared from 10%, 20% and 40% salbutamol sulphate/chitosan co-spray dried systems produced with and without crosslinking agent. Discs were also prepared from physical mixes of 40% crystalline salbutamol sulphate and either 60% spray dried chitosan produced with or without crosslinking agent or milled

chitosan. Morimoto et al. (2000) used phosphate buffered saline pH 7 when investigating *in vitro* release of salmon calcitonin from microspheres for potential pulmonary delivery. Nielson et al. (1981) described the alveolar subphase pH in the lungs of anesthetized rabbits as 6.92. Therefore isotonic phosphate buffer pH 7 was chosen as the dissolution medium for the *in vitro* salbutamol sulphate/chitosan release experiments. Co-spray dried systems and physical mixes of salbutamol sulphate with spray dried chitosan gave considerably slower release than discs prepared from pure drug alone or discs prepared from physical mixes of salbutamol sulphate and milled chitosan. The results are shown in Figure 6.21.

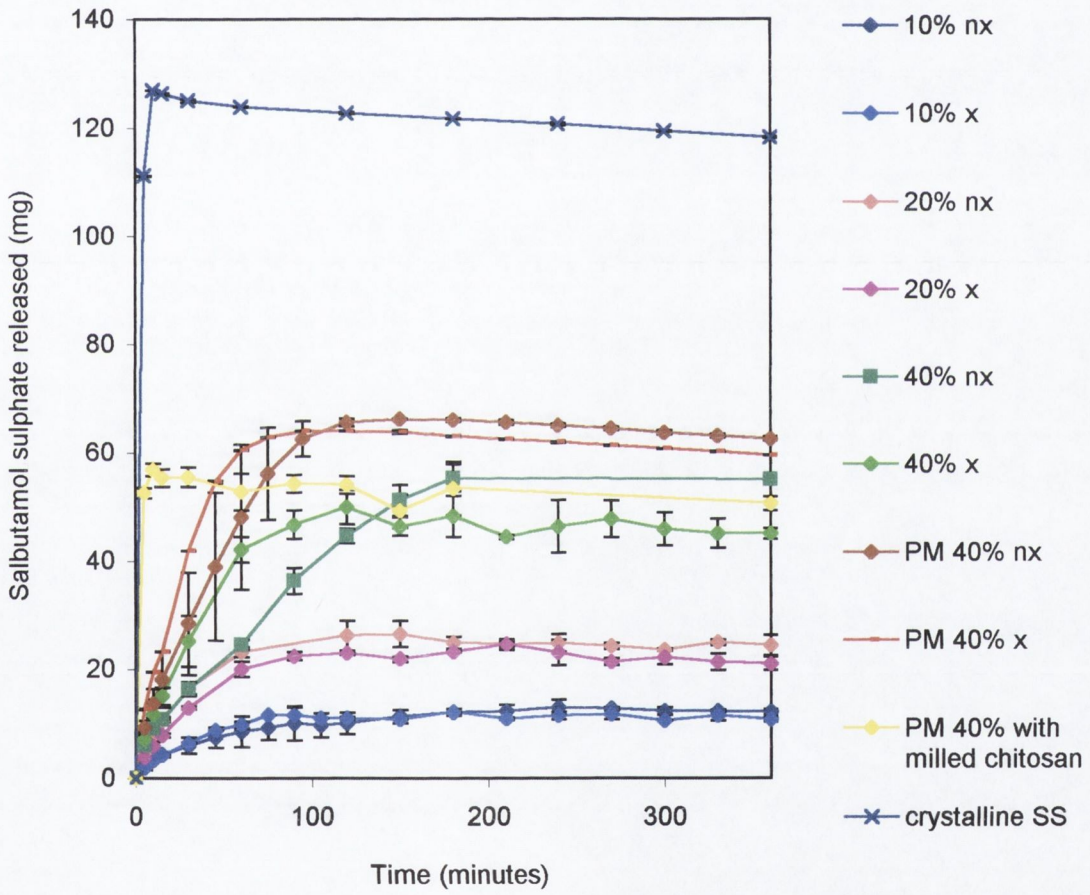

Figure 6.21 Release of salbutamol sulphate from compressed discs. 10% nx = spray dried not crosslinked 10% salbutamol sulphate/chitosan, 10% x = spray dried crosslinked 10% salbutamol sulphate/chitosan, 20% nx = spray dried not crosslinked 20% salbutamol sulphate/chitosan, 20% x = spray dried crosslinked 20% salbutamol sulphate/chitosan, 40% nx = spray dried not crosslinked 40% salbutamol sulphate/chitosan, 40% x = spray dried crosslinked 40% salbutamol sulphate/chitosan, PM 40% nx = physical mix of 40% crystalline salbutamol sulphate/spray dried not crosslinked chitosan, PM 40% x = physical mix of 40% crystalline salbutamol sulphate/spray dried crosslinked chitosan, PM 40% with milled chitosan = physical mix 40% crystalline salbutamol sulphate/milled chitosan, SS = salbutamol sulphate.

Release was complete for most systems by 100 minutes with all systems showing complete release by 210 minutes. The amount of drug released was in proportion to the amount present in the mixes.

Many models have been used in the literature to examine drug release from controlled drug delivery systems. Modelling release from a system should provide an insight into the mechanism of release and allow predictions to be made about the potential release patterns of the system being investigated.

The experimental release profiles of salbutamol sulphate/chitosan systems were initially fitted to the square root law (Equation 6.4), which is derived from the Higuchi equations (Higuchi, 1963) shown in Equation 6.1 and Equation 6.2. Equation 6.1 describes release by diffusion from a homogeneous matrix whereby the release involves diffusion through the matrix into the surrounding medium. It was initially derived by Higuchi (Higuchi, 1961) for release from an ointment base containing finely dispersed drugs.

$$W = \sqrt{Dt(2A - C_s)C_s} \qquad \text{Equation 6.1}$$

where W is the amount of drug released after time t per unit exposed area, D is the diffusivity of the drug in the homogeneous matrix media, A is the total amount of drug present in the matrix per unit volume and C_s is the solubility of the drug in the matrix substance.

Equation 6.2 is used to describe release from granular matrix systems whereby drug is leached by the dissolution medium which penetrates the matrix through pores, cracks and intergranular spaces, dissolving the drug and then releasing it by diffusion through these solvent-filled pores.

$$W = \sqrt{\frac{D_0 \varepsilon}{\tau}(2A - \varepsilon C_s)C_s t} \qquad \text{Equation 6.2}$$

where W is the amount of drug released per unit surface area, D_0 is the diffusion coefficient of the drug in the dissolution media, ε is the porosity of the matrix, τ is a tortuosity factor, A is the content of drug in the insoluble matrix, C_s is the solubility of the drug in the dissolution media and time is t.

When C_s is much less than A then Equation 6.2 can be simplified to Equation 6.3.

$$W = \sqrt{2DAC_s \frac{\varepsilon}{\tau} t} \qquad \text{Equation 6.3}$$

Equation 6.3 can be simplified to Equation 6.4

$$W = kt^{0.5} \qquad \text{Equation 6.4}$$

where W is the mass of drug released at time t per unit exposed area and k is a constant, $\sqrt{2DAC_s\frac{\varepsilon}{\tau}}$.

Since the equation was derived from the flux from an infinitely deep matrix, the equation will not remain valid when the drug reservoir is significantly depleted. Therefore only the experimental data for approximately the first 60% release, of salbutamol sulphate, was fitted to the Higuchi model as shown in Figure 6.22. The k value, obtained from fitting the salbutamol sulphate release from salbutamol/chitosan spray dried systems to the Higuchi model, increased with salbutamol sulphate loading (A). For both the 10 and 40% systems the crosslinked systems tended to give higher k values. Higher values were also obtained from discs prepared from physical mixes of salbutamol sulphate with spray dried crosslinked chitosan than physical mixes with non-crosslinked chitosan.

Table 6.12 shows the k values as well as the Model Selection Criteria (MSC) and Coefficient of Determination (CoDet) values obtained by MicroMath® Scientist® for fitting of salbutamol sulphate release to the Higuchi model.

The data did not fit the Higuchi model particularly well with model selection criterion values (MSC) generally below three. The Higuchi model is based on several assumptions, one being that there is no change in the dimensions of the matrix during drug release. During the chitosan/salbutamol sulphate release studies the discs were observed to swell by 1.2 to 1.6 times their original diameters. Table 6.10 shows the diameters measured immediately following the release experiments.

Table 6.10 Average diameters of discs of salbutamol sulphate/chitosan following release experiments.

System	Average Disc Diameters (mm) (n=3)	
	Systems containing non crosslinked chitosan	Systems containing crosslinked chitosan
Spray dried salbutamol sulphate 10%/chitosan	17	20
Spray dried salbutamol sulphate 20%/chitosan	17	21
Spray dried salbutamol sulphate 40%/chitosan	17	21
Physical mix of crystalline salbutamol sulphate 40%/spray dried chitosan	15	18.5

Note: All discs were 13 mm in diameter prior to release experiments.

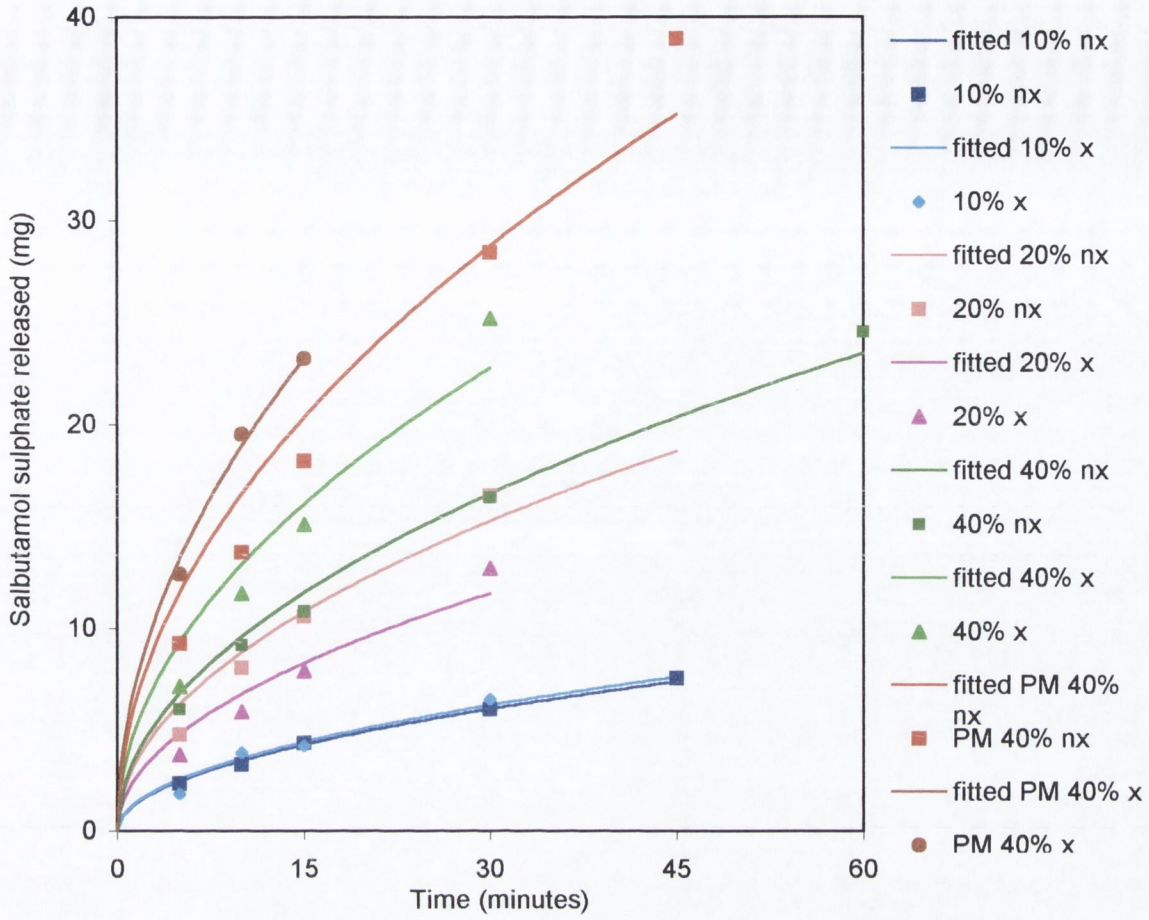

Figure 6.22 Salbutamol sulphate release data from salbutamol sulphate/chitosan systems fitted to the Higuchi model. 10% nx = spray dried not crosslinked 10% salbutamol sulphate/chitosan, 10% x = spray dried crosslinked 10% salbutamol sulphate/chitosan, 20% nx = spray dried not crosslinked 20% salbutamol sulphate/chitosan, 20% x = spray dried crosslinked 20% salbutamol sulphate/chitosan, 40% nx = spray dried not crosslinked 40% salbutamol sulphate/chitosan, 40% x = spray dried crosslinked 40% salbutamol sulphate/chitosan, PM 40% nx = physical mix of 40% crystalline salbutamol sulphate/spray dried not crosslinked chitosan, PM 40% x = physical mix of 40% crystalline salbutamol sulphate/spray dried crosslinked chitosan.

Schwartz et al. (1968) found the release of drug into aqueous media from wax matrices to give acceptably linear first order semi-log plots with slopes that were apparently independent of the concentration of drug embedded in the wax matrix. Therefore the data was fitted to the first order equation shown in Equation 6.5.

$$W = W\infty \times \left(1 - e^{-kt}\right) \qquad \text{Equation 6.5}$$

where W is weight released at time t, $W\infty$ is the weight released at infinity and k is the release rate constant.

From Figure 6.21 it is apparent that complete release has occurred by 210 minutes therefore only data up to and including time point 210 minutes was used for fitting to the first order model. Figure 6.23 shows the data fitted to the first order equation. The physical mixes shown were fitted by fixing the weight released at infinity to 60 mg, the total amount present.

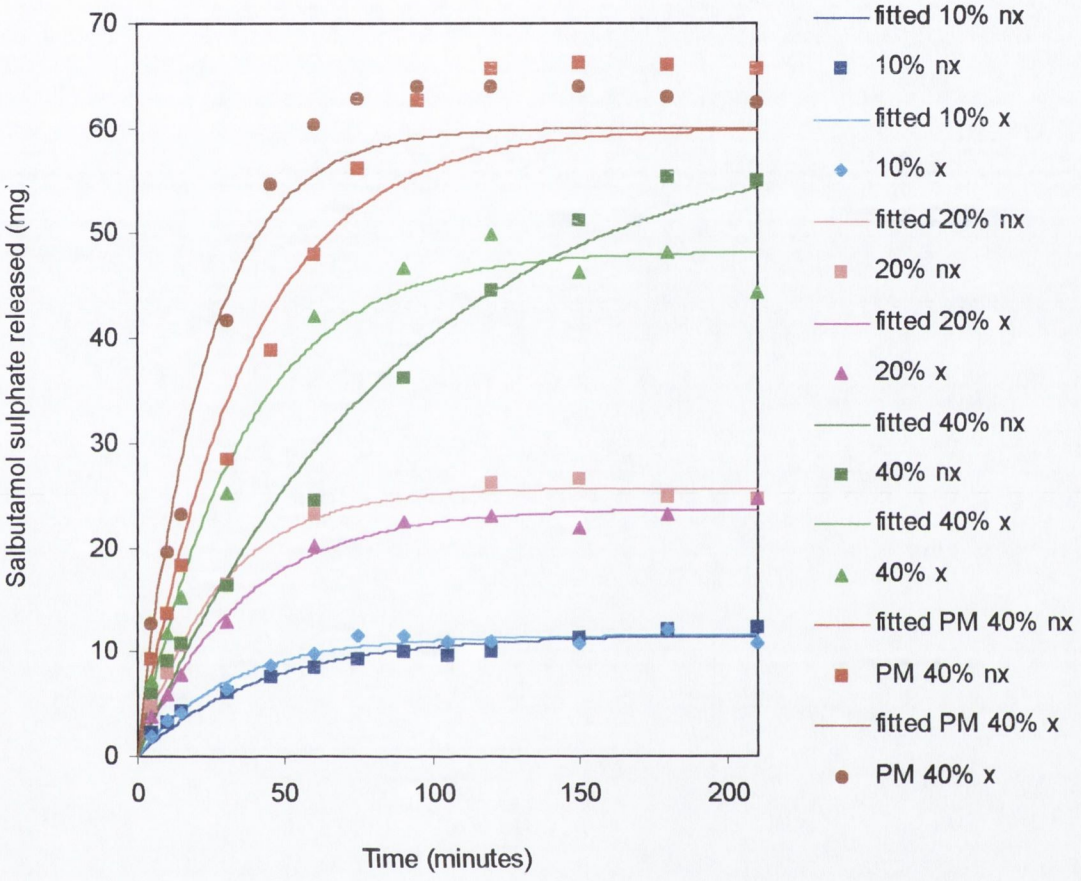

Figure 6.23 Salbutamol sulphate release data from salbutamol sulphate/chitosan systems fitted to the first order equation. 10% nx = spray dried not crosslinked 10% salbutamol sulphate/chitosan, 10% x = spray dried crosslinked 10% salbutamol sulphate/chitosan, 20% nx = spray dried not crosslinked 20% salbutamol sulphate/chitosan, 20% x = spray dried crosslinked 20% salbutamol sulphate/chitosan, 40% nx = spray dried not crosslinked 40% salbutamol sulphate/chitosan, 40% x = spray dried crosslinked 40% salbutamol sulphate/chitosan, PM 40% nx = physical mix of 40% crystalline salbutamol sulphate/spray dried not crosslinked chitosan, PM 40% x = physical mix of 40% crystalline salbutamol sulphate/spray dried crosslinked chitosan.

The rate constant *k* is reasonably similar for all systems, again the crosslinked 10%, 40% and physical mix systems showed higher *k* values than the corresponding non-crosslinked systems (Table 6.11). For both the 10% and 20% systems, less than 100% drug was

released by the time the profiles reached a plateau. Overall the fit was better, average MSC values being 3.5 compared to 2.9 for the Higuchi fit. From Figure 6.21 it appeared that there was a tendency for profiles to peak and decline, which could reflect degradation of the drug over time. Therefore the data was fitted to Equation 6.6, an equation describing the difference between two exponentials, one representing release of the drug and the other representing degradation of the drug.

$$W = Wm(e^{-KDt} - e^{-KRt}) \qquad \text{Equation 6.6}$$

where W is the weight released at time t, Wm is the total weight released, k_D is the degradation rate constant and k_R is the release rate constant.

Figure 6.24 shows the data fitted to the biexponential equation. The release rate constants, k_R were quite similar to the rate constant, k, in the first order fitted data (Table 6.11). There was no real improvement over the first order fit when the average MSC values were compared.

An alternative approach to the modelling of polymeric systems is the general power law expression described by Sinclair and Peppas (1984) and Ritger and Peppas (1987). This model was developed to model transport in glassy polymers and therefore was considered applicable to our systems. The model is only considered valid for up to 60% release. Equation 6.7 shows the equation describing the model.

$$\frac{W}{W_\infty} = kt^n \qquad \text{Equation 6.7}$$

where k is the diffusional constant and n is the diffusional exponent.

Equation 6.7 rearranges to Equation 6.8 which in turn rearranges to Equation 6.9.

$$W = W_\infty kt^n \qquad \text{Equation 6.8}$$

$$W = k' t^n \qquad \text{Equation 6.9}$$

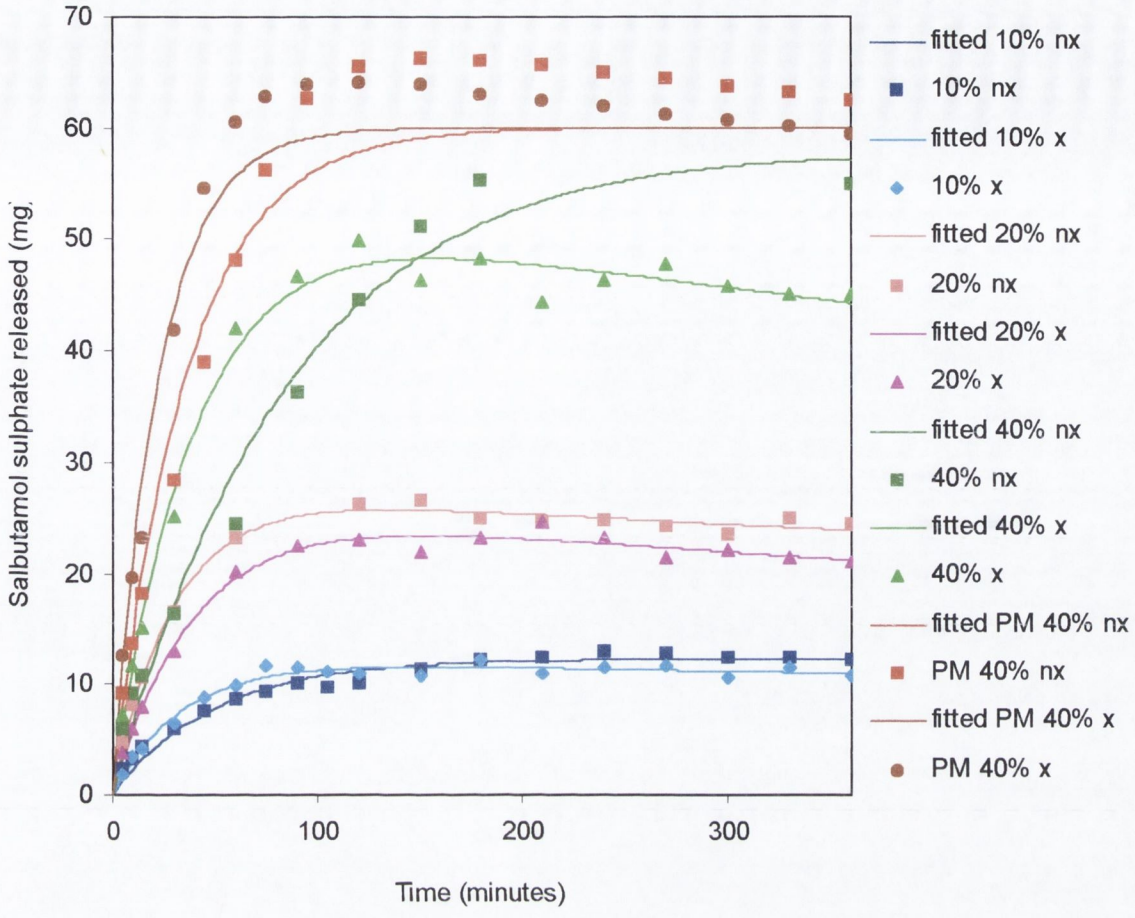

Figure 6.24 Salbutamol sulphate release data from salbutamol/chitosan systems fitted to a biexponential equation. 10% nx = spray dried not crosslinked 10% salbutamol sulphate/chitosan, 10% x = spray dried crosslinked 10% salbutamol sulphate/chitosan, 20% nx = spray dried not crosslinked 20% salbutamol sulphate/chitosan, 20% x = spray dried crosslinked 20% salbutamol sulphate/chitosan, 40% nx = spray dried not crosslinked 40% salbutamol sulphate/chitosan, 40% x = spray dried crosslinked 40% salbutamol sulphate/chitosan, PM 40% nx = physical mix of 40% crystalline salbutamol sulphate/spray dried not crosslinked chitosan, PM 40% x = physical mix of 40% crystalline salbutamol sulphate/spray dried crosslinked chitosan.

The release data was fitted to the general power law expression and is shown in Figure 6.25. If the Higuchi matrix diffusional model (Fickian) holds then a value of 0.5 would be obtained for n in Equation 6.7. Values of greater than 0.5 indicate anomalous diffusion (Ritger and Peppas, 1987). This is generally indicative of a system which swells. The closer the value obtained is to 1, the closer the release is to zero order. Equation 6.9 gave a better fit for the salbutamol sulphate release data than any of the other models previously described, the average MSC being 5.2. The values of n were greater than 0.5 and in all cases the value of n was higher for the crosslinked than non-crosslinked equivalent system. These higher values for n for the crosslinked discs are consistent with greater swelling

during release (see Table 6.10). The diffusional constant, k, tended to increase with salbutamol sulphate loading. Table 6.11 and Table 6.12 show a summary of the statistics and parameter estimates produced by MicroMath® Scientist® for the release profiles fitted to the models discussed.

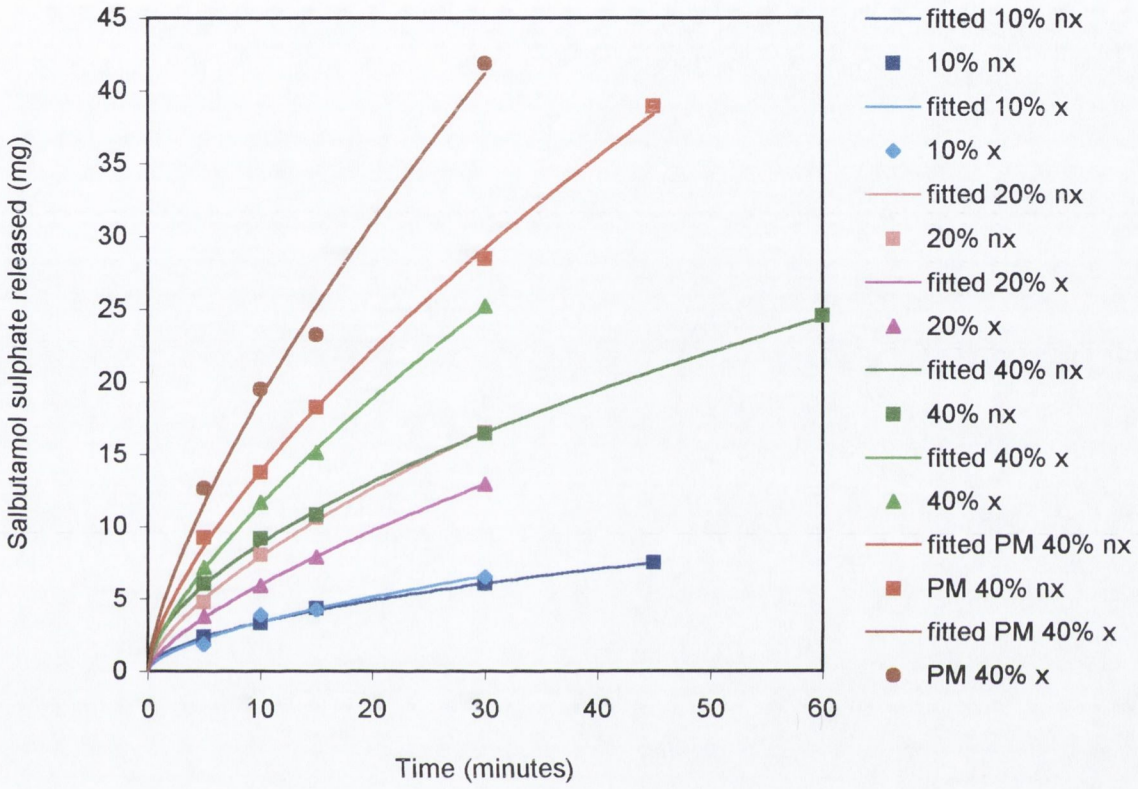

Figure 6.25 Salbutamol sulphate release data from salbutamol sulphate/chitosan systems fitted to the general power law expression. 10% nx = spray dried not crosslinked 10% salbutamol sulphate/chitosan, 10% x = spray dried crosslinked 10% salbutamol sulphate/chitosan, 20% nx = spray dried not crosslinked 20% salbutamol sulphate/chitosan, 20% x = spray dried crosslinked 20% salbutamol sulphate/chitosan, 40% nx = spray dried not crosslinked 40% salbutamol sulphate/chitosan, 40% x = spray dried crosslinked 40% salbutamol sulphate/chitosan, PM 40% nx = physical mix of 40% crystalline salbutamol sulphate/spray dried not crosslinked chitosan, PM 40% x = physical mix of 40% crystalline salbutamol sulphate/spray dried crosslinked chitosan.

Table 6.11 MicroMath® Scientist® goodness of fit and parameter values for release data fitted to the first order and the biexponential model. MSC is the Model Selection Criterion and CoDet is the Coefficient of Determination

	1st order Model				Biexponential Model				
System	***K (min^{-1})***	***W∞***	**MSC**	**CoDet**	***K_D (min^{-1})***	***K_R (min^{-1})***	***Wm***	**MSC**	**CoDet**
10%	0.0239	11.54	2.894	0.959	$2.52e^{-19}$	0.0204	12.23	2.947	0.962
10% XX	0.0321	11.55	3.435	0.976	0.00031	0.0296	12.23	3.433	0.977
20%	0.0363	25.69	4.508	0.993	0.00038	0.0335	27.37	4.655	0.994
20% XX	0.0284	23.67	4.400	0.992	0.00059	0.0254	26.15	4.170	0.989
40%	0.0115	58.97	3.451	0.979	$8.7e^{-5}$	0.0114	60*	3.484	0.979
40% XX	0.0285	48.32	3.602	0.982	0.00053	0.0250	53.52	4.049	0.988
PM 40%	0.0277	60*	2.768	0.990	$4.82e^{-19}$	0.0277	60*	2.651	0.944
PM 40% XX	0.0435	60*	3.175	0.988	4.82^{-19}	0.0435	60*	3.057	0.962
Average	0.029		3.529	0.982	0.000271	0.0271		3.56	0.97

*Upper limit set at 60mg, the theoretical maximum amount present.

Table 6.12 MicroMath® Scientist® goodness of fit and parameter values for release data fitted to the general power law expression and the Higuchi model. MSC is the Model Selection Criterion and CoDet is the Coefficient of Determination

	General Power Law Expression				Higuchi Model		
System	***K' (mg/min^n)***	***n***	**MSC**	**CoDet**	***K (mg/min$^{0.5}$)***	**MSC**	**CoDet**
10%	0.9854	0.5330	5.520	0.998	1.0994	4.918	0.995
10% XX	0.8361	0.6048	2.286	0.963	1.1343	2.263	0.937
20%	1.6830	0.6725	5.659	0.999	2.7866	2.318	0.940
20% XX	1.1720	0.7051	6.963	1.000	2.1358	2.084	0.925
40%	2.3850	0.5680	6.094	0.999	3.0313	3.935	0.987
40% XX	2.2560	0.7080	6.384	0.999	4.1544	2.058	0.923
PM 40%	2.8834	0.6800	5.401	0.998	5.2480	2.452	0.942
PM 40% XX	3.6890	0.7090	3.374	0.987	5.9900	3.520	0.985
Average			5.210	0.993		2.944	0.954

6.10.2. *In vitro* release from microparticles

Release experiments were carried out for the 10% crosslinked and non-crosslinked spray dried salbutamol sulphate/chitosan systems. The release profiles obtained are shown in Figure 6.26. It is evident that release was very rapid. Greater than 90% of salbutamol sulphate was released from the non-crosslinked salbutamol sulphate/chitosan microparticles in the first 5 minutes and 100% release occurred within 5 minutes for the crosslinked microparticles. In light of the previous disc studies this is not surprising. In the case of diffusion from the discs the maximum distance was 450 μm (discs were 0.9 mm in depth). In contrast the average diffusional distance in the particles was 0.8 μm (average radius of 100 particles). Therefore the diffusional distance in the microparticle system was approximately 563 times shorter than in the disc systems. The half life of release from the particles was approximately 2.5 minutes for the crosslinked system and just over 2.5 minutes for the non-crosslinked system. There was no significant difference between release from crosslinked versus non-crosslinked systems. The decrease in release over time may reflect filter holder retention or degradation of the drug.

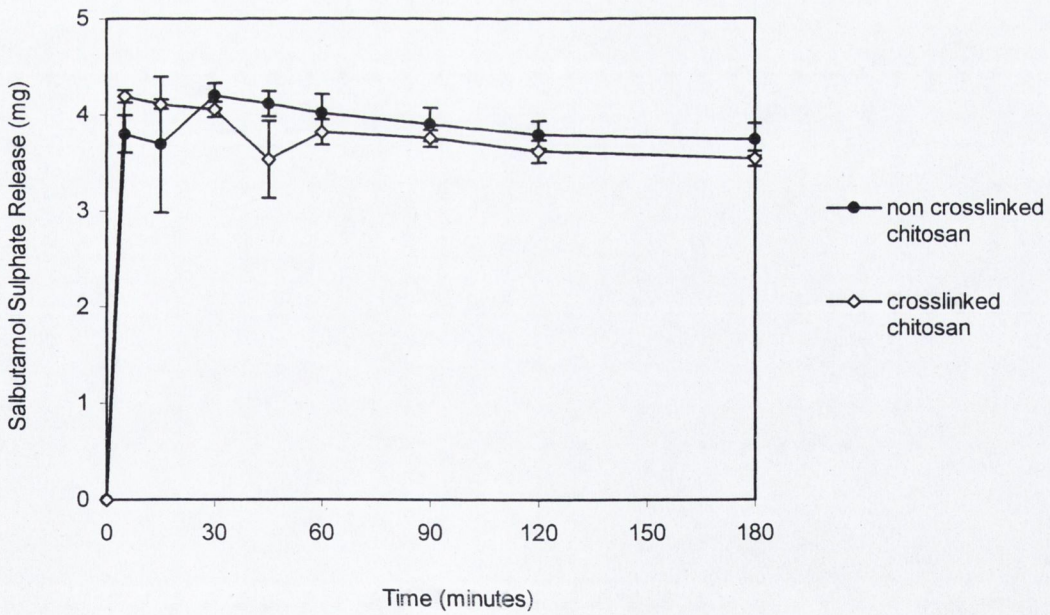

Figure 6.26 Release data for co-spray dried salbutamol sulphate 10%/chitosan and co-spray dried crosslinked salbutamol sulphate 10%/chitosan microspheres.

6.10.3. Conclusion

Spray dried chitosan particles either crosslinked or not crosslinked are unlikely to give any clinically significant retardation in release for a freely soluble drug like salbutamol sulphate (1 to 10 parts of solvent required to dissolve 1 part of solute, B.P. 2002). However since spray dried chitosan can retard the release of this freely soluble drug over the drug alone, investigation of less readily soluble drug systems for sustained release could yield more clinically significant findings. The reason for the increased swelling of the crosslinked chitosan over the non-crosslinked chitosans is unclear. Chitosans exhibit a high level of inter and intra-molecular hydrogen bonding. It is likely that crosslinking with formaldehyde disrupts some of the hydrogen bonding that is present in non-crosslinked chitosans thus resulting in a less tightly bound structure.

6.11. Chitosan/PEG systems for "stealth effect"

In section 6.9 it was demonstrated that chitosan with the model drug salbutamol sulphate achieved reasonable respirable fractions (without the use of a flow aid). For a controlled release inhalation formulation to be effective it must first reach the deep lung and then be retained in the lung for a prolonged period to release the active. The ability of biodegradable particles to escape detection and uptake by alveolar macrophages and cross the epithelium lining will determine the success of a sustained release drug delivery system. Chitosans favourable characteristics, namely the fact that it is mucoadhesive, biodegradable and has been shown to enhance the penetration of large molecules across mucosal surfaces by causing transient opening in tight junctions (Illum, 1998), make it an obvious choice as a carrier for lung delivery for systemic action. It has been shown already in this chapter that spray drying chitosan can result in microparticles of a size which would deposit in the deep lung. Therefore chitosan appears an ideal carrier for lung delivery of therapeutic agents for systemic action. Recently Carrión-Recio et al. (2002) investigated chitosan microspheres prepared by a microencapsulation technique as potential pulmonary delivery systems. They incorporated the model proteins insulin and fluorescein isothiocyanate labeled bovine serum albumin as model compounds and found the chitosan microspheres to have suitable morphological and aerodynamic properties for lung delivery. To deliver a sustained action, however, it is vital that chitosan is not quickly phagocytosed by the alveolar macrophages.

"Stealth" drug delivery systems can be prepared by modification of their surface with hydrophilic, flexible and non-ionic polymers such as PEG (Gref et al., 1994; Torchillin,

1998; Tobío et al., 1998). Microspheres composed of chitosan and PEG could possibly combine the mucoadhesive and permeability enhancing properties of chitosan with the stealth properties of PEG. Therefore chitosan/PEG microspheres were produced by spray drying with a view to determining their physicochemical properties prior to the possible inclusion of a drug. Phagocytosis of chitosan containing microspheres by the murine macrophage cell line J774A.1 was investigated.

Co-spray dried chitosan/PEG 4000 systems containing 10%, 20% and 30% PEG 4000 by weight of total solids were investigated. The systems were spray dried as 0.2% w/v solutions from 1% w/v acetic acid. Spray drying parameters are given in Appendix I.

6.11.1. Chitosan/PEG 4000 systems

XRD scans of chitosan/PEG 4000 10%, 20% and 30% PEG systems are shown in Figure 6.27. The spray dried chitosan/PEG 4000 10% system was completely amorphous. Peaks indicative of crystalline PEG 4000 were visible in the physical mix of chitosan/PEG 4000 10% indicating that 10% PEG in a system is detectable by XRD (Figure 6.27 scan b). The spray dried 20% and 30% PEG showed some crystalline PEG 4000 but in both cases the intensities were reduced implying a reduction in crystallinity on spray drying.

DSC scans of spray dried chitosan/PEG systems are shown in Figure 6.28. The DSC scan of spray dried chitosan/PEG 10% (Figure 6.28, scan a) showed a small endotherm in the PEG melting region indicating the possibility of some crystalline PEG. This contrasted with XRD analysis which showed the absence of crystalline PEG peaks. The spray dried chitosan/PEG 4000 20% system showed an endotherm in the PEG melting region, with a lower onset and peak melting temperature and a smaller enthalpy change than the equivalent physical mix. The crystalline PEG present is likely to be a mix of once folded and extended chain crystal forms, indicated by the temperature of melting and the shape of the melting endotherm (Figure 6.28 scan b). The 30% PEG system also showed the presence of some crystalline PEG 4000. The melting endotherm due to crystalline PEG again occurred at a lower onset and peak temperature and the enthalpy change was much smaller than the equivalent physical mix. The lower melting temperature implies that the crystalline PEG that was present was the once folded metastable conformation (Chatham, 1985 and Kambe, 1980).

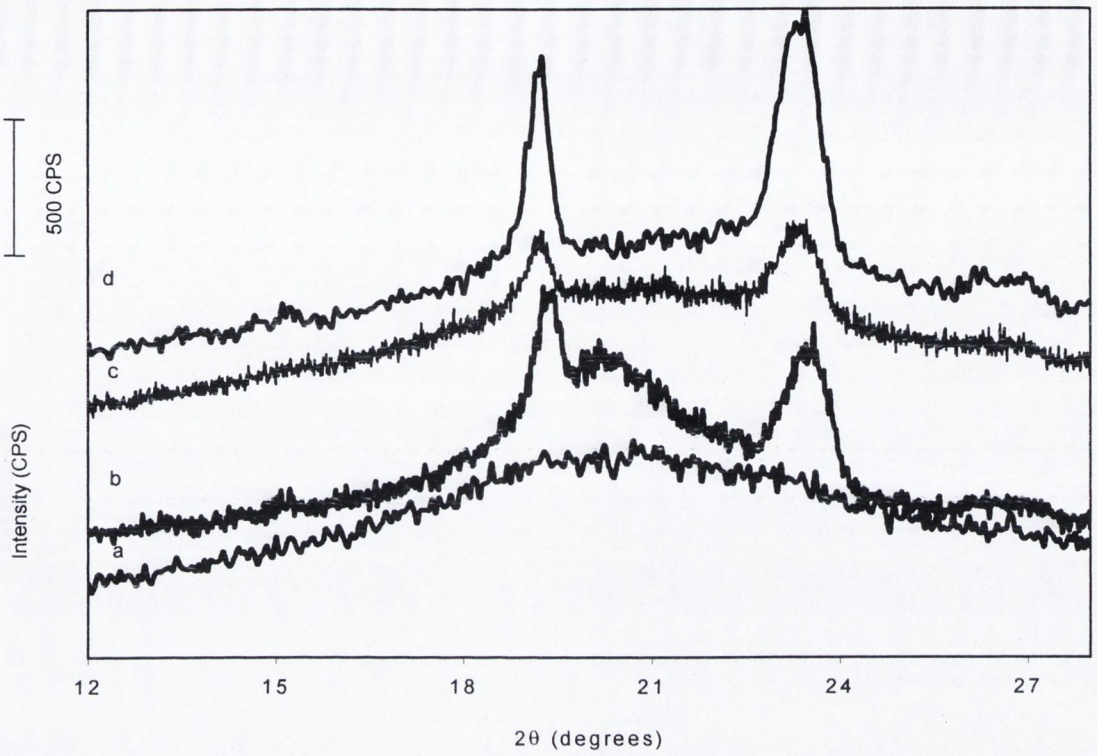

Figure 6.27 XRD scans of (a) spray dried chitosan/PEG 4000 10%; (b) physical mix of chitosan/PEG 4000 10%; (c) spray dried chitosan/PEG 4000 20% and (d) spray dried chitosan/PEG 4000 30%.

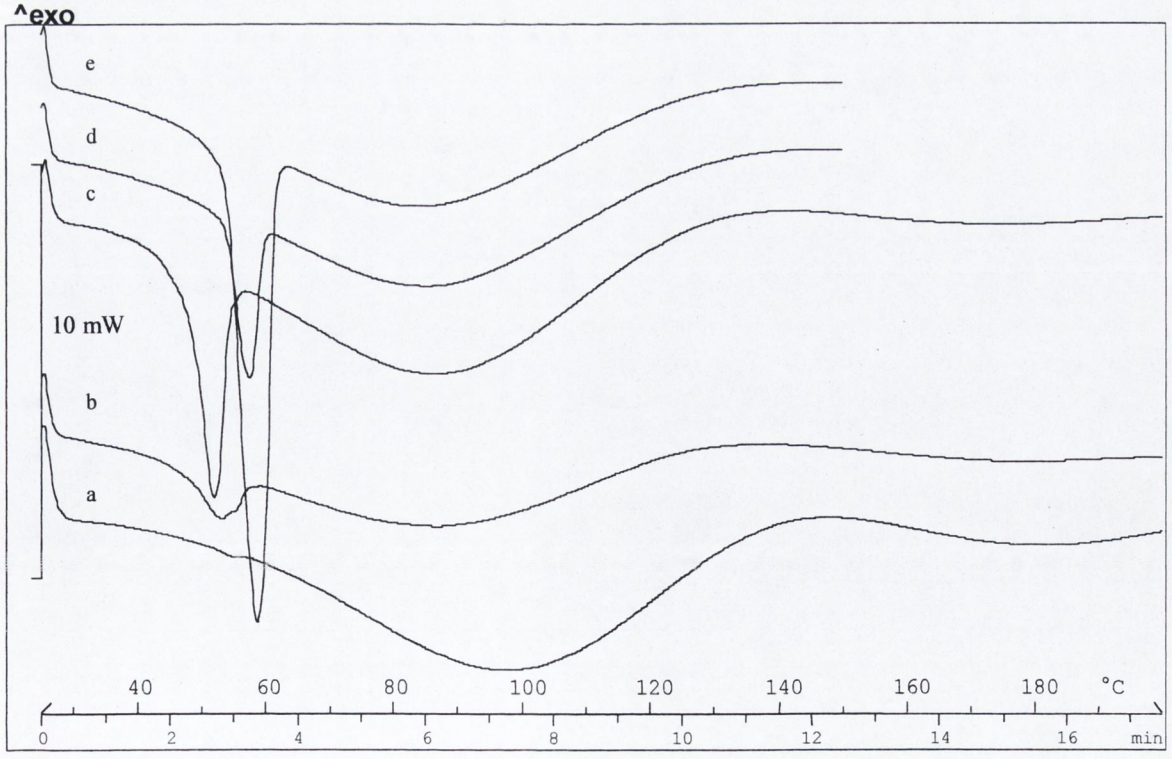

Figure 6.28 DSC scans of (a) spray dried chitosan/PEG 4000 10%; (b) spray dried chitosan/PEG 4000 20%; (c) spray dried chitosan/PEG 4000 30%; (d) physical mix of chitosan/PEG 4000 10% and (e) physical mix of chitosan/PEG 4000 30%.

SEM micrographs of spray dried chitosan/PEG systems are shown in Figure 6.29. Particles had roughened folded surfaces and were 0.5 - 4μm in diameter (similar in particle size to chitosan spray dried alone from acetic acid).

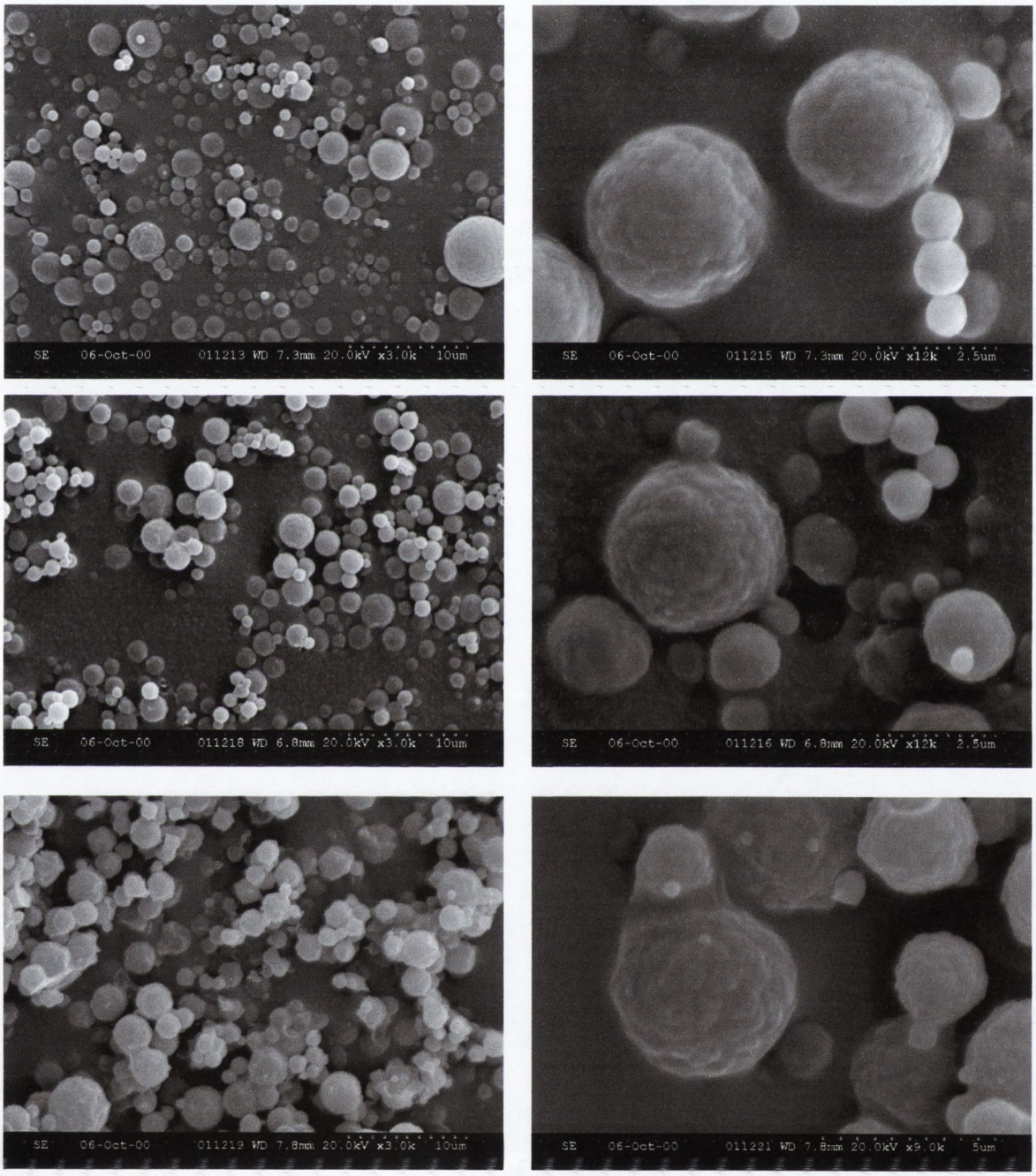

Figure 6.29 SEM micrographs of spray dried chitosan/PEG 4000 10% (top); spray dried chitosan/PEG 4000 20% (middle) and spray dried chitosan/PEG 4000 30% (bottom).

6.11.2. Phagocytosis study

6.11.2.1. Introduction

Biodegradable polylactic-co-glycolic acid (PLGA) microspheres have been suggested as an ideal carrier system to target drugs into phagocytic cells such as macrophages (Walter et al., 2001). PLGA microspheres have been shown to be phagocytosed by the murine macrophage cell line J774A.1 by Wang et al. (1999) and therefore were used as a positive control in this experiment. Negative controls consisted of wells of cells to which dulbecco's modified eagles media (DMEM) without the microparticles was added. Spray dried chitosan and spray dried chitosan/PEG microspheres (consisting of 10, 20 and 30% PEG 4000) were investigated with respect to phagocytosis by the macrophage cell line using the method previously described by Kimura et al. (1994) and Wang et al. (1999) as outlined in Chapter 2.

6.11.2.2. Results of phagocytosis experiments

A photograph of the negative control is shown in Figure 6.30. The cells had a granular appearance with dark spherical bodies visible in some cells. The positive control is shown in Figure 6.31. Many microspheres are visible consistent with practically every cell having phagocytosed at least one microsphere with at least 10-15 particles present in many cells. The photograph of the positive control, shown in Figure 6.31, was taken after washing the cells three times with buffer to remove non-phagocytosed microspheres. Following washing of the cells, the microspheres which remain were shown by Wang et al. (1999), using transmission electron microscopy, to be consistent with phagocytosed rather than surface adhered microspheres. Cells to which chitosan had been added are shown in Figure 6.32. This photograph shows the cells prior to washing three times with buffer so that the appearance of the chitosan particles can be observed. Figure 6.33 shows the cells to which the chitosan particles had been added and then washed off. Particles of chitosan were no longer detectable, consistent with non-phagocytosis of chitosan by the cells. The photographs were all taken following 1 hour of incubation with the microspheres. Similar observations were observed at 24 hours.

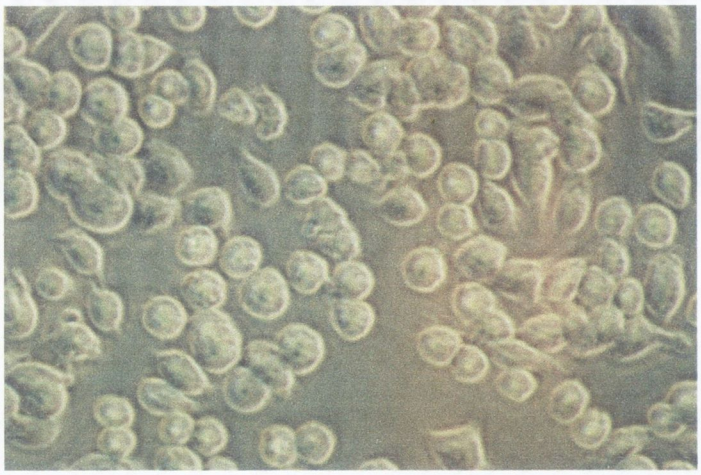

Figure 6.30 Photograph of J774A.1 cells to which no particles had been added (negative control).

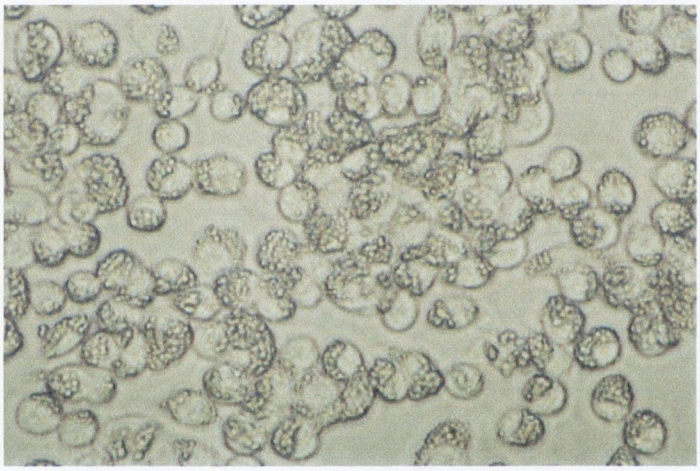

Figure 6.31 Positive control: J774A.1 cells following incubation with PLGA microspheres (following washing with buffer to remove non-phagocytosed particles).

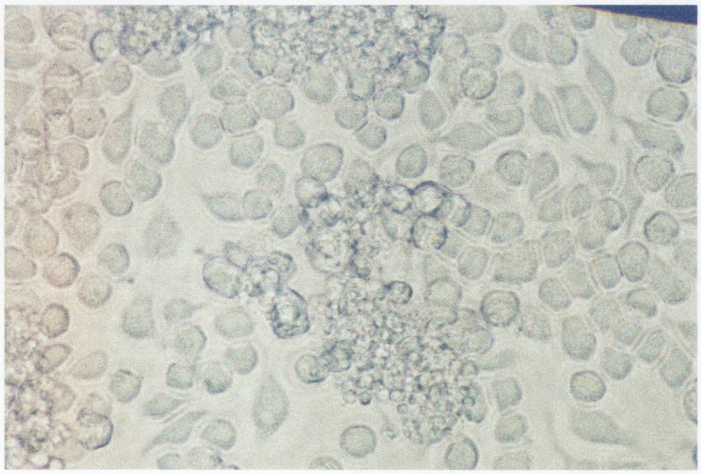

Figure 6.32 J774A.1 cells following incubation with chitosan microspheres (prior to washing with buffer to remove non-phagocytosed particles).

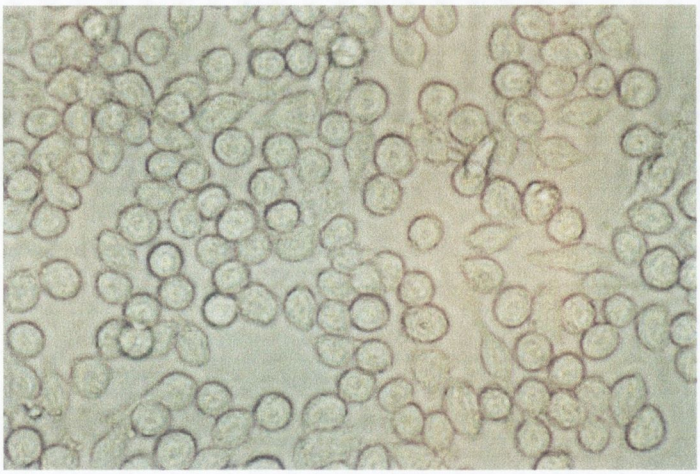

Figure 6.33 J774A.1 cells following incubation with chitosan microspheres (following washing with buffer to remove non-phagocytosed particles).

Cells which had been incubated with chitosan/PEG composite microspheres gave similar results to chitosan alone i.e. phagocytosis was not observed. It was expected that the chitosan microspheres would be phagocytosed and that the presence of PEG in chitosan/PEG microspheres might affect the number of microspheres phagocytosed (i.e. reduce the number of microspheres phagocytosed or stop phagocytosis altogether). During the study it was observed that in some areas of the wells, chitosan particles clumped on top of the monolayer making washing with phosphate buffer less effective.

From these preliminary studies it was concluded that the murine macrophage cell line did not phagocytose chitosan and therefore incorporation of PEG 4000 into chitosan microspheres was not necessary to render it "stealth". This finding implies that chitosan should be able to avoid the reticuloendothelial system and therefore act as a delivery system for sustained action. Banerjee et al. (2002) recently reported chitosan nanoparticles to have a "stealth" effect when injected intravenously in mice. They radiolabelled their chitosan and observed that the nanoparticles readily evaded the reticuloendothelial system resulting in long circulation times in the blood.

Although the J774.1A cell line is used for general phagocytosis studies, it is not in fact a lung macrophage cell line and therefore other methods to study phagocytosis for potential lung delivery might be more appropriate. Alternative methods for the study of phagocytosis of these systems could involve the use of an intratracheal rat model (Enna and Schanker, 1972), which can be used to study the absorption and metabolism of drugs by the pulmonary system. Evora et al. (1998) used lung macrophages obtained by intratracheal lavage of Wistar rats to investigate phagocytosis of microparticles intended for delivery. There are also two human derived respiratory epithelium cell lines, Calu-3

and A549, although these are not macrophage cell lines they have properties consistent with submucosal gland serous cells and type II pulmonary epithelial cells respectively. Foster et al. (2001) investigated microparticulate uptake of fluorescent polystyrene microspheres of differing sizes and surface chemistry using these two human cell lines and found that A549 cells appeared to have more phagocytic activity than Calu-3 cells. Perhaps it would be more appropriate in future work to use A549 cells or macrophages from intratracheal lavage of rats for phagocytosis of particles destined for the lung. The effect of crosslinking on phagocytosis of chitosan needs to be determined.

GENERAL DISCUSSION

7.1 Introduction

From a pharmaceutical processing point of view spray drying has a number of unique characteristics:

- the ability to dry a liquid feed to a dry powder in a one step process,
- the ability to produce spherical particles with good flow characteristics,
- the ability to induce phase changes,
- the rapid drying can be used for reasonably heat labile materials.

There has been limited investigations of two component systems, most work having focused on single component systems. It would be beneficial to be able to better understand the impact of the spray drying process on the physicochemical properties of such composite materials. Towards this end, this thesis examined a range of two component systems of interest in pharmaceutical formulation. Two component spray dried systems could be:

- two drugs,
- a drug plus an excipient,
- two excipients,
- a drug and a polymer, or
- two polymers.

7.2 Crystallinity of systems spray dried alone

In the course of the thesis a range of individual single component systems were spray dried. The materials investigated, their molecular weights, DSC melting temperatures, DSC enthalpy changes of melting of the unprocessed materials, and estimated glass transition temperatures (T_g) are shown in Table 7.1. Estimated glass transition temperatures were based on Equation 7.1 (Hancock and Zografi, 1994; Brittain, 1999).

$$T_g = (0.7)(T_m) \qquad \text{Equation 7.1}$$

where T_g is the glass transition temperature and T_m is the melting temperature in degrees Kelvin.

Table 7.1 Table showing molecular weights, DSC melting temperatures, DSC enthalpy of melting values and estimated glass transition temperatures for the different materials investigated in this thesis.

Materials investigated	**Molecular weight**	**Melting temperature (T_m)**	**Enthalpy change of melting**		**Estimated† Glass Transition Temperature**
			J/g	**KJ/mole**	
α-anhydrous lactose (spray dried lactose melts as the anhydrous α-form)	342.3	217°C 490K	115	39.4	70°C 343K
PEG 4000	3856	58°C 331K	192	740.4	-41°C 232K
PEG 20,000	22,869	62°C 335K	178	4070.7	-39°C 234K
PEO 300,000	547,649	63°C 336K	176	96,386.2	-38°C 235K
Chitosan	165,000	—	—	—	—
BFMT	421.4	229°C 502K	109	45.9	78°C 351K
Salbutamol sulphate	576.7	200°C 473K	165	95.2	58°C 331K
Salbutamol base	239.3	157°C 430K	210	50.2	28°C 301K
Ipratropium bromide monohydrate	430.4	237°C 510K	245	105.4	84°C 357K
Budesonide	430.5	262°C 535K	89	38.3	102°C 375K
Formoterol fumarate dihydrate	828.9	140°C 413K	*	*	16°C 289K (based on melting of racemate A)

†Estimated glass transition based on Equation 7.1 (Hancock and Zografi, 1994; Brittain, 1999)

*melting endotherms appear to overlap with the dehydration endotherm and degradation peaks therefore integration of the melting endotherm was not possible.

When spray dried as single component systems six out of the eleven materials shown in Table 7.1 were X-ray amorphous. These systems were lactose, bendroflumethiazide, salbutamol sulphate, budesonide, formoterol fumarate and chitosan. One of the systems, chitosan, was amorphous prior to spray drying and remained amorphous following spray drying. Five materials showed peaks indicative of crystallinity following spray drying. These materials were PEG 4000, PEG 20,000, PEO 300,000, salbutamol base and ipratropium bromide. PEGs are semicrystalline materials and exhibit a T_g which depends

on the molecular weight of the sample (Craig, 1995). In the molecular weight range of 10^2-10^7 the T_g varies from approximately –98°C to –17°C depending on molecular weight (Craig, 1995). The very low T_gs of these compounds indicates that at room temperature the materials are likely to have recrystallised. Salbutamol base has an estimated T_g of 28°C indicating that a low level of moisture could plasticise this material and result in a lowering of the glass transition temperature to room temperature allowing the material to convert to the rubbery state and recrystallise. While salbutamol base showed peaks indicative of crystallinity by XRD, DSC showed the presence of an exotherm indicative of some amorphous material having been produced on spray drying. Crystallinity may have arisen during preparation for XRD analysis. Ipratropium bromide also did not form an X-ray amorphous material on spray drying. DSC of the spray dried material failed to show an exotherm indicative of the presence of any amorphous material. From DSC of the crystalline starting material it was observed that ipratropium bromide had the largest enthalpy change associated with its melting when compared to the other systems. This may suggest that the crystalline form of this material is quite physically stable and therefore may be less likely to form an amorphous system. Spray drying of ipratropium bromide from aqueous solution resulted in predominantly the anhydrous form. The anhydrous forms of pseudopolymorphs are generally less stable than their monohydrate counterparts (Haleblian, 1975). Spray drying generally produces a higher energy form, thus it is not surprising that spray drying ipratropium bromide resulted in the formation of the anhydrous form. Spray drying from ethanolic solution (95%) resulted in some reduction in the amount of hydrate present, but the reduction was not as pronounced as when ipratropium bromide was spray dried from aqueous solution. Spray drying from ethanolic solution (95%) utilises a lower inlet temperature than spray drying from aqueous solution (77-79°C compared to 150-153°C), therefore the temperature drop would not have been as dramatic within the evaporating chamber which could affect the crystallinity of the resultant system. The ipratropium bromide spray dried from ethanolic solution may have been able to crystallise to the more stable monohydrate form during the less extreme drying cycle utilised for its production.

The structures of the materials which formed amorphous phases on spray drying (as determined by XRD) are shown in Figure 7.1 and those which did not form amorphous phases are shown in Figure 7.2. The structures were compared in order to ascertain if structure affected whether an amorphous phase was produced on spray drying.

Lactose (left = α-lactose, right = β-lactose)

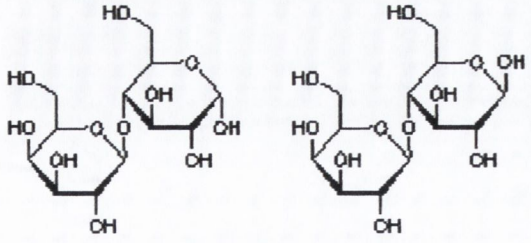

Bendroflumethiazide

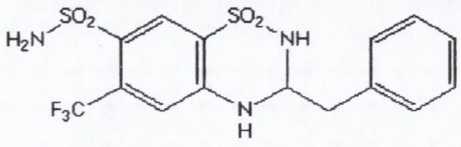

Salbutamol sulphate

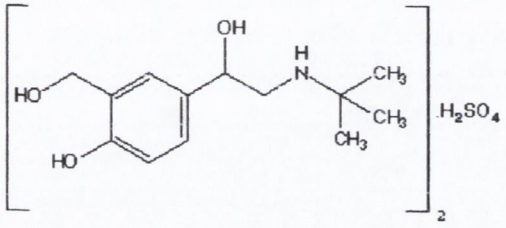

Budesonide

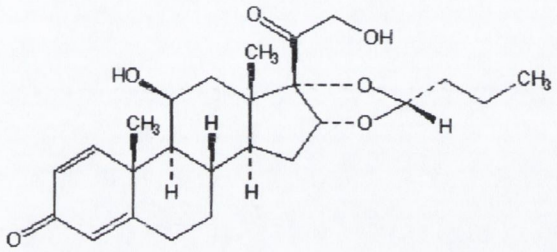

Formoterol fumarate dihydrate

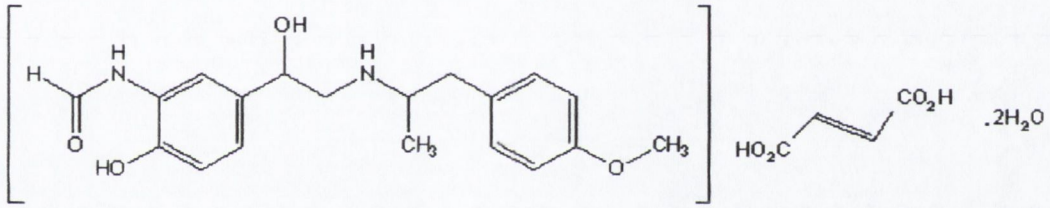

Figure 7.1 Structures of the materials which were X-ray amorphous on spray drying.

Salbutamol as the sulphate formed an X-ray amorphous phase, however as the base it showed peaks indicative of crystallinity. Therefore the salt form of salbutamol appeared to favour the formation of an amorphous phase on spray drying. Salbutamol base could only be spray dried from ethanolic solution due to its lack of aqueous solubility. The lower inlet temperatures utilised when spray drying from ethanol 95% may have resulted in a slower drying time or a less extreme drying process thereby allowing some of the salbutamol base to recrystallise. Although salbutamol sulphate formed a completely amorphous phase when spray dried from ethanol, unlike salbutamol base, the results can not be directly compared since salbutamol sulphate was not as soluble in ethanol as the base and therefore ethanol 75% was used as the solvent, not ethanol 95%. Additionally the feed concentration was much lower when spray drying salbutamol sulphate from ethanol compared to spray drying the base from ethanol (0.6% w/v compared to 2.5% w/v). Kawashima et al. (1983b) found that the temperature at which a pyrabarbital complex was spray dried had a

significant effect on the predominant crystal form of the resulting powder. They observed a greater degree of amorphism when a feed was dried at a temperature of 145°C as opposed to a temperature of 85°C. They attributed this to the more rapid drying that occurs at higher temperatures. The inlet and outlet temperatures used in this work when spray drying salbutamol base from ethanol (95%) were 77-79°C and 48-50°C respectively. The inlet and outlet temperatures used when spray drying salbutamol sulphate from ethanol (75%) were 100-102°C and 60-64°C respectively, the higher temperature being necessary to evaporate the larger water content in the solvent. The larger temperature drop that occurred when spray drying salbutamol sulphate from ethanol (75%) could have affected the crystallinity of the resultant system.

PEG/PEO structures (molecular weight depending on the number of repeat units, n)

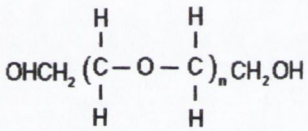

salbutamol base

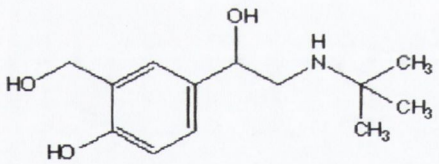

Ipratropium bromide monohydrate

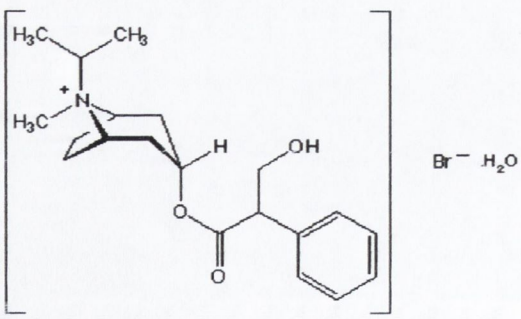

Figure 7.2 Structures of the materials which were not X-ray amorphous on spray drying.

All the systems studied in this thesis apart from the PEG/PEO polymers consisted of ring structures. Previously when Corrigan et al. (1984) spray dried a range of thiazide diuretics they found that the larger molecular weight compounds formed amorphous phases more

readily than the lower molecular weight thiazides. Amorphous systems produced from the higher molecular weight thiazides were more physically stable than amorphous systems produced from the lower molecular weight thiazides. The PEG/PEO polymers do not contain large side groups and this might explain why they are less likely to form amorphous systems on spray drying. Bodmeier and Chen (1988) described linear macromolecular polymers without bulky side groups, such as polylactic acid, as having strong and extensive intermolecular bonding coupled with adhering stiffness of the polymeric chains leading to strong chain interactions. They used these facts to explain the difficult disruption of a liquid filament into individual particles resulting in fibrous spray dried material. In addition to the low T_g of PEG/PEO polymers, the lack of bulky side chains associated with the polymers may be responsible for their retainment of crystallinity on spray drying.

Table 7.2 shows DSC details of the spray dried materials together with their T_g estimates and experimental T_gs, where available. T_gs of salbutamol sulphate and lactose were estimated at 58°C and 70°C respectively and therefore DSC may not have detected them due to absorbed water also being lost in this region. Ward and Schultz (1995) micronised salbutamol sulphate using an air jet micronisation technique. XRD showed peaks indicative of crystallinity. They found only minor differences in XRD peak intensities between micronised and unmicronised material which they first attributed to preferred orientation within the sample. DSC did however detect an endotherm at 64°C which they attributed to the T_g of amorphous salbutamol sulphate and a small exothermic peak at 85°C consistent with crystallisation of the amorphous material. A melting endotherm occurred at 202°C, close to the melting temperature of the crystalline salbutamol sulphate starting material of 200°C (T_m). The melting endotherm of the spray dried salbutamol sulphates produced for this thesis occurred at the lower temperature of approximately 160°C by DSC (heating rates of 10°C/minute were used both in this thesis and by Ward and Schultz (1995)). The T_g obtained experimentally by Ward and Schultz (1995), on heating their micronised material, was in good agreement with the predicted T_g of 60°C based on $0.7(T_m)$ in degrees Kelvin. It is possible that crystalline material present in their sample acted as seed crystals promoting the recrystallisation of any amorphous material present and therefore a recrystallisation exotherm was observed. Their material melted at 202°C, similar to the melting temperature of crystalline starting material (200°C), while in this thesis spray dried salbutamol sulphate melted at a lower temperature (approximately 160°C) and showed broad endotherms. Therefore it is possible that X-ray amorphous

spray dried salbutamol sulphate is relatively stable on heating and the broad "melting" at 160°C is melting of the amorphous form.

Table 7.2 Table showing onset temperatures and enthalpy changes of exotherms of the spray dried materials where visible by DSC, DSC melting temperatures of the spray dried materials ($T_{m\ SD}$), DSC enthalpy changes for both the spray dried and the starting materials, estimated glass transition temperatures based on Equation 7.1 (Hancock and Zografi, 1994; Brittain, 1999) and experimental glass transition temperatures found either in this thesis or in the literature.

Spray dried materials investigated	**Exotherm onset temperature**	**Exotherm enthalpy change**	**$T_{m\ SD}$**	**Enthalpy change of melting (J/g)**		**Glass transition temperature (T_g)**	
				Spray dried material	**Crystalline material**	**Estimated**	**Experimental**
Lactose	169°C 442K	109	217°C 490K	111	115	70°C 343K	104°C 377K (Elamin et al., 1995)
PEG 4000	---	---	56°C 329K	173	192	-41°C 232K	-17 to-98°C 175-256K (Craig, 1995)
PEG 20,000	---	---	68°C 341K	184	178	-39°C 234K	
PEO 300,000			61°C 334K	139	176	-38°C 235K	
Chitosan	---	---	---	---	---	---	---
BFMT	163°C 436K	47.8	220°C 493K	79	109	78°C 351K	120°C 393K
Salbutamol sulphate	---	---	169°C 442K (aq) 166°C 439K (EtOH)	44 (aq) 31 (EtOH)	165	58°C 331K	64°C 337K (Ward and Schultz, 1995)
Salbutamol base	63°C 336K	45	157°C 430K	197	210	28°C 301K	---
Ipratropium bromide	---	---	233°C 506K (aq) 231°C 504K (EtOH)	108 (aq) 111 (EtOH)	245	84°C 357K	---
Budesonide	113°C 386K	38	262°C 535K	90	89	102°C 375K	90°C 363K

aq=spray dried from aqueous solution, EtOH=spray dried from ethanolic solution.

The glass transition of budesonide was observed experimentally at approximately 90°C which was close to the theoretical estimate of 102°C. BFMT had an estimated glass transition of 78°C (351K) yet by DSC the transition appeared to occur at approximately 120°C (393K). Kerc and Srcic (1995) describe T_g/T_m values for pharmaceuticals as ranging from between 0.59 to 0.86. The T_g/T_m ratio of BFMT's experimentally determined T_g is 0.78 which is within the range described by Kerc and Srcic (1995).

7.3 Crystallinity of co-spray dried systems

Spray dried lactose is probably the most commonly used metastable amorphous excipient in pharmaceutical manufacturing (Schmitt et al., 1999). Chidavaenzi et al. (2001) investigated co-spray dried lactose/PEG 4000 systems since it is not uncommon in pharmaceutical technology to spray granulate formulations that comprise of lactose and polyethylene glycol as excipients. During the spray granulation process amorphous forms of excipients or drugs can be produced and therefore Chidavaenzi et al. (2001) were interested in determining whether lactose/PEG 4000 systems readily formed amorphous phases. Given that co-spray drying with PVP had been shown to promote the formation of amorphous materials (Corrigan et al., 1985) Chidavaenzi et al. thought PEG might act in a similar manner. Chidavaenzi et al. (2001) found crystalline β-lactose present in lactose/PEG 4000 systems when 12% PEG 4000 was spray dried by weight of lactose (10.7% by weight of total solids) but not when 1, 2 or 4% PEG 4000 was present (by weight of lactose). We found β-lactose present when 5% PEG 4000 (by weight of total solids) was spray dried with lactose but found it to be absent for 10, 20 and 30% PEG 4000 systems. Chidavaenzi et al. (2001) found some crystalline α-lactose monohydrate present in all their spray dried lactose/PEG 4000 systems. None of the systems spray dried in the current work showed the initial presence of α-lactose monohydrate. All co-spray dried lactose/PEG 4000 systems prepared for this thesis showed a reduction in PEG 4000 crystallinity on spray drying, the 10% PEG 4000 system appearing to consist of completely amorphous PEG 4000. The 10% PEG 4000 system also contained the least crystalline lactose. Interestingly any crystalline lactose which was detected in the 5% system was present as β-lactose while any crystalline lactose which was detected in the 20% or 30% systems was present as α-anhydrous lactose. On storage PEG 4000 and lactose recrystallised, storage at higher humidities resulting in recrystallisation to α-lactose monohydrate. An attempt was made to fit the recrystallisation of lactose to lactose monohydrate using the Avrami equation (Avrami, 1940). Jouppila et al. (1997) fitted the

recrystallisation of amorphous lactose in freeze-dried skim milk at relative humidities of 66.2% and greater to the Avrami equation. They measured increases in X-ray peak intensity at 19°, 20° and 22° 2θ. They attributed the peak at 19° 2θ to α-lactose monohydrate, stable anhydrous α-lactose and an anhydrous mix of α and β lactose in a molar ratio of 5:3. The peak at 20° 2θ was attributed to α-lactose monohydrate and anhydrous α/β lactose 5:3 mix. The peak at 22° 2θ was attributed to other lactose forms not including α-lactose monohydrate. When fitting their data they obtained K values of 2.7 x 10^{-2} $hours^{-1}$ (0.684 $days^{-1}$), 1.2 x 10^{-3} $hours^{-1}$ (0.028 $days^{-1}$) and 2.6 x 10^{-3} $hours^{-1}$ (0.062 $days^{-1}$) for peaks at 19°, 20° and 22° 2θ respectively for recrystallisation at 24°C and 76% RH. The rate of recrystallisation of amorphous lactose found in this thesis was 0.369 $days^{-1}$. However the peak measured in this thesis, at 16.4° 2θ, is specific to monohydrate lactose rather than a mix of monohydrate with other anhydrous forms. Increases in X-ray peak intensity at 19°, 20° and 22° 2θ could not be measured for co-spray dried lactose/PEG systems due to interference from crystalline PEG peaks which occur in the same region. Jouppila et al. investigated recrystallisation of amorphous lactose in skimmed milk powder which contains impurities such as salts and other carbohydrates. These impurities could affect the recrystallisation rates of amorphous lactose by acting either as nucleation sites or as inhibitors of crystallisation. Schmitt et al. (1999) investigated recrystallisation of amorphous lactose produced by spray drying solutions of lactose. They monitored recrystallisation by gravimetry. They reported much faster recrystallisation rates than those found either in this thesis or by Jouppila et al. (1997). A recrystallisation rate of 0.064 min^{-1} (67.104) $days^{-1}$ was reported for samples stored at 25°C and 62.6% RH. The stages in recrystallisation of amorphous lactose involve recrystallisation first to anhydrous lactose followed by recrystallisation to the monohydrate form (Chapter 3, section 3.4.1, Figure 3.13). Weight loss occurs when amorphous lactose recrystallises and since it initially recrystallises to the anhydrous form, Schmitt et al. obtained the rate for recrystallisation to anhydrous lactose. The recrystallisation monitored in this thesis was recrystallisation to the monohydrate form. The peak at 16.4° 2θ is representative of the monohydrate only and therefore recrystallisation rates were expected to be slower. Methods of production of amorphous material can affect the later recrystallisation rates since the method of production can affect the number of surviving nuclei (Chatham, 1985). Briggner et al. (1994) performed experiments to investigate the effect of the surface area of saturated salt solution and the available surface area of powder on the recrystallisation time of amorphous lactose. They described recrystallisation of lactose as a co-operative process, the amorphous material absorbing water, transporting it

throughout the powder bed and recrystallisation occurring when the entire bed was saturated (measured by isothermal microcalorimetry). They found that the delay in observing a recrystallisation peak was due to both the available surface area of the saturated salt solution and the powder bed (if both are large then recrystallisation was rapid, while if either was reduced the delay in recrystallisation increased). When comparing recrystallisation rates between samples, similar sized powder beds and similar areas of saturated salt solutions should therefore be used.

Co-spray drying lactose with 5% PEG 4000 resulted in a retardation of lactose crystallisation to lactose monohydrate while higher PEG 4000 concentrations appeared to accelerate recrystallisation. PEG 4000 included at concentrations above 5% may act as a plasticiser and therefore be responsible for the increased crystallisation rates. Chidavaenzi et al. (2001) found the presence of lactose monohydrate in all their co-spray dried systems. None of the lactose/PEG co-spray dried systems in the work for this thesis showed the initial presence of the monohydrate but on storage did recrystallise to the monohydrate. It is probable that Chidavaenzi et al. did not analyse their spray dried samples early enough following spray drying and that the material had already recrystallised and produced some monohydrate by the time they analysed the samples.

PEG 4000 has been shown on numerous occasions to aid in the dissolution of poorly soluble drugs. The fact that spray drying with lactose resulted in some cases in amorphous PEG, and at other concentrations in PEG of reduced crystallinity implied that co-spray drying PEG 4000 with poorly soluble drugs may result in higher energy drug/PEG systems which might show enhanced solubility and dissolution characteristics. Co-spray drying BFMT with PEG 4000, PEG 20,000 and PEO 300,000 resulted in completely amorphous systems with respect to drug and polymer over the concentration of polymer studied of 10%-30% by weight of total solids. This contrasted with the spray dried lactose/PEG systems in which crystalline PEG was clearly evident when present in concentrations of 20 and 30%. Higher dissolution rates were observed for the BFMT/PEG systems compared with micronised BFMT alone, with the spray dried 10% PEG-containing system giving 2-3 fold higher initial rates. Co-precipitates of hydroflumethiazide and PEG resulted in systems in which both the drug and the PEG were crystalline (Corrigan and Timoney, 1976). There are only a few examples of solid dispersions of PEG-drug systems where the drug is rendered amorphous, and these systems had much lower weight fractions of drug than the systems in this thesis. The drugs which were reported to be rendered amorphous when prepared as solid dispersions with PEG by either the melt or solvent evaporation methods (not by spray drying) were ritonavir (Law et al, 2001), nifedipine

(Chutimaworapan et al., 2000), griseofulvin (Aldén et al., 1992), tolbutamide (Chatham, 1985) and BFMT (Frontini and Mielck, 1997a). Co-spray drying PEG/BFMT systems not only resulted in amorphous drug but also amorphous PEG. Crystalline PEG 4000 was not detected in the co-spray dried salbutamol sulphate/PEG 4000 systems when included as 5% by weight of total solids. Higher PEG 4000 contents (20% and 40% PEG) resulted in evidence of some PEG crystallinity although the peak intensities were greatly reduced in comparison to equivalent physical mixes. Lactose, BFMT and salbutamol sulphate all formed amorphous phases when spray dried alone, yet when PEGs were co-spray dried with these materials they differed in crystallinity with respect to PEG. Table 7.3 shows the solubilities, molecular weights, melting temperatures by DSC and enthalpy change by DSC of the crystalline unprocessed drugs.

Table 7.3 Table showing physicochemical properties of lactose monohydrate, BFMT and salbutamol sulphate.

Drug	Aqueous solubility†	Ethanolic solubility†	Molecular weight	Melting point	Enthalpy change of melting (KJ/mole)
Lactose (based on melting of α-lactose)	Freely soluble	Practically insoluble	342.3	217°C 490K	39.4
BFMT	Practically insoluble	Soluble	421.4	229°C 502K	45.9
Salbutamol sulphate	Freely soluble	Slightly soluble	576.7	200°C 473K	95.2

† Ph. Eur. (2002)

The main difference between the three is their solubilities. Lactose and salbutamol sulphate are freely soluble in water while BFMT is sparingly soluble. Bendroflumethiazide is soluble in alcohol while lactose is practically insoluble and salbutamol sulphate is only slightly soluble in alcohol (Ph.Eur., 2002). The aqueous solubilities indicate the different hydrophilicities of the three components. Another difference was in the method of manufacture, BFMT/PEG systems were spray dried from ethanolic solvent while lactose/PEG and salbutamol sulphate/PEG systems were spray dried from aqueous solution. However PEG 4000 spray dried alone was spray dried from ethanolic solution and the resultant powder was crystalline.

Chidavaenzi et al. (2001) describe that added materials can act as inhibitors of crystallisation by hindering chain diffusion and packing resulting in a higher percentage of amorphous and imperfectly crystalline materials. BFMT resulted in amorphous PEG and PEO when PEG and PEO were included as 10, 20 and 30%. Salbutamol sulphate co-spray dried with PEG polymers did promote some reduction in polymer crystallinity but the extent depended on the concentration of polymer and molecular weight. Lactose/PEG co-spray dried systems resulted in X-ray amorphous PEG when PEG was included at concentrations of 10% (by weight of total solids) but at higher concentrations crystalline PEG was present. The larger and more rigid structure of BFMT may hinder chain diffusion and packing more than the structure of salbutamol sulphate or lactose thereby resulting in amorphous systems over a wider PEG concentration range.

Table 7.4 summarises the crystallinity of the BFMT/PEG 4000, salbutamol sulphate/PEG 4000 and lactose/PEG 4000 systems with respect to PEG 4000

Table 7.4 Table summarising crystallinity of PEG 4000 in BFMT/PEG 4000, salbutamol sulphate/PEG 4000 and lactose/PEG 4000 systems.

System	Percentage PEG 4000 by weight of total solids				
	5%	10%	20%	30%	40%
BFMT/PEG	---	a	a	a	---
Lactose/PEG	a*	a	c	c	---
Salbutamol sulphate/PEG	a	---	c	---	c

a= amorphous, c = peaks indicative of crystallinity

* crystallinity suggested by XRD but not by DSC.

Compatible blends of amorphous materials exhibit a single T_g that is intermediate to the T_g values of the individual components (Hancock and Zografi, 1994). The low T_gs of PEGs and PEOs indicate that these materials are likely to act as plasticisers and this has been shown in the current work for systems containing 10, 20 and 30% PEG (with either lactose or BFMT). Considering the glass transition behaviour of amorphous solids in terms of polymer free volume theory, the glass transition of a mix of two components ($T_{g\,mix}$) can be determined by Equation 7.2.

$$T_{g\,mix} = (\emptyset_1)(T_{g1}) + (\emptyset_2)(T_{g2}) \qquad \text{Equation 7.2}$$

where Ø is the volume fraction of each component.

Equation 7.2 assumes perfect volume additivity at T_g and no specific interaction between the two components. Since Ø is equal to $(\Delta_\alpha)(w)/\rho$ (where Δ_α is the thermal expansivity of T_g, , w is the weight faction and ρ is the true density of the material) then Equation 7.2 can be written as Equation 7.3.

$$T_{g\,mix} = \frac{[(w_1)(T_{g1}) + (K)(w_2)(T_{g2})]}{[w_1 + (K)(w_2)]} \qquad \text{Equation 7.3}$$

where $K = (\rho_1)(\Delta_{\alpha 2})/(\rho_2)(\Delta_{\alpha 1})$

Equation 7.3 is the Gordon-Taylor equation (Gordon and Taylor, 1952). Kelley and Bueche (1961) derived an identical equation to the Gordon-Taylor equation based on viscosity and free volume effects. Hancock and Zografi (1994) describe that since $\Delta_\alpha \times T_g$ is approximately constant, K can be calculated from the densities of the two components using Equation 7.4.

$$K = (\rho_1)(T_{g1})/(\rho_2)(T_{g2}) \qquad \text{Equation 7.4}$$

The $T_{g\ mix}$ was determined for BFMT/PEG 4000, lactose/PEG 4000 and salbutamol sulphate/PEG 4000 systems containing 10%, 20% and 30% PEG 4000. True densities were taken as 1.5 g/cm^3 for lactose (Handbook of Pharmaceutical Excipients, 1994), 1.18 g/cm^3 for PEG 4000 (Handbook of Pharmaceutical Excipients, 1994), 1.27 g/cm^3 for salbutamol sulphate (based on experimental true density measurements performed as described in Chapter 2) and 1.54 g/cm^3 for BFMT (based also on experimental true density measurements). Experimentally derived glass transition temperatures were used when available. An experimental T_g was not available for PEG 4000 and therefore the estimated T_g of -41°C was used (based on equation 7.1).

Table 7.5 shows the $T_{g\ mix}$ data calculated for BFMT/PEG 4000, lactose/PEG 4000 and salbutamol sulphate/PEG 4000 mixed systems. The $T_{g\ mix}$ values for the BFMT/PEG 4000 systems were in good agreement with the values obtained experimentally using modulated DSC in Chapter 4. Experimentally obtained values were 83°C, 69°C and 45°C for the 10%, 20% and 30% PEG/BFMT systems.

Table 7.5 Table showing the estimated glass transition of a mix of two components systems ($T_{g\ mix}$) determined from Equation 7.3 using the *K* value obtained from Equation 7.4.

PEG content in mix	BFMT/PEG 4000 $T_{g\ mix}$	lactose/PEG 4000 $T_{g\ mix}$	salbutamol sulphate/ PEG 4000 $T_{g\ mix}$
10% PEG	361.3K (88.3°C)	349.9K (76.8°C)	321.5K (48.5°C)
20% PEG	335.7K (62.7°C)	327.6K (54.6°C)	307.5K (34.5°C)
30% PEG	314.7K (41.8°C)	308.8K (35.8°C)	294.9K (21.9°C)

The trend would suggest that BFMT/PEG systems would be more stable at room temperature than lactose/PEG systems which would be more stable than salbutamol sulphate/PEG systems with respect to recrystallisation. This trend was reasonably consistent with the crystallinity of PEG found in these systems as shown in Table 7.4. The closer the T_g is to the actual storage temperature the more unstable the system will be. The Kauzmann temperature is generally accepted as the temperature below which translational and rotational motions cease on pharmaceutically relevant time scales (Hancock et al., 1995). Metastable amorphous materials are expected to be physically stable when stored at a temperature less than or equal to their Kauzmann temperature. The Kauzmann temperature of a material is generally ~50K below the T_g of the material (Hancock et al., 1995; Zhou et al., 2002). Table 7.6 shows the estimated Kauzmann temperatures of the mixed PEG 4000 systems (based on T_g – 50K (Hancock et al., 1995; Zhou et al., 2002)). The materials should be stored at or below their Kauzmann temperatures in order to maintain their metastable state.

Table 7.6 Table showing estimated Kauzmann temperatures for BFMT/PEG 4000, lactose/PEG 4000 and salbutamol sulphate/PEG 4000 mixes. Kauzmann temperatures were calculated as T_g - 50K.

PEG content in mix	BFMT/PEG 4000 Kauzmann temperatures	lactose/PEG 4000 Kauzmann temperatures	salbutamol sulphate/ PEG 4000 Kauzmann temperatures
10% PEG	311.3K (38.0°C)	299.9K (26.9°C)	271.5K (-1.5°C)
20% PEG	285.7K (12.7°C)	277.6K (4.6°C)	257.5K (-15.5°C)
30% PEG	264.7K (-8.3°C)	258.8K (-14.2°C)	244.9K (-28.1°C)

The Kauzmann temperatures in Table 7.6 indicate that at room temperature the salbutamol sulphate/PEG 4000 systems and the lactose/PEG 4000 20% and 30% systems will not be

stable. The lactose/PEG 4000 10% should be stable. Analysis of this system showed it to be the most X-ray amorphous of all the lactose/PEG 4000 systems. The BFMT/PEG 4000 10% should also be stable at room temperature since it has a Kauzmann temperature of 38°C. The 20% and 30% PEG/BFMT systems have Kauzmann temperatures below room temperature and therefore are likely to be unstable. These systems had not however recrystallised by the time they were initially analysed.

The $T_{g\ mix}$ values and the Kauzmann temperatures were calculated for salbutamol sulphate/lactose mixed systems and are shown in Table 7.7. The T_g values used in the calculations were the experimentally derived T_gs shown in Table 7.2. The $T_{g\ mix}$ and Kauzmann temperature values increase as the lactose content increases. The salbutamol sulphate/lactose spray dried systems were all amorphous when analysed by XRD which is consistent with the high $T_{g\ mix}$ and Kauzmann temperature values calculated for these systems.

Table 7.7 Table showing $T_{g\ mix}$ and Kauzmann temperatures for salbutamol sulphate/lactose systems.

System	$T_{g\ mix}$	Kauzmann temperatures
salbutamol sulphate/lactose 5%	338.5K (65.5°C)	288.5K (15.5°C)
salbutamol sulphate/lactose 20%	343.4K (70.4°C)	293.4K (20.4°C)
salbutamol sulphate/lactose 40%	350.4K (77.4°C)	300.4K (27.4°C)

Salbutamol and ipratropium bromide mixed systems were spray dried for this thesis since combination products containing these two components are available on the market (Combivent^{TM}, a pressurised metered dose inhalation formulation). Co-spray drying ipratropium bromide (which does not readily form an amorphous phase alone) with salbutamol sulphate resulted in X-ray amorphous composites regardless of whether aqueous or ethanolic solvent was used. Co-spray drying ipratropium bromide with salbutamol base resulted in systems with increasing amorphous content as the amount of ipratropium bromide in the mix was increased, with a 2:1 salbutamol base:ipratropium bromide system being completely amorphous.

$T_{g\ mix}$ and Kauzmann temperatures were calculated for salbutamol sulphate:ipratropium bromide and salbutamol base:ipratropium bromide systems. The results are shown in Table 7.8. The true densities of salbutamol base and ipratropium bromide monohydrate used in the calculation of the $T_{g\ mix}$ and Kauzmann temperatures were 1.27 g/cm^3 and 1.35 g/cm^3 respectively (derived experimentally using pycnometry as described in Chapter 2). From Table 7.8 it is apparent that the salbutamol sulphate:ipratropium bromide systems

have relatively high $T_{g\ mixes}$ and that ipratropium bromide acts as an antiplasticising agent, i.e. it increases the T_g. Kauzmann temperatures for the salbutamol sulphate:ipratropium bromide systems were close to room temperature. This indicates that these systems are likely to be relatively stable at room temperature. Analysis of spray dried composites of these systems showed them to be amorphous, consistent with the predicted stability. The salbutamol base:ipratropium bromide systems had lower $T_{g\ mix}$ values and lower Kauzmann temperatures. As the weight ratio of ipratropium bromide in the systems was increased the $T_{g\ mix}$ values increased. The 2:1 system had the highest $T_{g\ mix}$ value and it was the only salbutamol base:ipratropium bromide co-spray dried system to appear totally amorphous by XRD. The low $T_{g\ mix}$ values and the low Kauzmann temperatures of the salbutamol base:ipratropium bromide systems indicate that these systems will be unstable at room temperature. This is consistent with the observed crystallinity of the 10:1 and 5:1 co-spray dried systems. The very low Kauzmann temperatures of these systems indicates that they are likely to recrystallise even if stored under refrigeration.

Table 7.8 Table showing calculated $T_{g\ mix}$ and Kauzmann temperatures for salbutamol sulphate:ipratropium bromide systems based on experimentally derived T_g of salbutamol sulphate (Ward and Schultz, 1995) and estimated T_g of ipratropium bromide based on Equation 7.1 (Hancock and Zografi, 1994; Brittain, 1999).

System	$T_{g\ mix}$	Kauzmann temperatures
salbutamol sulphate:ipratropium bromide 10:1	338.6K (65.6°C)	288.6K (15.6°C)
salbutamol sulphate:ipratropium bromide 5:1	340.0K (67.0°C)	290.0K (17.0°C)
salbutamol sulphate:ipratropium bromide 2:1	343.1K (70.1°C)	293.1K (20.1°C)
salbutamol base:ipratropium bromide 10:1	304.6K (31.6°C)	254.6K (-18.4°C)
salbutamol base:ipratropium bromide 5:1	307.8K (34.8°C)	257.8K (-15.2°C)
salbutamol base:ipratropium bromide 2:1	315.3K (42.3°C)	265.3K (-7.7°C)

Co-spray drying another drug:drug combination, formoterol fumarate:budesonide systems resulted in X-ray amorphous systems. $T_{g\ mix}$ and Kauzmann temperature values were calculated for formoterol fumarate and budesonide systems. The experimentally determined T_g of budesonide and the estimated T_g of formoterol fumarate were used in the calculation of the $T_{g\ mix}$ values (T_gs are shown in Table 7.2 and Table 7.1). The true density values used in the calculation of $T_{g\ mix}$ values were 1.20 g/cm^3 and 1.27 g/cm^3 for formoterol fumarate and budesonide respectively (Tajber, 2002). The $T_{g\ mix}$ and Kauzmann temperatures for these systems are shown in Table 7.9.

Table 7.9 Table showing calculated $T_{g\ mix}$ and Kauzmann temperatures for formoterol fumarate:budesonide systems. The T_g of budesonide was the experimentally derived value shown in Table 7.2 and the formoterol fumarate T_g value was estimated using Equation 7.1 based on the melting of the A racemate since it appeared to be the predominant form present.

System	$T_{g\ mix}$	Kauzmann temperatures
Formoterol fumarate:budesonide 6:100	357.5K (84.5°C)	307.5K (34.5°C)
Formoterol fumarate:budesonide 6:400	361.6K (88.6°C)	311.6K (38.6°C)

The $T_{g\ mix}$ and Kauzmann temperatures of formoterol fumarate:budesonide systems indicate that formoterol fumarate:budesonide systems should be stable at room temperature, consistent with the experimental findings. The higher formoterol fumarate content results in a slightly lower $T_{g\ mix}$, i.e. it act as a plasticising agent.

All two component systems, consisting of components which produce amorphous materials when spray dried alone, consisted of completely amorphous composites i.e. co-spray dried salbutamol sulphate/lactose systems, chitosan/salbutamol sulphate systems and formoterol fumarate:budesonide systems were all X-ray amorphous, the components when spray dried alone also being X-ray amorphous. Co-spray drying systems where one or both components are crystalline when spray dried alone resulted in an increased amount of amorphous material i.e. lactose/PEG, BFMT/PEG, salbutamol sulphate/PEG, salbutamol sulphate/ipratropium bromide and salbutamol base/ipratropium when co-spray dried all showed a reduction in crystallinity of a material which when spray dried alone remained crystalline. The stability of an amorphous system consisting of two components depends on whether the T_g of one component is high enough to result in a $T_{g\ mix}$ that is sufficiently high that the Kauzmann temperature of the mix is higher than the storage temperature.

The Gordon-Taylor equation may be useful in predicting the likelihood that a two component composite will become amorphous on processing. Furthermore the Gordon-Taylor equation appears to be useful in predicting the likely physical stability of amorphous drug polymer composites and indicates that even polymers with apparently low T_gs may be stabilised by a suitable drug with a sufficiently high T_g.

Zhou et al. (2002) produced amorphous forms of several model compounds and determined their Kauzmann temperatures experimentally, which were generally in agreement with the T_g – 50K values of the compounds. Zhou et al. (2002) described that one of their model amorphous systems, ritonavir, showed excellent physical stability above its Kauzmann temperature. This indicated that although the Kauzmann temperature is a

useful parameter, knowledge of the Kauzmann temperature alone is not adequate to understand the physical stability of an amorphous system. Zhou et al. (2002) stated that configurational entropy and molecular mobility values as a function of temperature need to be assessed in addition to T_g and Kauzmann temperatures. They concluded from their work that compounds with high T_gs, high configurational entropy barriers, high Kauzmann temperatures and low molecular mobilities are expected to show the greatest stability. The measurement of molecular mobility is beyond the scope of this thesis and further studies could address its possible role.

Co-spray drying PEG 4000 with the amorphous polymer chitosan resulted in amorphous systems only when PEG was included as 10% by weight of solids. Concentrations of PEG higher than 10% resulted in peaks being visible by XRD indicative of the presence of some crystalline PEG. Chitosan remained amorphous in the co-spray dried composites. The glass transition temperature of chitosan could not be determined experimentally and was not available in the literature. An estimate of the T_g could not be calculated since the melting temperature of chitosan was not known (melting temperatures of rigid-rod-type polymers are not generally determinable (Lee et al., 2000; Kim et al., 1994)).

Co-spray dried BFMT/PEO 300,000 10% at feed concentrations of 2.5% w/v resulted in a system which consisted of particles which were not uniform in appearance. Bodmeier and Chen (1988) described the formation of fibres when spray drying polylactic acid/drug solutions and attributed the fibre formation to insufficient forces being available to break the liquid filament into polymeric droplets. They performed studies that indicated the successful dispersion of the filament into droplets depended strongly on the type of polymer used and to a lesser extent on the viscosity of the spray dried solution. Clarke et al. (1998) described fibre formation when spray drying polylactic co-glycolic systems and described that spray drying at lower feed concentrations was necessary to achieve microparticles. Co-spray dried BFMT/PEO 300,000 10% at feed concentrations of 0.8% w/v (total solids) resulted in microspherical particles.

EDXA was performed on the morphologically non-homogeneous 2.5% w/v feed concentration produced BFMT/PEO system and was consistent with BFMT being uniformly present. It was evident that the two components were not physically separate. The composite nature of the spray dried product makes spray drying a possible method of producing intimate mixtures of components. This represents an advantage of spray drying two component or multi-component systems, particularly when there is a significant difference in the proportion of the two components, in that a more uniform mix will be

obtained than in a conventional mechanical mixing process. A particular pharmaceutical application is the production of inhalation products containing more than one active.

7.4 Spray dried systems for inhalation

Spray drying is known for its ability to produce fine microspherical powders with good flow properties and therefore should prove a useful method of production for inhalation products, especially for the production of powders for dry powder inhalers. Co-spray drying drug/drug systems or drug/excipient systems should result in composite particles, thereby overcoming mixing problems. In chapter 5 and 6 various drugs and excipients were spray dried, and for systems with acceptable morphology and particle size, as evidenced by SEM, twin stage impinger (TSI) experiments were performed. Spray dried salbutamol base, ipratropium bromide and salbutamol base:ipratropium bromide composites were of unsuitable morphology for TSI analysis (i.e. individual spheres or non-aggregated particles were not present). These systems were interestingly predominantly crystalline on spray drying.

Figure 7.3 shows a bar chart of the respirable fractions obtained for the various spray dried systems analysed by TSI. The red bars represent materials which were not X-ray amorphous and the blue bars represent materials which were X-ray amorphous.

The chitosan containing systems showed the highest respirable fractions (TSI) of all the co-spray dried systems and these materials were amorphous. Figure 7.4 shows a plot of the respirable fractions obtained, expressed as a percentage, versus feed concentrations of the various spray dried systems. The white circle symbols represent the respirable fractions (TSI) obtained when chitosan containing-systems were analysed, their feed concentration being 0.2% w/v. For a particular group of two component systems the same feed concentration was used for all weight ratios, for example, all salbutamol sulphate/PEG 4000 systems were spray dried at a feed concentration of 2.5% w/v. However different feed concentrations were used across groups depending on the solubility of the different components. One system, the salbutamol sulphate/lactose 20% system was spray dried at two different feed concentrations, as 10% w/v and as 2.5% w/v solutions (represented by the circles in Figure 7.4). The difference in respirable fractions was large (13.5% for the 10% w/v feed solution compared to 25.7% for the 2.5% w/v feed solution) and was consistent with the change in particle size as observed by SEM.

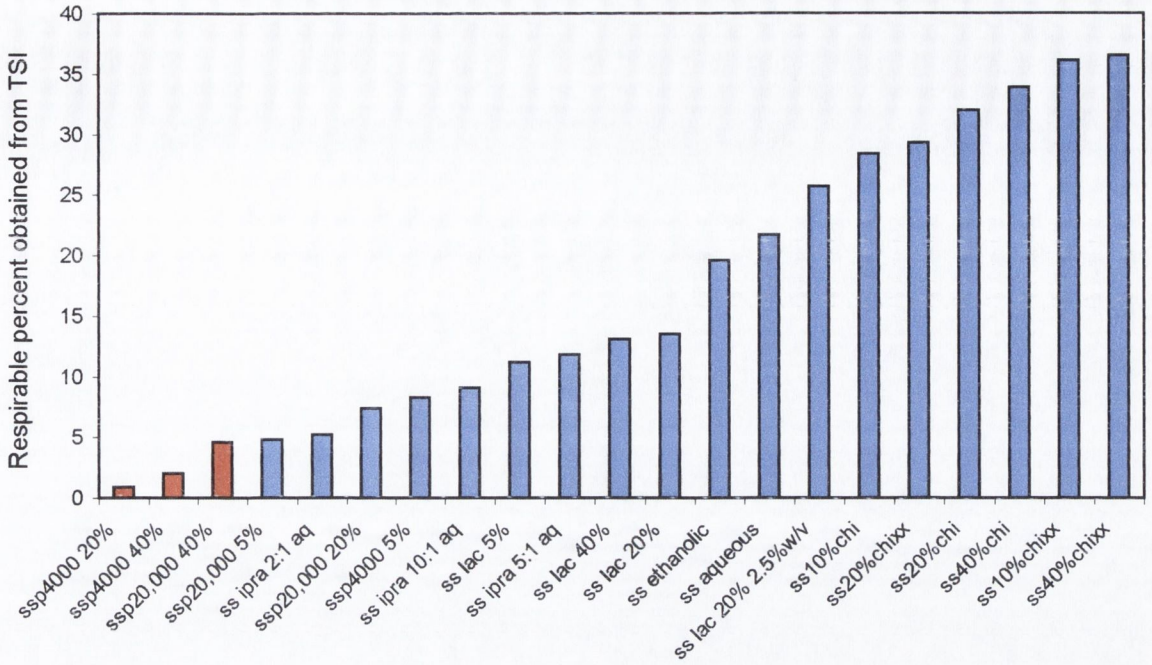

Figure 7.3 Bar chart showing respirable fraction expressed as a percent, obtained for the various spray dried systems analysed by TSI. ssp4000 = salbutamol sulphate/PEG 4000, ssp20,000 = salbutamol sulphate/PEG 20,000, ss ipra = salbutamol sulphate:ipratropium bromide, aq = spray dried from aqueous solution, ss ethanolic = salbutamol sulphate spray dried from ethanolic solution, ss aqueous = salbutamol sulphate spray dried from aqueous solution, ss lac = salbutamol sulphate/lactose systems, ss lac 20% 2.5% w/v = the salbutamol sulphate/lactose 20% system which was spray dried at the lower feed concentration of 2.5% w/v, sschi = salbutamol sulphate/chitosan systems and sschixx = salbutamol sulphate/crosslinked chitosan systems. The red bars represent materials which were not X-ray amorphous and the blue bars represent materials which were X-ray amorphous.

Feed concentration is only likely to impact on respirable fraction if it results in an aerodynamic particle size outside the range which would be deposited in the lower impinger. Spray dried salbutamol sulphate systems are represented by the square symbols in Figure 7.4. One system was spray dried as a 10% w/v aqueous solution and the other as a 0.6% w/v ethanolic solution. Both systems gave statistically similar respirable fractions ($P = 0.6$ in a two sample t-test). When the salbutamol sulphate particles spray dried from the two different solvents were compared the particle size of the system spray dried at the lower feed concentration of 0.6% w/v from ethanolic solution resulted in particles 1 to 3 μm in diameter while the aqueous spray dried system resulted in particles 1 to 7 μm in diameter (by SEM). Particles of an aerodynamic particle size < 6.3 μm deposit in the lower stage of the impinger. Both systems must have had an aerodynamic particle size below the cut off diameter of 6.3 μm in order to result in similar deposition by TSI.

Chitosan/salbutamol sulphate co-spray dried systems showed particles sizes of 1-4 μm. While SEM showed spray dried salbutamol sulphate and co-spray dried chitosan/salbutamol sulphate systems to have particles which should all be in the respirable range, SEM does not determine the aerodynamic diameter which is affected by density, flow properties, surface energies etc. TSI results showed most ratios of co-spray dried chitosan/salbutamol sulphate systems to have significantly superior deposition to spray dried salbutamol sulphate alone.

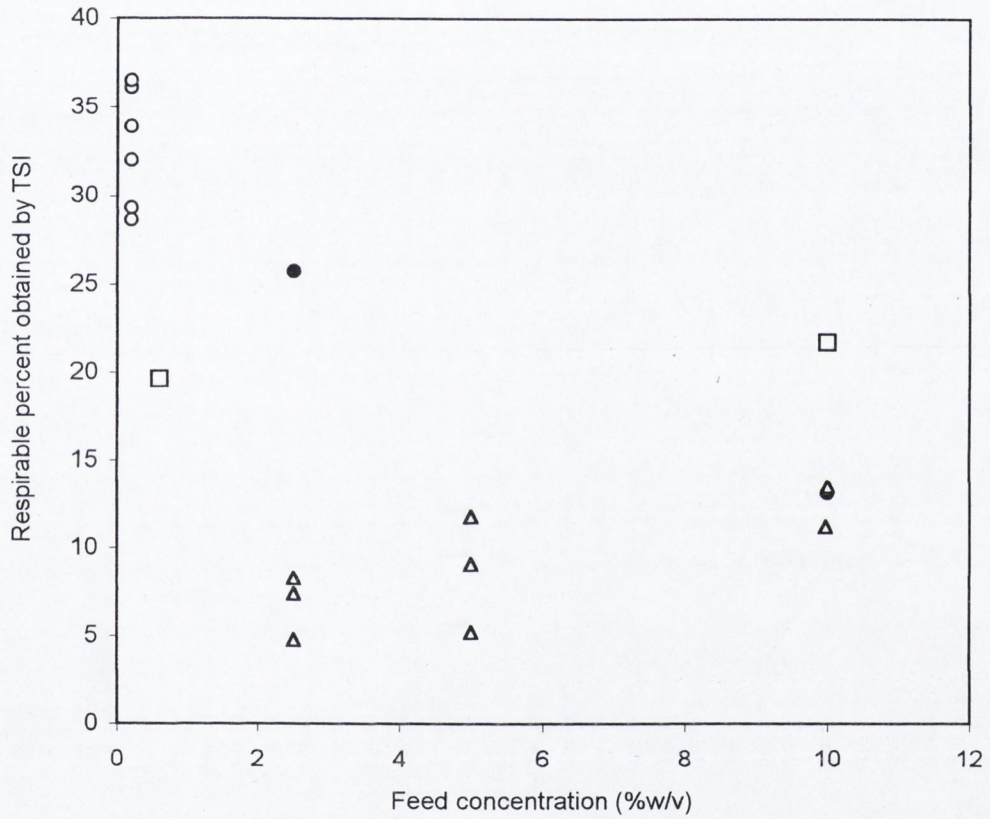

Figure 7.4 Chart showing respirable fraction, expressed as a percentage, versus feed concentration employed during the spray drying of various systems. ○ = chitosan containing systems, ● = salbutamol sulphate/lactose 20% systems spray dried at the two different feed concentrations, □ = spray dried salbutamol sulphates (salbutamol sulphate spray dried from ethanol was spray dried at the lower feed concentration and salbutamol sulphate spray dried from aqueous solution was spray dried at the higher feed concentration); Δ = other spray dried systems.

Salbutamol sulphate/lactose 20% systems spray dried at feed concentrations of 2.5% w/v and 10% w/v resulted in particle sizes of 2 to 10 and 1 to 20 μm respectively. A significant amount of the 10% w/v spray dried systems particles were apparently larger

than the TSI upper/lower stage cut off of 6.3 μm and therefore this system resulted in a lower respirable fraction than the 2.5% w/v system.

It has been shown that the surface morphology of a carrier can affect the respirable fractions of a drug (Kawashima et al., 1988; Zeng et al., 2000), due to different strengths of adhesion between the drug and the carrier. Zeng et al. (2000) found that increasing either the surface smoothness or the elongation ratio of lactose crystals increased the potentially respirable fraction of salbutamol sulphate from dry powder inhalers.

The adhesion of particles is a surface phenomenon and therefore the morphology of the surface will have a significant effect on the adhesion of particles (Ganderton and Jones, 1992). Amorphous materials behave in a different manner to crystalline materials and this influences interactions including the powders cohesiveness and adhesion between the powder and other phases (Briggner et al., 1994). The spray dried systems prepared for this thesis differed in their surface morphology. Figure 7.5 shows SEM micrographs of various spray dried systems displaying the different particle morphologies that were obtained.

No trends in particle morphology with respect to deposition were observed for the spray dried systems analysed. Particle morphologies of the salbutamol sulphate/chitosan systems differed from each other depending on the weight ratio of salbutamol sulphate included in the composite. The 40% salbutamol sulphate/chitosan systems, whether crosslinked or non-crosslinked, consisted of collapsed particles while other weight ratios consisted of spherical convoluted particles (Figure 7.5 scan h and g respectively). TSI results, however, of the different weight ratios, which showed very different particle morphologies, gave respirable fractions which were not statistically different. Of the three weight ratios of salbutamol sulphate:ipratropium bromide studied, two of the systems, the 10:1 and 5:1 systems, showed spherical shaped particles with indentations. The 2:1 system showed predominantly smooth spherical particles. All three weight ratios showed particles of similar diameters. TSI results of the three different systems were not statistically different from one another despite the differences in particle morphology/surface topography.

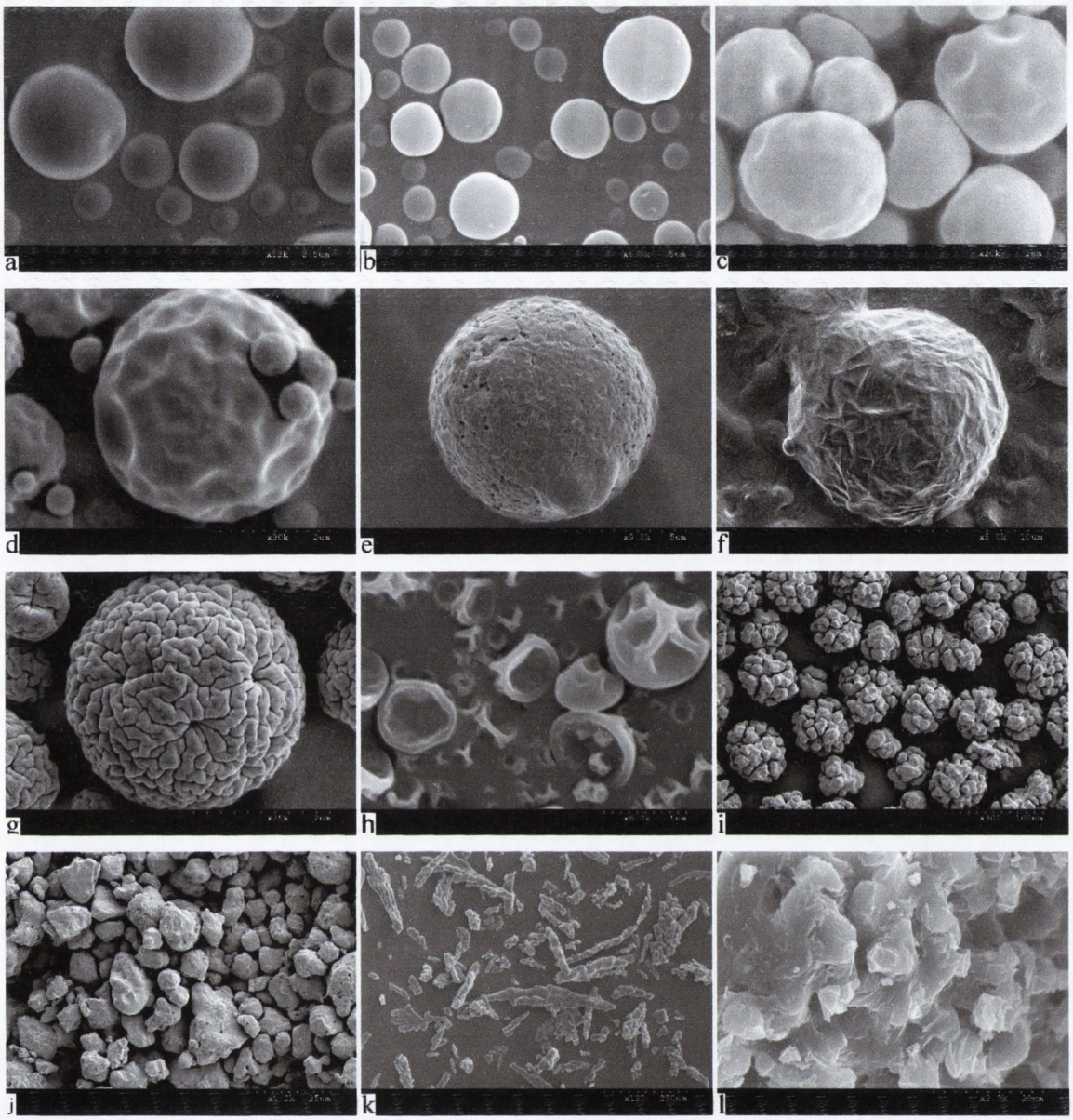

Figure 7.5 SEM micrographs of various different spray dried systems. (a) salbutamol sulphate:ipratropium bromide 2:1 from aqueous solution; (b) formoterol fumarate:budesonide 6:100; (c) salbutamol sulphate:ipratropium bromide 10:1 from aqueous solution; (d) salbutamol sulphate spray dried from aqueous solution; (e) salbutamol sulphate/PEG 4000 20%; (f) salbutamol sulphate/PEG 20,000 20%; (g) salbutamol sulphate 10%/chitosan; (h) salbutamol sulphate 40%/chitosan; (i) PEG 4000 (outlet temperature 45-46°C) ; (j) ipratropium bromide spray dried from aqueous solution; (k) PEG 4000 (outlet temperature 41-44 °C) and (l) salbutamol base:ipratropium bromide 10:1.

Vidgrén et al. (1989) produced spray dried sodium cromoglycate particles for inhalation. The spray dried systems had a mean diameter of 2.81 μm (+/- 0.04 μm) compared to mechanically micronised material which had a mean diameter of 3.81 μm (+/- 0.08). The proportion of spray dried particles in the 0.3-3.3 μm size range was approximately twice the proportion of mechanically micronised particle in this range. While particles in the

0.3-3.3 μm size range are not necessary for the action of drugs designed to act locally, for example drugs which relax the bronchial smooth muscle, the proportion of particles in this size range would be important for a therapeutic agent which was intended for systemic action. Vidgrén et al. studied the effect of humidity on the *in vitro* deposition of the amorphous spray dried material compared to the micronised crystalline material. The spray dried amorphous form was more affected by the air moisture than the crystalline micronised form. At humidities greater than 60% RH the amorphous material formed aggregates which greatly decreased the *in vitro* deposition. X-ray diffraction of the spray dried material exposed to greater than 60% RH showed peaks indicative of crystallinity. The micronised material was less affected by changes in humidity. Further study is required into the physical stability of the spray dried powders for inhalation produced in the current work. The effects of temperature and relative humidity on the twin stage impinger deposition need to be considered.

Spray dried chitosan/salbutamol sulphate systems gave high *in vitro* respirable fractions. Carrión-Recio et al. (2002) investigated chitosan microspheres prepared by a double emulsion microencapsulation technique as potential pulmonary delivery systems. They incorporated the model proteins insulin and fluorescein isothiocyanate labelled bovine serum albumin as model compounds and found the chitosan microspheres to have suitable morphological and aerodynamic properties for lung delivery. The aerodynamic particle sizes of the chitosan systems ranged between 3.5 and 18 μm depending on the aqueous phase composition and stirring rate employed in their preparation. Williams et al. (1998) investigated spray dried chitosan for use in pressurised metered dose inhalers and found spray dried chitosans to be compatible with the non-CFC propellant P134a. From the preliminary work with chitosan/salbutamol sulphate co-spray dried systems in this thesis it appears that spray drying is a successful method for the production of chitosan powders for DPIs and may also prove useful in the production of powders for inclusion in pMDIs.

Chitosan has been used as an excipient for sustained release delivery systems (Nigalaye et al., 1990; Takeuchi et al., 2000; Dangprasirt and Pongwai, 1998; Giunchedi et al., 1998; Ganza-Gonzalez et al., 1999). Chitosan co-spray dried with the model drug salbutamol sulphate was shown in this thesis to result in microparticles with good deposition in the lower impinger of the twin stage impinger. Co-spray dried salbutamol sulphate/chitosan systems, prepared with and without crosslinking, showed some delayed release of salbutamol sulphate, however the delayed release did not appear to be such as to be likely to show clinical significance. Salbutamol sulphate is a freely soluble drug, perhaps investigations using a less soluble drug would show more significant results. The inclusion

of protein/peptide therapeutics in chitosan composites for potential lung delivery for systemic action, thus avoiding the necessity of parenteral administration, needs to be investigated.

For sustained lung delivery the therapeutic agent, once delivered to the alveoli, must avoid phagocytosis by the alveolar macrophages (Edwards et al., 1997; Evora et al., 1998). In order to reduce or avoid phagocytosis in the lungs the creation of spray dried microspherical chitosan/PEG systems as "stealth" chitosan carriers was attempted. Neither chitosan alone nor chitosan/PEG composite particles appeared to be readily phagocytosed by the phagocytic cell line J774A.1, and therefore the inclusion of PEG did not appear necessary. Banerjee et al. (2002) recently showed that chitosan nanoparticles avoided phagocytosis by reticuloendothelial cells *in vivo*. These results are consistent with the "stealth" effect of spray dried chitosan particles found in this thesis.

Chitosan has been studied for use in the intranasal administration of proteins and peptides. Vila et al. (2002) produced biodegradable nanoparticles as potential protein carriers for nasal administration. One of the systems consisted of chitosan nanoparticles containing either insulin or tetanus toxoid while a second system consisted of chitosan-coated polylactic acid-glycolic acid (PLGA) nanoparticles with encapsulated tetanus toxoid. Vila et al. (2002) chose chitosan for use in their nanoparticles due to its mucoadhesive and permeability enhancing properties. The nanoparticles made of pure chitosan were found to be stable upon incubation with lysozyme and were capable of improving the nasal absorption of insulin as well as resulting in local and systemic immune responses to tetanus toxoid, following intranasal administration. The coating of PLGA nanoparticles with chitosan also improved the stability of the PLGA particles in the presence of lysozyme and enhanced the nasal transport of the encapsulated tetanus toxoid. A third system produced by Vila et al. (2002) consisted of polyethylene glycol (PEG)-coated polylactic acid nanoparticles. They found that PEG coating improved the stability of PLA nanoparticles in the gastrointestinal fluids and helped the transport of encapsulated tetanus toxoid across the intestinal and nasal mucosae. Intranasal administration of these nanoparticles provided high and long-lasting immune responses.

Since chitosan appears an ideal carrier for therapeutics to the deep lung for systemic action it is likely that more research will focus on chitosan for inhalation in the future. Not only is it biodegradable and mucoadhesive but it appears stable to lysozyme and invisible to macrophages. The cationic nature of chitosan should also prove useful for incorporation of anionic compounds.

7.5 Main findings

- Spray drying can produce systems containing amorphous PEG.
- Spray drying can produce high energy drug/PEG systems.
- Spray drying ipratropium bromide results in different solid state forms depending on the solvent used.
- Spray drying budesonide results in an amorphous form.
- Co-spray dried lactose/PEG systems differed in crystallinity with respect to both PEG and lactose depending on the concentration of PEG in the mix. PEG of reduced crystallinity is formed in each system with the 10% PEG system being amorphous with respect to PEG. PEG recrystallises to the once folded conformation followed by conversion to the more stable extended chain form on storage. Lactose converts to anhydrous crystalline lactose followed by conversion to the monohydrate form only. PEG in concentrations of 5% appears to slow the recrystallisation of lactose to lactose monohydrate while in concentrations of 10% and 20% the rates of recrystallisation to the monohydrate form were increased with respect to lactose alone.
- Co-spray drying two component systems results in decreased crystallinity of the resultant mixes compared to physical mixes.
- The Gordon-Taylor equation may be useful in predicting the likelihood that a two component composite will become amorphous on processing.
- The Gordon-Taylor equation may be useful in predicting the stability of amorphous two component systems.
- Most spray dried amorphous systems were observed to be microspherical, the exceptions being spray dried salbutamol base:ipratropium bromide 2:1, which consisted of fused aggregates, and chitosan/salbutamol sulphate 40% systems, which consisted of collapsed spheres.
- Spray drying is a useful method of obtaining composite microspherical particles in the inhalable range.
- Chitosan may be a useful excipient for delivery of therapeutics to the deep lung for systemic activity.

7.6 Future Work

- Further investigations into the application of the Gordon-Taylor equation to predict the formation of stable amorphous composites should be explored together with the impact of molecular mobility on the stability of such composites.
- Further study is required into the physical stability of spray dried powders for inhalation. The effects of temperature and relative humidity on the twin stage impinger deposition need to be considered.
- The effect of mixing of spray dried systems with coarse carrier particles could be investigated to determine whether increased respirable fractions would be obtained.
- Use of different types and concentrations of crosslinking agents on the ability of chitosan to prolong release could be evaluated.

REFERENCES

REFERENCES

Ahlneck, C. and Zografi, G., The molecular basis of moisture effects on the physical and chemical stability of drugs, Int. J. Pharm., 62 (1990) 87-95.

Aiedeh, K., Gianasi, E., Orienti, I. and Zecchi, V., Chitosan microcapsules as controlled release systems for insulin, J. Microencapsulation, 14 (1997) 567-576.

Aldén, M., Tegenfeldt, J. and Sjokvist, E., Structure of solid dispersions in the system polyethylene glycol-griseofulvin with additions of sodium dodecyl sulphate, Int. J. Pharm., 83 (1992) 47-52.

Angberg, M., Lactose and thermal analysis with special emphasis on microcalorimetry, Thermochimica Acta, 248 (1995) 161-176.

Artursson, P., Lindmark, T., Davis, S. S. and Illum, L., Effect of chitosan on the permeability of monolayers of intestinal epithelial cells (Caco-2), Pharm. Res., 11, 9 (1994) 1358-1361.

Avrami, M., Kinetics of phase change. II. Transformation-time relations for random distribution of nuclei., J. Chem. Phys., 8 (1940) 212-214.

Bailey, F. E. and Koleske, J. V., Polyethylene Oxide, Academic Press, New York, 1976.

Banerjee, T., Mitra, S., Singh, A. K., Sharma, R. K. and Maitra, A., Preparation, characterisation and biodistribution of ultrafine chitosan nanoparticles, Int. J. Pharm., 243 (2002) 93-105.

Bernkop-Schnürch, A., Chitosan and its derivatives:potential excipients for peroral peptide delivery systems, Int. J. Pharm., 194 (2000) 1-13.

Black, D. B. and Lovering, E. G., Estimation of the degree of crystallinity in digoxin by X-ray and IR methods, J. Pharm. Pharmac., 29 (1977) 684-687.

Bodmeier, R. and Chen, H., Preparation of biodegradable polylactide microparticles using a spray drying technique, J. Pharm. Pharmacol., 40 (1988) 754-757.

Briggner, L-E., Buckton, G., Bystrom, K. and Darcy, P., The use of isothermal microcalorimetry in the study of changes in crystallinity induced during the processing of powders, Int. J. Pharm., 105 (1994) 125-135.

Brittain, H. G., Polymorphism in pharmaceutical solids, Marcel Dekker, New York, (1999).

British Pharmacopoeia, The Stationery Office, Great Brittain (2002).

Broadhead, J., Rouan, E. S. K. and Rhodes, C. T., The spray drying of pharmaceuticals, Drug Dev. Ind. Pharm., 18 (1992) 1169-1206.

Broadhead, J., Rouan, S. K. E. and Rhodes, C. T., The deposition of spray-dried β-galactosidase from dry powder inhaler devices, Drug Dev. Ind. Pharm., 22, 8 (1996) 813-822.

Buckley, C. P. and Kovacs, A. J., Melting behaviour of low molecular weight poly(ethylene-oxide) fractions. I. Extended chain crystals, Progr. Colloid & Polymer Sci, 58 (1975) 44-52.

Buckton, G. and Darcy, P., The influence of additives on the recrystallisation of amorphous spray-dried lactose, Int. J. Pharm., 121 (1995) 81-87.

Buckton, G. and Darcy, P., The use of gravimetric studies to assess the degree of crystallinity of predominantly crystalline powders, Int. J. Pharm., 123 (1995b) 256-271.

Buckton, G. and Darcy, P., Water mobility in amorphous lactose below and close to the glass transition temperature, Int. J. Pharm., 136 (1996) 141-146.

Buma, T. J. and Wiegers, G. A., X-Ray Powder Patterns of Lactose and Unit Cell Dimensions of β-Lactose, Neth. Milk & Dairy J., 21 (1967) 208-213.

Byron, P. R., Determinants of drug and polypeptide bioavailability from aerosols delivered to the lung, Adv. Drug Deliv. Rev. 5 (1990) 107-132.

Cal, S., Rogríguez-Puente, B., Souto, C., Concheiro, A., Gomez-Amoza, J. L. and Martínez-Pacheco, R., Comparison of a spray-dried α-lactose monohydrate with a fully hydrated roller-dried β-lactose, Int. J. Pharm., 136 (1996) 13-21.

Calvo, P., Remuñán-López, C., Vila-Jato, J. L. and Alonso, M. J., Chitosan and chitosan/ethylene oxide-propylene oxide block copolymer nanoparticles as novel carriers for proteins and vaccines, Pharm. Res., 14, 10 (1997) 1431-1436.

Carrión-Recio, D., Alonso, M. J., Vila-Jato, J. L. and Remuñán-López, C., Development of chitosan microspheres for pulmonary drug delivery, Proc. 4th World Meeting of Pharmaceutics, Biopharmaceutics and Pharmaceutical Technology, ADRITELF/APGI/APV, Florence, April (2002).

Chatham, S.M., Characterisation of molten filled hard gelatin capsules, Ph.D Thesis, University of London (1985).

Chawla, A., Taylor, K. M. G., Newton, J. M. and Johnson, M. C. R., Production of spray dried salbutamol sulphate for use in dry powder aerosol formulation, Int. J. Pharm., 108 (1994) 233-240.

Chenite, A., Buschmann, M., Wang, D., Chaput, C. and Kandani, N., Rheological characterisation of thermogelling chitosan/glycerol-phosphate solutions, Carbohydrate Polymers, 46 (2001) 39-47.

Chidavaenzi O. C., Buckton, G., Koosha F. and Pathak, R., The use of thermal techniques to assess the impact of feed concentration on the amorphous content and polymorphic forms present in spray dried lactose, Int. J. Pharm., 159 (1997) 67-74.

Chidavaenzi O. C., Buckton, G. and Koosha F., The effect of co-spray drying with polyethylene glycol 4000 on the crystallinity and physical form of lactose, Int. J. Pharm., 216 (2001) 43-49.

Chiou, W. L. and Niazi, S., Phase diagram and dissolution-rate studies on sulfathiazole-urea solid dispersions, J. Pharm. Sci., 60 (1971) 1333-1337.

Chiou, W. L. and Riegelman, S., Pharmaceutical applications of solid dispersion systems, J. Pharm. Sci., 60 (1971) 1281-1301.

Chutimaworapan, S., Ritthidej, G. C., Yonemochi, E., Oguchi, T. and Yamamoto, K., Effect of water-soluble carriers on dissolution characteristics of nifedipine solid dispersions, Drug Dev. Ind. Pharm., 26 (2000) 1141-1150.

Clarke, N., O'Connor, K. and Ramtoola, Z., Influence of formulation variables on the morphology of biodegradable microparticles prepared by spray drying, Drug Dev. Ind. Pharm., 24 (1998) 169-174.

Colthorpe, P., Farr, S. F., Taylor, G., Smith, I. J. and Wyatt, D., The pharmacokinetics of pulmonary delivered insulin : a comparison of intratracheal and aerosol administration to the rabbit, Pharm. Res., 9 (1992) 764-768.

Conte, U., Conti, B., Giunchedi, P. and Maggi, L., Spray dried polylactide microsphere preparation:Influence of the technological parameters, Drug Dev. Ind. Pharm., 20 (1994) 235-258.

Corrigan, O. I. and Timoney, R. F., The influence of polyvinylpyrrolidone on the dissolution properties of hydroflumethiazide, J. Pharm. Pharmac., 27 (1975) 759-764.

Corrigan, O. I. and Timoney, R. F., The influence of polyethylene glycols on the dissolution properties of hydroflumethiazide, Pharm. Acta Helvetiae, 51 (1976) 268-271.

Corrigan, O. I., Murphy, C. A. and Timoney, R. F., Dissolution properties of polyethylene glycols and polyethylene glycol-drug systems, Int. J. Pharm., 4 (1979) 67-74.

Corrigan, O. I., Holohan, E. M. and Sabra, K., Physicochemical properties of spray dried drugs:Phenobarbitone and hydroflumethiazide, Drug Dev. Ind. Pharm., 9 (1983) 1-20.

Corrigan, O. I. and Holohan, E. M., Amorphous spray-dried hydroflumethiazide polyvinylpyrrolidone systems:physicochemical properties, J. Pharm. Pharmacol., 36 (1984) 217-221.

Corrigan, O. I., Holohan, E. M. and Sabra, K., Amorphous forms of thiazide diuretics prepared by spray-drying, Int. J. Pharm., 18 (1984) 195-200.

Corrigan, O. I., Holohan, E. M. and Reilly, M. R., Physicochemical properties of indomethacin and related compounds co-spray dried with polyvinylpyrollidone, Drug. Dev. Ind. Pharm., 11 (1985) 677-695.

Corrigan, O. I., Mechanisms of dissolution of fast release solid dispersion, Drug Dev. Ind. Pharm., 11 (1985) 697-724.

Corrigan, O. I., Retardation of polymeric carrier dissolution by dispersed drugs:factors influencing the dissolution of solid dispersions containing polyethylene glycols, Drug Dev. Ind. Pharm., 12 (1986) 1777-1793.

Corrigan, O. I., Thermal analysis of spray dried products, Thermochimica Acta, 248 (1995) 245-248.

Craig, D. Q. M., Characterisation of the solid and solution state properties of drug dispersions in polyethylene glycols, Ph.D Thesis, School of Pharmacy, University of London (1989).

Craig, D. Q. M., Polyethylene glycols and drug release, Drug Dev. Ind. Pharm., 16 (1990) 2501-2526.

Craig, D. Q. M., A review of thermal methods used for the analysis of the crystal form, solution thermodynamics and glass transition behaviour of polyethylene glycols, Thermochimica Acta, 248 (1995) 189-203.

Craig, D. Q. M., The mechanisms of drug release from solid dispersions in water-soluble polymers, Int. J. Pharm., 231 (2002) 131-144.

Cullity, B. D., Elements of X-ray diffraction, 2nd Edition, Addison-Wesley, London, (1978).

Curotto, E. and Aros, F., Quantitative determination of chitosan and the percentage of free amino groups, Analytical Biochemistry, 211 (1993) 240-241.

Dangprasirt, P. and Pongwai, S., Development of diclofenac sodium controlled release solid dispersion powders and capsules by freeze drying technique using ethylcellulose and chitosan as carriers, Drug Dev. Ind. Pharm., 24 (10) (1998) 947-953.

Darcy, P. and Buckton, G., The influence of heating/drying on the crystallisation of amorphous lactose after structural collapse, Int. J. Pharm., 158 (1997) 157-164.

Dodane, V. and Vilivalam, V. D., Pharmaceutical applications of chitosan, PSTT, 1, 6 (1998) 246-253.

Doff, H. D., Brownen, F. L. and Corrigan, O. I., Determination of α-impurities in the β-polymorph of inosine using infra-red spectroscopy and x-ray powder diffraction, Analyst, 111 (1986) 179-182.

Doherty, C. and York, P., Accelerated stability of an X-ray amorphous frusemide-polyvinylpyrrolidone solid dispersion, Drug Dev. Ind. Pharm., 15 (1989) 1969-1987.

Drapier-Beche, N., Fanni, J., Parmentier, M. and Vilasi, M., Evaluation of lactose crystalline forms by non-destructive analysis, J. Dairy Sci., 80 (1997) 457-463.

Dubois, J-L. and Ford, J. L., Similarities in the release rates of different drugs from polyethylene glycol 6000 dispersions, J. Pharm. Pharmacol., 37 (1985) 494-495.

Edwards, D. A., Hanes, J., Caponetti, G., Hrkach, J., Ben-Jebria, A., Eskew, M. L., Mintzes, J., Deaver, D., Lotan, N. and Langer, R., Large porous particles for pulmonary drug delivery, Science, 276 (1997) 1868-1870.

Elamin, A. A., Sebhatu, T. and Ahlneck, C., The use of amorphous model substances to study mechanically activated materials in the solid state, Int. J. Pharm., 119 (1995) 25-36.

Enna, S. J. and Schanker, L. S., Absorption of saccharides and urea from the rat lung, Am. J. Physiol., 222 (1972) 409-414.

European Pharmacopoeia, 4th Edition, 2002.

Evora, C., Soriano, I., Rogers, R. A., Shakesheff, K. M., Hanes, J. and Langer, R., Relating the phagocytosis of microparticles by alveolar macrophages to surface chemistry: the effect of 1,2-dipalmitoylphosphatidylcholine, J. Control. Release, 51 (1998) 143-152.

Fell, J. T. and Newton, J. M., The production and properties of spray dried lactose, Pharmaceutica Acta Helvetiae, (1971) 425-430.

Foster, K. A., Yazdanian, M. and Audus, K. L., Microparticulate uptake mechanisms of in-vitro cell culture models of the respiratory epithelium, J. Pharm. Pharmacol., 53 (2001) 57-66.

Frontini, R. and Mielck, J. B., Determination and quantification of BFMT and its degradation products using HPLC, J. Liq. Chromatography, 15, 14 (1992) 2519-2528.

Frontini, R. and Mielck, J. B., Formation of formaldehyde in PEG and in poloxamer under stress conditions, Int. J. Pharm., 114 (1995) 121-123.

Frontini, R. and Mielck. J., Interactions between bendroflumethiazide and water soluble polymers. I. Solubility of bendroflumethiazide in water from solid dispersions and formation of associates under climatic stress, Eur. J. Pharm. and Biopharm., 43 (1997a) 185-191.

Frontini, R. and Mielck. J., Interactions between bendroflumethiazide and water soluble polymers. II. Factors promoting drug-polymer associations, Eur. J. Pharm. and Biopharm., 43 (1997b) 309-314.

Frontini, R. and Mielck. J., Interactions between bendroflumethiazide and water soluble polymers. III. Chemical degradation, Eur. J. Pharm. and Biopharm., 44 (1997c) 85-88.

Fukuoka, E., Makita, M. and Yamamura, S., Glassy state of pharmaceuticals. II. Bioinequivalence of glassy and crystalline indomethacin, Chem. Pharm. Bull., 35, 7 (1987) 2943-2948.

Ganderton, D and Jones, T., Advances in Pharmaceutical Sciences, 6, Chapter 5, (1992).

Ganza-González, A., Anguiano-Igea, S., Otero-Espinar, F. J. and Méndez, J. B., Chitosan and chondroitin microspheres for oral-administration controlled release of metoclopramide, Eur. J. Pharm. and Biopharm., 48 (1999) 149-155.

Genta, I., Pavanetto, F., Conti, B., Giunchedi, P. and Conte, U., Improvement of dexamethasone dissolution rate from spray-dried chitosan microspheres, S.T.P. Pharma Sci., 5 (3) (1995) 202-207.

Giron, D., Thermal analysis and calorimetric methods in the characterisation of polymorphs and solvates, Thermochimica Acta, 248 (1995) 1-59.

Giunchedi, P., Genta, I., Conti, B., Muzzarelli, R. A. A. and Conte, U., Preparation and characterisation of ampicillin loaded methylpyrrolidinone chitosan and chitosan microspheres, Biomaterials, 19 (1998) 157-161.

Giunchedi, P., Juliano, C., Gavini, E., Cossu, M. and Sorrenti, M., Formulation and in vivo evaluation of chlorhexidine buccal tablets prepared using drug-loaded chitosan microspheres, Eur. J. Pharm. and Biopharm., 53 (2002) 233-239.

Gonda, I., Inhalation therapy with recombinant human deoxyribonuclease I, Adv. Drug Deliv. Rev., 19 (1996) 37-46.

Gordon, M. and Taylor, J. S., Ideal co-polymers and the second order transitions of synthetic rubbers. 1. Non-crystalline co-polymers, J. Appl. Chem., 2 (1952) 493-500.

Gref, R., Minamitake, Y., Peracchia, M. T., Trubetskoy, V., Torchillin, V. and Langer, R., Biodegradable long-circulating polymeric nanospheres, Science, 263 (1994) 1600-1603.

Guillory, J. K., Hwang, S. L. and Lach, J. L., Interactions between pharmaceutical compounds by thermal methods, J. Pharm. Sci., 58 (1969) 301.

Gunsel, W. C. and Lachman, L., Comparative evaluation of tablet formulations prepared from conventionally-processed and spray-dried lactose, J. Pharm. Sci., 52 (1963) 178-182.

Haleblian, J. and McCrone, W., Pharmaceutical applications of polymorphism, J. Pharm. Sci., 58 (1969) 911-929.

Haleblian, J., Characterisation of habits and crystalline modification of solids and their pharmaceutical applications, J. Pharm. Sci., 64 (1975) 1269-1288.

Hallworth, G. W. and Westmoreland, D. G., The twin impinger: a simple device for assessing the delivery of drugs from metered dose pressurized aerosol inhalers, J. Pharm. Pharmacol., 39 (1987) 966-972.

Hancock, B. C. and Zografi, G., The relationship between the glass transition temperature and the water content of amorphous pharmaceutical solids, Pharm. Res., 11 (1994) 471-477.

Hancock, B. C., Shamblin, S. L. and Zografi, G.,Molecular mobility of amorphous pharmaceutical solids below their glass transition temperatures, Pharm. Res., 12, 6, (1995) 799-806.

Hancock, B. C. and Zografi, G., Characteristics and significance of the amorphous state in pharmaceutical systems, J. Pharm. Sci., 86 (1997) 1-11.

Hancock, B. C. and Parks, M., What is the true solubility advantage of amorphous pharmaceuticals? Pharm. Res., 17 (2000) 397-404.

The Handbook of pharmaceutical excipients, 2nd edition, Editors Wade, A. and Weller, P. J., (1994).

Harris, J. M. and Zalipsky, S., Poly(ethylene glycol):Chemistry and Biological Applications, American Chemical Society, Washington DC, (1997).

Hassan, E. E., Parish, R. C. and Gallo, J. M., Optimised formulation of magnetic chitosan microspheres containing the anticancer agent, oxantrazole, Pharm. Res., 9 (1992) 390-397.

Hassan, S. M., A stability-indicating assay for bendrofluazide using high-performance liquid chromatography, Chromatographia, 17, 2 (1983) 101-103.

He, P., Davis, S. S. and Illum, L., Chitosan microspheres prepared by spray drying, Int. J.Pharm. 187 (1999) 53-65.

Heelan, B. A. and Corrigan, O. I., In vitro analysis of the release of incorporated agents from sodium caseinate microspheres, J. Microencapsulation, 14, 1 (1997) 63-78.

Hickey, A. J., Pharmaceutical Inhalation Aerosol Technology, Marcel Dekker, (1992).

Hickey, A. J., Inhalation Aerosols. Physical and Biological Basis for Therapy, Marcel Dekker, (1996).

Higuchi, T., Rate of release of medicaments from ointment bases containing drugs in suspension, J. Pharm. Sci., 50, 2 (1961) 874-875.

Higuchi, T., Mechanism of sustained-action medication, J. Pharm. Sci., 52, 12 (1963) 1145-1149.

Higuchi, W. I., Diffusional models useful in biopharmaceutics, J. Pharm. Sci., 56 (1967) 315-324.

Hirai, A., Odani, H. and Nakajima, A., Determination of degree of deacetylation of chitosan by ^{1}H NMR spectroscopy, Polymer Bulletin, 26 (1991) 87-94.

Hume-Rotherly, W. and Raynor, G. V., The structure of metals and alloys, Institute of Metals, London, 1954.

Illum, L., Hunneyball, I. M. and Davis, S. S., The effect of hydrophilic coatings on the uptake of colloidal particles by the liver and by peritoneal macrophages, Int. J. Pharm., 29 (1986) 53-65.

Illum, L., Farraj, N. F. and Davis, S. S., Chitosan as a novel nasal delivery system for peptide drugs, Pharm. Res., 11, 8 (1994) 1186-1189.

Illum, L., Chitosan and its use as a pharmaceutical excipient, Pharm. Res., 15, 9 (1998) 1326-1331.

Jameela, S. R. and Jayakrishnan, A., Glutaraldehyde crosslinked chitosan microspheres as a long acting biodegradable drug delivery vehicle: studies on the *in vitro* release of mitoxantrone and *in vivo* degradation of microspheres in rat muscle, Biomaterials, 16 (1995) 769-775.

Jouppila, K., Kansikas, J. and Roos, Y. H., Glass Transition, Water Plasticization, and Lactose Crystallisation in Skim Milk Powder, J. Dairy Sci., 80 (1997) 3152-3160.

Kambe, Y., Thermal behaviour of poly(ethylene oxide) as revealed by differential scanning calorimetry, Polymer, 21 (1980) 352-355.

Kaur, R., Grant, D. J. W. and Eaves, T., Comparison of polyethylene glycol and polyoxyethylene stearate as excipients for solid dispersion systems of griseofulvin and tolbutamide I: Phase equilibria, J. Pharm. Sci., 69, 11 (1980) 1317-1321.

Kawashima, Y., Lin, S. Y. and Takenaka, H., Polymorphism and drug release behaviour of spray-dried microcapsules of sulfamethoxazole with polysaccharide gum and colloidal silica, Drug Dev. Ind. Pharm., 9, 8 (1983) 1445-1463.

Kawashima, Y., Lin, S-Y., Ueda, M., Takenaka, H. and Ando, Y., Direct preparation of solid particulates of aminopyrine-barbital complex (pyrabital) from droplets by a spray-drying technique, J. Pharm. Sci., 72, 5 (1983b) 514-518.

Kawashima, Y., Serigano, T., Hino, T., Yamamoto, H. and Takeuchi, H., Effect of surface morphology of carrier lactose on dry powder inhalation property of pranlukast hydrate, Int. J. Pharm., 172 (1998) 179-188.

Kelley, F. N. and Bueche, F., Viscosity and glass temperature relations for polymer diluent systems, J. Polym. Sci., 50 (1961) 549-556.

Kerč, J. and Srčič, S., Thermal analysis of glassy pharmaceuticals, Thermochimica Acta, 248 (1995) 81-95.

Khankari, R. K. and Grant, D. J. W., Pharmaceutical hydrates, Thermochimica Acta, 248 (1995) 61-79.

Khor, E., Methods for the treatment of collagenous tissues for bioprostheses, Biomaterials, 18 (1997) 95-105.

Kimura H., Ogura Y., Moritera, T., Honda, Y., Tabata, Y. and Ikada, Y., In vitro phagocytosis of polylactide microspheres by retinal pigment epithelial cells and intracellular drug release, Current Eye Research, 13, 5 (1994) 353-360.

Kin, S. S., Kim, S. J., Moon, Y. D., and Lee, Y. M., Thermal characteristics of chitin and hydroxypropyl chitin, Polymer, 35, 15 (1994) 3212-3216.

Klug, H. P. and Alexander, L. E., X-ray diffraction procedures for polycrystalline and amorphous materials, Wiley Interscience, 2nd edition, (1974).

Kovacs, A. J., Gonthier, A. and Straupe, C., Isothermal growth, thickening and melting of poly(ethylene oxide) single crystals in the bulk, J. Pol. Sci.: Symposium, 50 (1975) 283-352.

Kovacs, A. J., Straupe, C. and Gonthier, A., Isothermal growth, thickening and melting of poly(ethylene oxide) single crystals in the bulk. II., J. Pol. Sci.:Polymer Symposium, 59 (1977) 31-54.

Kurita, K., Tomita, K., Tada, T., Ishii, S., Nishimura, S-I. and Shimoda, K., Squid chitin as a potential alternative chitin source:Deacetylation behaviour and characteristic properties, J. Polymer Sci., Part A:Polymer Chemistry, 31 (1993) 485-491.

Lacasse, F. X., Filion, M. C., Phillips, N. C., Escher, E., McMullen, J. N. and Hildgen, P., Influence of surface properties at biodegradable microsphere surfaces : effects on plasma protein adsorption and phagocytosis, Pharm. Res., 15, 2 (1998) 312-317.

Law, D., Krill, S. L., Schmitt, E. A., Fort, J. J., Qiu, Y., Wang, W. and Porter, W. R., Physicochemical considerations in the preparation of amorphous ritonavir-poly(ethylene glycol) 8000 solid dispersions, J. Pharm. Sci., 90 (2001) 1015-1025.

Ledwidge, M. T., Draper, S. M., Wilcock, D. J. and Corrigan, O. I., Physicochemical characterisation of diclofenac N-(2-hydroxyethyl)pyrrolidine:anhydrate and dihydrate crystalline forms, J. Pharm. Sci., 85 (1996) 16-21.

Lee, S., Rao, S. P., Moon, M. H. and Giddings, J. C., Determination of mean diameter and particle size distribution of acrylate latex using flow field-flow fractionation, photon correlation spectroscopy, and electron microscopy, Anal. Chem., 68 (1996) 1545-1549.

Lee, S. J., Kim, S. S. and Lee, M. Y., Interpenetrating polymer network hydrogels based on poly(ethylene glycol) macromer and chitosan, Carbohydrate Polymers, 41 (2000) 197-205.

Lehr, C-M., Bouwstra, J. A., Schacht, E. H. and Junginger, H. E., In vitro evaluation of mucoadhesive properties of chitosan and some other natural polymers, Int. J. Pharm., 78 (1992) 43-48.

Leuner, C., Dressman, J., Improving drug solubility for oral delivery using solid dispersions, Eur. J. Pharm. and Biopharm., 50 (2000) 47-60.

Lim, L. Y. and Wan, L. S. C., Heat treatment of chitosan films, Drug Dev. Ind. Pharm., 21 (1995) 839-846.

Lin, S-L., Menig, J. and Lachman, L., Interdependence of physiological surfactant and drug particle size on the dissolution behaviour of water-insoluble drugs, J. Pharm. Sci., 57 (1968) 2143-2148.

Lin-Vien, D., Colthup, N. B., Gateley, W. and Graselli, J. G., The Handbook of Infrared and Raman Characteristic Frequencies of Organic Molecules, Academic Press, (1991).

Lueβen, H. L., de Leeuw, V. J., Langemeÿer, M. W. E., de Boer, A. B. G., Verhoef, J. C. and Junginger, H. E., Mucoadhesive polymers in peroral peptide drug delivery, VI. Carbomer and chitosan improve the intestinal absorption of peptide drug buserelin *in vivo*, Pharm. Res., 13 (1996) 1668-1672.

Lucas, P., Anderson, K. and Staniforth, J. N., Protein deposition from dry powder inhalers:Fine particle multiplets as performance modifiers, Pharm. Res., 15, 4 (1998) 562-569.

Martin, A. M., Physical pharmacy, 4th edition, Lea & Febiger (1993).

Masters, K., Spray drying handbook, 4th edition, (1985).

Matsuda, Y., Kawaguchi, S., Kobayashi, H. and Nishijo, J., Polymorphism of phenylbutazone by a spray drying method, J. Pharm. Pharmacol., 32 (1980) 579-580.

Matsuda, Y., Kawaguchi, S., Kobayashi, H. and Nishijo, J., Physicochemical characeterisation of spray-dried phenylbutazone polymorphs, J. Pharm. Sci., 73, 2 (1984) 173-179.

Meares, P., Polymers - structure and bulk properties, van Nostrand, London (1965).

Mi, F-L., Tan, Y-C., Liang, H-F. and Sung, H-W., In vivo biocompatibility and degradability of a novel injectable-chitosan-based implant, Biomaterials, 23 (2002) 181-191.

Miura, T., Usami, M., Tsuura, Y., Ishida, H. and Seino, Y., Hypoglycemic and hypolipidemic effect of chitosan in normal and neonatal streptozotocin-induced diabetic mice, Biol. Pharm. Bull., 18 (1995) 1623-1625.

Morén, J., Newhouse, M. T. and Dolovich, M. B., (editors)Aerosols in Medicine. Principles and Diagnosis, Elsevier, (1985).

Morimoto, K., Katsumata, H., Yabuta, T., Iwanaga, K., Kakemi, M., Tabata, Y. and Ikada, Y., Gelatin microspheres as a pulmonary delivery system: evalutation of salmon calcitonin absorption, J. Pharm. Pharmacol., 52 (2000) 611-617.

Morris, K. R., Newman, A. W., Bugay, D. E., Ranadive, S. A., Singh, A. K., Szyper, M., Varia, S. A., Brittain, H. G. and Serajuddin, A. T. M., Characterisation of humidity-dependent changes in crystal properties of a new HMG-CoA reductase inhibitor in support of its dosage form development, Int. J. Pharm., 108 (1994) 195-206.

Najib, N. M. and Suleiman, M. S., Characterisation of a diflunisal polyethylene glycol solid dispersion system, Int. J. Pharm., 51 (1989) 225-232.

Nernst, W and Brunner, E., Theorie der reaktionsgeschwindigkeit in heterogenen systemen, A. Phys. Chem., 47 (1904) 56-102.

Newman, A. W. and Brittain, H. G., Particle morphology:optical and electron microscopies, in Physcial Characterisation of pharmaceutical solids, Brittain, H. G. (Editor), Marcel Dekker, New York, (1995) 127-156.

Nguyen, N-A. T., Ghosh, S., Gatlin, L. A. and Grant, D. J., Physicochemical characterisation of the various solid forms of carbovir, an antiviral nucleoside, J. Pharm. Sci., 83 (1994) 1116-1123.

Nielson, D. W., Goerke, J. and Clements, J. A., Alveolar subphase pH in the lungs of anesthetized rabbits, Proc. Natl. Acad. Sci., USA, 78, 11 (1981) 7119-7123.

Nigalaye, A. G., Adusumilli, P. and Bolton, S., Investigation of prolonged drug release from matrix formulations of chitosan, Drug, Dev. Ind. Pharm., 16 (1990) 449-467.

Nishioka, Y., Kyotani, S., Okamura, M., Miyazaki, M., Okazaki, K., Ohnishi, S., Yamamoto, Y. and Ito, K., Release characteristics of cisplatin chitosan microspheres and effect of containing chitin, Chem. Pharm. Bull., 38 (1990) 2871-2873.

Nyqvist, H., Saturated salt solutions for maintaining specified relative humidities, Int. J. Pharm. Tech. & Prod. Mfr., 4, 2 (1983) 47-48.

Ohya, Y., Cai, R., Nishizawa, H., Hara, K. and Ouchi, T., Preparation of PEG-grafted chitosan nanoparticles as peptide drug carriers, S.T.P. Pharma Sci., 10, 1 (2000) 77-82.

Patton, J. S., Trinchero, P. and Platz, R. M., Bioavailability of pulmonary delivered peptides and proteins: g-interferon, calcitonins and parathyroid hormones, J. Control. Release, 28 (1994) 79-85.

Paul, W., and Sharma, C. P., Chitosan, a drug carrier for the 21st century: a review, S.T.P. Pharma Sciences, 10, 1, (2000) 5-22.

Phadnis, N. V. and Suryanarayanan, R., Simultaneous quantification of an enantiomer and the racemic compound of ibuprofen by X-ray powder diffractometry, Pharm. Res., 4, 9 (1997) 1176-1180.

Pharmaceutical handbook:incorporating the "Pharmaceutical pocket book", Pharmaceutical Press, London, 19th edition (1980).

Portero, A., Remuñán-López, C. and Vila-Jato, J. L., Effect of chitosan and chitosan glutamate enhancing the dissolution properties of the poorly water soluble drug nifedipine, Int. J. Pharm., 175 (1998) 75-84.

Reed-Hill, R. E., Physical metallurgy principles, Van-Nostrand, Princetown, NJ (1964).

Reisman, A., Phase equilibria:Basic principles, applications, experimental techniques, 19, in Physical chemistry:A series of monographs, Ed. Loebl, E. M., Academic Press, New York (1970).

Remuñán-López, C. and Bodmeier, R., Mechanical, water uptake and permeability properties of crosslinked chitosan glutamate and alginate films, J. Control. Rel., 44 (1997) 215-225.

Ritger, P. L. and Peppas, N. A., A simple equation for description of solute release II. Fickian and anomalous release from swellable devices, J. Control. Rel., 5 (1987) 37-42.

Ritthidej, G. C., Chomto, P., Pummangura, S. and Menasveta, P., Chitin and chitosan as disintegrants in paracetamol tablets, Drug Dev. Ind. Pharm., 20 (1994) 2109-2134.

Sawayanagi, Y., Nambu, N. and Nagai, T., Directly compressed tablets containing chitin or chitosan in addition to lactose or potato starch, Chem. Pharm. Bull., 30 (1982a) 2935-2940.

Sawayanagi, Y., Nambu, N. and Nagai, T., Enhancement of dissolution properties of griseofulvin from ground mixtures with chitin and chitosan, Chem. Pharm. Bull., 30 (1982b) 4464-4467.

Sawayanagi, Y., Nambu, N. and Nagai, T., Enhancement of dissolution properties of prednisolone from ground mixtures with chitin and chitosan, Chem. Pharm. Bull., 31 (1983) 2507-2509.

Schmitt, E. A., Law, D. and Zhang, G. Z., Nucleation and crystallization kinetics of hydrated amorphous lactose above the glass transition temperature, J. Pharm. Sci., 88 (1999) 291-296.

Schwartz, J. B., Simonelli, A. P. and Higuchi, W. I., Drug release from wax matrices I, Analysis of data with first-order kinetics and with the diffusion-controlled model, J. Pharm. Sci., 57 (1968) 274-277.

Sebhatu, T. and Alderborn, G., Relationships between the effective interparticulate contact area and the tensile strength of tablets of amorphous and crystalline lactose of varying particle size, Eur. J. Pharm. Sci., 8, 4, (1999) 235-242.

Sekiguchi, K. and Obi, N., Studies on absorption of eutectic mixture 1. A comparison of the behaviour of eutectic mixture of sulfathiazole and that of ordinary sulfathiazole in man, Chem. Pharm. Bull., 9 (1961) 866-872.

Shell, J. W., X-ray crystallographic applications in pharmaceutical research II, J. Pharm. Sci., 52 (1963) 24-29.

Sinclair, G. W. and Peppas, N. A., Analysis of non-Fickian transport in polymers using simplified exponential expressions:J. Membrane Sci., 17 (1984) 329-331.

Smith, G. W., Melting behaviour for eutectic-forming binary systems, Mol. Cryst. Liq. Cryst., 42 (1977) 307-318.

Stubberud, L., Forbes, R.T., The use of gravimetry for the study of the effect of additives on the moisture-induced recrystallisation of amorphous lactose, Int. J Pharm., 163, (1998) 145-156.

Sugimoto, M., Morimoto, M., Sashiwa, H., Saimoto, H. and Shigemasa, Y., Preparation and characterisation of water-soluble chitin and chitosan derivatives, Carbohydrate Polymers, 36 (1998) 49-59.

Tachibana, T and Nakamura, A., A method for preparing an aqueous colloidal dispersion of organic materials by using water-soluble polymers: dispersion of beta-carotene by polyvinylpyrrolidone, Kolloid-Z. Polym., 203 (1965) 130-133.

Tajber, L., Personal communication (2002).

Takenaka, H., Kawashima, Y. and Lin, S. Y., Polymorphism of spray-dried microencapsulated sulfamethoxazole with cellulose acetate phthalate and colloidal silica, montmorillonite, or talc, J. Pharm. Sci., 11 (1981) 1256-1260.

Takeuchi, H., Yamamoto, H., Toshiyuki, N., Tomoaki, H., Kawashima, Y., Enteral absorption of insulin in rats from mucoadhesive chitosan-coated liposomes, Pharm. Res., 13 (1996) 896-901.

Takeuchi, H., Yasuji, T., Yamamoto, H. and Kawashima, Y., Spray-dried lactose composite particles containing an ion complex of alginate-chitosan for designing a dry-coated tablet having a time-controlled releasing function, Pharm. Res., 17 (2000) 94-99.

Tan, S. C., Khor, E., Tan, T.K. and Wong, S. M., The degree of deacetylation of chitosan: advocating the first derivative UV-spectrophotometry method of determination, Talanta, 45 (1998) 713-719.

Tanaka, Y., Tanioka, S., Tanaka, M., Tanigawa, T., Kitamura, Y., Minami, S., Okamoto, Y., Miyashita, M. and Nanno, M., Effects of chitin and chitosan particles on BALB/c mice by oral and parenteral administration, Biomaterials, 18 (1997) 591-595.

Taylor, L. S. and Zografi, G., Spectroscopic characterisation of interactions between PVP and indomethacin in amorphous molecular dispersions, Pharm. Res., 14 (1997) 1691-1698.

Timsina, M. P., Martin, G. P., Marriot, C., Ganderton, D. and Yianneskis, M., Drug delivery to the respiratory tract using dry powder inhalers, Int. J. Pharm., 101 (1994) 1-13.

Tobío, M., Gref, R., Sánchez, A., Langer, R. and Alonso, M. J., Stealth PLA-PEG nanoparticles as protein carriers for nasal administration, Pharm. Res., 15, 2 (1998) 270-275.

Torchillin, V. P., Polymer-coated long-circulating microparticulate pharmaceuticals, J. Microencapsulation, 8, 9 (1998) 1-19.

Tozaki, H., Komoike, J., Tada, C., Maruyama, T., Terabe, A., Suzuki, T., Yamamoto, A. and Muranishi, S., Chitosan capsules for colon-specific drug delivery: Improvement of insulin absorption from the rat colon, J. Pharm. Sci., 86, 9 (1997) 1016-1021.

United States Pharmacopeia 24, United States Pharmacopeial Convention, Rockville, Maryland (2000).

Upadrashta, S. M., Katikaneni, P. R. and Nuessle, N. O., Chitosan as a tablet binder, Drug Dev. Ind. Pharm., 18 (1992) 1701-1708.

Vachoud, L., Zydowicz, N. and Domard, A., Physicochemical behaviour of chitin gels, Carbohydrate Research, 326 (2000) 295-304.

Vanbever, R., Mintzes, J. K., Wang, J., Nice, J., Chen, D., Batycky, R., Langer, R. and Edwards, D. A., Formulation and Physical Characterisation of Large Porous Particles for Inhalation, Pharm. Res., 16, 11 (1999) 1735-1742.

Venkataram, S. and Rogers, J. A., Characteristics of drug-phospholipid coprecipitates I: Physical properties and dissolution behavior of griseofulvin-dimyristoylphosphatidylcholine systems, J. Pharm. Sci., 73 (1984) 757-761.

Verdonck, E., Schaap, K. and Thomas, L. C., A discussion of the principles and applications of modulated temperature DSC (MTDSC), Int. J. Pharm., 192 (1999) 3-20.

Vidgrén, P., Vidgren, M. and Paronen, P., Physical stability and inhalation behaviour of mechanically micronised and spray dried disodium cromoglycate in different humidities, Acta Pharmaceutica Fennica 98 (1989) 71-78.

Vila, A., Sánchez, A., Tobío, M., Calvo, P. and Alonso, M. J., Design of biodegradable particles for protein delivery, J. Control. Rel., 78 (2002) 15-24.

Vromans, H., Bolhuis, G. K., Lerk, C. G., Kussendrager, K. D. and Bosch, H., Studies on tableting properties of lactose, Part 6, Consolidation and compaction of spray dried amorphous lactose, Acta Pharm. Suec., 23 (1986) 231-240.

Wang, D., Robinson, D. R., Kwon, G. S. and Samuel, J., Encapsulation of plasmid DNA in biodegradable poly(D,L-lactic-co-glycolic acid) microspheres as a novel approach for immunogene delivery, J. Control. Rel., 57 (1999) 9-18.

Walter, E., Dreher, D., Kok, M., Thiele, L., Kiama, S. G., Gehr, P. and Merkle, H. P., Hydrophilic poly(DL-lactide-co-glycolide) microspheres for the delivery of DNA to human-derived macrophages and dendritic cells, J. Control. Rel., 76 (2001) 149-168.

Ward, G. H. and Schultz, R. K., Process-induced crystallinity changes in albuterol sulfate and its effect of powder physical stability, Pharm. Res., 12 (1995) 773-779.

Williams, R. O., Barron, M. K., Alonso, M. J. and Remuñán-López, C., Investigation of a pMDI system containing chitosan microspheres and P134a, Int. J. Pharm., 174 (1998) 209-222.

Zeng, X. M., Martin, G. P. and Marriott, C., The controlled delivery of drugs to the lung, Int. J. Pharm., 124 (1995) 149-164.

Zeng, X. M., Martin, G.P., Marriott, C. and Pritchard, J., The influence of carrier morphology on drug delivery by dry powder inhalers, Int. J. Pharm., 200 (2000) 93-106.

Zhou, D., Zhang, G. G. Z., Law, D, Grant, D. J. W. and Schmitt, E. A., Physical stability of amorphous pharmaceuticals:Importance of configurational thermodynamic quantities and molecular mobility, J. Pharm. Sci., 91, 8 (2002) 1863-1872.

Zong, Z., Kimura, Y., Takahashi, M. and Yamane, H., Characterisation of chemical and solid state structures of acylated chitosans, Polymer, 41 (2000) 899-906.

APPENDICES

APPENDIX I

Table 1 PEG 4000 spray drying conditions. All PEG systems were spray dried from ethanol 95%.

Spray Drier	System	Inlet Temp (°C)	Outlet Temp (°C)	Pump Rate (%)	Air Flow (nl/hr)	Aspirator Rate (%)
Büchi 190	PEG 4000 5% w/v	74	53-54	25	500	Unknown
Büchi 190	PEG 4000 2.5% w/v	71-72	45-46	25	500	Unknown
Büchi 191	PEG 4000 2.5% w/v	76	51-53	25	600	85
Büchi 191	PEG 4000 2.5% w/v	76	45	40	600	90
Büchi 191	PEG 4000 2.5% w/	75-76	43-44	30	600	70
Büchi 191	PEG 4000 2.5% w/v	75-76	41	30	600	60
Büchi 191	PEG 4000 2.5% w/v	77	31-32	70	600	85
Büchi 191	PEG 4000 2.5% w/v	71	46	5	500	100
Büchi 191	PEG 4000 2.5% w/v	71	40-41	50	600	100

Table 2 PEG 20,000 and PEO 300,000 spray drying conditions. Systems were spray dried from ethanol 95%.

Spray Drier	System	Inlet Temp (°C)	Outlet Temp (°C)	Pump Rate (%)	Air Flow (nl/hr)	Aspirator Rate (%)
Büchi 191	PEG 20,000 1% w/v	78	47-48	45	600	100
Büchi 191	PEO 300,000 0.5% w/v	78-79	52-55	30	600	100

Table 3 Spray drying conditions for lactose and lactose/PEG 4000 (containing 5, 10, 20, 30% PEG 4000 by weight of solids) systems spray dried using the Büchi 190. Systems were prepared using deionised water. The lactose used in the preparation of all solutions for spray drying was lactose monohydrate.

System	Inlet temperature (°C)	Outlet temperature (°C)	Pump setting (dial)	Air flow rate (l/hr)
Lactose	123	81-84	5	600
Lactose/PEG containing 5% PEG by weight of total solids spray dried as a 10% w/v solution	116	76-78	5	600
Lactose/PEG containing 10% PEG by weight of total solids spray dried as a 10% w/v solution	116	76-78	5	600
Lactose/PEG containing 20% PEG by weight of total solids spray dried as a 10% w/v solution	116	76-78	5	600
Lactose/PEG containing 30% PEG by weight of total solids spray dried as a 10% w/v solution	116	75-78	5	600

Table 4 BFMT and BFMT/PEG 4000 spray drying conditions. All systems were spray dried as 2.5% w/v solutions from ethanol 95% using a Büchi 191 spray drier.

System	Inlet temperature (°C)	Outlet temperature (°C)	Pump setting (%)	Air flow rate (l/hr)	Aspirator rate (%)
BFMT	78-79	58-62	20	600	100
BFMT/PEG 4000 containing 10% PEG by weight of BFMT	78-79	57-62	20	600	100
BFMT/PEG 4000 containing 20% PEG by weight of BFMT	78-79	56-60	20	600	100
BFMT/PEG 4000 containing 30% PEG by weight of BFMT	79-80	60-62	20	600	100
BFMT/PEG 4000 containing 90% PEG by weight of BFMT	71-72	42-45	45	600	100

Table 5 BFMT and BFMT/PEG 20,000 spray drying conditions. All systems were spray dried as 2.5% w/v solutions from ethanol 95% using a Büchi 191 spray drier.

System	Inlet temperature (°C)	Outlet temperature (°C)	Pump setting (%)	Air flow rate (l/hr)	Aspirator rate (%)
BFMT/PEG 20,000 containing 10% PEG by weight of BFMT	78-79	53-55	25	600	85
BFMT/PEG 20,000 containing 20% PEG by weight of BFMT	78-80	55-57	25	600	85
BFMT/PEG 20,000 containing 30% PEG by weight of BFMT	78-80	52-54	25	600	85

Table 6 BFMT and BFMT/PEO 300,000 spray drying conditions. All systems were spray dried from ethanol 95% using a Büchi 191 spray drier.

System	Inlet temperature (°C)	Outlet temperature (°C)	Pump setting (%)	Air flow rate (l/hr)	Aspirator rate (%)
BFMT/PEO 300,000 containing 10% PEG by weight of BFMT spray dried as a 2.5% w/v solution	78-79	53-55	25	600	85
BFMT/PEO 300,000 containing 10% PEG by weight of BFMT spray dried as a 0.8% w/v solution	78-79	52-54	25	600	85
BFMT/PEO 300,000 containing 30% PEG by weight of BFMT spray dried as a 0.8% w/v solution	78-79	52-54	25	600	85

Table 7 Spray drying conditions for salbutamol and ipratropium bromide systems using the Büchi 190.

System	Inlet Temp (°C)	Outlet Temp (°C)	Pump Rate (%)	Air Flow (nl/hr)
Salbutamol sulphate spray dried as a 10% w/v aqueous solution	150-152 °C	75-78 °C	7	650
Ipratropium bromide spray dried as a 5% w/v aqueous solution	150-153 °C	102-104 °C	7	700
Salbutamol sulphate:Ipratropium bromide 10:1 spray dried as a 5% w/v aqueous solution	150-152 °C	100-102 °C	7	650
Salbutamol sulphate:Ipratropium bromide 5:1 spray dried as a 5% w/v aqueous solution	150-153 °C	99-103 °C	7	700
Salbutamol sulphate:Ipratropium bromide 2:1 spray dried as a 5% w/v aqueous solution	150-153 °C	99-100 °C	7	650
Salbutamol base spray dried as a 2.5% w/v solution from ethanol (95%)	77-79 °C	48-50 °C	6	500
Ipratropium bromide was spray dried as a 2.5% w/v solution from ethanol (95%)	77-79 °C	55-56 °C	6	500
Salbutamol BP:Ipratropium bromide 10:1 spray dried as a 2.5% w/v solution from ethanol (95%)	77-78 °C	54-56 °C	6	500
Salbutamol BP:Ipratropium bromide 5:1 spray dried as a 2.5% w/v solution from ethanol (95%)	76-78 °C	52-56	6	500
Salbutamol BP:Ipratropium bromide 2:1 spray dried as a 2.5% w/v solution from ethanol (95%)	75-79	56-58	6	500

Table 8 Continuation of spray drying conditions for salbutamol and ipratropium bromide systems using the Büchi 190.

System	Inlet Temp (°C)	Outlet Temp (°C)	Pump Rate (%)	Air Flow (nl/hr)
Salbutamol sulphate spray dried as a 0.6% w/v solution from ethanolic solvent consisting of 75% ethanol and 25% water	100-102	60-64	6	500
Salbutamol sulphate:Ipratropium bromide 10:1 system spray dried as a 0.94% w/v solution from ethanolic solvent consisting of 84% ethanol and 16% water	87-94	60-66	6	500
Salbutamol sulphate:Ipratropium bromide 5:1 system spray dried as a 2.5% w/v solution from ethanolic solvent consisting of 85% ethanol and 15% water	95-96	64-70	6	500
Salbutamol sulphate:Ipratropium bromide 2:1 system spray dried as a 0.5% w/v solution from ethanolic solvent consisting of 89% ethanol and 11% water	85-88	60-64	6	500

Table 9 Spray drying conditions for budesonide and formoterol fumarate dihydrate systems using the Büchi 191.

System	Inlet Temp (°C)	Outlet Temp (°C)	Pump Rate (%)	Air Flow (nl/hr)	Aspirator rate (%)
Budesonide (spray dried as a 2.5% w/v solution)	78-79	52-56	30	600	100
Formoterol fumarate dihyrate:budesonide 6:100 (spray dried as a 1.75% w/v solution*)	78-79	52-56	30	600	100
Formoterol fumarate dihyrate:budesonide 6:400 (spray dried as a 2.5% w/v solution)	78-79	52-56	30	600	100

*The 6:100 system was spray dried as a 1.75% w/v feed solution since the formoterol fumarate dihydrate was not soluble at a higher concentration.

Table 10 Spray drying conditions for salbutamol sulphate/lactose and salbutamol sulphate/PEG systems spray dried using a Büchi 191 spray drier.

System	Inlet Temp (°C)	Outlet Temp (°C)	Aspirator Rate (%)	Pump Rate (%)	Air Flow (nl/hr)
Salbutamol sulphate/lactose 5% (total solids 10% w/v)	150	104-105	100	10	600
Salbutamol sulphate/lactose 20% (total solids 10% w/v)	150	103-105	100	10	600
Salbutamol sulphate/lactose 20% (total solids 2.5% w/v)	150	98-103	100	10	600
Salbutamol sulphate/lactose 40% (total solids 10% w/v)	150	103-104	100	10	600
Salbutamol sulphate/PEG 4000 5% (total solids 2.5% w/v)	150	91-97	100	18	600
Salbutamol sulphate/PEG 4000 20%(total solids 2.5% w/v)	150	92-97	100	18	600
Salbutamol sulphate/PEG 4000 40%(total solids 2.5% w/v)	150	95-98	100	18	600
Salbutamol sulphate/PEG 20,000 5% (total solids 2.5% w/v)	150	100-105	100	18	600
Salbutamol sulphate/PEG 20,000 20% (total solids 2.5% w/v)	150	90	100	18	600
Salbutamol sulphate/PEG 20,000 40% (total solids 2.5% w/v)	150	96-100	100	18	600

Table 11 Spray drying conditions for chitosan and chitosan/salbutamol sulphate systems spray dried using a Büchi 191 spray drier.

System	Inlet Temp (°C)	Outlet Temp (°C)	Aspirator Rate (%)	Pump Rate (%)	Air Flow (nl/hr)
Chitosan 0.2% w/v solids in 1% acetic acid	140	89-91	100	15	600
Chitosan 0.2% w/v solids in 1% acetic acid containing 1.6% v/v of a 1% formaldehyde solution as a crosslinking agent	140	91-92	100	15	600
Chitosan 0.12% w/v solids in 0.8% HCl	140	90-92	100	15	600
Chitosan/salbutamol sulphate 10% (total solids 0.2% w/v)	140	98-100	100	15	600
Chitosan/salbutamol sulphate 20% (total solids 0.2% w/v)	140	92-98	100	15	600
Chitosan/salbutamol sulphate 40% (total solids 0.2% w/v)	140	90-92	100	15	600
Chitosan/salbutamol sulphate 10% (total solids 0.2% w/v spray dried from 1% acetic acid containing 1.6% v/v of a 1% formaldehyde solution as a crosslinking agent)	140	92-94	100	15	600
Chitosan/salbutamol sulphate 20% (total solids 0.2% w/v spray dried from 1% acetic acid containing 1.6% v/v of a 1% formaldehyde solution as a crosslinking agent)	140	90-93	100	15	600
Chitosan/salbutamol sulphate 40% (total solids 0.2% w/v spray dried from 1% acetic acid containing 1.6% v/v of a 1% formaldehyde solution as a crosslinking agent)	140	82-88	100	15	600
Chitosan/PEG 4000 (10%) spray dried at 0.2% w/v solutions from 1% acetic acid	160	109-110	85	10	600
Chitosan/PEG 4000 (20%) spray dried at 0.2% w/v solutions from 1% acetic acid	160	106-110	85	10	600
Chitosan/PEG 4000 (30%) spray dried at 0.2% w/v solutions from 1% acetic acid	135	93	85	10	600

APPENDIX II

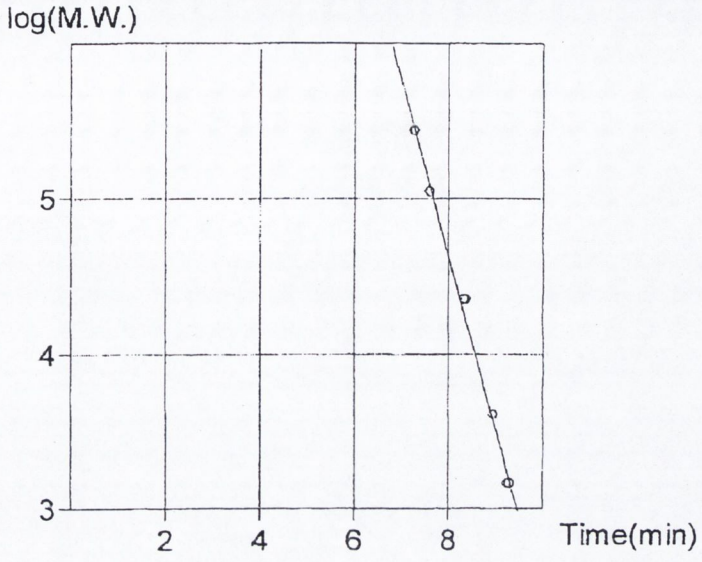

Figure 1 GPC sample calibration curve of PEG/PEO standards.

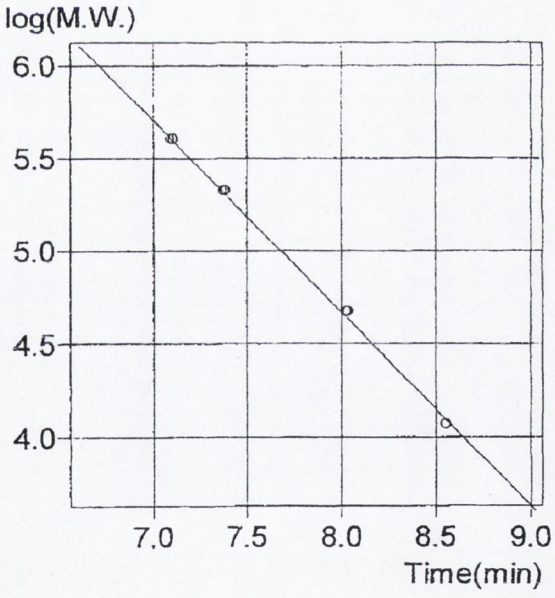

Figure 2 GPC sample calibration curve of pullulan standards for chitosan molecular weight determination.

APPENDIX III

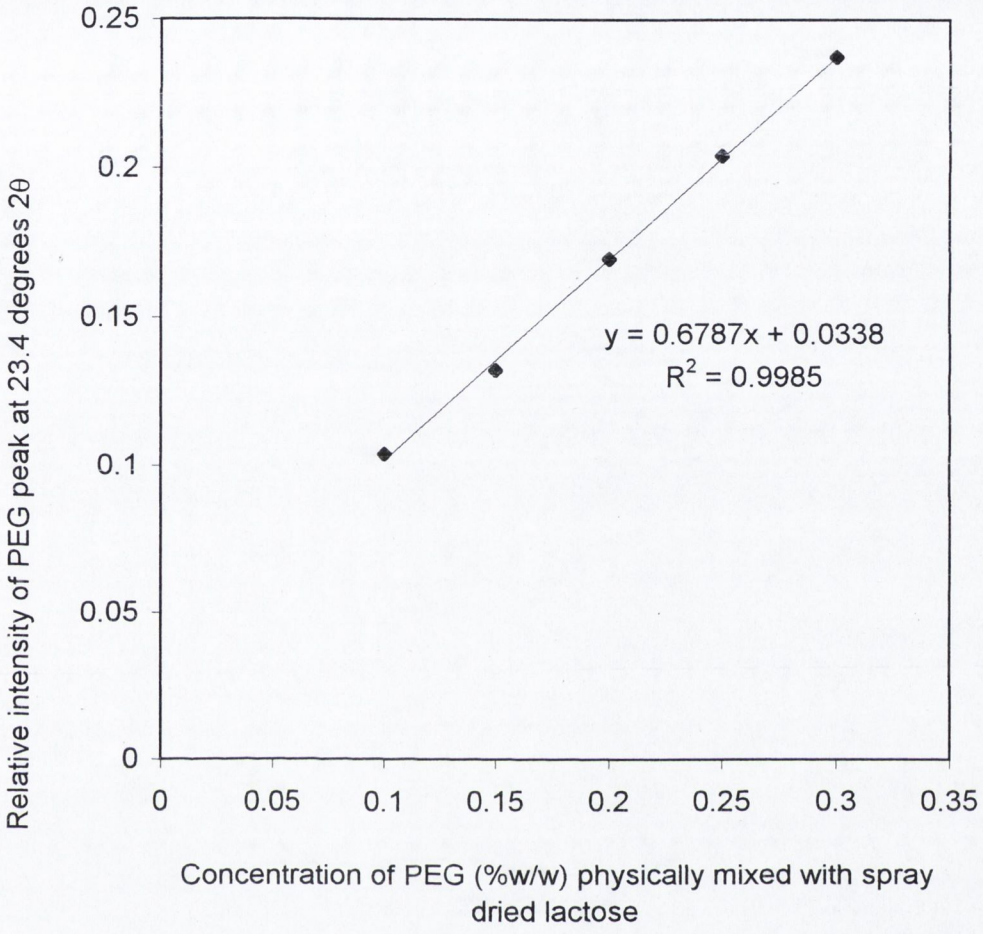

Figure 1 Calibration curve of PEG XRD peak height intensity at 23.4° 2θ in PEG/spray dried lactose physical mixes.

APPENDIX IV

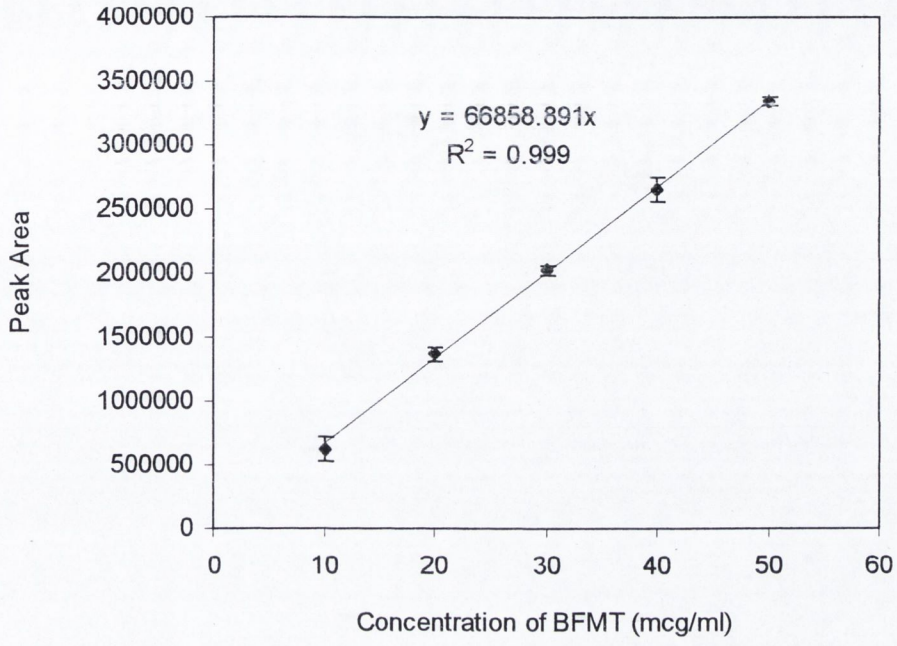

Figure 1 Sample HPLC calibration curve of BFMT.

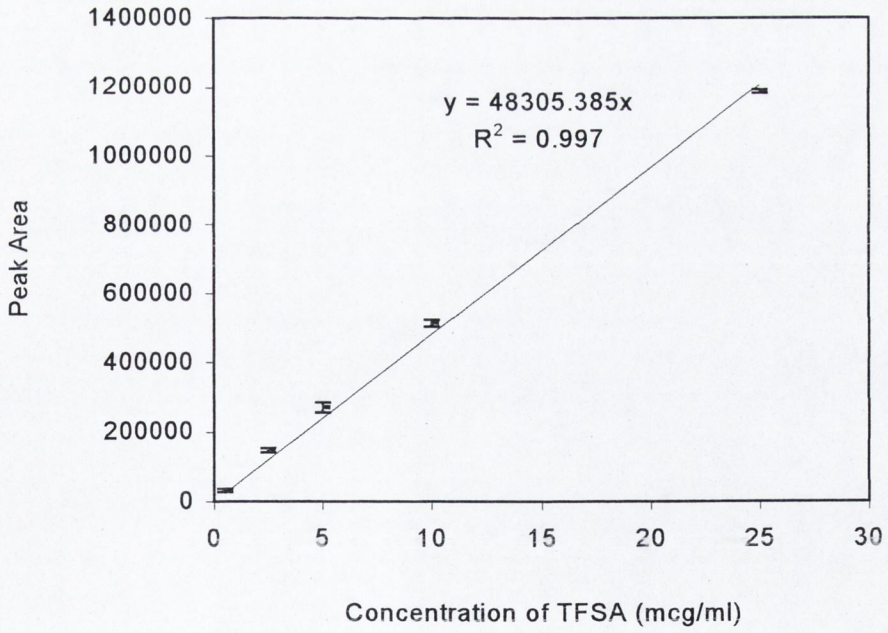

Figure 2 Sample HPLC calibration curve of TFSA.

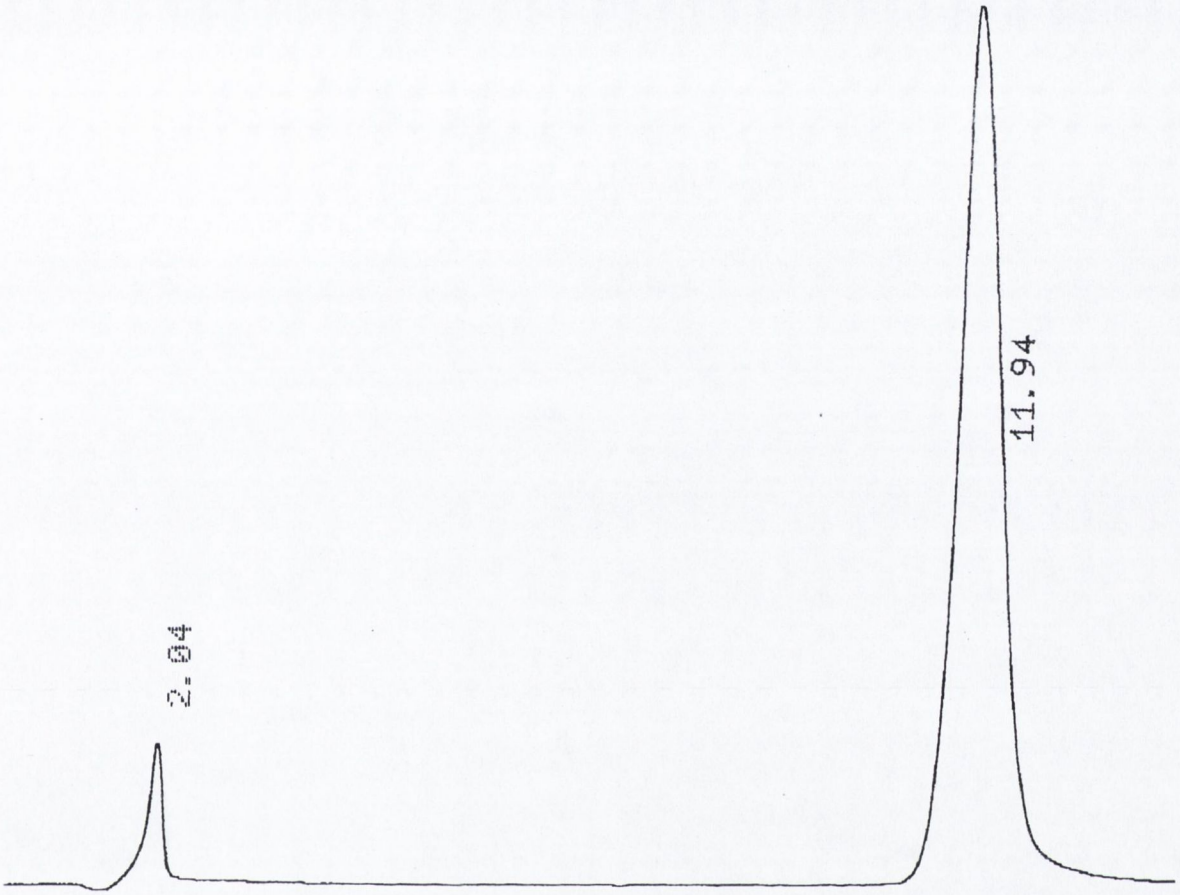

Figure 3 Sample HPLC chromatogram of BFMT (peak at 2.04 is the solvent peak, peak at 11.94 is due to BFMT). HPLC methods are described in Chapter 2.

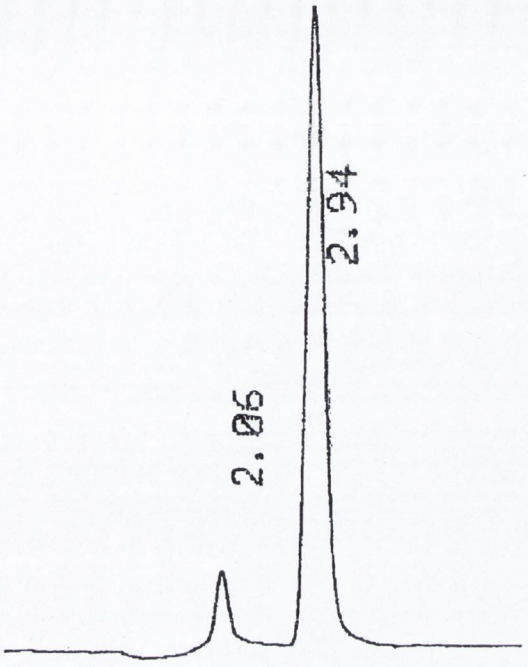

Figure 4 Sample HPLC chromatogram of TFSA (peak at 2.06 is solvent peak, peak at 2.94 is due to TFSA). HPLC methods are described in Chapter 2.

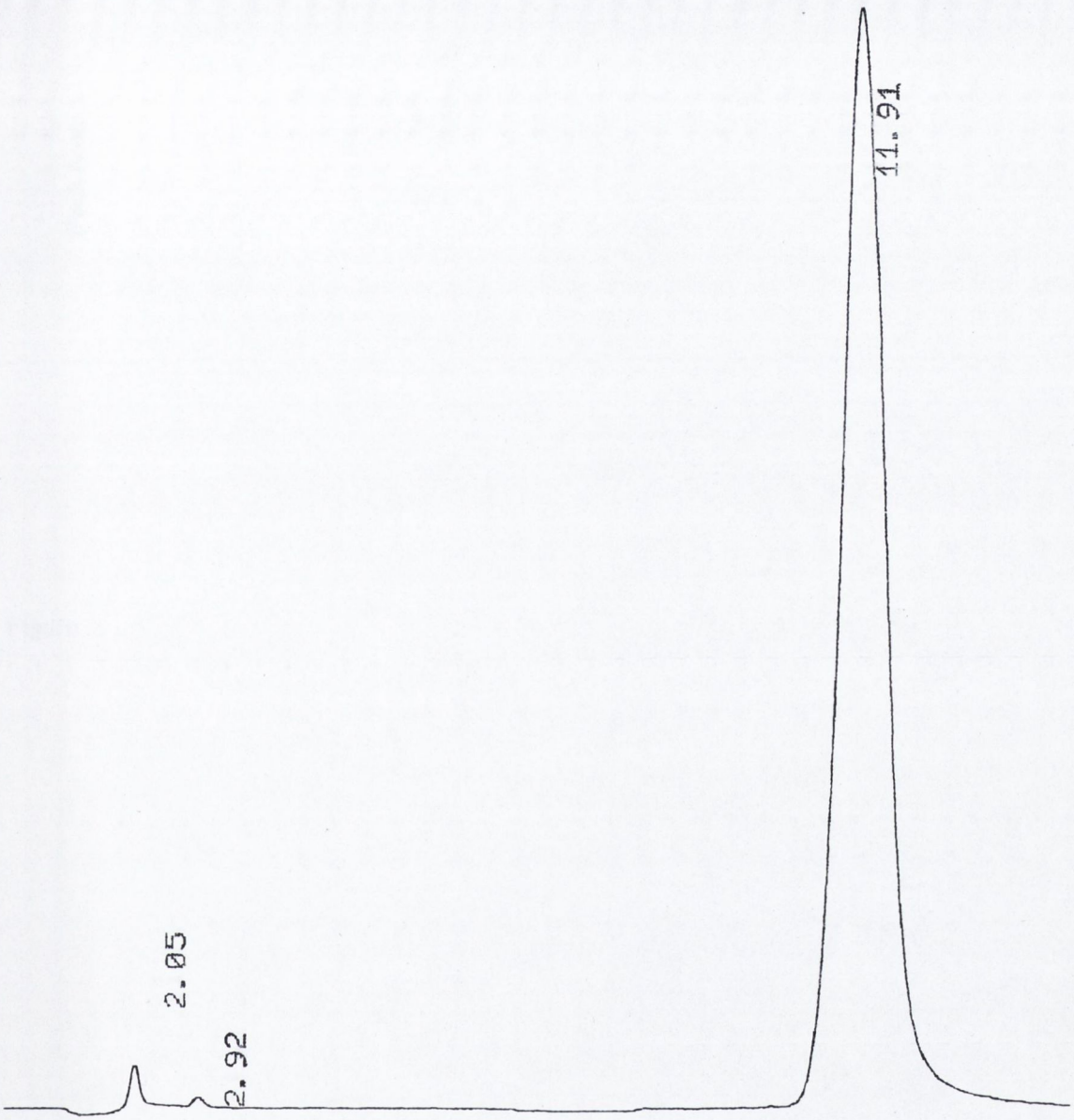

Figure 5 Sample HPLC chromatogram of BFMT and TFSA (at 11.91 and 2.92 respectively). HPLC methods are described in Chapter 2.

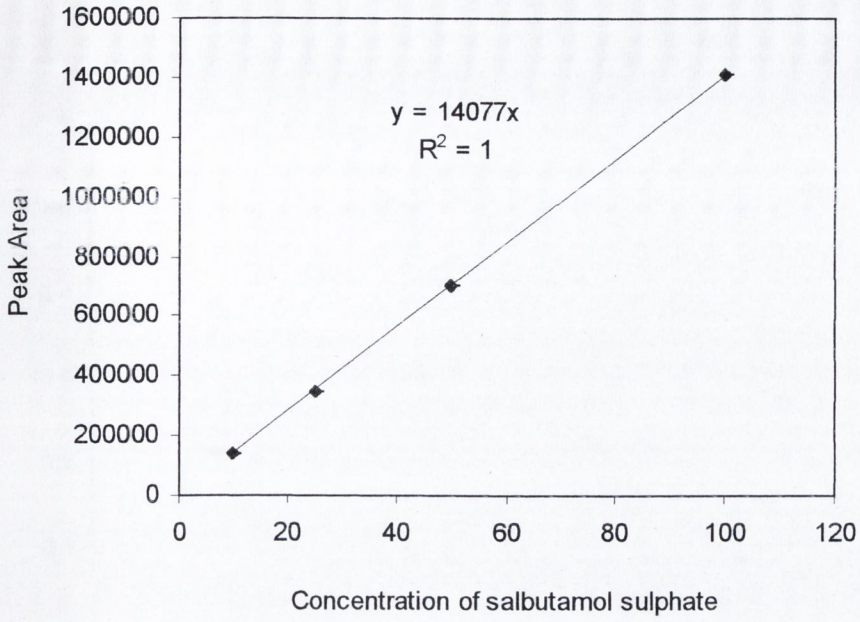

Figure 6 Sample HPLC calibration curve of salbutamol sulphate.

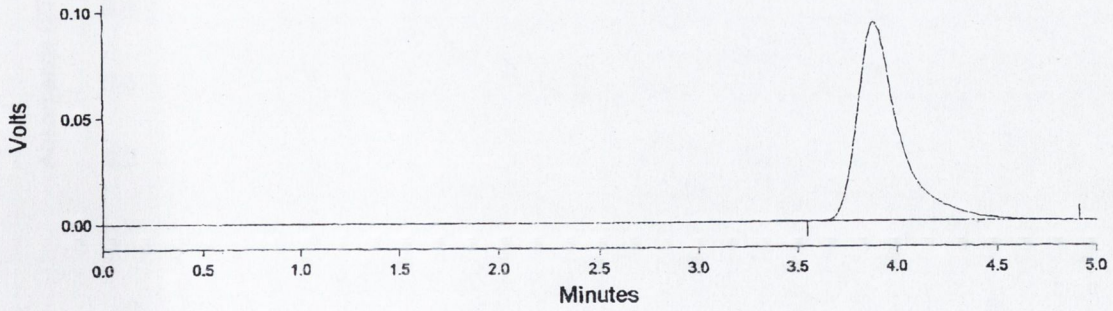

Figure 7 Sample HPLC chromatogram of salbutamol sulphate. HPLC methods are described in Chapter 2.

APPENDIX V

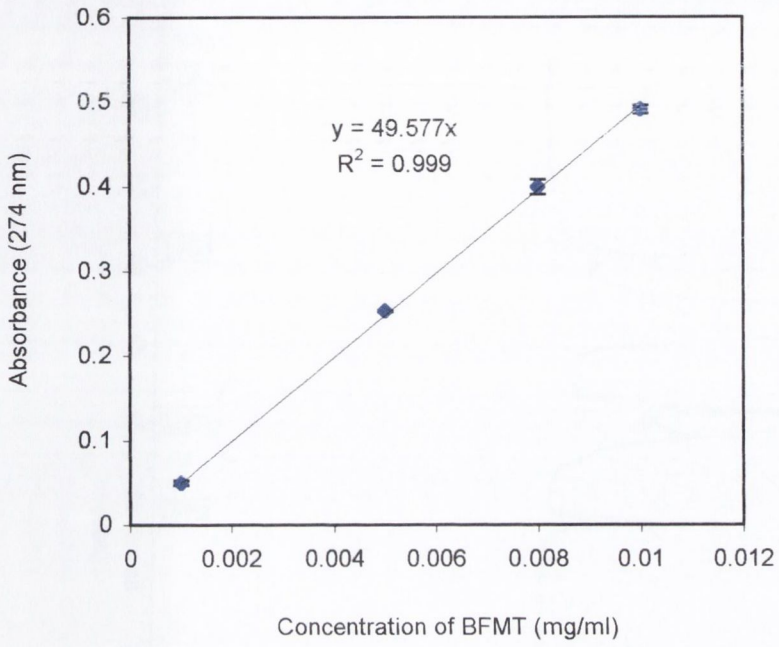

Figure 3 Sample UV calibration curve for BFMT.

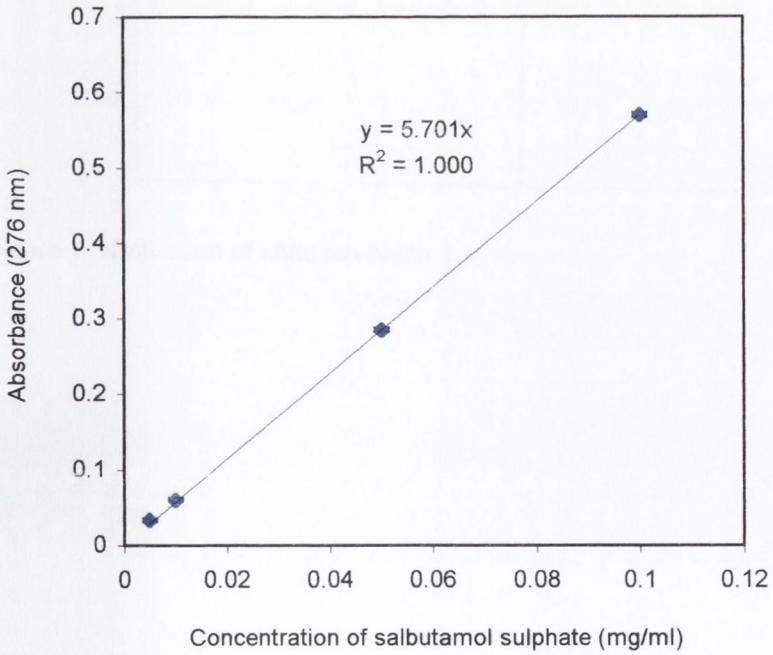

Figure 2 Sample UV calibration curve of salbutamol sulphate.

APPENDIX VI

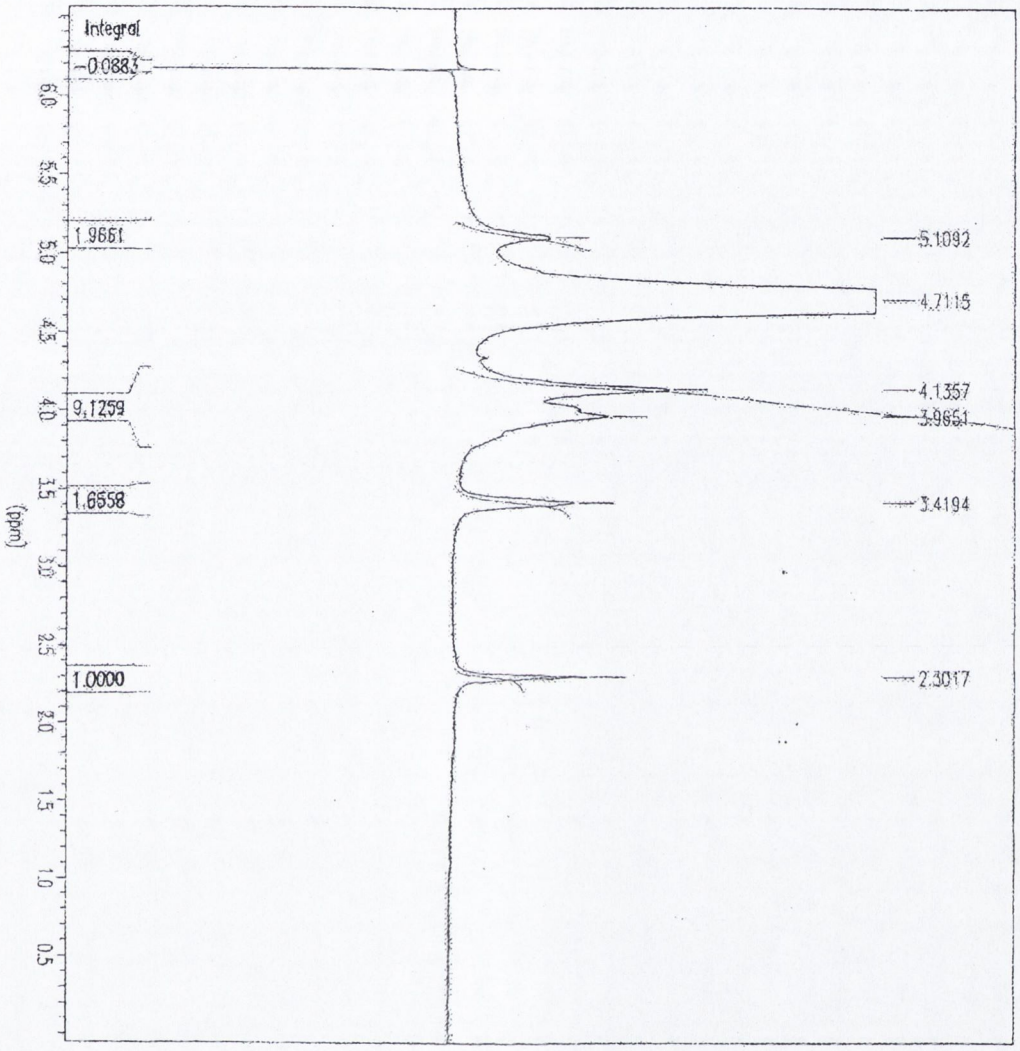

Figure 1 NMR scan of chitosan batch 1.

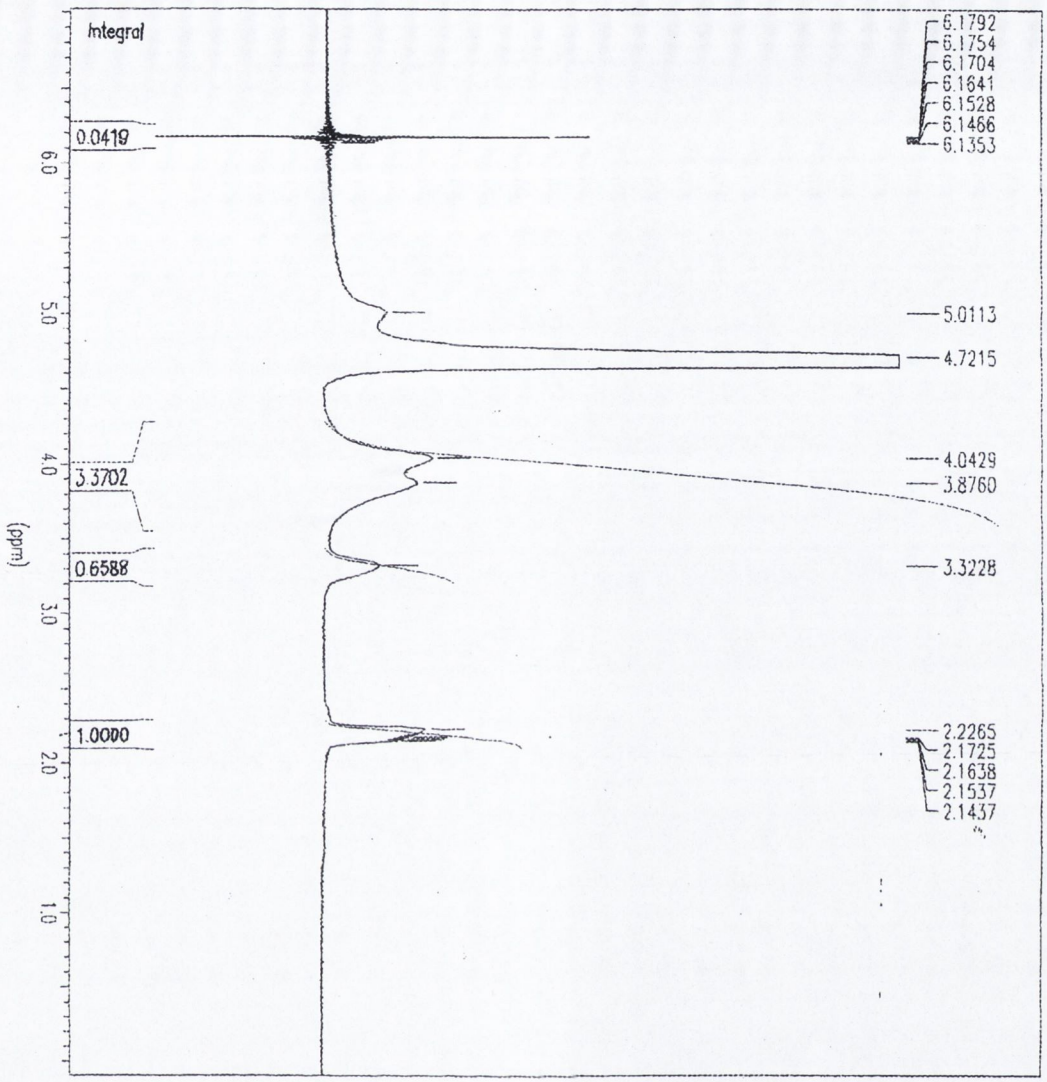

Figure 2 NMR scan of spray dried chitosan batch 1.

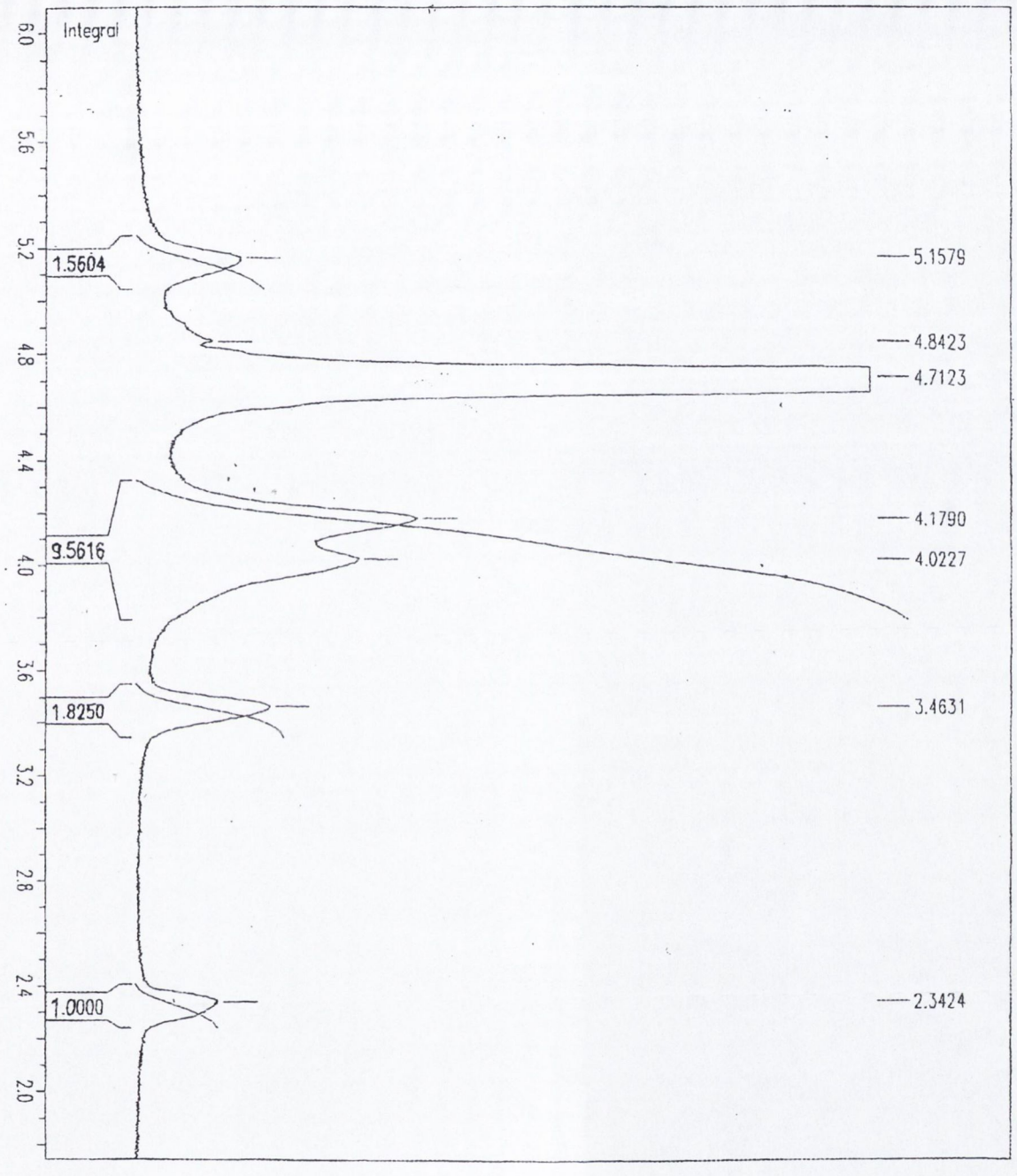

Figure 3 NMR of chitosan batch 2.

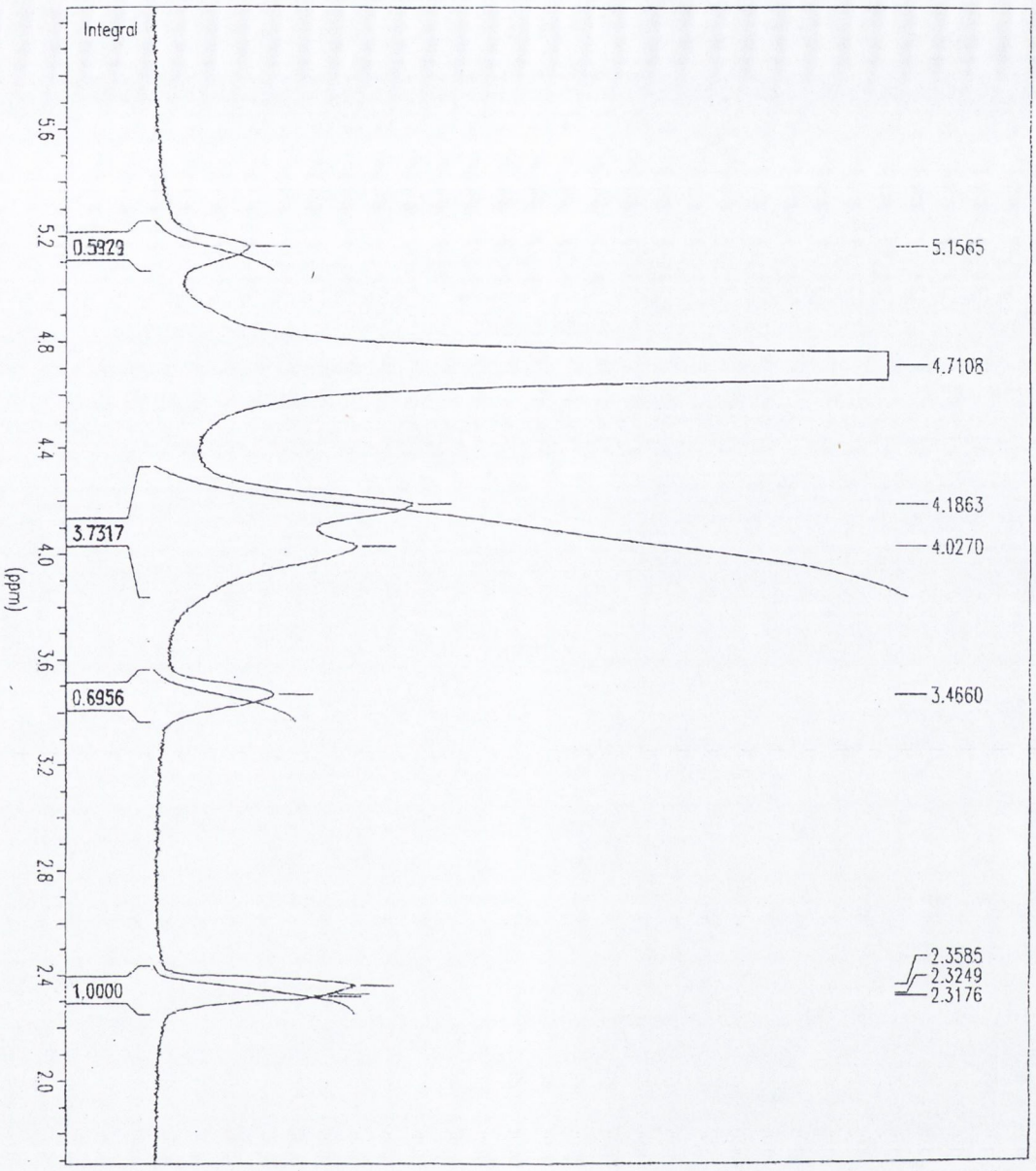

Figure 4 NMR scan of spray dried chitosan batch 2.

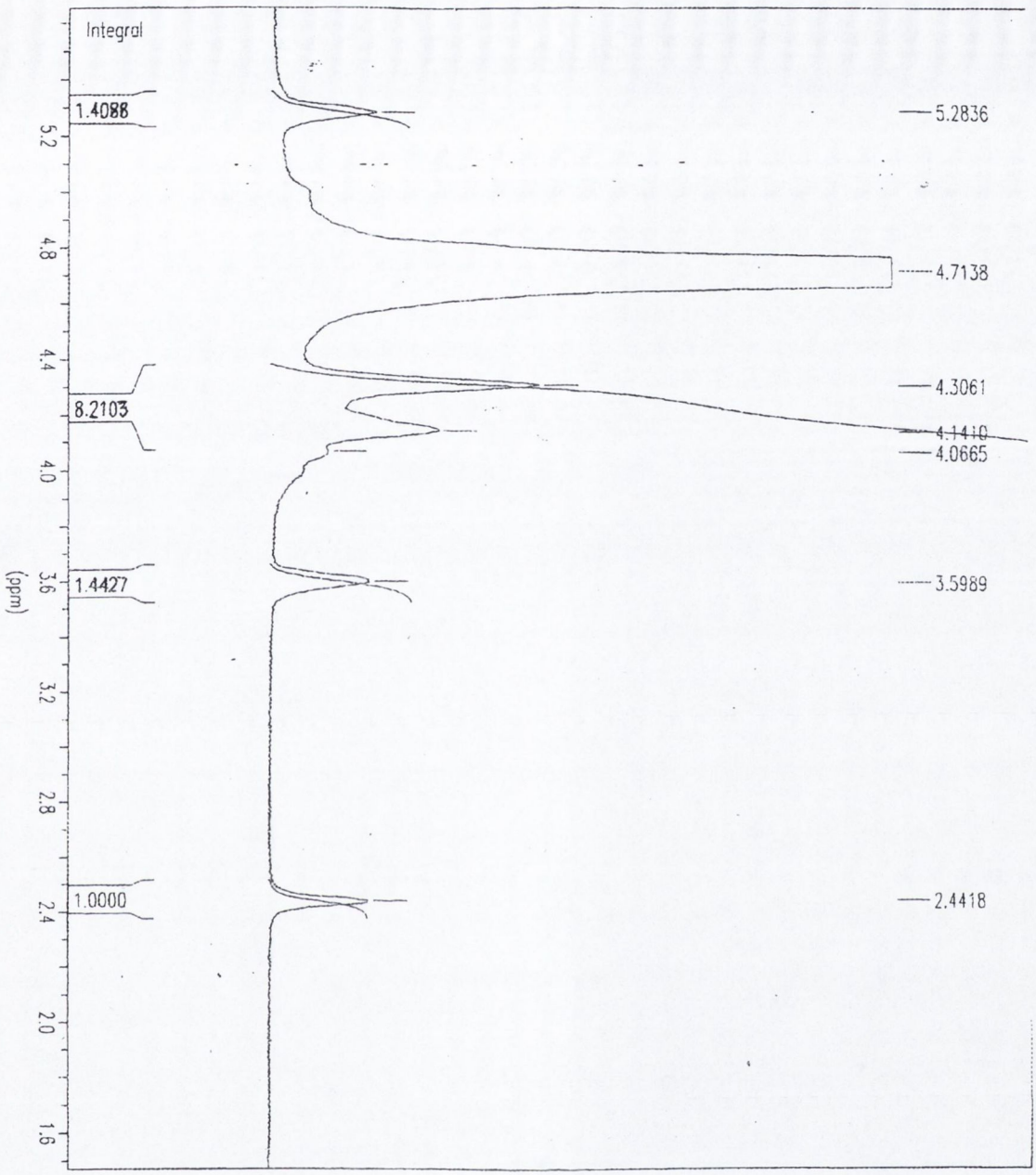

Figure 5 NMR scan of chitosan spray dried from HCl.

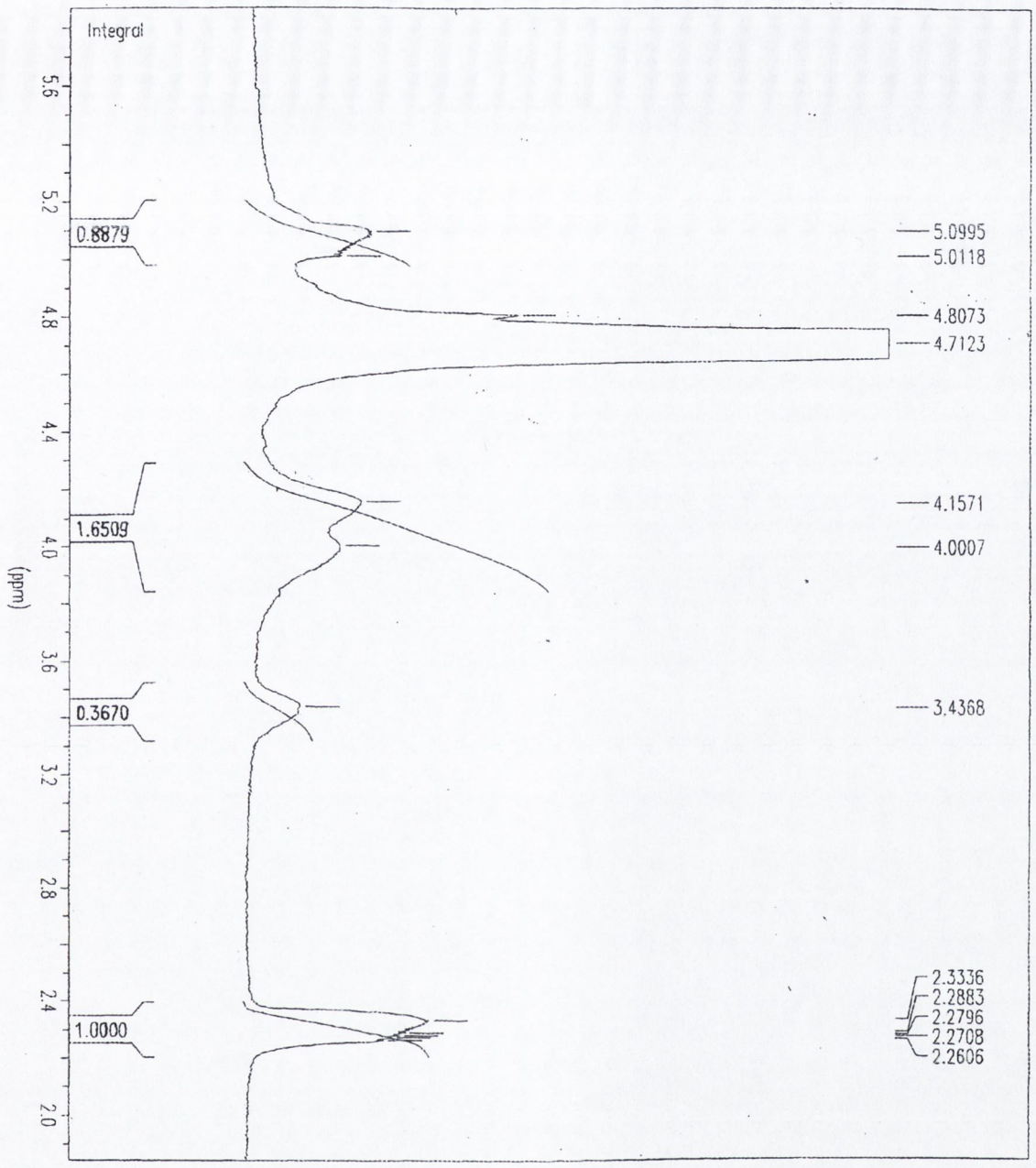

Figure 6 NMR scan of spray dried crosslinked chitosan.

APPENDIX VII

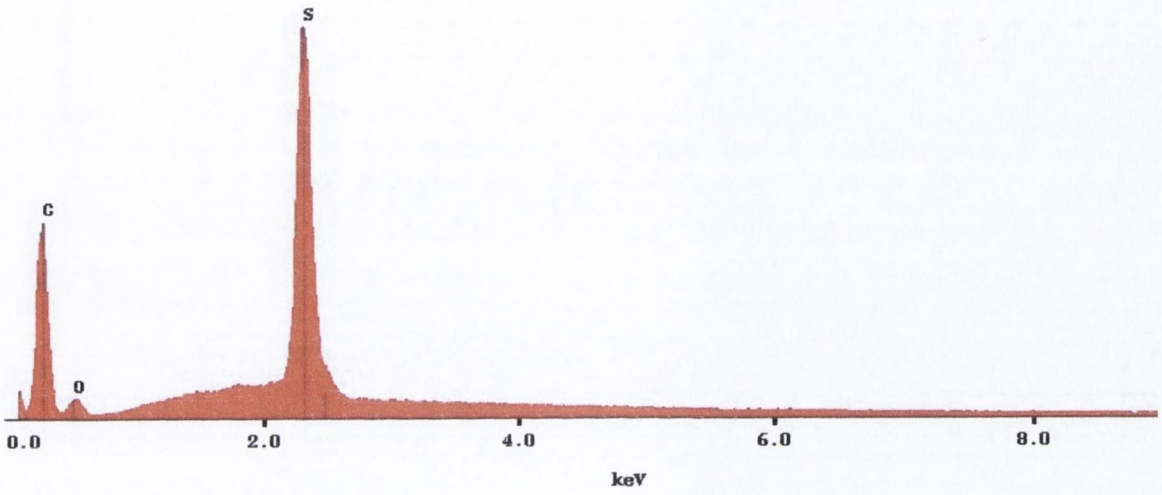

Figure 1 EDXA scan of spray dried salbutamol sulphate.

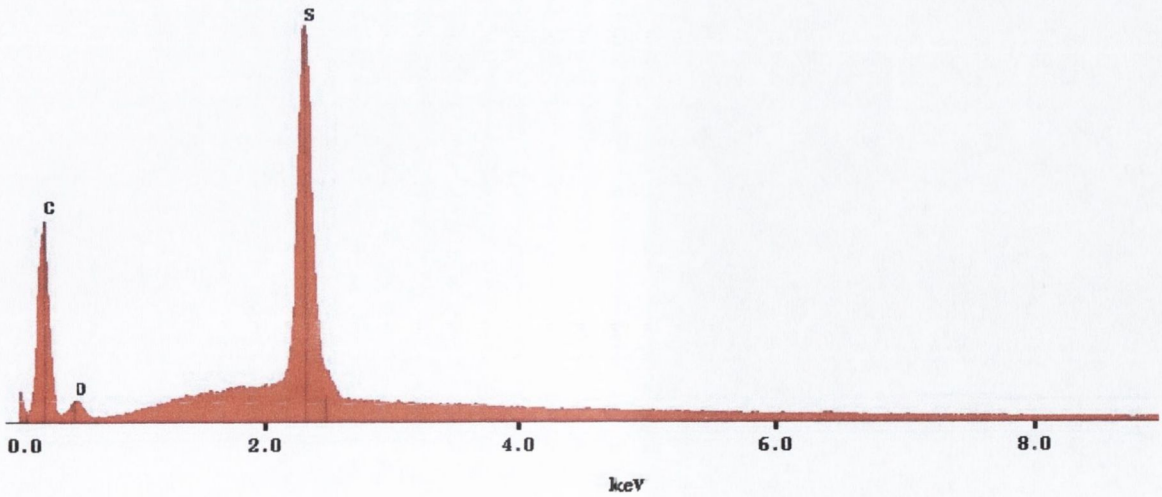

Figure 2 EDXA scan of a disc of a physical mix of 40%salbutamol sulphate/60%chitosan raw materials.

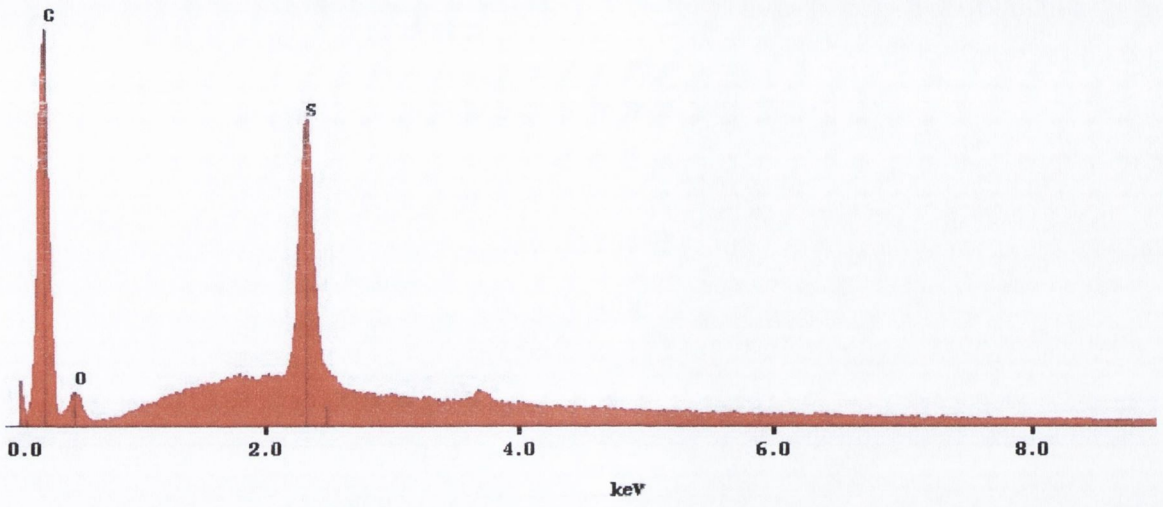

Figure 3 EDXA scan of a disc of co-spray dried 40%salbutamol sulphate/60%chitosan mix.

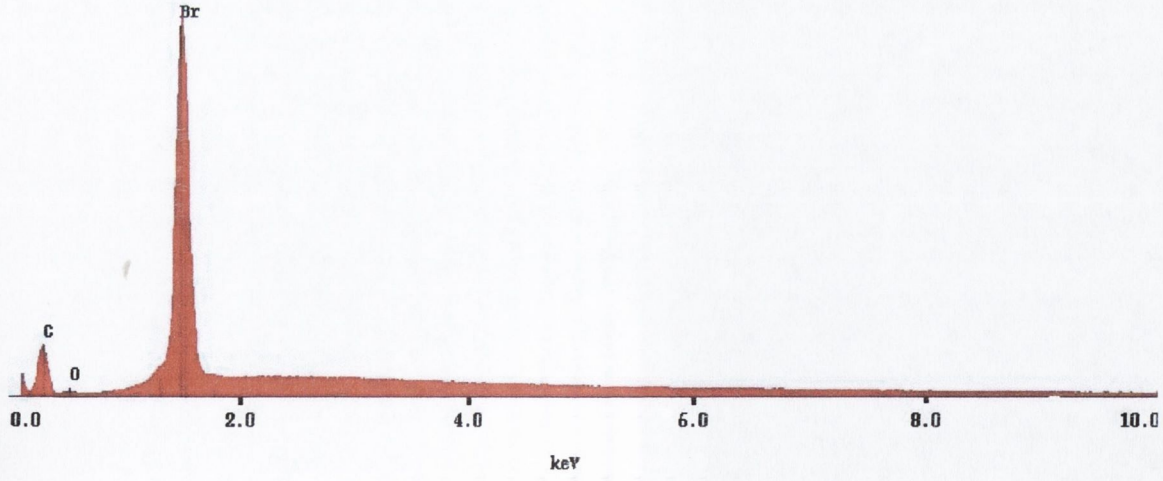

Figure 4 EDXA scan of a disc of ipratropium bromide starting material.

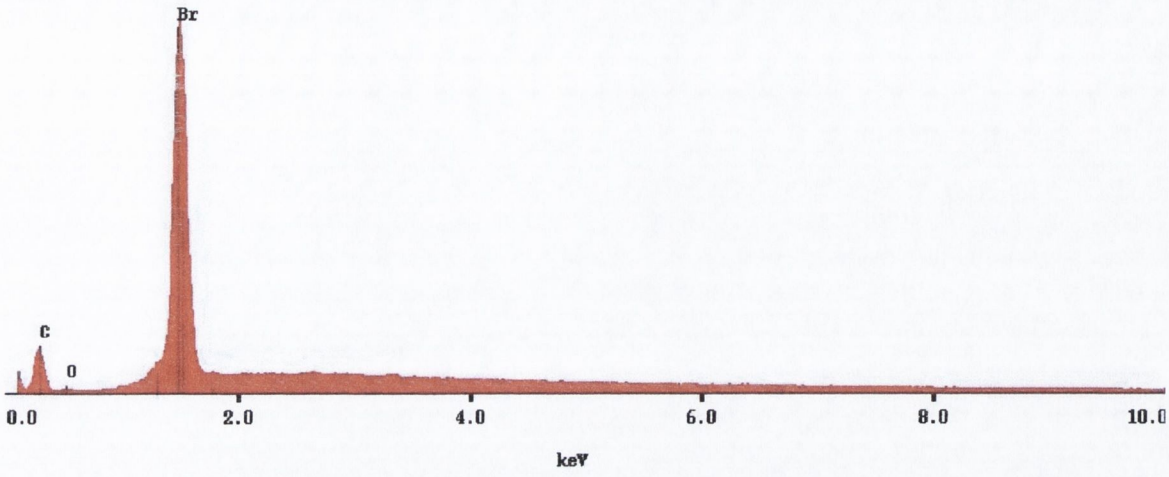

Figure 5 EDXA of a disc of ipratropium bromide spray dried from aqueous solution.

APPENDIX VIII

Figure 1 FTIR spectrum of salbutamol sulphate starting material.

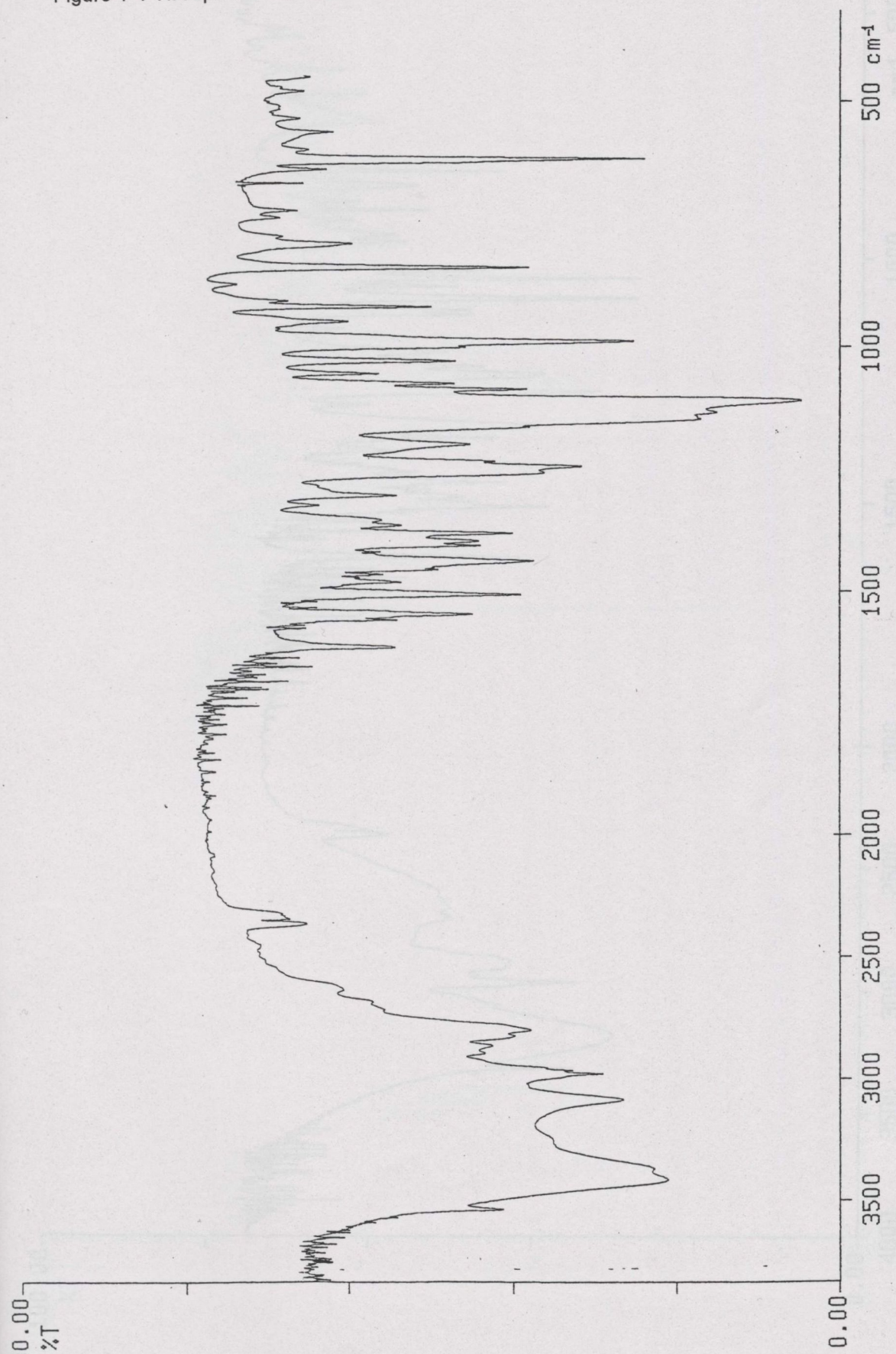

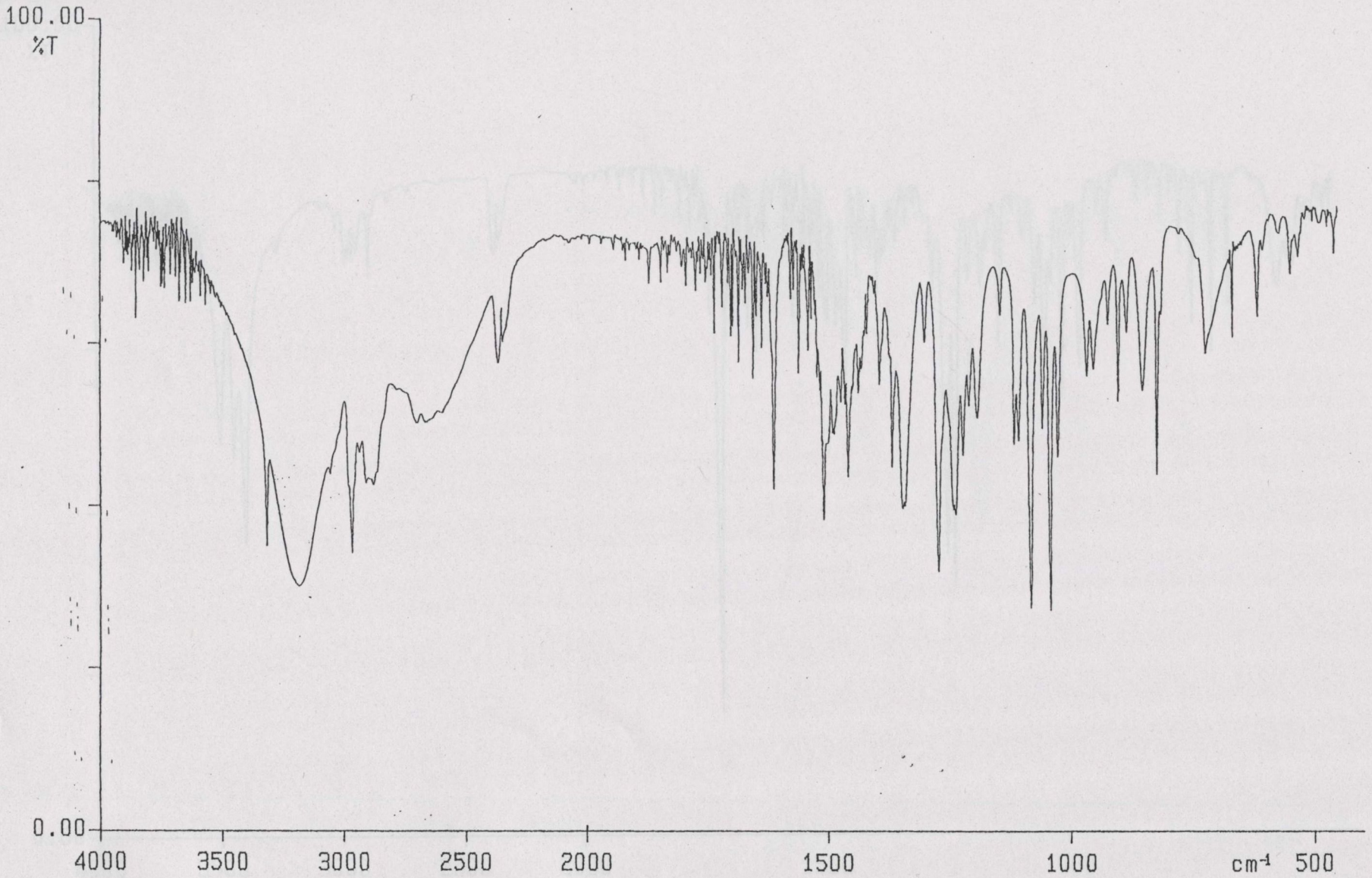

Figure 2 FTIR spectrum of salbutamol base starting material.

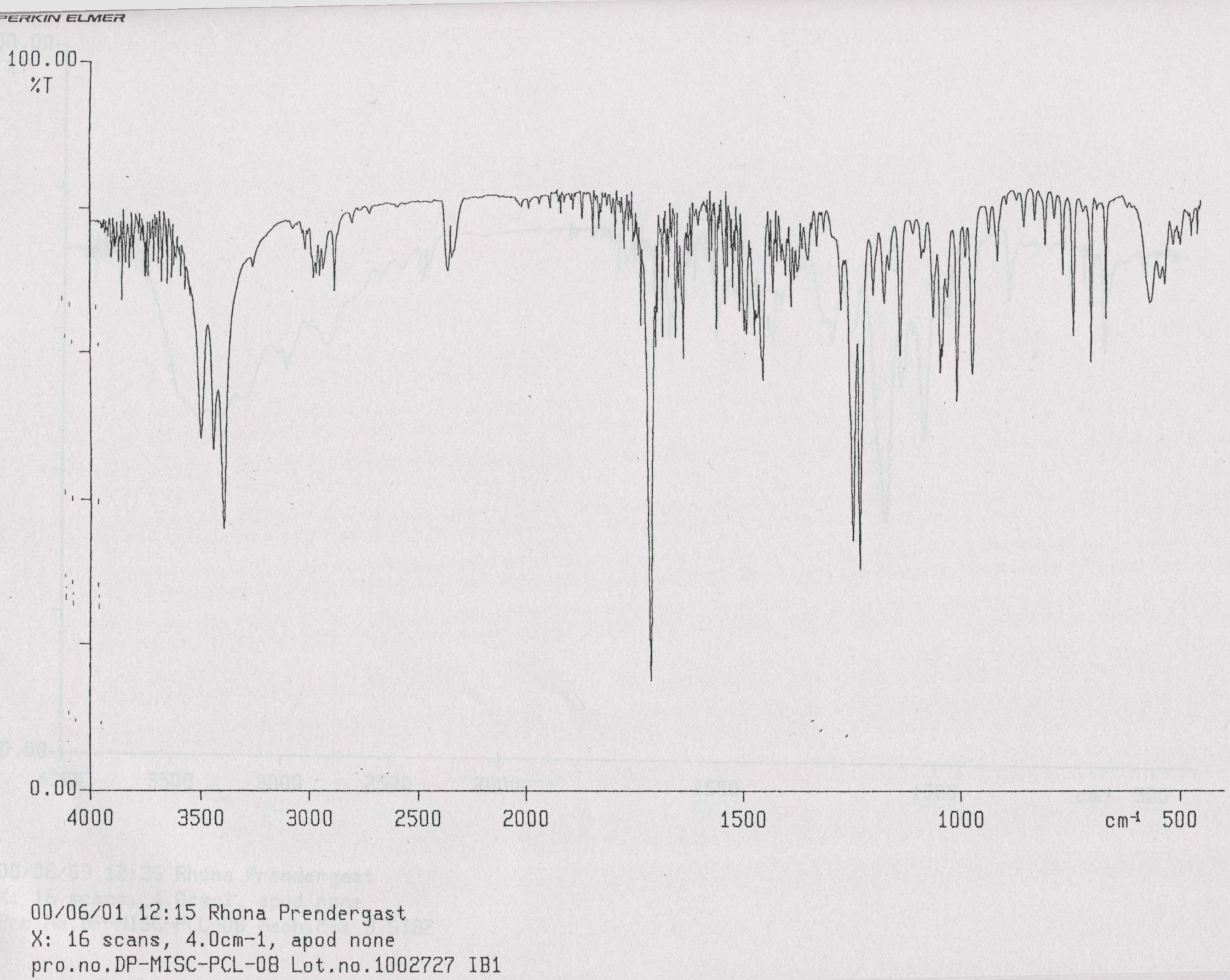

Figure 3 FTIR spectrum of ipratropium bromide monohydrate starting material.

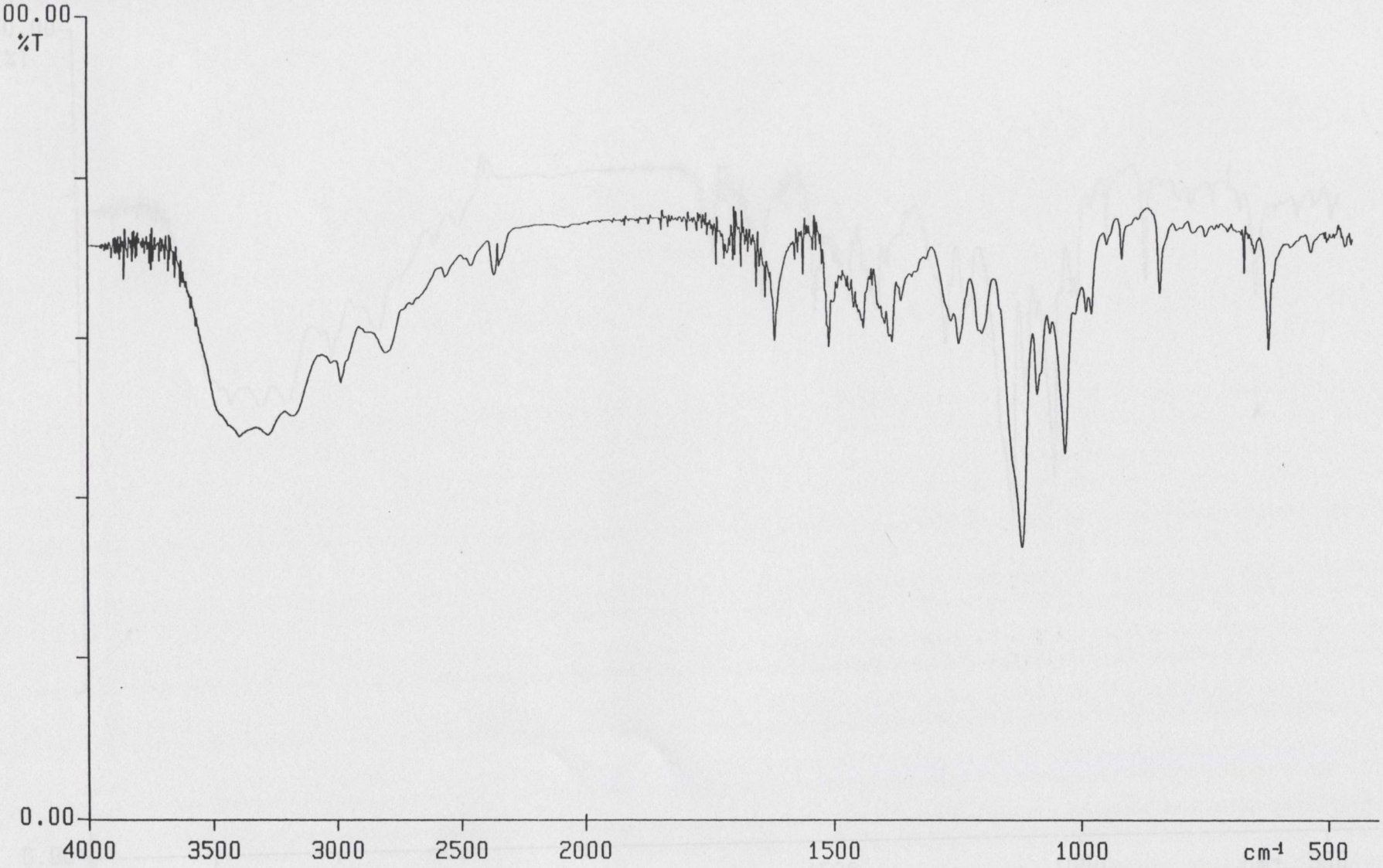

Figure 4 FTIR spectrum of a physical mix of salbutamol sulphate:ipratropium bromide 10:1.

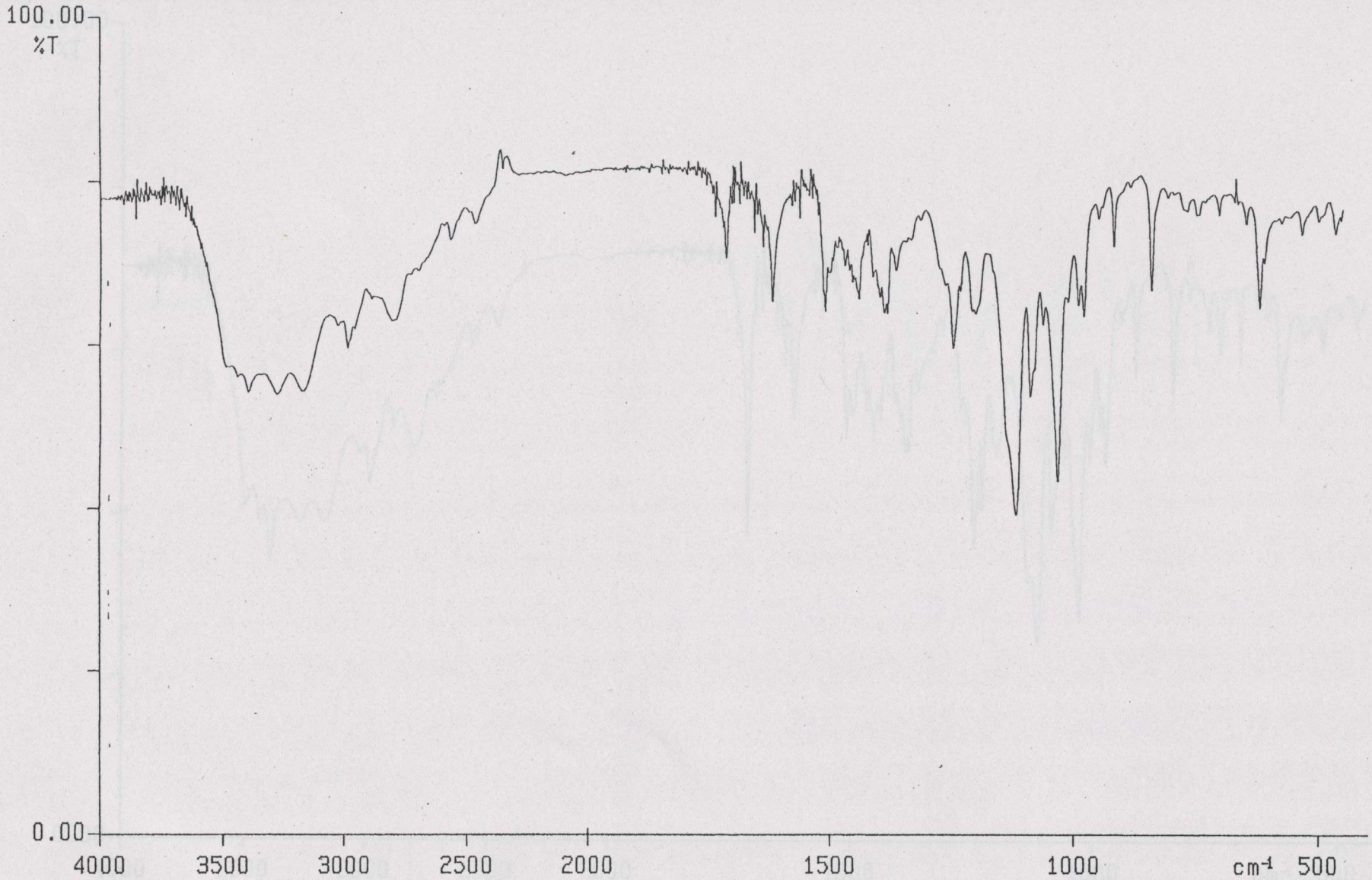

Figure 5 FTIR spectrum of a physical mix of salbutamol sulphate:ipratropium bromide 5:1.

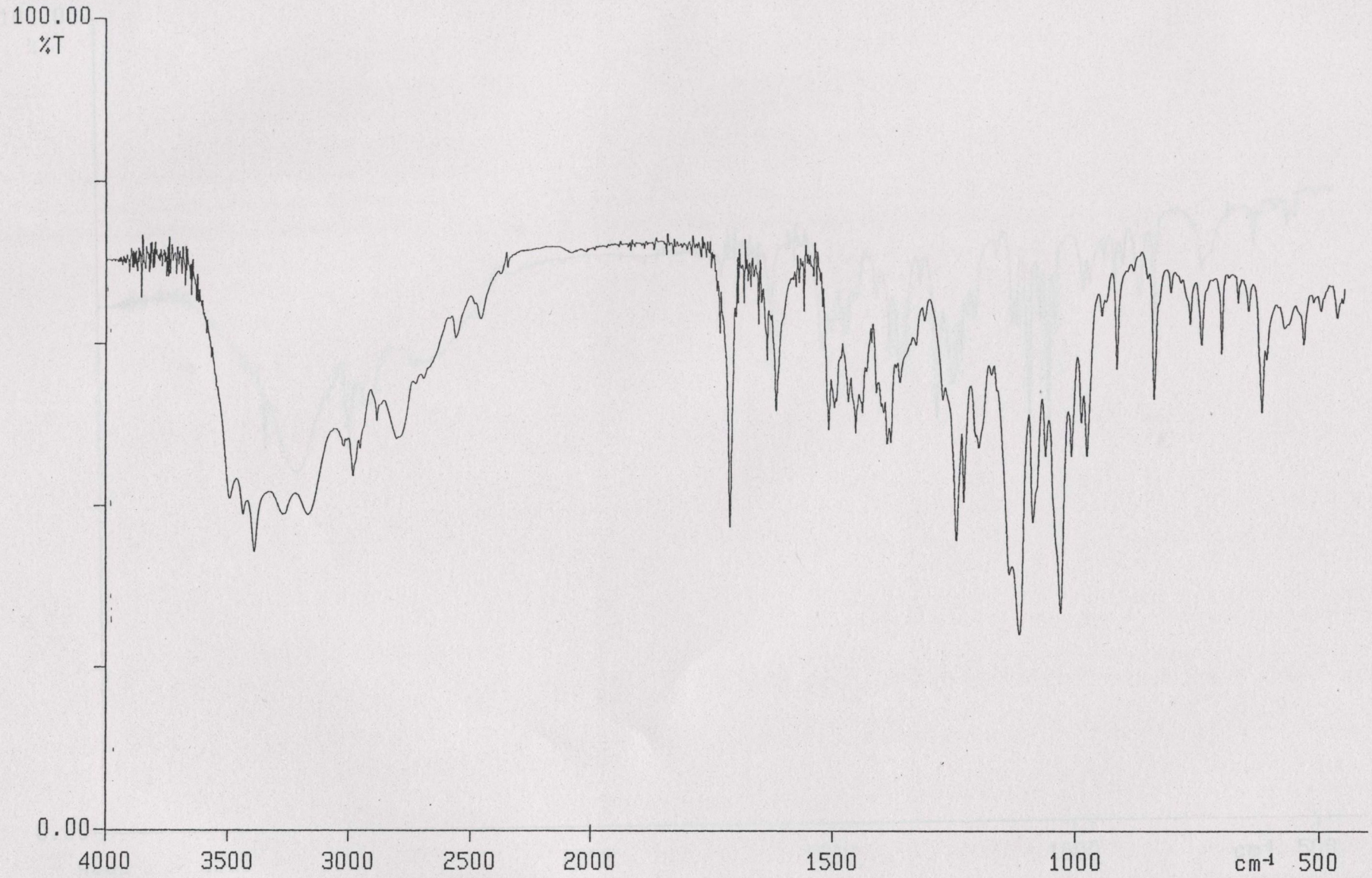

Figure 6 FTIR spectrum of a physical mix of salbutamol sulphate:ipratropium bromide 2:1.

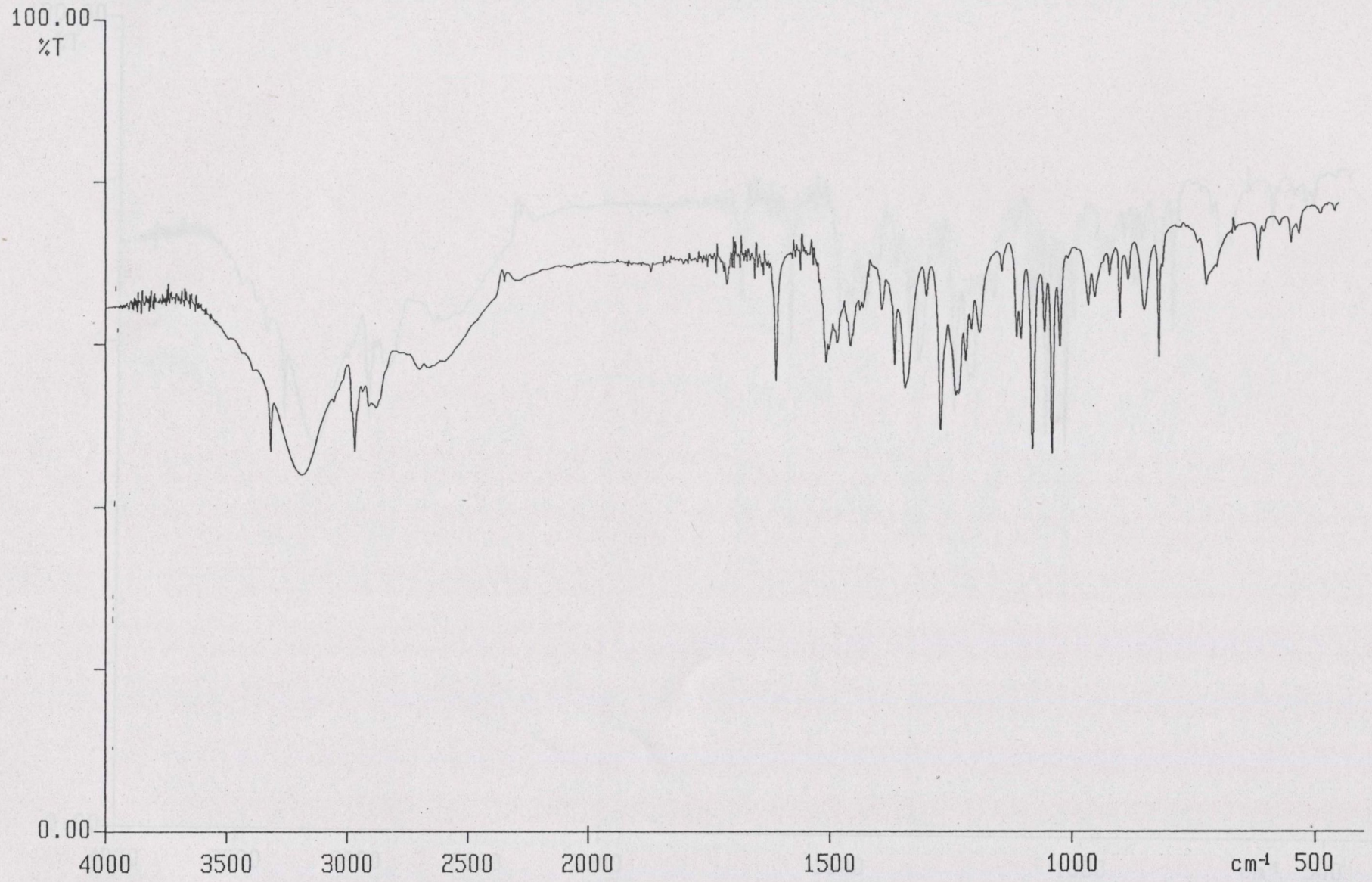

Figure 7 FTIR spectrum of a physical mix of salbutamol base:ipratropium bromide 10:1.

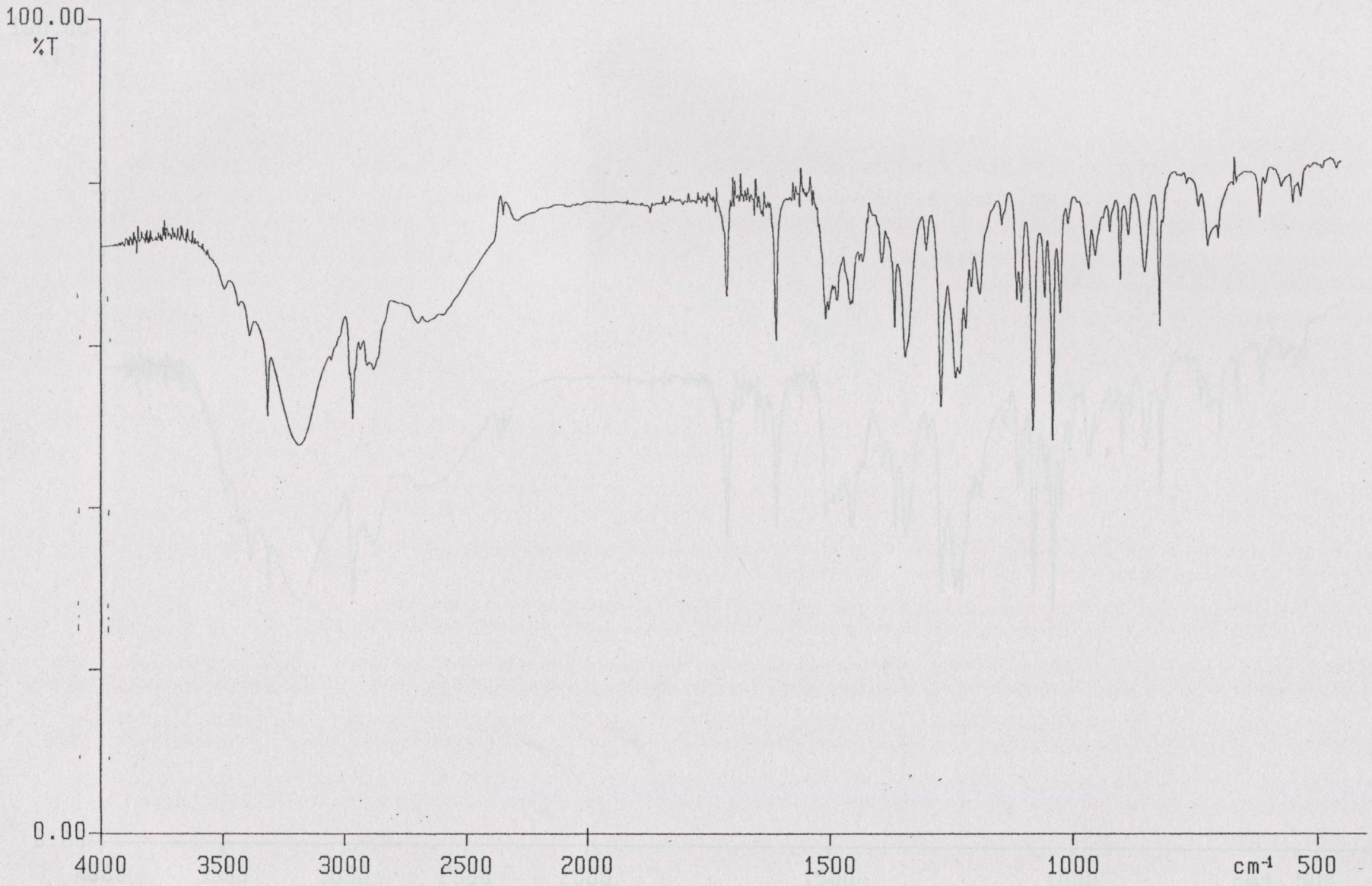

Figure 8 FTIR spectrum of a physical mix of salbutamol base:ipratropium bromide 5:1.

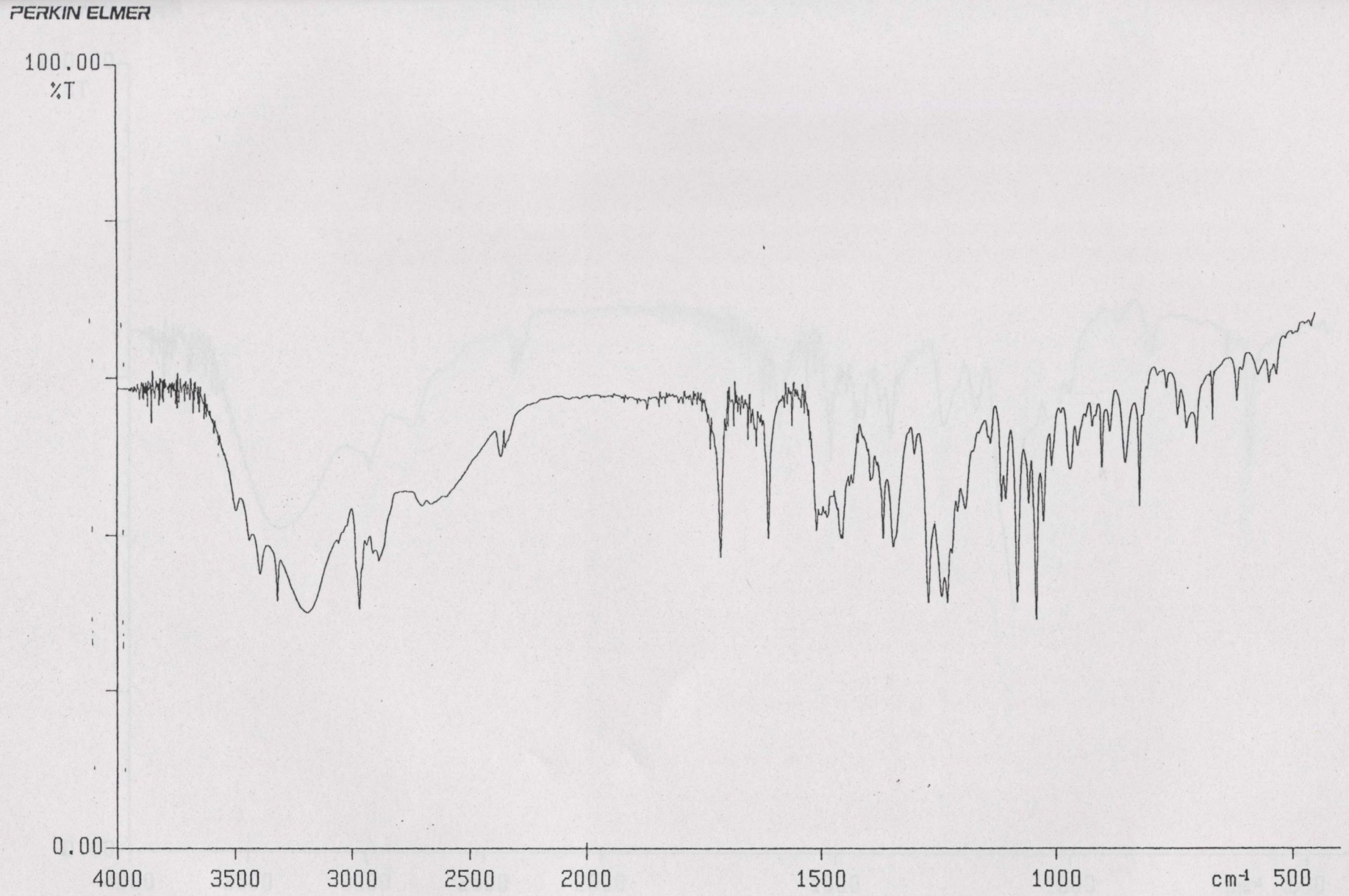

Figure 9 FTIR spectrum of a physical mix of salbutamol base:ipratropium bromide 2:1.

Figure 10 FTIR spectrum of salbutamol sulphate spray dried from aqueous solution.

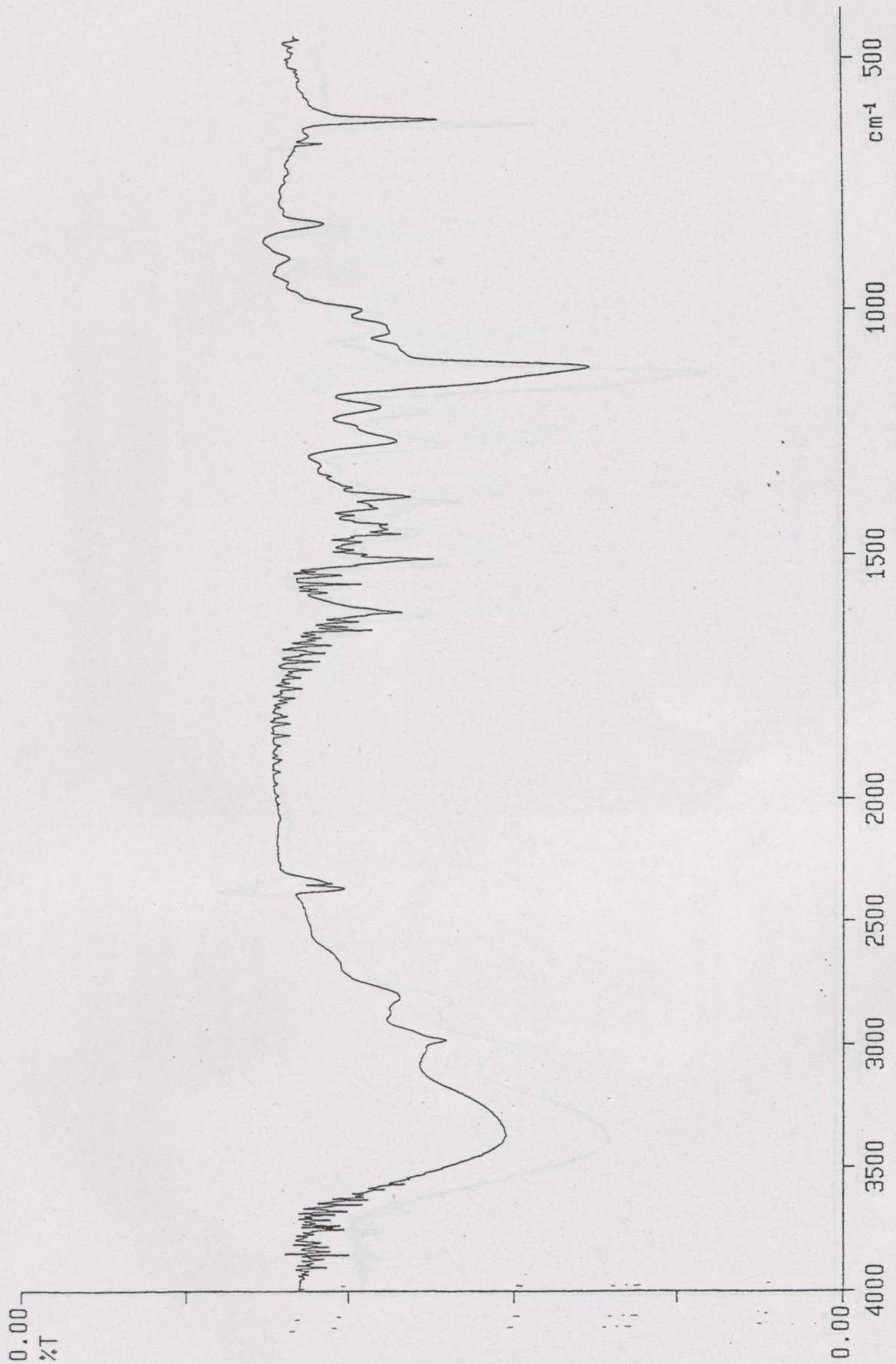

Figure 11 FTIR spectrum of salbutamol sulphate spray dried from ethanolic solution.

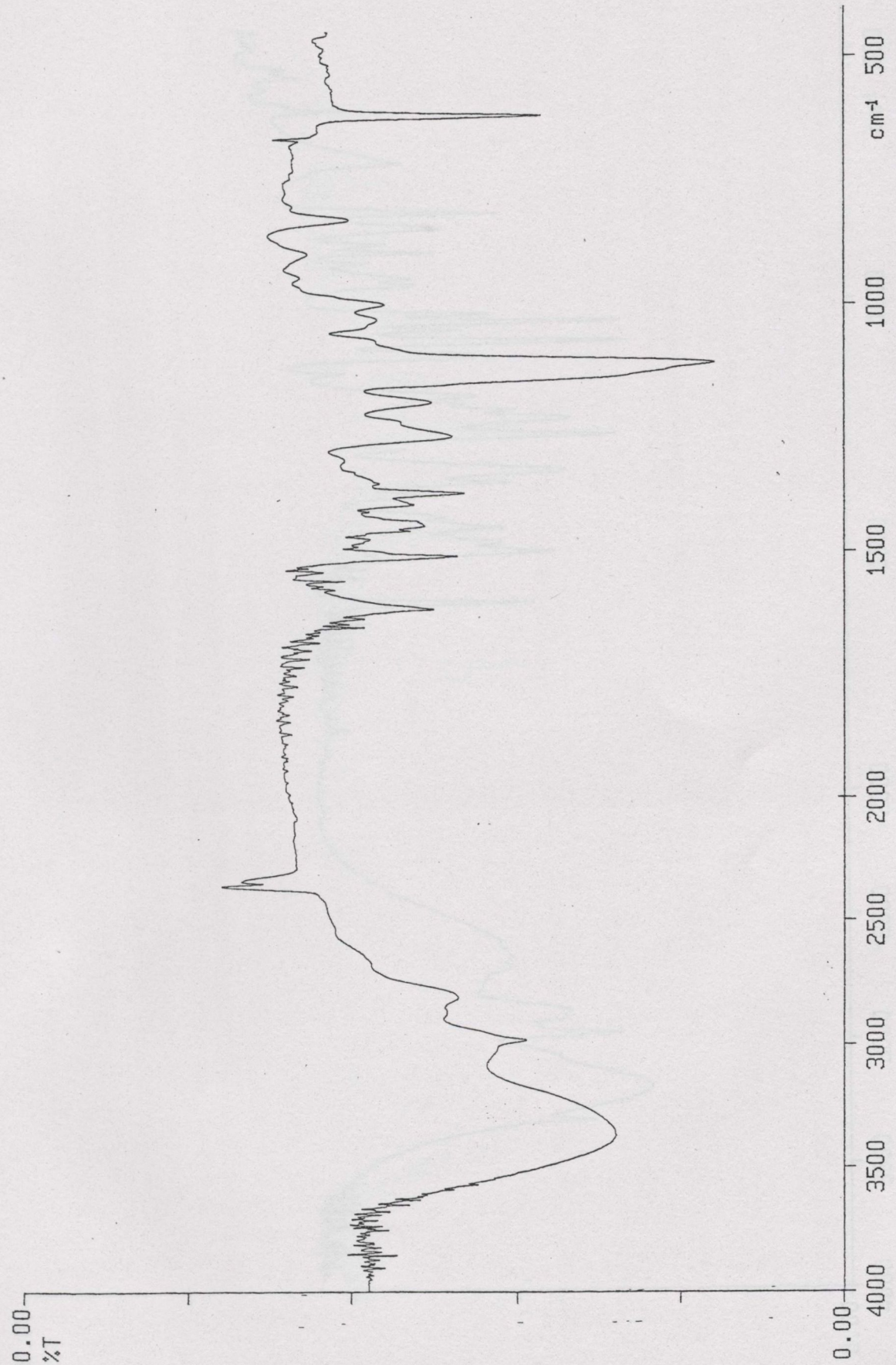

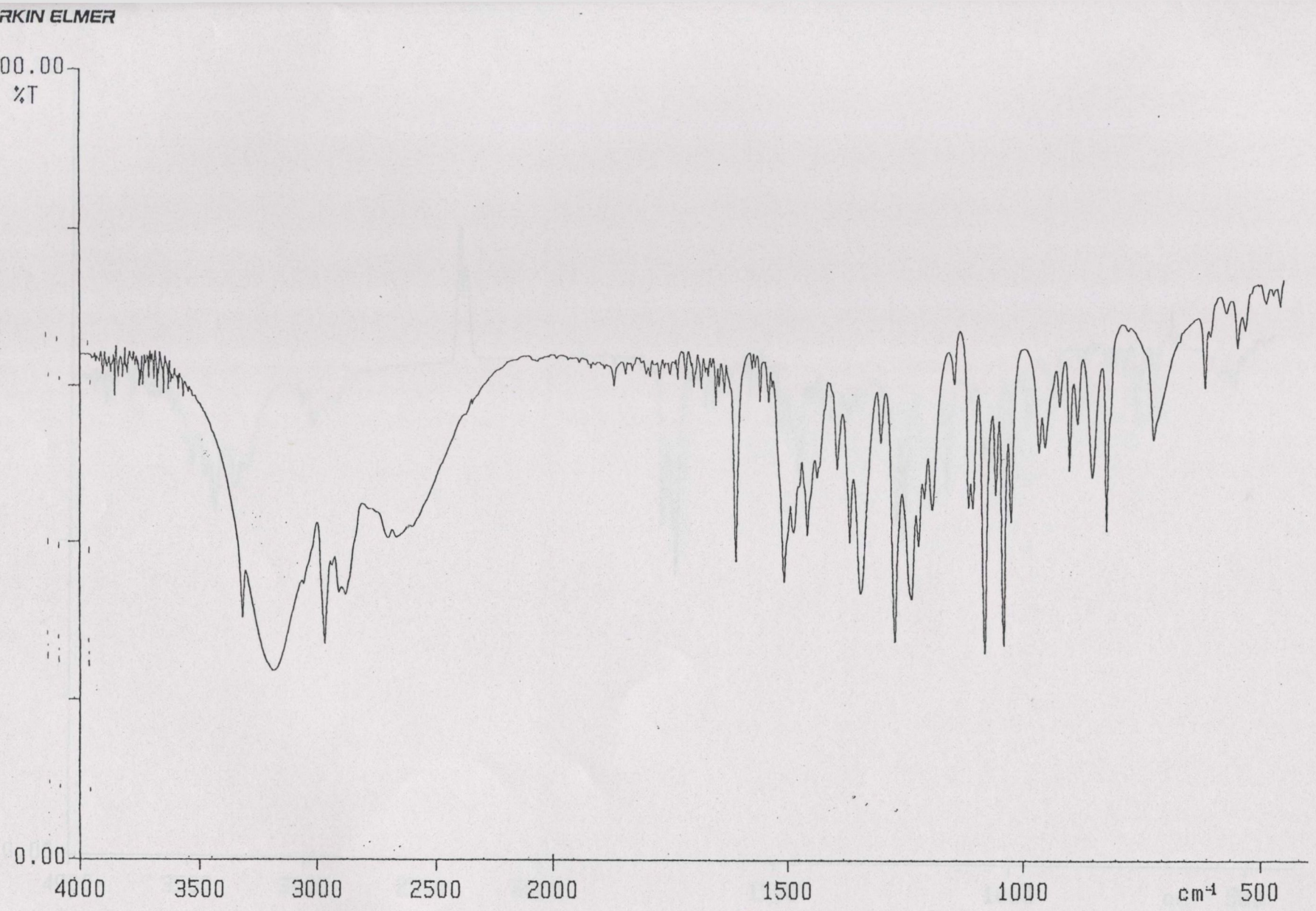

Figure 12 FTIR spectrum of spray dried salbutamol base.

Figure 13 FTIR spectrum of ipratropium bromide spray dried from aqueous solution.

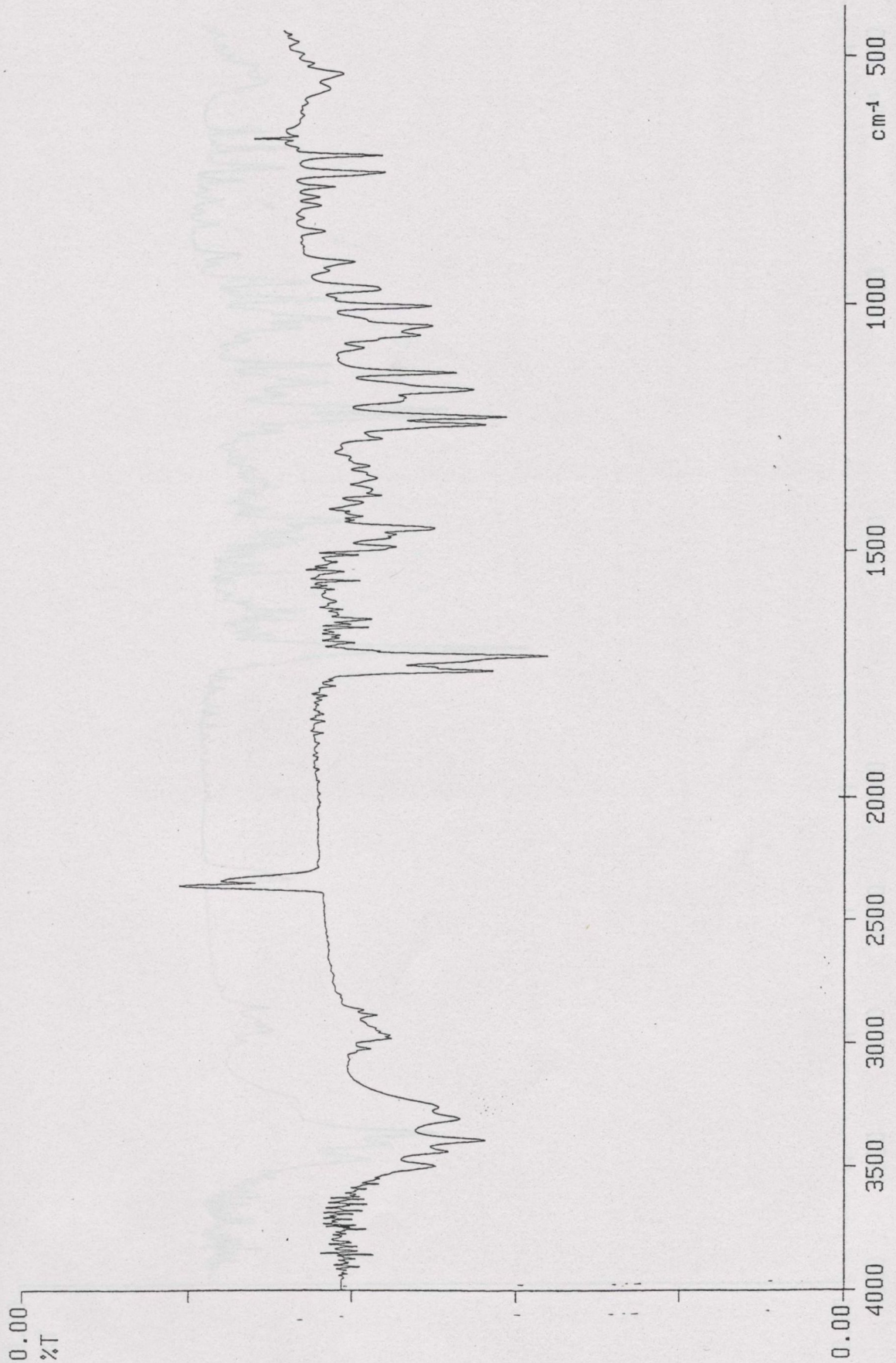

Figure 14 FTIR spectrum of ipratropium bromide spray dried from ethanolic solution.

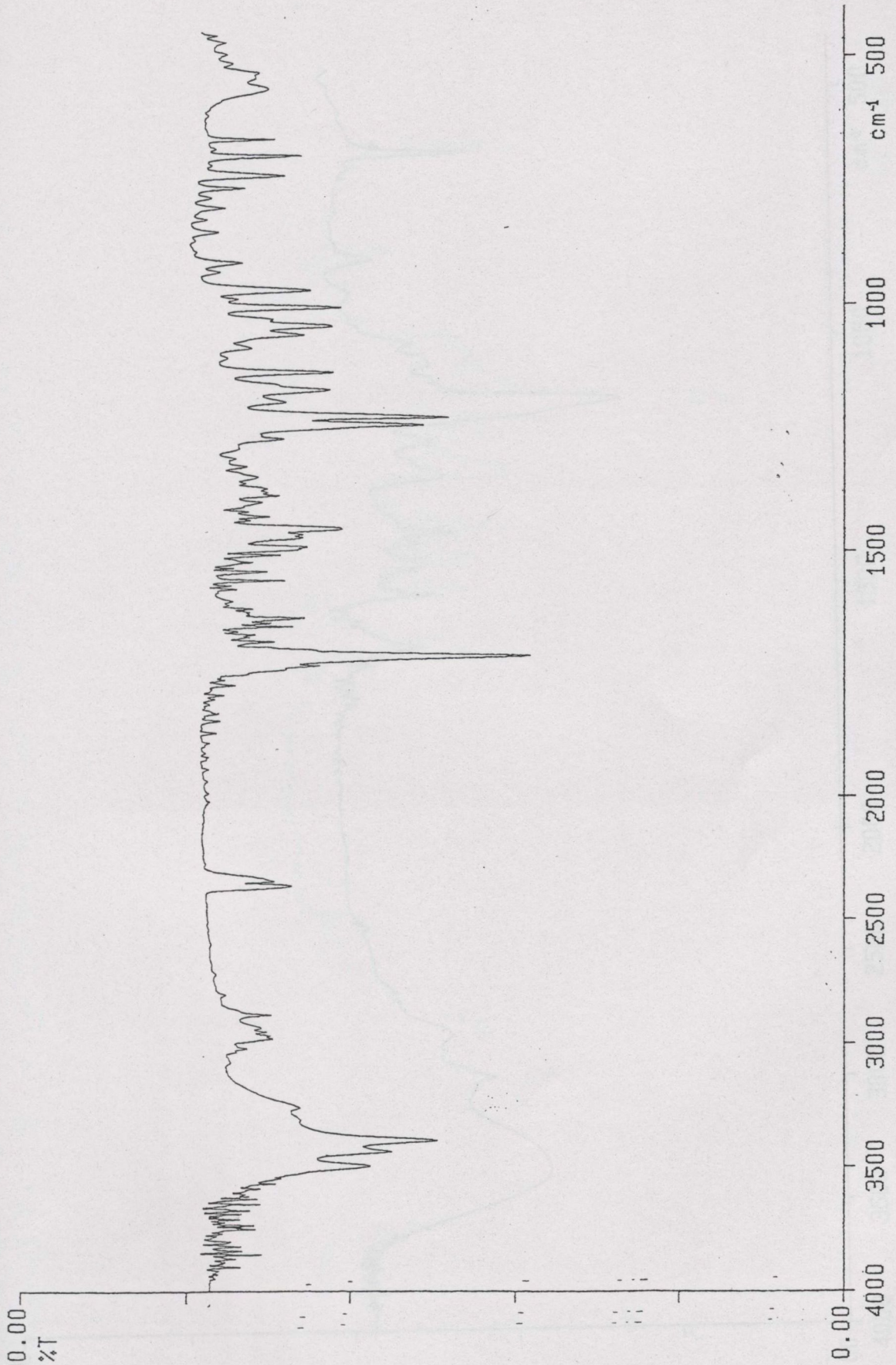

Figure 15 FTIR spectrum of salbutamol sulphate:ipratropium bromide 10:1 spray dried from aqueous solution.

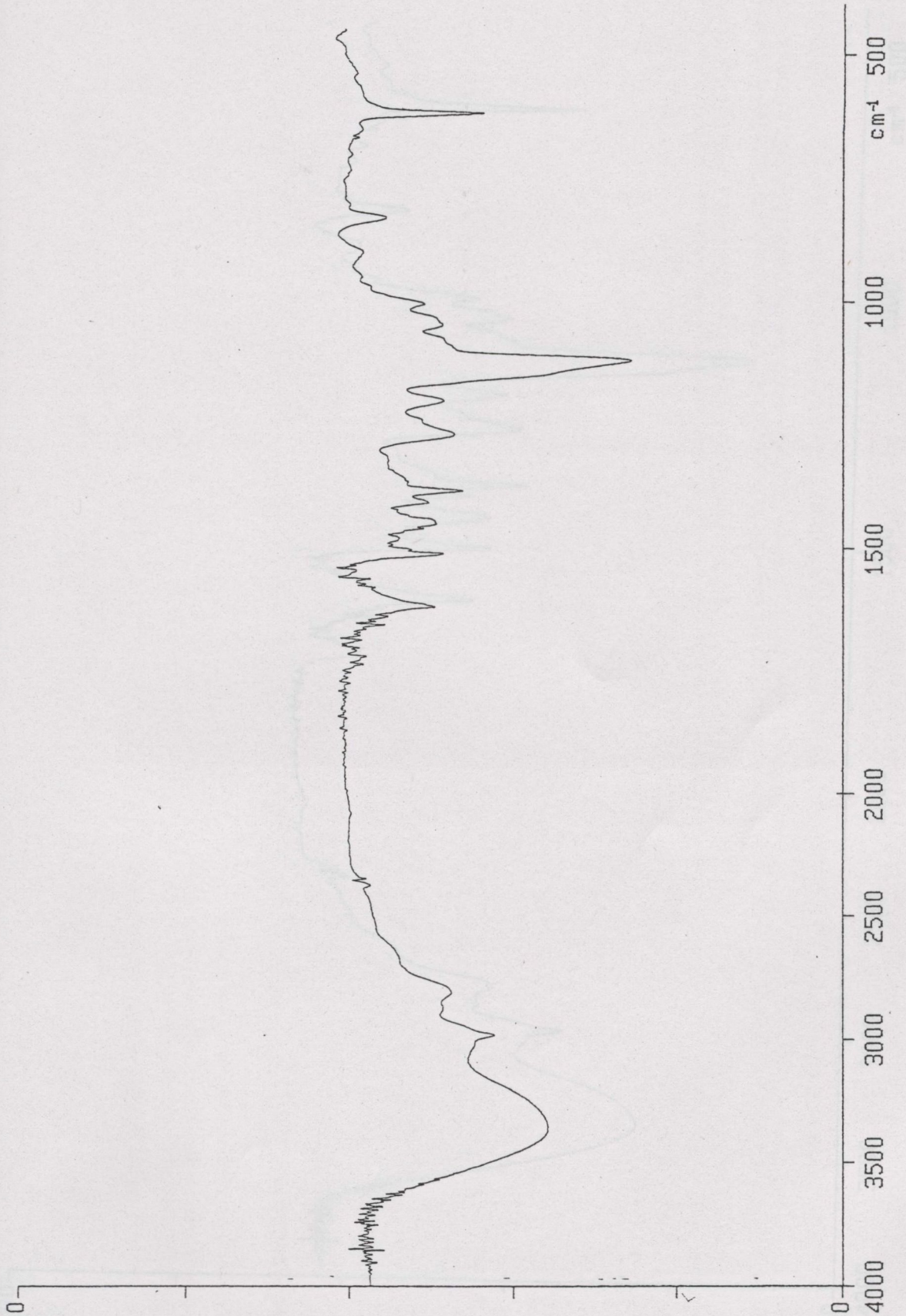

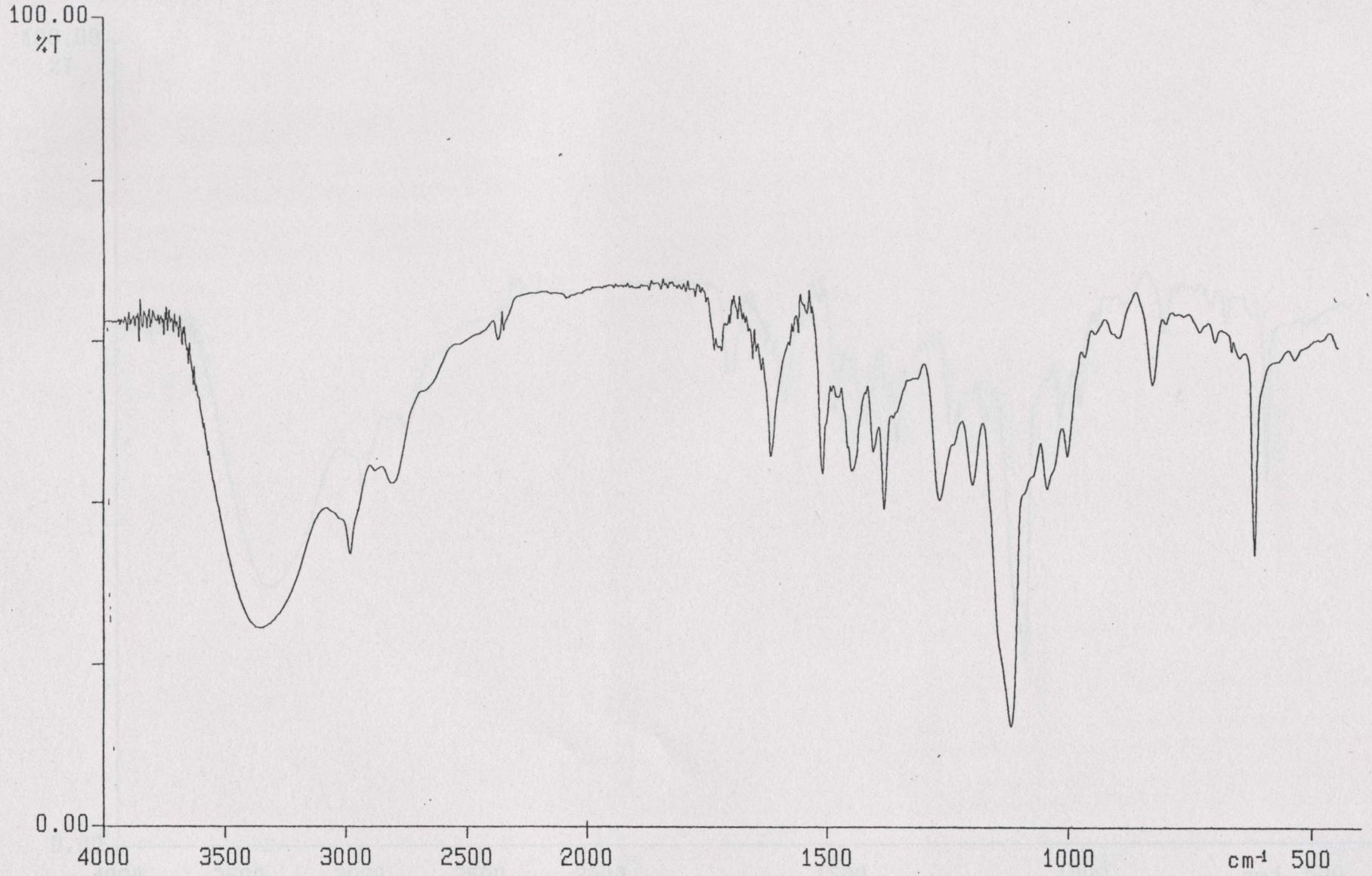

00/07/18 14:42 Rhona Prendergast
X: 16 scans, 4.0cm-1
Pro.No.DP-MISC-PCL-08,Ratio5:1,SDSS:IBW2

Figure 16 FTIR spectrum of salbutamol sulphate:ipratropium bromide 5:1 spray dried from aqueous solution

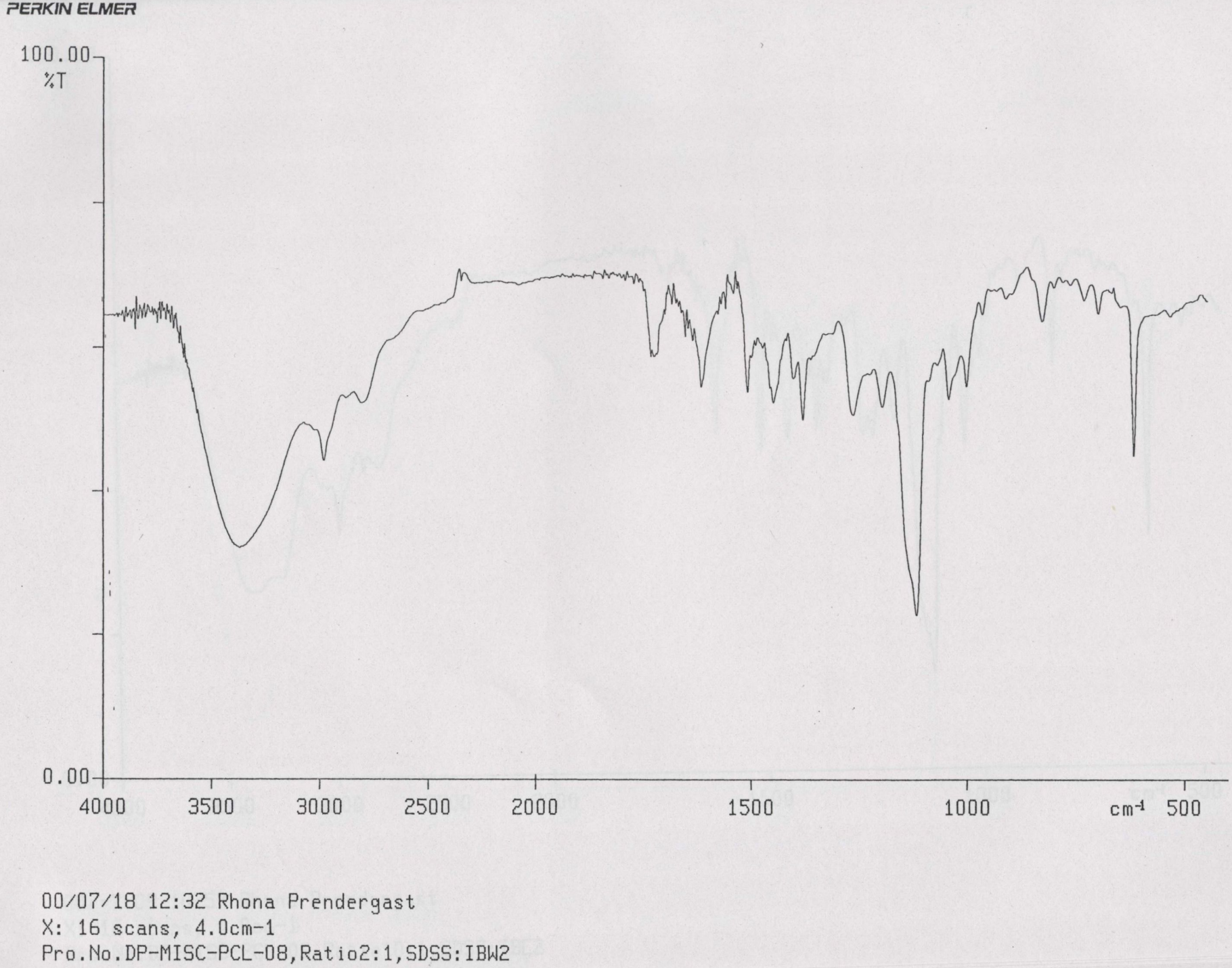

Figure 17 FTIR spectrum of salbutamol sulphate:ipratropium bromide 2:1 spray dried from aqueous solution.

Figure 18 FTIR spectrum of salbutamol sulphate:ipratropium bromide 10:1 spray dried from ethanolic solution.

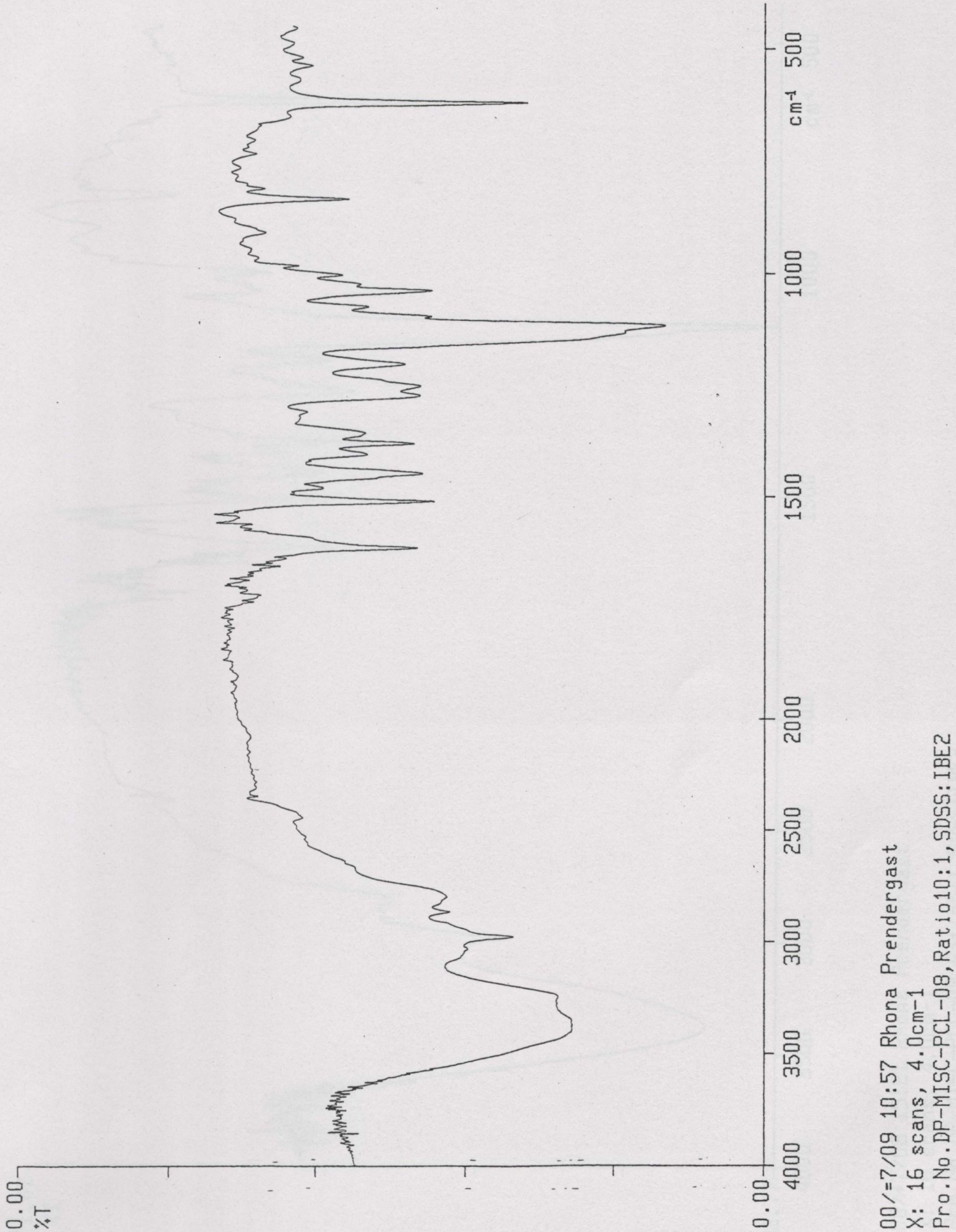

Figure 19 FTIR spectrum of salbutamol sulphate:ipratropium bromide 5:1 spray dried from ethanolic solution.

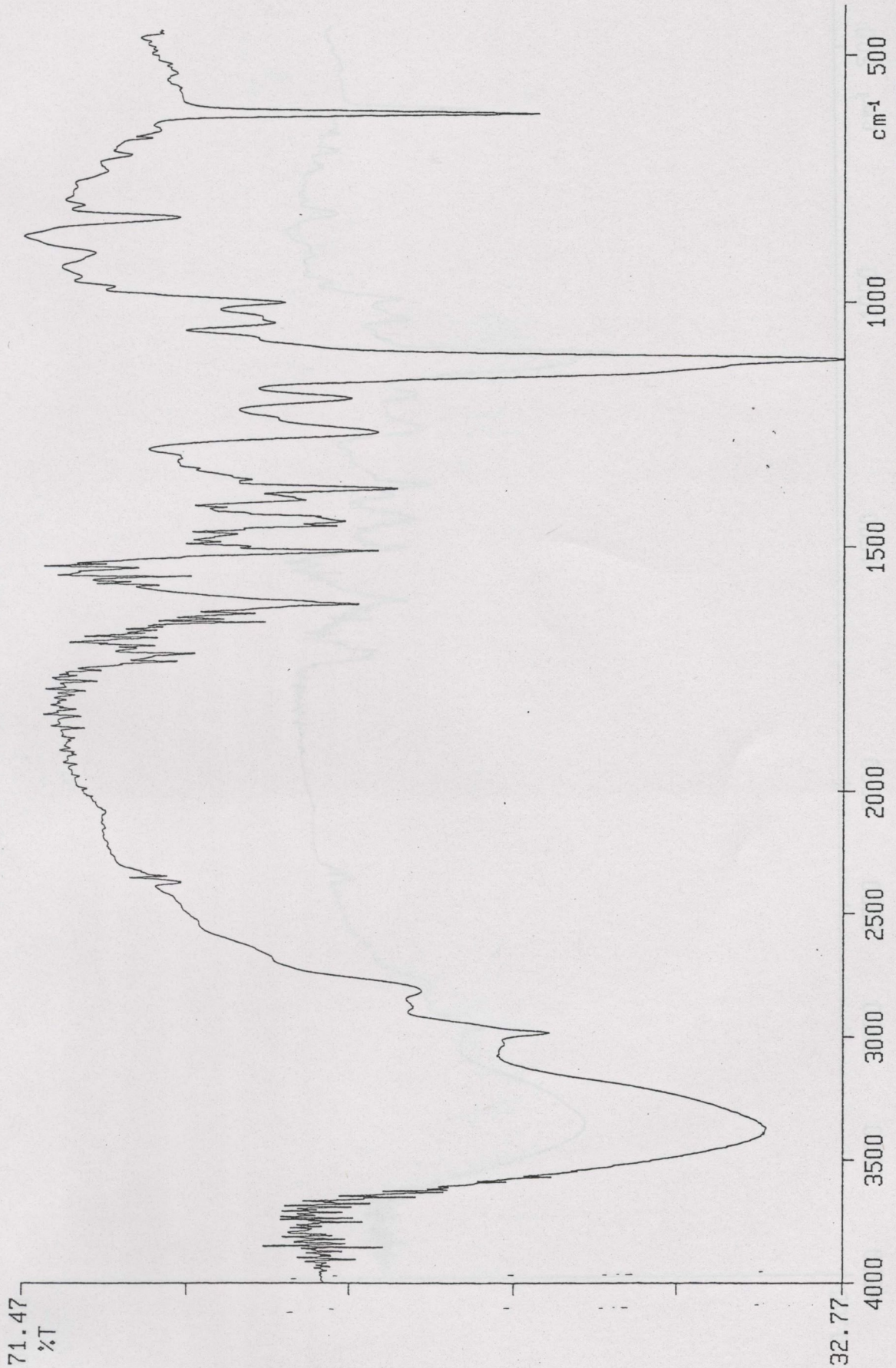

Figure 20 FTIR spectrum of salbutamol sulphate:ipratropium bromide 2:1 spray dried from ethanolic solution.

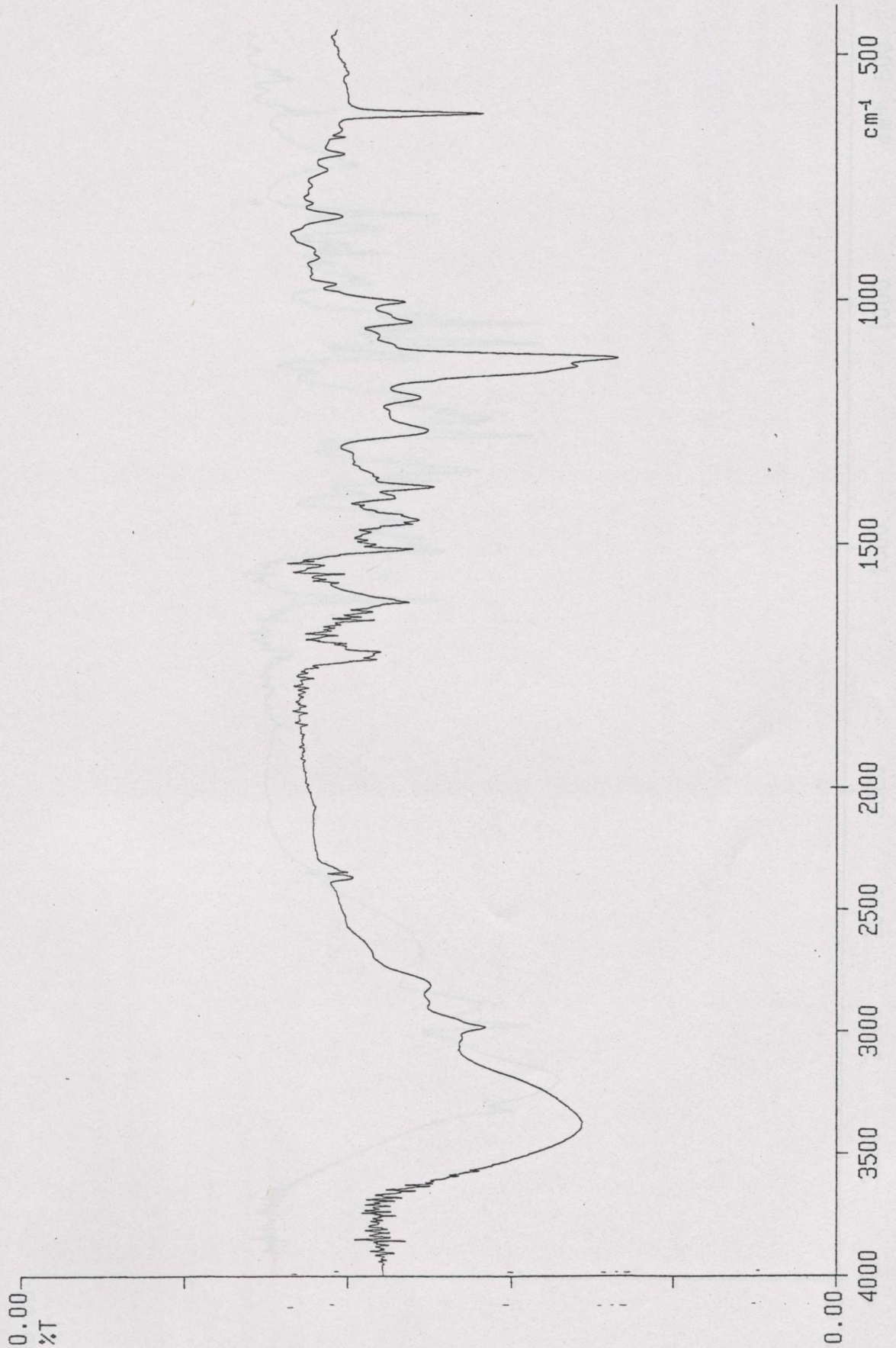

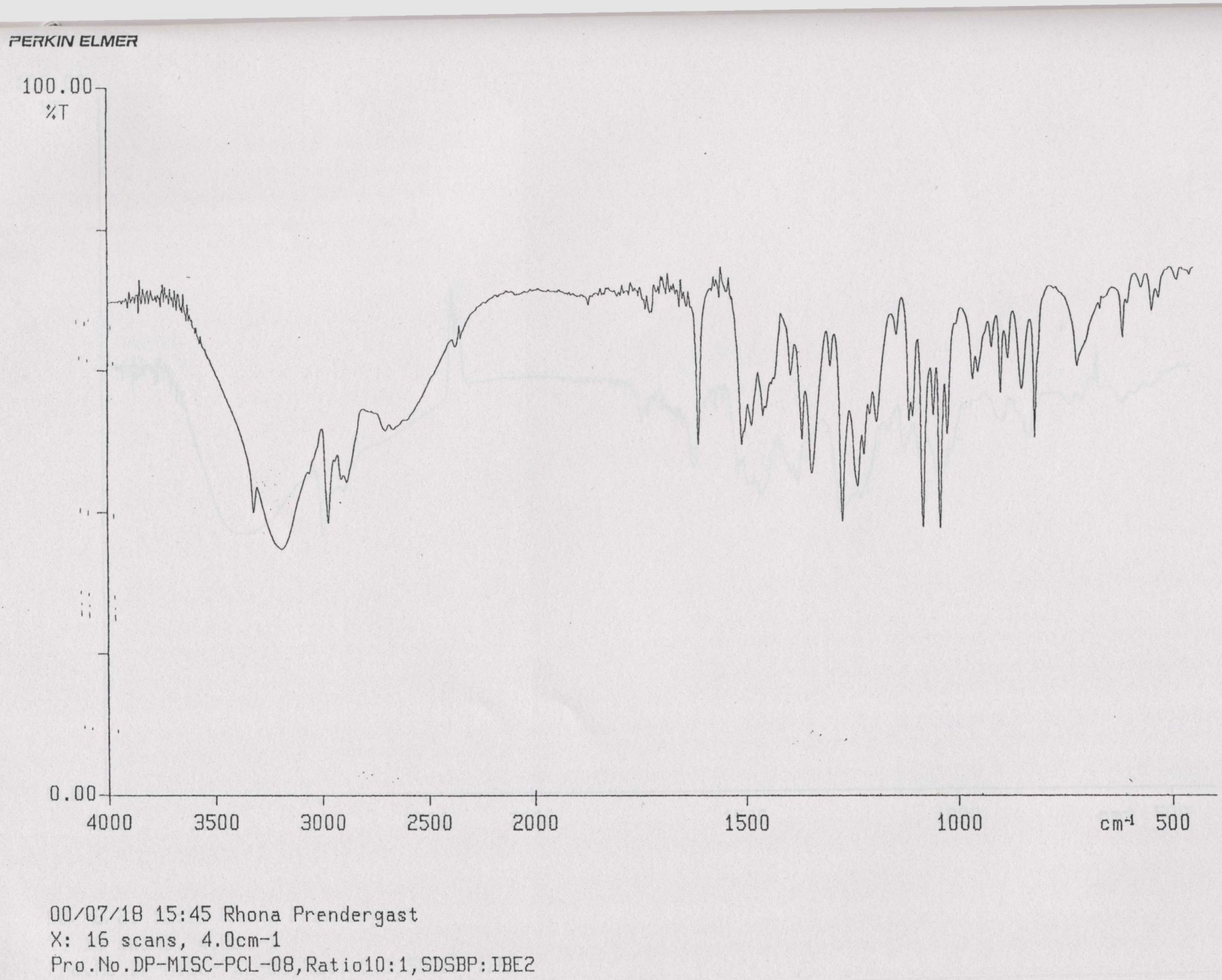

Figure 21 FTIR spectrum of spray dried salbutamol base:ipratropium bromide 10:1.

Figure 22 FTIR spectrum of spray dried salbutamol base:ipratropium bromide 5:1.

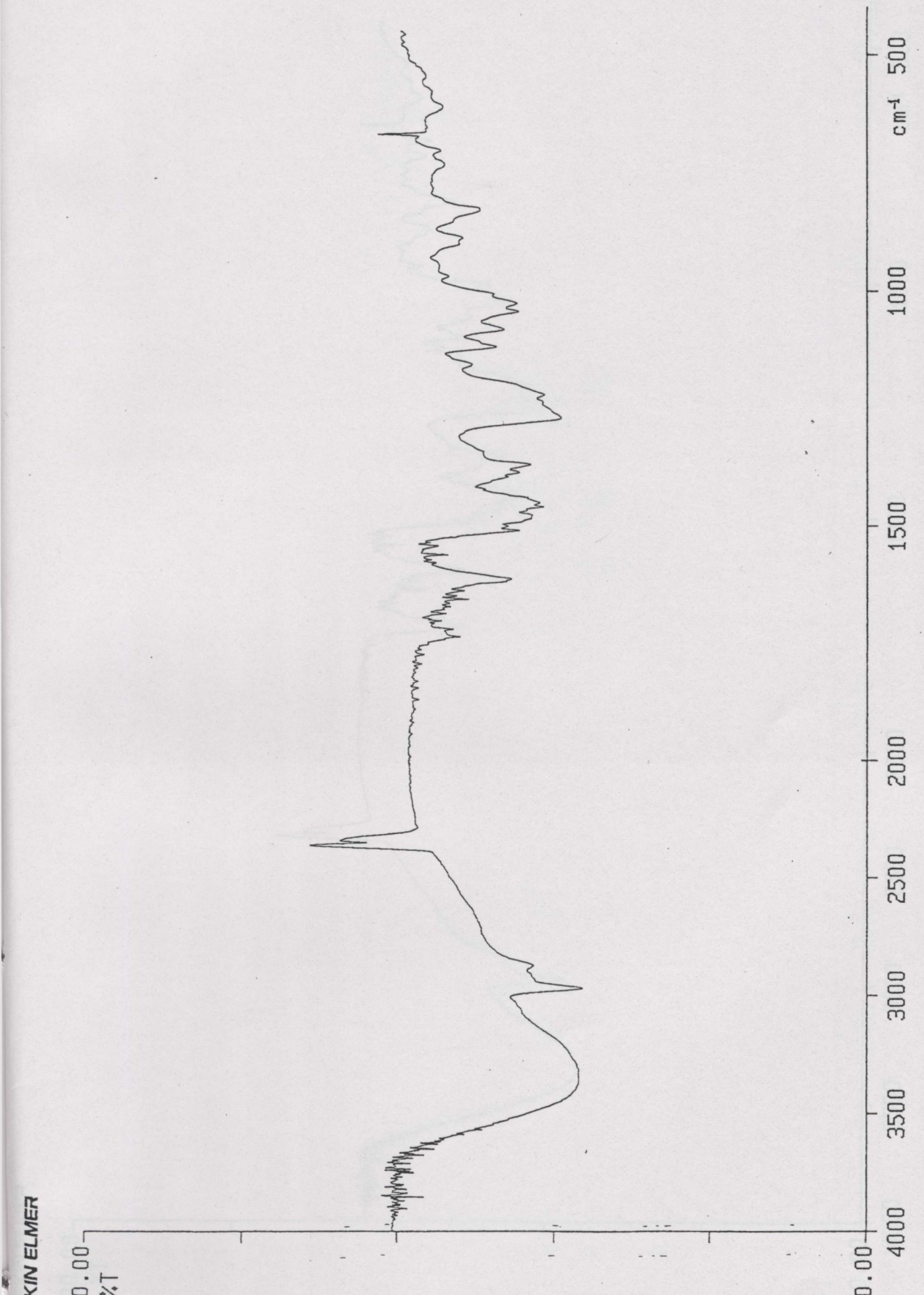

Figure 23 FTIR spectrum of spray dried salbutamol base:ipratropium bromide 2:1.

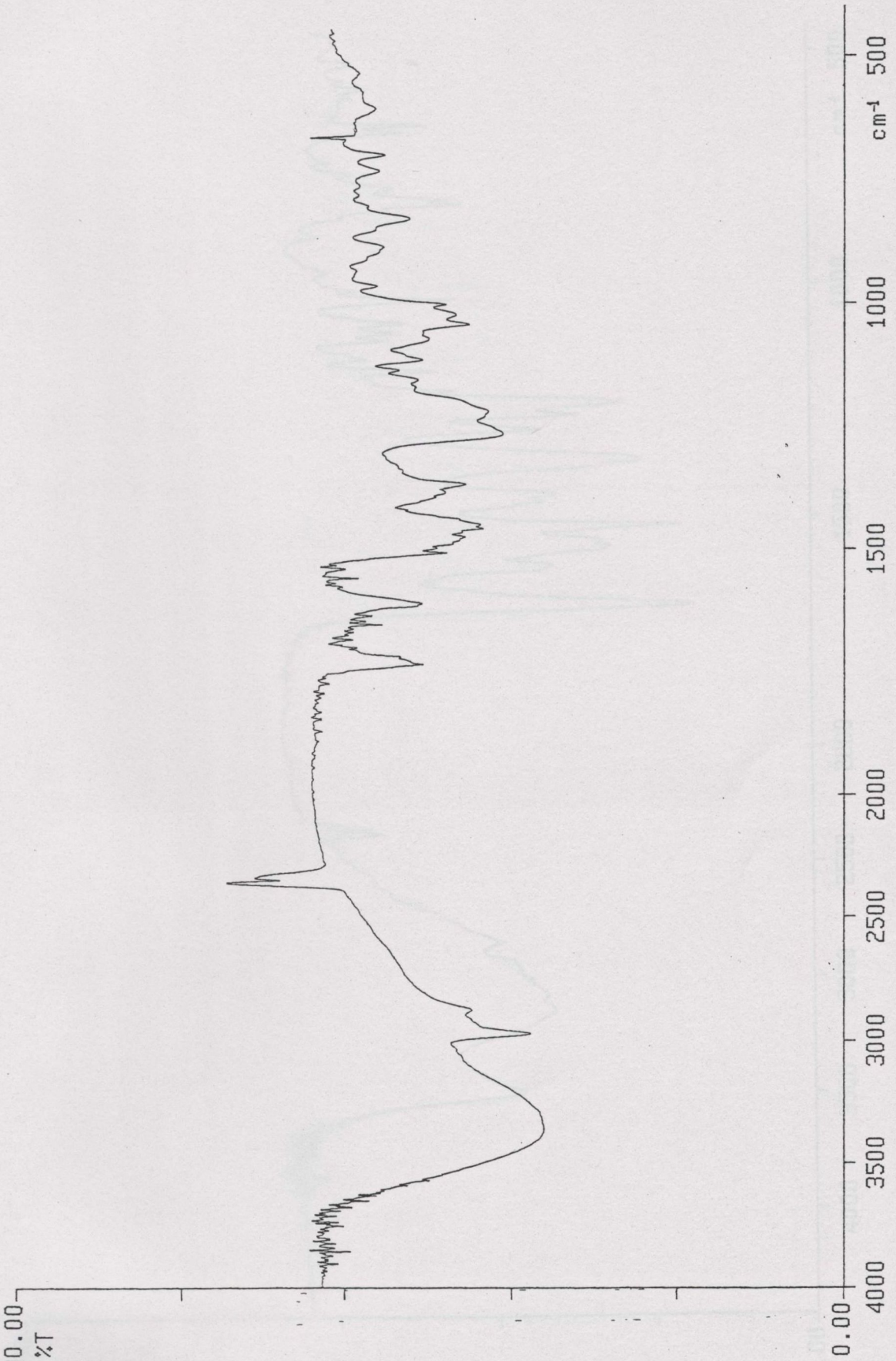

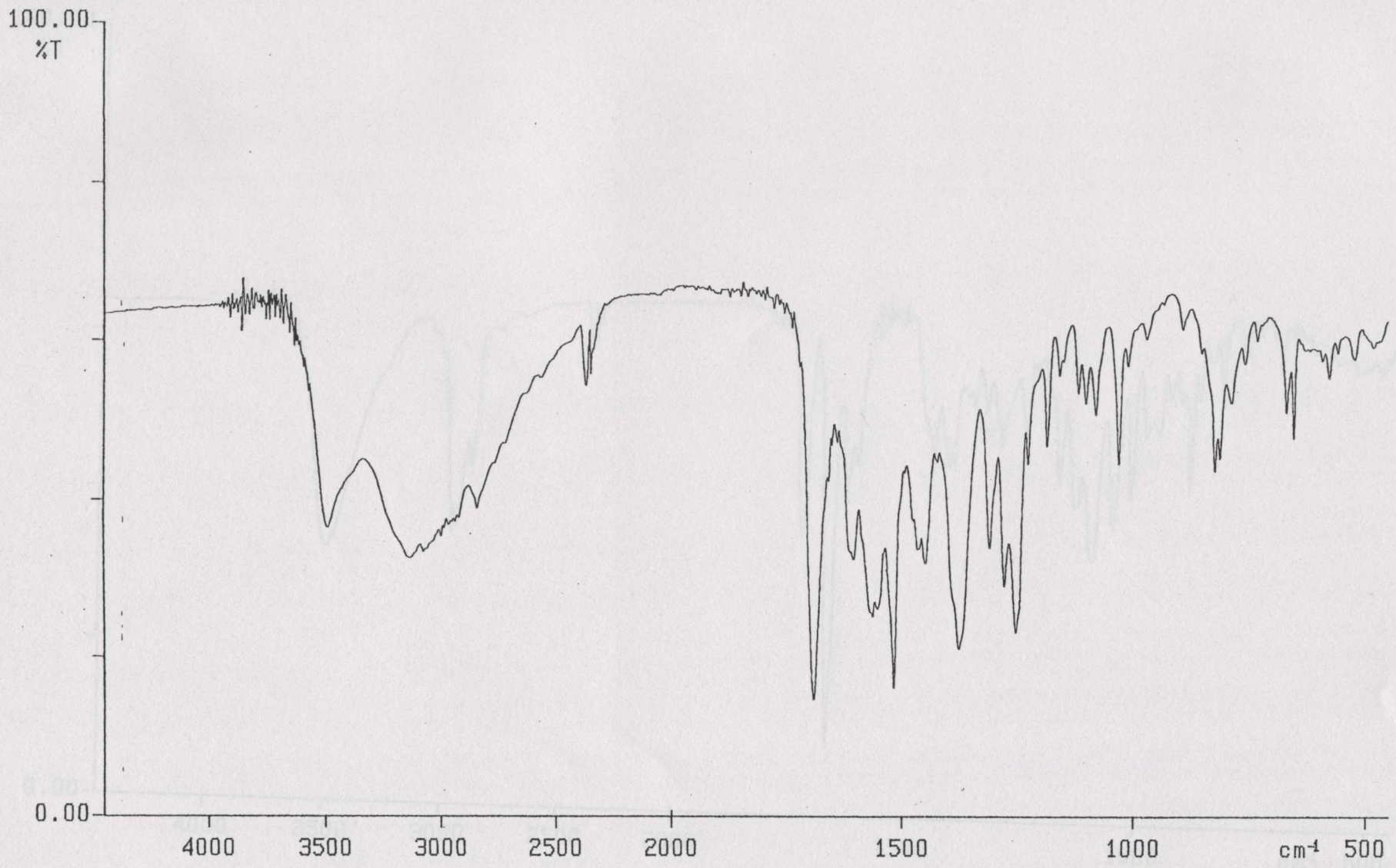

Figure 24 FTIR spectrum of formoterol fumarate dihydrate starting material.

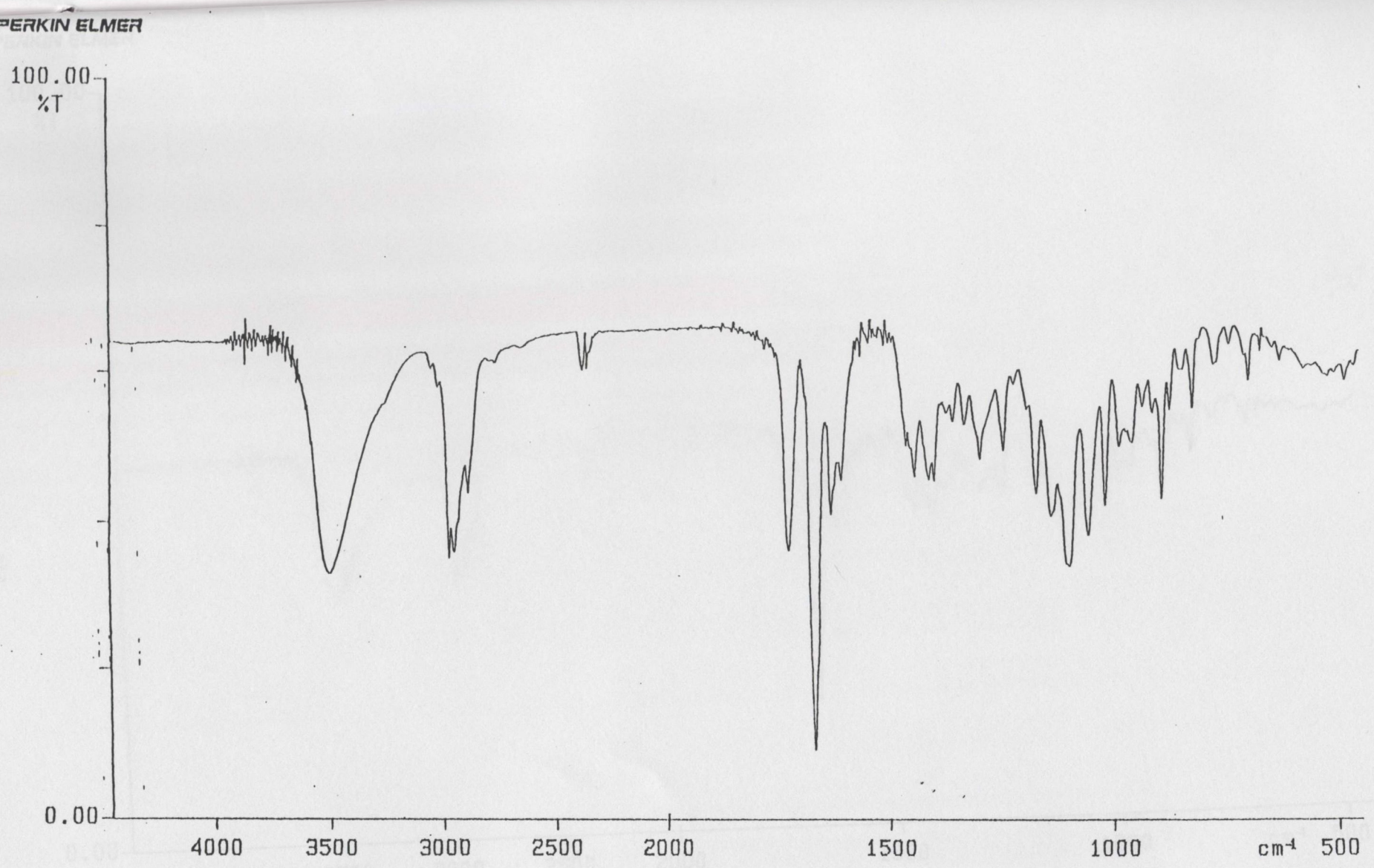

Figure 25 FTIR spectrum of budesonide starting material.

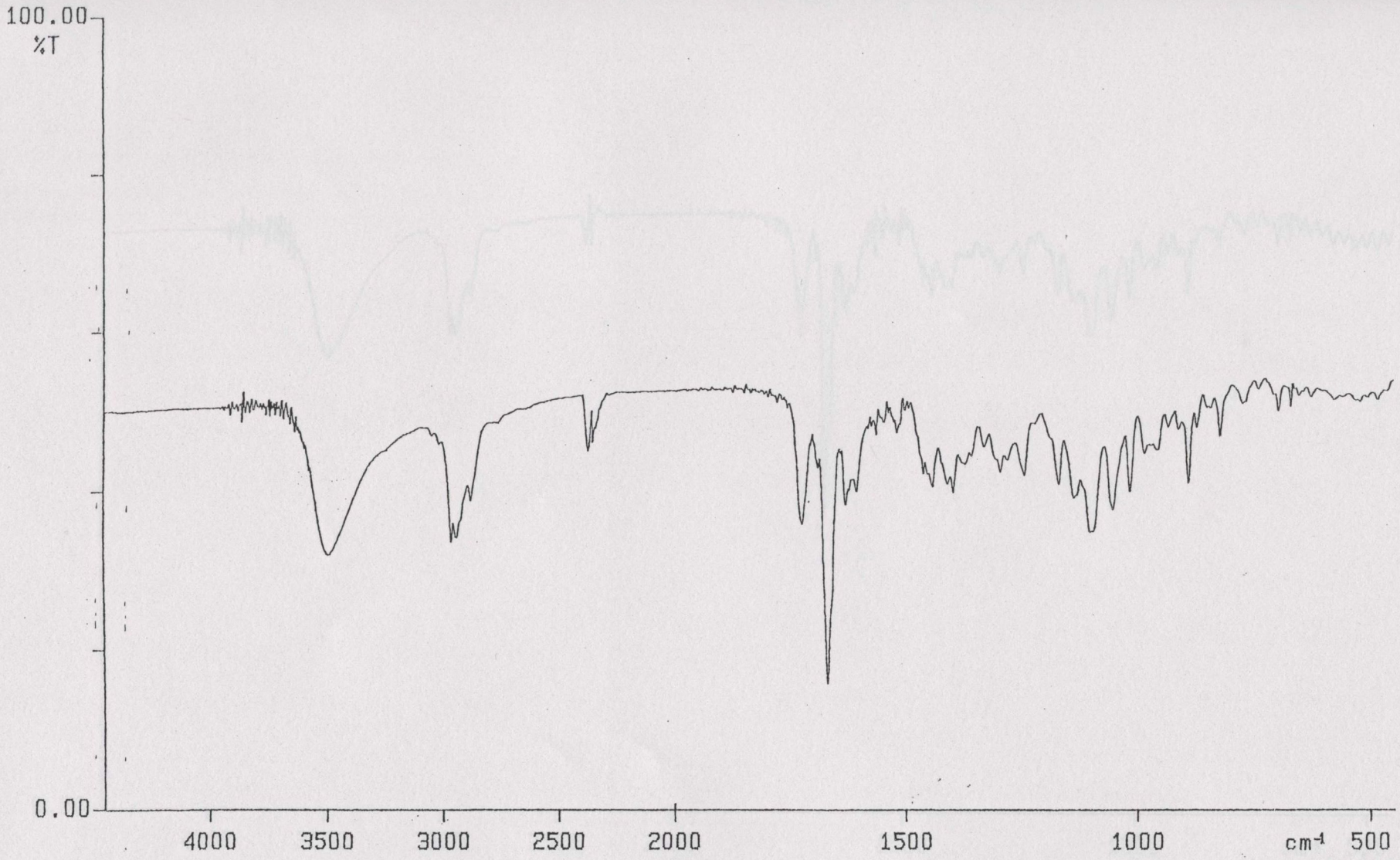

Figure 26 FTIR spectrum of a physical mix of formoterol fumarate dihydrate:budesonide 6:100.

Figure 27 FTIR spectrum of a physical mix of formoterol fumarate dihydrate:budesonide 6:400.

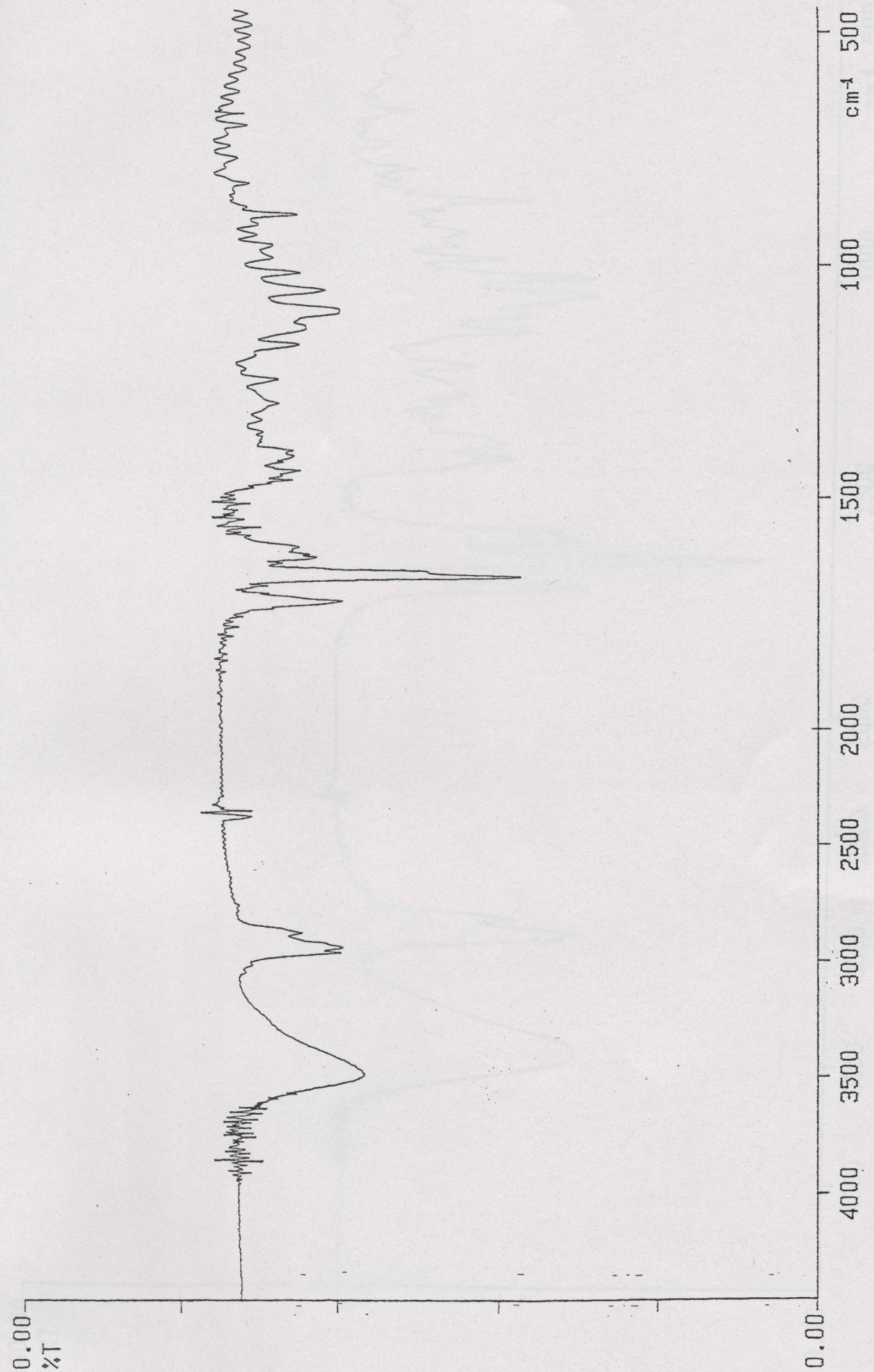

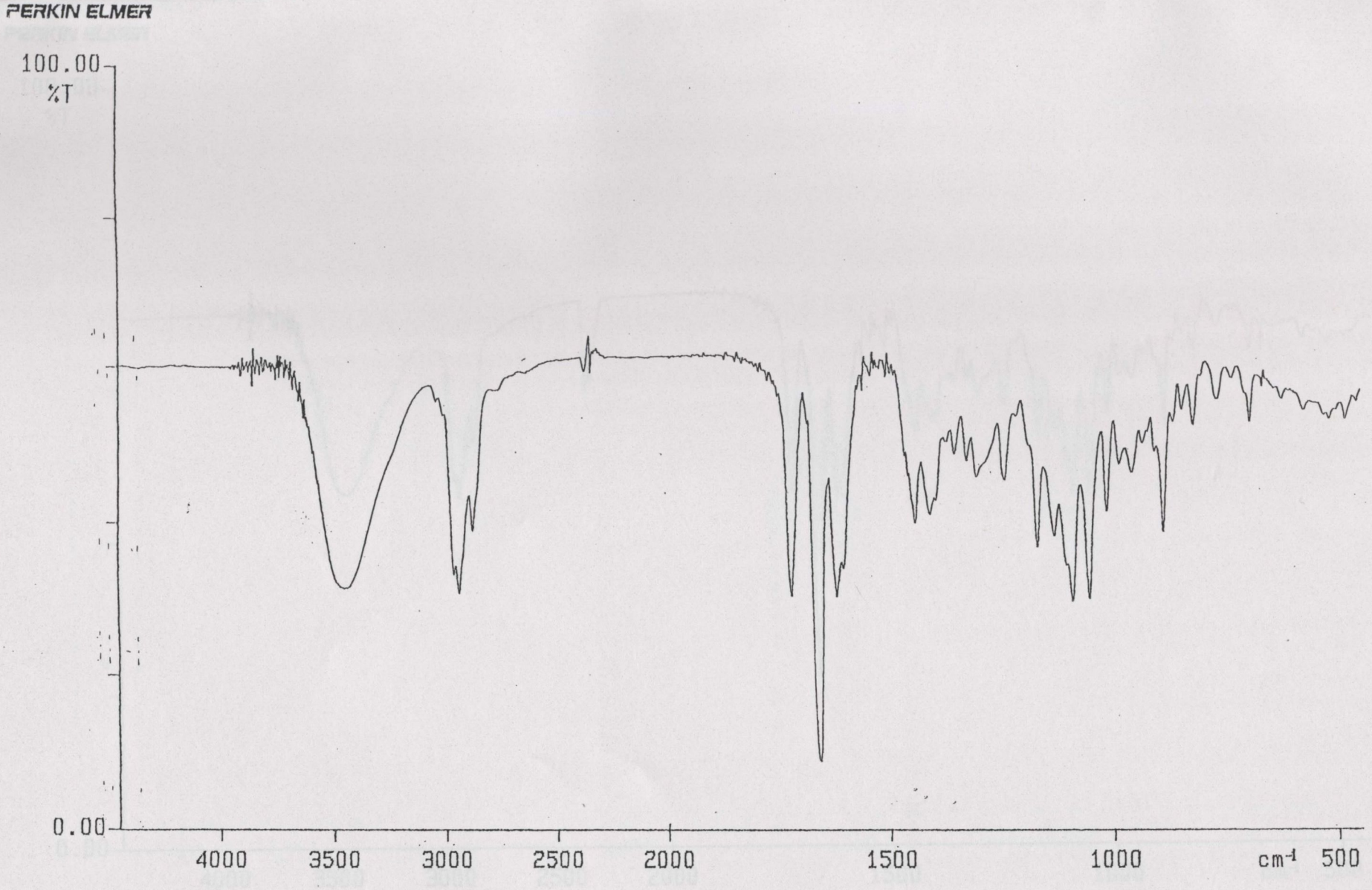

Figure 28 FTIR spectrum of spray dried budesonide.

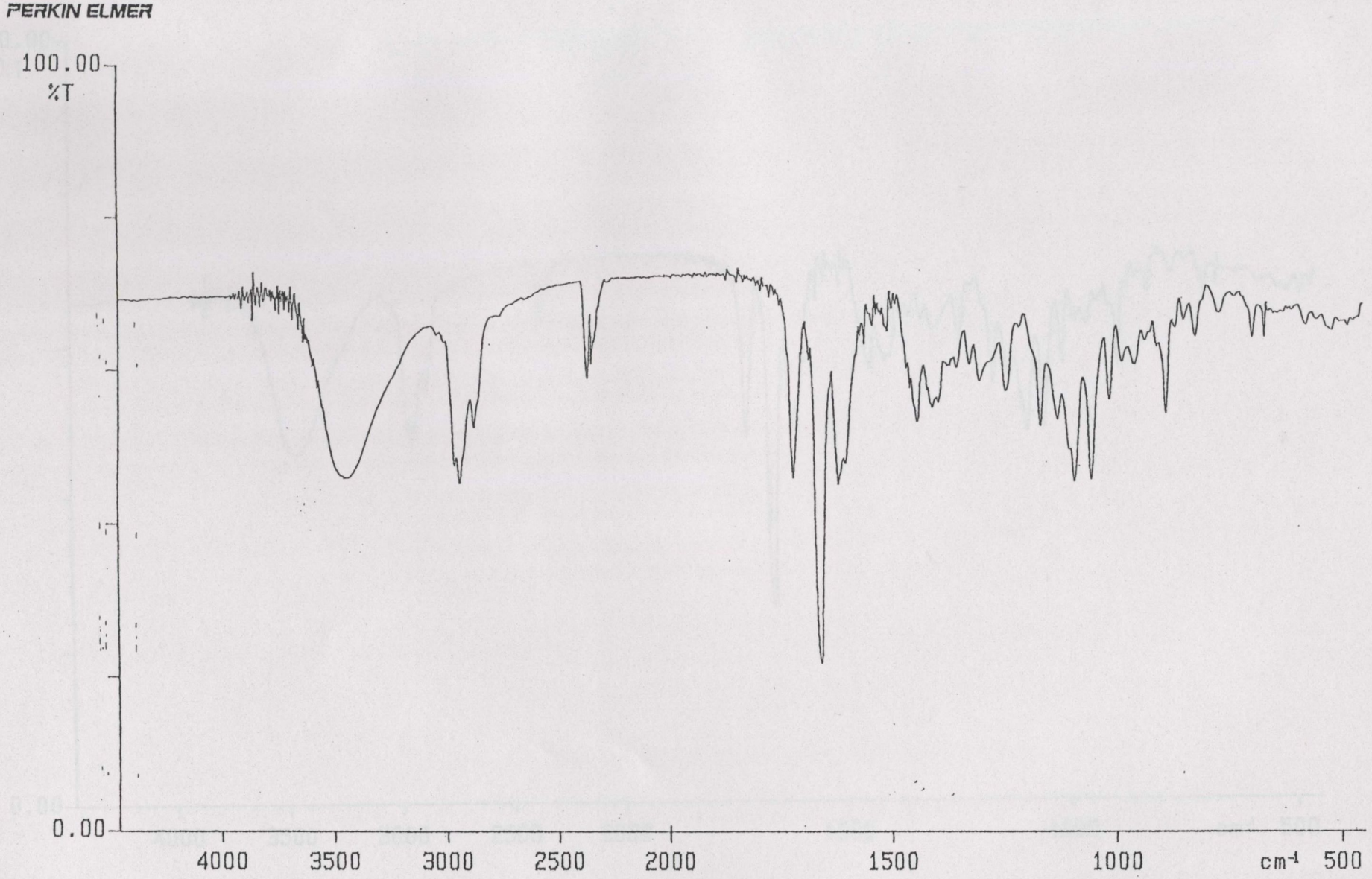

Figure 29 FTIR spectrum of spray dried formoterol fumarate:budesonide 6:100.

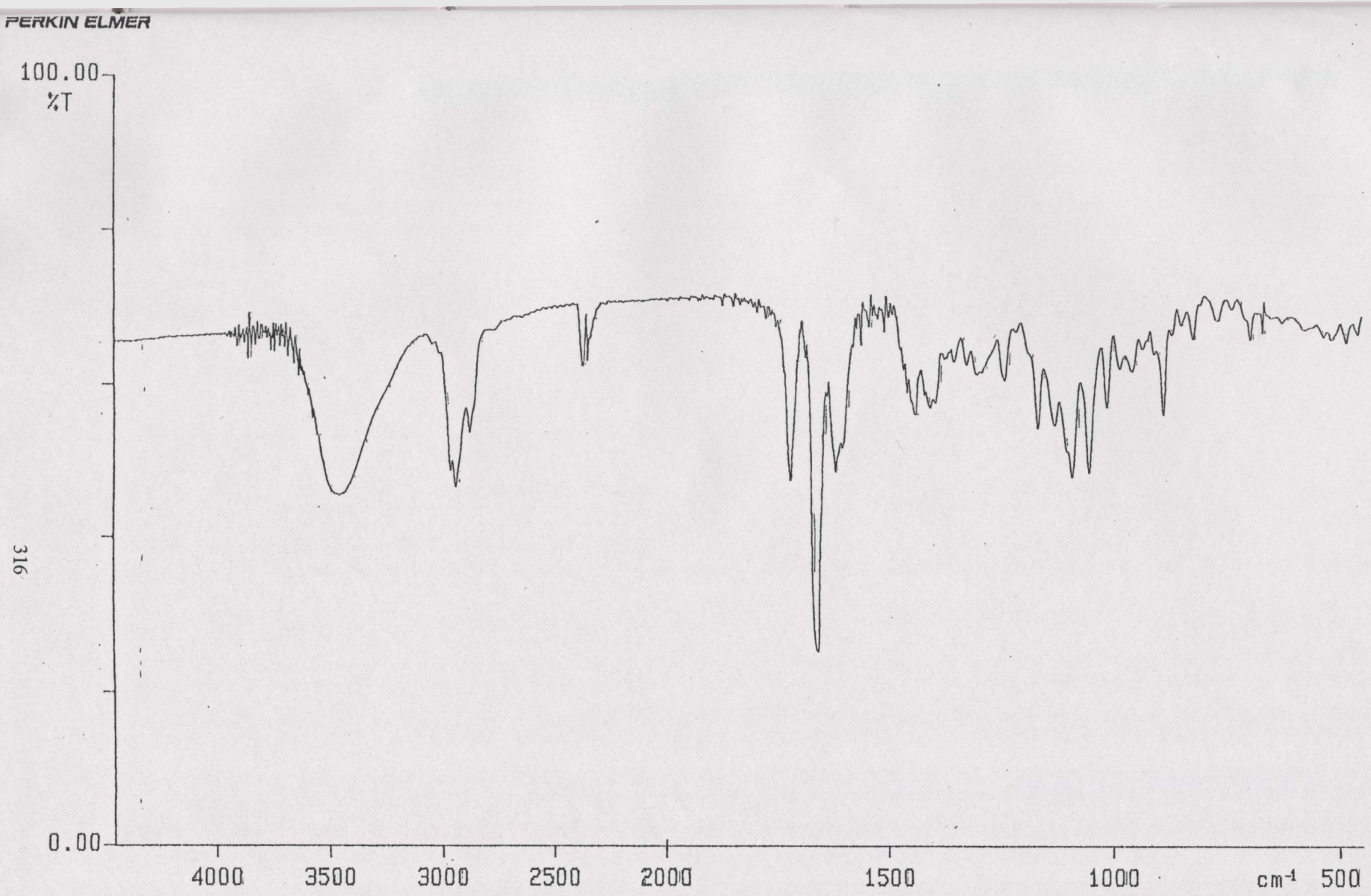

Figure 30 FTIR spectrum of spray dried formoterol fumarate:budesonide 6:400.